

Explorations of Photoelectron Spectroscopy



THE UNIVERSITY OF
WESTERN
AUSTRALIA

Peter Watson

Supervisor: Dr Duncan A. Wild

This thesis is presented for the degree of Doctor of Philosophy

of The University of Western Australia

School of Molecular Sciences

Date of submission: 28/01/2021

Declaration

I, Peter Watson, certify that:

This thesis has been substantially accomplished during enrolment in this degree.

This thesis does not contain material which has been submitted for the award of any other degree or diploma in my name, in any university or other tertiary institution.

In the future, no part of this thesis will be used in a submission in my name, for any other degree or diploma in any university or other tertiary institution without the prior approval of The University of Western Australia and where applicable, any partner institution responsible for the joint-award of this degree.

This thesis does not contain any material previously published or written by another person, except where due reference has been made in the text and, where relevant, in the Authorship Declaration that follows.

This thesis does not violate or infringe any copyright, trademark, patent, or other rights whatsoever of any person.

This thesis contains only sole-authored work, some of which has been published and/or prepared for publication.



Peter Watson, 27/01/2021

Acknowledgments

The author would like to formally acknowledge the Danish Centre for Materials Crystallography.

As with all theses, there are an innumerable number of people who have helped me along this long journey to where I find myself now. First and foremost, to my supervisors Duncan Wild, Allan McKinley and Dino Spagnoli; To Dino; I would like to thank you for your collegiality and support in what has been a tough last few months in my candidature.

To Allan; thank you for your guidance and good cheer throughout my time at UWA. Your steady hand and knowledge of academia have proved invaluable to help me grow as a young researcher and you have proven time and again to be a fount of knowledge and technical expertise when handling our spectrometer.

To Duncan; I would like to thank you from the bottom of my heart. I could not have asked for a more generous supervisor. As new PhD student in the group, I never felt like I couldn't pursue the questions I wanted to pursue or take on work outside my project such as my time in the UWA Student Guild and Senate and becoming an AFHEA. You've been a pleasure to work alongside and I've always enjoyed coming into the lab and your relish for discovery has rubbed off on me.

To the member of the Wild Group and Phys Chem Supergroup; Tim, Christian, Hayden, James, Manon, Damian, Hannah, Max and Matt. You're all wonderful chemists and damn fine friends. From the Cheers playlist, to our own language. There is truly no group quite like us.

To my family who have supported me throughout my life; my parents, Carol and

Daniel; my sister Megan, the boys George and Henry. Mum, you've always been the biggest fighter in my corner. Your tenacity has always been an inspiration to me. Dad, you've instilled in me the joy of building something and using my hands and an appreciation of the beauty of the world around us. You've helped me grow into the man I am today.

To my late grandmother Greta, I wish I could've shown you this work, and you had got to see me graduate from my doctorate. I hope I make you proud.

Finally, to Pheobe, you are my northern star and my guiding light. No matter how far from you I go, you will always be in my heart. You continue to be everything I could want in a partner and more, every day.

Abstract

This thesis explores the computational and experimental approaches to characterisation of weakly bound anion-molecule van der Waals (vdW) complexes. The review of literature establishes the theoretical basis for computational methods employed in the thesis and demonstrates the power of anion photoelectron spectroscopy (PES) in elucidating structure-energy relationships (be they investigations of reaction profiles or binding motifs), gas phase microsolvation and photodynamics. The aim of the work described in this thesis explores the improvement of the anion PES spectrometer housed at the University of Western Australia from a practical standpoint as well as seeking to extend robust ab initio methods to larger chemical systems.

The first results chapter of the thesis utilises anion PES and ab initio methods to investigate the reaction of methyl iodide (CH_3I) with oxygen. A photoelectron spectrum is presented with a broad band assigned to two conformers of the $\text{O}_2^- \cdots \text{CH}_3\text{I}$ complex as well as peaks resulting from the formation and dissociation of as of yet unreported $\text{I}^- \cdots \text{CH}_3\text{OO}$ complex. Methylperoxy, as the simplest alkylperoxy radical in particular, is of atmospheric importance as an intermediate in the formation of carbonyl compounds. Complex structures and energetics have been calculated using MP2 methods and Weizmann (W1w) energies respectively. In the case of the superoxide (O_2^-) complexes term energies of the neutral excited states are included in the ground state vertical detachment energies (VDE) to yield transitions from the ground state anion to excited state neutral complexes.

The following results chapter establishes the applicability of double-hybrid density functional theory (DH-DFT) methods in accurate determination of photoelectron detachment energies for halide-molecule vdW complexes. Comparisons between DSD-PBEP86-D3BJ calculated VDEs for complexes between halides and O_2 , N_2 ,

HCCH, C₂H₄ and formic acid show good agreement in predicting experimental spectra. These methods are then extended to investigate the interactions with unsaturated hydrocarbons, namely halide-propene complexes, with comparisons to new experimental spectra drawn.

The third results chapter utilises the established DH-DFT methods to explore hydrocarbons of increasing degrees of unsaturation. Presented are photoelectron spectra of halide-1,3-butadiene complexes. In addition to investigating binding motifs of these complexes, halide solvation by 1,3-butadiene is investigated with additional spectra presented for X⁻…(C₄H₆)_n (X = Cl, Br, I and n = 1-3, 1-3 and 1-7 respectively). In the case of iodide-1,3-butadiene solvation stepwise stability of solvation show increases at n = 5 and n = 7, representing a partially filled and filled first solvation shell respectively.

Finally, a number of phosphorus hydride-molecule (PH₂⁻…M) complexes are investigated computationally using DH-DFT and W2w energies to identify targets for spectroscopy. Phosphorus containing compounds have become of astrochemical interest in recent years due to their potential as biosignatures. Complexes with CH₄, C₂H₄, HCCH, CO₂, H₂S and NH₃ are presented along with their associated structures, complex stabilisation energies and electron affinities. We note in particular the barrierless formation of the phosphino formate anion (PH₂COO⁻) as an ideal sink in extraterrestrial atmospheres such as Venus.

Contents

1	Introduction	1
1.1	Photoelectron Spectroscopy	2
1.1.1	Photoelectron Spectroscopy	2
1.1.2	ZEKE Spectroscopy	3
1.1.3	Slow Electron Velocity Map Imaging (SEVI) Spectroscopy . .	7
1.2	Computational Methods	17
1.2.1	Principles of Computational Chemistry	17
1.2.2	<i>Ab initio</i> Methods	24
1.2.3	Multireference Methods and Treatment of Excited States . .	33
1.2.4	Density Functional Theory	41
1.2.5	Jacob's Ladder	45
1.2.6	London Dispersion	52
1.2.7	Basis Sets	54
1.2.8	Vibronic Simulations	57
1.2.9	Summary	60
2	Materials and Methods	62
2.1	Computational Approaches	62
2.1.1	<i>Ab Initio</i> Calculations	62
2.2	Existing TOF-PES Spectrometer	69
2.2.1	Gas Mixing Station	69
2.2.2	Time of Flight Photoelectron Spectroscopy	71

2.2.3	Laser	87
2.2.4	SEVI	88
2.3	TOF-PES Modifications During Candidature	94
2.3.1	New Gas Mixing Station	94
2.3.2	Piezo Nozzle Source	95
2.3.3	New Electron Flight Tube	96
2.3.4	SEVI Reconfiguration	97
2.3.5	Summary	100
3	Iodide-Methylperoxy Complexes	103
3.1	Introduction	103
3.2	Methods	106
3.3	Results and Discussion	106
3.4	Summary	114
4	Halide-Propene Complexes	116
4.1	Introduction	116
4.2	Methods	119
4.2.1	Experimental Methods	119
4.2.2	Computational Methods	121
4.3	Results and Discussion	122
4.3.1	Benchmarking DH-DFT Methods	122
4.3.2	Halide-Propene Complexes	127
4.4	Summary	140
5	Halide-Butadiene Complexes	141
5.1	Introduction	141
5.2	Methods	143
5.2.1	Experimental Methods	143
5.2.2	Computational Methods	144

5.3 Results and Discussion	146
5.3.1 Computational Results	146
5.3.2 Time-Of-Flight Mass Spectrometry	148
5.3.3 Photoelectron Spectra	153
5.4 Summary	161
6 Phosphorus Containing Complexes	163
6.1 Introduction	163
6.2 Methods	165
6.3 Results and Discussion	168
6.3.1 PH ₂ ⁻ ...CH ₄ Complexes	168
6.3.2 PH ₂ ⁻ ...C ₂ H ₄ Complexes	172
6.3.3 PH ₂ ⁻ ...HCCH Complexes	175
6.3.4 PH ₂ ⁻ ...CO ₂ Complexes	179
6.3.5 PH ₂ ⁻ ...H ₂ S Complexes	184
6.3.6 PH ₂ ⁻ ...NH ₃ Complexes	187
6.4 Summary	189
7 Conclusions	192
References	195
A Tables and Data: Methylperoxy Radical Complexes	231
B Tables and Data: Double-Hybrid Benchmarking	278
C Tables and Data: Halide-Propene Complexes	408
D Tables and Data: Halide-Butadiene Complexes	429
E Tables and Data: PH₂⁻ Complexes	485

F Additional Appendices	596
F.1 List of Publications	596
F.2 SEVI Chamber Volume	598

List of Figures

1.1	Transitions in photodetachment anion PES	3
1.2	Comparison between conventional PES, ZEKE and SEVI spectroscopy.	4
1.3	Simplified schematic of ZEKE spectroscopy.	5
1.4	Illustrative example of SEVI spectroscopy	8
1.5	Illustrative example of autodetachment dynamics	11
1.6	A representation of the H_2^+ ion.	19
1.7	A plot of a) ψ_+ and b) ψ_- along the internuclear axis of H_2^+	23
1.8	Plot of divergence of Møller-Plesset (MP) energy at higher order.	31
1.9	Representation of the inactive, active and virtual orbitals of a Complete Active Space Self Consistent Field Theory (CASSCF) calculation.	36
1.10	Representation of Jacobs Ladder.	44
2.1	Computational conformer screening protocol	63
2.2	Illustrative anion and neutral potential energy surfaces.	65
2.3	Schematic of the current configuration of the gas mixing station.	69
2.4	Schematic of the existing TOF-PES at the commencement of candidature.	72
2.5	Gas dynamics of a supersonic expansion.	73
2.6	Velocity distribution of the background gas compared to the skimmed gas distributions.	75
2.7	Potential energy surfaces of an example dissociative electron attachment process.	76

2.8 Schematic of the mass gate and ion decelerator.	80
2.9 Time-of-flight mass spectrum of a CH ₃ I:O ₂ :Ar gas mix.	82
2.10 Magnetic field lines of the magnetic bottle spectrometer.	83
2.11 Example calibration photoelectron spectra of I ⁻	90
2.12 Schematic of the existing SEVI spectrometer at the commencement of candidature.	91
2.13 Schematic of the double walled μ -metal shielding.	92
2.14 Schematic of the current configuration of the gas mixing station. . . .	95
2.15 Schematic of the piezo nozzle installed in the Wild Group TOF-PES. .	96
2.16 Schematic of the reconfigured SEVI spectrometer.	102
3.1 O ₂ :CH ₃ I:CH ₂ Br ₂ :Ar Mass Spectrum	107
3.2 Iodide-Methylperoxy PES	108
3.3 MP2 O ₂ MeI Structures	110
3.4 Fitted Iodide-Methylperoxy PES	112
3.5 O ₂ MeI Reaction Pathway	115
4.1 Structures of halide-molecule complexes	124
4.2 Halide-Propene Optimised Structures	128
4.3 CH ₂ Br ₂ :C ₃ H ₆ :Ar Mass Spectrum	130
4.4 CH ₃ I:C ₃ H ₆ :Ar Mass Spectrum	132
4.5 CCl ₄ :C ₃ H ₆ :Ar Mass Spectrum	133
4.6 Chloride-Propene PES	135
4.7 Bromide-Propene PES	136
4.8 Simulated Bromide-Propene Photoelectron Spectrum	138
4.9 Iodide-Propene PES	139
5.1 Butadiene Complex Starting Geometries	145
5.2 Halide-butadiene Optimised Structures	147
5.3 CCl ₄ :C ₄ H ₆ :Ar Mass Spectrum	149

5.4 CH ₂ Br ₂ :C ₄ H ₆ :Ar Mass Spectrum	151
5.5 CH ₃ I:C ₄ H ₆ :Ar Mass Spectrum	152
5.6 Chloride-Butadiene PES	154
5.7 Bromide-Butadiene PES	156
5.8 Iodide-Butadiene PES	157
5.9 Iodide-2-butadiene Optimised Structures	159
5.10 Solvation Energies of vdW Complexes	160
5.11 Hypothetical 6-coordinate complex	161
6.1 PH ₂ …CH ₄ optimised structures	169
6.2 PH ₂ …C ₂ H ₄ optimised structures	173
6.3 Simulated PH ₂ ⁻ …C ₂ H ₄ spectra	176
6.4 PH ₂ …HCCH optimised structures	177
6.5 Simulated PH ₂ ⁻ …HCCH spectrum	178
6.6 PH ₂ …CO ₂ optimised structures	180
6.7 Potential energy scans of the PH ₂ ⁻ …CO ₂ complex.	182
6.8 Simulated PH ₂ ⁻ …CO ₂ spectra	183
6.9 PH ₂ …H ₂ S and HS…PH ₃ optimised structures	186
6.10 Simulated HS ⁻ …PH ₃ spectrum	187
6.11 PH ₂ …NH ₃ optimised structures	188
6.12 Simulated PH ₂ ⁻ …NH ₃ spectrum	190
A.1 $^2P_{3/2} \leftarrow ^1S$ Iodide PES	276
A.2 Bare Iodide Peak from within Iodide-Methylperoxy PES	277
C.1 Example Chloride PES	410
C.2 Additional Cl-Propene PES	411

Chapter 1

Introduction

Long-range van der Waals (vdW) interactions are ubiquitous in chemistry, known to be fundamental channels in the formation and cleavage of bonds,¹ in the binding of macromolecular structures such as proteins,² and present in intermediates in both atmospheric and extraterrestrial chemical contexts.^{3–7} Ewing suggests that the definition of vdW or weakly bound complexes are interchangeable, and refers to systems where interactions involve competitive dispersion, hydrogen-bonding and electric multipole interactions.⁸ A simplistic classification is based upon typical bond lengths found in vdW complexes (2–5 Å),⁹ and in most cases this is a sufficient indicator of weaker interaction, however as vdW complexes are considered here primarily as transition states in chemical reactions it is more appropriate to classify them based upon their complex dissociation energy (D_0 , which are typically less than 30 kJ mol⁻¹ to 40 kJ mol⁻¹).^{10–12} Regardless, the properties of these systems (their energetics and geometries) are intrinsically tied to their geometric and electronic structure. These properties can therefore be elucidated by means of spectroscopy and verification through the modelling of electronic structure.

This chapter represents a review of literature surrounding both the experimental and theoretical methodologies used in the investigation of weakly bound clusters, namely photoelectron spectroscopy (PES) and computational chemical methods. Where literature is directly applicable to one of the systems studied within this

work, it will be discussed as part of the introduction to the relevant chapter.

1.1 Photoelectron Spectroscopy

1.1.1 Photoelectron Spectroscopy

Spectroscopy, in all its forms is one of the most powerful techniques in modern physical chemistry for elucidating the geometric and electronic structure of chemical species. Photoelectron spectroscopy (PES), the focus of this work, targets stable chemical species with photons lying within regions of the electromagnetic spectrum of sufficient energy to detach electrons such that their kinetic energies can be measured (Equation 1.1)

$$E_B = h\nu - E_K \quad (1.1)$$

where the electron binding energy (E_B) is determined by measuring the kinetic energy (E_K) of electrons produced during a photodetachment event. By measuring this kinetic energy and knowing the energy carried by the incident photon ($h\nu$), Koopman's theorem is then utilised to determine the energy associated with the orbital from which this electron was ejected.¹³

First demonstrated by Brehm *et. al.*,¹⁴ anion photoelectron spectroscopy probes negatively charged analogues and determines their electron binding energies, representative of the electron affinity of the corresponding neutral. Coupling photoelectron spectrometers with mass selection techniques of sufficient mass resolution allows for separation of a gas-phase mixture and interrogation of specific species by PES techniques.¹⁵ Since its advent, anion PES has become an efficient method for spectroscopic analysis. The technique has seen use in determination of the electronic binding energies of molecular anions and radicals,^{16–24} metal complexes and clusters^{25–31} and loosely bound van der Waals systems,^{32–39} as well as exploring photochemical processes,^{40–43} bonding interactions^{12,44,45} and transition state chem-

istry.^{46–48} Additionally, improvements in experimental design including moving to a pulsed experimental regime⁴⁹ and increased energy resolution have allowed discrete transitions of not only electronic but also vibrational and even rotational states^{22,50} to be observed. These and further examples are discussed in more detail in the following sections including the variants of PES by which they were performed.

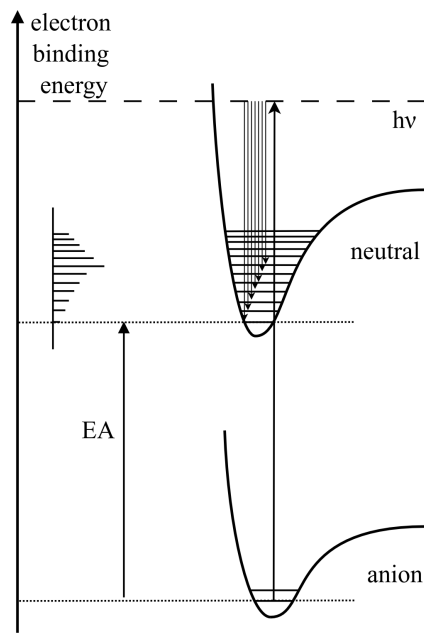


Figure 1.1: Transitions in photodetachment anion PES

1.1.2 ZEKE Spectroscopy

Threshold Spectroscopy

In general, reduction of broadening in photoelectron kinetic energy can be categorised by those driven by the molecular beam (thermal and Coulombic effects),⁵¹ those of the light source and experimental design. Much of the broadening resulting from a light source in modern spectroscopic applications has been circumvented by the use of laser sources as opposed to broader sources with a suitable monochromator.⁵² However photoelectron detection in anion PES has previously been limited by the larger radial velocities of fixed wavelength detection schemes. The highest respective resolutions of these apparatus are 50 cm^{-1} for the hemispherical

analyser,⁵³ $40\text{--}80\text{ cm}^{-1}$ for conventional time-of-flight photoelectron spectroscopy (TOF-PES)⁵⁴ and 150 cm^{-1} for magnetic bottle TOF-PES.⁵⁵ Previous work within the Wild Group, utilising a TOF-PES apparatus based on designs by Wiley and McLaren¹⁵ and Cheshnovsky,⁵⁶ has recorded $\text{Cl}^-\cdots\text{N}_2$ complexes with an associated kinetic energy full-width half maximum (FWHM) of 0.21 eV (1690 cm^{-1}).⁵⁷ Given the spin-orbit splitting of the 2P states of chloride is 0.109 eV (879 cm^{-1}), separation of even electronic states is not possible with the existing apparatus.

Threshold spectroscopy techniques, where tuneable light sources excite photoelectrons to energies near the photodetachment region, offer a means by which to reduce photoelectron radial velocities. These include both zero electron kinetic energy (ZEKE) and SEVI spectroscopy. A simplified schematic adapted from Schlag⁵⁸ is presented in Figure 1.2⁵⁹ and shows the various detachment schemes for these techniques.

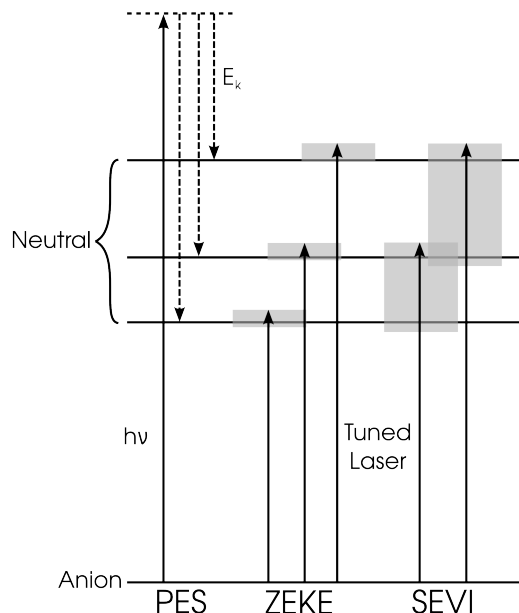


Figure 1.2: Comparison between conventional PES (left), ZEKE (centre) and SEVI (right) spectroscopy. Adapted from Osterwalder *et al.* (via Schlag)⁶⁰

ZEKE Spectroscopy

ZEKE spectroscopy offers one avenue for attaining higher resolution PES than conventional methods. By tuning the energy of the incident photon to near threshold wavelength (as shown in Figure 1.2), electrons are promoted to high-lying Rydberg states in which the high orbital angular momentum (ℓ) improves their stability and increases their lifetime.⁶¹ Species in these states can then be ionised by a pulsed electric field to increase the photodetachment volume and allow for detection at a micro-channel plate (MCP).⁶² Tuning photon wavelengths such that laser energies are above threshold levels extracts both ZEKE and non-ZEKE kinetic energy electrons, with the latter being similar in nature to conventional PES. Furthermore, due to their spherical expansion, by passing the photoelectrons through an orifice some of the kinetic electrons carrying velocity components perpendicular to the path of the beam may be blocked and their signal can then be reduced with respect to that of the ZEKE electrons⁵⁸ This expansion also leads to pairs of non-ZEKE signals corresponding to the leading and tailing surfaces of the sphere.

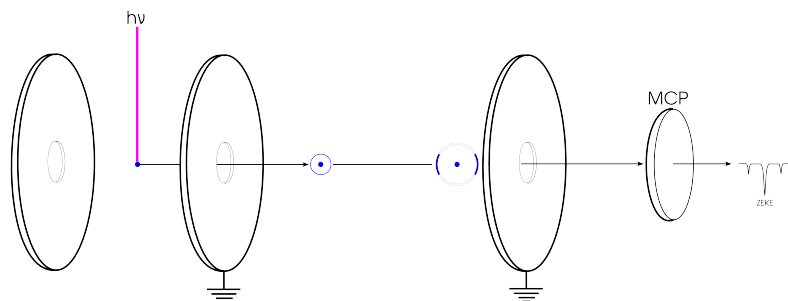


Figure 1.3: Simplified schematic of ZEKE spectroscopy.

Comparing the accuracy of determined ionisation potentials of benzene between conventional PES ($74\,536.0(1200)\text{ cm}^{-1}$) and ZEKE spectroscopy ($74\,556.1(3)\text{ cm}^{-1}$) the associated error reported for ZEKE methods is 0.25 % of that associated with conventional PES.^{63,64} At this level of resolution not only is vibrational structure observed but there is potential for observable rotational structure in the spectra⁶² (at the time of writing the highest resolution of recorded ZEKE spectra has been

reported to be 0.15 cm^{-1} in the spectrum of NO⁶⁵). ZEKE spectroscopy, however, is often difficult to implement experimentally, particularly in timing the extraction pulse and minimising the impact of stray electric and magnetic fields.⁴⁶

The Wigner threshold law,⁶⁶ given in Equation 1.2, describes the photodetachment cross section (analogous to the probability of detachment) with respect to quantum angular momentum (ℓ) of the orbital and energy of the incident photon ($h\nu$). In ZEKE spectroscopy experiments from anion states, only detachment of $\ell = 0$ electrons is possible with significant cross-sections, whereas for $\ell \geq 1$ these cross-sections are very small. Neumark *et al.* demonstrated the potential power of this in showing detachment from *s*-orbital environments in the specific cases of Si₂⁻ and Si₄⁻ respectively,^{67,68} however this is largely restrictive in the applicability of anion ZEKE.

$$\sigma \propto (h\nu + E_{th})^{\ell + \frac{1}{2}} \quad (1.2)$$

In attempts to benefit from both high kinetic energy resolution provided by anion ZEKE and flexibility of conventional PES the groups of Cheshnovsky and Neumark developed photoelectron action at constant energy (PEACE)⁶⁹ and SEVI⁶⁰ spectroscopy respectively. SEVI will be detailed in the following section however PEACE will be reviewed here. PEACE spectroscopy utilises a Wiley-McLaren time-of-flight mass spectrometer (TOF-MS) with a collinear magnetic bottle photoelectron spectrometer optimised for collection of low energy electrons. By designing the instrument to be collinear, Cheshnovsky *et al.* reduce the effect of Doppler broadening present in orthogonal instruments. Their designs also include a decelerating region allowing not only compensation for the energy of the molecular beam, but for the energy of the incident photon to be above threshold whilst still preserving the collection of slow electrons. This higher energy regime coupled with the magnetic bottle design circumvents the high number of photodetachment events statistically necessary for some threshold experiments. While PEACE spectroscopy has delivered

energy resolutions of 1.0 meV, the corresponding proof-of-concept SEVI experiments delivered a ten-fold improvement in resolution.⁶⁰

1.1.3 SEVI Spectroscopy

Whereas previously discussed anion PES spectroscopic techniques measure electron kinetic energy *temporally*, SEVI spectra determine kinetic energy *spatially*. The technique is built upon other photoelectron imaging experiments, where photoelectrons are produced via thermionic emission rather than photodetachment.⁷⁰ Considering a detachment process, photoelectrons are ejected radially from a point in space where photons of sufficient energy interact with a chemical species, be that an anion, neutral or cation. As opposed to ZEKE experiments where photoelectrons are removed from Rydberg states of the neutral by an electrostatic pulse, photoelectrons in SEVI typically undergo direct photodetachment at near threshold energies (with their photodetachment cross-section governed by Equation 1.2). Following detachment, photoelectrons of various kinetic energies form nested spheres centred on the point of detachment. Under ideal conditions, these can then be extracted by an electrostatic lens and their position detected on a position sensitive MCP. The position of the photoelectron collisions on the detector is then determined by projection of these nested spheres onto the screen where the radial density of the photoelectrons in the plane of the screen is correlated with the intensity at that position and the radial position is correlated with photoelectron kinetic energy (see Figure 1.4).

Seminal work by Eppink and Parker⁷¹ demonstrated that with an appropriate velocity map imaging (VMI) lens design consisting of a set of repeller, extractor and ground ring electrodes and suitable applied voltages, photoelectrons ejected from different positions within the laser beam profile but with the same angle spacing, could be mapped to the same position on the detector. This compensated for distortions in the final image resulting from the photoelectron ejection and vastly improved the

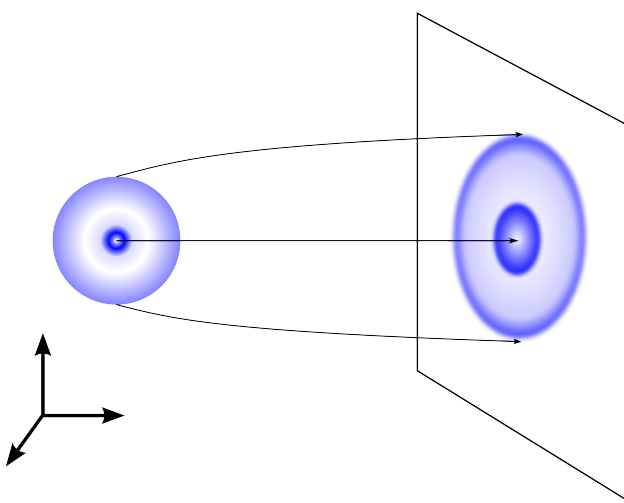


Figure 1.4: Illustrative example of SEVI spectroscopy. Two nested spheres and projected onto a screen surface forming concentric circles.

ultimate resolution of these spectra. In addition to energy information that can be drawn from SEVI images, information on the bonding environment can be determined based on the distribution of photoelectrons.⁷² As an example when ejected from *s* and *p* type orbitals, the ejected photoelectrons form *p* waves and interfering *s* and *d* waves respectively ($\ell' = \ell \pm 1$).⁷³ The intensity of the photoelectron angular distribution (PAD) is then represented by the Cooper-Zare equation (Equation 1.3 for a single photon process) as a function of the angle between photoelectron ejection and the polarisation axis of a linearly polarised light source:⁷⁴

$$I(\theta) = \frac{\sigma_{tot}}{4\pi} [1 + \beta P_2(\cos \theta)] \quad (1.3)$$

where P_2 is the second order Legendre polynomial such that $P_2(\cos \theta) = \frac{1}{2}(3\cos^2 \theta - 1)$, σ_{tot} is the total photodetachment cross section and β is the anisotropy parameter. The β parameter ranges from -1, for perpendicular (\perp) photodetachment corresponding to detachment at near threshold kinetic energies from a *p* orbital with inclusion of *s* and *d* partial waves, to 2 for parallel (\parallel) photodetachment representing a detachment from a pure *s* orbital.⁷⁵ This allows qualitative statements to be made regarding the degree of hybridisation present in a chemical system and has been used to assign peaks with photoelectron spectra by inferring the molecular

bonding environment.^{76,77} The β parameter at higher kinetic energies (ε) is then determined by a mixed $s\&p$ model ($|\psi_{sp}\rangle = \sqrt{1-f}|s\rangle + \sqrt{f}|p\rangle$):⁷⁸

$$\beta = \frac{2Z\varepsilon + 2A\varepsilon^2 - 4\varepsilon \cos(\delta_2 - \delta_0)}{A^{-1} + 2A\varepsilon^2 + Z\varepsilon} \quad (1.4)$$

where $Z = (1-f)B/Af$, A and B represent scaling factors of $\ell+1$ and $\ell-1$ waves and $\cos(\delta_2 - \delta_0)$ represents the phase shift between s and d partial waves. A similar interpretation can then also be applied to the mixing of higher $p\&d$ states ($|\psi_{pd}\rangle = \sqrt{1-f}|p\rangle + \sqrt{f}|d\rangle$).⁷⁹

The flexibility and power with which properties of a chemical system could be interrogated allowed for a suite of SEVI spectrometers to be constructed in the years following the publication of designs of the Eppink-Parker VMI lens. A number of notable examples of SEVI spectrometers and their applications will be detailed and the design outlined in the context of those purposes.

The first published example of an anion photoelectron VMI spectrometer is that of the Sanov Group.^{80,81} The design in this case comprised both orthogonal extraction of ions and photoelectron detachment with an MCP along the time-of-flight (TOF) axis and after the laser intersection region and utilising a fixed wavelength Nd:YAG laser light source. Studies with this apparatus appear focussed on the PADs produced by photodetachment rather than the discrete binding energies themselves. However as a proof-of-concept, photoelectron VMI offered good energy resolution with reported typical reported electron affinities of small radicals to meV range (ie $E_a(C_5H_4N) = 1.48(2)$ eV, VDE(Biacetyl)= 1.12(5) eV).^{75,82} Sanov *et al.* also derived much of the methodology for interpretation of PADs in photoelectron VMI spectra, including the application of mixed $s\&p$ and $p\&d$ models described previously^{75,79} and the fitting of anisotropy parameters from two photon processes (with inclusion of a fourth order Legendre polynomial).⁸³

The first true SEVI spectrometer, being that spectra were taken with near threshold photon energies, was that of the Neumark Group, built as improvements upon an

existing VMI spectrometer.^{60,84} The spectrometer utilised a collinear design where gas mixtures are introduced via a pulsed piezo nozzle at 20 Hz with typical backing pressures of 140 kPa to 550 kPa. Under the initial designs, this SEVI spectrometer achieved energy resolutions of $\frac{\Delta KE}{KE} = 7\%$ with best performance at higher kinetic energies.⁶⁰ However while energy resolution improved with higher eKE, the authors noted that the larger photoelectron images were prone to interference from electric fields from the edge of the detector. In general though, peaks resulting from low eKE photoelectrons showed FWHM of 1.1 cm^{-1} , comparable to ZEKE spectroscopy.

Later improvements were made to the SEVI spectrometer in the Neumark Group. These included the addition of an RF octupole ion trap in the source region of the spectrometer.⁸⁵ By trapping the produced ions (in this case C_5^-) and introducing pulses of buffer gas to the ion trap, the ion temperature can be reduced from 59(2) K to 10(2) K. The corresponding improvement in resolution under what was termed “cryo-SEVI” is represented by the reduction in FWHM of the ${}^1\Sigma_g^+ \leftarrow {}^2\Pi_{1/2}$ transition from 13.3 cm^{-1} to 6.3 cm^{-1} . Further improvements were later made to the VMI lens of the Neumark SEVI spectrometer. In addition to the existing Eppink-Parker design, four guarding electrodes, two between each of the existing electrodes were included.⁷⁷ The new 7-ring lens operated similarly to before with spacings between the electrodes of $10 \text{ M}\Omega$, resistively coupling the chain. The guarding electrodes offered a more uniform electric field gradient within the lens as well as increasing the total length of the lens without increasing the impact of fringe field effects. This offered further improvements in energy resolution with reported calibration spectra of O^- and F^- yielding threshold ($eKE = 5 \text{ cm}^{-1}$) FWHM of 1.2 cm^{-1} . The overall optimal resolution of the spectrometer with improved VMI lens design is then determined as $\frac{\Delta KE}{KE} = 1.4\%$.

A notable application of the SEVI spectrometer in the Neumark Group is that of the photoelectron spectra of iodide-nucleobase weakly bound clusters.^{40,86,87} These compounds were of particular interest as representative moieties to understand the mechanism by which ionising radiation damages DNA.⁸⁸ In addition to observing

direct photodetachment and determining the electron binding energies, molecular anions of uracil and thyamine can form dipole bound states (DBS) where electrons are promoted to high-lying resonant states near threshold.⁸⁹ Similarly to Rydberg states, where electrons are bound by the formation of a cation, electrons in DBSs are, as the name suggests, bound by the strength of the dipole in the corresponding neutral. As a result, candidates for dipole-bound states typically require a dipole of at least 2.5 D with the electron trapped in the resulting $1/r^2$ potential.⁹⁰ The presence of these DBSs in molecules are of interest as they represent channels for electron capture and anion formation. The opportunity for charge-transfer within the cluster, as seen with $I^- \cdots (H_2O)_4$ clusters, is similarly appealing for studying gas- and condensed phase reactions.⁹¹

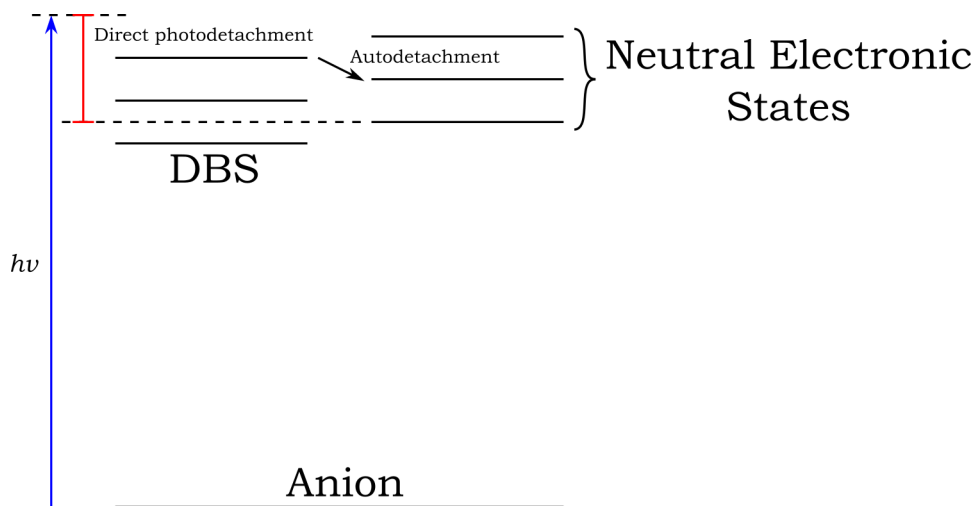
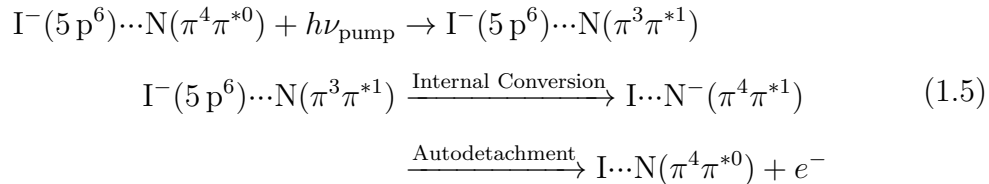


Figure 1.5: Comparison between direct photodetachment (red) and, were a resonant transition to a DBS is available, autodetachment via a DBS (black). The energy levels shown represent vibrational energy levels of the DBS and neutral electronic state respectively. Photon energy ($h\nu$) is represented by the blue arrow.

From the perspective of PES experiments however, the excitation to a DBS typically corresponds to a sharp increase in the photodetachment cross-section of a species.⁹⁰ Where a resonant excitation to a DBS is located, the species may then undergo photoelectron autodetachment where upon ejection of a photoelectron from the DBS, the change in energy to the neutral species is small and low kinetic energy electrons are produced (see Figure 1.5).⁹² Previous photoelectron spectroscopy ex-

periments on uracil and thyamine by Hendricks determined their electron affinities to be 93 meV and 69 meV respectively.^{88,93} In the case of the iodide-nucleobase clusters, excitation may also proceed via a valence-bound excited state of the nucleobase (Equation 1.5). With both photoelectron decay dynamics available, two-photon PES where the wavelength dependence of the excitation laser allowed for selection of these channels and a time delayed photodetachment photon could then interrogate the relaxation of the excited states.^{40,86,94,95} Additional examples of these photodynamics and the photofragmentation of these clusters have also been demonstrated for iodide-thymine and iodide-cytosine clusters by Dessent *et al.*⁹⁶



To the writer's knowledge, the highest resolution SEVI spectrometer that has been reported to date is that of Cavanagh and Gibson.⁹⁷ While VMI lens design considerations are no doubt integral in the construction of a SEVI spectrometer, the observation made by Cheshnovsky that control of the molecular beam profile and velocity is paramount appears to be true in general also.⁵⁶ As well as inclusion of guarding electrodes to the VMI lens, the design of the Cananagh and Gibson spectrometer is optimised for mass spectrometry resolution and by correlation, energy resolution. The main design considerations are the considerable length of the spectrometers TOF path (2 m), coaxial ion injection and VMI axis, low ion beam energy of 500 eV and the inclusion an ion buncher module.⁹⁸ Cavanagh and Gibson also note the need for strict control of applied voltages and minimisation of interfering field effects.⁹⁷ This is further demonstrated in that due to the beam energy being comparatively lower, while the effect of Doppler broadening may be reduced, similarly smaller voltages in the ion buncher, requiring a buncher voltage of ~ 35 V) to

reduce a 500 eV beam of O⁻ from 80 mm in length to 2 mm over the TOF path.⁹⁷ In the same sense an absolute effect imparted by interfering fields are relatively greater at smaller beam energies.

Ultimately however, the reported energy resolution of the Cavanagh and Gibson design spectrometer is $\frac{\Delta KE}{KE} = 0.38\%$, an approximately 70 % improvement in resolution compared to Neumark.^{60,97} It is worth noting however that the design choices suggest that the intention of the spectrometer is to provide extremely high resolution spectra on small molecular anions,^{99–101} to the point where spin-orbit states of these small anions may resolved. In contrast the spectrometer in the Neumark group appears much more flexible in its design scope and, in addition to the photodetachment dynamics described previously, is employed to investigate larger polyaromatic hydrocarbons,^{76,77,102} transition metal oxide clusters^{48,103,104} and weakly bound systems^{40,47} where RF cooling is necessitated.

Recently the Cavanagh and Gibson spectrometer has been used to undertake an extensive study of the photodetachment dynamics of the cyanomethide anion CH₂CN⁻.¹⁰⁵ In this case, cyanomethide exhibit similar DBS behaviour to that described previously and the high resolution of the Cavanagh and Gibson instrument allowed for classification of multiple photodetachment channels inclusive of energy redistribution through vibrational and rotational states of the neutral. Similar, high resolution SEVI spectrometers have also been constructed in recent years by the groups of Lai-Sheng Wang,¹⁰⁶ Zichao Tang^{44,107} and Carl Lineberger.^{108,109}

Other notable examples of VMI photoelectron spectrometers are those of the Fielding and Verlet Groups.^{110,111} The Fielding VMI spectrometer also utilises an electrospray ionisation source (ESI) source which allowed for ions to be produced from solution rather than directly in the gas phase.¹¹² The energy resolution of the instrument under this regime was demonstrated via photodetachment from an iodide anion with a photon energy of 4.61 eV. The corresponding FWHM of transitions to the ²P_{3/2} (*eKE* = 1.5 eV) and ²P_{1/2} (*eKE* = 0.6 eV) states are approximately 90 meV and 60 meV respectively. By using an ESI source, new opportunities for spectroscopy

of typically inaccessible species are available. Injecting biologically relevant compounds for spectroscopy in a buffer medium allows for control of the deprotonation and replication of biological pH conditions. Examples from the Fielding Group that followed from the construction of the VMI spectrometer include the characterisation of vertical detachment energies (VDE)s of analagous compounds to green and cyan fluorescent protein chromophores used in *in vivo* imaging experiments.¹¹³ Further investigation of the photodynamics of such systems showed that for the chromophore *p*-hydroxybenzylidene-2,3-dimethyl-imidazolinone (HBDI), resonant transitions similar to those described here previously for iodide-nucleobase clusters, competed with direct photodetachment and were possible channels of photoactivation.¹¹⁴

Verlet, seeking to perform combined orthogonal photoelectron and photofragmentation spectroscopy and two-photon experiments, sought to reduce the electric field gradient in the VMI lens as it deflected the ion beam as it passed through.¹¹⁵ The designed VMI lens was similar conceptually to a 3-electrode VMI lens (although nominally was a 2-electrode lens), however between the extractor and what would typically be a grounded electrode, was a resistive glass tube that made up the photoelectron flight tube.¹¹¹ Initial testing of the VMI lens design operated the lens at -300 V with a nominal resolution of $\frac{\Delta KE}{KE} = 8\%$, however this field gradient could be reduced. By biasing the front face of the detector ($+75\text{ V}$) to ensure electron collisions were of sufficient energy for detection, the potential difference of the VMI lens could be reduced to -75 V . Where fringe field effects can effect the properties of the species in question, minimising their impact can become important. Verlet's low extraction field VMI lens was also demonstrated to operate only on a 9 V battery, with a field gradient of $<0.5\text{ V cm}^{-1}$. At these field gradients, the fields created by normal operating voltages of the subsequent photofragment detector (1 kV) reduced the resolution of the parallel VMI lens to 14% .¹¹¹ The spectrometer would however be utilised in a number of studies investigating reaction mechanisms,^{116,117} electron transfer from valence-bound to dipole-bound states,^{118,119} and bonding characterisation¹²⁰ using a combination of polarisation angle, photon energy and pump-probe

delay PES.

With key design elements of a small and smooth electric gradient at the point of photodetachment, VMI lens designs have been taken to further extremes. Garand *et al.* in recent years have constructed a 3-potential, 38-electrode lens with the intention of smooth electric field gradients.¹²¹ The design utilises sets of resistively coupled electrodes to reduce the voltage over the full length of the photoelectron flight tube similar to Verlet's VMI lens. Whereas other designs focus the photoelectrons and then allow them to drift towards the detector, these designs appears to guide the photoelectrons over the entire region, albeit with decreasing field gradients.

Image Processing

While spectrometer designs have now been discussed at length, a crucial step in the processing of data from SEVI spectroscopy is the reconstruction of the 3D photoelectron distribution from the 2D image. Methods of 3D reconstruction often involve the implementation of an inverse Abel transform¹²² (Equation 1.6) however this method requires cylindrical symmetry and accurate centering algorithms. Hence it often suffers from amplification of noise (particularly centreline noise) and requires smoothing.^{123,124} Basis set expansion (BASEX) methods, assume the image is made up of an expansion of a “well-behaved basis set” and handles noise more appropriately than that of direct inverse Abel transform. They do however still rely on cylindrical symmetry and centreline noise is not eliminated.^{123,125} Both methods use the cylindrical symmetry of the PAD to transform a 2D image in Cartesian coordinates to a 3D projection An alternative to overcome the shortcomings of BASEX methods is polar BASEX (pBASEX) which transform the image directly from Cartesian to polar coordinates before determining expansions of polar functions. This method delivers the benefits of handling of noise demonstrated by BASEX methods while transforming centreline noise to that of a centred dot such that it does not interfere with the rings representative of photoelectron signal.^{123,126} pBA-

SEX methods also prove to be significantly less costly than BASEX methods. In the development of pBASEX, a test image produced from the (1+1') multiphoton ionisation of para-difluorobenzene, processed on a 1.7 GHz Pentium IV processor recorded computational times of 1.3 s and 64.0 s for pBASEX and BASEX methods respectively.¹²⁶ A further review of inverse Abel methods demonstrated an improvement of an order of magnitude between BASEX and pBASEX methods for images up to 10^4 pixels.¹²⁷ pBASEX has subsequently have become the most popular method for image processing in SEVI spectroscopy.¹²⁸

$$f(r, z) = -\frac{1}{\pi} \int_r^\infty \frac{dF(y, z)}{dy} \frac{1}{\sqrt{y^2 - r^2}} dy \quad (1.6)$$

Alternative onion peeling algorithms¹²⁴ are computationally faster and more intuitive to implement. Their reconstruction begins on the edges of the image and they accumulate noise as they progress inwards.¹²⁶ Combining the ideas of pBASEX and onion peeling algorithms into polar onion peeling (POP) reduces the noise for larger radii and subsequently the noise accumulation moving inward, however currently implementation of POP methods are not optimal and the increased computational cost does not outweigh the sacrificed accuracy with respect to pBASEX methods.¹²³ Experimental comparisons between these direct reconstruction methods has been made for SEVI spectra of Au^- , which suggests similar performance between onion peeling, POP, BASEX and pBASEX methods with radial widths ranging from 1.72 to 2.5 pixels.¹⁰⁶ The Hansen and Law method for both the forward and inverse Abel transforms is expressed via the standard linear state-variable model as a set of differential equations. It offers the benefits of being robust and efficient in image processing as it does not require a good basis set to begin with (unlike BASEX methods).^{129,130} Whereas many groups have developed in-house codes for data analysis, the open-source PyAbel module developed by Hickstein *et al.* implements all the algorithms described above, offering the flexibility of a typical Python environment to analyse VMI images.¹²⁷ The developers note that images

up to 50,001x50,001 pixels can be processed using a desktop workstation (3.4 GHz Intel i7-6700 processor, 32GB RAM).¹²⁷

Recently a different approach to the reconstruction of photoelectron distributions has been proposed.¹²⁸ Maximum Entropy Velocity Legendre Reconstruction (MEVELER) rather than directly transforming the 2D imaging to a 3D distribution, determines the most *likely* 3D distribution to produce a given 2D image. As a result it requires no smoothing and introduces fewer artefacts than pBASEX methods for both model¹²⁸ and experimental data.^{50,128}

1.2 Computational Methods

The following section outlines the theoretical foundation that underpins the computational methods used in this thesis. It serves as a broad introduction into this research area of chemistry and assumes little to no prior knowledge of the field. The intention is that a reader, or a student, seeking to understand the rationale in the choices in theoretical approaches made, should broadly reconcile these concepts after reading. This section covers the early ideas in theoretical chemistry, *ab initio* methods inclusive of Hartree-Fock and post-HF methods up to and including Coupled Cluster methods, density functional theory and some more practical applications in the context of PES. Texts that are referenced in this section and provide further detail on these topics include those by Lowe and Peterson¹³¹ and Foresman and Frisch¹³² for general overviews, Bartlett,¹³³ for coupled cluster methods, Roos¹³⁴ for multireference methods and Parr and Yang¹³⁵ for density functional theory.

1.2.1 Principles of Computational Chemistry

The Schrödinger equation

The advent of the era of quantum chemistry can be depicted with the derivation of the Schrödinger equation,¹³⁶ solutions to which allow the determination of a wide

range of physical and chemical properties. In its simplest form, the time-independent Schrödinger equation can be expressed as:

$$\hat{H}|\Psi\rangle = E|\Psi\rangle \quad (1.7)$$

Here the equation related the classical description with the wave description of a system where the energy eigenvalue of the system is given by E and the non-relativistic Hamiltonian \hat{H} , is represented by the potential and kinetic operators:

$$\hat{H} = \frac{-\hbar^2}{2m} \nabla^2 + V(\mathbf{r}) \quad (1.8)$$

In the determination of the energy associated with given arrangements of atoms and electrons, changes in energy can be interpreted as either inputs or outputs from a chemical system. For the simplest of 2-body systems such as the hydrogen atom the solutions to the Schrödinger equation can be determined exactly. However extension beyond this to many-body problems requires approximation of solutions.

The Born-Oppenheimer Approximation

In a many-body problem with M atoms and N electrons, the Hamiltonian of the system can be written:

$$\hat{H} = \underbrace{\sum_{i=1}^N \sum_{i>j}^N \frac{1}{r_{ij}}}_{(1)} - \underbrace{\sum_{i=1}^N \frac{1}{2} \nabla_i^2}_{(2)} - \underbrace{\sum_{i=1}^N \sum_{A=1}^M \frac{Z_A}{r_{iA}}}_{(3)} + \underbrace{\sum_{A=1}^M \sum_{B>A}^M \frac{Z_A Z_B}{R_{AB}}}_{(4)} - \underbrace{\sum_{A=1}^M \frac{1}{2m_A} \nabla_A^2}_{(5)} \quad (1.9)$$

where Z_M and m_M are the charge and mass the nuclei of atom M and the separation between particles is given by r_{ij} , r_{iA} and R_{AB} for electron-electron, electron-atom and atom-atom pairs respectively. The terms of the Hamiltonian represent:

- (1) the potential energy between a pairs of electrons (i and j) in the system;

- (2) the kinetic energy of electrons in the system;
- (3) the pairwise potential energy between the nuclei (A and B) and electrons in the system;
- (4) the potential energy between pairs of nuclei in the system; and finally
- (5) the kinetic energy of nuclei in the system.

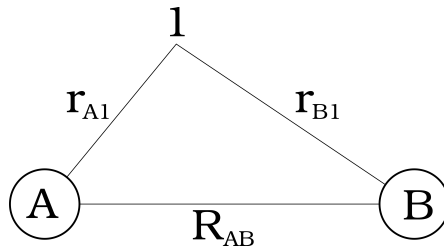


Figure 1.6: A representation of the H_2^+ ion.

Considering the H_2^+ ion shown in Figure 1.6 we are able to produce a Hamiltonian of the system that describes the motion of both protons and the electron. Yet as the mass ratio between a proton and electron is large ($\frac{m_e}{m_{\text{A},\text{B}}} \approx 1836$) the velocities of the nuclei relative to the electron can be approximated to zero, separating and thus removing the ∇_A^2 and ∇_B^2 terms. This is the Born-Oppenheimer approximation¹³⁷ where the resulting Hamiltonian represents the energy associated with an electron moving through the field generated by the nuclei. In this case that is the potential from the two protons R_{AB} distance apart.

$$\hat{H}_{elec}|\psi(\mathbf{r}_1)\rangle = E_{elec}|\psi(\mathbf{r}_1)\rangle \quad (1.10)$$

and

$$E_{elec} + E_{nuc\ rep} = E_{elec} + \frac{1}{R_{AB}} \quad (1.11)$$

In many cases the solutions to Equation 1.10 provide an adequate description of a system. However in instances where nuclear motion and electronic motion are coupled (i.e. rovibronic transitions) the inclusion of the nuclear Hamiltonian is

needed.¹³⁸ In the same sense that the energy of electrons is described by their motion through a field generated by the nuclei, conversely, the energy of the nuclei can be described by their motion through the field generated by the motion of electrons. Therefore the electronic energy can be included in the nuclear Hamiltonian operator:

$$\hat{H}_{nuc}(\mathbf{r}_A, \mathbf{r}_B) = -\frac{1}{2m_A}\nabla_A^2 - \frac{1}{2m_B}\nabla_B^2 + E_{elec} + \frac{1}{R_{AB}} \quad (1.12)$$

$$\hat{H}_{nuc}(\mathbf{r}_A, \mathbf{r}_B)\psi(\mathbf{r}_A, \mathbf{r}_B) = E_{nuc}\psi(\mathbf{r}_A, \mathbf{r}_B) \quad (1.13)$$

As the solutions equation 1.13 include electronic, vibrational, translational and rotational energy, they are also solutions to the system as a whole but the total wavefunction is then given by the product of the electronic and nuclear wavefunctions.

$$\hat{H}_{nuc}|\psi_{nuc}\rangle = E_{tot}|\psi_{nuc}\rangle \quad (1.14)$$

where:

$$\Psi = \psi_{elec}(\mathbf{r}_N, \mathbf{R}_M)\psi_{nuc}(\mathbf{R}_M) \quad (1.15)$$

Note that while the H_2^+ ion has been used an example, Equations 1.14 and 1.15 hold true for larger cases.

Solving the Schrödinger Equation by the Linear Variation Method

In attempting to solve the electronic Schrödinger equation for the H_2^+ ion, a choice of function for the description of the molecular orbitals are required. One can imagine that in the simplest case the wavefunction of H_2^+ could be described by the combination of the two 1s orbitals of the hydrogen atoms. Where the wavefunction (ψ) includes contributions from higher order orbitals, the general case for a description is the result of a linear combination of these contributing atomic orbital

wavefunctions (ϕ_i).

$$\psi = \sum_i c_i \phi_i \quad (1.16)$$

where c_i is the set of coefficients for the contributions of ϕ_i .

The Schrödinger equation is then able to be solved via the linear variation method which suggests that the average value of \hat{H} over a normalised, acceptable function ϕ is the upper bound for the lowest eigenvalue of \hat{H} . As ϕ approaches the true wavefunction ψ , \bar{E} must also approach the lowest energy state.

$$\frac{\int \psi^* \hat{H} \psi d\tau}{\int \psi^* \psi d\tau} = \frac{\int (\sum_i c_i^* \phi_i^*) \hat{H} (\sum_i c_i \phi_i) d\tau}{\int (\sum_i c_i^* \phi_i^*) (\sum_i c_i \phi_i) d\tau} = \bar{E} \quad (1.17)$$

and therefore at the minimum value of \bar{E} :

$$\frac{\partial \bar{E}}{\partial c_i} = 0 \quad (1.18)$$

Performing this differentiation, a general formulation of the partial derivative $\partial \bar{E} / \partial c_i$ is:

$$c_1(H_{i1} - \bar{E}S_{i1}) + c_2(H_{i2} - \bar{E}S_{i2}) + \dots + c_n(H_{in} - \bar{E}S_{in}) = 0 \quad (1.19)$$

where $\int \phi_i \hat{H} \phi_j d\tau \equiv H_{ij}$ and $\int \phi_i \phi_j d\tau \equiv S_{ij}$. The set of solutions for partial derivatives with respect to each c_i can then be expressed as a set of homogeneous linear equations whose non-trivial solutions (solutions other than $c_1 = c_2 = \dots = c_n = 0$) exist for discrete values of \bar{E} . This is known as the secular determinant

$$\begin{vmatrix} H_{11} - \bar{E}S_{11} & H_{12} - \bar{E}S_{12} & \dots & H_{1n} - \bar{E}S_{1n} \\ H_{21} - \bar{E}S_{21} & H_{22} - \bar{E}S_{22} & \dots & H_{2n} - \bar{E}S_{2n} \\ \vdots & \vdots & & \vdots \\ H_{n1} - \bar{E}S_{n1} & H_{n2} - \bar{E}S_{n2} & \dots & H_{nn} - \bar{E}S_{nn} \end{vmatrix} = 0 \quad (1.20)$$

Revisiting the H_2^+ ion, we can express the secular determinant of the combination of the two 1s orbitals centred on A and B as:

$$\begin{vmatrix} H_{AA} - \bar{E}S_{AA} & H_{AB} - \bar{E}S_{AB} \\ H_{BA} - \bar{E}S_{BA} & H_{BB} - \bar{E}S_{BB} \end{vmatrix} = 0 \quad (1.21)$$

which is further simplified by firstly noting that the electron occupying $1s_A$ is equivalent in energy to it occupying $1s_B$; secondly that given the 1s basis function is real it follows that $S_{AB} = S_{BA}$ and $H_{AB} = H_{BA}$; and thirdly if our basis function is normalised ($\int \psi^* \psi dv = 1$), $S_{AA} = S_{BB} = 1$:

$$\begin{vmatrix} H_{AA} - E & H_{AB} - ES_{AB} \\ H_{AB} - ES_{AB} & H_{AA} - E \end{vmatrix} = 0 \quad (1.22)$$

The non-trivial solution that satisfies 1.22 is $c_A = \pm c_B$. In also satisfying the normality requirement such that $c_A^2 + c_B^2 + 2c_A c_B S_{AB} = 1$ the resulting wavefunctions:

$$\psi_+ = \frac{1}{\sqrt{2(1 + S_{AB})}} (1s_A + 1s_B) \quad (1.23)$$

and;

$$\psi_- = \frac{1}{\sqrt{2(1 - S_{AB})}} (1s_A - 1s_B) \quad (1.24)$$

represent the high and low energy solutions to the Schrödinger equation. They are the result of the constructive or destructive interference respectively between the two phases of the 1s atomic orbital, known chemically as the σ bonding and σ^* anti-bonding orbitals.

Anti-symmetry and the Pauli Exclusion Principle

Early atomic spectra experiments by Dutch physicist Pieter Zeeman demonstrated the splitting of spectral lines of earth metals such as sodium under the effect of strong magnetic fields.¹³⁹ Later in 1925, when rationalising this phenomenon with

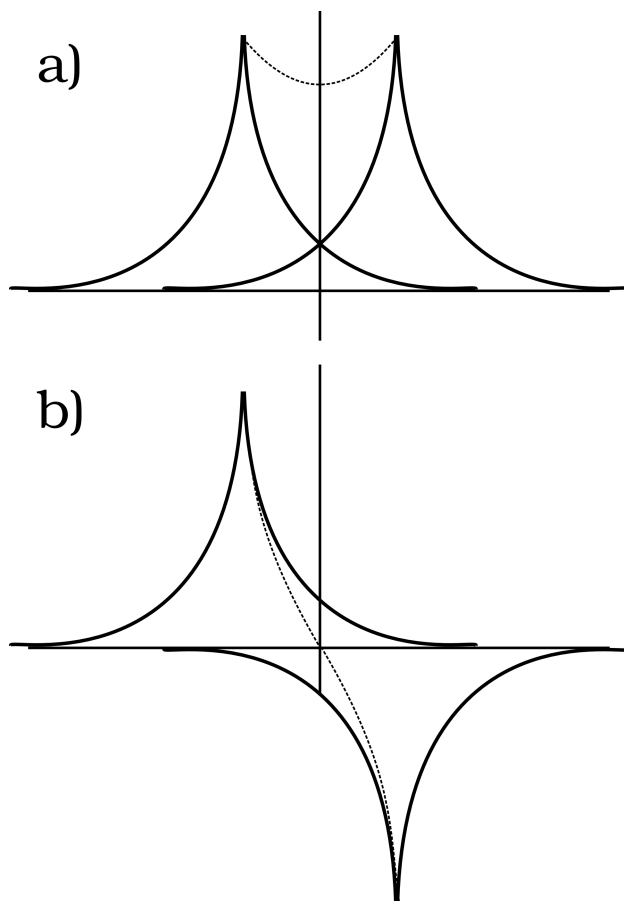


Figure 1.7: A plot of a) ψ_+ and b) ψ_- along the internuclear axis of H_2^+ .

the existing quantum numbers describing the electron shell (n) and orbital angular momentum (l), Wolfgang Pauli proposed the intrinsic angular momentum number present in elementary particles (termed ‘spin’ and denoted s).¹⁴⁰ In addition to this property Pauli postulated that the total wavefunction for two identical particles with half integer spin such as electrons is antisymmetric with respect to exchange.

$$\Psi(\dots, \mathbf{r}_A, \dots, \mathbf{r}_B, \dots) = -\Psi(\dots, \mathbf{r}_B, \dots, \mathbf{r}_A, \dots) \quad (1.25)$$

Many-electron systems and Slater Determinants

As demonstrated previously in the case of the H_2^+ ion, the solving of the Schrödinger equation quickly becomes cumbersome with all but the simplest systems described by convenient basis functions. A general formation of an N -electron wavefunction (Ψ) whose molecular orbitals ($\chi_i(\mathbf{x}_i)$) are a linear combination of atomic orbitals is

a Slater Determinant:¹⁴¹

$$\begin{aligned}\Psi(\mathbf{x}_1, \mathbf{x}_2, \dots, \mathbf{x}_N) &= \widehat{A} \chi_1(\mathbf{x}_1) \chi_2(\mathbf{x}_2) \dots \chi_N(\mathbf{x}_N) \\ &= \frac{1}{\sqrt{N!}} \begin{vmatrix} \chi_1(\mathbf{x}_1) & \chi_2(\mathbf{x}_1) & \dots & \chi_N(\mathbf{x}_1) \\ \chi_1(\mathbf{x}_2) & \chi_2(\mathbf{x}_2) & \dots & \chi_N(\mathbf{x}_2) \\ \vdots & \vdots & \ddots & \vdots \\ \chi_1(\mathbf{x}_N) & \chi_2(\mathbf{x}_N) & \dots & \chi_N(\mathbf{x}_N) \end{vmatrix} \quad (1.26)\end{aligned}$$

where \widehat{A} is the antisymmetrisation operator defined as:

$$\widehat{A} = \frac{1}{N!} \sum_P (-1)^p \widehat{P} \quad (1.27)$$

where \widehat{P} is the permutation operator.

The benefit of expressing the wavefunction in this way is that some matrix B , which is the matrix A with any two rows interchanged, has a determinant that is the negative of the determinant of A . That is to say $|A| = -|B|$, and that the Slater determinant is antisymmetric with respect to exchange, thus satisfying the Pauli exclusion principle.

1.2.2 *Ab initio* Methods

Hartree-Fock

The Hartree-Fock method^{142–144} applies the variational method to determine the energy of a system using both an average of the electron-electron interaction and single Slater determinant. The Hartree-Fock equations (1.28) consist of the Fock operator (\widehat{F}), this Slater determinant expression of the wavefunction (ϕ_i) and the set of eigenvalues (ϵ_i).

$$\widehat{F} \phi_i = \epsilon_i \phi_i \quad (1.28)$$

$$\widehat{F}(1) = -\frac{1}{2}\nabla_1^2 - \sum_{\mu} \frac{Z_{\mu}}{r_{\mu 1}} + \sum_{j=1}^n (2\widehat{J}_j - \widehat{K}_j) \quad (1.29)$$

where the Fock operator expresses the electron-electron interaction of the Hamiltonian as the Coulomb operator (\widehat{J}) and the exchange operator (\widehat{K}). The Coulomb operator determines the potential between one electron in the mean-field of each other electron while the exchange operator gives the exchange interaction between two electrons in the system.

$$\widehat{J}_j = \int \phi_j^*(2) \frac{1}{r_{12}} \phi_j(2) d\tau(2) \quad (1.30)$$

$$\widehat{K}_j \phi_i(1) = \int \phi_j^*(2) \frac{1}{r_{12}} \phi_i(2) d\tau(2) \phi_j(1) \quad (1.31)$$

By iteratively updating the contribution coefficients of the atomic orbitals (c_i in Equation 1.16) and the Fock operator, the Hartree-Fock equations approach a self-consistent field (SCF) which describes both the one-electron wavefunction and energy of the system. Expressing the Hartree-Fock equations as matrices, Roothaan and Hall provided a generalised form for solving for the wavefunction and energy of a system in the restricted, closed-shell case (termed Restricted Hartree-Fock (RHF)).¹⁴⁵

$$\mathbf{Fc} = \boldsymbol{\epsilon} \mathbf{Sc} \quad (1.32)$$

where \mathbf{F} is the Fock operator, \mathbf{c} is the set of orbital coefficients, $\boldsymbol{\epsilon}$ is the set of energy eigenvalues and \mathbf{S} is the overlap integral between the atomic orbitals.

The determination of solutions to the Fock equations for a given system then follows:

1. Determine an initial guess of the 1-electron molecular orbitals for a given system

2. Formulate the Fock matrix from the set of molecular orbitals
3. Diagonalise the Fock matrix
 - If the resulting change in energy is smaller than a given tolerance the energy is deemed to be ‘converged’ and the calculation is complete
 - Else return to 2 and update the Fock matrix using a new set of MOs

For cases where not all electrons are paired, Restricted Open Shell Hartree-Fock (ROHF) and Unrestricted Hartree-Fock (UHF) were developed by Roothaan *et. al.*¹⁴⁶ and Pople and Nesbet,¹⁴⁷ respectively. ROHF still treats the electrons as pairs bar one in the case of a doublet, two in the case of a triplet and so on whereas UHF formulates two sets of Hartree-Fock equations for the α ($+\frac{1}{2}$) and β ($-\frac{1}{2}$) spins.

$$\mathbf{F}^\alpha \mathbf{c}^\alpha = \epsilon^\alpha \mathbf{S}^\alpha \mathbf{c}^\alpha \quad \mathbf{F}^\beta \mathbf{c}^\beta = \epsilon^\beta \mathbf{S}^\beta \mathbf{c}^\beta \quad (1.33)$$

In the determination of properties of a given system via Hartree-Fock methods, the spin expectation valueⁱ $\langle S^2 \rangle$ that is calculated can be interpreted to examine the degree of contribution from higher spin states than the true eigenfunction. While restricted methods (RHF and ROHF) are able to calculate $\langle S^2 \rangle$ exactly due to the constrained spatial distribution of the orbitals, the unconstrained nature of UHF methods can lead to differences in the spatial coordinates of pairs of α and β electrons. This is known as spin-contamination and is the result of contributions from other electronic states than the one in question. Systems with multiple unpaired electrons are prone to higher levels of spin contamination and are best treated by approximating wavefunctions for each contributing state.

While both ROHF and UHF are appropriate for open-shell systems, both have considerations for their applicability in quantum chemistry. Initial considerations are with respect to the computational cost, be that hardware or time required for the

ⁱIn quantum mechanics the expectation value of an operator \mathbf{A} is defined as $\langle \psi | \mathbf{A} | \psi \rangle$.

calculation, where ROHF is more expensive relative to UHF. Further considerations informing the choice of method vary between chemical problems. For most open-shell cases where both α and β electrons are necessary, for example in the description of bonding, typically UHF wavefunctions are used. In other cases, where spin-contamination is a concern, ROHF may be more appropriate.

A significant detractor for Hartree-Fock methodology is that as it determines the electron-electron interaction using a self-consistent field, it fails to account for interaction between discrete electrons. The energy associated with dynamical electron correlation, the instantaneous Coulomb repulsion between electrons occupying the same spatial orbitals, is the correlation energy and is defined by Löwdin¹⁴⁸ as “the difference between the exact eigenvalue of the Hamiltonian and its expectation value in the Hartree-Fock approximation for the state under consideration”, or:

$$E_{tot} = E_{HF} + E_{corr} \quad (1.34)$$

Although Hartree-Fock methods account for significant amounts of the total energy of a system and include the interaction of two electrons of the same spin with respect to exchange, opposite spin electron correlation energy in even the simplest systems such as the H₂ molecule can be determined to be on the order of an electronvolt (-1.06 eV for H₂¹⁴⁹). When bonding is measured on scales of kJ mol⁻¹, accurate determination of electron correlation energy via post-Hartree-Fock methods is required. These methods seek to capture electron correlation by expressing the wavefunction as a combination of electron configurations, thereby including contributions from excited states.

Configuration Interaction

The most natural extension to Hartree-Fock methods that include electron correlation is configuration interaction. Configuration interaction (CI)¹⁵⁰ includes in the wavefunction both the Hartree-Fock wavefunction, and weighted contributions from

*n*th-order excited state configurations of this Hartree-Fock wavefunction. The wavefunction is then expressed as:

$$\Psi_{CI} = \Psi_{HF} + \sum_{ia} t_i^a \Psi_{i \rightarrow a} + \sum_{ijab} t_{ij}^{ab} \Psi_{ij \rightarrow ab} + \dots \quad (1.35)$$

where t is the weighting factor of that configuration.

Taken to its extreme, where all electrons are excited and all configurations are included, Equation 1.35 becomes known as full CI. While full CI includes all the electron correlation energy for the chosen basis set, it is prohibitively expensive computationally for all but the smallest systems.¹⁵¹ As a result, configuration interaction is typically truncated at a given number of excitations be that single, double, triple and so on, with nomenclature expressing this truncation (for example the inclusion of singly and doubly excited configurations is CISD). This truncation however, at anything but full CI, results in the method no longer being size-extensiveⁱⁱ and no longer appropriate for calculating the energy of separation in the making a breaking of bonds. Alternate methods that capture electron correlation whilst maintaining size-extensivity are detailed in the following sections.

Møller-Plesset Perturbation Theory

A special case of Rayleigh-Schrödinger perturbation theory,¹³⁶ MP perturbation theory¹⁵³ supposes that the true Hamiltonian of a system can be decomposed into the simpler Hartree-Fock Hamiltonian ($\hat{H}_{(0)}$) and some scaled perturbing operator (\hat{V}) that accounts for the electron correlation of the system.

$$\hat{H} = \hat{H}_{(0)} + \lambda \hat{V} \quad (1.36)$$

The nomenclature of MP theory is then expressed by the *n*th-order of the perturbation, with each written as MP*n*.^{154–157}

ⁱⁱSize-extensivity, first described in this context by Pople and Binkley,¹⁵² requires that the sum of energies of two components *A* and *B* must be equal in energy to the energy of *A* and *B* calculated together (ie. $E(A + B) = E(A) + E(B)$).

0th-order:

$$E^{(0)} = \langle \Psi_0 | \hat{H}_{(0)} | \Psi_0 \rangle = \sum_i \epsilon_i \quad (1.37)$$

1st-order:

$$E^{(1)} = \langle \Psi_0 | \hat{H} | \Psi_0 \rangle \quad (1.38)$$

$$E^{HF} = E^{(0)} + E^{(1)} \quad (1.39)$$

2nd-order:

$$E^{(2)} = E^{HF} - \sum_{s \neq 0} \frac{\left| \langle \Psi_0 | \hat{V} | \Psi_s \rangle \right|^2}{E_s - E_0} = E^{HF} - \frac{1}{4} \sum_{ijab} \frac{|\langle ij || ab \rangle|^2}{\epsilon_a + \epsilon_b - \epsilon_i - \epsilon_j} \quad (1.40)$$

3rd-order:

$$E^{(3)} = E^{(2)} - \sum_{st} \frac{\langle \Psi_0 | \hat{V} | \Psi_s \rangle \langle \Psi_s | \hat{V} | \Psi_t \rangle \langle \Psi_t | \hat{V} | \Psi_0 \rangle}{(E_s - E_0)(E_t - E_0)} \quad (1.41)$$

4th-order:

$$\begin{aligned} E^{(4)} &= E^{(3)} - \sum_{stu} \frac{\langle \Psi_0 | \hat{V} | \Psi_s \rangle \langle \Psi_s | \hat{V} | \Psi_t \rangle \langle \Psi_t | \hat{V} | \Psi_u \rangle \langle \Psi_u | \hat{V} | \Psi_0 \rangle}{(E_s - E_0)(E_t - E_0)(E_u - E_0)} \\ &= E^{(3)} - \sum_{stu} \frac{t_s \hat{V}_{st} \hat{V}_{tu} t_u}{\epsilon_a + \epsilon_b + \epsilon_c - \epsilon_i - \epsilon_j - \epsilon_k} \\ &= E^{(3)} - \sum_{stu} \frac{|\mathbf{u}_t|^2}{\epsilon_a + \epsilon_b + \epsilon_c - \epsilon_i - \epsilon_j - \epsilon_k} \end{aligned} \quad (1.42)$$

This power series can continue to n th-order however the increasing number of correlation terms are difficult to derive alone. For MP7 and MP8 this constitutes 221 (141 unique) and 918 (583 unique) terms, respectively.¹⁵⁸ Given the increasing number of n -electron correlations required for higher order perturbation theory, the computational cost of MP methods scales non-linearly with respect to their order. Table 1.1 summarises the cost of MP n methods with increasing order. Noting that in some cases where some contributions are small, for example the 3-electron correlation contribution in MP4, these are omitted to reduce computational cost.

Table 1.1: Computational cost of a number of MP n methods. $O(M^n)$ refers to the number of orbitals (O) and basis functions (M).¹⁵⁸

Method	Computational Cost
MP2	$O(M^5)$
MP3	$O(M^6)$
MP4(SDQ)	$O(M^6)$
MP4(SDTQ)	$O(M^7)$
MP5	$O(M^8)$
MP6	$O(M^9)$

When assessing MP methods efficacy to recover electron correlation energy, comparisons to full CI calculations have shown to be convergent with increasing order.^{159,160} However as percentages of full CI, the diminishing returns with respect to increasing order and corresponding cost prove MP methods less efficient than other post-HF approaches to electron correlation.¹⁵⁸ Additionally, differences between MP and full CI energies have been shown to not only oscillate due to the coupling of new correlation effects at even n , but also diverge at higher n . The oscillation also demonstrates the non-variational nature of MP theory as the true energy of the system does not represent a lower bound. Handy and Somasundram¹⁶¹ demonstrated such an effect, considering the water molecule with MP theory up to 48th order, however as shown in Figure 1.8, MP n energies of the neon atom further diverge at higher order.

Owing to their comparatively low computational cost and avoidance of divergent behaviour, lower order MP methods have become popularised in recent decades. MP2 calculations have been shown to account for 92.4% of the total correlation energy on average for a variety of molecules (percentage correlation accounted for ranging from 82% to 98%).¹⁶² As such, for many chemical applications they are suitable, though when considering weaker interactions or multireference systems where non-dynamical correlation becomes important,^{163,164} the inheritance of issues from single reference HF methods present in MP n make them inadequate descriptors.

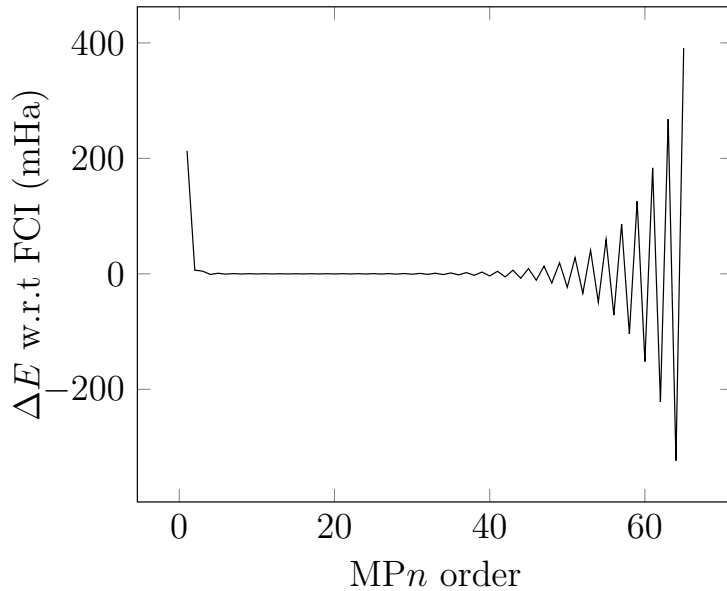


Figure 1.8: Plot of divergence of MP energy at higher order for Ne atom¹⁶⁵

Coupled Cluster Methods

Coupled Cluster (CC) methods approach the problem of electron correlation interaction by including excitations from the ground state via an exponential excitation operator, $e^{\hat{T}}$. This exponential ansatz can then be expanded as a Taylor series where each term includes the n -orbital cluster operator (\hat{T}_n).

$$\Psi_{CC} = e^{\hat{T}}\psi_0 = \left[1 + \hat{T} + \frac{\hat{T}^2}{2!} + \frac{\hat{T}^3}{3!} + \dots \right] \psi_0 \quad (1.43)$$

$$\hat{T}_n = \left(\frac{1}{n!} \right)^2 \sum_{ab\dots}^2 \sum_{ij\dots}^{occ} t_{ab\dots}^{ij\dots} \hat{a}_i^\dagger \hat{a}_j^\dagger \dots \hat{a}_b \hat{a}_a \quad (1.44)$$

where $\hat{a}_{i,j,\dots}^\dagger$ and $\hat{a}_{a,b,\dots}$ represent *creation* and *annihilation* operators respectively. When applied to the Slater determinant both operators represent the creation of newly occupied orbitals and the annihilation of those vacated with each excitation.ⁱⁱⁱ

Applying Equation 1.43 to the Schrödinger equation (Equation 1.7) the expression for the energy can be determined as:

ⁱⁱⁱFor a given pair of creation and annihilation operators, i and a , the anticommutation relation for the mixed product is $a_i^\dagger a_a + a_a a_i^\dagger = \delta_{ai} = 0$ where δ_{ai} is the Kronecker delta and $a \neq i$ are representations of respective occupied and virtual orbitals

$$\langle \Psi_0 | \hat{H} e^{\hat{T}} | \Psi_0 \rangle = E \langle \Psi_0 | e^{\hat{T}} | \Psi_0 \rangle = E \quad (1.45)$$

or, by substituting the power series from 1.43:

$$\langle \Psi_0 | \hat{H} \left(1 + \hat{T} + \frac{\hat{T}^2}{2!} + \frac{\hat{T}^3}{3!} + \dots \right) | \Psi_0 \rangle = E \quad (1.46)$$

and then distributing terms:

$$\langle \Psi_0 | \hat{H} | \Psi_0 \rangle + \langle \Psi_0 | \hat{H} \hat{T} | \Psi_0 \rangle + \left\langle \Psi_0 | \hat{H} \frac{\hat{T}^2}{2!} | \Psi_0 \right\rangle + \left\langle \Psi_0 | \hat{H} \frac{\hat{T}^3}{3!} | \Psi_0 \right\rangle + \dots = E \quad (1.47)$$

By recognising that \hat{H} and \hat{T} are two-electron and one-electron operators respectively, the Slater-Condon rules^{141,166} can be applied. These state that for two Slater determinants differing by more than two orbitals, the Hamiltonian must be zero. As such the \hat{T}^3 term, representing three-fold excitations, must be zero. This is also true for any following terms, allowing Equation 1.47 to be truncated but remain formally exact at two-fold excitations.

$$\langle \Psi_0 | \hat{H} | \Psi_0 \rangle + \langle \Psi_0 | \hat{H} \hat{T} | \Psi_0 \rangle + \left\langle \Psi_0 | \hat{H} \frac{\hat{T}^2}{2!} | \Psi_0 \right\rangle = E \quad (1.48)$$

In the discussion of CC methods, the n -order cluster operator (\hat{T}) has been treated to include all excitations. However, similarly to CI and MP methods, the computational cost of CC methods is restricted to a manageable size by inclusion of only a given number of excitations. Each inclusion is denoted S, D, T, Q and so on for single, double, triple and quadruple excitations and scales non-linearly with the inclusion of higher excitations. While comparatively more accurate than corresponding CI and MP methods, CC methods are significantly more costly. Between CCSD and CCSDT the cost scales with respect to $O(M^6)$ and $O(M^8)$ per iteration.^{167,168} For some systems however, CCSD proved to be inaccurate, and with limited computational resources it was necessary to develop cheaper inclusions of

triple excitations. This lead to the development for the perturbative inclusion of triple excitations.¹⁶⁹

The inclusion of the triples correction, denoted (T), is made possible by the observed relationship between CC and MP methods. CCSD includes terms that are identical to those contributions in MP2 (Equation 1.40) and MP3 (Equation 1.41). As such, triple excitations can be included perturbatively in CCSD(T) via contributions in the same form as MP4 methods (Equation 1.42) and MP5.

Due to the strong performance of CCSD(T) in recent years and accuracy in describing closed shell systems,^{170–172} it has become “the gold standard of quantum chemistry”. However CCSD(T) is reliant on a sufficiently accurate Hartree-Fock approximation of the overall wavefunction and when considering systems where single reference are no longer appropriate this performance quickly deteriorates. When considering bond breaking and biradical systems, while using an UHF reference can improve the description of these systems, inclusion of the open-shell singlet state can be problematic when approximated with a wavefunction possessing less spin contamination.¹⁷³ Approaches that have been shown to circumvent these issues vary, but can include:

- treating triple and higher order excitations non-perturbatively;¹⁷⁴
- applying de-excitation operators to a single-reference excited state termed equation-of-motion (EOM) coupled cluster methods;¹⁷⁵ and
- utilising multiple Slater determinants to form the reference wavefunction, known collectively as *multireference methods*.

1.2.3 Multireference Methods and Treatment of Excited States

Multiconfigurational Self Consistent Field Theory

Where a system consists of multiple states that are degenerate, or near degenerate, it is often desirable to include contributions from these states within the calculation.

Whereas in a configuration interaction calculation the coefficients of these contributions are optimised (see Equation 1.35), the wavefunction itself is unchanged from the Hartree-Fock wavefunction (Ψ_{HF}). Considering the example of H₂ dissociation, the wavefunction can be described as $\Psi = (\sigma_g)^2$ when bonded. As the separation between atoms increases however, the contribution of the σ_g orbital decreases and the corresponding contribution of the anti-bonding σ_u orbital increases. As such the wavefunction over all internuclear distance space can best be described as $\Psi = C_1(\sigma_g)^2 + C_2(\sigma_u)^2$. Multiconfigurational self consistent field (MCSCF) theory optimises both the coefficients of the atomic orbitals to improve the included wavefunctions but also the C_i coefficients of the contributing configuration state function (CSF)s.

This approach is applicable for simple systems but when considering multiple bonds and multiple contributing configurations a more formalised approach is needed. A general expression for the MCSCF wavefunction is as follows:

$$|0\rangle = \sum_m c_m |m\rangle \quad (1.49)$$

This is not to be confused with Equation 1.16 which expresses the wavefunction as a combination of atomic orbitals. Rather, the total MCSCF wavefunction ($|0\rangle$) is itself a linear combination of each contributing CSF, $|m\rangle$.

The tool used to describe this behaviour is second quantisation^{iv}. Using annihilation and creation operators, the Hamiltonian is then defined as:

$$\hat{H} = \sum_{pq} \langle \psi_p | \hat{h} | \psi_q \rangle \hat{a}_p^\dagger \hat{a}_q + \frac{1}{2} \sum_{pqrs} \langle pr | qs \rangle \hat{a}_p^\dagger \hat{a}_r^\dagger \hat{a}_s \hat{a}_q \quad (1.50)$$

where the one-electron operator represents the excitation of one electron from p to q and the two-electron operator includes a second electron excitation from r to s . In a spin-independent formalism ($\sigma \in \alpha, \beta$) these are often represented as *excitation*

^{iv}In brief, second quantisation is a linear combination of Slater determinants projected onto the orthonormal basis of single excitation operators (Fock space).

operators:

$$\hat{E}_{pq} = \sum_{\sigma} (\hat{a}_{p\sigma}^{\dagger} \hat{a}_{q\sigma}) \quad (1.51)$$

$$\hat{E}_{pq,rs} \equiv \hat{E}_{pq}\hat{E}_{rs} - \delta_{rq}\hat{E}_{ps} = \sum_{\sigma,\sigma'} (\hat{a}_{p\sigma}^{\dagger} \hat{a}_{r\sigma'}^{\dagger} \hat{a}_{s\sigma'} \hat{a}_{q\sigma}) \quad (1.52)$$

The molecular orbital components that are described in the Hamiltonian themselves represent an excitation $\psi_p \leftarrow \psi_q$ in the case of the one-electron integral and pairs of excitations interacting with each other ($\psi_p \leftarrow \psi_q, \psi_r \leftarrow \psi_s$).

$$\langle \psi_p | \hat{h} | \psi_q \rangle = \int \frac{1}{2} \nabla \psi_p^*(\mathbf{r}) \psi_q(\mathbf{r}) + \psi_p^*(\mathbf{r}) v(\mathbf{r}) \psi_q(\mathbf{r}) d\mathbf{r}^3 = h_{pq} \quad (1.53)$$

$$\langle pr | qs \rangle = \int \int \psi_p^*(\mathbf{r}_1) \psi_r^*(\mathbf{r}_2) \frac{1}{r_{12}} \psi_r(\mathbf{r}_1) \psi_s(\mathbf{r}_2) = g_{pqrs} \quad (1.54)$$

This allows the Hamiltonian in MCSCF to be expressed as a combination of excitation operators for interacting CSFs and the one- and two- electron integrals h_{ij} and g_{ijkl} respectively.

$$\hat{H} = \sum_{i,j} h_{ij} \hat{E}_{ij} + \frac{1}{2} \sum_{i,j,k,l} g_{ijkl} (\hat{E}_{ij} \hat{E}_{kl} - \delta_{jk} \hat{E}_{il}) \quad (1.55)$$

The corresponding MCSCF energy as a solution to the Schrödinger equation is the expectation value:

$$E = \langle \Psi | \hat{H} | \Psi \rangle = \sum_{i,j} h_{ij} D_{ij} + \sum_{i,j,k,l} g_{ijkl} P_{ijkl} \quad (1.56)$$

where the coefficients c_m from 1.49 are contained in the density matrices **D** and **P**.

CASSCF

In practice, MCSCF calculations are vastly more demanding than single reference methods, as each CSF is in itself a full-CI calculation. To date, the MCSCF cal-

culation with the largest number of active electrons that has been completed is the chromium dimer, consisting of 28 correlated electrons and equating to 2.8×10^9 CSFs.^{176,177} Given that in most chemically important interactions, core electrons are largely unaffected by bonding, the problem can be reduced in scope. This is done by reducing the orbitals considered to those where the interactions are taking place or where the desired electronic configurations can still be described in a restricted scope. These termed the ‘*active space*’ shown in Figure 1.9 for a CASSCF(8,6) calculation of O₂. The remaining orbitals are either core or non-interacting (termed ‘*inactive*’) or unoccupied (or ‘*virtual*’).

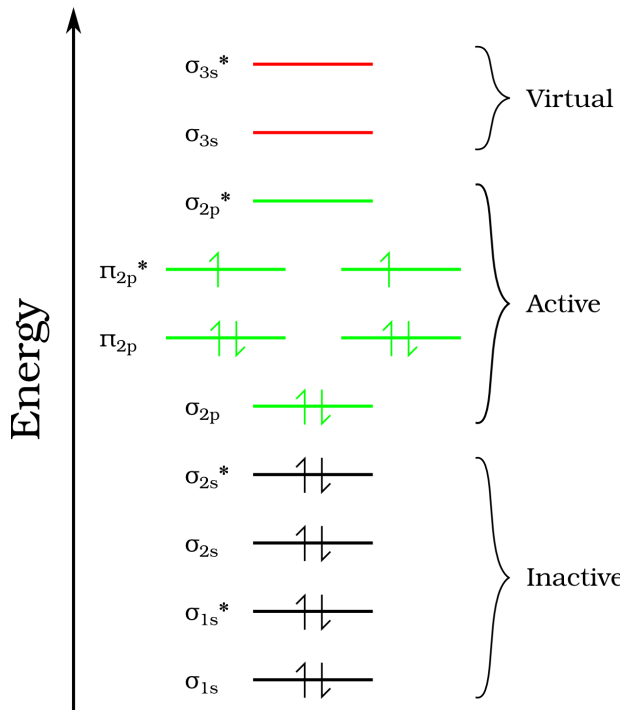


Figure 1.9: Representation of the inactive, active and virtual orbitals of a CASSCF calculation. In this case the calculation is CASSCF(8,6) for an O₂ molecule where the 2p electrons only are included in the active space.

This variant of MCSCF, referred to as CASSCF, reduces the dimension of the problem such that the number of configurations N_{CAS} is given by the Weyl formula:¹³⁴

$$N_{\text{CAS}} = \frac{2S+1}{n+1} \binom{n+1}{N/2-S} \binom{n+1}{N/2+S+1} \quad (1.57)$$

where N is the number of electrons in n active orbitals with a total spin of S . When referring to CASSCF methods, the active space and number of electrons within it are denoted CASSCF(N,n). Further, not necessarily all CSFs are included in the CASSCF wavefunction, only those within the active space. The CASSCF wavefunction is then nominally an average of a number of near-degenerate states to capture non-dynamic correlation effects;^{178,179} however, the user may select an individual CSF by adjusting the weighted contribution of these states to formally calculate the energy of an excited state. Despite the reduction in computational cost, the limitation in size of CASSCF calculations is currently typically between $n = 12 - 16$.¹³⁴

While CASSCF calculations perform well for systems where non-dynamical correlation is important, by being the multireference equivalent of Hartree-Fock methods, they similarly omit dynamic correlation effects. Additionally as the CSFs that are included are truncated as opposed to a full-CI calculation, the calculation is no longer size extensive. Configuration interaction of the multireference wavefunction can be performed to recover dynamic correlation effects however these calculations are similarly prohibitively costly. Perturbation theory can be utilised in multireference methods as an alternative to configuration interaction and is equivalent to MP methods in single reference wavefunction methods

Multireference Perturbation Theory

In the same sense that single reference perturbation theory considers the interactions between the first-order wavefunction with the excited space, multireference perturbation theory considers the interactions between a CASSCF root state with higher order excitations. In Rayleigh-Schrödinger Perturbation Theory (RS-PT) the Hamiltonian is expressed as two component parts, \hat{H}_0 and \hat{H}_1 , where \hat{H}_0 has some known wavefunction as an eigenvalue and \hat{H}_1 represents a perturbative contribution. The total Schrödinger equation is then expressed for some λ as:

$$(\hat{H}_0 + \lambda \hat{H}_1) \Psi_\lambda = E_\lambda \Psi_\lambda \quad (1.58)$$

where both Ψ_λ and E_λ can be represented by a Taylor expansion and $\langle \Psi_\lambda | \Psi^{(0)} \rangle = 1$. The solutions to the Schrödinger equation is then given by Equation 1.59, but is highly dependant on the choice of zeroth-order Hamiltonian (\hat{H}_0).

$$\begin{aligned} E_{2n} &= \langle \Psi_n | \hat{H}_0 | \Psi_n \rangle \\ E_{2n+1} &= \langle \Psi_n | \hat{H}_1 | \Psi_n \rangle \\ (\hat{H}_0 - E_0) \Psi_{n+1} &= - \left(\hat{H}_1 \Psi_n - \sum_{k=1}^{n-1} E_k \Psi_{n-k} \right) \end{aligned} \quad (1.59)$$

Complete Active Space Perturbation Theory Second Order (CASPT2) formulates Equation 1.59 as matrix equations where the elements are determined by utilising excitation operators of the form described in Equations 1.51 and 1.52 to produce a CI Hamiltonian in the form of Equation 1.50. The RS-PT equation is given of the form:

$$(\hat{H}_0 - E_0) \Psi^{(1)} = -(\hat{H} - E_0) \Psi^{(0)} = \Psi^{(RHS)} \quad (1.60)$$

The excitation operators are classed as internal, semi-internal and external excitations with orbitals denoted (t, u, v, x) , (i, j, k, l) and (a, b, c, d) for the active, inactive and virtual spaces respectively.

- *Internal* excitations are those from the inactive to the active space or within the active space ($\hat{E}_{tiuv}, \hat{E}_{tiuj}$).
- *Semi-internal* excitations consist of excitations from the inactive and active spaces to the virtual space in the field of internal excitations ($\hat{E}_{atuv}, \hat{E}_{aitu}, \hat{E}_{tiau}, \hat{E}_{tiaj}$).
- *External* excitations consist of pairwise excitations both to the virtual space ($\hat{E}_{atbu}, \hat{E}_{aibt}, \hat{E}_{aibj}$).

As these operators span all one- and two-electron operators present in the Hamiltonian, it is referred to as the first-order interacting space. The first-order wavefunction $\Psi^{(1)}$ then lies within this space and is of the form:

$$\Psi^{(1)} = \sum_{KP} t_P^{(K)} \hat{X}_P^{(K)} \Psi^{(0)} \quad (1.61)$$

where $\hat{X}_P^{(K)} \in \{\hat{E}_{tuvj}, \hat{E}_{tiuj}, \dots, \hat{E}_{bjai}\}$.

Higher order contributions can then be represented as projections onto the first-order interacting space:

$$\sum_{LQ} A_{PQ}^{(KL)} t_Q^{(L)} = u_P^{(K)} \quad (1.62)$$

with:

$$\begin{aligned} A_{PQ}^{(KL)} &= \langle \Psi^{(0)} | (\hat{X}_P^{(K)})^\dagger (\hat{H}_0 - E_0) \hat{X}_Q^{(L)} | \Psi^{(0)} \rangle \\ u_P^{(K)} &= -\langle \Psi^{(0)} | (\hat{X}_P^{(K)})^\dagger \hat{H} | \Psi^{(0)} \rangle \end{aligned} \quad (1.63)$$

Although solvable, these equations still represent elements of a full CI Hamiltonian matrix and the expense of the method is correlated with the number of Slater Determinants. It is possible however, to choose an operator that is sufficiently simple that it remains solvable whilst still avoiding linear dependencies that arise from excitations from active orbitals with low occupations to highly occupied active orbitals, and differing excitation types do not couple. Additionally, when operating on a non-active space, this operator should replicate MP2 methods. These requirements can be met by choosing a Fock-type operator and defining \hat{H}_0 as:

$$\hat{H}_0 = \hat{P}_{CAS} \hat{F} \hat{P}_{CAS} + \hat{P}_{SD} \hat{F} \hat{P}_{SD} \quad (1.64)$$

where \hat{P} are projection operators onto the relevant spaces and where:

$$\widehat{F} = \sum_{pq} F_{pq} \widehat{E}_{pq} \quad (1.65)$$

with some set of orthonormal orbitals.

CASPT2 methods have been utilised in calculating energies and geometries for ground and excited states of a number of organic molecules, including a number of conjugated hydrocarbons such as acrolein and *cis* and *trans* buta-1,3-diene.¹⁸⁰ A number of studies have used CASPT2 methods to compliment or reinterpret photo-electron spectroscopy experiments.¹⁸¹ Ivanov *et. al.* investigated a number of lanthanum clusters (La_n^- $n = 1, 3 - 7$) utilising density functional theory to determine cluster structures followed by CASSCF/CASPT2 single point energies to determine vertical detachment energies.¹⁸² The challenge with investigating lanthanide species in this case is the complicated valence orbital structure resulting from *f*-shell contributions to the MOs. CASPT2 becomes necessary in these cases as the energy of many of these near degenerate orbitals need to be determined accurately to describe electron detachment processes adequately. Similarly, photoelectron spectroscopy experiments coupled with CASPT2 calculations have been used by Weichman *et. al.* to characterise the electronic structure of samarium oxide (SmO).¹⁸³ These calculations have the added benefit of representing a simple diatomic and allow CASPT2 geometry optimisations to become viable.

The challenges in each case are that the restrictions on the size of the active space (typically up to 20 active orbitals) and the scaling of the method as a result.¹⁸⁴ Additionally, as the choice and ordering of active space can greatly effect the output of any given calculation, CAS methods do not operate as “black boxes” compared with traditional single reference calculations and care must be taken in executing any of these methods. CASPT2 is also prone to intruder states, which result from near zero energy denominators in the expansion of the perturbed Hamiltonian.¹⁸⁵ The effect of these intruder states can be treated by applying a shift to these energies (termed the ionization potential-electron affinity (IPEA) shift), however this is viewed as an

empirical correction and varies depending on the type of system it applies to.¹⁸⁶

An analogous method to CASPT2 which seeks to avoid the impact of intruder states is n -electron valence state perturbation theory (NEVPT2). NEVPT2, developed by Angeli and co-workers,^{187–189} utilises a Dyall Hamiltonian¹⁹⁰ for \hat{H}_0 containin a two-electron operator \hat{H}_v :

$$\begin{aligned}\hat{H}^D &= \color{red}{\hat{H}_i} + \color{blue}{\hat{H}_v} + \color{purple}{C} \\ &= \sum_i^{\text{core}} \epsilon_i E_{ii} + \sum_r^{\text{virt}} \epsilon_r E_{rr} + \sum_{ab}^{\text{act}} h_{ab}^{\text{eff}} E_{ab} + \frac{1}{2} \sum_{abcd}^{\text{act}} \langle ab|cd \rangle (E_{ac} E_{bd} - \delta_{bc} E_{ad}) \\ &\quad + 2 \sum_i^{\text{core}} h_{ii} + \sum_{ij}^{\text{core}} (2 \langle ij|ij \rangle - \langle ij|ji \rangle) - 2 \sum_i^{\text{core}} \epsilon_i\end{aligned}\quad (1.66)$$

While NEVPT2 methods are superior in the sense that they are size extensive and do not suffer from intruder states, they are not invariant with respect to choice of active space. This is due to the formal assignment of orbitals in the inactive and active spaces and as such, further care must be taken in choosing the active space to appropriately determine energies.¹⁹¹

Nevertheless NEVPT2 has seen continual improvements to its formulation in the last decade¹⁹² and found use in a number of anion photoelectron spectroscopy studies, particularly in the calculation of small metal clusters such as titanium di-germanium (TiGe_2^-)¹⁹³ and manganese sulfide (MnS^-).¹⁹⁴

1.2.4 Density Functional Theory

So far in discussing methodologies for solving the Schrödinger equation each approach has sought to determine an expression for the wavefunction of the system. However, it may be appropriate to consider the electronic structure of a system in a semi-classical manner, that being the density of electrons as a function of spatial and spin coordinates $\rho(\mathbf{r})$ (the Thomas-Fermi model).¹⁹⁵

$$\rho(\mathbf{r}) = \int |\psi(1, 2, \dots, N)|^2 d\mathbf{r} \quad (1.67)$$

Under this model the Hamiltonian expressed in Equation 1.9 is recontextualised such that the terms are expressions of the electron density. The potential energy between pairs of nuclei and electrons (term (3)) is then called the external potential $v_{ext}(\vec{r})$, and by treating the electron density as an inhomogeneous electron gas, Hohenberg and Kohn demonstrated that no two $v_{ext}(\vec{r})$ could be derived from the same density (ρ).¹⁹⁶ From this, the authors also suggested that it follows that one could derive the other terms from *ab initio* methods and determine the energy of the system for a unique electron density mapped by some functional. Some guess of electron density ρ with energy E would then lie higher in energy than that of the exact E_0 , allowing the use of the variational principle (Equation 1.17) to solve for the exact density ρ_0 . This represents an attractive alternative to traditional wavefunction methods as it avoids the steep scaling with respect to the number of basis functions of high level methods such as coupled cluster. The problem then becomes to determine a robust functional that maps ρ to E without an undue reliance on a Hamiltonian that is reminiscent of wavefunction methods. The remaining terms in the Hamiltionian (Equation 1.9) are then expressed as components of the functional. These include the kinetic energy contribution ($T[\rho]$), the pairwise nuclei-electron attraction ($E_{ne}[\rho]$) and the Coulomb and exchange terms of the electron-electron repulsion ($J[\rho]$ and $K[\rho]$ respectively). In seminal work by Kohn and Sham, it was proposed that the electron density can be expressed as the sum of probability densities of a set of orbitals similar to a Slater determinant (Equation 1.68).¹⁹⁷

$$\rho = \sum_i^n |\phi_i|^2 \quad (1.68)$$

A result of this is that the kinetic energy term $T[\rho]$ can be determined differentiating this set of Kohn-Sham orbitals (Equation 1.69).

$$T_S = \sum_{i=1}^n \langle \phi_i | -\frac{1}{2} \nabla^2 | \phi_i \rangle \quad (1.69)$$

With this, the underlying formulation of density functional theory is near complete, having adequately captured all but one element of the Born-Oppenheimer approximated Hamiltonian. Yet to be fully included, however, are elements of electron correlation and exchange. These are partially accounted for in $J[\rho]$ and $K[\rho]$ however non-classical contributions are more generally captured in an exchange-correlation functional $E_{xc}[\rho]$.

$$E_{DFT}[\rho] = T_S[\rho] + E_{ne}[\rho] + J[\rho] + E_{xc}[\rho] \quad (1.70)$$

As the form of this exchange-correlation functional is unknown, a great number of functionals have been formulated to approximate it, often themselves splitting this term into exchange ($E_x[\rho]$) and correlation ($E_c[\rho]$) components. Such an explosion in available approaches and the significant reduction in computational cost with respect to *ab initio* methods has lead to density functional theory (DFT) on the whole becoming arguably the most popular computational method today.¹⁹⁸ In fact, the great number of approximate functionals now available in modern DFT methods has lead to what has been termed by Perdew as a “functional zoo”.¹⁹⁹ Typically a functional is given some general parameterisation and then optimised or trained against accurate *ab initio* or experimentally determined quantities. While proven to be effective, the result is one where the choice of functional can be of great importance when approaching a chemical problem as functionals are optimised to perform in broad areas of chemistry (main group thermochemistry, reaction barrier heights, UV-vis spectroscopy, non-covalent and transition metal interactions).²⁰⁰ As of yet the exact form of $E_{xc}[\rho]$ is not known, and unlike *ab initio* methods there is not a systematic way to improve upon functional performance. However, in an effort to replicate this behaviour, theoreticians have adopted the biblical analogy of “Jacob’s Ladder” coined by Perdew (see Figure 1.10), where the increasing sophis-

tication of the exchange-correlation functional will allow for the ascension from hell (represented by Hartree-Fock theory) to the heaven of a complete description of the Schrödinger equation.²⁰¹ Within the analogy each rung represents a distinct change in the parameterisation approach and each will be described briefly here with relevant functionals detailed in Chapter 2. Two distinct approaches have been taken in DFT functional development; those that exhibit exact behaviour with respect to the underlying physical properties in question and those that follow a semi-empirical approach by fitting parametrised functionals to model systems calculated with high level *ab initio* methods.²⁰²

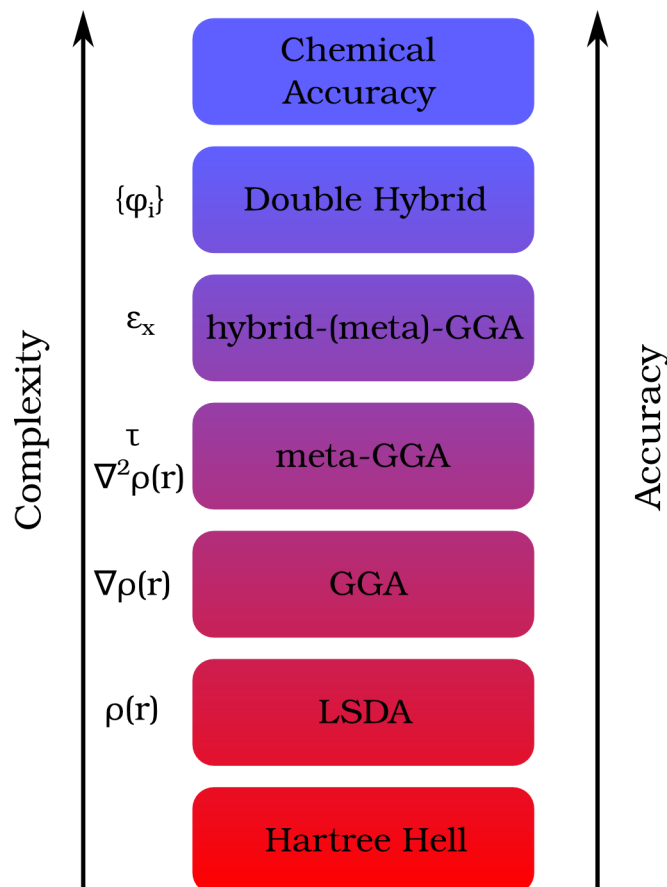


Figure 1.10: Representation of Jacobs Ladder adapted from Peng et al.²⁰³ Each rung describes a different level of parametrisation of DFT functionals beginning with the lowest rung denoted Hartree Hell, through to the heaven of Chemical Accuracy. Each rung is described in Section 1.2.5.

1.2.5 Jacob's Ladder

Local Spin Density Approximation (LSDA)

The lowest and simplest approach to parametrising Kohn-Sham density functional theory is the Local Spin Density Approximation. As detailed in Equations 1.69 and 1.70, while the kinetic energy terms of a given functional can be derived from the Kohn-Sham orbitals, it is not clear what an appropriate exchange-correlation functional would be. In the local density approximation, by treating the density as a homogeneous electron gas with a given exchange-correlation energy $\epsilon_{xc}(\rho)$ yields the following functional:

$$E_{xc}^{LSDA}[\rho_\alpha, \rho_\beta] = \int \rho(\mathbf{r}) \epsilon_{xc}(\rho_\alpha, \rho_\beta) d\mathbf{r} \quad (1.71)$$

Under LSDA the exchange and correlation terms in $\epsilon_{xc}(\rho)$ are separated into their respective terms. The Dirac exchange energy is then given by:¹³⁵

$$E_x[\rho_\alpha, \rho_\beta] = \frac{1}{2}(E_x[2\rho_\alpha] + E_x[2\rho_\beta]) \quad (1.72)$$

$$\epsilon_x(\rho) = -\frac{3}{4} \left(\frac{3}{\pi} \right)^{1/3} \rho(\mathbf{r})^{1/3} \quad (1.73)$$

and the exchange potential is:

$$v_x^{LDA}(\mathbf{r}) = -\left(\frac{3}{\pi} \rho(\mathbf{r}) \right)^{1/3} \quad (1.74)$$

The correlation terms, however, are not directly derived from the density alone as they need account for both the position \mathbf{r} but also both spin cases of the particles in question. An expression of the correlation functional inclusive of the spin-polarisation (ζ) would therefore be of the form:

$$\epsilon_c[\rho^\alpha, \rho^\beta] = \int \rho \epsilon_c(\rho, \zeta) d\mathbf{r} \quad (1.75)$$

and incorporate the pairwise interaction between particles within the expression of density. Early attempts at describing ϵ_c were only derived analytically in high and low density cases ($r \gg 1, r \ll 1$), however work by Vosko, Wilk and Nusair proposed a description of ϵ_c :²⁰⁴

$$\epsilon_c^{VWN}(r_s, \zeta) = \epsilon_c^0(r_s) + \alpha(r_s) \left[\frac{f(\zeta)}{f''(0)} \right] \left[\left(1 + f''(0) \frac{\epsilon_c^1(r_s) - \epsilon_c^0(r_s)}{\alpha(r_s)} \right) \zeta^4 \right] \quad (1.76)$$

and following interpolation of Monte Carlo calculations yielded a numerical description for both ϵ_c^1 and ϵ_c^0 :

$$\begin{aligned} \epsilon_c(r_s) = & \frac{A}{2} \left(\ln \left(\frac{x}{X(x)} \right) + \frac{2b}{Q} \arctan \left(\frac{Q}{2x+b} \right) - \frac{bx_0}{X(x_0)} \left(\ln \left(\frac{(x-x_0)^2}{X(x)} \right) \right. \right. \\ & \left. \left. + \frac{2(b+2x_0)}{Q} \arctan \left(\frac{Q}{2x+b} \right) \right) \right) \end{aligned} \quad (1.77)$$

Table 1.2: Parameterisation of the VWN correlation functional $\epsilon_c(r_s)$.

Parameter	$\epsilon_c^0(r_s)$	$\epsilon_c^1(r_s)$
x	$\sqrt{r_s}$	
$X(x)$	$x^2 + bx + c$	
Q	$\sqrt{4c - b^2}$	
A	0.0621814	$1/2(0.0621814)$
x_0	-0.409286	-0.743294
b	13.0720	20.1231
c	42.7198	101.578

Together this forms the SVWN functional with a Slater exchange functional and establishes a common naming convention for non-empirical DFT functionals.

Generalised Gradient Approximation (GGA)

As chemical systems are almost always represented by an electron density that doesn't demonstrate the same homogeneity required by LSDA methods, these functionals fail for describing all but the simplest of systems. This manifests in the over

estimation of interaction energies and resulting shortening of bonds with the helium dimer being a notable example.²⁰² Rather, by including in the exchange-correlation functional components of the density gradient $\nabla\rho(\mathbf{r})$, this inhomogeneity can begin to be captured. This yields an exchange functional which includes an Inhomogeneity Correction Factor (ICF) (g_x^{GGA}) as a power series (Equation 1.79).²⁰⁵

$$E_x^{GGA} = -\frac{3}{2}\left(\frac{3}{4\pi}\right)^{1/3} \int \rho^{4/3} g_x^{GGA} d\mathbf{r} \quad (1.78)$$

$$g_x^{GGA}(u) = \sum_{j=0}^N c_{x,j} u^j \quad (1.79)$$

and

$$u = \frac{\gamma \frac{|\nabla\rho|^2}{\rho^{8/3}}}{1 + \gamma \frac{|\nabla\rho|^2}{\rho^{8/3}}} \quad (1.80)$$

Similar arguments are then taken with the problem of the correlation functional, with the inclusion of contributions from same and opposite electron spins.

$$E_c^{GGA} = E_{c\alpha\beta}^{GGA} + \sum_{\sigma} E_{c\sigma\sigma'}^{GGA} \quad (1.81)$$

For opposite spin:

$$E_{c\alpha\beta}^{GGA} = \int \rho \epsilon_{c\alpha\beta}[\rho_{\alpha}, \rho_{\beta}] g_{c\alpha\beta}^{GGA}(s_{avg}^2) d\mathbf{r} \quad (1.82)$$

While for the same spin case:

$$E_{c\sigma\sigma'}^{GGA} = \int \rho \epsilon_{c\sigma\sigma}[\rho_{\sigma}] g_{c\sigma\sigma}^{GGA}(s_{\sigma}^2) d\mathbf{r} \quad (1.83)$$

where $g_{c\alpha\beta}^{GGA}$ and $g_{c\sigma\sigma}^{GGA}$ have analogous terms to $g_x^{GGA}(u)$ in Equation 1.79.

All together, a number of exchange and correlation GGA functionals have been developed by the groups of Becke, Perdew, Yang and Parr and combining the respective components yield a number of popular functionals. These include the PBE and

PW91 functionals for both correlation and exchange,^{206,207} the B88 exchange functional which is commonly combined with the LYP functional to form BLYP,^{208,209} and the P86 correlation functional.²¹⁰

meta-GGA

Occupying the third rung of Jacob's Ladder are the meta-GGA functionals. LSDA and GGA functionals, depending on the density and density gradient, do not accurately describe delocalisation of same-spin electrons and overestimate the exchange energy as a result. This can be addressed with the inclusion of exact exchange (see Hybrid Functionals), however meta-GGA functionals approach this problem by inclusion of the kinetic energy density (Equation 1.84) to circumvent the need to calculate exact exchange from Hartree-Fock methods.

$$\tau_\sigma = \frac{\nabla^2 \rho_\sigma}{2} - \sum_{i=1}^{n_\sigma} \phi_{i,\sigma}^*(\mathbf{r}) \nabla^2 \phi_{i,\sigma}(\mathbf{r}) \quad (1.84)$$

The resulting exchange functional E_x^{mGGA} , is then similar to a GGA functional with a modified ICF:

$$E_x^{mGGA} = -\frac{3}{2} \left(\frac{3}{4\pi} \right)^{1/3} \int \rho^{4/3} g_x^{mGGA} d\mathbf{r} \quad (1.85)$$

$$g_x^{mGGA}(w, u) = \sum_{i=0}^{N_t} \sum_{j=0}^N c_{x,ij} w^i u^j \quad (1.86)$$

where $t_\sigma = \frac{3}{5} (6\pi^2)^{2/3} \frac{\rho_\sigma^{5/3}}{\tau_\sigma}$ and $w = \frac{t_\sigma - 1}{t_\sigma + 1}$.

Notable meta-GGA functionals include the PKZB²¹¹ and TPSS²¹² functionals which performed well in atomisation energies, determination of barrier heights but often did not describe long-range dynamic correlation well. This was addressed to a degree by a number of empirical, meta-GGA Minnesota functionals developed by Truhlar *et al.* (with a good example being the M06-L functional).²¹³

Hybrid Functionals

A systemic failing of the first three rungs of Jacob's Ladder are that the functionals presented are local. This manifests in Self Interaction Error (SIE), where a given electron interacts with the entirety of the electron density, and therefore with itself. SIE is present even in calculations of one electron systems such as the hydrogen atom.²⁰² Systems that are prone to SIE include rare gas dimers and dimeric radical cations ($(\text{NH}_3)_2^+$).²¹⁴ Additionally, in systems where dynamical correlation (and particularly long-range correlation) is important for good descriptions of that system, local DFT methods also under perform.

In these systems, the empirical “hybrid” functionals are proposed. These include mixing in a complement of Hartree-Fock exchange into the exchange functional (Equation 1.87). By their nature these functionals require tuning to large training sets, with standardised testing sets developed for this purpose.

$$E_{xc}^H = c_x E_x^{HF} + (1 - c_x) E_x^{DFT} + E_c^{DFT} \quad (1.87)$$

A popular and widely used example for main group thermochemistry is the global hybrid GGA Becke, 3-parameter, Lee-Yang-Parr (B3LYP) functional.²¹⁵

$$E_{xc}^{B3LYP} = E_x^{LSDA} + a_0(E_x^{exact} - E_x^{LSDA}) + a_x \Delta E_x^{B88} + a_c \Delta E_c^{LYP} \quad (1.88)$$

or as $\Delta E_c^{LYP} = E_c^{LYP} - E_c^{LSDA}$ the B3LYP functional is often expressed as:

$$E_{xc}^{B3LYP} = (1 - a_0) E_x^{LSDA} + a_0 E_x^{exact} + a_x \Delta E_x^{B88} + (1 - a_c) E_c^{LSDA} + a_c E_c^{LYP} \quad (1.89)$$

where the three empirical parameters are $a_x = 0.20$, $a_0 = 0.72$ and $a_c = 0.81$.

Early testing of B3LYP and comparative studies with existing functionals suggested that B3LYP performs well for thermochemical calculations for a range of

small molecules.^{216,217} With comparable computational cost to Hartree-Fock methods, B3LYP was quickly adopted for general use, however it does suffer from a number of systematic deficiencies. Namely, B3LYP often contains a large Basis set superposition error (BSSE), resulting in erroneous thermochemical properties or conformers.^{218,219} Similarly, as B3LYP does not accurately account for long-range dispersion, van der Waals interactions and some intramolecular interactions are not accounted for, with the unbound benzene dimer being a notable early example.²²⁰

A number of extensions to GGA and meta-GGA functionals were also developed, with notable examples being the global hybrid meta-GGA M06, M06-HF and M06-2X functionals.^{200,221} Each of these contain 27 %, 100 % and 54 % Hartree-Fock exchange respectively and are as many as 35 parameters. The inclusion of Hartree-Fock exchange in the suite of Minnesota functionals aided the performance of these functionals for long-range and charge transfer purposes. However there existed a growing opposition to the “overparametrising” and increasingly empirical nature of DFT functionals, with advocates desiring a return to a simpler functional description reliant on a more accurate description of the electron density.²²² The ultimate goal to replicate wavefunction methods and be “right for the right reasons” resulting in the growth of a number of double-hybrid functionals.²²³

Double-Hybrid Functionals

In an effort to improve on the robustness of DFT methods, Stefan Grimme proposed a fifth rung of Jacob’s Ladder. Occupying this rung would be a range of semi-empirical functionals that include not only Hartree-Fock exchange but also electron correlation from *ab initio* methods in the exchange-correlation functional. With computational cost still be an important consideration in functional design, correlation energy would be drawn from perturbation theory (from Görling and Levy)²²⁴ and comparable *in cost* to MP2 methods.²²⁵ The first proposed functional is denoted B2PLYP and has the form:

$$E_{xc}^H = c_x E_x^{HF} + (1 - c_x) E_x^{DFT} + a E_c^{DFT} + b E_c^{PT2} \quad (1.90)$$

with nominally $a = 1 - b = 1 - c_c$.

As the correlation term, however, is derived from perturbation theory, it contains a similar overestimation of exchange that is present in the E_x^{HF} term. To account for this and improve on performance further, the E_c^{PT2} term can be separated into scaled same and opposite spin terms similar to spin-component scaled MP2 (SCS-MP2):²²⁶

$$E_c^{PT2} = c_o E_{\alpha\beta}^{PT2} + c_s (E_{\alpha\alpha}^{PT2} + E_{\beta\beta}^{PT2}) \quad (1.91)$$

The inclusion of the DSD (dispersion corrected, spin-component scaled, double hybrid) component in lower rungs of Jacob's Ladder, in many cases this is the result of serendipitous error cancellation. In the initial parametrisation of DSD double hybrids, Kozuch and Martin²²⁷ note that the LSDA functional vastly improves comparable to GGA functionals; however, this is due to the overestimation of correlation and underestimation of exchange. The authors also note that while performance is largely unaffected by choice of exchange functional, the popular LYP functional suffers under a DSD parameterisation compared to others such as P86.

Testing against large databases by the groups of Goerigk and Grimme²²⁸ yielded systematic improvement of functional performance moving from GGAs (rung 2) through to the double hybrids. These functionals, while largely semi-empirical, offer the currently most robust treatment of physical properties within chemical systems. For weakly bound systems however, where long-range interactions are most important, tuning of functional parameters can often only provide satisfactory performance at the expense of overestimation at intramolecular bonding distances. As a result, across the suite of functionals comprising Jacob's Ladder, long-range dispersion corrections are included.

1.2.6 London Dispersion

In approaching the challenge of accounting for long-range dispersion interactions, which are of particular importance to dimer formation, covered here are the commonly used semi-empirical methods. These methods includes an atom-pairwise correction to the existing functional which is damped such that, at typical intramolecular bonding distances the functional dominates and at larger interatomic distances such as those in long-range interactions, the dispersion corrections contributes and is tuned appropriately. The dispersion correction takes the form:

$$E_{disp}^{AB} = -s_n \sum_{AB} \sum_{n=6,8,10,\dots} \frac{C_n^{AB}}{R^n} f_{damp}^{(n)} \quad (1.92)$$

where R is the atom-pairwise interatomic distance, s_n are scaling parameters tuned for a given functional. The C_n^{AB} coefficients are dispersion coefficients and are representative of dipole-dipole (C_6^{AB}), dipole-quadrupole (C_8^{AB}) and dipole-octapole and quadrupole-quadrupole (C_{10}^{AB}) interactions. These C_n^{AB} functions can themselves be determined formally from experimental or theoretical measurements for atomic polarisabilities using the Casimir-Polder expression^v.²²⁹

The damping function $f_{damp}^{(n)}$ can take several forms. The most commonly used early form of a dispersion correction, Grimme's D2 correction expresses the damping function as:

$$f_{damp} = \frac{1}{1 + e^{-d(R_{AB}/R_0 - 1)}} \quad (1.93)$$

where R_0 is the atomic vdW radii.²³⁰ The dispersion coefficients (C_6^A) in this case are computed from atomic polarisabilities and first ionisation potentials.

Grimme's later D3 correction offer two improvements to D2. Firstly, the inclusion of a $1/R^8$ term thereby including higher order multipole contributions to dispersion (the quadrupole-quadrupole and dipole-octapole contributions can be included by

^v $C_6^{AB} = \frac{3}{\pi} \int_0^\infty \alpha_A(i\omega) \alpha_B(i\omega) d\omega$, $C_8^{AB} = 3C_6^{AB} \sqrt{Q_A Q_B}$ and $Q_A = \sqrt{Z_A} \frac{\langle r_A^4 \rangle}{\langle r_A^2 \rangle}$

proper scaling of s_8) and secondly, the parameterisation of C_n terms such that atoms in varying coordination states are accounted for.

$$f_{damp}^{(n)} = \frac{1}{1 + 6\left(\frac{R_{AB}}{s_{r,n}R_0}\right)^{-a_n}} \quad (1.94)$$

where $a_6 = 12$, $a_8 = 14$ and typically $s_{r,8} = 1$. This is denoted D3(0) as the damping function is such that as $R \rightarrow 0$, $E_{disp} \rightarrow 0$. An alternative that tends towards non-zero dispersion at small interatomic distances is Becke-Johnson (BJ) damping. As dispersion is non-zero at shorter distances, D3(BJ) typically transitions smoothly into regions where the exchange-correlation functional accounts for these effect, more so than traditional D3(0) damping.²³¹

$$f_{damp}^{(n)} = \frac{R_{AB}^n}{R_{AB}^n + (a_1 R^0 + a_2)^n} \quad (1.95)$$

In the dispersion correction schemes discussed thus far, the expressions have drawn upon calculated dispersion coefficients and while these have been updated in D3(0) they are still predetermined and drawn upon when calculating the E_{disp} . As a result the E_{disp} has only been dependant on the pairwise interatomic distances. The most contemporary dispersion correction, termed D4, seeks to include the effect of atomic charges in the dispersion coefficients, determining them simultaneously to the energy of the functional.^{232,233} This is done by integrating the Casimir-Polder equation:

$$C_6^{AB} = \sum_{A,ref=1}^{N^{A,ref}} \sum_{B,ref=1}^{N^{B,ref}} \frac{3}{\pi} \int_0^\infty d\omega \alpha^{A,ref}(i\omega, z^A) W_A^{A,ref} \alpha^{B,ref}(i\omega, z^B) W_B^{B,ref} \quad (1.96)$$

Here $\alpha^{A,ref}$ are scaled reference polarisabilities based on effective charges (z^A). This process removes the need for adjusted dispersion coefficients such as those in D3(0) by actively accounting for changes to polarisability and charge density on atoms within a given system prior to inclusion in a D3(BJ) form of E_{disp} .

While it can be seen that somewhat systematic improvements can be made on the dispersion correction in that higher order multipole interactions may be included, it is the choice of correction coupled with the choice of exchange-correlation functional that is important. Where the exchange-correlation functional is chosen to include lone-range effects, use of a less sophisticated dispersion correction may yield better functional performance, with ω B97X-D as a good example employing a modified version of D2 dispersion (utilising the D3(0) damping function for $n = 6$ only).²³⁴ The intention is to avoid “double counting,” an effect that is already included in the parameterisation of the functional. As a result modern semi-empirical functional design (for hybrid and double-hybrids) may include optimisation of both the exchange and correlation contributions in tandem with the s_n parameters.

1.2.7 Basis Sets

In approaching the determination of solutions to the many-body Schrödinger equation it has been shown that in addition to the simplification of the problem, the choice of basis functions (collectively known as a basis set) that describe the atomic orbitals is crucial. As a reflection of a model physical system, the accurate description of orbitals is paramount in helping distinguish meaningful results from those that are artefacts of basis set choice. The most rudimentary basis sets are those consisting of Slater-type orbitals (STOs)²³⁵

$$R(n, Z, s) = r^{n-1} e^{\frac{-(Z-s)r}{n}} \quad (1.97)$$

In general, the considerations for the choice of basis set are that of accuracy and computational cost, the latter of which manifests as the result of both the number of basis functions and complexity of their description. STOs, as solutions to the Schrödinger equation for the hydrogen atom, accurately reflect the cusp behaviour (i.e. as $r \rightarrow 0$) near the nucleus of atoms. These functions, however, are not easily differentiable and suffer from higher computational cost. Alternatively, Gaussian

functions can be used to represent the atomic orbitals (denoted Gaussian-type orbitals (GTOs)) and while they do not readily display appropriate cusp behaviour without inclusion of additional functions, they do show good tail (increasing r) behaviour and can be fitted to STOs at typical bonding distances.²³⁶ GTOs are also advantageous in terms of their cost in that pairs of Gaussians can be combined into a single Gaussian function and by repeating this process the calculation at hand is greatly simplified. This property lends well to linear combination of atomic orbitals (LCAO) methods and GTOs have seen universal use in modern computational chemistry software. By representing atomic orbitals as a linear combination of Gaussian functions, additional functions can be readily included to account for polarisation and long-range effects.

The quality of basis sets in general are denoted by the number of polarisation functions included ($n = D, T, Q, 5, \dots$) with a perfect description of the atomic orbitals being the complete basis set (CBS) (ie $n \rightarrow \infty$). Basis sets as they are described, use notation that represents the number of basis functions and a reduced number of ‘contracted’ functions, with the understanding that core electrons are largely unaffected by interactions in bonding. This notation can vary but for the purposes used within this thesis basis sets are describe with the number of functions contained within rounded brackets and contracted functions within square brackets. Taking Dunning’s cc-pVDZ-PP basis set for Ga-Kr as an example (drawn from the Basis Set Exchange);²³⁷ the basis set is represented by $(8s7p7d)/[4s3p2d]$.²³⁸ Augmented basis sets then include an additional diffuse function at each ℓ in both the uncontracted and contracted sets (ie $(9s8p8d)/[5s4p3d]$). The basis functions themselves comprise a number of primitive Gaussians which are denoted, again for a contracted aug-cc-pVDZ-PP (81811,7711,711).

Dunning’s correlation consistent (‘cc’) basis sets in particular, have been designed with the intention that they converge with increasing quality in both HF and correlation energy. These basis sets have become popular for use in post-HF methods as their consistency allows for extrapolation to the CBS. One such method

termed Weizmann methods (see Equation 2.1), utilises an extrapolation shown by Halkier *et. al.*²³⁹ where, given the energies of given cardinal numbers (X, Y) may be expresses as $E_X^{corr} = E_{XY}^{corr} + AX^{-3}$, a two-point extrapolation yields the energy at the CBS. Early Weizmann methods, denoted W1 and W2, extrapolated the energy components being the SCF and CC energies from up to quadruple- and quintuple- ζ basis set respectively.^{240,241} Later extensions W3 and W4,^{242,243} as well as the high-accuracy extrapolated ab initio thermochemistry (HEAT) protocol,²⁴⁴ have since become standards for highly accurate (3σ accuracy of 1 kJ mol^{-1} for small molecules in W4) thermochemical calculations and the general framework has been extended in recent decades as increasing computational resources have become available.²⁴⁵ Often also these extrapolated energies form the benchmark sets used in validating DFT functionals.²⁴⁶

Dunning's basis sets utilise a general contraction scheme where “*all primitives may contribute to each of several contracted basis functions*”.²⁴⁷ The alternate def2 basis sets, designed by the Ahlrichs' group, utilised a segmented contraction scheme with the intention of reducing the number of primitives and correspondingly computational cost whilst still delivering comparable performance.^{248,249} Segmented contraction schemes as opposed to general contraction schemes, allow primitives to only contribute to a single contracted function, thereby ‘segmenting’ the basis set into parts and avoiding doubling up on functions in the contracted set.²⁵⁰ This is evident when comparing the contracted cc-pVTZ and def2-TZVP basis sets (again for Ga-Kr) where the number of primitives are ((20)(20)(20)1(20)1,(13)(13)1(13)1,811,1) and (842111,64111,5111,1).²³⁷ Inclusion of an effective core potential (ECP) reduces the total number of primitives in the Dunning basis set to 69 however this is still nearly double that of the def2 basis. As computational cost scales with the number of basis functions, ultimately it is the choice of the chemist to determine that the basis set of choice is fit for purpose in a given context.

1.2.8 Vibronic Simulations

Franck-Condon Principle

Given that electronic structure methods allow for electronic structure to be calculated for a given geometric structure, it is a natural extension that one could calculate a VDE of a given state and geometry by repeating the energy calculation on the new potential energy surface with the same methods and basis set. Including vibrational energy components and determining the energy difference between pairs of alike minima on the anion and neutral potential energy surfaces yields a determination of electron affinity (E_a) (ie. $E_a = (E_{\text{Neut}} + zpe_{\text{Neut}}) - (E_{\text{Ani}} + zpe_{\text{Ani}})$). While this is fit for the purpose of determining the thermochemistry of the system, it does not provide any information on the probability of a given vibronic transition. The probabilities may be determined by the Franck-Condon principle (Equation 1.98), where the probability of a given transition ($j \leftarrow i$) is proportional to the degree of overlap between the two states.^{251,252} While both nuclear and electronic components of these wavefunctions may be included, it is assumed that vibronic transitions occur in accordance with the Born-Oppenheimer approximation, that is all transitions between potential energy surfaces are vertical excitations.

$$P_{j \leftarrow i} \propto |\langle \psi_j | \mu | \psi_i \rangle|^2 \quad (1.98)$$

where μ is the electronic dipole moment operator between the two states. By separating the electronic and nuclear wavefunctions, the overlap in electronic wavefunctions can determine the electronic dipole moment operator, from which the photodetachment cross-section can be determined. By then determining the overlap in the nuclear wavefunctions a series of Franck-Condon factors (FCFs) can be determined. Together these factors can be used to predict vibronic transitions based on; 1) the probability of a given electronic transition; 2) the FCFs then determine the probability of transitions to vibrational states given similarities in geometry; and 3) the energy difference of the transition ($E_{j \leftarrow i}$).

$$I(\omega) = \sum_{i,j} P_{j \leftarrow i} \delta(\omega - E_{j \leftarrow i}) \quad (1.99)$$

For a multidimensional harmonic oscillator, the total wavefunction is a product of the individual vibrational wavefunctions (at all quanta).

$$\chi_{\nu_1, \nu_2, \dots, \nu_N}(\mathbf{Q}) = \prod_{a=1}^N \chi_{a, \nu_a}(Q_a) \quad (1.100)$$

As the modes in each state and their magnitude of displacement are different in order to determine the FCFs and predict spectra, the two coordinate systems need to be transformed to be comparable. There are two approaches to this:

1. The Parallel Approximation: Under the Parallel Approximation the change in \mathbf{Q} ($\Delta\mathbf{Q}$) is simply applied to one of the states such that the axis are rotated to align. The assumption of the parallel approximation is that the normal modes, representative of the curvature of the potential energy surface, do not change significantly between the two states. Typically, this rotation would be in the coordinate system used is the upper electronic state to preserve the nodal overlap of the states.²⁵³
2. Duschinsky Rotations: Whereas the parallel approximation represents a transform of the coordinate system describing the modes of one state to align with the other, Duschinsky rotations represent a transform of the normal modes themselves. The idea proposed by Duschinsky is that normal modes of one state could be represented by a linear combination of the normal modes of the other by the transform $\vec{Q}' = S \cdot \vec{Q}'' + \vec{d}$.²⁵⁴ Here the transform from the normal mode basis of \vec{Q}'' comprises a transform of nuclear coordinates \vec{d} and the application of some rotation of the normal modes expressed by S .

Both methods are suitable for the calculation of rigid molecules; however, in cases where low frequency modes are present such as in vdW complexes or free rotors exist in the molecule, care need be taken to approach these problems appro-

priately.²⁵⁵ While some quantum chemistry codes have this functionality in-built, the work described in this thesis utilises *ezSpectrum 3.0*²⁵⁶ (now known as *ezFCF*) to determine FCFs from electronic structure outputs.

Calculating PADs and Anisotropy Parameters

In the previous discussion of predicting vibronic transitions the only requirements to determine FCFs are the structures and a description of the normal modes of the two states. This interpretation relies on Koopman's theorem for the interpretation on the photodetachment process, that being that the orbital description of the removal of the photoelectron corresponds to the orbital description of the neutral wavefunction (ionised anion wavefunction). In practice however this is not the case, instead a Dyson orbital, representing the overlap between the anion wavefunction and the photodetached neutral wavefunction, is preferable as it allows for the relaxation of the occupied orbitals whilst still retaining a one-electron description.²⁵⁷

$$\phi^d(\mathbf{r}_1) = \sqrt{N} \int \psi_i^n(\mathbf{r}_1, \dots, \mathbf{r}_n) \psi_j^{n-1}(\mathbf{r}_2, \dots, \mathbf{r}_n) d\mathbf{r}_2 \dots d\mathbf{r}_n \quad (1.101)$$

In addition to being able to calculate FCFs in a similar fashion to the procedure described above, the anisotropy parameter and subsequent PAD can be determined from the electronic dipole moment of a transition. Under a plane-wave model, a modified Cooper-Zare Equation (1.3) expresses the cross-section as:

$$\frac{d\sigma}{d\Omega_k} = \frac{4\pi^2 k E}{c} \langle \phi^d | \hat{\mu} | \psi_k^{el} \rangle \quad (1.102)$$

where the plane-wave of $\psi_k^{el} = \frac{1}{(2\pi)^{3/2}} e^{i\mathbf{k}\mathbf{r}}$. By characterising the plane-wave as a combination of contributing partial-waves, a quantitative assignment of PADs can be made under the *s&p* model.⁷⁸ For most anion PES experiments, this suffices as a method of determining the PAD and β parameter. This is due to the fact that, upon photodetachment, the photoelectron is assumed to be ejected in a non-interacting environment with the residual molecule. However this is not the case. Exemplified

in the photodetachment of neutrals to cations, the photoelectron is ejected within the potential of the residual and forms a Coulomb wave (where the formal charge of the molecule is Z and where $Z = 0$ yields the plane-wave model behaviour). While not immediately apparent in the context of anion PES, in photodetachment to DBSs photodetachment modelled under a Coulomb wave model may produce formal charges less than 1. This was demonstrated by Gozem *et al.* for photodetachment cross-sections of formaldehyde, ethylene, acetylene, butene, 1-butyne, methanol and propyne.²⁵⁸

1.2.9 Summary

This chapter has outlined the theoretical and conceptual foundation for the works undertaken in this thesis. This includes illustration the notable power and flexibility of photoelectron spectroscopy in the characterisation and study of chemical species. Magnetic bottle time-of-flight photoelectron spectroscopy, which is the subject of the works within this thesis, benefits from the highly efficient collection of photoelectrons produced during photodetachment. However, this is at the expense of spectral energy resolution, and this technique often cannot resolve near degenerate neutral electronic or vibrational states. VMI photoelectron spectrometers offer one way to circumvent the causes of spectral broadening in traditional by recording the spatial distribution of photoelectrons on a detector screen. Taken to its extreme, slow electron velocity map imaging (SEVI) utilises tunable laser radiation to perform photodetachment at energies that lie just above the photodetachment threshold of a given transition, thereby further reducing broadening effects.

Also established in this Chapter are the fundamental concepts underlying the computational methods employed in this thesis; from the solving of the Schrödinger equation for a simple system such as H_2^+ , through to multireference problems. While *ab initio* methods are highly robust and accurate (particularly coupled cluster methods), they scale poorly with the number of basis functions and are quickly become

too demanding on computational resources to be feasibly undertaken. Alternatively, density functional theory (DFT) methods provide much more scalable approaches to chemical problems but at the expense of accuracy. It is then pertinent to determine methods that both scale at low computational cost, but provide comparable results to experimental observables.

Chapter 2

Materials and Methods

2.1 Computational Approaches

2.1.1 *Ab Initio* Calculations

Calculation Protocols

The approach taken in many of the studies detailed herein is well established amongst previous work in the Wild Group^{259–263} and is detailed here in Figure 2.1. Where methodology differs or is adapted for specific cases those details are provided in the appropriate chapters General and universal (within this work) considerations are described here. An initial set of conformers is proposed based on rudimentary chemical understanding; this can be from a combination of properties of the constituent molecules such as known dipole and electrostatic interactions, steric drivers such as pockets within structures and proposed valence orbital geometries. The conformers are then optimised using *ab initio* methods (typically MP2) with Dunning’s augmented correlation-consistent polarised valence basis sets, denoted here as AVnZ.^{264,265} These basis sets have been selected above the former cc-pVnZ sets as the additional diffuse functions are required to adequately describe weak interactions.²³⁸ Where appropriate for heavier atoms such as bromine and iodine, the corresponding basis sets that include an ECP are used to account for relativistic

effects and reduce computational cost.^{238,266} As $\Delta E/\Delta \mathbf{r}$ is low near van der Waals minima, the geometric convergence criteria used in these calculations is similarly tight (VTight in Gaussian 09: RMS Force $< 1 \times 10^{-6}$).²⁶⁷

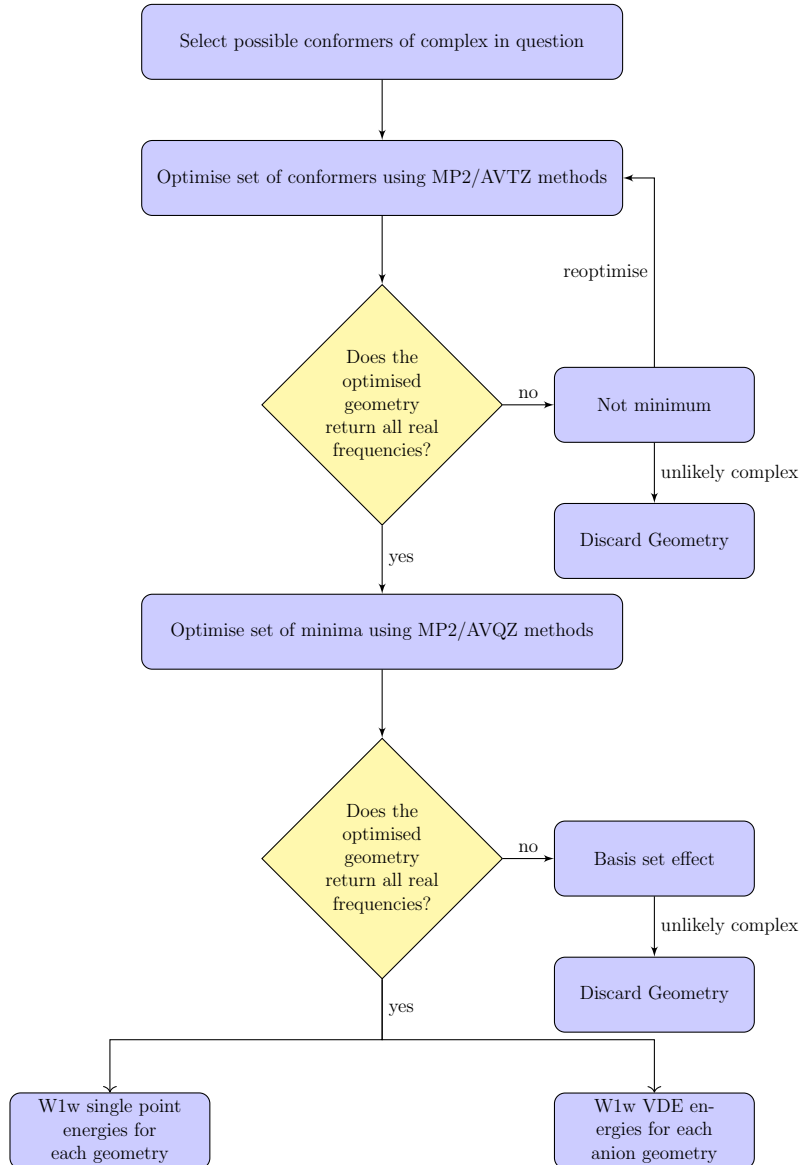


Figure 2.1: Protocol followed for screening of complex conformers and determination of complete basis set limit energies.

Typically beginning with MP2/AVTZ calculations, conformers that produce all real harmonic frequencies and are local minima are then re-optimised using AVQZ basis sets. Those stationary points that produce one or more imaginary harmonic modes are either classified as *n*th order transition states (based on the number of imaginary modes, implying the structure is a maximum in that coordinate) or used to

inform new guesses to include in the set of conformers. Stationary point geometries that are shown to be minima in both MP2/AVTZ and MP2/AVQZ calculations are then used as geometries in suitable Weizmann theory (Wn) calculations as per Equation 2.1.

$$E_{\infty} = E_L + \frac{E_L - E_{L-1}}{\left(\frac{L}{L-1}\right)^{\alpha} - 1} \quad (2.1)$$

where L is the cardinal number (i.e. AVLZ) of the basis sets being used and α is the appropriate exponent. Wnw methods are often used in this work and correspond to Weizmann methods adapted for Dunning's augmented basis sets. For W1w, $L = T, Q$ for extrapolating the SCF energy and CCSD contribution and D, T for extrapolating the perturbative triple (T) contribution. These are increased to $L = Q, 5$ and T, Q respectively for W2w. In both W1w and W2w methods, $\alpha = 5$ for SCF extrapolations, however for coupled cluster extrapolations $\alpha = 3.22$ and 3 for W1w and W2w respectively.

Whether by MP2, CC, Wn or other methods, the thermodynamics of the system of interest can be determined by examining the difference in energy at critical points on the potential energy surface. Shown in Figure 2.2, the electronic dissociation energy (D_e) of both the anion and neutral complexes can be found by finding the difference between the sum of the energies of the consituent species and that of the complex. This can be corrected to complex dissociation energy (D_0) by the inclusion of the difference in vibrational zero point energies, typically drawn from the highest available frequency calculation for that complex. Similarly, the experimentally comparative value electron stabilisation energy (E_{stab}) can be determined by either the difference in the E_a between the complex and the bare anion, or by the difference in the D_0 of the anion and neutral complexes. Additionally, VDEs can also be calculated by performing a single point energy calculation of the anion complex geometry on the corresponding neutral potential energy surface and determining the difference in energy between the two.

As much of the published work herein and within the Wild Group investigates the halide-molecule complexes, it is necessary to calculate the E_a of both of the 2P states of the halide. Methods such as those described above will determine the E_a of the barycentre between these two states, however to accurately reflect experiment these are artificially split into their respective spin-orbit states. This is done by assuming that the spin-orbit coupling between the 2P states is essentially unperturbed upon formation of the complex, and a correction can be applied to the barycentre E_a yielding the $^2P_{3/2}$ and $^2P_{1/2}$ energies. Further improvement upon computational methods can be made by calibrating the calculated E_a of the bare halide against accurately determined experimental energies. Assuming that this error is systematic to the choice of method, the difference between these may then be applied to calculated complex E_a thereby correcting them.

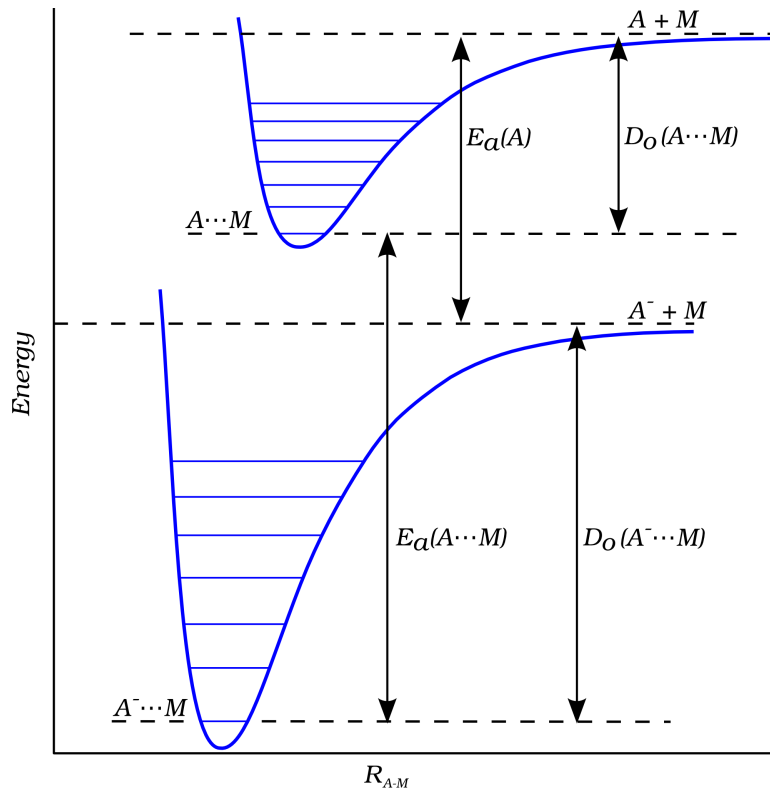


Figure 2.2: Illustrative anion and neutral potential energy surfaces of interacting A with some solvent M . E_a are the electron affinities of the complex stabilisation energies and bare A , and D_0 are the respective complex stabilisation energies of the anion and neutral complexes.

Further levels of screening can be included to improve upon structural informa-

tion by following a Pople diagram^{268,269} and using either larger basis sets or higher levels of theory however these can become prohibitively expensive. For larger van der Waals systems that have low energy gradients with respect to changes in geometry, low level Weizmann methods that utilise DFT functionals for geometry optimisations can be suitable, provided they adequately describe long-range interactions.^{240,241,243} In this work, these functionals include the spin-component-scaled double-hybrid functional (DSD-PBEP86-D3BJ) parameterised by Kozuch and Martin (and particularly the 2013 parameterisation).^{227,270} The functional has been selected for its robust performance across a wide range of chemistries via the GMTKN55 database.²²⁸ In this set the weighted total mean absolute deviation (WTMAD) is calculated in two ways; 1) as an average value over the 55 data sets (WTMAD-1), and 2) where each test set is weighted respectively and scaled by the number of energies within that set (WTMAD-2, see Equation 2.2).

$$\text{WTMAD-2} = \frac{1}{\sum_{i=1}^{55} N_i} \sum_{i=1}^{55} N_i \frac{56.84 \text{ kcal mol}^{-1}}{|\Delta E|_i} MAD_i \quad (2.2)$$

In general, functionals belonging to the ‘fifth rung’ of Jacob’s Ladder performed best in the GMTKN55 test set and of these the DSD-PBEP86-D3BJ functional performed best with WTMAD-1 and WTMAD-2 values of 1.46 kcal mol⁻¹ and 1.69 kcal mol⁻¹ respectively.²²⁸

The functional is of the form expressed in Equation 1.91, parameterised in Gaussian 09 utilising the *IOps* commands; `b2plyp(semidirect) iop(3/125=0220005200, 3/78=0440004400, 3/76=0310006900, 3/74=1004) empiricaldispersion=gd3bj`. The empirical dispersion parameters are a truncated form of Equation 1.95²⁷¹ given by:

$$E_D^{BJ} = -\frac{1}{2} \sum_{A \neq B} s_6 \frac{C_6^{AB}}{R_{AB}^6 + (a_1 R_{AB}^0 + a_2)^6} + s_8 \frac{C_8^{AB}}{R_{AB}^8 + (a_1 R_{AB}^0 + a_2)^8} \quad (2.3)$$

where $R_{AB}^0 = \sqrt{\frac{C_8^{AB}}{C_6^{AB}}}$. Each of the empirical dispersion parameters are then set as environmental variables when executing Gaussian 09.

Within the *IOps* parameterisation, 3/74 chooses the PBE exchange functional (1000) with P86 correlation (+4), other commands are summarised below:

Table 2.1: Parameterisation of the DSD-PBEP86-D3BJ functional and where each parameter is set with respect to Gaussian 09.²⁶⁷

Parameter	Value	Set By
c_X	0.31	iops - 3/76
c_c	0.44	iops - 3/78
c_o	0.52	iops - 3/125
c_s	0.22	iops - 3/125
s_6	0.48	Environmental Variable
s_8	0.00	Environmental Variable
R_{AB}^6	0.00	Environmental Variable
a_1	0.00	Environmental Variable
a_2	5.60	Environmental Variable

It is worth noting that as s_8 is set to zero, the second term in Equation 2.3 disappears, leaving only the s_6 term.

In addition to the optimisation convergence criteria and the parameters above, as DFT methods undergo a numerical integration at each step, the integration grid used is an important consideration on the accuracy. Pruned grids are defined by a number of points surrounding each atom and denoted (m, n) , where m is the number of radial shells surrounding each atom and n is the number of points per shell. In Gaussian 09 the default grid is denoted **Fine** is (75,302). However typically for cases where low energy vibrational modes are important, as is the case in van der Waals complexes, an **UltraFine** (99,590) grid is required. This would later become the default grid in Gaussian 16.

While Dunning's augmented basis sets have been used in *ab initio* calculations, for DFT methods these and additional basis sets are tested. As it has been used in the parameterisation of the DSD-PBEP86-D3BJ functional, Ahlrich's def2-QZVP functional is also used here.^{248,272} For bromine the def2-QZVP basis set is represented by (24s20p10d2f1g)/[11s7p4d2f1g] with primitives ((11)411111111/(10)511111/7111/11/1)

and is considerably cheaper than the corresponding aug-cc-pVQZ set. While def2-QZVP bases also include an ECP for iodine, the default basis for bromine is an all electron set.

Computational Resources

Calculations in this thesis have been completed utilising comparatively modest computational resources. At the commencement of candidature, calculations have been undertaken using two local workstations. These workstations are comprised of *Intel i7-3770K 3.5GHz* and *i7-4790K 4.0GHz* CPUs respectively, both with 8 threads. Each workstation also contains 32 GB of RAM with additional virtual memory accessible. During candidature, a high-performance computing (HPC) cluster was constructed within the University of Western Australia. Each of the computing nodes within the cluster consisted of 12 cores (24 hyperthreaded) and 24 GB of memory. As a shared facility however, walltimes for use of these nodes were restricted through the Torque queuing system for short (8 h), long (72 h) and vlong (480 h) jobs.

For aspects of the project that require high throughput calculations at lower computational cost such as the initial screening of conformer sets, the HPC cluster is suitable for most systems. Where necessary, harmonic frequency calculations can be undertaken numerically such that they may be restarted. Those calculations that require significant resources within the scope of this project (ie Wnw energy calculations) are then reserved for use on the local workstations where they are not limited by walltime.

Calculations as part of this work have been completed utlising primarily Gaussian 09²⁶⁷ for geometry optimisations and harmonic frequency calculations. For the CC single point energy calculations required for Wnw energy extrapolations, both Gaussian and CFOUR²⁷³ have been used. Finally, where multireference (NEVPT2) methods have been used, these energies have been calculated in ORCA 4.1.2.^{274,275}

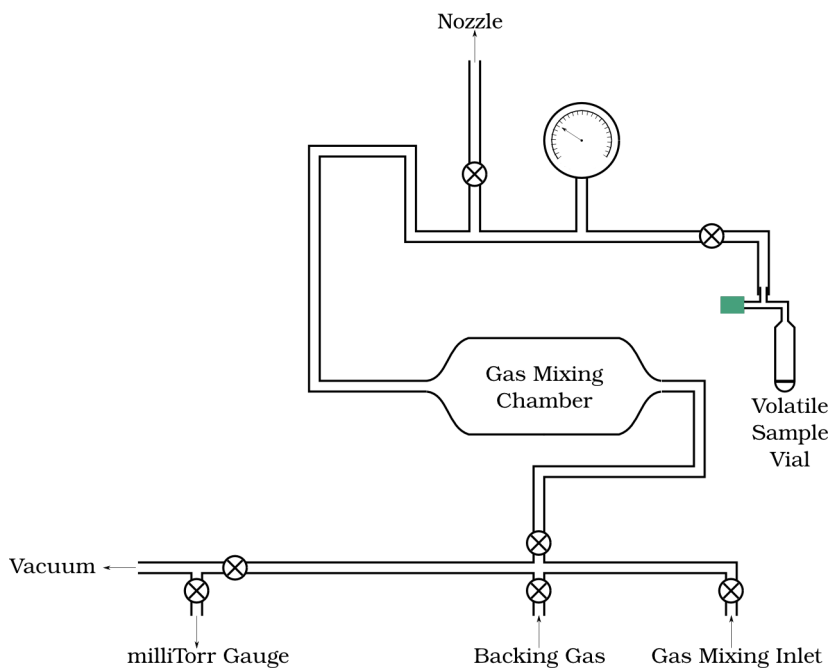


Figure 2.3: Schematic of the current configuration of the gas mixing station.

2.2 Existing TOF-PES Spectrometer

2.2.1 Gas Mixing Station

Prior to injection into the TOF-PES spectrometer, gases are prepared and stored in the gas mixing station. The gas mixing station consists of a central vessel approximately 1400 cm^3 (2 s.f) in volume connected to a series of inlets and outlets by 1/4" *Swagelock* stainless steel tubing. Since the commencement of candidature, the station has undergone changes in design and scope (see Section 2.3.1). The original gas mixing station (shown in Figure 2.3), featured two inlets with Teflon lines leading to source gases and one sample vial for liquid sources. The station also featured a high pressure gauge allowing the user to estimate the quantity of source gases introduced to the chamber and a mTorr vacuum gauge. Vacuum on the station is reached via a rotary pump that feeds through a liquid nitrogen cold trap with typical pressure of 30 mTorr to 70 mTorr.

Under typical operation, halide precursors (CH_3I , CH_2Br_2 , CH_2Cl_2) are degassed via a freeze-pump-thaw method prior to opening to the evacuated vessel. For liquid

samples with higher vapour pressures, the sample vial is placed in an ice-water (0°C), ice-salt water (approx. -11°C) or dry ice-acetone (-78°C) to control the introduction of precursor to the station. The Antoine equation²⁷⁶ is used to estimate the vapour pressure of the solution at decreased temperature:

$$\log p = A - \frac{B}{C + T} \quad (2.4)$$

Table 2.2 provides examples of the constants used in the Antoine equation and the vapour pressure of relevant liquids under each condition.

Table 2.2: Antoine coefficients and calculated vapour pressures p_T (in Torr for a given T in $^{\circ}\text{C}$) for a variety of common liquid sources and temperatures used as part of experiment. A and B are both in Torr and C is in $^{\circ}\text{C}$. Antoine coefficients have been determined by fitting to experimental data from *a*: Stull,²⁷⁷ *b*: Heisig²⁷⁸ and *c*: Hull.²⁷⁹ NA: temperature is below the melting point of the substance.

	<i>A</i>	<i>B</i>	<i>C</i>	p_{-78}	p_{-11}	p_0	p_{10}	p_{25}
				Torr				
Acetone ²⁸⁰	7.02447	1161.0	224.00	0	37	69	116	230
Ethanol ²⁸⁰	8.04494	1554.3	222.65	0	5	12	23	59
Water ²⁸⁰	7.94917	1657.5	227.02	NA	NA	4	9	24
Formic Acid ^a	7.68304	1748.8	263.71	NA	NA	NA	20	42
CS ₂ ²⁸¹	6.94194	1168.6	241.53	1	75	127	198	361
1,3-butadiene ^b	6.85871	935.5	239.76	12	588	905	1297	2115
Cyclopentadiene ^c	7.10081	1199.8	244.10	1	90	153	239	439
CH ₂ Cl ₂ ^a	7.06792	1138.5	230.90	0	78	137	220	416
CHCl ₃ ²⁸⁰	6.95470	1171.0	226.23	NA	33	60	99	197
CCl ₄ ²⁸⁰	6.93390	1242.4	230.00	NA	18	34	57	115
CH ₂ Br ₂ ^a	7.38040	1546.8	244.82	NA	6	12	20	44
CH ₃ I ^a	6.95389	1145.9	238.30	NA	82	140	218	400

Once the halide precursors are introduced the inlet taps can be used to control the introduction of partial pressures of the complexing gas (typically no more than 50 kPa) and argon backing gas. The total pressure inside the gas mixing station during operation is 450 kPa such that gas mixes are made to approximately 1:10:100 ratio of precursor, complex gas and argon.

2.2.2 Time of Flight Photoelectron Spectroscopy

Construction of the original TOF-PES in the Wild Group was completed in 2008²⁸² with subsequent improvements by a number of Wild Group members.^{283–288} At the time of commencement of candidature the apparatus featured the existing capability of conventional time-of-flight PES, with construction of a SEVI spectrometer coupled to the TOF-MS near completion (shown in Figure 2.4).²⁸⁹ As research within the Wild Group had focussed on the study of weakly bound halide-molecule vdW complexes, the spectrometer has been designed with simplicity and low temperature operation in mind. It consists of a source and extraction chamber, time-of-flight mass spectrometer chamber with adjoining electron flight tube and the SEVI section with each section separated by gate valves. This section will outline the design and operation of each of these sections as they form part of the existing spectrometer.

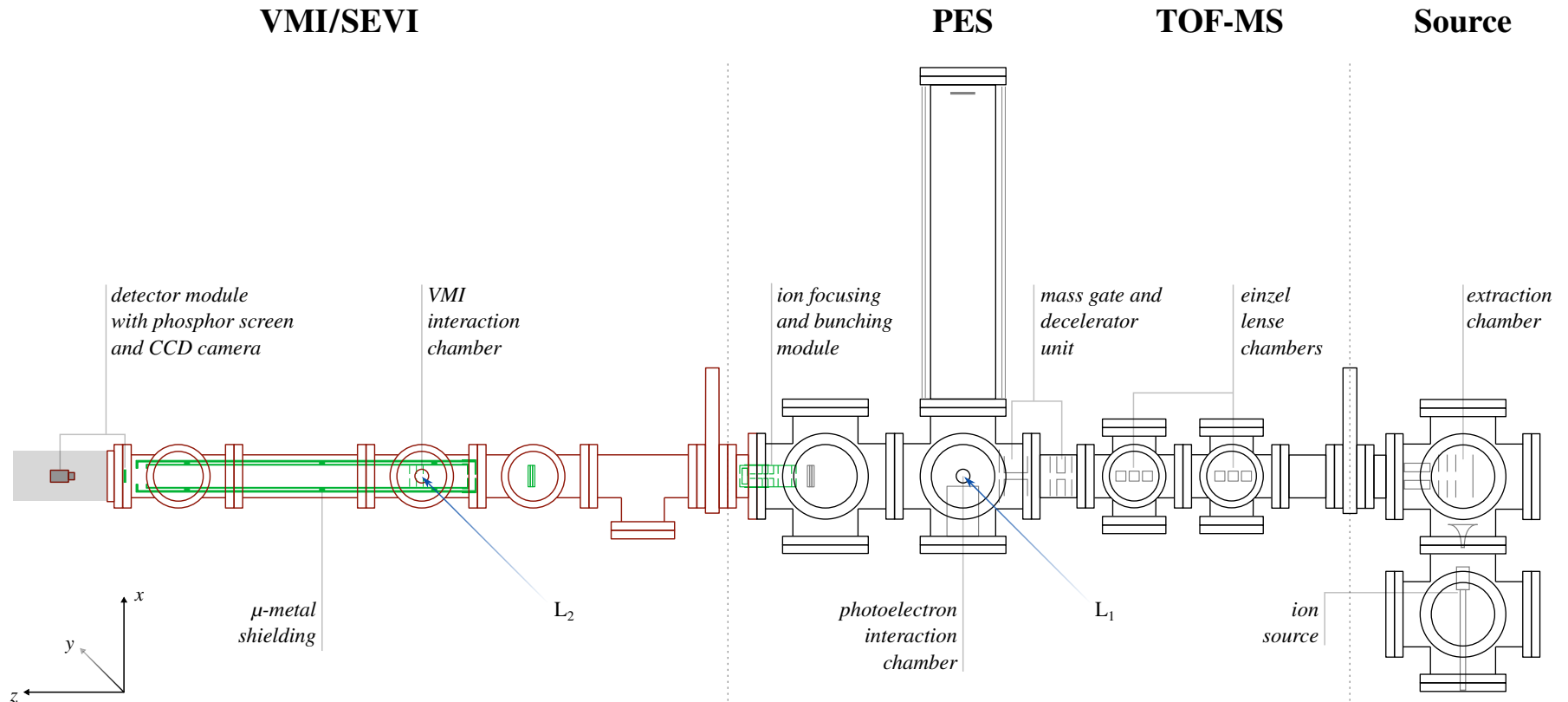


Figure 2.4: Schematic of the existing TOF-PES at the commencement of candidature. The spectrometer consists of (right to left) the source and extraction chamber, Wiley-McLaren TOF-MS, time-of-flight photoelectron spectrometer and the slow electron velocity map imaging spectrometer. L₁ and L₂ represent the laser intersection regions for conventional and SEVI PES respectively. Sections shown in colour represent the most recently constructed elements, the SEVI spectrometer (red) and the interior components including an ion buncher, MCP ion detector and μ -metal shielding.²⁸⁹

Source and Extraction Chamber and Complex Generation

The source chamber is where three key actions are performed in the process of any experiment. It is where gas mixtures are injected into the spectrometer, anions and the subsequent vdW complexes of interest are formed and where these complexes are extracted into the TOF-MS. The source chamber, a ISO250-K 6-way cross, is maintained at high vacuum by a *Diffstak 250/2000P* diffusion pump (backed by an *Edwards E2M40* rotary pump) adjoining the base of the chamber. In addition to the joint to the extraction chamber the remaining flanges include a viewing window and access flange, active ion (pressure) gauge denoted AIG1, liquid nitrogen cold trap and the nozzle with necessary gas, coolant and electrical feedthroughs.

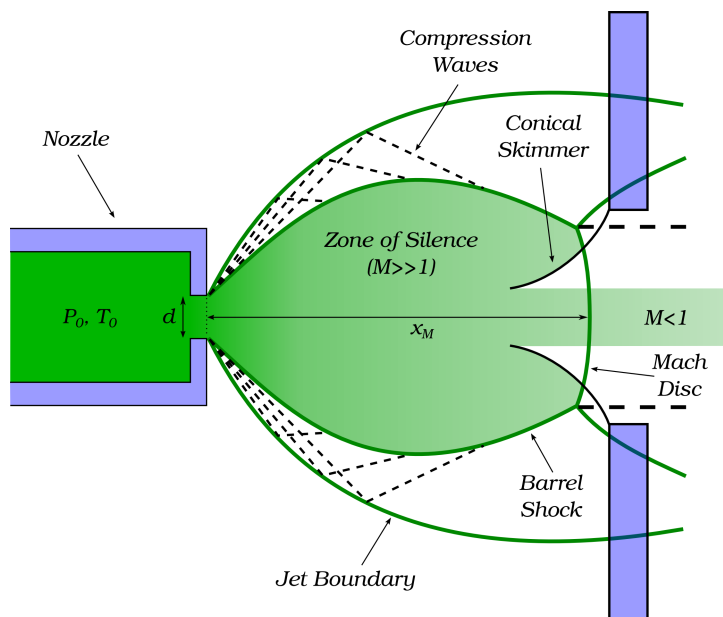


Figure 2.5: Gas dynamics of a supersonic expansion. Adapted from *Havenith*.²⁹⁰

Gas mixtures are introduced via a *Parker Hannifin General Valve Series 9* solenoid nozzle pulsed at 10 Hz. When injected, the expanding gas mixture cools adiabatically which corresponds to a rapid decrease in the speed of sound (a). Given that the diameter of the nozzle orifice is 0.8 mm and the backing pressure of the gas mixture is much larger than the vacuum within the chamber ($P_0/P_b \geq 2$), the injected gas forms a supersonic expansion (see Figure 2.5).²⁹⁰ Under these conditions the Mach number ($M = v/a$) increases rapidly from the point of expansion before

decreasing until $M = 1$ some distance x_M from the nozzle orifice. At this point a shock wave known as a Mach disk is formed perpendicular to the direction of flow. The region between the orifice and the Mach disk within the expansion where $M \gg 1$ is referred to as the zone of silence. Due to the large backing pressure, the translational components of molecules within the expansion are predominantly carried in the direction of the expansion. While gases may also have a radial component of translational motion, for those travelling on or near the axis of the expansion this component is small. By placing a skimmer (tip diameter 3 mm) coaxially to the expansion and within the zone of silence, the molecular beam is collimated and the expansion is disrupted such that the Mach disk cannot form. The distance x_M , in an axisymmetric expansion can be estimated for a monoatomic ideal gas by Equation 2.5. In practice, x_M may be overestimated by Equations 2.5, however provided that the skimmer is within the zone of silence the beam can be adequately collimated.

$$x_M = 0.67d\sqrt{\frac{P_0}{P_b}} \quad (2.5)$$

Gas mixtures used in the Wild Group contain the species in questions in dilute mixtures of argon. The use of argon and other noble gases as bulk gases in molecular beam experiments have been shown to improve cooling efficiency via collisional cooling.²⁹¹ Classically, the internal energy of the polyatomic components is partitioned into translational, vibrational and rotational components, whereas the monoatomic gases include only a translational component. As kinetic energy is redistributed between the monoatomic and polyatomic molecules within the gas mixture, the vibrational and rotational components of the polyatomic gas is reduced.¹³ Combined with the skimmer this produces a low temperature, narrowly-distributed velocity distribution within the gas mix. In the example provided in Figure 2.6 NH₃ is seeded within Xe, here the gas velocities would be comparably lower than if neon or argon were used. This is attributed to the larger atomic mass of xenon with respect to argon or neon, as the equal transfer of kinetic energy to each of these noble gases

corresponds to decreasing velocities. Argon however is notably cheaper than xenon and still allows for typical beam temperatures of less than 100 K.²⁹²

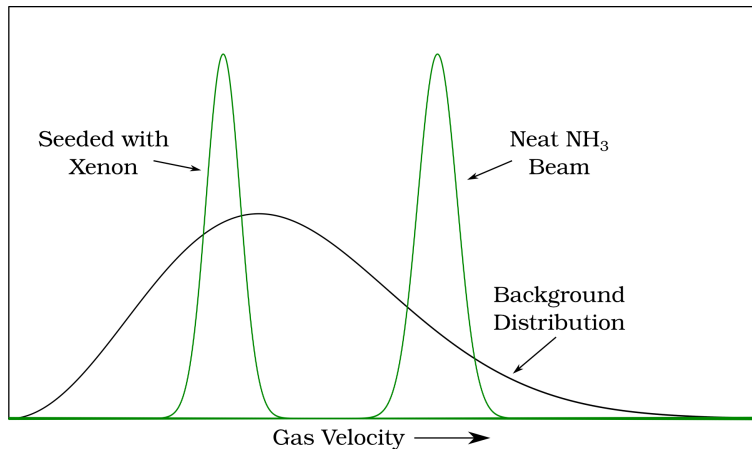
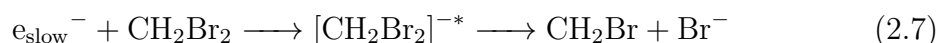
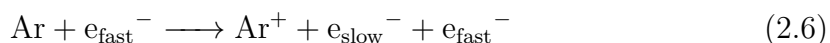


Figure 2.6: Velocity distribution of the background gas (black trace) compared to the skimmed gas distributions of NH₃ and NH₃ in Xe (green traces). Adapted from Christen.²⁹¹

Simultaneous to injection into the source chamber, the gas pulse is intersected by a stream of electrons to form charged species. These electrons are generated by thermionic emission from a rhenium wire (*Goodfellow*, $\varnothing = 0.2$ mm). Within the source module, the rhenium wire is connected between two insulated posts and connected to a constant current power supply. Surrounding the exterior of the wire is a Wenhelt shield, to which a negative potential is applied. The detached electron beam is then focussed with an einzel lens to increase the electron density in the region of the supersonic expansion.

These fast electrons interact with the argon backing gas to produce slow and scattered electrons as per Equation 2.6. The subsequent slow electrons can then be captured by the halide precursor to form halide anions by dissociative electron attachment (Equation 2.7).



Dissociative electron attachment has been used extensively in spectroscopy and

molecular beam experiments.²⁹³ An example of the dynamics of this process is shown in Figure 2.7 for a hypothetical simple case of a molecule XY with a dissociative anion channel. In this case, the energy difference between the ground vibrational state displaced geometries and the corresponding energy on the dissociative anion channel, represents the bounds of electron energies (denoted ϵ_1 and ϵ_2) that produce dissociative electron attachment. The intersection between the anion and neutral states and the energy difference to this conformation represents the minimum energy ($\epsilon = E^\dagger$) required to produce ions. The benefit in this case spectroscopically is that the bond dissociation energy (BDE) is upper bounded by the sum of this energy and the E_a of the dissociated anion component ($BDE \leq E^\dagger + E_a$).²⁹⁴

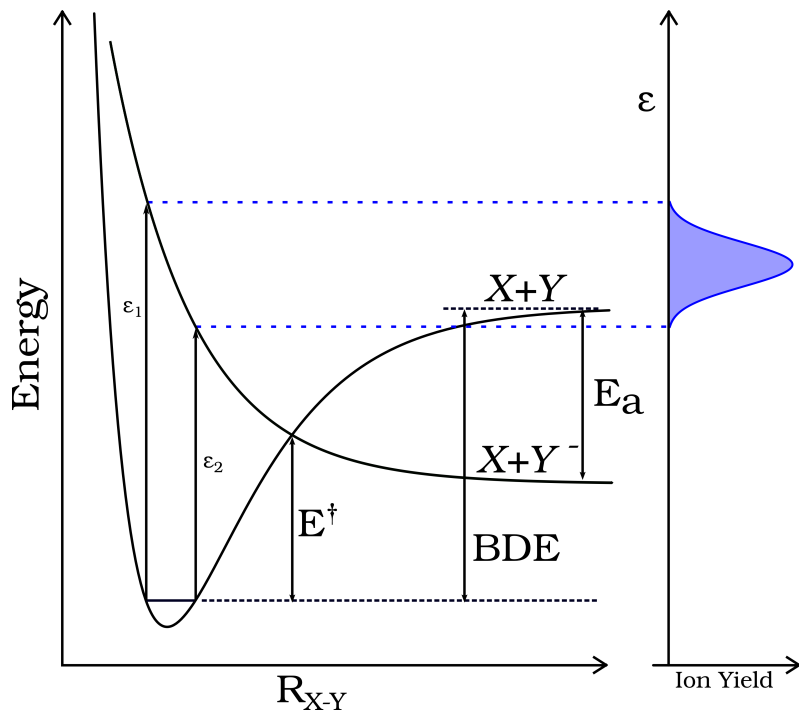


Figure 2.7: Potential energy surfaces of an example dissociative electron attachment process. The molecule XY is excited by an electron with energy ϵ to the dissociative XY^- surface. Here E_a is the electron affinity of Y and E^\dagger is the barrier to formation of the dissociative channel.

The example shown in Figure 2.7 is one such example of dissociative electron attachment. Other examples include where the anion surface is similarly bound much like the neutral surface or may be metastable in the excited region. These intensity of transitions to these bound states are then proportional to the Franck-Condon

overlap of the corresponding wavefunctions. As an example, this has been shown by Wnorowska *et al.* for a range of halocarbon derivatives of nitrobenzene where the ion yield shows a number of peaks where ϵ corresponds to these transitions.²⁹⁵

After passing through the electron beam and undergoing dissociative electron attachment, the gas pulse enters the extraction chamber. Similarly to the source chamber, the extraction chamber consists of an ISO100-K 6-way cross evacuated by a *Speedivac E04* diffusion pump (backed by the same *Edwards E2M40* rotary pump). The *Speedivac* features an in-built liquid nitrogen cold trap which can be automatically filled by a purpose built monitoring circuit. Housed within the chamber are a set of steel plates (termed TOF plates) that extract anions from the gas pulse by imparting a large negative voltage. The chamber, as well as connecting to the source chamber, TOF-MS flight tube and *Speedivac*, features flanges that provide for electrical feedthroughs that connect to the TOF plates, access for maintenance and cleaning, and an active ion gauge. The active ion gauge is situated on the opposite flange to the source chamber connection and, although not currently operational, allows for determination of gas velocity distributions similar to those in Figure 2.6. It is hoped that this data could inform the user as to the expansion dynamics in the experiment and help to optimise complex production.

To account for expansion of the gas pulse and ensure that anions arrive coincidentally during mass spectrometry, the second (front) of the two primary TOF plates is held at a voltage approximately 90 % of that applied to the rear plate. This is referred to as ‘space focussing’ and is optimised by tuning the voltage applied to the front plate with respect to peak width from the corresponding time-of-flight mass spectrum. It has also been found throughout experimental work within the Wild Group that coating these plates in graphite improves their longevity when in use by decreasing adsorbed gases to the steel. The third and final plate is grounded to prevent interference with equipment along the time-of-flight axis. To decrease the flight path from the nozzle orifice to the extraction region, a cylindrical housing was machined that would extend into the extraction chamber as opposed to sitting level

with the flange.

Both the *Diffstak* and *Speedivac* pump at rates of 2000 L s^{-1} and 600 L s^{-1} , maintaining a pressure of 5×10^{-8} Torr at rest and a typical operation pressure of 1×10^{-5} Torr to 5×10^{-5} Torr within the chambers. When performing experiments on gases that readily adsorb to the interior of the chamber, the use of both cold traps in the source and extraction chambers respectively improves the pumping efficiency and minimises adsorption within the TOF-MS. This reduces the need for regular cleaning within the TOF-MS and in turn prolongs the duration during which experiments can be undertaken on these gases. It has also been found, however, that use of the source chamber cold trap while beneficial, typically corresponds to pressure increases during shutdown procedures. This is in response to a reduction in the cooling efficacy of the trap and subsequent desorption of gases from the exterior surface of the trap.

Ion Flight Tube

The TOF-MS flight tube consists of a series of 6" *Conflat* flange chambers. These are (in order), a straight chamber, two 4-way crosses and another straight chamber adaptor from 6" to 8" that connects the laser intersection region. The nominal length of each of these chambers is 8.64" (219.46 mm) however it is difficult to measure a precise flight path length directly. This is due to the adjustment in joints for the alignment of the flanges and subsequent spacers that sit between some joints from the original construction.^{282,283} When combined with the difficulty to determine precise start and end points between the TOF plates and laser intersection region, it is more convenient to calibrate the mass spectrum for some arbitrary path length (see Section 2.2.2). While this chamber and the photoelectron flight tube chamber is not gated, this section houses (and is pumped primarily by) an *Edwards EXT255H* turbomolecular pump at a rate of 250 L s^{-1} . The photoelectron flight tube is then pumped by a *Kyky FF 160/620E* turbomolecular pump at a rate of 600 L s^{-1} .

From the TOF plates, and moving along the ion flight axis, the anion beam is

redirected and focussed using a series of electrostatic optics. The first of these, still within the extraction chamber, is two pairs of plates set parallel to the ion beam path and perpendicular to each other. These *X-Y* deflection plates can be controlled at voltages of ± 100 V and are able to steer the ion beam along the flight tube. As the ion flight tube axis is orthogonal to the axis of the supersonic expansion, the *X-Y* deflection plates can also be used to counteract the velocity of the gas pulse. This becomes important downfield along the TOF axis as drift of the ion beam over the longer path length can make beam alignment difficult.

In addition to the *X-Y* deflection plates, the ion beam is focussed using electrostatic optics called Einzel lenses.^{296,297} Each of these lenses consists of three collinear cylindrical sections, where the outer cylinders are grounded and the centre section is held at a high negative voltage. As the electric field within the cylinders is cylindrically symmetrical, the negative voltage imparts a larger repulsive force on ions that are radially further from the axis of the beam. The first Einzel lens is housed immediately after the gate valve and within the ion flight tube. As the beam is charged, these optics are important to adjust for any Coulombic expansion of the ion pulse (the repulsion of like charged species)²⁹⁸ as well as residual radial trajectories. Coulombic expansion will be present throughout the trajectory of the ion beam and as such a second Einzel lens provides additional adjustment downfield.

Previous development within the Wild Group also included the construction of an ion decelerator based on designs by Kopczynski.^{289,299} This unit also feature a mass gate and a second set of *X-Y* deflection plates all mounted following the downfield Einzel lens. A schematic of the mass gate and ion decelerator is shown in Figure 2.8.

The mass gate consists of three sets of two stainless steel rings with nickel mesh (90% transmittance, *Industrial Netting # BM0700-01 N*) clamped between them. The outer sets of rings are grounded while the centre set is held at a high negative voltage (1 kV to 5 kV), necessarily higher than that of the TOF voltage applied. This high voltage serves to repel all anions that approach the gate while the grounded

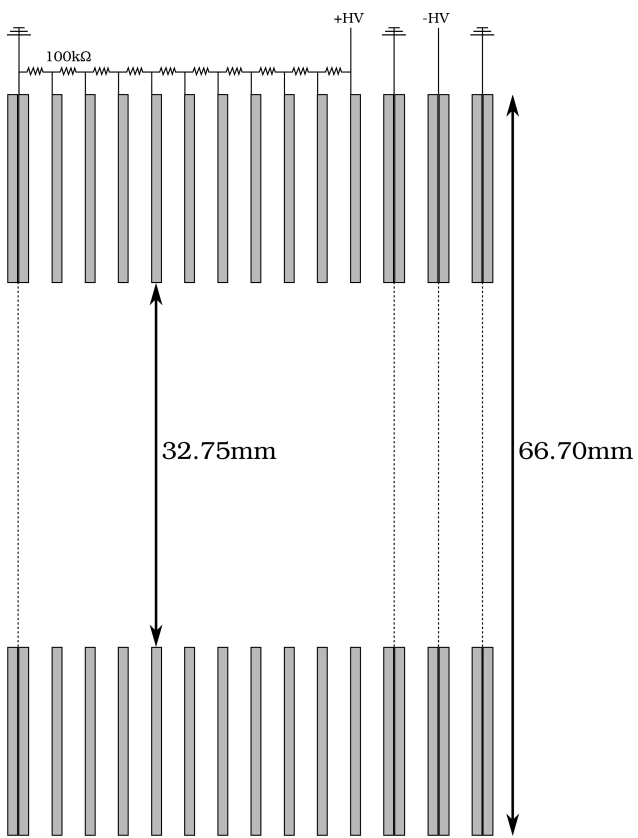


Figure 2.8: Schematic of the mass gate and ion decelerator based on designs by Kopczynski.^{289,299} The mass gate features three pairs of plates with mesh clamped between each set. The outer pairs are grounded while the centre set is at a high negative voltage. The ion decelerator features 10 sets of plates with an 11th pair of grounded plates, each plate is connected by a $100\text{ k}\Omega$ resistor.

outer plates prevent interference from the resulting electric field. By switching the centre voltage off, approaching anions are allowed to pass and by controlling the timing and breadth of the switching pulse allows the ion beam to be mass selected.

The ion decelerator similarly consists of a set of 10 coaxial stainless steel rings ($\varnothing_{inner} = 32.75\text{ mm}$, $\varnothing_{outer} = 66.70\text{ mm}$) set 2 mm apart in a Teflon casing. An 11th pair of rings, with mesh clamped between them is then grounded. Each of the rings is connected as part of a chain with ten $100\text{ k}\Omega$ resistors separating each. The voltage applied to the first ring is then stepped downwards to ground along the each of the successive rings at a rate of approximately 10% each step. This produces a linearly decreasing electric field within the ion decelerator that reduces the kinetic energy of the ion beam. The ion decelerator is switched on at a high positive voltage as ions

enter the interior region within the stack but have passed the first ring. Provided that the applied voltage is not significantly higher than that of the TOF plates, the beam is decelerated but not gated.

Laser Intersection Region and Photoelectron Flight Tube

As the path length can be approximated and E_K can be equated from the voltage applied to the TOF plates, an approximate arrival time can be determined by use of Equation 2.8. Given that certain masses are expected to be present within the ion beam, in particular the halide anions, and coupled with the isotopic abundances of these ions, peaks can be identified. After which, the mass spectrum can be calibrated against the function in Equation 2.8 and the remaining spectral features assigned by deduction based on the constituent components within the gas mix.

$$E_K = \frac{1}{2}M\frac{d^2}{t^2} \implies t = \sqrt{\frac{Md^2}{2E_K}} \quad (2.8)$$

Ions are detected in the region after the laser intersection by a Chevron configuration MCP (*Burle APD 3025MA*, $\varnothing = 25$ mm) housed on a sliding stage to raise and lower the detector. Raising the detector allows for the ion beam to proceed through to the SEVI section of the spectrometer. When detecting anions, the front face of the MCP is grounded while the rear face is held at 1700 V and the anode at 1750 V. The MCP is designed such that each collision with the detector creates a cascade of up to 10^6 electrons and allows for higher sensitivity of detection.⁵¹

The mass resolution of the instrument can be determined by the equation $m/\Delta m$ where Δm is the FWHM of the a peak within the mass spectrum. This can be determined graphically by analysing the peak in software or by fitting a Gaussian function to the peak where $\Delta m = 2\sqrt{2\ln 2}\sigma$ and σ is the standard deviation of the Gaussian function. An example mass spectrum is included in Figure 2.9 from previously studied X...O₂ complexes with resolutions of select peaks presented in Table 2.3.³⁰⁰

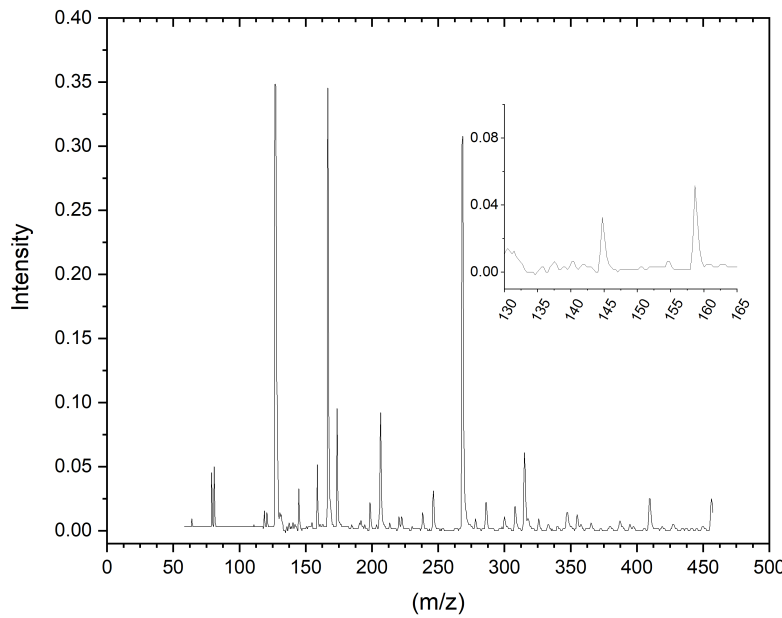


Figure 2.9: Time-of-flight mass spectrum of a $\text{CH}_3\text{I}:\text{O}_2:\text{Ar}$ gas mix with trace CH_3I , 40 kPa O_2 and made up to 450 kPa with Ar.

Table 2.3: Determined mass spectrum resolution with respect to m/z ratio for a selection of species present. Adapted from previous experimental data.³⁰⁰

Species	m/z	$m/\Delta m$
$^{79}\text{Br}^-$	79	137.84
$^{81}\text{Br}^-$	81	147.19
$^{127}\text{I}^-$	127	84.18
$^{127}\text{I}^- \cdots \text{Ar}$	167	170.84
$^{127}\text{I}^- \cdots \text{CH}_3\text{I}$	269	203.68

As shown in Table 2.3, typically mass resolution increases with increasing m/z . This is predominantly due to the lower velocities that higher mass ions carry, however it is also expected that larger masses reduce the impact of Coulombic expansion within the ion beam. We note also the resolution of the $^{127}\text{I}^-$ peak, as this is noticeably lower than the preceding and following peaks in the table listed. The reduction in resolution is attributed to a high anion yield, subsequent larger impacts of charge density within the peak and saturation of the MCP. This may be important should complexes of interest have similar m/z ratios to bare halide peaks used for calibration, as they may be obscured as a result. Largely however, the mass resolution of the TOF-MS spectrometer is fit for the purposes described here and

can separate peaks with nominal m/z differences of 1.

The photoelectron spectrometer is a conventional TOF magnetic bottle spectrometer based on designs of Cheshnovsky.⁵⁶ The photoelectron flight tube consists of a cylindrical chamber approximately 1.625 m in length wrapped in a coiled solenoid with spacing between the coil of 5 mm (325 turns). Under normal operations a 5 A current is passed through the solenoid which yields a magnetic field strength according to the Biot-Savart relationship ($B = \mu_0 n I$) of 1.28 mT (where n is the number of turns of wire per metre). The magnetic bottle is created by a modified 8" flange on the laser intersection region with an insert that a series of rods each tipped with a neodymium disk magnet ($\text{Nd}_2\text{Fe}_{14}\text{B}$) can be inserted. Each of these magnets are 11.90 mm, 14.76 mm and 19.72 mm respectively and are numbered for reference in descending size order. The combination and proximity of the permanent magnet with the activated solenoid maps the curvature of the disk magnets' field to the parallelised field of the solenoid, forming the magnetic bottle (see Figure 2.10). The polarity of the magnets when installed on the rods is not consistent however, and when swapping between them often the polarity of the solenoid must be reversed to avoid the formation of divergent fields. Surrounding the photoelectron flight tube are two additional tubes of μ -metal shielding intended to attenuate any intrusive magnetic fields from nearby equipment and the Earth's magnetic field.

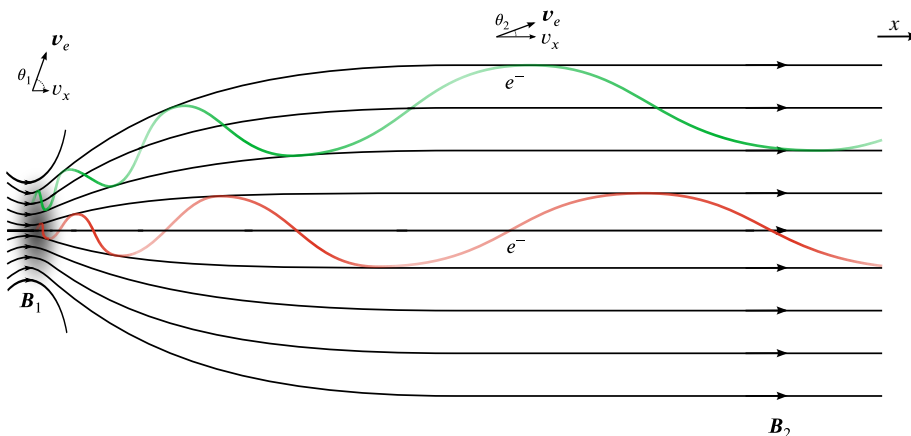


Figure 2.10: Magnetic field lines of the magnetic bottle spectrometer. Courtesy of Marcus Kettner.²⁸⁹

Upon intersection of the anion beam with laser light, photoelectrons are ejected radially from the point of intersection carrying kinetic energy as per Equation 1.1. These photoelectrons follow and precess around the magnetic field lines of the magnetic bottle, ultimately travelling parallel to each other along the field of the solenoid and along the axis of the photoelectron flight tube until their time of flight is detected at the far end. This mode of operation has been shown to collect over 98 % of ejected photoelectrons.⁵⁶ The photoelectron flight times can be estimated in a similar manner to the ion flight times in the mass spectrometry experiment ($t = \sqrt{\frac{m_e \ell^2}{2E_e}}$) where E_e and m_e are the kinetic energy and the mass of the ejected photoelectron. As indicated in Figure 2.10, this results in a distribution in the flight path lengths of the ejected photoelectrons which serves as a source of broadening of the photoelectron time of flight signal. However as shown by Cheshnovsky, the primary source of signal broadening is the velocity of the anions given by:⁵⁶

$$\Delta E_e = 4\sqrt{\frac{m_e}{m_i} E_e E_i} \quad (2.9)$$

where m_e and m_i are the masses of the photoelectron and ion respectively and E_n are their energies. Using this formula, a photoelectron ejected from an iodide anion with 1500 eV of energy by a 266 nm laser pulse representing a ${}^2P_{3/2} \leftarrow {}^1S$ transition would lead to ΔE_e of 0.41 eV. The inclusion of the ion decelerator module is one method intended to address this resolution limitation of conventional PES as described in Section 1.1.1.

The photoelectron detector used in these experiments is a *Burle APD 3040MA* MCP ($\phi = 40$ mm, 10 μm pore size) that operates in the same manner as the ion detectors described previously. To improve the efficiency of low energy photoelectron detection a grounded mesh is placed 25 mm in front of the front face of the MCP which is then biased at 200 V. This serves to provide acceleration of photoelectrons as they pass the grounded mesh and ensure that collisions with the detector are recorded. The rear plate and anode of the MCP are then held at 2300 V and 2500 V

respectively. The analogue signal produced by the MCP is amplified by a *VT120A Ortec Fast Pre-Amplifier*, subsequently digitised by an *Ortec Constant Fraction Discriminator (CFD)* and then recorded in 2 ns time bins by a multiscaler card (*P7888 Fast Comtec GmbH*) installed in a local workstation.

In practice, a TOF-PES spectrum is simply a histogram of collision events with respect to time of flight. These can be over any number of laser shots however typically experiments in the Wild Group record spectra for 10,000 shots (at 10 Hz this yields 1000 s per spectrum). t_0 in this case is triggered by the laser pulse being directed onto a fast silicon photodiode (*Thorlabs, SM05PD2A*) after passing through the laser intersection region. To calibrate the spectrometer the photoelectron spectra of anions with known binding energies are recorded (in this case Cl^- , Br^- and I^-), and their electron kinetic energy is plotted against the inverse of their times of flight squared (E_e vs. $1/t^2$). This calibration is then used to transform the x -axis of each spectrum from a TOF domain to one in electron kinetic energy which can then also be expressed as the electron binding energy of the species by subtracting it from the photon energy of the laser. Given the coordinate transform from TOF to E_e the resultant time bins must undergo a Jacobi transform of their energies as per Equation 2.10.

$$\int_a^b I(t) dt = \int_{\alpha}^{\beta} I(t(E_e)) \frac{dt}{dE_e} dE_e$$

$$\frac{dt}{dE_e} = \frac{-t^3}{m_e \ell^2}$$
(2.10)

As the Jacobian here includes a constant factor of $-1/m_e \ell^2$ this can be removed via normalisation of the intensities, however the t^3 factor included results in a sizable increase in intensity for slow photoelectrons (those closer in binding energy to that of the laser photon energy). While this factor can improve the asymmetry of individual peaks and better reflect the relative populations of the 2P states of the halogen present in raw photoelectron spectra (see Figure 2.11), noise near

threshold binding energies can become prohibitively difficult to remove. Similarly, those species with lower binding energies will result in spectral features that are suppressed in comparison to those closer to the laser photon energy. Tuning the laser wavelength such that it is sufficiently above the binding energy but not too far above to eliminate any spectral features is the balance sought in these experiments and in general when investigating halide clusters a fixed wavelength of 266 nm is sufficient for these needs. We also note the impact of power broadening on the shape of the peaks within the photoelectron spectra. While the spectral resolution is low, and it is believed that this is not a significant source of error in peak assignments, it should be considered when assessing the quality of the data.

After transforming a given spectrum the peaks corresponding to the VDE can be selected from the peak maximum graphically. Alternatively the peaks may be fitted with a Gaussian function to determine both the VDE and FWHM of the peak. Given that the resolution of the existing TOF-PES is low, it is often difficult to separate electronic states with smaller energy separation, namely the 2P states of chlorine. To allow for these states to be separated it has become practice within the Wild Group to fit a pair of Gaussians to these peaks within the experimental spectrum.⁵⁷ These fits, utilise the known spin-orbit splitting of the 2P states of chlorine (0.109 eV) and the 2:1 intensity ratio of the assumed peaks arising from the state degeneracy for $J = 3/2$ and $1/2$ to minimise the number of fitting parameters necessary.^{57,301}

$$I = Ae^{-\frac{(E_{BE}-VDE)^2}{2\sigma^2}} + \frac{1}{2}Ae^{-\frac{(E_{BE}-VDE-0.109)^2}{2\sigma^2}} \quad (2.11)$$

where E_{BE} in this case represents the electron binding energy of the $^2P_{3/2}$ state. The E_{stab} is then determined from the shift in binding energy between the $^2P_{3/2}$ states of the halide and corresponding complex.

2.2.3 Laser

The light source used in photoelectron spectroscopy experiments in the Wild Group is a Nd:YAG (Neodymium-doped Yttrium Aluminium Garnate $\text{Y}_3\text{Al}_5\text{O}_{12}$) laser. For fixed wavelength experiments on halide-molecule complexes, 266 nm (4.6611 eV) photon energy is typically used. This is generated from a *Spectra Physics Quanta-Ray Pro* laser via production of the second harmonic (532 nm, 2.3305 eV) which is passed through a β -barium borate crystal (BBO) and frequency doubled to produce the desired photon energy. The laser operates in line with the frequency of the TOF-MS experiment (10 Hz) and the pulse width of the produced photons is 5 ns with energy outputs of approximately $250 \text{ mJ pulse}^{-1}$ and $650 \text{ mJ pulse}^{-1}$ for the 266 nm and 532 nm respectively. Where a lower energy regime is required the 532 nm laser pulse may be used directly.

In being redirected to the laser intersection region, the laser pulse is polarised such that the polarisation axis (normal to the plane) corresponds to the x -axis (see Figure 2.4 for reference). The energy density output from the laser is much higher than that required for photodetachment and as such the beam is attenuated by crossed polarisers so that the energy output to approximately 5 mJ pulse^{-1} to 10 mJ pulse^{-1} . Downfield, and above the laser intersection region, the beam is collimated by a telescopic lens and then trimmed by a series of two circular apertures such that the beam diameter is 3 mm to 5 mm.

Where tunable photon energy is required for threshold spectroscopy experiments, the laser pulse from the *Quanta-Ray Pro* can be used as a pump pulse for a *Syrah Cobra-Stretch* dye laser. Depending on the choice of laser dye (from those available in the Wild Group), the pump pulse can be either be 532 nm or the third harmonic 355 nm. The available photon energies and efficiencies of available dyes is summarised in Table 2.4.

In addition to the dye laser output photon energy, the pulse may also be frequency doubled to achieve photon energies higher than those of the fixed wavelength

Table 2.4: Accessible wavelengths by use of the *Syrah Cobra-Stretch* dye laser. Dyes listed are those currently available in the Wild Group.

Dye	λ_{range} nm	λ_{peak} nm	Efficiency %	c g L^{-1}	Solvent
$\lambda_{pump} = 355 \text{ nm}$					
BiBuQ	380-410	390	4.0	1.4	Ethanol:Toluene
DCM	605-665	640	14.0	0.3	Ethanol
Coumarin 480	452-500	473	17.0	0.4	Ethanol
Rhodamin 6G	563-597	574	16.0	0.6	Ethanol
Sulforhodamine B	582-620	596	14.0	0.3	Ethanol
$\lambda_{pump} = 532 \text{ nm}$					
DCM	602-660	627	28.0	0.3	Ethanol
	626-685	651	28.0	0.3	DMSO
Rhodamin B	558-614	596	27.0	0.2	Ethanol
Pyridin 2	691-751	718	20.0	0.18	Ethanol
Rhodamin 6G	559-576	566	30.3	0.09	Ethanol
Sulforhodamine B	585-600	591	27.0	0.2	Ethanol

266 nm pulse.

2.2.4 SEVI

The SEVI spectrometer has been previously constructed and adjoined to the existing TOF-PES in the Wild Group and schematics of the spectrometer are included in Figure 2.12.²⁸⁹ The design of this spectrometer was itself based on those by Cavanagh⁹⁷ which feature a collinear ion and photoelectron beam, and a 3-element VMI lens similar to that of Eppink-Parker.⁷¹

The SEVI spectrometer consists of a series of standard 6" Conflat chambers separated from the TOF-PES by a second gate valve. Commencing from the gate valve, these chambers include two Tee pieces (*Kurt Lesker T-0600S*) which provide for the electrical feedthroughs required for the VMI lens and a secondary MCP ion detector. This second detector is a *Tectra GmbH MCP-25-D-S-A* MCP ($\phi = 18.8 \text{ mm}$, $6 \mu\text{m}$ pore size). Similarly to the ion detector used in conventional TOF experiments, the front face of the MCP is grounded and the back face and detecting anode are held at 1800 V and 2300 V. Both MCPs do not provide positional data of the anion beam,

however the beam position can be estimated and optimised by taking the mean of voltages applied to the X - Y deflection plates when the intensity of the mass spectrum begins to decrease. The benefit of the smaller diameter of the second MCP in this regard is that by extension the corresponding beam profile impacting the detector is similarly narrow and centralised. Such beam dynamics are important in adequately guiding the anion beam through the spectrometer for SEVI experiments.

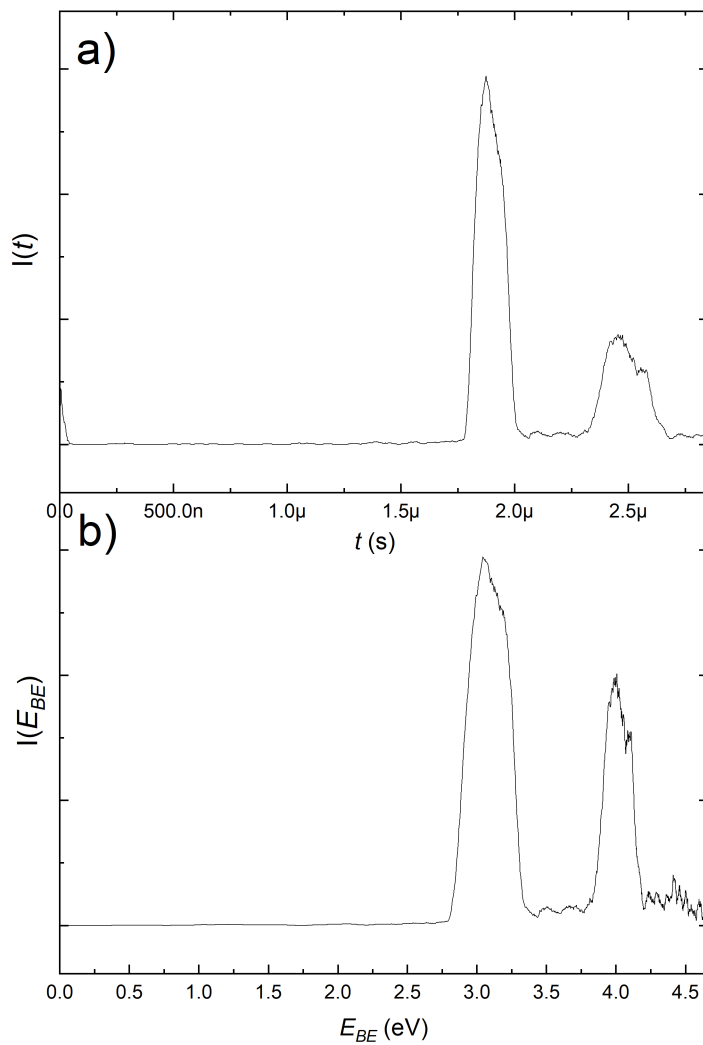


Figure 2.11: Photoelectron spectra of I^- showing the $^2P_{3/2}$ and $^2P_{1/2}$ peaks used for calibration. a) includes intensity as a function of the photoelectron TOF ($I(t)$) while b) plots intensity as a function of electron binding energy (E_{BE}). It can be seen that the incorporation of the Jacobian addresses the relative intensity of the peaks as well as, to a degree, their asymmetry but does also increase the impact of noise in the spectrum.

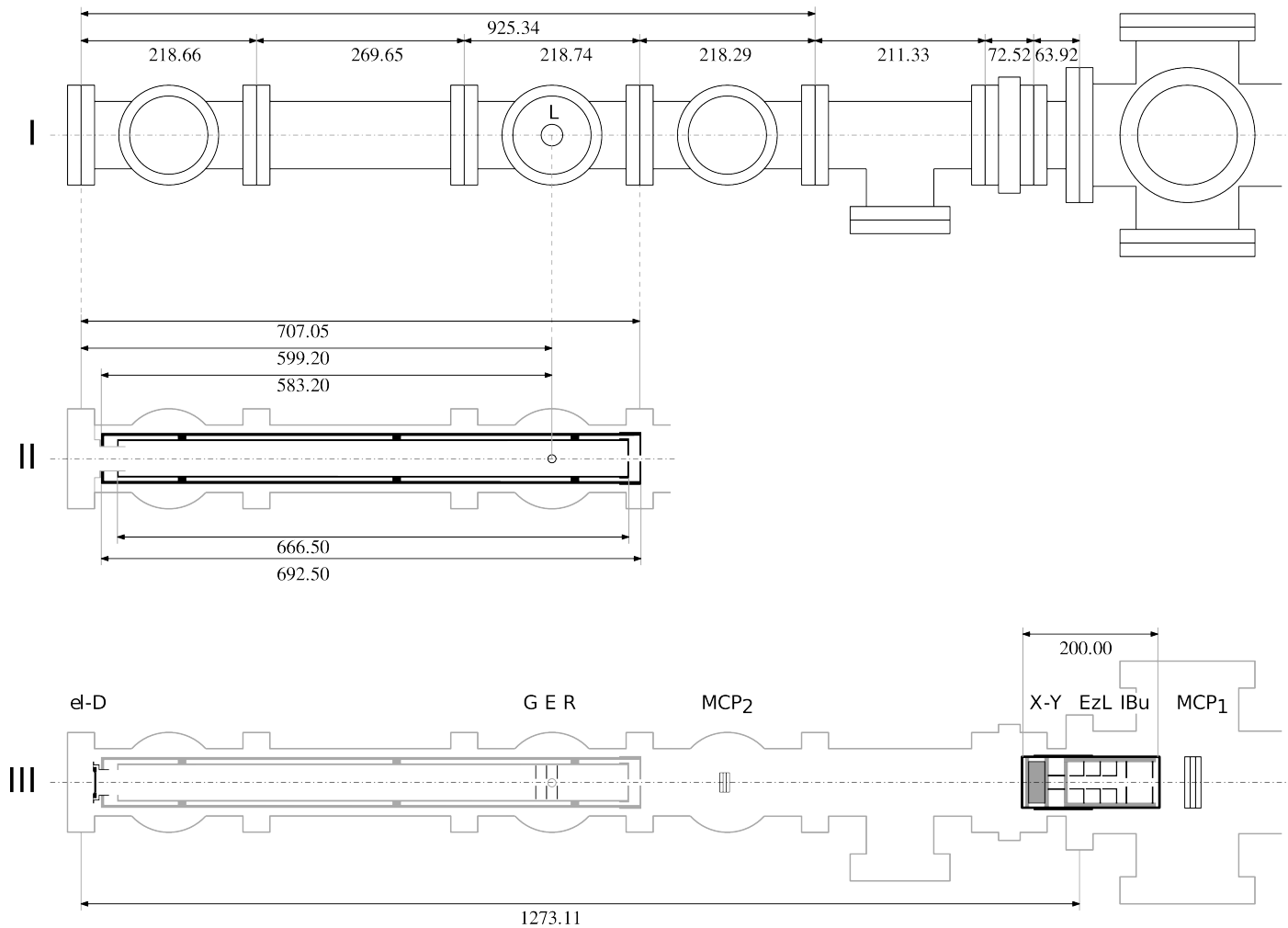


Figure 2.12: Schematic of the existing SEVI spectrometer at the commencement of candidature courtesy of Marcus Kettner. All measurements are in mm. I) features the arrangement of 6" Conflat vacuum chambers that make up the spectrometer. II) illustrates the dimensions of the double-walled μ -metal shielding that makes up the photoelectron flight tube and where it is located in the spectrometer. III) details (*left to right*) the electron detector (el-D), ground, extractor and repeller plates of the VMI lens (G, E, and R), the MCP detector and an electrostatic optics module that contains an additional set of X-Y deflection plates, einzel lens and ion buncher.

These chambers are immediately followed by a 4-way cross (*Kurt Lesker C-0600S*) as the laser intersection region, a straight nipple (*Kurt Lesker FN-0600*) and a further 4-way cross. These three chambers are housed within the μ -metal shielding that makes up the photoelectron flight tube. Mounted to the top of the laser intersection region chamber is an optics tower constructed from 20 mm square extruded aluminium. To the second 4-way cross is mounted an active ion gauge to monitor the vacuum in the SEVI section of the spectrometer and an additional turbomolecular pump. This turbomolecular pump (*Leybold Turbovac 151*, 150 L s^{-1}) is then backed by an *Edwards 2M18* rotary pump and maintains a pressure of 1.5×10^{-8} Torr at rest.

The photoelectron flight tube has been described previously,²⁸⁹ and consists of a 692.50 mm long, double-walled μ -metal cylinder that rests within the vacuum chamber. The cylinder is capped at each end. On the leading end cap a 6.00 mm orifice is bored that the ion beam passes through. The cap on the detection end of the flight tube has a wider hole bored ($\phi = 52.00$ mm), used to locate the photoelectron flight tube on the detector flange. 109.3 mm from the end of the assembly perpendicular to the cylindrical axis, a hole has been bored through the entire assembly ($\phi = 10$ mm) for the laser pulse to pass through. The photoelectron flight path length is then 583.20 mm to the end of the assembly, noting that a short additional length would be included as part of the screen flange.

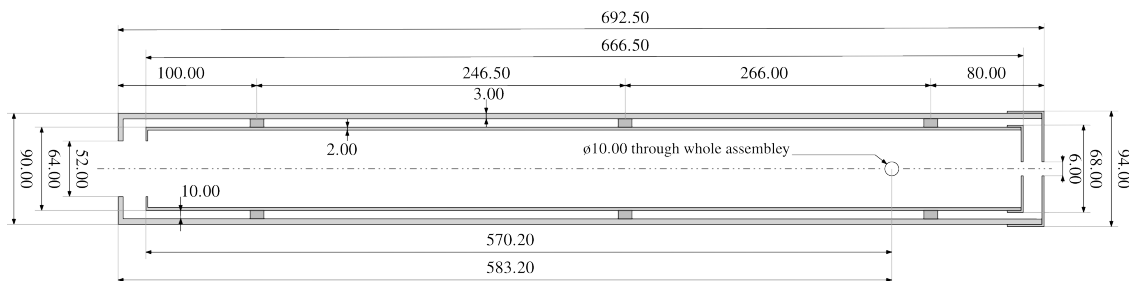


Figure 2.13: Schematic of the double walled μ -metal shielding that makes up the photoelectron flight tube for SEVI spectrometry. Courtesy of Marcus Kettner.²⁸⁹

The VMI lens is housed within the μ -metal shielding and consists of a ground, extractor and repeller plate based on designs by Cavanagh.⁹⁷ The VMI lens has

an aperture on the repeller plate ($\phi = 3\text{ mm}$) through which the ion beam can pass. Once entering the lens the laser intersection region then lies between the repeller and extractor plates. The apertures on the extractor and ground plates are wider ($\phi = 15\text{ mm}$) to allow for the radial velocities and expansion of the detached photoelectrons. Previous work within the Wild Group using *SIMION*³⁰² has optimised the ratio of the voltages applied to the repeller (V_R) and extractor (V_E) to be $V_E/V_R = 0.681$.²⁸⁹

The photoelectron detector is designed to illuminate a phosphor screen for image capture by a CCD camera (*IDS UI-2140RE-M-GL*). The detector is made up of a MCP ($\phi = 43.5\text{ mm}$, $12\text{ }\mu\text{m}$ pore size) with a ceramic scintillator underneath. The scintillator is made of an amorphous terbium-activated gadolinium oxysulfide ($\text{G}_{32}\text{O}_{2}\text{S:Tb}$) material that emits between 360 nm to 680 nm with peak emission of 545 nm (green).³⁰³ The average decay time for phosphorescence to 10 % intensity is 1 ms which is fit for purpose in a 10 Hz experiment. The screen assembly was manufactured and integrated into a $6''$ Conflat flange by *El-Mul Technologies Ltd* for ready incorporation into the SEVI spectrometer.

In use the front face of the MCP is grounded, though can be held at high voltage (500 V to 800 V) to repel incoming anions and pulsed to ground when electrons are due to arrive. The back face and phosphor screen are then held at a maximum of 2000 V and 6000 V respectively (the recommend back face voltage is $<1800\text{ V}$). To avoid discharge between and damage to the elements of the MCP the difference between the back face and the phosphor screen cannot exceed 4000 V (recommended $<3500\text{ V}$). As a result, when energising the detector the voltage is stepped up accordingly to operate within these limits.

At the commencement of candidature the SEVI spectrometer was not yet operational. At that time ions had successfully been steered through the spectrometer to the phosphor screen. This was evidenced by a consistent signal on the screen that could be repositioned by adjusting voltages applied to the *X-Y* deflection lens in the SEVI spectrometer. Further, anion photodetachment was confirmed by adjust-

ing the input voltages to the SEVI MCP, switching it from anion detection mode to neutral detection. By adjusting the timing of the laser pulse, a signal appeared in the same position suggesting that photodetachment had indeed occurred. However, when switching back to anion detection mode, it was at that time impossible to discriminate between the anion signal and that of any potential photoelectrons. Additionally, the position of the anion signal was off-centre on the screen. This was deemed to be of concern given that the assembly was collinear and downfield drift of the anions suggested either residual translational velocities from the gas pulse (orthogonal to the SEVI axis) or unintended impact from the electrostatic optics. Part of the work within this thesis seeks to devise strategies to address these issues and these are detailed in Section 2.3.4.

2.3 TOF-PES Modifications During Candidature

2.3.1 New Gas Mixing Station

The current configuration of the gas mixing station is shown in Figure 2.14. Improvements made to the station include the addition of a second sample vial, a second gas inlet, a bubbler and an additional line between the vacuum and nozzle that bypasses the mixing vessel. The line between the nozzle and vacuum allow for isolation of the gas mixing station while the nozzle is evacuated or vented. The additional sample vial allows for gas mixes to be made from liquid sources with high vapour pressures (e.g. acetone, ethanol) while still being able to introduce a halide precursor. Where a gas source is still used, the additional sample vial may hold a second halide precursor. Considering the low energy resolution of conventional TOF-PES and subsequent difficulty in resolving the 2P peaks of chloride complexes due to their lower spin-orbit splitting, inclusion of a second halide precursor can be advantageous by allowing for energy calibration against bromide or iodide.

The bubbler has been included in the gas mixing station for use when liquid

samples with low vapour pressures are being investigated. This similarly allows both sample vials be used for multiple halide precursors. A pair of 2-way valves immediately preceding and following the bubbler, allow for the bubbler to be bypassed when not in use. While promising, to date the bubbler has not been used in experiment.

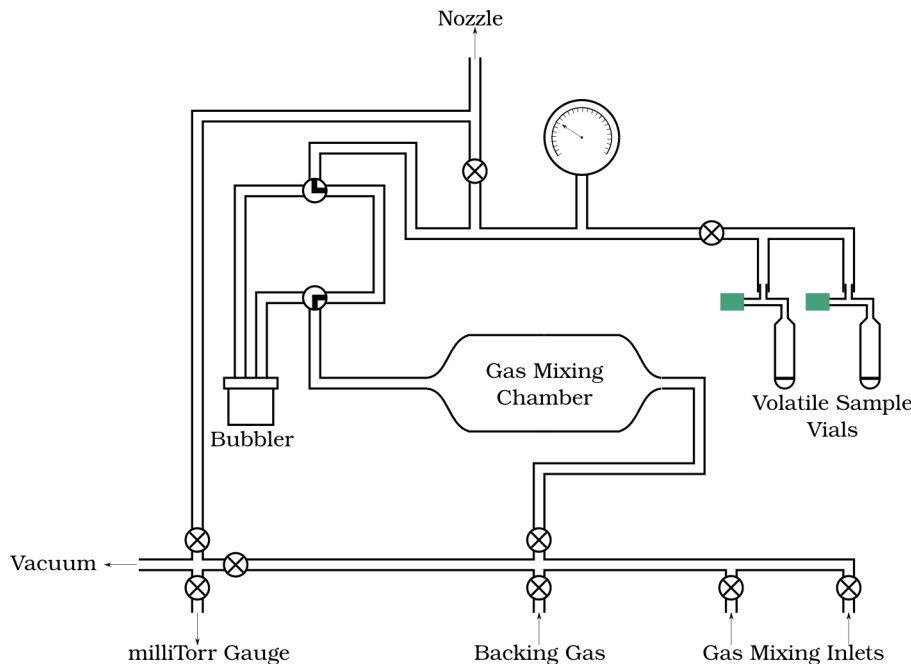


Figure 2.14: Schematic of the current configuration of the gas mixing station.

2.3.2 Piezo Nozzle Source

In order to achieve consistent and reproducible photoelectron spectra, the dynamics of the inject gas pulse must be highly stable. During candidature, the existing TOF-PES spectrometer included a solenoid nozzle (*Parker Hannifin General Valve Series 9*), which while suitable for initial experimental work, was susceptible to electrical noise and “double-pulsing”. Additionally, given the mechanical components within the nozzle, the solenoid design deteriorated over time.

To improve upon these elements, a piezoelectric valve nozzle was constructed to replace the solenoid valve. Designs of the piezo nozzle are based upon those by Proch and Trickl³⁰⁴ but most similar to those by Schießer and Schäfer.³⁰⁵ The

nozzle resembles a short cylindrical vessel with a long tube with an orifice at one end extending from one side. On the other side is a 1/4" *Swagelock* gas connection and a BNC coaxial feedthrough (MHV). Internally, a plunger is mounted to a piezodisk translator and extends down the length of the stem piece with an O-ring sealing the orifice from the inside. When a potential is applied the piezo disk flexes inwards, withdrawing the plunger from the orifice and allowing gas to pass into the background vacuum. The design of the nozzle is shown in Figure 2.15.

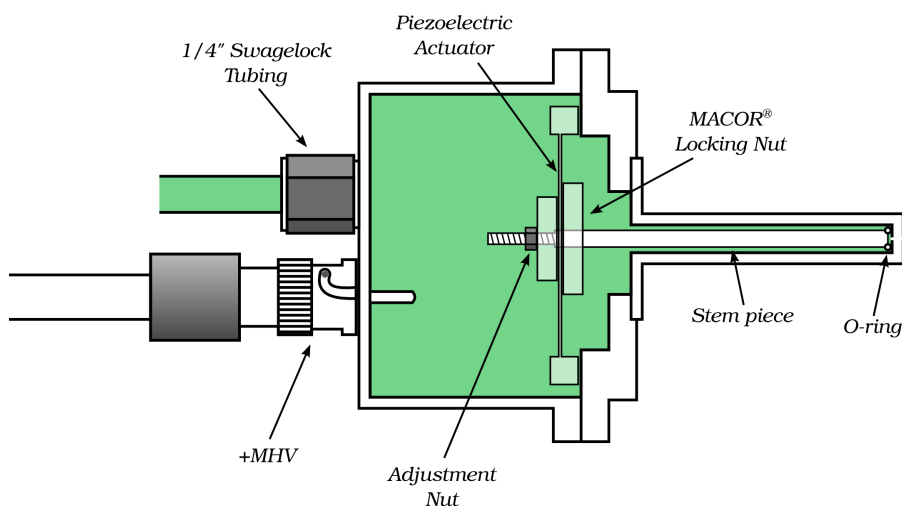


Figure 2.15: Schematic of the piezo nozzle installed in the Wild Group TOF-PES. The design of the nozzle assembly is based on designs by Proch and Trickl³⁰⁴ and similar to those of Schießer and Schäfer³⁰⁵ albeit with the reduced length of the nozzle stem from 210 mm to 47 mm.

2.3.3 New Electron Flight Tube

During candidature, it was identified that the current flowing through the solenoid surrounding the photoelectron flight tube of the TOF-PES (5 A) was causing the coil to heat up. It was speculated that this heat would disrupt the uniformity of the magnetic field. Additionally, to improve the mapping of the magnetic bottle to the parallelised magnetic field, the photoelectron flight tube was due to be reduced in diameter such that it could be slipped within the 8" flange and brought closer to the laser intersection region. This choice was to align the design of the PES spectrometer with those of Cheshnovksy.⁵⁶

To address the heating issue present in the existing photoelectron flight tube without compromising the strength of the generated magnetic field, the solenoid was rewound, reducing the spacing between turns from 5 mm to 2 mm. This effectively increased the number of turns per metre from 200 to 500. The constant current supply was correspondingly reduced from approximately 5 A to 1 A which effectively halved the strength of the magnetic field to 0.628 mT. While weaker than the previous field this is still suitable for PES spectroscopy. Details of these changes are provided in published work from Corkish *et al.*³⁰⁶

2.3.4 SEVI Reconfiguration

In order to address the challenges in obtaining photoelectron spectra from the existing SEVI spectrometer, the design of the spectrometer was altered. As noted in Section 2.2.4, while photodetachment could be confirmed by switching the photoelectron detector to a neutral detector, separating any photoelectrons produced was impossible while the anion signal was also impacting the detector. Additionally, the anion signal was being detected off-centre on the photoelectron detector, which suggested that either residual radial velocities were present or unintended electrostatic effects were playing a role in the beam direction after entering the μ -metal shielding.

Whereas the existing SEVI spectrometer was collinear similar to designs of Cavanagh,⁹⁷ Neumark,⁸⁵ and Wang,³⁰⁷ the redesign of the SEVI spectrometer is such that the photoelectron flight tube is orthogonal to the TOF axis and reminiscent of designs by Verlet.⁸⁵ The reconfiguration largely utilises existing vacuum chambers from the SEVI spectrometer, however to facilitate the rotation of the photoelectron flight tube an additional 6" Conflat 6-way cross was purchased (*Kurt Lesker C6-0600S*). This was adjoined to the existing TOF-PES at the gate valve with the extruded aluminium optics tower and bottom flange window being transposed from the existing 4-way cross. The length of the photoelectron flight tube necessitated that the straight nipple and 4-way cross be joined to the 6-way cross in the direc-

tion of the x -axis. As with the existing arrangement, the 4-way cross housed the phosphor screen flange as well as both the *Turbovac* pump and active ion gauge. Of the remaining two Tee chambers, one was joined after the 6-way cross in the z -direction and provided for the second MCP to be moved after the laser intersection region. The other Tee chamber was originally not due to be utilised in the new arrangement, however as the μ -metal assembly was equal in length to the interior of the chambers that housed it, there was not available space to house the required electrical feedthroughs for the VMI lens. By including the Tee chamber the issue of space is resolved and reduces the risk of electrical shorting between the feedthroughs and high voltage cabling. The total volume of the reconfigured SEVI spectrometer is estimated using measurements from schematics and is approximately 12.5 L (see Appendix F.2).

Having rotated the photoelectron flight tube, an additional 10 mm hole needed to be drilled through the assembly orthogonally to the existing hole. When working with the workshop within the Department of Physics at UWA to machine this hole, it was determined that the existing hole was not wholly circular. For this reason when positioning the assembly within the spectrometer, the original set is used as the laser intersection region where the beam diameter should be much less than the aperture. This leaves the true 10 mm aperture to ensure the greatest likelihood of guiding the ion beam through the assembly.

In part, the motivation for reorientation the photoelectron flight tube was to address practical challenges with the existing setup. As the μ -metal shielding assembly is located on the photoelectron detector flange by resting on the end cap, opening and resealing the detector flange whilst maintaining the positioning the shielding was difficult. By rotating the photoelectron flight tube, the assembly could then be removed through the 6-way cross. While the inclusion of the additional Tee chamber provided the necessary space for the VMI lens electrical feedthroughs, it resulted in the inability to readily remove the shielding. Nor could this chamber be rotated such that the Tee aligned with the photoelectron flight axis, as it would prohibit the

opening gate valve. As such it is recommended that the chamber be removed from the 6-way cross as if it were a flange for maintenance access. Should locating the μ -metal shielding on the photoelectron detector flange be difficult, it is also recommended that the ion gauge be removed in preference to the *Turbovac* to access this region of the spectrometer.

To address the issue of ion beam drift present in previously collinear experiments, the removal of both of the 6", Tee chambers following the gate valve seeks to bring the laser intersection region closer to the last set of *X-Y* deflection plates and einzel lens. The intention here is to improve the effect that the electrostatic optics have on the ion beam by reducing the length over which they must correct the ion beam. By placing the MCP detector after the 6-way cross chamber, whether the ion beam is successfully guided through the μ -metal assembly can be confirmed. Currently the detector is energised in anion-detecting mode such that the front face is grounded, the back face is held at -1800 V with the detector held at -1850 V . Though not available with the current setup, the MCP can be biased such that the front face, back face and detector are held at -1800 V , ground and 50 V respectively. By doing so, the MCP can operate in a neutral-detecting mode and be used to confirm that photodetachment is occurring.

By reorientating the photoelectron flight tube, the issue of anion detection on the photoelectron detector is believed to be removed entirely, as the anion beam will continue in the *z*-direction shown in Figure 2.16. Considering the case of a photoelectron detachment from a iodide anion (${}^2P_{3/2} \leftarrow {}^1S$) using a 266 nm laser pulse, the photoelectron kinetic energy is therefore 1.601 eV . Assuming a photoelectron path length of 599.20 mm based on the distance between the laser intersection region and the end of the μ -metal shielding, the flight time is then $0.798\text{ }\mu\text{s}$. If the beam energy is 1500 eV and the velocity of the reference frame of the ejected photoelectron in the *z*-direction is the same, in the same period of time the photoelectron will have drifted 38.1 mm , nearing the edge of the detector. However by applying the VMI lens voltage (at 1000 V) this drift is reduced dramatically to 1.5 mm . While we

may expect that the beam velocities may impact on the resolution of the instrument, the reduction in anion signal is deemed favourable. Further improvements to the spectrometer design would include use of the ion decelerator and ion buncher modules.

2.3.5 Summary

In the following Chapters, several studies of anion-molecule vdW complexes are presented. In Chapter 3, $\text{CH}_3\text{O}_2\text{I}^-$ complexes are formed from gas mixtures with higher partial pressures of O_2 . As the methylperoxy radical represents an important atmospheric intermediate, these complexes are studied via magnetic bottle photoelectron spectroscopy to determine the structure of the complex (be that $\text{O}_2^- \cdots \text{CH}_3\text{I}$ or $\text{I}^- \cdots \text{CH}_3\text{OO}$), and the strength of the non-covalent interaction. These experiments are then complemented with MP2/AVQZ geometry optimisations and harmonic frequency calculations followed by CCSD(T)/CBS energies via the W1w protocol and NEVPT2 term energies.

In Chapter 4, halide-propene complexes are investigated similarly with photoelectron spectroscopy. As propene represents a size of molecule approaching what is computationally feasible given the resources available, a number of previously studied halide-molecule complexes for which both experimental and CCSD(T)/CBS data is available, are used as a benchmark to test the applicability of the DSD-PBEP86-D3BJ double-hybrid functional.

In Chapter 5, the DSD-PBEP86-D3BJ functional is then applied to the larger halide- $(\text{C}_4\text{H}_6)_n$ complexes for $n_{\text{I}} = 1, 2$, $n_{\text{Br}}, n_{\text{Cl}} = 1$. Photoelectron spectra are then presented for $\text{Cl}^- \cdots (\text{C}_4\text{H}_6)_n$, $\text{Br}^- \cdots (\text{C}_4\text{H}_6)_n$ and $\text{I}^- \cdots (\text{C}_4\text{H}_6)_n$ complexes demonstrating the binding motifs, strength of interaction and demonstrating gas-phase anion solvation.

Finally in Chapter 6, a number of photoelectron spectra of phosphorous hydride-molecule complexes predicted through DSD-PBEP86-D3BJ geometry optimisations

and harmonic frequency calculations, W2w energies and vibronic simulations are presented. Recent observation of PH₃ in extraterrestrial environments, make it an attractive spectroscopic target. However, the high toxicity of PH₃ presents challenges for laboratory spectroscopic studies. By using computational methods, promising spectroscopic targets may be identified for future photoelectron spectroscopy experiments.

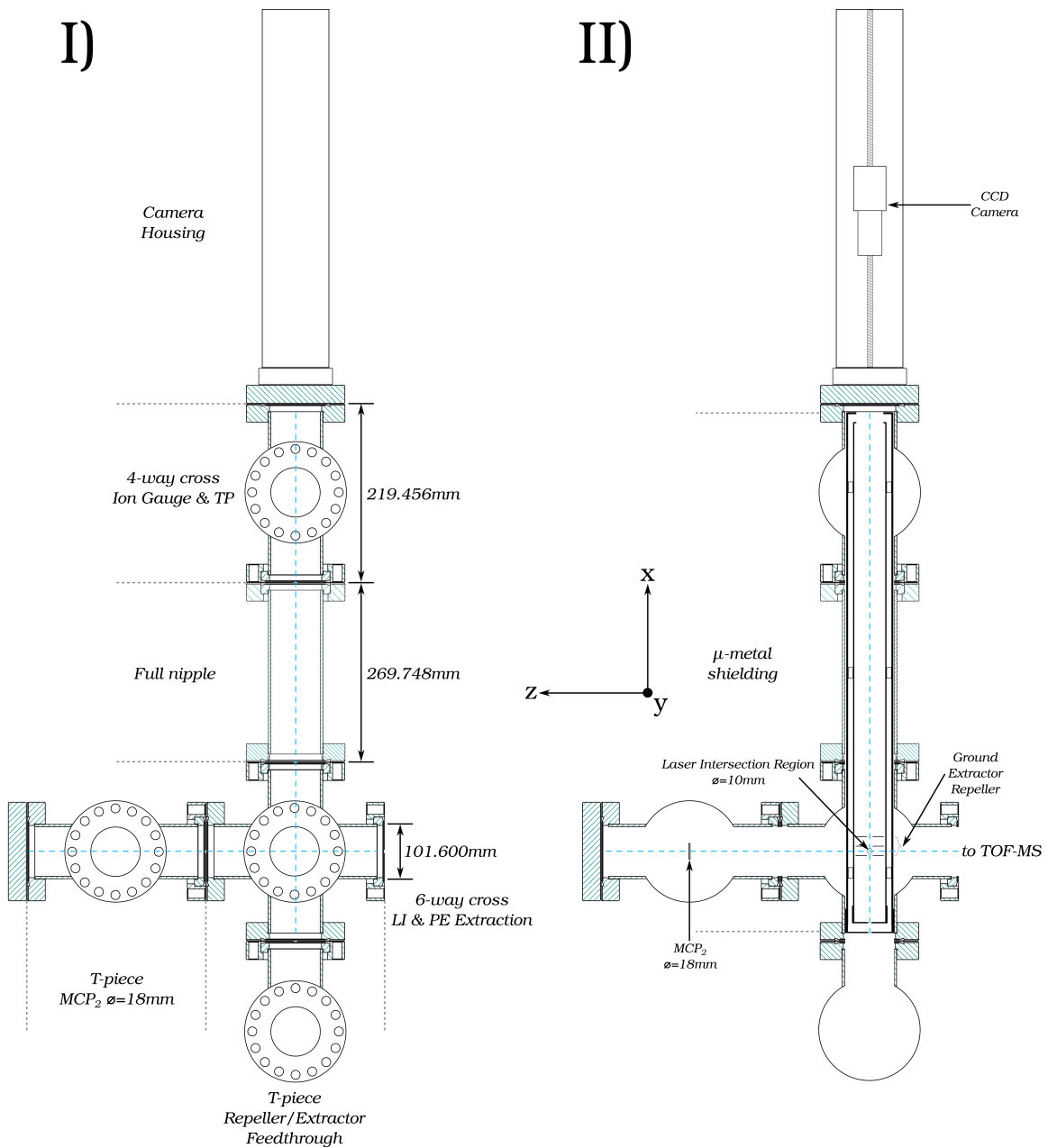


Figure 2.16: Schematic of the reconfigured SEVI spectrometer. Individual chambers are adapted from existing schematics from *Kurt Lesker*. All measurements are in mm. I) features the arrangement of 6" Conflat vacuum chambers that make up the spectrometer. The design is similar to that of Figure 2.12 however the photoelectron flight tube is rotated 90°. This is facilitated by the inclusion of a 6-way cross. II) shows the reconfigured components within the SEVI spectrometer.

Chapter 3

Iodide-Methylperoxy Complexes

3.1 Introduction

The methylperoxy radical (CH_3OO) represents an important intermediate in stratospheric and tropospheric chemistry. The formation of this species comes from several sources, including the abstraction of hydrogen from methane by OH and other radical species to form the CH_3 radical, followed by the mediated reaction with atmospheric O_2 to form CH_3OO as shown in the following scheme:



Despite being the simplest and most abundant alkyl peroxy radical in the atmosphere, studies differ in the degree to which methylperoxy radicals contribute to the tropospheric methanol budget.^{308,309} What is evident from this debate is that further understanding of the reaction pathways, whether they proceed via trioxides and Criegee intermediates,³¹⁰ and the impact of complexation on these dynamics is necessary.³⁰⁹

Methylperoxy radicals under atmospheric conditions are largely unreactive, however are facile to reaction with other atmospheric radicals (NO , NO_2 , HO_2 , O_3)³¹¹

with common products including the corresponding carboxylic acids, aldehydes and ketones. The mechanisms and kinetics of these reactions have been studied extensively via photolytic production of the radical species and monitoring the production of CH₃OO by UV-vis spectrometry,^{312,313} multiplexed photoionization mass spectrometry³⁰⁹ and pulsed laser-induced fluorescence³¹⁴ as notable examples.

The earliest electronic structure studies of ROO radicals began with the work of Hunziker and Wendt,^{315,316} characterising the near infrared $\tilde{A} \leftarrow \tilde{X}$ transition of CH₃OO as 7375(6) cm⁻¹. Later cavity ring down spectroscopy (CRDS) experiments offered an approximately ten-fold improvement on the accuracy of the energy of this transition to 7382.8(5) cm⁻¹ as well as the ability to probe rotational structure of the radical.^{317,318} The first photoelectron spectra of the methyl- and ethyl- hydroperoxide anions by Blanksby et al.,³¹⁹ determined the adiabatic electron affinities (E_a) of the corresponding neutral species to be 1.161(5) eV and 1.154(4) eV respectively. Blanksby's work also showed good agreement in the determination of $\tilde{A} \leftarrow \tilde{X}$ transition albeit at lower energy resolution. Other experimental work on the CH₃OO radical include photodissociation studies using PES,³²⁰ infrared spectroscopic studies in both the matrix,^{321,322} and later gas phase.^{318,323}

Computationally, studies of the CH₃OO radical, and by extension ROO radicals in general, are numerous. Accompanying the published experimental work are electronic structure calculations utilising a range of density functional,^{322–325} ab initio³²⁶ and composite methods.³¹⁹ Gao et al. determined E_a for CH₃OO using B3LYP, BLYP, BP86, BPW91 functionals. The determined values ranged from 0.99 eV to 1.15 eV and although outside of the experimental uncertainty, demonstrated the use of these functionals in determining electron affinities of larger alkylperoxy radicals. While the use of CCSD and QCISD methods by Li et al.³²⁶ did not appear to offer great improvement in determining the electron affinity of the CH₃OO radical, it is noted that the $\angle(C - O - O)$ in the ¹A' state of the anion appeared to be susceptible to higher order electron correlation effects, and QCISD was selected for the subsequent Franck-Condon simulations.

The effect of complexation between ROO and partner species, to the authors' knowledge has not been studied outside of kinetic experiments noted previously, while methylperoxy-molecule partners have been investigated theoretically. These include the reactions of CH₃OO with atmospheric methanol and hydroxy methyl radicals via M06-2X and MP2 methods followed by QCISD(T) and CCSD(T) energetics.³²⁷ Similarly the reaction of CH₃OO with atomic iodine has been examined on the neutral triplet and singlet surfaces using B3LYP followed by *ab initio* single point energies.³²⁸ Both studies detail a number of structures exhibiting binding to both the methyl pocket and peroxy substituent of the radical. Particularly in the study of the singlet I⁻ ···CH₃OO, reaction is favoured via relatively stable binding of iodine to the peroxy ($\Delta E_{Elec+ZPE} = -81.91 \text{ kJ mol}^{-1}$) and the lowest subsequent barrier from this intermediate of 115.37 kJ mol⁻¹. However no such intermediate species were calculated on the triplet surface. Were these to be determined to be stable they may represent attractive spectroscopic targets.

Anion photoelectron spectroscopy has been shown be a powerful technique in elucidating electronic structure of weakly bound species and van der Waals complexes.^{14,46,329} The spectroscopic benefit of the technique is two-fold; the relative stability of the negatively charged complex formed with respect to the neutral allows for the production of greater quantities of the species in question, whilst the detached photoelectrons representing vibronic transitions to the neutral potential energy surface still allow for a detailed determination of neutral electronic structure. An additional benefit of utilising formally charged species is that they may be separated by mass spectroscopy prior to photoelectron detachment. In this work we present the first photoelectron spectrum of an anion-methylperoxy complex (I···CH₃OO), representative of a pre-reaction adduct of halogen and methylperoxy radicals, and support experiment with high level *ab initio* methods.

3.2 Methods

At the time of these experiments, the TOF-PES spectrometer was that of the original design described in Chapter 2. Previous spectroscopic work has produced the CH₃OO radical in a supersonic expansions via the formation of CH₃.³³⁰ In this work, a gas mixture similar to previous halide-oxygen work³⁰⁰ of 100 kPa O₂ in 450 kPa argon seeded with CH₃I and CH₂Br₂ was passed through an electron beam to produce iodide anions via slow electron attachment.

The structures and energies of the CH₃O₂I conformers have been optimised using MP2 methods with Dunning's aug-cc-pVnZ (n=T,Q) basis sets in Gaussian09^{238,264,267,331} These geometries (shown in Figure 3.3) have been determined to be minima by harmonic frequency calculations at the same level of theory. The energies of each conformer at the CBS are then determined using CFOUR single point energies and Weizmann (W1w) methods as per Equation 2.1.

To determine VDEs for the excited O₂⁻ ...CH₃I complex, CASSCF³³² followed by NEVPT2¹⁸⁷ single point energies were determined using ORCA.^{275,333} The active space used was restricted to include only the oxygen *p*-electrons, such that the excitations are local to O₂⁻.³³⁴ These term energies are then included additively with ground state W1w VDEs, yielding “pseudo-W1w” VDEs for detachment to excited neutral states.

3.3 Results and Discussion

Mass spectra produced from the O₂:CH₃I:CH₂Br₂:argon gas mix are presented in Figure 3.1a and 3.1b. Complete peak assignments for both spectra are included in Appendix A (page 232), however key assignments are discussed here. In the low *m/z* range (Figure 3.1a), the mass spectrum is dominated by a pair of peaks resulting from ⁷⁹Br⁻ and ⁸¹Br⁻ respectively, however additional peaks at 32 *m/z* and 64 *m/z* are present. These are assigned to the bare superoxide anion O₂⁻ and dimer cluster

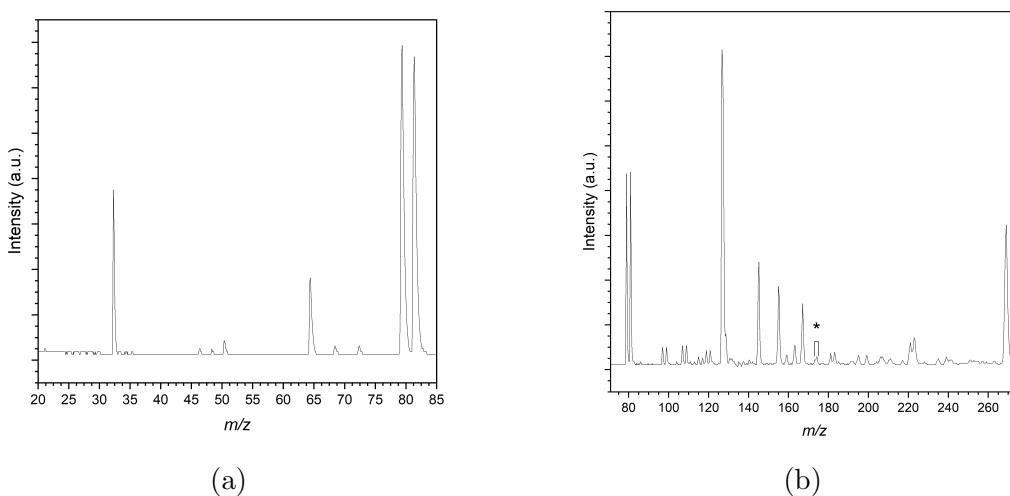


Figure 3.1: Mass spectra from $\text{O}_2:\text{CH}_3\text{I}:\text{CH}_2\text{Br}_2:\text{argon}$ gas mix at a) low m/z and b) high m/z ratios. The peak of interest is marked with *.

$([\text{O}_2\cdots\text{O}_2]^-)$ respectively. While photoelectron spectra of these mass peaks are not recorded there exist in literature numerous examples of O_2^- cluster formation via electric discharge and direct attachment of low kinetic energy electrons^{335–338} In the high m/z range (Figure 3.1b), common halide solvation with H_2O , N_2 and Ar is present with additional peaks at $221/223$ m/z and 267 m/z assigned to $\text{Br}^-\cdots\text{CH}_3\text{I}$ and $\text{I}^-\cdots\text{CH}_3\text{I}$ respectively.

The peak of interest in the spectrum lies at 173.9 m/z (Figure 3.1b), corresponding to CH_3IO_2^- and is believed to be the result of two competing van der Waals complexes in a number of conformers; $\text{I}^-\cdots\text{CH}_3\text{OO}$ and $\text{O}_2^-\cdots\text{CH}_3\text{I}$. While previous work within the Wild Group has formed halide-molecule complexes readily in the gas phase by simple association,^{57,173,339} the presence of a relatively intense O_2^- peak in the mass spectrum suggests that more complex dynamics may be present. The spectrum contains a broad feature between 1.7 eV to 2.4 eV as well as more intense peaks at 3.01 eV , 3.50 eV and 4.01 eV . The intense peaks are assigned to the $^2P_{3/2}$ (I^\bullet) \leftarrow 1S (I^-), $^3A''$ ($\text{I}^\bullet\cdots\text{CH}_3\text{OO}$) \leftarrow $^2A''$ ($\text{I}^-\cdots\text{CH}_3\text{OO}$) (photodetachment from a perturbed I^-) and $^2P_{1/2}$ (I^\bullet) \leftarrow 1S (I^-) transitions respectively. The presence of I^- photodetachment in this mass peak suggests complex formation and dissociation within the timescale of the experiment, with dissociation occurring after the

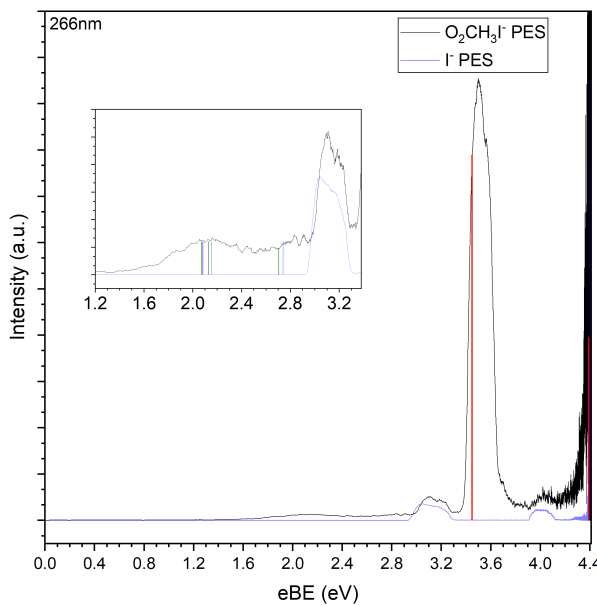


Figure 3.2: Photoelectron spectra of CH_3IO_2^- . The blue trace represents the I^- calibration spectrum and computational vertical detachment energies are shown as stick spectra for vDW1 $\text{O}_2^- \cdots \text{H}_3\text{Cl}$ (green), vDW2 $\text{I}^- \cdots \text{H}_3\text{COO}$ (red), and vDW3 $\text{O}_2^- \cdots \text{ICH}_3$ (blue).

potential is applied to the TOF plates but before detection (792.00 μs to 831.96 μs after the nozzle pulse). The broad feature present may be from several sources. Previous photoelectron spectra of CH_3OO include a number of vibronic transitions from the recorded E_a (1.161(5) eV) to higher energy bands ($T_e = 0.914(5)$ eV),³¹⁹ however CH_3OO^- is not present in the mass spectrum (Figure 3.1a) and the higher E_a of I^- suggests that charge transfer is not favoured in the $\text{I}^- \cdots \text{CH}_3\text{OO}$ complex. This band is tentatively assigned to correspond to detachment to excited states of O_2 within the $\text{O}_2 \cdots \text{CH}_3\text{I}$ complex.

The most stable anion structures of the respective complexes on the basis of the complex dissociation energy (D_0), are those where O_2^- is bound to the methyl pocket of the CH_3I (vDW1, $D_0 = 63.3 \text{ kJ mol}^{-1}$) and I^- is similarly bound in the methyl pocket of the CH_3OO (vDW2, $D_0 = 45.5 \text{ kJ mol}^{-1}$). These structures have also been calculated as minima in the triplet neutral state and are in addition to those previously determined by Zhang et al.³²⁸ Higher energy minima have also been calculated on the anion potential energy surface (vDW3), where O_2^- is bound via a

halogen bonding interaction however this lies only 3.3 kJ mol^{-1} above vdW1. The W1w barrier to total internal rotation of CH_3I was also determined by a transition state search and is 47.3 kJ mol^{-1} for $\text{vdW1} \rightarrow \text{vdW3}$. These interactions appear to be dominated by electrostatic interactions, however moving through the TS2 transition state, the interaction between the π -orbital of the O_2^- with the electron density of the iodine within CH_3I may represent a degree of covalency. Previously modelled electrostatic potential surfaces of CH_3I show regions of reduced electron density in the methyl pocket and formation of a σ -hole.³⁴⁰ Regarding the σ -hole in particular, the authors denote an α angle as the supplement of the angle of attack of a given nucleophile ($\alpha = 180 - \angle_{\text{C-X-Nu}}$), using α as a proxy for the size of the σ -hole. For CH_3I $\alpha \leq 40^\circ$, whereas the corresponding supplement of the $\angle_{\text{X-C-H}}$ is 72.0° and the solid angle created by the methyl group rotor is 3.99 sr. Collisionally this would suggest that nucleophilic attack via the methyl group (vdW1) is favoured compared to the halogen bonding interaction (vdW3).

In treatment of the iodide complexes, the calculated VDE is adjusted for the spin-orbit splitting of the iodine to a pair of perturbed 2P states. The associated vertical detachment energies (VDEs) of the $\text{I}^- \cdots \text{CH}_3\text{OO}$ are 3.449 eV and 4.391 eV for the perturbed $^2P_{3/2}$ and $^2P_{1/2}$ states respectively, with the former showing very good agreement with the experimental peak position of 3.50 eV. The degree of perturbation, shown by the stabilisation in electron binding energy in the complex compared to the I^- peak (E_{stab}), is representative of the difference in complex dissociation energies (D_0) between the anion and neutral complexes. The $^2P_{3/2}(\text{I}^\bullet) \leftarrow ^1S(\text{I}^-)$ and $^3A''(\text{I}^\bullet \cdots \text{CH}_3\text{OO}) \leftarrow ^2A''(\text{I}^- \cdots \text{CH}_3\text{OO})$ assigned peaks within the experimental photoelectron spectrum can be further addressed by deconvolution by three Gaussians representing the differing flight path lengths to the detector (towards, perpendicular and away). By taking the centre of the lowest eBE Gaussian (fastest and more direct photoelectrons) the peak positions of the respective transitions can be determined as 3.06 eV and 3.46 eV. All fitting parameters are also provided in Appendix A (page 276). While the complex detachment shows excellent agreement

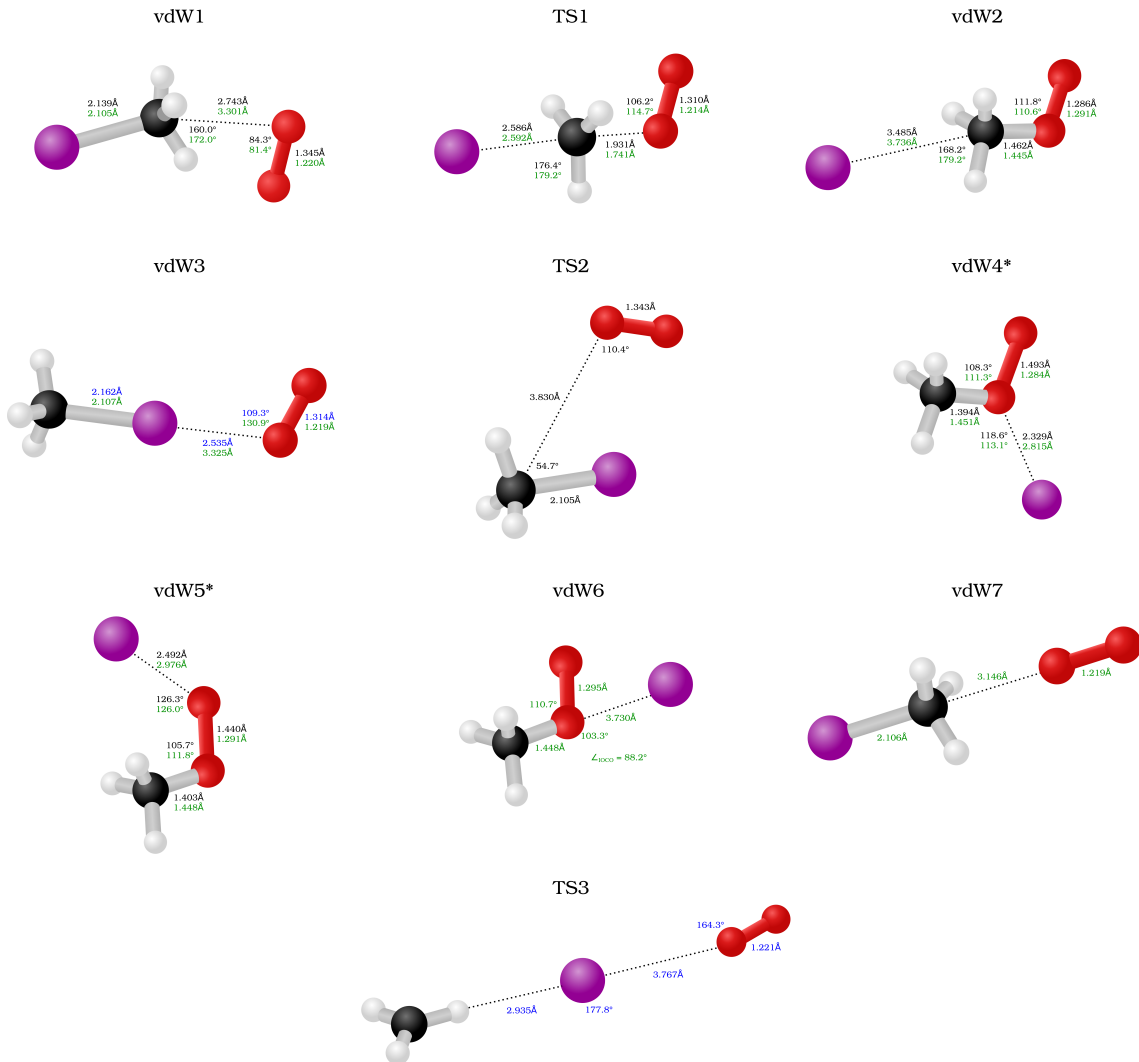


Figure 3.3: MP2/pVQZ calculated geometries for the $\text{O}_2^- \cdots \text{CH}_3\text{I}$ and $\text{I}^- \cdots \text{CH}_3\text{OO}$ complexes. Anion parameters are shown in black and blue, neutral parameters are shown in green. * pVQZ geometries of the vdW4 and vdW5 anion complexes were determined to be transition states and the pVTZ geometric parameters are reported here.

with calculated W1w results, the assigned dissociated iodide peak also agrees precisely within experimental resolution with the literature value, further supporting the proposition that this results from complex dissociation within the timescale of the experiment.³⁴¹

The E_{stab} value also serves as a good proxy to infer the strength of electrostatic interaction as these interaction dominate the binding of anion van der Waals complexes. By this metric the iodide-methylperoxy complex ($E_{stab} = 0.40$ eV) is similarly bound compared to other iodide-molecule complexes with values of 0.40 eV, 0.41 eV, 0.48 eV and 0.44 eV/0.43 eV for $I^- \cdots CH_3CHO$,³⁴² $I^- \cdots CH_2O$,³⁰⁶ $I^- \cdots (H_2O)(CH_3CH_2)$ ³⁴³ and $I^- \cdots CH_3COCH_3$ ^{339,344} respectively. $I^- \cdots (H_2O)(CH_3CH_2)$ also corresponds in mass to $CH_3IO_2^-$ however experiments where they have been observed required addition of these solvent molecules to the gas mixture in similar quantities as the halide precursor. For this reason and that this feature is only present in this suite of experiments at higher partial pressure of O₂, these complexes have been ruled out as candidates in the photoelectron spectrum.³⁰⁰

Franck-Condon factors were also modelled with Duschinsky rotations for photodetachment from the vdW2 complex using *ezSpectrum 3.0*²⁵⁶ at a temperature approximating the molecular beam (50 K). These transitions are included as a stick spectrum in Figure 3.4b with full FCF factors provided in Appendix A (page 275). Given the similarity in geometries between and anion and neutral vdW2 complexes, the most intense transition belongs to that of the ADE. Other intense transitions include those with vibrational quanta in the vdW intermolecular modes and CH₃ rotation ($\omega_1-\omega_4$). Additional weak features at 3.58 eV and 3.62 eV then correspond to the C–O stretch ($\omega_6 = 946\text{ cm}^{-1}$) and O–O stretch ($\omega_6 = 1279\text{ cm}^{-1}$). Though it is unlikely, the ω_6 band transitions may be evidenced in the experimental spectrum by the peak shoulder at approximately 3.57 eV.

Previous computational work has found that accurate determination of the electron affinity of the superoxide anion is difficult, and that the piecewise inclusion of non-dynamical correlation effects are necessary.^{174,335} We note that the use of W1w

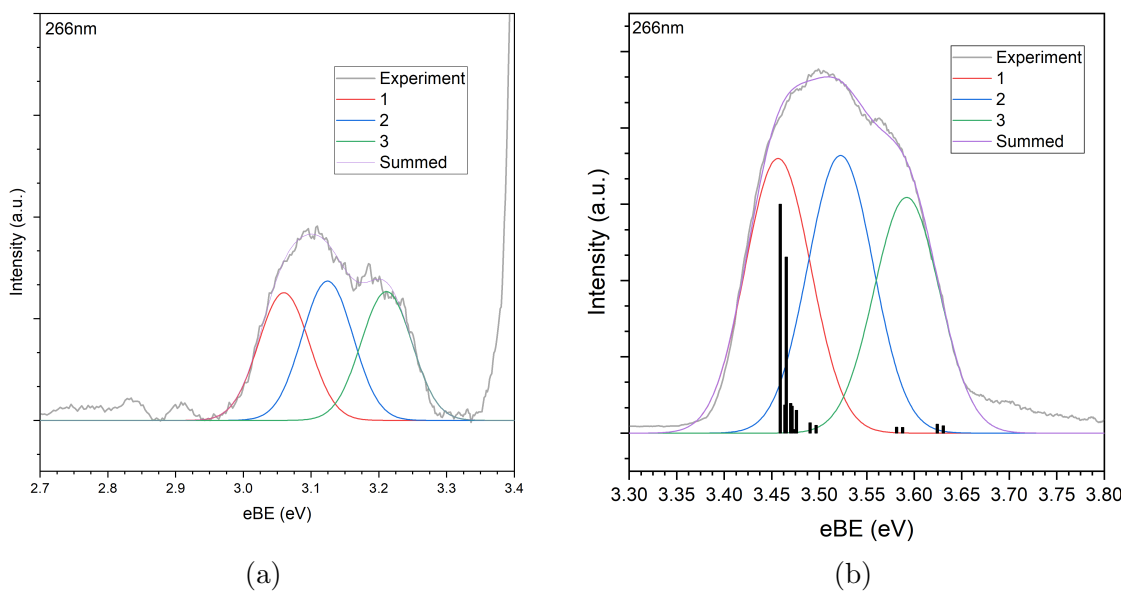


Figure 3.4: Deconvoluted peaks from within the $173.9\text{ }m/z\text{ }(\text{CH}_3\text{O}_2\text{I}^-)$ photoelectron spectrum. Each spectrum consists of three Gaussians representing flight paths directly towards, perpendicular to, and away from the detector. (a) Peak assigned to the $^2P_{3/2}\text{ (I}^\bullet\text{)} \leftarrow ^1S\text{ (I}^-\text{)}$ ($eBE = 3.06\text{ eV}$) transition. (b) Peak assigned to the $^3A''\text{ (I}^\bullet \cdots \text{CH}_3\text{OO}) \leftarrow ^2A''\text{ (I}^- \cdots \text{CH}_3\text{OO)}$ ($eBE = 3.46\text{ eV}$) transition. A stick spectrum, generated from calculated Franck-Condon factors (FCFs) is included.

methods determine the $\text{O}_2^- E_a$ to be 0.438 eV . Comparing the O=O bond length in both the anion and neutral we see that the MP2/pVQZ optimisations agree with experiment in the case of the anion but is longer for the neutral. The corresponding change in W1w energy in this region is small (0.006 eV) and the difference between the experimental ADE and that determined by W1w is attributed to inclusion of an anharmonic vibrational correction and those included by Neograday.¹⁷⁴ While this E_a is outside the experimental error determined by Lineberger, W1w methods are deemed acceptable for comparison with our experiment and that previous work within our group has supported their application in these cases. The VDE determined the energy associated with the O_2^- geometry in the $^3\Sigma_g$ state is significantly larger (0.907 eV), but is representative of a large geometry change and corresponds to the most probable Franck-Condon transition.

In the case of detachment to excited singlet states of the superoxide anion, W1w methods determine the $^1A' \leftarrow ^2A''$ transitions of the vdW1 and vdW3 complexes

to be 2.337 eV and 2.256 eV respectively. Both detachments do not show suitable agreement with the broad band present in the spectrum which is most intense at 2.1 eV. This may be due to the (T) contribution to the W1w energies, as typically this contribution is overestimated in singlet biradical species.¹⁷³

Noting that these VDEs are the most probable vibronic transitions, these pseudo-W1w VDEs show sufficient agreement with the broad band present in the photoelectron spectrum and allow assignment of the band to numerous ${}^1A'$ states of the superoxide complex.

Table 3.1: Calculated complex dissociation energies, electron affinities and vertical detachment energies of CH₃OOI complexes. For CCSD(T) and W1w methods, vibrational contributions are included from MP2/auc-cc-pVQZ harmonic frequencies.

State	E_{W1w} E_h	E_{CASCF} E_h	E_{NEVPT2} E_h	VDE_{W1w} eV	T_e eV	VDE_{W1w+T_e} eV
vdW1: O ₂ ⁻ ... H ₃ Cl						
${}^2A''$	-485.1158986					
${}^3A''$	-485.0706155	-483.9503739	-484.7751402	1.187		
${}^1A'$	-485.0283714	-483.9269082	-484.7426175	2.337	0.885	2.072
${}^1A'$		-483.9306004	-484.7406084		0.940	2.127
${}^1A'$		-483.9032413	-484.7193407		1.518	2.705
vdW3: O ₂ ⁻ ... ICH ₃						
${}^2A''$	-485.1147113					
${}^3A''$	-485.0704565	-483.9518727	-484.772859	1.163		
${}^1A'$	-485.0302549	-483.9262601	-484.7390006	2.256	0.921	2.084
${}^1A'$		-483.929307	-484.7364286		0.991	2.154
${}^1A'$		-483.9016634	-484.7148893		1.577	2.740

While the superoxide complex is present in the photoelectron spectrum, the iodide complex is dominant. The formation of CH₃OO is the result of competing S_N2 and electron transfer (ET) mechanisms. Where the difference in E_a between the nucleophilic O₂⁻ and bare iodide is greater than the bond dissociation energy of H₃C-I, the ET channel can compete with S_N2 .³⁴⁵ The calculated thermodynamics (ΔG_{W1w}^{298K}) of these competing channels in the O₂⁻ + CH₃I reaction are shown in Figure 3.5. The ET transition state represents a 4A CH₃...I⁻...O₂ complex (TS3), and while the surface intersection with the doublet state is not located, ΔG_{W1w}^{298K} for this complex represents the *minimum* energy required for ET to proceed. As the bar-

riers for S_N2 and ET respectively are 51.5 kJ mol^{-1} and $\geq 75.5 \text{ kJ mol}^{-1}$, and vdW1 is more stable than vdW2, it would suggest that the S_N2 mechanism for formation of $\text{I}^- \cdots \text{CH}_3\text{OO}$ is favoured. Additionally, the enthalpy and Gibbs energy contributions to TS3 at 298 K are $116.2 \text{ kJ mol}^{-1}$ and $-14.2 \text{ kJ mol}^{-1}$ respectively. This indicates that this transition state is further unfavoured at lower temperatures such as those found in the supersonic expansion of the molecular beam ($\sim 10 \text{ K}$). With respect to the experimental conditions, the production of CH_3 radicals as a biproduct of the formation of I^- via dissociative electron attachment in a higher partial pressure of O_2 leads to the production of CH_3OO . The subsequent formation of $\text{I}^- \cdots \text{CH}_3\text{OO}$ complexes observed in the mass spectrum is believed to be largely contributed by direct association. However the dissociation of the complex in the timescale of the experiment cannot rule out the S_N2 pathway entirely as the exothermicity of the reaction would drive dissociation of $\text{I}^- \cdots \text{CH}_3\text{OO}$ where complex formation prior to mass spectrometry undergoes significant collisional cooling and stabilisation.

3.4 Summary

The anion photoelectron spectra of two competing complexes $\text{O}_2^- \cdots \text{CH}_3\text{I}$ and $\text{I}^- \cdots \text{CH}_3\text{OO}$ are presented. *Ab initio* methods (W1w and NEVPT2) have been utilised to rationalise the features present in the experimental spectrum, corresponding to the $^3A'' \leftarrow ^2A''$ transition in the iodide-methylperoxy complex (3.46 eV) and transitions from the $^2A''$ to numerous $^1A'$ states of two superoxide-methyliodide complexes. The thermodynamics of formation have also been investigated computationally, and while direct addition of oxygen to methyl radicals a likely source of CH_3OO , two competing mechanisms (S_N2 and ET) are also contributors albeit with S_N2 favoured. Timescales on which spectroscopy is performed are long by comparison to these processes, however producing these complexes *in situ* may be of interest for future work to probe their dynamics of formation.

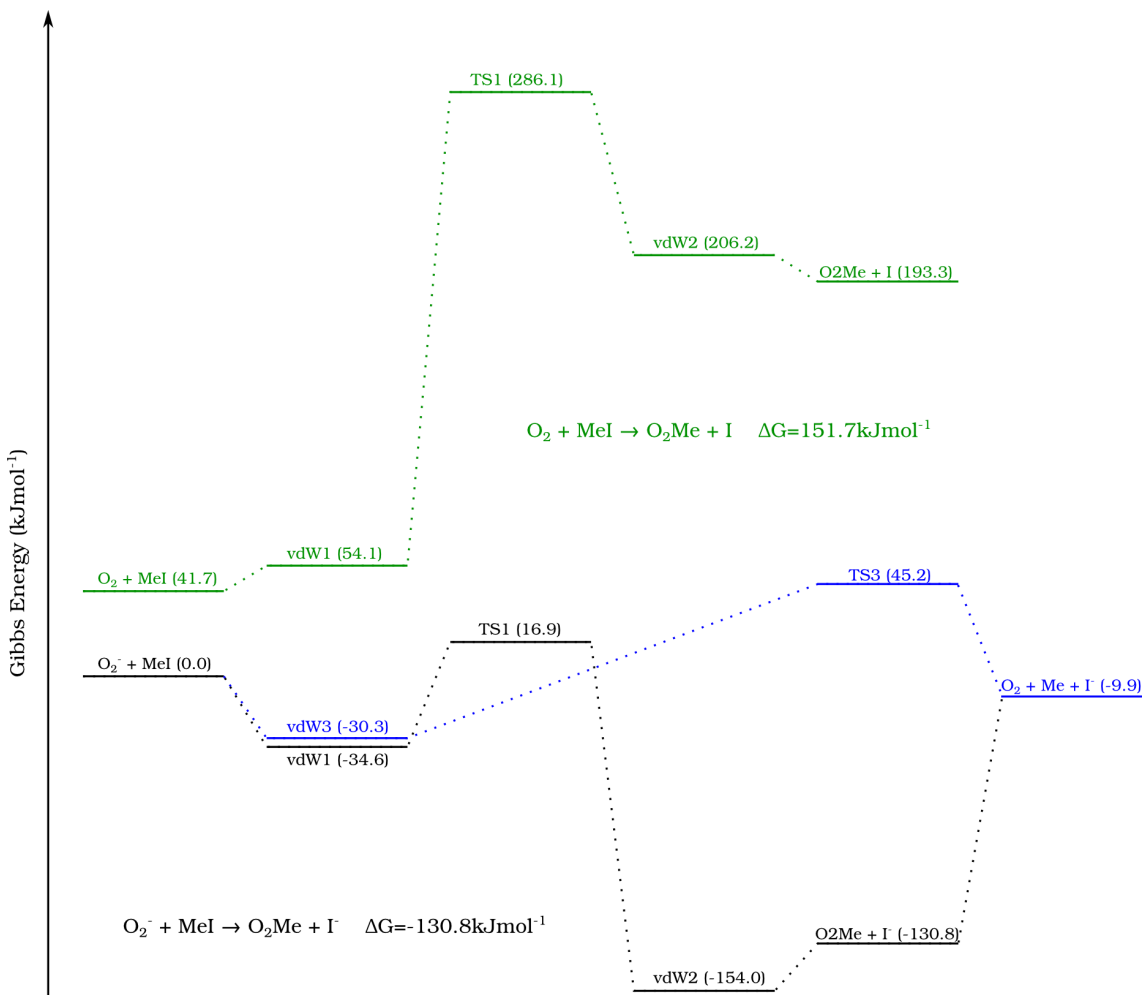


Figure 3.5: Reaction pathways of the superoxide (O_2^-) and methyliodide complex formation. Substitution via an S_N2 mechanism in the anion ground ${}^2A''$ state is denoted in black and in the neutral ${}^2A''$ state in green. Electron transfer, proceeding via a halogen bonded $\text{O}_2^- \cdots \text{ICH}_3$ (vdW3) through TS3 (4A) is shown in blue.

Chapter 4

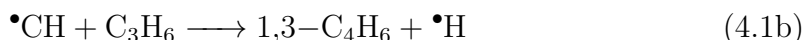
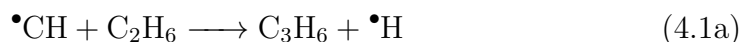
Halide-Propene Complexes

4.1 Introduction

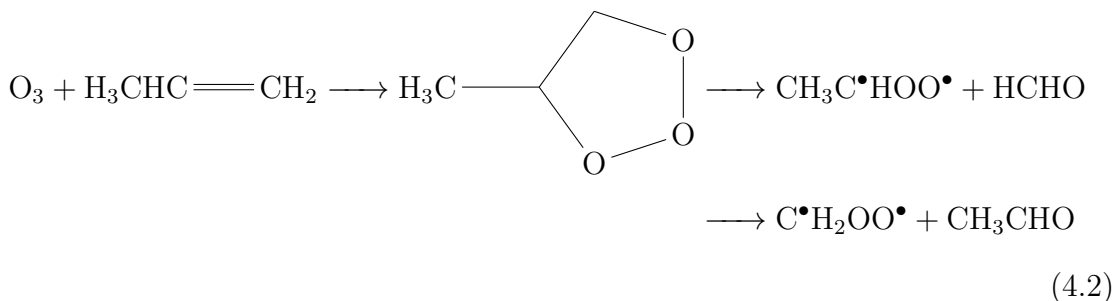
Propene represents an important atmospheric, industrial, and extraterrestrial hydrocarbon as an extension of the chemistry displayed by ethene and an intermediate in reactions to produce both longer and substituted hydrocarbons. Industrially, propene undergoes polymerisation to form polypropylene, a common plastic with U.S production capacity of 7.8 Tg yr^{-1} . Production of polypropylene relies on a Ziegler-Natta catalyst and can be done in the form of slurry or the gas-phase.³⁴⁶ Taking the example of gas-phase polymerisation, a minor route in global production, heterogeneous co-catalysts TiCl_4 and MgCl_2 are used, presenting the potential for chlorine-propene complex formation as catalyst degradation would likely lead to the release of chlorine radicals into the reaction vessel.³⁴⁷

The detection of propene in both the atmospheres of Titan and the interstellar medium (ISM) in the Taurus Molecular Cloud (TMC-1) place propene as an important pre in a bottom-up approach to the formation of long-chain hydrocarbons in extraterrestrial environments (see Equations 4.1a-4.1c).^{348,349} The basis of this process is the bimolecular reaction of the methylidyne radical ($\bullet\text{CH}$) with ethane to produce propene and atomic hydrogen with further reactions building upon the size of the carbon chain.³⁵⁰ As an example the methylidyne radical ($\bullet\text{CH}$) has been

investigated spectroscopically using VUV synchrotron photoionisation mass spectrometry, producing a mixture of 1,3-butadiene, 1,2-butadiene and 1-butyne as photolysis products. The ethynyl radical ($\cdot\text{C}_2\text{H}$) participates in similar processes of hydrocarbon growth and has been investigated extensively, particularly by pulsed Laval nozzle experiments.^{351–353}



Tropospherically, propene undergoes oxidation via two primary mechanisms. Models of smog chambers suggest that reaction with hydroxy radicals (HO^\bullet) and O_2 leads to the production of aldehydes (methanal and ethanal) and hydroperoxyl (HO_2).³⁵⁴ Atmospheric models determining the fate of volatile organic compounds (VOC) indicate direct reaction with ozone again leads to production of two primary aldehydes but also Criegee biradicals as demonstrated by:³⁵⁵



These reactions occur in the troposphere, and given ideal conditions, the latter can lead to net ozone production;³⁵⁵ however, the impact of halogen radicals in this region ultimately results in ozone depletion³⁵⁶ via reactions with bromine shown in reactions 4.3a, 4.3b and 4.3c. While the largest flux of propene (and other VOCs) into the atmosphere is from the chemical industry and petroleum sources

(32-62 Tg yr⁻¹) both propene and bromine are readily sourced from the oceans into the marine boundary layer (MBL), albeit in much lower amounts (propene: 0.5 Tg yr⁻¹).³⁵⁷ Given the free-radical addition to alkenes, the interaction between a halogen radical and propene in the vdW region could activate propene to reaction with hydroxyl radicals and oxygen, or ozone as per the reactions suggested previously (Equation 4.2), and hence understanding the structure and reactivity of these complexes is a worthwhile endeavour.



Similarly the radical intermediates of the $\bullet\text{OH} + \text{C}_3\text{H}_6$ reaction have been studied via (2+1) REMPI spectroscopy, utilising 193 nm radiation to produce the photolysis products ($\bullet\text{C}_3\text{H}_6\text{OH}$).³⁵⁸ At the time of writing, halogen-propene complexes have scarcely been studied, with the only published work on propene complexes believed to be that of Xu³⁵⁹ and Peebles^{360,361} who recorded the rotational spectrum and modelled the propene-SO₂ complex respectively. Xu³⁵⁹ reports the structure of the propene-SO₂ complex where the propene carbon backbone lies parallel with the plane of the SO₂. This reflects a similar conformation to that of the halogen-acetylene complexes and may therefore be indicative of dispersion interaction.²⁵⁹ Modelling work involving a combination of distributed multipole analysis (DMA) and atom-atom potentials was undertaken by Peebles and the resulting structures agree with the parallel plane conformation though different structures as to the rotation of the SO₂ molecule in this plane.^{360,361} Considering that this work is rather inexpensive computationally, with DMA being completed using only Hartree-Fock theory and 6-31G** basis sets, it is difficult to take any of the determined structures as definitive. However as these structures are not radically different from those

determined from experiment, general conclusions as to complex interaction can still be made.

Given the role that halogen radical chemistry plays atmospherically, and that halogen-propene vdW complexes represent model systems for these pre-reaction adducts, their structure and stability warrants further exploration. This chapter features two different studies of halide-molecule complexes. The first applies a double-hybrid functional to previously studied halide-molecule systems in order to benchmark the functional against previous experimental and *ab initio* methods. This is discussed briefly in Section 4.2.2 to rationalise its selection as a computational method. The second then employs these methods and photoelectron spectroscopy in the study of a number of halide-propene clusters, to determine their electron binding energies and the nature of the non-covalent interactions present. The purpose of these studies is to:

1. extend the capacity of accurate photoelectron spectroscopy predictions made via computational methods within reasonable computational cost; and
2. investigate the substituent effects present in larger unsaturated hydrocarbons on interactions with halides and halogens by comparison to previous halide-ethene complexes using anion PES.

4.2 Methods

4.2.1 Experimental Methods

Halide-propene gas mixtures were prepared by exposing halide sources to the evacuated gas mixing station followed by injection of 50 kPa of propene gas sourced from a local hardware store (*Tradeflame, TF/Ultra Gas MAPP*, 400 g). The duration of exposure is governed by the vapour pressures determined in Table 2.2, with the halide sources CCl_4 , CH_2Br_2 and CH_3I open to vacuum for 10 s each at 25 °C for CCl_4 and CH_2Br_2 and –11 °C (ice-salt water bath) for CH_3I . The gas mixture is then made

up to an operational backing pressure of 450 kPa with argon. Each halide source was prepared by degassing though at least 2 freeze-pump-thaw cycles to ensure that residual solvents (acetone, ethanol) are removed. As the atomic mass of C₃H₆ is 42 amu, the ³⁷Cl⁻...C₃H₆ complex is expected to have an *m/z* value of approximately 79. To reduce the impact of residual ⁷⁹Br contaminating the complex peak in the mass spectrum, bromide experiments were conducted first, followed by iodide and then chloride spectra. It was not deemed appropriate to begin experiments with chloride spectra as recently concluded spectra had also been of the bromide complexes. This contaminating effect was sought to be reduced further by repeatedly flushing the gas mixing station with a backing pressure (450 kPa) of Ar; however, it was not eliminated entirely as spectra of ⁸¹Br⁻ were also used for the purposes of calibration.

The spectrometer in the Wild Group has been described in detail in Chapter 2, and the configuration of the spectrometer at the time of these experiments included the upgraded gas mixing station, photoelectron flight tube, and piezoelectric nozzle. Typical operating parameters of the TOF-MS include electron filament current of 3.85 A provided by a constant current laboratory power supply (*TTi EL155*), and beam energy of -1500 V. Mass spectra were calibrated using bare halide peaks identified by their approximate TOF timing and isotopic abundances, where available multiple halides were used for this calibration and, in the case of the iodide experiments, the inclusion of the bromide-79,81 doublet was necessary. Similarly, PES spectra of bare halides were taken and used to calibrate PES spectra of the associated complexes. For each of the chloride complexes, the deconvolution procedure described in Equation 2.11 was used for the purpose of verification of the ²P_{3/2,1/2} Cl \leftarrow ¹S Cl⁻ transition, however the respective bromide and iodide spectra form the calibration.

4.2.2 Computational Methods

To test the applicability of the DSD-PBEP96-D3BJ functional for the purposes used in this work, a number of representative halide-molecule complexes were optimised and compared to previous computational and experimental studies. The complexes selected are the halide complexes with O₂, N₂, acetylene, ethene and both the *cis*- and *trans*-formic acid isomers.^{34,57,259,300,362–364} As these complexes have been investigated previously, starting geometries were chosen from those already optimised using *ab initio* methods rather than a traditional search of conformer space. These were then reoptimised using the DSD-PBEP86-D3BJ functional with def-2QZVP and AVnZ ($n = T, Q$) basis sets followed by confirmation of minima by harmonic frequency calculations. Associated D_0 values are then determined for both the anion and neutral minima by comparison of the correspond energies of the monomer species. VDEs for these complexes were calculated similarly to previous *ab initio* methods, by calculating the energy of the neutral complex at the geometry of the anion. The energy difference between the neutral single-point energy and the anion minima then represents the barycentre of the neutral electronic state and is artificially split into the two states analogous to the 2P states of the halogen. These values are also corrected for differences between the methods used here and experimental $^2P_{3/2,1/2} \leftarrow ^1S$ photodetachment transitions of the bare halides. A summary of the resulting corrected and shifted VDEs is provided in Table 4.2 with all cartesian coordinates, geometries, VDEs, harmonic frequencies provided in Appendix B.

The results of these calculations are presented and discussed in further detail in Section 4.3.1 however in general those values calculated using Dunning basis sets were more suitable. Considering the computational cost of the halide-propene calculations, and that the employed calibration protocol to experimental halide photodetachment corrected for deficiencies in the basis set, the smaller basis sets (def-2QZVP and AVTZ) were selected for the exploratory work.

4.3 Results and Discussion

4.3.1 Benchmarking DH-DFT Methods

In almost all cases, the minima determined via *ab initio* methods previously have been confirmed by the double-hybrid functional showing the same bonding motifs. While interatomic distances can be compared for the complexes present, the energy gradients of these minima are low given the strength of vdW interactions in general and relatively large geometry changes typically are not reflective of true behaviour. In all cases, it is more appropriate to consider regions of interaction rather than discrete bond lengths as even small thermal contributions can result in large deviations from equilibrium structures. We approach vdW complexes here in this manner; however, much work has been undertaken to characterise the roaming pathways of gas-phase interactions.³⁶⁵ Regardless, comparing typical bond lengths between *ab initio* results and those from DH-DFT methods show that the latter approximate the values to a high degree. As an example, comparing the $\text{I}^- \cdots \text{N}_2$ 1A_1 complex, previous CCSD(T)/AVTZ geometries calculate an I–N interatomic distance of 4.057 Å with a CBS D_0 of 7.0 kJ mol⁻¹. The corresponding DSD-PBEP86-D3BJ/AVQZ interatomic distance and D_0 are 4.048 Å and 8.1 kJ mol⁻¹ which shows excellent agreement with CC values. These example D_0 energies lie outside the arbitrarily set threshold for chemical accuracy in non-covalent interactions (≤ 0.1 kcal mol⁻¹); however this difference is approximately 11 meV and well within the spectroscopic resolution of the PES spectrometer.

All DSD-PBEP86-D3BJ structures are presented in Figure 4.1. It should be noted that the structures presented correspond to minima on their respective potential energy surfaces, however all the structures presented for the halide-oxygen complexes are determined to be transition states in all basis sets. The calculation of these complexes in particular have presented difficulties previously as the multireference character of the system can lead to spin contamination of the SCF wavefunction and erroneous exaggeration of the perturbative contribution in CCSD(T).³⁰⁰ These

effects have been attributed to higher order electrostatic contributions, particularly in the anion complex, where the appropriate bent anion structure is determined via inclusion of ion-quadrupole and ion-hexadecapole contributions. This can be addressed to a degree with robust coupled cluster methods by use of analytic gradients as opposed to finite differences; however, in benchmarking the double-hybrid functional here, error superposition cannot be excluded without full decomposition of the respective energy contributions. Rather, the approach taken here is to alter the choice of basis set. Given that the original DSD-PBEP86-D3BJ functional has been parameterised to mimic CCSD(T) electronic behaviour and optimised with Ahlrichs def-2 basis sets, to avoid any systematic error in basis set design, a basis set from this family should also be chosen.^{227,270} However in the original design of Dunning basis sets additional augmentation functions are included to improved the dipole polarisabilities of group 18 elements, this also extends to group 17 halides also.²³⁸ Similar improvements to the calculated polarisability of fluorine and other atomic polarisability have been shown in the design of Ahlrich def-2 basis sets with additional diffuse functions (mean unsigned error of 0.5%).³⁶⁶

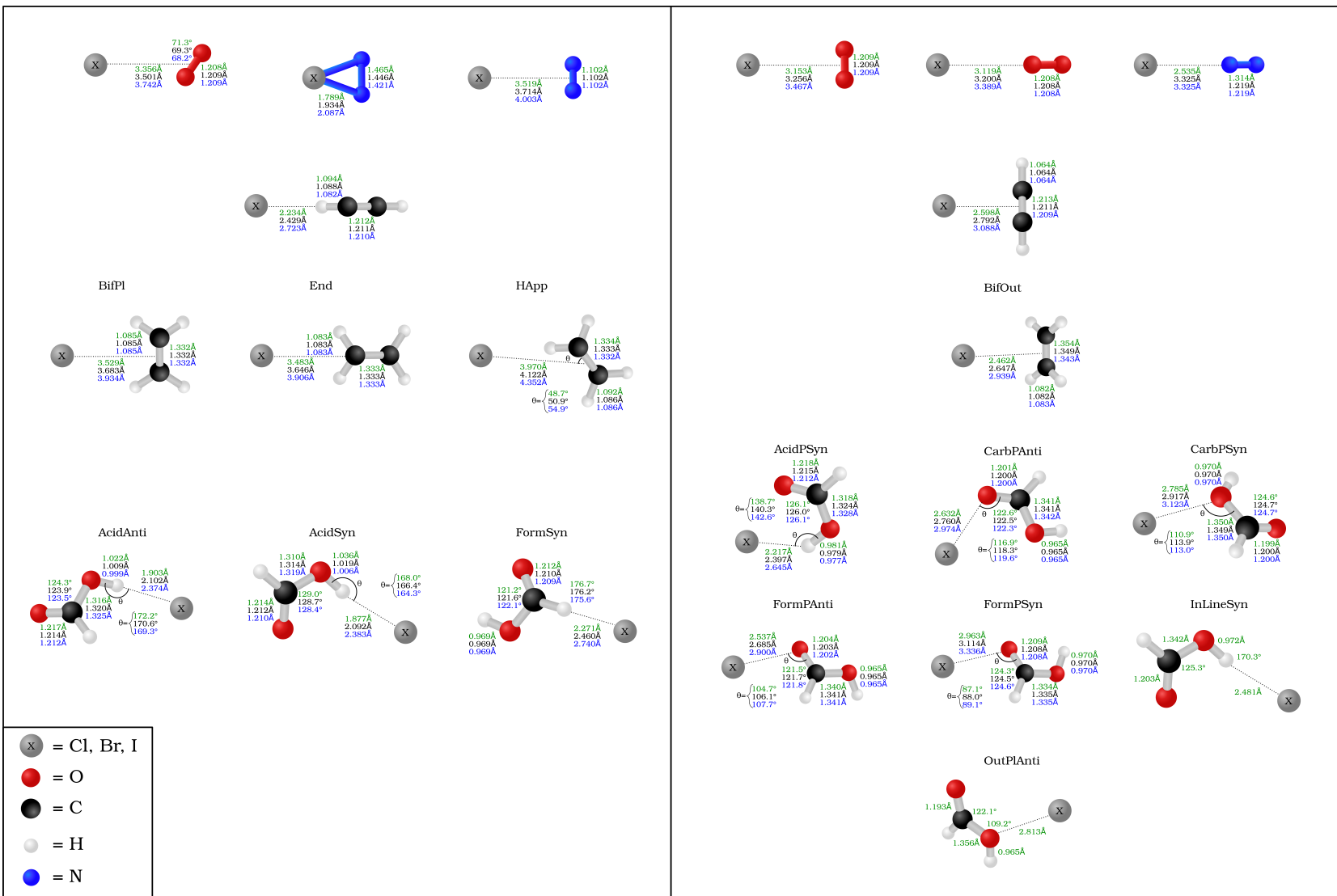


Figure 4.1: Structures of halide-molecule complexes calculated from DSD-PBEP86-D3BJ functional using AVQZ basis sets. Complete data sets, including for def-2QZVP and AVTZ basis sets are provided in Appendix B.

To test the dependence in this troublesome case, the XO_2 complexes (where $\text{X} = \text{Cl}, \text{Br}$ or I) were reoptimised using both inclusion of diffuse functions in the Alhrich's set but also additional diffuse functions in the already augmented Dunning basis set, denoted def-2QZVPD and dAVTZ respectively (shown in Table B1).³⁶⁷ In the anion complexes, inclusion of additional diffuse functions in the def-2QZVPD basis set yielded all real modes that showed good agreement with previously calculated CCSD(T)/AVTZ frequencies. The corresponding doubly augmented (dAVTZ) basis set, however, did not produce qualitatively the same result, and yielded a transition state. Should force constants be calculated at each step of the geometry optimisation, however, dAVTZ basis sets yield appropriate results. This suggests that the optimisation procedure rather than the basis set produces these results, however, becoming overly reliant on a full harmonic calculation at each optimisation step quickly become impracticable. There may still be a basis set effect contributing to the performance of the dAVTZ basis set as nominally, the AV n Z bases used for chlorine and other 3rd row elements, include reparameterised d -functions.²⁶⁵ It should be noted that the number of primitives in both the AV(T+d)Z and dAVTZ basis sets are equal, however, the values of their exponents are not, reflecting the reparameterisation in literature.²⁶⁵ Using the *MolSSI* basis set exchange Python API module, the additional functions to form the doubly augmented d-aug-cc-pV(T+d)Z basis set was generated for chlorine and is provided in Appendix C.^{237,367} Optimising the XO_2 anion complex with this basis set similarly yields qualitatively incorrect harmonic frequencies and requires the determination of second derivatives at each optimisation step.

Overall, while users should be aware that the inclusion of additional diffuse functions to an Ahlrich basis set is preferable for troublesome cases, the number of primitives with respect to the Dunning bases here (albeit comparing the TZ and QZ quality bases), is not preferable. Secondly, while outside the scope of this work, the intention of performing calculations on these geometries with AVTZ and AVQZ basis sets was that future energy decomposition (via methods such as SAPT2) could lead

Table 4.1: Comparison of the calculated harmonic frequencies of the $\text{Cl}^- \cdots \text{O}_2$ complex for DSD-PBEP86-D3BJ and a number of basis sets with CCSD(T)/AVTZ. In almost all basis sets, second derivatives are required to qualitatively replicate CC harmonic frequencies.

$\text{Cl}^- \cdots \text{O}_2 C_s$						
	AV(T+d)Z	dAVTZ	dAV(T+d)Z	def-2QZVP	def-2QZVPD	CCSD(T)/AVTZ
# Primatives	264	264	324	305	335	
ω_1	119 <i>i</i>	119 <i>i</i>	119 <i>i</i>	126 <i>i</i>	15	14
ω_2	55	56	56	57	57	58
ω_3	1566	1566	1566	1587	1602	1591
	w. CalcAll					
ω_1	25	25	25	24		
ω_2	62	62	62	61		
ω_3	1580	1580	1580	1599		

to the formulation of extrapolation protocols that would exceed the thermodynamic accuracy of the functionals.³⁶⁸ A number of existing protocols have been developed in recent years, however these have typically used the cc-pVnZ bases.^{369–373}

While the structures show the same binding motifs in each of the halide-molecule complexes, for the purposes of this work the most appropriate experimental comparison is that of the VDEs. For each of the halide-molecule complexes these VDEs are compared with both experiment and previous *ab initio* methods to determine the viability of the DSD-PBEP86-D3BJ functional in this context. These VDEs are summarised in Table 4.2 for the AVQZ basis set. In most cases, the double-hybrid used achieves comparable performance to the *ab initio* methods and in some cases ($\text{X}^- \cdots \text{HCCH}$ complexes) appears to perform better. There are examples amongst the test suite, namely the formic acid complexes, where the double-hybrid does perform poorly, particularly for the $\text{Br}^- \cdots \text{syn-HCOOH}$ complex where the experimental ${}^2P_{3/2}$ peak is 4.23 eV while the value for the double-hybrid is 4.47 eV. Despite the encouraging performance of the double-hybrid in these cases, the calibration protocol used in determine detachment energies corrects for systematic errors in the choice of method and basis set (see Appendix B). However as this difference can be accounted for by calibration of the method against experimental photodetachment of the bare halides, the difference between the AVQZ VDEs and those from the AVTZ calculations is small. Given this, and the appreciable increase in computa-

tional cost for larger systems, the exploratory study of halide-propene complexes will include use of the def-2QZVP and AVTZ basis sets.

Table 4.2: Comparison between literature computational (VDE_{Comp}), experimental (VDE_{Exp}) and VDEs determined as part of this work (VDE_{DH-DFT}) for XM complexes ($X = \text{Cl}, \text{Br}, \text{I}$ and $M = \text{O}_2, \text{N}_2, \text{HCCH}, \text{C}_2\text{H}_4, \text{syn-HCOOH}$ and anti-HCOOH).

Complex	Computational Method	VDE_{Comp}	VDE_{Exp}	$VDE_{DH-DFT/AVQZ}$
$\text{Cl}^- \cdots \text{O}_2^{34,300}$	CCSD(T)/CBS	3.66 3.77	3.66 3.77	3.65 3.76
$\text{Br}^- \cdots \text{O}_2^{300}$	CCSD(T)/CBS	3.40 3.85	3.43 3.90	3.40 3.85
$\text{I}^- \cdots \text{O}_2^{300}$	CCSD(T)/CBS	3.09 4.03	3.12 4.06	3.09 4.03
$\text{Cl}^- \cdots \text{N}_2^{57}$	CCSD(T)/CBS	3.69 3.80	3.72 3.83	3.68 3.79
$\text{Br}^- \cdots \text{N}_2^{362}$	CCSD(T)/CBS	3.41 3.86	3.42 3.92	3.42 3.88
$\text{I}^- \cdots \text{N}_2^{362}$	CCSD(T)/CBS	3.08 4.02	3.07 3.92	3.10 4.04
$\text{Cl}^- \cdots \text{HCCH}^{259}$	CCSD(T)/CBS	4.04 4.15	4.1 [†]	4.13 4.24
$\text{Br}^- \cdots \text{HCCH}^{259}$	CCSD(T)/CBS	3.72 4.18	3.81 4.28	3.78 4.24
$\text{I}^- \cdots \text{HCCH}^{259}$	CCSD(T)/CBS	3.33 4.28	3.43 4.37	3.36 4.30
$\text{Br}^- \cdots \text{C}_2\text{H}_4^{363}$	CCSD(T)/CBS	3.52 3.98	3.57 4.05	3.51 3.97
$\text{I}^- \cdots \text{C}_2\text{H}_4^{363}$	CCSD(T)/CBS	3.17 4.11	3.19 4.12	3.17 4.11
$\text{Cl}^- \cdots \text{syn-HCOOH}^{364}$	CCSD(T)/CBS	4.75 4.86	4.67 4.78	4.79 4.92
$\text{Br}^- \cdots \text{syn-HCOOH}^{364}$	CCSD(T)/CBS	4.24 4.70	4.23 4.69	4.47 4.96
$\text{I}^- \cdots \text{syn-HCOOH}^{364}$	CCSD(T)/CBS	3.69 4.63	3.75 4.68	3.71 4.68
$\text{Cl}^- \cdots \text{anti-HCOOH}^{364}$	CCSD(T)/CBS	5.12 5.23	5.07 5.18	5.13 5.24
$\text{Br}^- \cdots \text{anti-HCOOH}^{364}$	CCSD(T)/CBS	4.63 5.08	4.62 5.08	4.65 5.13
$\text{I}^- \cdots \text{anti-HCOOH}^{364}$	CCSD(T)/CBS	4.07 5.01	4.08 5.05	4.07 5.03

[†]: Experimental spectra were not deconvoluted into the two 2P peaks of the Cl in this case.

4.3.2 Halide-Propene Complexes

Computational Results

The optimised structures from the conformer search of the halide/halogen-propene complexes are shown in Figure 4.2. The anion complexes consist of two primary minima, where the halide is bound by coordinating to hydrogen atoms of the propene. These structures represent the bidentate (BiDent) and bifurcated (Bif) structures and are bound with D_0 values between 23.8 kJ mol^{-1} and 30.4 kJ mol^{-1} . In each case the chloride complex is the most strongly bound given that the charge density of the anion decreases moving down the group 17 elements. An additional structure, where the halide appends to the carbene hydrogen, is also optimised for the chloride

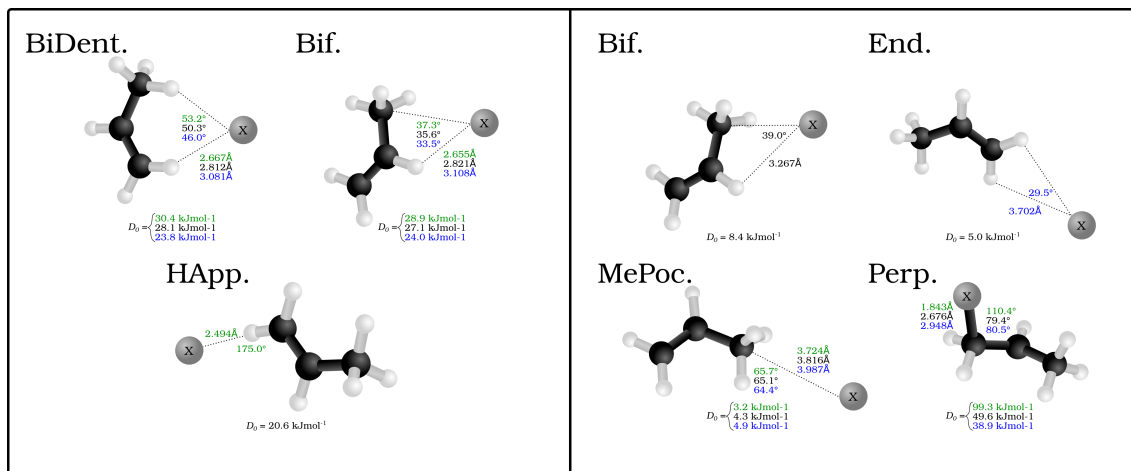


Figure 4.2: Optimised structures of the $\text{X}\cdots\text{C}_3\text{H}_6$ anion (left) and neutral (right) complexes. Structures are calculated with the DSD-PBEP86-D3BJ functional with AVTZ basis sets, with structural differences for the chloride (green), bromide (black) and iodide (blue) complexes. Associated D_0 values are included for each structure.

complex. This suggests that in regions where the electron density is more polarisable, anions with higher charge density are more suited to these interactions. As noted in Section 4.3.1, where the only available electrostatic interactions are those of carbene hydrogens as in the halide-ethene complexes, these interactions can compete with the ion-induced dipole interaction of the alkene. Noting that the hydrogen appended complexes are minima for each halide (excluding the $\text{I}^-\cdots\text{C}_2\text{H}_4/\text{AVQZ}$), they are also similarly stable to that of the $\text{Cl}^-\cdots\text{C}_3\text{H}_6$ hydrogen appended complex. In these structures, the ion-induced dipole interaction of similar strength to the hydrogen appended structure ($D_0 \approx 20 \text{ kJ mol}^{-1}$) however when they are available in propene, a purely electrostatic interaction is more stable.

A similar number of neutral complexes have been optimised for the halogen-propene complexes (also in Figure 4.2). While a selection of these are minima in the bromine and iodine complexes, namely the bifurcated (Bif) and carbene appended (End), the two structures that yield minima in all halogens are those where the halogen rests inside the methyl group pocket (MePoc) or interacts with the π -system of the propene (Perp). The MePoc structures are weakly bound ($D_0 = 3.2 \text{ kJ mol}^{-1}$ to 4.9 kJ mol^{-1}) as is expected for vdW complexes, and we note that the D_0 halide trend establish inverts for the corresponding halogens. This is attributed to the

polarisability of the halogen atoms in each case, with those that are more diffuse and polarisable able to form stronger transient interactions. Those complexes where the halogen is interacting with the π -system are bound stronger than even the corresponding halide complexes. For the bromine and iodine complexes the D_0 values are 49.6 kJ mol^{-1} and 38.9 kJ mol^{-1} respectively and the halogen is bound equidistant from the two unsaturated carbons. In the chlorine complex however there is a distinct contraction of the C–Cl distance to 1.843 \AA and the $\angle_{\text{X}-\text{C}=\text{C}}$ increases to 110.4° as the chlorine binds with the terminal carbon forming a 1-chloropropyl radical. The associated D_0 of this complex is significantly higher (99.3 kJ mol^{-1}) and representative of an intermediate for the free-radical addition of chlorine to the alkene. This insertion agrees with previous theoretical studies in that gas-phase chlorine insertion occurs preferentially on the terminal carbon and that the Cl–C distance and $\angle_{\text{Cl}-\text{C}-\text{C}}$ angle correspond to literature MP2/AVDZ structures.^{374–376}

Time-Of-Flight Mass Spectrometry

The mass spectra produced from each of the gas mixtures are presented in Figures 4.3, 4.4 and 4.5 in the chronological order in which they were recorded. Regarding the systems studied, these represent the bromide, iodide, and chloride gas mixtures respectively for the reasoning outlined in Section 4.2. Full mass spectral assignment are outlined in Appendix C (page 409), however, important peak and features will be described here.

Figure 4.3 is the mass spectrum produced from the $\text{CH}_2\text{Br}_2:\text{C}_3\text{H}_6:\text{Ar}$ gas mixture. Immediately apparent are the two sets of calibration peaks corresponding to the $^{35,37}\text{Cl}^-$ and $^{79,81}\text{Br}^-$ anions. There is also a peak at 77 m/z which corresponds in mass to $^{35}\text{ClC}_3\text{H}_6^-$ is assigned to the formation of the $^{35}\text{Cl}^- \cdots \text{C}_3\text{H}_6$ complex. This complex formation also contributes to the now unequal intensities of the bromide peaks, highlighted in the inset of Figure 4.3, as the corresponding ^{37}Cl complex isobaric with the ^{79}Br peak. While not the intended spectroscopic target in this gas mixture, PES spectra of the 77 m/z peak were recorded in case later experiments

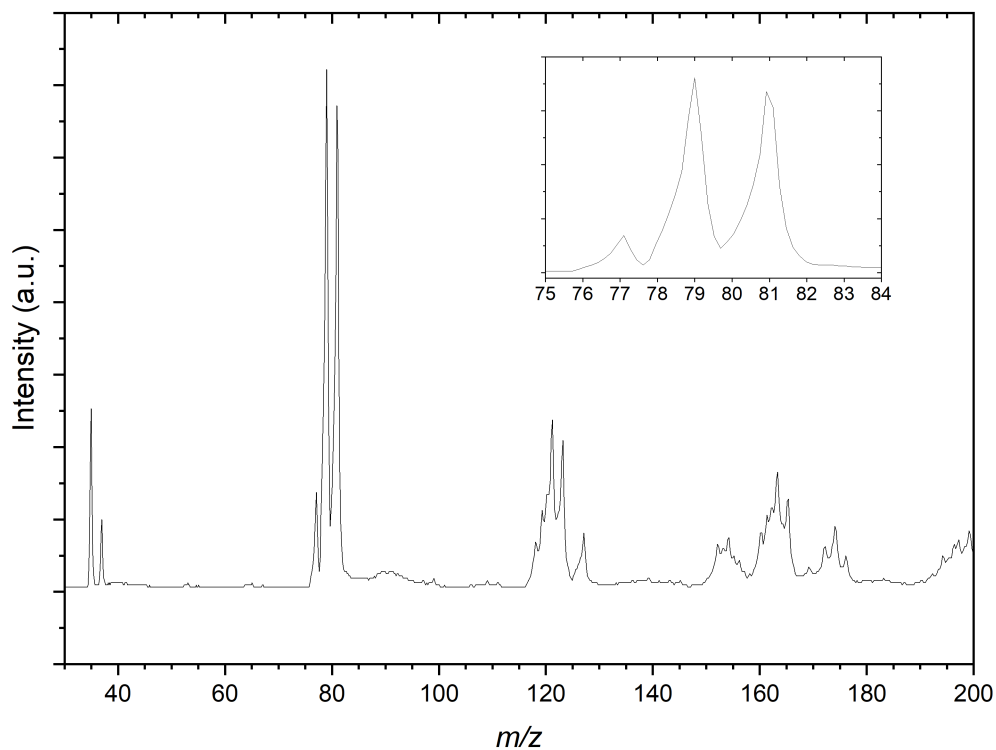


Figure 4.3: Mass spectrum resulting from the $\text{CH}_2\text{Br}_2:\text{C}_3\text{H}_6:\text{Ar}$ gas mixture. The spectrum shows mass peaks resulting from the bare Cl^- anions and propene complexes with Cl^- and Br^- . Inset: the bare Br^- is believed to be isobaric with the $^{37}\text{Cl}^-\cdots\text{C}_3\text{H}_6$ complex.

on the CCl_4 gas mixture proved unsuccessful. These are included in Appendix C (page 411) along with corresponding a deconvoluted Cl^- PES spectrum.

A number of other structures are present in the mass spectrum in the regions of 115-125 m/z and 150-175 m/z . These peaks are taken to be a combination of several isotopic combinations of CCl_4 and a similar contaminant CHCl_3 from previous experiments. For the region of 115-125 m/z , combinations of CHCl_3^- here expected but not assigned as the vdW complex $\text{Cl}^- \cdots \bullet\text{CHCl}_2$, would result in peaks with m/z values of 118, 120, 122 and 124 respectively. The $^{81}\text{Br}^- \cdots \text{C}_3\text{H}_6$ complex would be expected to have a m/z value of 123 and there is a peak in this structure that indeed does. As this peak appears sufficiently resolved, PES spectra of this mass peak would not be expected to contain other contaminant complexes, however when undertaking photodetachment within such a congested region this should be kept in mind. The other structures within the mass spectrum which are similarly congested are made up of what is believed to be likewise isotopic combinations of $\text{Cl}^- \cdots \text{CHCl}_3$ and $\text{Cl}^- \cdots \bullet\text{CCl}_3$ (with $(n_{35}, m_{37}) = (4, 0), (3, 1), (2, 2), (1, 3)$ and $(0, 4)$). These species are not typically expected to be formed under normal dissociative electron attachment conditions, however a breakdown of the piezo disk crystal over time is associated with small arcing within the nozzle module. This may have acted as a discharge source within the gas mixture to produce more exotic anionic species.

Comparatively, the mass spectrum of the $\text{CH}_3\text{I}:\text{C}_3\text{H}_6:\text{Ar}$ gas mixture (Figure 4.4) is not significantly congested. In the lower m/z range shown, the residual bromide anion peaks are still detected however the spectrum is now dominated by the iodide signal. These three peaks are used for a preliminary calibration that is then improved upon with inclusion of the next most intense signal at 269 m/z representing the $\text{I}^- \cdots \text{CH}_3\text{I}$ complex commonly seen in previous CH_3I gas mixtures.³⁷⁷ The other peaks within the mass spectrum represent these two primary iodide sources solvated by propene molecules, with $\text{I}^- \cdots (\text{C}_3\text{H}_6)_n$ and $\text{I}^- \cdots (\text{CH}_3\text{I})(\text{C}_3\text{H}_6)_n$ ($n = 1-3$) present.

Finally the mass spectrum of the $\text{CCl}_4:\text{C}_3\text{H}_6:\text{Ar}$ gas mix is presented in Figure 4.5. There is a congested 117-125 m/z region in the mass spectrum similar to that

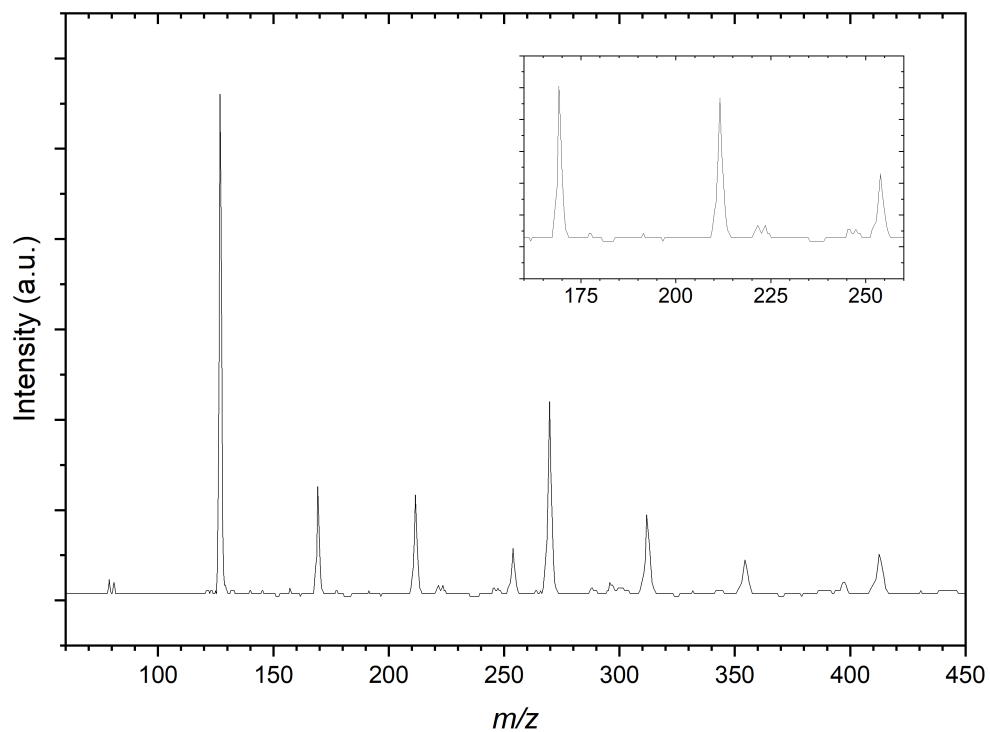


Figure 4.4: Mass spectrum resulting from the $\text{CH}_3\text{I}:\text{C}_3\text{H}_6:\text{Ar}$ gas mixture. The spectrum shows mass peaks resulting from the bare Br^- anions and propene complexes with I^- . Inset: highlighted the peaks at $169, 211$ and 254 m/z assigned to the $\text{I}^- \cdots (\text{C}_3\text{H}_6)_n$ ($n = 1-3$) complexes.

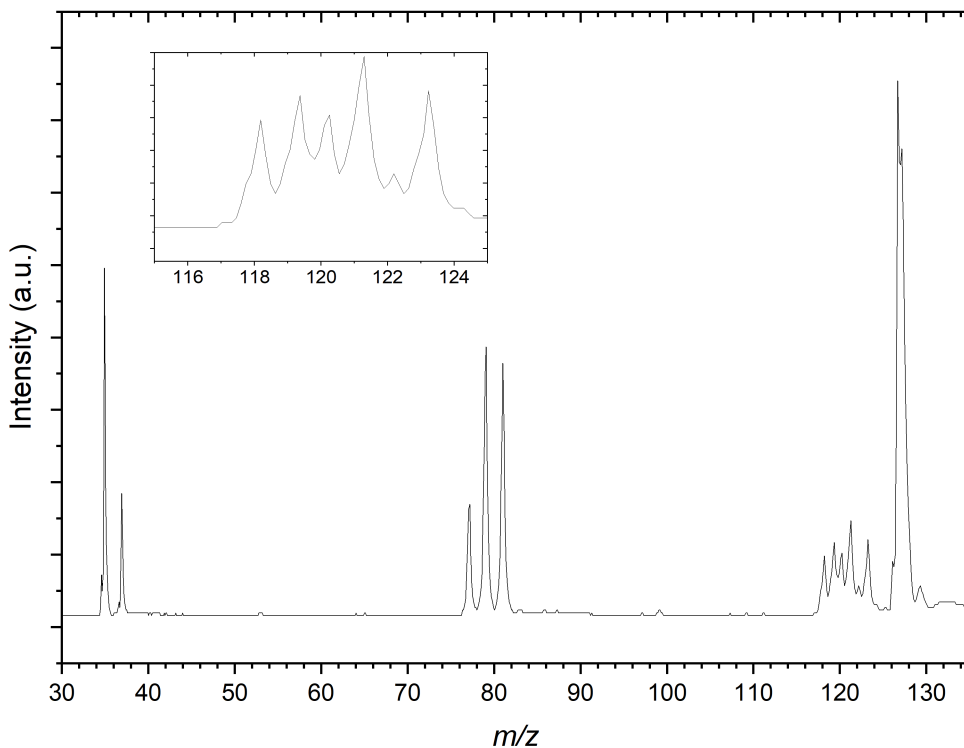


Figure 4.5: Mass spectrum resulting from the $\text{CCl}_4:\text{C}_3\text{H}_6:\text{Ar}$ gas mixture. The spectrum shows mass peaks resulting from the bare halides and propene complexes with both Cl^- and Br^- . Inset: highlighted the peaks at $118\text{--}124$ m/z assigned to the $\text{Br}^-\cdots\text{C}_3\text{H}_6$ and $\text{Cl}^-\cdots(\text{C}_3\text{H}_6)_2$ complexes.

of Figure 4.3 however this is significantly more resolved than for the previous spectrum. The resolution in this region in the presented spectrum does not adequately resolve these peaks. This is attributed predominantly due to the optimisation of space focussing of the TOF plates and einzel lenses for the calibration peaks. It is because of this resolution and congestion that a number of the peaks are assigned to complexes of bromide and argon as well as the previously noted $\text{Cl}^-\cdots(\text{C}_3\text{H}_6)_2$ complexes. The mass range is restricted here by comparison to the CH_3I gas mixture however there are clear formation of both the $^{35}\text{Cl}^-\cdots\text{C}_3\text{H}_6$ and $^{81}\text{Br}^-\cdots\text{C}_3\text{H}_6$, distinct from contaminant isobaric species.

Photoelectron Spectra

Each of the photoelectron spectra were calibrated against accurately determined electron binding energy (E_{BE}) values of resolved 2P transitions of the bare halides.

For the spectra taken of mass signals in Figure 4.3 the $^{81}\text{Br}^-$ signal was used, whereas for the mass spectra in Figures 4.4 and 4.5 I^- forms the calibration. Each spectrum is calibrated using Equation 4.4 and the recorded TOF values from these calibration spectra. Each calibration is then detailed in Table C4 (page 410). There is often slight variation in the calibration spectra between days of PES experiments. This is due to the reoptimisation of the TOF-PES parameters to maximise the ion signal in the mass spectrum. Even small changes in the beam alignment, typically to account for the deposition of gases on the metallic components and subsequent interference in their electric field properties, can affect the total path length of the photoelectrons and the region of photodetachment within the magnetic bottle.

$$E_{BE} = h\nu - \left(\frac{A}{TOF^2} + B \right) \quad (4.4)$$

The photoelectron spectrum of the 77 m/z peak from Figure 4.5 is shown in Figure 4.6. The spectrum consists of a single broad feature that is attributed to transitions to the two perturbed 2P states of the chlorine. A pair of Gaussian functions is fitted to the spectrum as per Equation 2.11 with an R^2 value of 0.9848. While the intensities of the fit are arbitrary and are normalised for the purposes of presentation here, the σ value from the fit is 85.6(4) meV. The determined E_{BE} values for the perturbed $\text{Cl}^- \cdots \text{C}_3\text{H}_6$ states are then 3.89(1) eV and 4.00(1) eV respectively. This is indicative of a relatively strong vdW interaction as the E_{stab} of the chloride complex is 0.28 eV (27.1 kJ mol $^{-1}$). Comparing this experimental stabilisation with that of the DSD-PBEP86-D3BJ/AVTZ values, the closest calculated VDE belongs to the bifurcated structure ($E_{stab}=27.5$ kJ mol $^{-1}$). While it is tempting to therefore assigned the detachment to this conformer, the resolution of the experiment is such that this is not conclusive. Given the similarity in the D_0 values for the bidentate and bifurcated structures, the formation of the complex is likely driven by collision theory and the orientation of the monomers under complex formation. Similarly, considering the solid angle of the approaching chloride to the

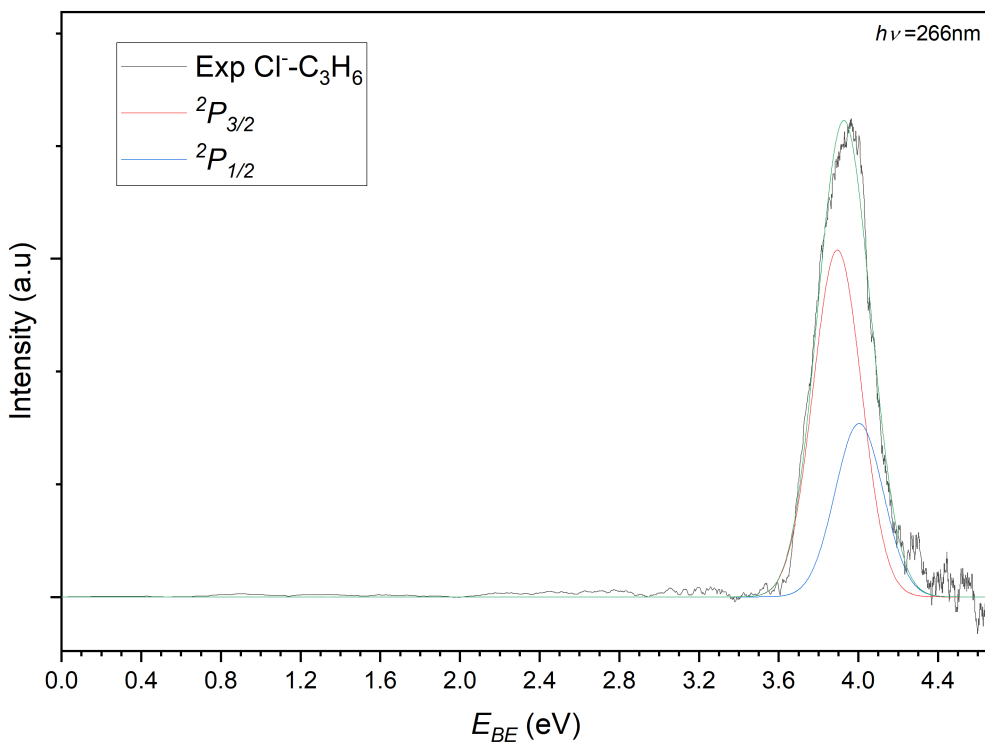


Figure 4.6: Photoelectron spectrum of the $77\text{ }m/z$ peak from Figure 4.5. The spectrum is deconvoluted into two gaussians representing the perturbed $^2P_{3/2}$ (red) and $^2P_{1/2}$ (blue) states of the $\text{Cl}^- \cdots \text{C}_3\text{H}_6$ complex.

propene, the interaction between the formal charge of the halide and the π -system of the propene would likely be repulsive and redirect the incoming halide to regions of attractive interaction. While the third hydrogen-appended structure is present of the chloride complex, it is relatively weaker bound, and would likely represent a meta-stable conformation.

In recording the bromide-propene spectrum, the $123\text{ }m/z$ peak in Figure 4.3 was targeted. The resulting PES is shown in Figure 4.7 and is attributed to the $^{81}\text{Br}^- \cdots \text{C}_3\text{H}_6$. These transitions are assigned similarly to the chloride complex and have E_{BE} values of 3.59 eV and 4.01 eV for transitions to the perturbed $^2P_{3/2}$ and $^2P_{1/2}$ states of the bromine. The E_{stab} of the complex is then determined to be 0.23 eV (22.2 kJ mol^{-1}), highlighting the relative strength of the interaction in the chloride complex. The inset of Figure 4.7 details the tailing features of the $^2P_{1/2}$ peak. Typically these features are more resolved than those of the $^2P_{3/2}$ peak as

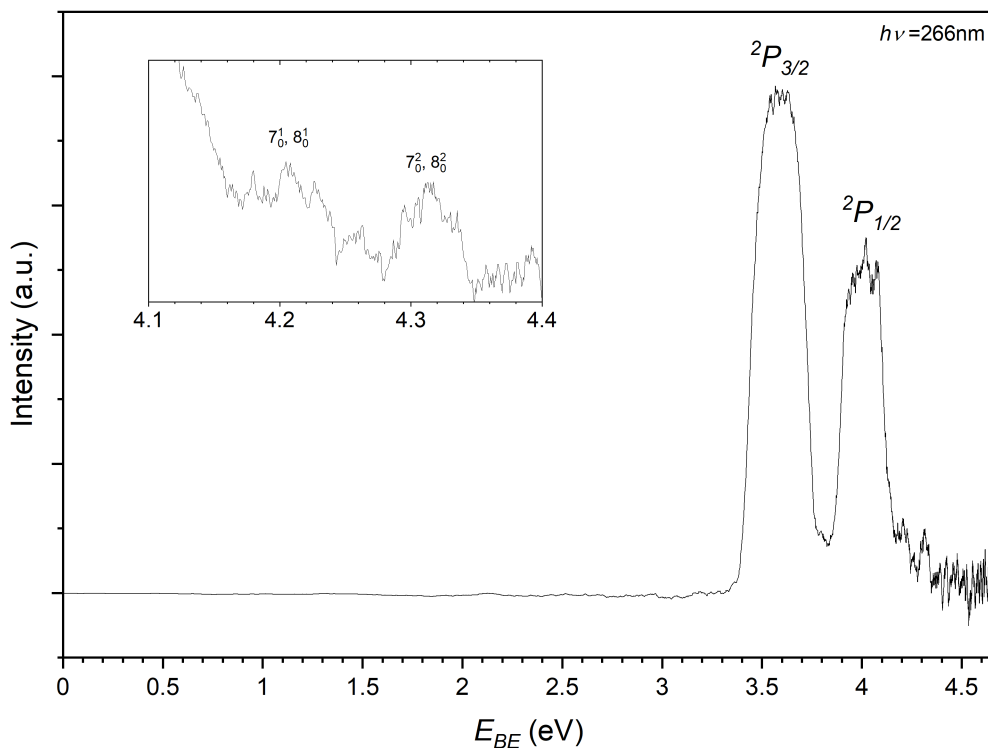


Figure 4.7: Photoelectron spectrum of the $123\text{ }m/z$ peak from Figure 4.3 assigned to photodetachment to the perturbed $^2P_{3/2}$ and $^2P_{1/2}$ states of the $\text{Br}^- \cdots \text{C}_3\text{H}_6$ complex. Inset: expanded view of the vibrational structure present at higher E_{BE} than the $^2P_{1/2}$ peak. This is tentatively assigned to progressions in the ω_7 (936 cm^{-1}) and ω_8 (942 cm^{-1}) modes.

the detector is less saturated and the features are closer to the photon energy. There are two features present in this region with E_{BE} values of 4.21 eV and 4.31 eV respectively. Within the main $^2P_{1/2}$ peak there is some additional structure with features at 4.02 eV and 4.08 eV . While less resolved, some structure is present within and shouldering the $^2P_{3/2}$. These transitions correspond to 3.62 eV and 3.79 eV .

As the bromide-propene complex has calculated bifurcated minima structures in the anion and neutral, the PES can be modelled with *ezSpectrum 3.0* and is presented in Figure 4.8.²⁵⁶ Full FCFs with Duschinsky rotations from these calculations are included in Table C21 (page 428) and as the spin-orbit states in this context only represent a change to the band origin, are only included for the $^2P_{3/2}$ however the vibronic behaviour is the same in both cases here. The band origin, corresponding to the adiabatic detachment energy (ADE), is 3.563 eV with the next transition at

3.616 eV corresponding well to the experimental feature within the main $^2P_{3/2}$ peak. This represents a 5_0^1 vibronic transition with the ω_5 (424 cm^{-1}) mode corresponding to a C–C–C bending mode of the propene. Notably the energy difference between this feature and the ADE corresponds to the same peak separation in the $^2P_{1/2}$ peak. Allowing for the assignment of these 4 features. The feature residing between the two perturbed 2P peaks has an E_{BE} of 3.79 eV and agrees well with the modelled 7_0^2 and 8_0^2 overtones ($E_{BE}=3.795\text{ eV}, 3.797\text{ eV}$). Here the ω_7 (936 cm^{-1}) and ω_8 (942 cm^{-1}) modes represent the C–CH₃ stretch and a number of coupled C–H bending modes. The same modes are assigned to this progression present in the $^2P_{1/2}$ peak (4.21 eV and 4.31 eV). This vibrational structure suggests that transitions to the bifurcated neutral, importantly from the corresponding anion complex, are indeed present. It is not clear whether the same structure is present for the bidentate complex as no corresponding neutral was optimised. Given the neutral geometry would represent a highly vibrationally excited analoge of the bidentate complex the VDE, while not an experimentally observable quantity, would then likely correspond to some potentially unbound excited state. Similarly to the chloride complex, it is expected that both complexes are observed experimentally and cannot be distinguished at the current resolution.

Finally the iodide-propene complex PES is recorded by photodetachment of the 169 m/z peak in Figure 4.4 and shown in Figure 4.9. As with the previous PES spectra for the chloride and bromide complexes, the spectrum features two main peaks representing detachment to the perturbed 2P states of the iodine in an I[−]…C₃H₆ complex. The E_{BE} of these peaks are determined to be 3.26 eV and 4.20 eV, equating to an E_{stab} value of 0.20 eV (19.4 kJ mol^{-1}). In the higher E_{BE} region from the $^2P_{1/2}$ peak similar vibrational structure can be seen to that of the bromide complex. Two bands are determined with one having E_{BE} values of 4.35, 4.40, 4.45 and 4.50 eV ($\Delta E_{BE} = 0.05\text{ eV} = 403\text{ cm}^{-1}$) corresponding to a progression in the C–C–C bend ($\omega_5 = 420\text{ cm}^{-1}$). The other band is only determined with two peaks 4.47 and 4.52 eV and is assigned to a combination band of the bending mode and a C–C–C

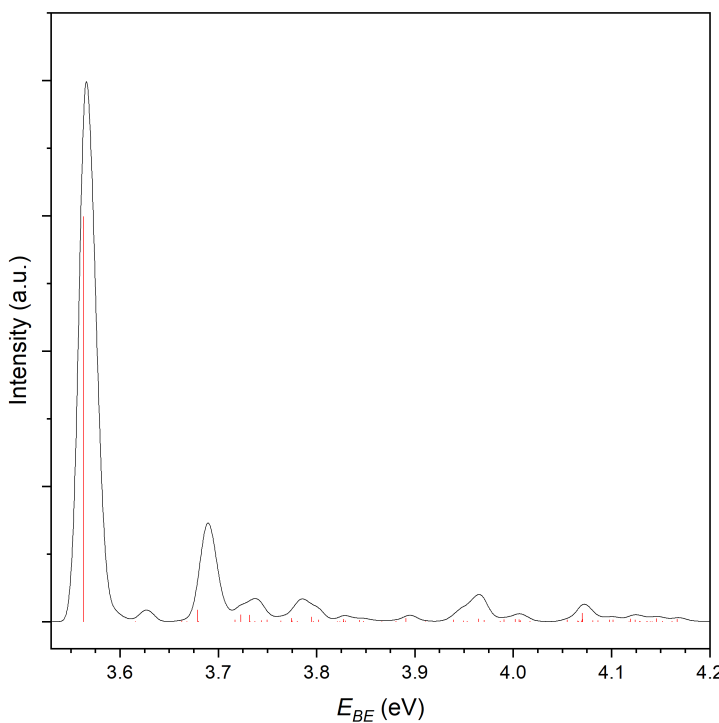


Figure 4.8: Simulated photoelectron spectrum for the $^2P_{3/2}$ photodetachment of the $\text{Br}^- \cdots \text{C}_3\text{H}_6$ complex. Stick spectra (red) represent the individual FCFs calculated. The black trace is a gaussian convolution with width, $\omega = 0.005$.

internal twisting mode ($\omega_3 = 160 \text{ cm}^{-1}$). Both transitions represent transitions to the complex where the halide is interacting with the π -system perpendicularly to the plane of the propene.

Collectively, the halide-propene complexes are bound by the electrostatic interaction of the anion, with the relatively strong D_0 values in each case dominated by the anion interaction. Moreover, the respective charge density of the anion correlates with the strength of the interaction. This is reflected by the E_{stab} values of 27.1 kJ mol^{-1} , 22.2 kJ mol^{-1} and 19.4 kJ mol^{-1} for the Cl^- , Br^- and $\text{I}^- \cdots \text{C}_3\text{H}_6$ respectively. In comparing the bidentate and bifurcated conformers of each of the halide complexes, the E_{stab} values indicate that those halides that are larger (Br , I), are sterically unfavoured in residing in the interacting regions when compared to the chloride complexes. The vibrational progressions present in the iodide and bromide complexes suggest that detachment from the bound anions, of which both the bifurcated and bidentate conformers are most likely, to a vibrationally excited

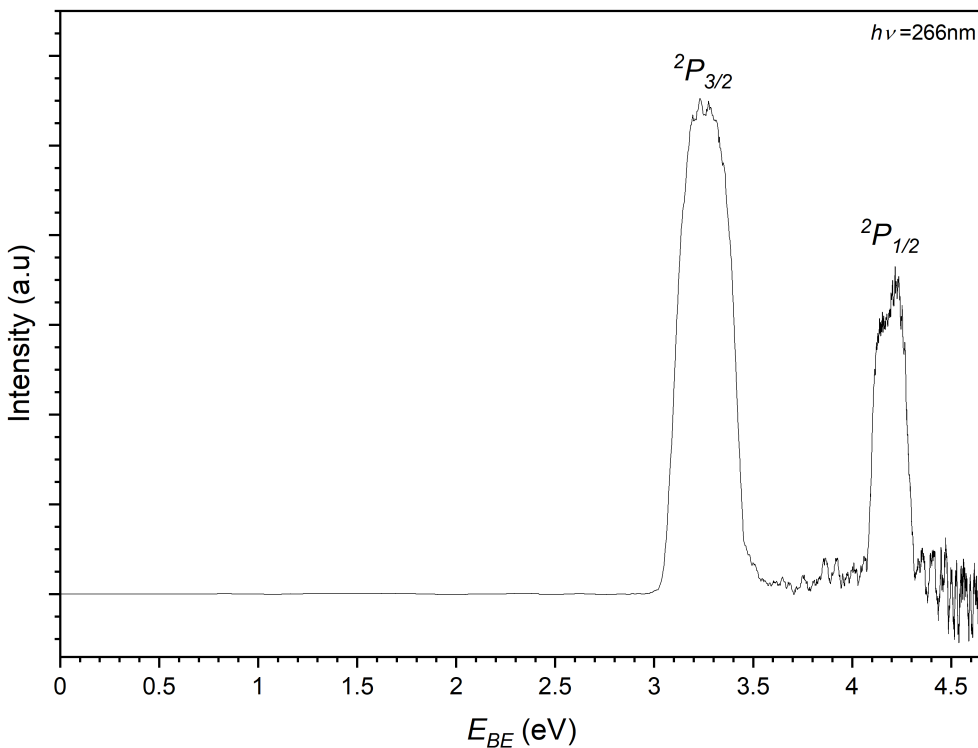


Figure 4.9: Photoelectron spectrum of the $169\text{ }m/z$ peak from Figure 4.4 assigned to photodetachment to the perturbed $^2P_{3/2}$ and $^2P_{1/2}$ states of the $\text{I}^- \cdots \text{C}_3\text{H}_6$ complex.

region of the neutral. Given that the most stable neutral complexes are those where the halogen interacts with the π -system reminiscent of a free-radical addition to the alkene, detachment to these states may serve to lock the halide in the vdW region prior to initiation. Here the use of anion PES allows for photodetachment to regions of the neutral potential energy surface that may not be typically accessible in neutral spectroscopy. These neutral interactions can also be compared to those of previously studied halide-alkene systems, namely the halide-ethene complexes.³⁶³ In these complexes, where the interaction dominated by the perturbation of the π -system, the strength of interaction is lower than when a purely hydrogen bonding environment is available. The E_{stab} values for the halide-ethene complexes are 0.21 eV (19.5 kJ mol^{-1}) and 0.13 eV (12.6 kJ mol^{-1}) for bromide and iodide respectively. The stability of the bromide complexes is not dissimilar, while there is a significant stabilising effect when increasing the length of the alkene in the iodide complexes. Again it is expected that the interaction is balanced by the charge

density of the anion and its size with respect to the physical interacting region.

4.4 Summary

To summarise, halide-propene complexes have been produced in the gas-phase and their photoelectron spectra are presented. The experimental E_{BE} values, representing transitions to perturbed 2P states of the halogen, are 3.89 eV and 4.00 eV, 3.59 eV and 4.01 eV, and 3.26 eV and 4.20 eV. DSD-PBEP86-D3BJ/AVTZ calculations have also been completed to determine structures of a number of anion and neutral complexes. To validate the double-hybrid for use in these cases, a suite of validation calculations were also completed for comparison with previously studied halide-molecule complexes. These generally showed good agreement with previous experiments however in troublesome cases, use of additional diffuse functions in an Ahlrich def-2QZVPD basis set was the only basis set to yield qualitatively correct harmonic frequencies. With all other basis sets, calculating second derivatives at each optimisation step was required. Each of the calculated halide-propene structures correspond to photodetachment from either a bidentate or bifurcated structure where the interaction is dominated by the electrostatics interaction of the anion and hydrogen atoms. Given the energy resolution of the PES spectrometer, the two conformers cannot be distinguished however vibrational structure in the $\text{Br}^- \cdots \text{C}_3\text{H}_6$ spectrum indicates that the bifurcated structure is present at least here. The most stable neutral conformers are those where the halogen interacts with the π -system of the C=C bond in each case. For the chlorine complex, this also results in insertion into the double bond at the terminal carbon, producing a 1-chloropropyl radical.

Chapter 5

Halide-Butadiene Complexes

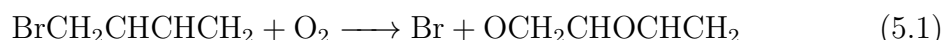
5.1 Introduction

In recent years, much interest has been generated as to the formation of large carbon aggregations from monomer units in the ISM. Unlike propene, direct observation of 1,3-butadiene has not been shown as of yet, but as 1,3-butadiene represents an important potential intermediate that reacts with radical species to produce larger carbon units (see Equation 4.1c), it still remains of astrochemical interest. Currently, butadiene is believed to form in extraterrestrial ices, particularly methane ices with the addition of monomer radical species.³⁷⁸ As the property of butadiene that supports this hydrocarbon growth is its degree of unsaturation, a number of studies have investigated the reaction of radical species with butadiene as pathways within this larger astrochemical process. Also noted in Chapter 4, the addition reaction of the ethynyl radical ($\bullet\text{C}_2\text{H}$) yields the formation of benzene, and similar mechanisms are proposed for the formation of produce nitrogen containing heterocycles and substituted naphthalenes.³⁵⁰ These include reactions with cyano ($\bullet\text{CN}$), phenyl ($\bullet\text{C}_6\text{H}_5$) and *meta*-tolyl ($\bullet\text{C}_7\text{H}_7$) radicals respectively.^{379–381}

Alternatively, butadiene is a notable product of combustion reactions and occurs from both anthropogenic sources in the burning of fuel mixtures as well as natural sources such as from forest fires.^{382,383} In combustion reactions, one such

mechanism for butadiene formation is from the decomposition of the C₈H₁₂ diradical which occurs on a picosecond timescale.³⁸² Once formed, it undergoes similar radical chemistry to produce larger carbon aggregates believed to be precursors to soot formation.³⁸⁴

Atmospherically, brominated butadiene radicals activate the oxidation of butadiene with a weaker Br–C bond forming a good leaving group and addition site on the neighbouring carbon, as illustrated in Equation 5.1.



The rate constant for this reaction is then $4.7 \times 10^{-13} \text{ cm}^{-3} \text{ molecule}^{-1} \text{ s}^{-1}$ at 298 K and 700 Torr.³⁸⁵ For the chlorinated analogue, the stronger Cl–H interaction is believed to favour hydrogen abstraction reactions and the formation of corresponding radicals. The experimentally measured rate constant for the reaction of chlorine atoms with butadiene here is $3.31 \times 10^{-10} \text{ cm}^{-3} \text{ molecule}^{-1} \text{ s}^{-1}$.³⁸³ The structure of these intermediates involve the insertion of the halogen into the C=C bond, bonding with the terminal carbon.

Despite the importance of butadiene radical interactions in both atmospheric and extraterrestrial environments, there are few studies investigating the geometric and electronic structure of these complexes. Halide-butadiene complexes represent good analogues of these systems as they utilise the different bonding motifs of the anion to spectroscopically investigate other regions of the neutral potential energy surface. Additionally, as the halides represent simple analogues or stand-ins for a number of anion-molecule interactions, investigating the structure of these complexes may provide insight into the radical chemistry present in extraterrestrial environments. While these reactions may be modelled as well behaved bimolecular systems, the role of gas-phase solvation may also be important in their structure and reactivity.³⁸⁶

Study of halide-butadiene systems may also provide insight into the pre-reaction vdW complexes of important synthetic reactions, namely the Diels-Alder reaction,

pericyclic reactions of dienes that form a suite of ring structures.³⁸⁷ The stereoselectivity of these products is governed by the structure of the pre-reaction adduct prior to the concerted ring-closing mechanism, and by substituting the dieneophile for a model anion may provide insight into these reactions.³⁸⁸

This chapter investigates a number of solvated halide-butadiene complexes using a combination of theoretical methods and anion photoelectron spectroscopy. The electronic structure of solvated systems is approached by the electronic stabilisation energy of each successive solvated butadiene molecule (denoted E_{solv}). From these energies and the binding motifs present, insight can be gained as to the structure of larger solvated species.

5.2 Methods

5.2.1 Experimental Methods

Gas mixtures were prepared by introduction of the relevant halide source followed by a partial pressure of 1,3-butadiene (*Sigma-Aldrich* >99 %, 100 g) and then made up to operational pressure (450 kPa). Each of the halide sources used correspond to those from previous halide-propene experiments (CCl_4 , CH_2Br_2 and CH_3I). When making up the gas mixtures, the lights were switched off to reduce any potential light-activated cycloadditions in the line of the gas mixing station. The clear teflon gas line that connected the gas mixing station to the piezo nozzle assembly was also covered in aluminium foil.

The original gas mixture, consisting of $\text{CH}_3\text{I}:\text{C}_4\text{H}_6:\text{Ar}$ was made with trace methyl iodide and a partial pressure of 30 kPa of 1,3-butadiene. This however did not yield significant intensities in the mass spectrum to perform PES and the gas mixture was remade with a higher partial pressure of 50 kPa. The improved intensities in the mass spectrum informed the later CH_2Br_2 and CCl_4 gas mixtures and this partial pressure of 1,3-butadiene remained unchanged. Similarly to halide-propene

experiments, trace amounts of each of the halide sources were introduced by exposure to the evacuated gas mixing station, guided by the calculated vapour pressures in Table 2.2.

In attempting to form larger clusters the beam energy was increased to -2200 V for the CH_3I gas mixture to improve the beam stability and the influence of stray fields. While this broadened the peaks presented, the associated reduction in energy resolution was acceptable to form highly solvated 1,3-butadiene complexes as the spin-orbit splitting of the 2P states of iodine is greatest of the selected halides. For the corresponding Br^- and Cl^- spectra, the beam energy was reduced to -1500 V to adequately resolve the 2P peaks and reduce the width of fitted Gaussian functions respectively. The timescale of the experiment is such that the voltage is applied to the TOF plates at $T_0 + 404.34\text{ }\mu\text{s}$ and the laser is Q-switched at $+22.91\text{ }\mu\text{s}$ relative to the TOF plates to intersect the laser pulse with I^- in the ion beam. This was particularly important for larger $\text{I}^- \cdots (\text{C}_4\text{H}_6)_n$ complexes as the correlation between the Q-switch timing and the ion TOF was used to guide temporal photodetachment searches.

PES spectra were analysed in two different approaches. For the Br^- and I^- PES spectra, where the 2P peaks are resolved, the peak positions are determined by averaging the E_{BE} values at half-maximum intensity for each peak. For the Cl^- spectra, the peak positions are determined by fitting a pair of Gaussian functions as per Equation 2.11.

5.2.2 Computational Methods

The DSD-PBEP86-D3BJ double-hybrid functional with def-2QZVP and AVTZ basis sets was used to perform a conformer search for both the *cis*- and *trans*-1,3-butadiene halide and halogen complexes. Starting geometries utilised a number of different bonding arrangements with respect to the double bonds of the butadiene molecules similarly to previously studied ethene and propene complexes.³⁶³ These

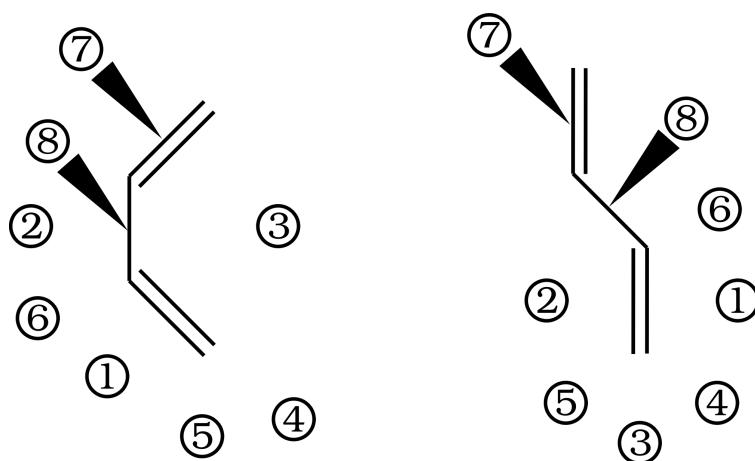


Figure 5.1: Starting geometries for the $X \cdots C_4H_6$ complexes. Each structure referred to in text is numbered by the location of the halide/halogen for both the *cis* (left) and *trans* (right) isomers.

included where the halide or halogen bifurcates the $C=C$ or $C-C$ bond, is bidentate coordinated by the butadiene, appends to a single hydrogen or is bound out-of-plane from the butadiene. Due to the number of these conformers each is numbered for *cis*- and *trans*-1,3-butadiene as per Figure 5.1 and referred to in text as such. The starting geometries are generally numbered with an order representing the bifurcation of a bond or bisection of an angle, followed by hydrogen-appended geometries, followed by out-of-plane interactions with a bond.

All structures were screened by harmonic frequency calculations using the associated basis set of their optimisation. For the *trans*-1,3-butadiene complexes, conformers were screened to be minima, however the *cis*-1,3-butadiene monomer is itself a transition state where the imaginary mode represents a rotation around the $C-C$ bond. For these complexes, while D_0 values are also reported as they provide an indication as to the relative stability of the complexes, the reduction in the imaginary mode compared to the monomer is also considered. Similar protocols to those used in Chapter 4 for the determination of VDEs of the respective complexes was then undertaken, with only halide-*trans*-butadiene complexes considered.

5.3 Results and Discussion

5.3.1 Computational Results

A number of both anion and neutral structures have been determined for the halide/halogen-butadiene complexes (Figure 5.2). For the anion complexes the minima are the 1, 2 and 4*trans* conformers, with the most stable for all three halides being the 2*trans*. In this conformer, the halide is bound to hydrogens attached to the 1 and 3 carbons in the butadiene. This electrostatic interaction is approximately ~30% more stable than the next conformer (1*trans*), where the halide bifurcates the C=C bond. Additional structures are also present in the bromide and chloride complexes, where the halide appends to a hydrogen on the terminal carbon. These structures exhibit similar bonding motifs to the halide-propene complexes, with the bidentate structure again for those complexes the most stable. Each of the halide structures also shows trends in their D_0 values that correspond to the halide-propene complexes, with the chloride complex the most stable and the iodide complex the least stable in each structure. Comparing the two bidentate complexes in the halide-propene and halide-butadiene complexes, the larger hydrocarbon chain is more stable. This is attributed to the ability of the diene to delocalise the donated electron density such that the charge density gradients are constructive, whereas in the propene complex the induced dipoles contain destructive vector components.

For the *cis*-butadiene complexes, while none of them are determined to be minima, the complexes are still stabilised compared to the monomer units. For the four structures present, each exhibit the same bonding motifs as their *trans* counterparts; either bifurcating a CC bond, bidentate coordination, or appending to a terminal hydrogen. Comparing the imaginary mode representing the rotation around the C–C bond in each of the complexes (in this case the Cl^- complexes) with that of the monomer ($182\text{i}\,\text{cm}^{-1}$), the 1*cis* ($163\text{i}\,\text{cm}^{-1}$), 2*cis* ($171\text{i}\,\text{cm}^{-1}$) and 5*cis* ($139\text{i}\,\text{cm}^{-1}$) structures do not significantly stabilise the rotation. The 2*cis* structure however has a frequency of $49\text{i}\,\text{cm}^{-1}$, as the two coordinating hydrogens lie on either side of the

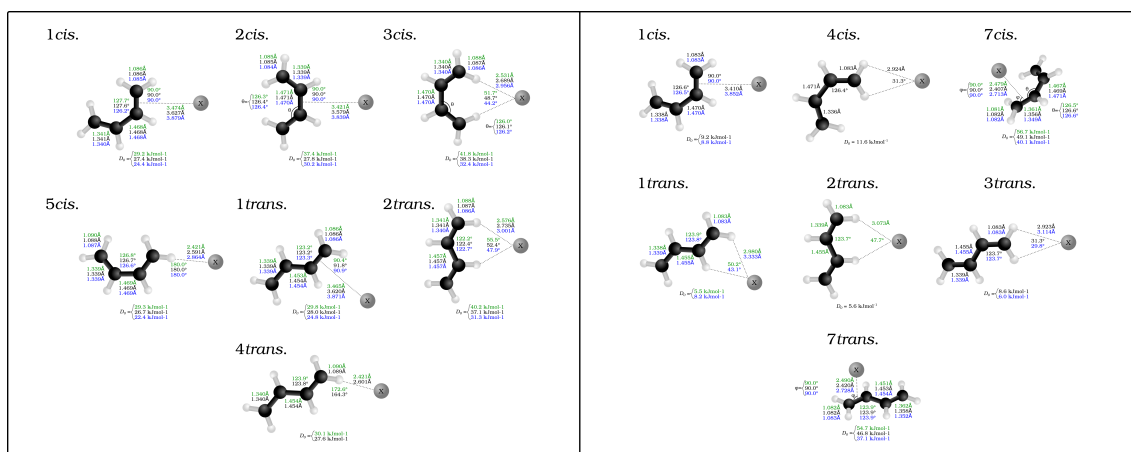


Figure 5.2: Optimised structures of the $X \cdots C_4H_6$ anion (left) and neutral (right) complexes. Structures are calculated with the DSD-PBEP86-D3BJ functional with AVTZ basis sets, with structural differences for the chloride (green), bromide (black) and iodide (blue) complexes. Associated D_0 values are included for each structure.

C–C bond and as such the complex formation stabilises the rotation. While still an imaginary mode for each of the halides studied here, an anion with higher charge density such as fluoride may yield a stabilised *cis*-butadiene complex.

In the neutral complexes each of the vdW complexes exhibit similar D_0 values to the comparative halide-propene complexes discussed in Chapter 4. The most stable neutral complexes are the *7cis* and *7trans* structures respectively, as the halogen exhibits similar interaction with the *pi*-system as the halogen-propene complexes. Despite the increase in complex stability in these cases, the *7cis* structure still retains the imaginary mode ($132i\text{ cm}^{-1}$) and it is not significantly stabilised with respect to the butadiene monomer. The *7trans* structure however is reminiscent of the prereaction adduct in radical activation of butadiene by bromine to produce peroxy radicals, as reported in the literature³⁸⁵ In both cases similarly to the inversion of halide/halogen stability in the propene complexes, the halogen-butadiene complexes are less stable than the corresponding propene complexes. This is likely due to a combination of delocalisation through the carbon chain reducing the bonding interaction at any given carbon.

5.3.2 Time-Of-Flight Mass Spectrometry

The mass spectra for the CCl_4 , CH_2Br_2 and CH_3I gas mixtures are presented in Figures 5.3, 5.4 and 5.5. Similar to the previous halide-propene suite of experiments, the mass spectra often contain residual halide sources from preceding gas mixtures. In this suite of experiments, the chronological order of experiments are those with CH_3I , CH_2Br_2 and finally CCl_4 . This was done to ensure that either residual Br^- or I^- would be present in the CCl_4 gas mixture for PES calibration. Each of the mass spectra were calibrated against the bare halide peaks present in each, which were themselves identified by their relative intensities and isotopic abundances. Full mass assignments are provided in Appendix D (page 430, 431 and 432). For those mass peaks that are assigned to highly solvated complexes, given that each of the mass spectra are calibrated against peaks at comparatively low m/z values, uncertainty of the calibration may effect the absolute m/z values for these complexes. However as solvation occurs in a stepwise fashion, the separation and relative intensities of peaks within bands of the mass spectrum can be assigned with respect to their neighbours. By commencing assignments at low, well-defined m/z values and proceeding in series, full assignment of the spectrum is then achieved.

The mass spectrum of the $\text{CCl}_4:\text{C}_4\text{H}_6:\text{Ar}$ gas mixture is shown in Figure 5.3. The spectrum shows clear mass peaks for the $^{35,37}\text{Cl}^-$, $^{79,81}\text{Br}^-$ and I^- ions. The spectrum also features a progression, marked by the red drop downs, of the $^{35,37}\text{Cl}^- \cdots (\text{C}_4\text{H}_6)_n$ ($n = 1-4$) complexes. These peaks are identified based upon the isotopic abundances of the underlying chloride ion and, at higher m/z values, the relative $\Delta m/z$ equalling the mass of a single butadiene unit. The highest of these (~ 250 m/z), is no longer well resolved when compared to the bare chloride. This effect is the result of the relative TOF plate voltages and adjustment of the relative space focussing of the molecular beam. While this may be improved upon by adjusting the voltage applied to the front TOF plate, for the purposes of these photoelectron spectroscopy experiments the effect is not appreciable. Immediately preceding each

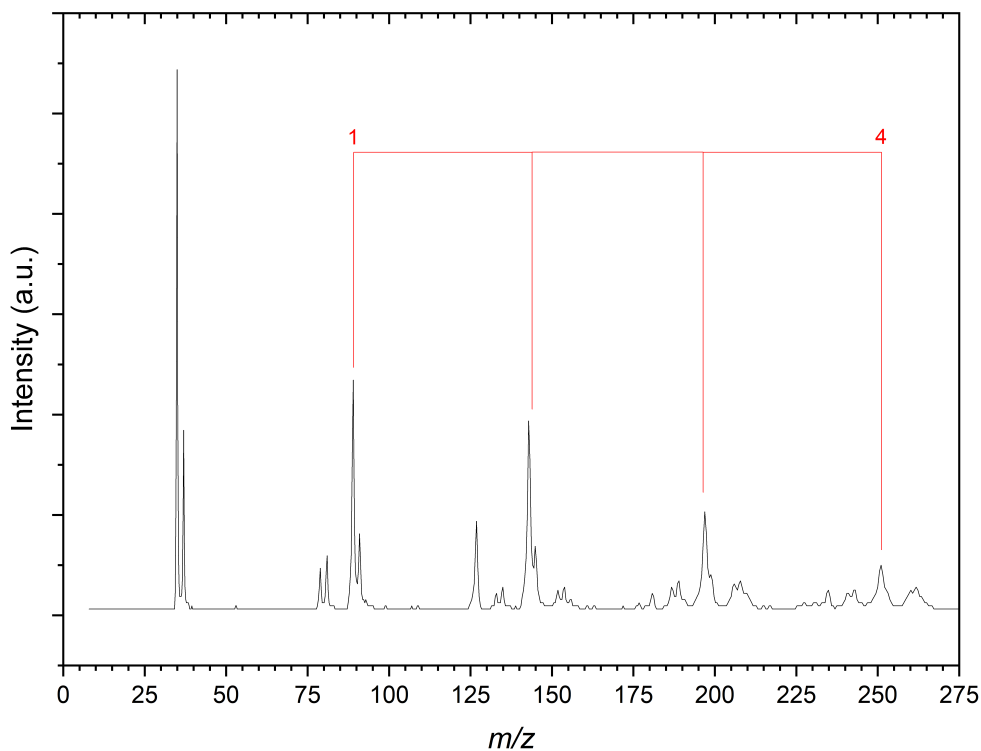


Figure 5.3: Time-of-flight mass spectrum produced from a $\text{CCl}_4:\text{C}_4\text{H}_6:\text{Ar}$ gas mixture (trace:50 kPa:400 kPa). The spectrum features a number of the desired $\text{Cl}^- \cdots (\text{C}_4\text{H}_6)_n$ complexes for $n \leq 4$, labelled by the red drop downs.

of the $^{35,37}\text{Cl}^- \cdots (\text{C}_4\text{H}_6)_n$, there are a number of spectral features that can be assigned to the respective butadiene solvated bromide complexes (for $n = 1-3$). The formation of these complexes is encouraging for later scheduled experiments, as are both peaks at 181 and 235 m/z which represent $\text{I}^- \cdots (\text{C}_4\text{H}_6)_n$ for $n \leq 2$. Immediately following the chloride-butadiene complexes (from $n = 2$), a number of $\text{Cl}^- \cdot (\text{CCl}_3) \cdot (\text{C}_4\text{H}_6)_n$ complexes with up to two butadiene molecules are present. PES spectra were not recorded of these species to confirm their structure though they do present interesting opportunities for future work in investigating a mixed solvent, gas-phase complex.

The mass spectrum from the $\text{CH}_2\text{Br}_2:\text{C}_4\text{H}_6:\text{Ar}$ gas mixture (Figure 5.4), shows good complex formation for a number of solvated bromide and iodide clusters. The space focussing of the TOF-PES results in poorer mass resolution for >275 m/z , however the same approach that was used to analyse the CCl_4 spectrum can be

taken here. There are two progressions of solvated bromide complexes denoted in Figure 5.4 by red and blue drop downs. The peaks indicated in red represent the $\text{Br}^- \cdots (\text{C}_4\text{H}_6)_n$ ($n = 1-5$) complexes and starting at 133 m/z with the monosolvated $^{79}\text{Br}^-$ complex. The blue peaks start at 173 m/z for $n = 0$ in a series of $^{79,81}\text{Br}^- \cdots (\text{CH}_2)^{81,79}\text{Br}(\text{C}_4\text{H}_6)_n$ complexes. The bromide-bromomethyl radical peak has previously been studied by anion PES however as with the $\text{Cl}^- \cdot (\text{CCl}_3)$ complexes, the butadiene solvated complexes offer an opportunity to study solvation in a competitive environment.

Particularly in these bromide-bromomethyl radical complexes, the relative intensities of the features in the mass spectrum increase with increasing butadiene solvation. This is believed to be a kinetic effect with a stark pressure dependence. The typical operating voltage of the piezo nozzle is $\sim 340\text{ V}$, with increases in the applied voltage required throughout a day of experiments as the background pressure slowly increases. However it was found in these butadiene experiments that the mass spectrum intensities comparing high and low m/z peaks was greatly dependent on the nozzle voltage. At low voltages, low m/z peaks such as the bare halides and monosolvated halides produced good mass spectrum intensities whereas increases in the nozzle voltage of up to 10 V reduced these intensities as the high m/z peaks became more intense. This suggests that in the source chamber the amount of halide anions produced by dissociative electron attachment becomes rate limiting as the increased local partial pressure of butadiene and the halomethane source readily solvate the anion and anion complexes.

Lastly, the mass spectrum of the $\text{CH}_3\text{I}:\text{C}_4\text{H}_6:\text{Ar}$ gas mixture is presented in Figure 5.5. The range of this spectrum is significantly larger than that of the corresponding bromide spectrum, with the largest spectral features recorded at 702 m/z . As with the previous mass spectra, the CH_3I spectrum consists of a number of solvated iodide-butadiene complexes as well as mixed-solvent complexes. These are shown in Figure 5.5 as red, blue and orange drop downs which represent $\text{I}^- \cdots (\text{C}_4\text{H}_6)_n$ ($n = 1-10$), $\text{I}^- \cdots (\text{CH}_3\text{I})(\text{C}_4\text{H}_6)_n$ ($n = 0-8$) and $\text{I}^- \cdots (\text{CH}_3\text{I})_2(\text{C}_4\text{H}_6)_n$ ($n = 0-5$) respec-

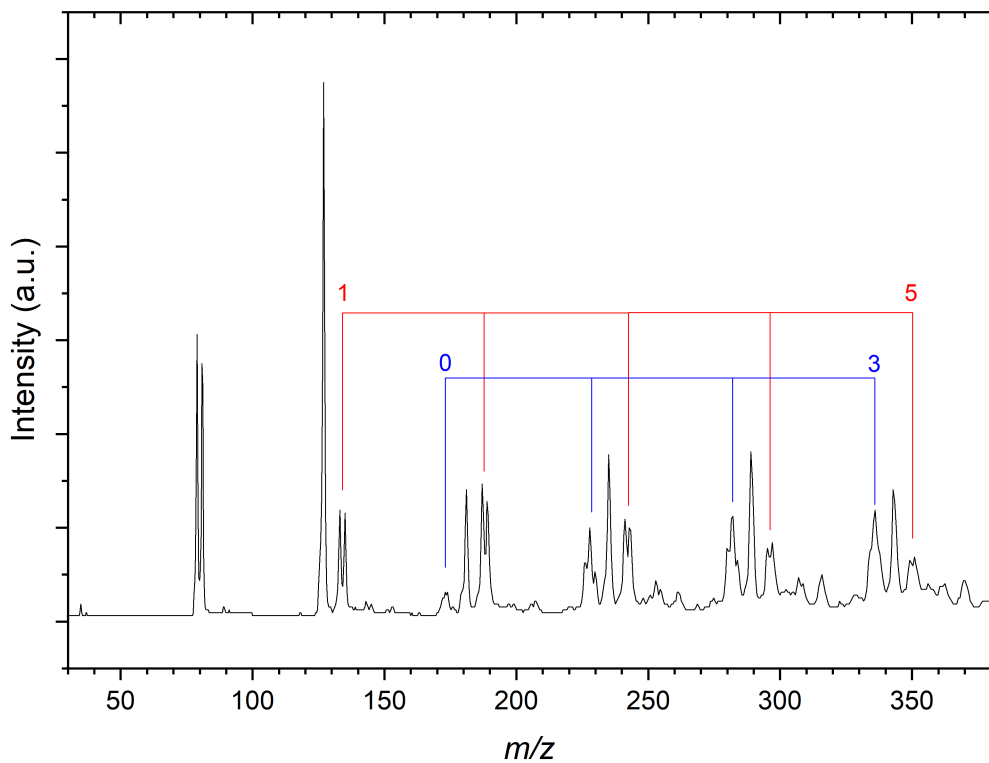


Figure 5.4: Time-of-flight mass spectrum produced from a $\text{CH}_2\text{Br}_2:\text{C}_4\text{H}_6:\text{Ar}$ gas mixture (trace:50 kPa:400 kPa). The spectrum features a number of the desired $\text{Br}^- \cdots (\text{C}_4\text{H}_6)_n$ complexes for $n \leq 5$, labelled by the red drop downs, as well as peaks attributed to $\text{Br}^- \cdots (\text{CH}_2\text{Br})(\text{C}_4\text{H}_6)_n$ ($n = 0-3$) complexes (blue drop downs).

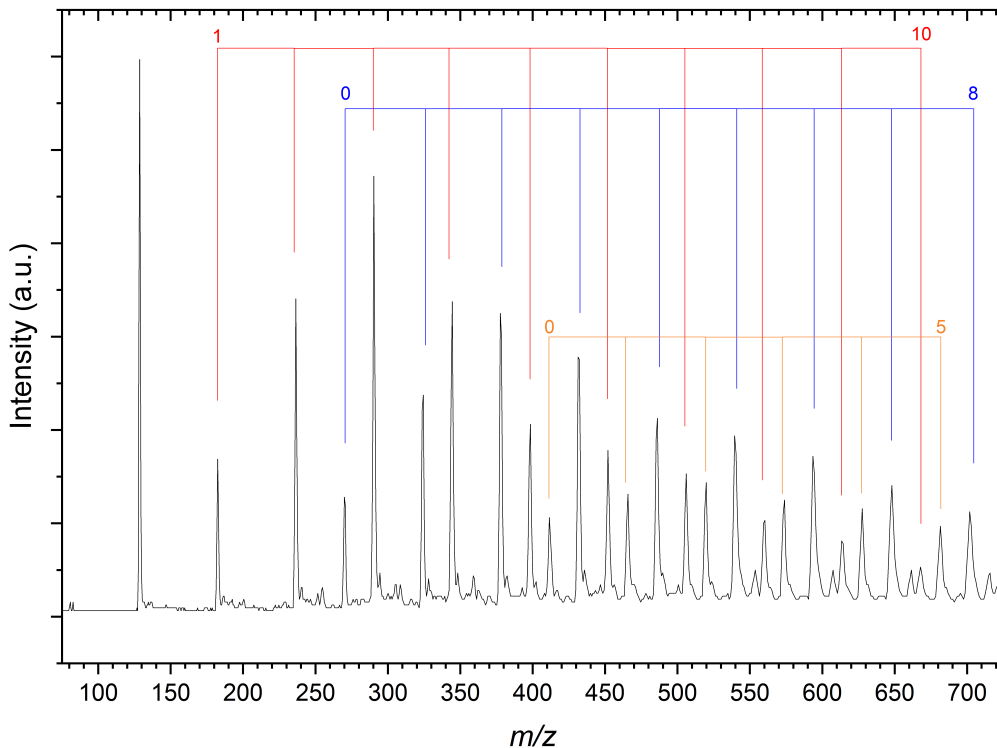


Figure 5.5: Time-of-flight mass spectrum produced from a $\text{CH}_3\text{I}:\text{C}_4\text{H}_6:\text{Ar}$ gas mixture (trace:50 kPa:400 kPa). The spectrum features a number of the desired $\text{I}^-\cdots(\text{C}_4\text{H}_6)_n$ complexes for $n \leq 10$, labelled by the red drop downs, as well as peaks attributed to $\text{I}^-\cdots(\text{CH}_3\text{I})(\text{C}_4\text{H}_6)_n$ ($n = 0-8$) complexes (blue drop downs) and $\text{I}^-\cdots(\text{CH}_3\text{I})_2(\text{C}_4\text{H}_6)_n$ ($n = 0-8$) complexes (orange drop downs).

tively. As with the mixed-solvent bromide complexes, the nozzle voltage appears to affect the relative intensities of the peaks within each band, with the most intense comprising the $n = 3$ complex in each case. The strong iodide mass peak in Figure 5.4 coupled with the strong solvation progression present in the CH_3I mass spectrum is indicative of the relatively large amount of CH_3I present in this gas mix.

At high m/z , the spectrum becomes increasingly congested as the number of permutations of the monomer units grows. In order to perform PES spectroscopy on peaks in this regime, similarly to their mass assignment, the Q-switch timing may be correlated against the ion TOF and used to predict Q-switch timing of these larger clusters. This is especially useful in performing spectroscopy on peaks where the mass spectrum is less intense and the contained anion complexes produce photoelectrons with TOF similar to those of the background ion noise.

5.3.3 Photoelectron Spectra

The photoelectron spectra of the $\text{Cl}^- \cdots (\text{C}_4\text{H}_6)_n$ $n = 0\text{-}3$ complexes are presented in Figure 5.6. Each of the spectra are fitted with two Gaussian functions as per Equation 2.11. The determined E_{BE} for each of the perturbed $^2P_{3/2}$ peaks are then presented in Table 5.1. As there are multiply solvated halides present in these spectra, the stepwise solvation energy (E_{solv}) is a measure of the successive electronic stabilisation (ΔE_{stab}) with each additional solvating molecule.

The E_{BE} of the $\text{Cl}^- \cdots \text{C}_4\text{H}_6$ complex is determined from peak fitting as $3.9962(6)$ eV but is reported to 3 s.f. Comparing the experimental E_{BE} (4.00 eV) with the VDE calculated from DSD-PBEP86/AVTZ calculations, the most probable anion structure is again the *2trans* complex (4.02 eV). The *1trans* and *4trans* conformers are structurally similar and have similar D_0 values and the corresponding VDE values are 3.88 eV and 3.93 eV, respectively. Given the quality of the fit in this case ($R^2 = 0.9826$), this is believed to be sufficiently different to assign the spectrum to the *2trans* structure. The E_{stab} of the complex is determined to be 39.0 kJ mol^{-1} which shows good agreement with the determined D_0 of the anion complex. The calculated E_{stab} is 34.6 kJ mol^{-1} , but represents the ADE rather than VDE. Extending this to the further solvated chloride-butadiene complexes, the E_{solv} show successive decreases with increasing degrees of solvation. These experimental E_{solv} energies are 27.6 kJ mol^{-1} and 20.9 kJ mol^{-1} respectively, indicating the stability in these anion complexes.

From the fitting of the experimental chloride-butadiene spectra, it is clear that the fitted Gaussian functions become narrower as the E_{BE} approaches the photon energy (i.e. low electron kinetic energy (E_{KE})). Fitting a linear regression through this data of E_{KE} against σ for each fit yields the function $\sigma = 9.7 \times 10^{-2}E_{KE} + 3.02 \times 10^{-2}$ ($R^2 = 0.9821$) and provides some predictive power as to the expected Gaussian width of a given transition. The corresponding dE/E_{KE} values range from 30 % to 64 % near threshold.

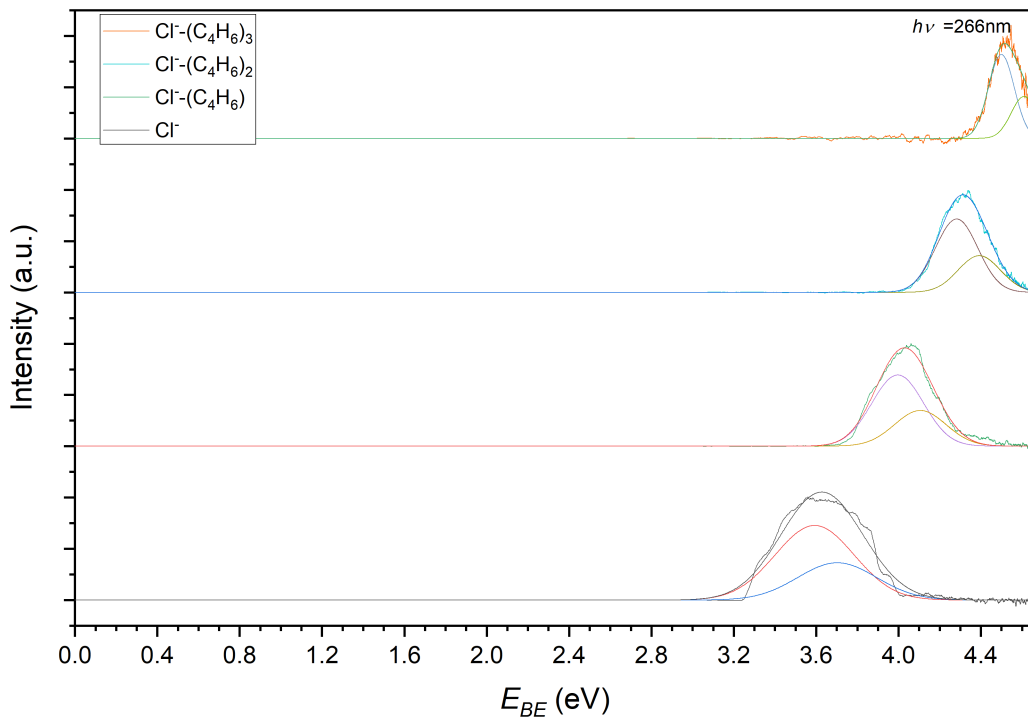


Figure 5.6: Photoelectron spectrum of $\text{Cl}^- \cdots (\text{C}_4\text{H}_6)_n$ ($n = 1-3$) complexes from Figure 5.3 assigned to photodetachment to the perturbed $^2P_{3/2}$ and $^2P_{1/2}$ states of each complex. Each complex is deconvoluted into two Gaussian functions representing the two 2P peaks. Note that the fit to the Cl^- spectrum is poorer further from the centroid of the Gaussian functions. This is likely due to power broadening as discussed in Chapter 2.2.2.

The photoelectron spectra from the $\text{Br}^- \cdots (\text{C}_4\text{H}_6)_n$ ($n = 1-3$) complexes are presented in Figure 5.7. The E_{BE} of the $n = 1$ complex is determined as 3.66 eV with a resulting E_{stab} of 0.31 eV (30.2 kJ mol⁻¹). Compared to the chloride complexes, the $\text{Br}^- \cdots \text{C}_4\text{H}_6$ calculated D_0 value does not agree as well with the VDE. Considering that the neutral complexes are generally more strongly bound moving down the group 17 elements, this deviation away from alignment is attributed to the more appropriate definition of the difference in D_0 values. This suggests that the VDE conformation in the neutral state is bound, albeit vibrationally excited. Of the neutral bromide vdW minima, the D_0 values range from 8.6 kJ mol⁻¹ to 11.6 kJ mol⁻¹. For the anion complexes, the *1trans* and *4trans* complexes have D_0 values of 28.0 kJ mol⁻¹ and 27.6 kJ mol⁻¹ respectively. As these are both less than the E_{stab} energy it suggests that photodetachment from these complexes, while possible would be to unbound states as only a negative D_0 in the neutral would produce such an E_{stab} .

Photoelectron spectroscopy of the iodide-butadiene complexes were successfully performed for up to 7 solvating butadiene molecules. This was helped by the larger spin-orbit splitting of the neutral iodide, bringing the E_{BE} of the $^2P_{3/2}$ peak for higher solvated complexes below that of the photon energy. These photoelectron spectra are presented in Figure 5.8 and the E_{BEs} of each peak presented in Table 5.1.

The E_{BE} of the perturbed $^2P_{3/2}$ peak is 3.27 eV and the calculated E_{stab} of the monosolvated complex is 0.21 eV (20.4 kJ mol⁻¹). Unlike the bromide complexes, D_0 values of both of the iodide complexes are greater than the E_{stab} from experiment and both theoretically possible photodetachment channels. As the *2trans* complex is significantly more stable and that the neutral D_0 values are ~ 8 kJ mol⁻¹, it suggests that it is still the most probable anion structure as the resulting E_{stab} values are closest to experiment.

As there are a number of solvated structures present for each of the halides, it is necessary to consider whether butadiene [4+2] Diels-Alder cycloaddition occurs

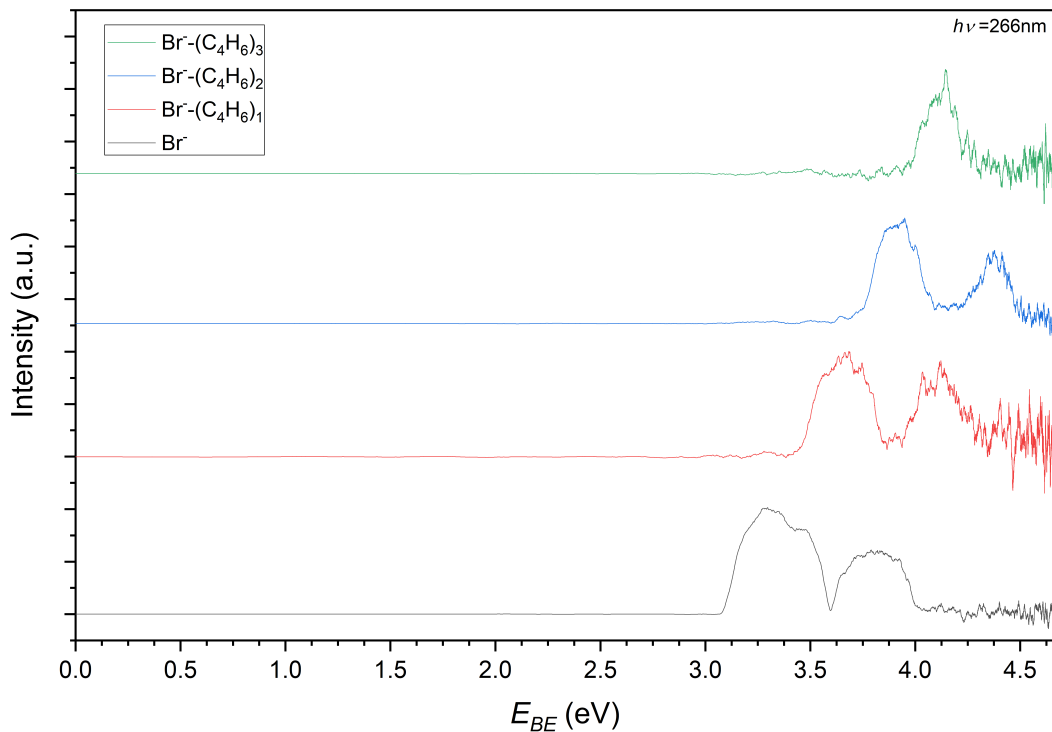


Figure 5.7: Photoelectron spectrum of $\text{Br}^- \cdots (\text{C}_4\text{H}_6)_n$ ($n = 0-3$) complexes from Figure 5.4 assigned to photodetachment to the perturbed $^2P_{3/2}$ and $^2P_{1/2}$ states of each complex. As with Figure 5.6, the asymmetry of the peaks is attributed to power broadening.

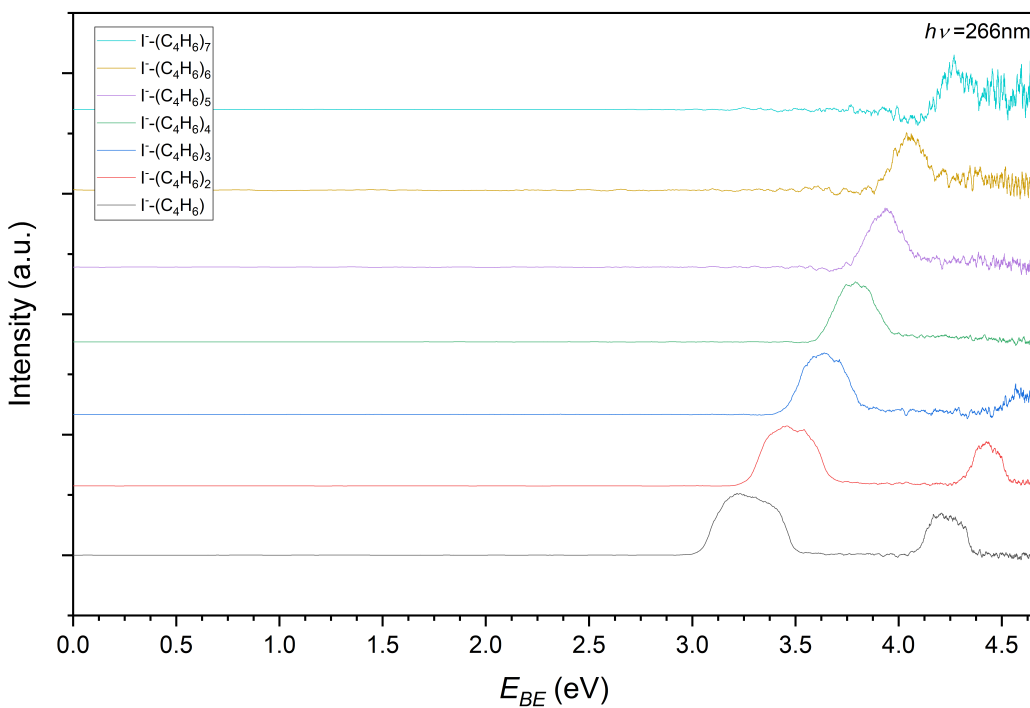


Figure 5.8: Photoelectron spectrum of $\text{I}^- \cdots (\text{C}_4\text{H}_6)_n$ ($n = 1-7$) complexes from Figure 5.5 assigned to photodetachment to the perturbed $^2\text{P}_{3/2}$ and $^2\text{P}_{1/2}$ states of each complex.

Table 5.1: Comparison between the experimental electronic binding energy (E_{BE}), stepwise solvation energy (E_{solv}) and calculated VDE for the halide-butadiene complexes (all in eV).

n	$\text{Cl} \cdots (\text{C}_4\text{H}_6)_n$			$\text{Br} \cdots (\text{C}_4\text{H}_6)_n$			$\text{I} \cdots (\text{C}_4\text{H}_6)_n$		
	E_{BE}	VDE_{Calc}	E_{solv}	E_{BE}	VDE_{Calc}	E_{solv}	E_{BE}	VDE_{Calc}	E_{solv}
0	3.59			3.34			3.06		
1	4.00	4.02	0.40	3.66	3.70	0.31	3.27	3.31	0.21
2	4.28		0.29	3.91		0.26	3.47	3.52	0.20
3	4.50		0.22	4.13		0.21	3.64		0.17
4							3.78		0.14
5							3.93		0.15
6							4.06		0.13
7							4.27		0.21

within the gas mixture. To investigate this, additional DSD-PBEP86-D3BJ calculations were performed on the iodide complex with the most probable product, 4-vinylcyclohexene. As the number of heavy atoms increased significantly in these larger complexes, the basis set used was the def-2TZVPD. The def-2 basis set was

chosen here based on the reliability of the def-2QZVPD basis set for troublesome cases (see Section 4.3.1). These were compared with a minimum structure representing the $\text{I}^- \cdots (\text{C}_4\text{H}_6)_2$ complex where the butadiene monomers interacted with the iodide similarly to the *2trans* conformer of the monosolvated complex. The results of these calculations are shown in Figure 5.9, where two minima and a transition state were determined for the 4-vinylhexene complex and one structure was determined for the trimer complex. The trimer structure is a transition state where the imaginary mode ($53\text{i}\,\text{cm}^{-1}$) represents a rotation of the butadiene monomers such that their interaction is not directly towards the iodide. The proposed offset arrangement of the butadiene monomers does still represent a good approximation of the trimer structure. Undertaking VDE calculations of the two iodide-4-vinylhexene complexes and the $\text{I}^- \cdots (\text{C}_4\text{H}_6)_2$ complexes yields distance values of 3.19 eV, 3.35 eV and 3.52 eV respectively. The D_0 values of the 4-vinylhexene complexes are also similar to those of the monosolvated iodide-butadiene complex, indicating that the degree of stabilisation is more dependant on the degree of solvation than the solvent molecule in this case. Compared with the experimental detachment (3.47 eV), only the trimer complex agrees reasonably with the experimental perturbed ${}^2P_{3/2}$ peak and the Diels-Alder product is subsequently ruled out from higher butadiene complexes for each halide.

In both the bromide and iodide complexes there is a similarly distinct decrease in the E_{solv} energy as there was in the chloride complexes. These energies are plotted against the number of solvating butadiene molecules, and compared with other larger halide clusters with H_2O , CO_2 and N_2O in literature in Figure 5.10.^{287,389,390} As noted by Markovich in comparing halide-water clusters, the E_{solv} energy decreases with each successive solvent molecule until a full solvation shell is filled. The onset of solvating molecules filling a second solvation shell is marked by a sharp increase in the E_{solv} for that number of molecules. In the case of the iodide-butadiene clusters this occurs at $n = 7$ and is indicative that the filled first solvation shell consists of 6 coordinated butadiene molecules. The E_{solv} for $n = 7$ is approximately equal to

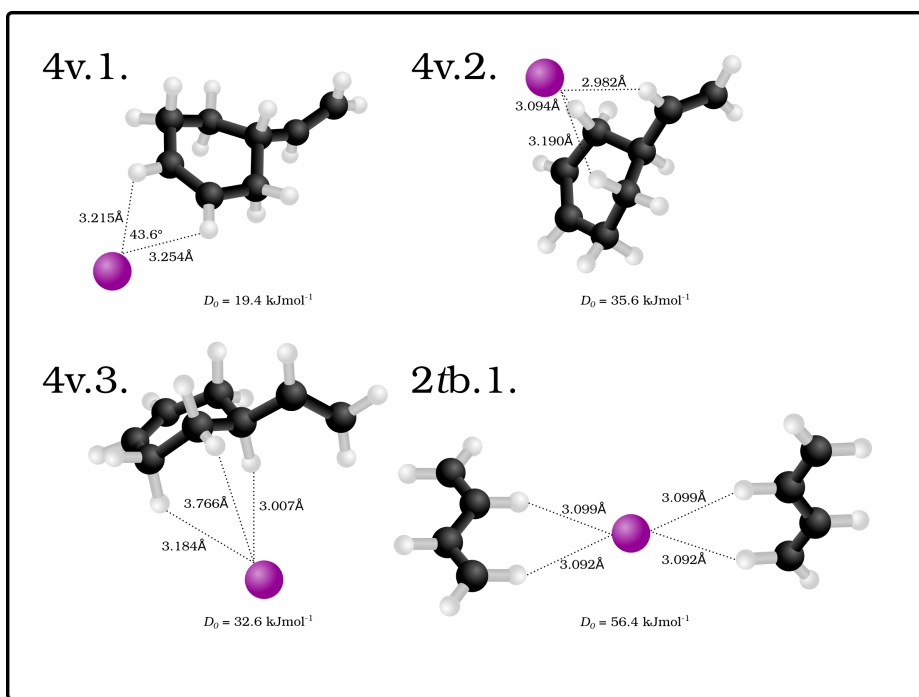


Figure 5.9: Optimised structures of the $\text{I}^- \cdots \text{C}_8\text{H}_{12}$ and $\text{I}^- \cdots (\text{C}_4\text{H}_6)_2$ anion complexes. Structures are calculated with the DSD-PBEP86-D3BJ functional with def-2QZVPD basis set. Associated D_0 values are included for each structure.

that of the monosolvated complex suggesting that the filling of the second solvation shell treats the complete first shell as a single unit, much like a bare iodide albeit shielded. Interestingly there is also present at $n = 5$ a small increase in the E_{solv} which suggests that the 4-coordinated complex may itself be a metastable structure.

Extending the bonding motifs present in the $\text{I}^- \cdots (\text{C}_4\text{H}_6)_{1,2}$ complexes, a hypothetical structure of the $\text{I}^- \cdots (\text{C}_4\text{H}_6)_6$ structure is presented in Figure 5.11. This structure is not optimised and the symmetry of the molecule means that the offset dihedral angle between opposite butadiene molecules results in a structure where there are instances where neighbouring butadiene molecules would be in a repulsive conformation. Nonetheless this the PES of this complex represents a significantly stabilised complex, experimentally difficult to produce in the gas-phase and perform spectroscopy on.

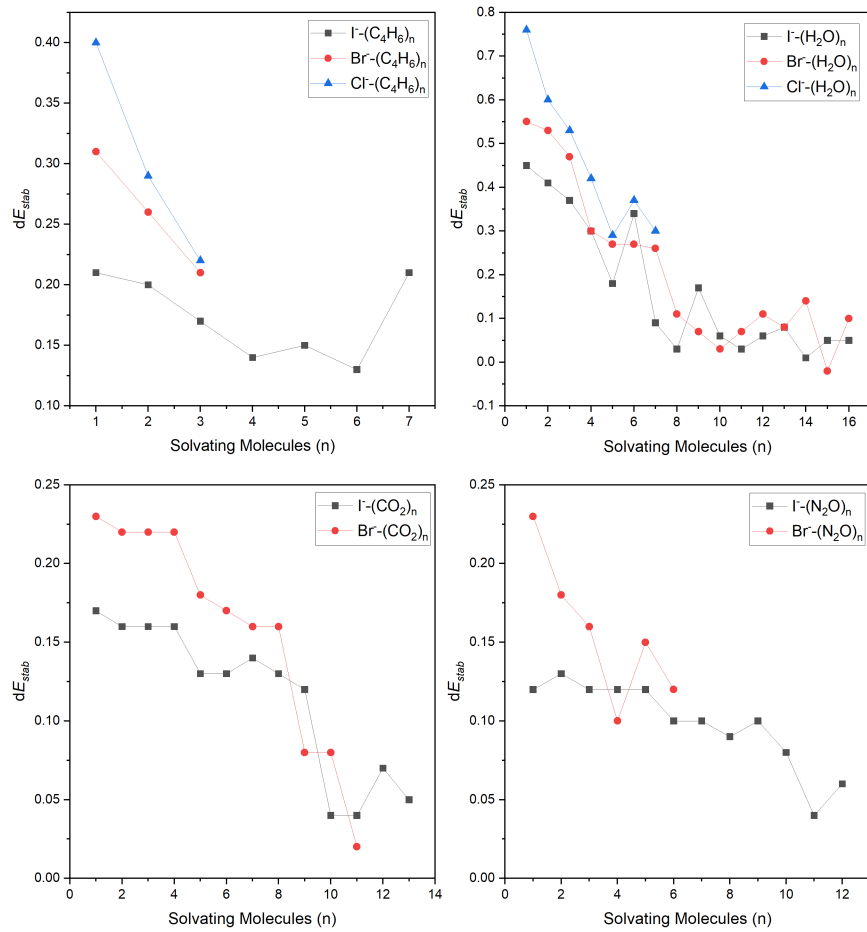


Figure 5.10: Comparison of trends in E_{solv} for a range of solvated halide complexes with butadiene, H_2O ,³⁹⁰ CO_2 ,³⁸⁹ and N_2O .^{287,389}

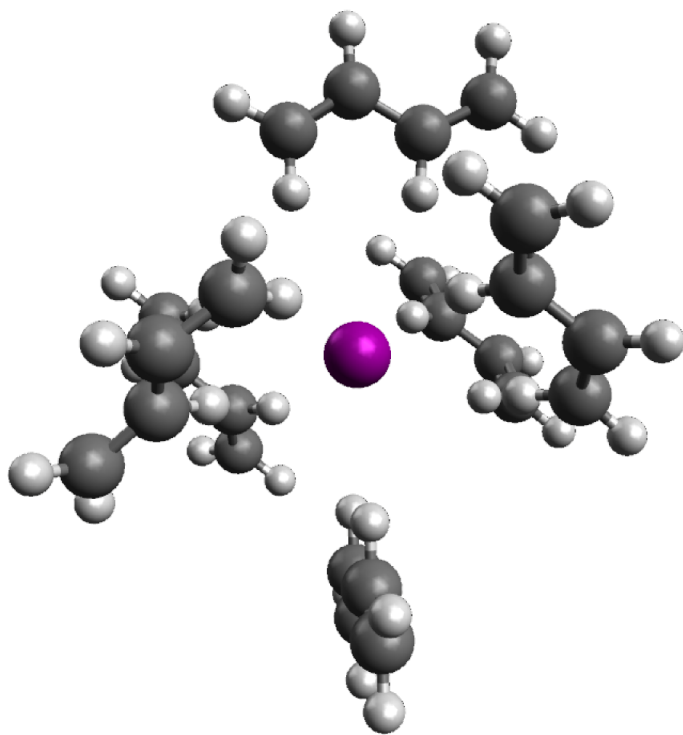


Figure 5.11: Hypothetical structure of the $\text{I}^- \cdots (\text{C}_4\text{H}_6)_6$ complex. The structure is not optimised, but utilises bonding motifs present in the dimer and trimer complexes. Image generated from *Avogadro v1.1.1*.³⁹¹

5.4 Summary

In summary, a number of $\text{X}^- \cdots (\text{C}_4\text{H}_6)_n$ ($\text{X} = \text{Cl}, \text{Br}, \text{I}; n \leq 3, 3, 7$ respectively) complexes have been formed in the gas-phase and their anion photoelectron spectra recorded. To complement these experimental results the structures of a number of vdW complexes have been calculated for each of the halide and halogen species with both *cis*- and *trans*-1,3-butadiene using the DSD-PBEP86-D3BJ functional. For the monosolvated complexes, the E_{stab} values decrease as the size of halide increases and from calculation are most stable when coordinated by bidentate hydrogens from the butadiene. The VDE of these complexes was determined as 4.00 eV, 3.66 eV and 3.27 eV for the Cl^- , Br^- and I^- complexes respectively. The difference in stabilisation trend with respect to the halide decreases as the number of solvating butadiene molecules increases with $n = 3$ near parity.

As the 1,3-butadiene may undergo a [4+2] cycloaddition, the iodide complex of

the product 4-vinylcyclohexene was also calculated. The VDE of this complex was found to be 3.35 eV whereas the trimer butadiene complex has a VDE of 3.52 eV, much more aligned to the experimental value of 3.47 eV.

Within the solvation of the iodide-butadiene complexes, the stepwise solvation energy generally decreases with the number of solvating butadiene molecules. There are two points where the solvation energy increases at $n = 5$ and $n = 7$ which are indicative that the $n = 4$ represents a metastable solvated iodide and the $n = 6$ represents a full solvation shell.

Chapter 6

Phosphorus Containing Complexes

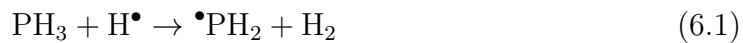
6.1 Introduction

Phosphorus containing molecules form the backbone of DNA and are fundamental in the exchange of energy within cells. Cosmically, elemental phosphorus is formed in late-life, carbon-rich stars (red giants)³⁹² and simple hydrides and phosphorus containing radicals (PH_3 , PN, CP, HCP, PO, and C_2P) have been shown to be present in the ISM and circumstellar envelope (CSE). Observational measurements have often relied upon detection of molecules from rotational transitions in the GHz range and in the case of phosphine (PH_3) in the CSE of IRC+10216 these represented the tentative assignment of the $J = 1 - 0$ transition³⁹³ followed by confirmation with the $J = 2 - 1$ spectral line at 266.9 GHz and 533.8 GHz respectively.³⁹⁴ For this reason previous computational work investigating a number of phosphorus containing compounds has been undertaken to determine dipole moments³⁹⁵ and spectral line lists to help detect and characterise these species.^{396,397}

The simple phosphorus hydride (PH_3) has been observed in extraterrestrial atmospheres of Jupiter and Saturn,^{398–400} in ices on Neptune and Uranus⁴⁰¹ and in the coma of comets.⁴⁰² Recent debate has also included whether PH_3 is present in the Venusian atmosphere also, with discussion centred on the observed concentration and possible spectral contamination by SO_2 .^{403,404} Regardless of the presence of

PH_3 on Venus, outside of the oxidation of this species to form organophosphates, the chemistry of phosphine is not fully understood and there is scope to determine additional reaction pathways of phosphorus hydride species.⁴⁰⁵ In these extraterrestrial environments PH_3 can undergo a number of reactions including:

Degradation by H-radicals;⁴⁰⁶



PH_3 reformation;⁴⁰⁷



Destruction by OH-radicals;⁴⁰⁸



and Destruction by *UV* radiation:



The rate constants for Equations 6.1 and 6.2 are $k_1 = 1.09 \times 10^{-10} \exp\left(\frac{-1048}{T}\right)$ and $k_2 = 3.7 \times 10^{-10} e^{\left(\frac{-340}{T}\right)}$ respectively. Therefore, within the temperate zone of Venus for example (50 km to 60 km), where atmospheric temperatures range from ~ 325 K to ~ 225 K,⁴⁰⁹ the associated rate constants of PH_3 destruction and reformation via H-radicals are $1.14 \times 10^{-10} \text{ cm}^3 \text{ s}^{-1}$ and $2.86 \times 10^{-12} \text{ cm}^3 \text{ s}^{-1}$ at 288 K. This alone suggests that PH_3 depletion is likely under these conditions, however its observation demands that other sources and sinks for atmospheric models be explored.

Experimentally, PH_3 has been shown to produce daughter phosphorus hydride ions under both dissociative electron attachment⁴¹⁰ and electric discharge sources.^{20,411} In the latter experiments, photoelectron spectra were recorded for both PH^- and PH_2^- with E_a values of 1.027(6) eV and 1.263(6) eV respectively. To further explore

their reactivity, a number of theoretical studies have investigated heats of formation of phosphorus hydrides⁴¹² as well as reactions of PH_2^- with $\text{CH}_3\text{CH}_2\text{Cl}$ ⁴¹³ and $\text{RPH}^- \cdots \text{CO}_2$ clusters ($\text{R} = \text{H}$, CH_3 , $\text{CH}_2=\text{CH}$ and C_6H_5).⁴¹⁴ While some experimental work has recently demonstrated the formation of phosphino formic acid PH_2COOH in binary $\text{PH}_3:\text{CO}_2$ ice mixtures reminiscent of sub solar planetary environments, with the corresponding formate anion synthesised from NaPH_2 and CO_2 , much of the clustering of phosphorus hydrides have not been thoroughly explored. Part of the lack of experimental work is the distinct hazards of working with PH_3 gas. It is flammable and acutely toxic with an LD_{50} in rats via gas inhalation of 10 ppm over 4 h.⁴¹⁵ As such, exploratory calculations offer an alternative route to investigate phosphorus hydride complexes and identify promising spectroscopic targets.

In this chapter, a number of PH_2^- vdW complexes are investigated using theoretical methods. Given that PH_2^- appears to readily form via both dissociative electron attachment and from discharge sources, these complexes represent a suite of anion-molecule pairs that are expected to form in TOF-PES experiments. The solvating molecules chosen are methane (CH_4),^{416,417} ethene (C_2H_4),⁴¹⁸ acetylene (HCCH),⁴¹⁹ CO_2 ,⁴²⁰ H_2S ,^{421,422} and NH_3 .⁴²³

6.2 Methods

Explorations of conformer space of $\text{PH}_2 \cdots \text{M}$ anion and neutral complexes have differed for each of the solvating molecules. As a general approach, starting geometries are sampled from expected critical points of monomer orientations. These include bonding between faces, vertices and edges of a polyhedron inscribed by the monomer (ie, tetrahedron for CH_4 , isosceles triangles for PH_2 , H_2S). From the original sample set, each conformer undergoes geometry optimisation with the DSD-PBEP86-D3BJ functional and Ahlrichs' def-2QZVP⁴²⁴ and Dunning's aug-cc-pVTZ basis sets.^{265,331} For P and S additional diffuse functions are included in the Dunning's basis set

(aug-cc-pV(T+d)Z), however, for the sake of brevity all Dunning's basis sets will be denoted AV n Z. Following geometry optimisation, minima were confirmed by harmonic frequency calculations, those AVTZ calculations that produced minima were then reoptimised with AVQZ basis sets. Conformers were also excluded from the search should their geometry optimisation tend them towards other conformers to avoid unnecessary calculations. Geometry optimisations and harmonic frequency calculations have been completed in Gaussian 09²⁶⁷ using the Pople HPC. Where appropriate, vibronic simulations have been undertaken determining FCFs using Duschinsky rotations in ezSpectrum 3.0.²⁵⁶

Previous calculations on halide-molecules complexes in the Wild Group apply a spin-orbit splitting based on the experimental spin-orbit states of the neutral halide. Additionally, to account for systematic errors in the calculation method, a shift based upon comparison between the calculated and experimented VDE is also applied. In the case of the polyatomic PH₂⁻, given the energy distribution between states includes a vibrational contribution and that there is significant change in the P–H bond length upon photodetachment (1.429 Å to 1.417 Å at DSD-PBEP86/AVQZ for the anion and neutral respectively), it is not appropriate to use the VDE for this calibration and rather the ADE is used. Test calculations on the isolated PH₂ anion and neutral utilising the DSD-PBEP86-D3BJ functional and high level *ab initio* single-point energies are presented in Table 6.1. These demonstrate that differences from the calculated ADE to the experimental ADE determined by Ervin *et. al.*²⁰ decrease remarkably with both more rigorous computational methods and basis set size. The smallest difference between experiment and theory corresponds to W2w energies with a calculated shift of 33 cm⁻¹. Not only is this difference significantly low but lies within the experimental uncertainty of 0.006 eV (48 cm⁻¹) as does the W1w energy. Given the relatively small clusters considered here, containing only up to 9 atoms or 4 heavy atoms in the cases of the PH₂⁻...C₂H₄ and PH₂⁻...CO₂ complexes respectively, single-point energies at W2w level of theory with structure and vibrational contributions from DSD-PBEP86-D3BJ/AVQZ calculations are pre-

sented from here onwards. Where appropriate, CC energies have been calculated utilising a local workstation to avoid the walltime limit set by the Pople HPC queuing system at UWA.

Table 6.1: Comparison between the experimental ADE of PH_2^- and a number of computational methods. DSD-PBEP86-D3BJ methods are presented with associated basis sets while other CC and Wnw methods utilise the structure and zpe from DSD-PBEP86-D3BJ/AVQZ calculation.

Computational Method	Basis Set	VDE_{Comp} eV	ADE_{Comp} eV	ADE_{Exp} eV	Shift cm^{-1}
DSD-PBEP86-D3BJ	def-2QZVP	0.696	1.062	1.263(6)*	-1621
	AVTZ	0.874	1.194		-553
	AVQZ	0.882	1.221		-335
CCSD(T) [†]	AVTZ	0.829	1.197	1.263(6)*	-530
	AVQZ	0.874	1.241		-180
CCSD [†]	AV5Z	0.782	1.253		-79
W1w [†]	N/A	0.902	1.268		44
W2w [†]	N/A	0.900	1.267		33

$$VDE_{Comp} = E_{\text{anion}} - (E_{\text{anion}}^- + zpe_{\text{anion}})$$

$$ADE_{Comp} = (E_{\text{neutral}} + zpe_{\text{neutral}}) - (E_{\text{anion}}^- + zpe_{\text{anion}})$$

*: From Ervin *et. al.*²⁰

[†]: These methods utilise DSD-PBEP86-D3BJ/AVQZ geometries and zpe.

In the case of the $\text{PH}_2^- \cdots \text{H}_2\text{S}$ complex, as the proton affinity of PH_3 and H_2S are $1522.0(63) \text{ kJ mol}^{-1}$ and $1470.42(25) \text{ kJ mol}^{-1}$ respectively,^{20,425} in some conformers proton transfer to a $\text{HS}^- \cdots \text{PH}_3$ complex is favoured. While this is discussed further in Section 6.3, the HS^- monomer was similarly benchmarked with full benchmark results in Appendix E (page 487). Prior to determination of the calibration shift the calculated ADEs are split to account for the spin-orbit splitting of the ${}^2\Pi$ state of SH given by $\Delta E_{SO} = \frac{A}{2}(j(j+1) - \ell(\ell+1) - s(s+1))$ with $A = -378.53 \text{ cm}^{-1}$.⁴²⁶ This is then benchmarked against the $R(0)$ transition ($18\,669.544(14) \text{ cm}^{-1} = 2.314\,668\,7(17) \text{ eV}$) from photodetachment microscopy⁴²⁵ with the W2w shift calculated as 54 cm^{-1} and is of similar quality to the PH_2^- benchmark.

6.3 Results and Discussion

The following section details the structures, energies and simulated photoelectron spectra for each of the dimer complexes. In each case the nature and strength of the bonding interaction, and in cases the likelihood of observing such a complex experimentally is discussed. For full geometries, energies, frequencies, Cartesian coordinates and FCFs please refer to Appendix E.

6.3.1 $\text{PH}_2^- \cdots \text{CH}_4$ Complexes

The optimised DSD-PBEP86-D3BJ/AVQZ $\text{PH}_2 \cdots \text{CH}_4$ anion and neutral complexes are presented in Figure 6.1. There are two anion minima and two neutral minima determined denoted 1a-b and 1c,e respectively. Structure 1d, while presented here, was confirmed to be a minimum at AVTZ but was a higher order saddle point when recalculated at AVQZ and def-2QZVP. In addition to the minima geometries presented, Figure 6.1 also includes D_0 values determined from $W2w$ energies (with DSD-PBEP86-D3BJ/AVQZ vibrational contributions). Additional structures which were either determined to be minima in AVTZ calculations but were not with AVQZ basis sets, or those that are minima under the def-2QZVP basis set but not Dunning basis sets are presented in Appendix E.

Regarding the anion structures, the two conformers represent PH_2^- anions with the hydrogen atoms facing towards or away from a C–H bond. These structures are similar to those previously calculated for $X^- \cdots \text{CH}_4$ ($X = F, Cl, Br, I$) using MP2 methods and 6-31++G(d,p) basis sets.⁴²⁷ In this work three geometries of the $X^- \cdots \text{CH}_4$ complex were optimised with the halide in each case bonding axially, facially, or bisecting the H–C–H angle. In all cases the axially bonded halide complex was the only minimum structure, and although the PH_2^- complex is not represented by a spherical charge distribution, exhibits the same interaction. A def-2QZVP minimum structure similar to 1a and 1b was also determined where the dihedral between H–P–H plane and the interacting hydrogen is close to orthogonal ($\theta_{H-P-HC} = 86.2^\circ$

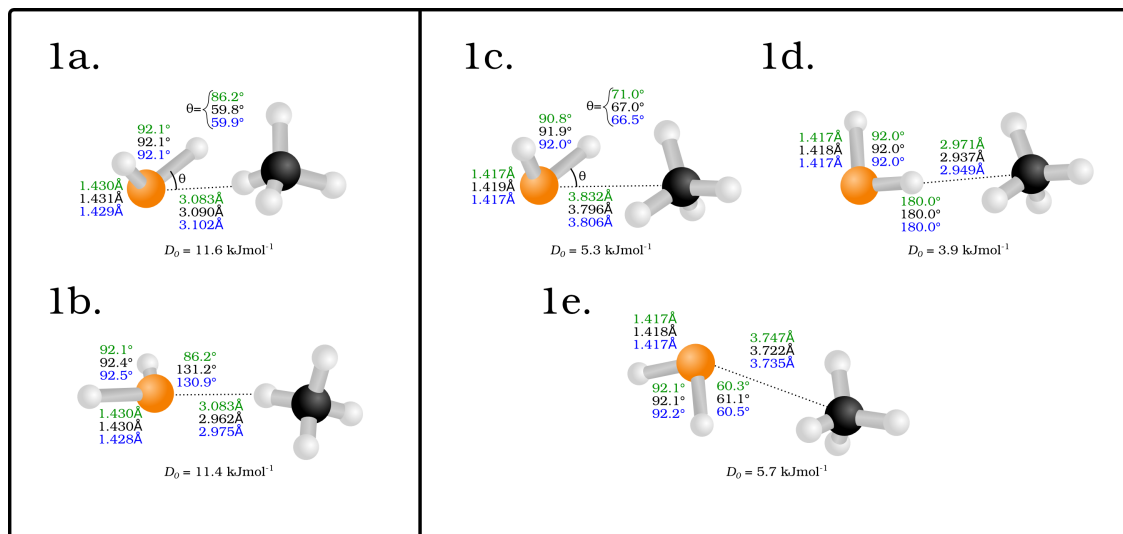


Figure 6.1: Optimised structures of the $\text{PH}_2\cdots\text{CH}_4$ anion (left) and neutral (right) complexes. Structures are calculated with the DSD-PBEP86-D3BJ functional and def-2QZVP (green), AVTZ (black) and AVQZ (blue) basis sets. Associated D_0 values are included for each structure from W2w methods.

for def-2QZVP). Optimisations from this geometry with AVTZ basis sets then diverge to either 1a or 1b. This appears to be reflective of the need for additional diffuse functions in basis set choice to adequately describe the polarisation of anions as discussed in Chapter 4. Both conformers appear to be dominated by the electrostatic interaction between charge localised on the phosphorus and the hydrogen of the methane; however, the orientation of the hydrogens on PH_2^- are staggered with respect to the non-interacting hydrogens of CH_4 . The strength of the interactions in the complexes are weak, with D_0 of 1a and 1b being 11.6 kJ mol^{-1} and 11.4 kJ mol^{-1} respectively. While 1a is slightly more stable than 1b the difference is negligible (0.2 kJ mol^{-1}). Additional structures were found to be stationary points comparable to both anion conformers albeit in an eclipsed orientation. These structures are denoted 1a* and 1b* respectively. They were found to be first-order transition states at AVTZ and were not reoptimised at AVQZ level. They have imaginary modes of $10i \text{ cm}^{-1}$ and $13i \text{ cm}^{-1}$ and a difference in energy at DSD-PBEP86-D3BJ/AVTZ of 1.3 cm^{-1} and 1.7 cm^{-1} with their corresponding minima for 1a* and 1b* respectively. As such both are considered free rotors around the axis of the CH–P interaction.

Whereas the anion structures are dominated by electrostatic interactions, the

minima neutral complexes comprise conformers interacting with faces (CH_3 pockets) rather than individual hydrogens. Both 1c and 1e have P–C distances that are comparable, if not slightly shorter, to the anion complexes with P–HC distances $\sim 3\text{\AA}$. Their D_0 values are also approximately half those of the anion complexes, being 5.3 kJ mol^{-1} and 5.7 kJ mol^{-1} respectively. Considering the 1d structure as a higher-order saddle point, with two low frequency imaginary modes representing rotations of the PH_2 both out-of-plane (32i cm^{-1}) and in-plane (20i cm^{-1}), it would suggest that this structure would move towards that of 1c following these modes. In the case of the 1e complex, the geometry suggests that a cooperative interaction between the lone pair on the phosphorus is interacting with the nearest hydrogen (labelled H3), while the carbon donates into the P–H bond. Natural Bond Orbital (NBO) analysis of the 1e complex in Table 6.2 shows the donation from the CH_4 to PH_2 consists of delocalisation from the $\sigma_{\text{C-H}3}$ orbital into a Rydberg orbital on the phosphorus with significant *d* and *f* contributions. Additional delocalisation into the $\sigma_{\text{P-H}8}^*$ orbital of the P–H bond pointing away from the complex. Conversely, the reciprocal interactions from the PH_2 into CH_4 consist of donation from the $\sigma_{\text{P-H}6}$ bond into Rydberg states of the carbon atom, two out-of-plane hydrogens and the $\sigma_{\text{C-H}2}^*$ orbital of the farside hydrogen. The same $\sigma_{\text{C-H}2}^*$ is also donated into, receiving electron density from the lone pair on the phosphorus. It should be noted that all of these interactions are weak, with the largest denoted at 0.33 kJ mol^{-1} , however they give an indication of the binding motif present in this complex beyond simple electrostatic or lone pair interactions point-to-point interactions.

Given that both anion structures are free rotors around the axis of the C–H bond the calculated W2w ADEs for these complexes have been determined for transitions to both neutral minima. For 1a the two ADEs for transitions to 1c and 1e are 1.324 eV and 1.321 eV , respectively, whereas these values are 1.332 eV and 1.328 eV for 1b. The VDEs for structures 1a and 1b at W2w level of theory are then 1.328 eV and 1.339 eV . Modelling the FCFs of these transitions yields values $|\det(S)|$ where S is the overlap matrix of the two states. In probable transitions this value is near 1,

Table 6.2: Intermolecular interaction NBO analysis for structure 1e.

	NBO_i	Occupancy	E_i (a.u.)	NBO_j	Occupancy	E_j (a.u.)	$E^{(2)}$ kJ mol ⁻¹
C–H…P	$\sigma(C1 – H3)$	0.99909	-0.61793	Ry(P7)	0.00016	1.14187	0.25
C–H…P–H	$\sigma(C1 – H3)$	0.99909	-0.61793	$\sigma^*(P7 – H8)$	0.00163	0.33465	0.33
H–P…C	$\sigma(H6 – P7)$	0.99772	-0.57057	Ry(C1)	0.00012	1.16498	0.21
H–P…H	$\sigma(H6 – P7)$	0.99772	-0.57057	Ry(H4)	0.00006	1.81723	0.13
H–P…H	$\sigma(H6 – P7)$	0.99772	-0.57057	Ry(H5)	0.00006	1.81723	0.13
H–P…C–H	$\sigma(H6 – P7)$	0.99772	-0.57057	$\sigma^*(C1 – H2)$	0.00049	0.54600	0.25
P–H…C	$\sigma(P7 – H8)$	0.99795	-0.57006	Ry(C1)	0.00012	1.16498	0.13
P…C–H	LP(P7)	0.99915	-0.57770	$\sigma^*(C1 – H2)$	0.00049	0.54600	0.33

indicating good overlap between the vibrational states of the anion and neutral. For transitions from both anion conformers to the 1e conformer the geometry change is large. The calculated $|det(S)|$ values for these transitions are both 0 which is indicative of negligible overlap between states. It is likely that photodetachment will still occur for these transitions however only for highly vibrationally excited states, at energies greater than the D_0 of the neutral. The conditions present in the vibronic simulation are those of the experiment, with temperatures set to 50 K and no hot-bands and minimal excitations in the final state present, albeit with those excitations in the full subspace. The more probable transitions are those from the anion conformers to 1c, with $|det(S)|$ values of 0.465 and 0.389 respectively. While again too low to model the photodetachment spectra, the associated ADEs of are 1.324 eV and 1.332 eV so these spectra may be distinguishable on an energy basis alone. Both atom reordering and extending the number of allowed vibrations in both the initial and target states similarly did not produce better overlap between states.

On the whole, while the $\text{PH}_2\cdots\text{CH}_4$ complexes are weakly bound, the D_0 values of the anion are larger than those of complexes observed previously in the Wild Group.³⁰⁰ The photoelectron spectra that result are likely to represent photodetachment to either highly vibrationally excited bound states or unbound conformers of the neutral.

6.3.2 $\text{PH}_2^- \cdots \text{C}_2\text{H}_4$ Complexes

For the complexes of $\text{PH}_2^- \cdots \text{C}_2\text{H}_4$, similar structures are minimised as those for the corresponding halide clusters (Figure 6.2). Those determined via *ab initio* methods have been determined recently within the Wild Group,³⁶³ and also described in Chapter 4. The anion complexes with C_2H_4 show similar orientation to those of the CH_4 complexes, with two minima (denoted 2a and 2b) where the $\text{C}=\text{C}$ bond is bifurcated by the PH_2^- . In these conformers, the hydrogens similarly face towards and away from the C_2H_4 and are orientated such that they lie out-of-plane of the C_2H_4 . An additional anion structure denoted 2c is appended to one of the hydrogens of the C_2H_4 with the $\text{H}-\text{P}-\text{H}$ bond similarly bisected by the plane of the C_2H_4 . In the neutral complexes, four minima were located; one structure similar to the 2b anion complex (2f); two where the PH_2 lies roughly perpendicular to the $\text{C}=\text{C}$ bond but out of the plane of the molecule (2e, 2g); and one where the phosphorus lies at an acute angle from the plane of the C_2H_4 (2d). Structures 2e and 2g are similar to those found in the $\text{X} \cdots \text{C}_2\text{H}_4$ neutral complexes. The bonding interaction in the anion and neutral complexes in this case is similar to that of the halide complexes. In the anions, the structures present would suggest that again, coordination with hydrogen atoms do dominate the interaction however the absence of an end-on structure (where a single CH_2 moiety is interacting with the anion), suggests that the interaction is only favoured where electron density does not destabilise a neighbouring hydrogen. As such comparing stability of complexes with differing bonding motifs in the halide and PH_2^- complexes, the D_0 values range from 23.1 kJ mol^{-1} to 18.1 kJ mol^{-1} for $\text{Cl}^- \rightarrow \text{I}^-$ in the bifurcated structure which similar to those of 2a and 2b (21.4 kJ mol^{-1} and 20.0 kJ mol^{-1} respectively). This is attributed to a charge-induced dipole interaction between the anion and the $\text{C}=\text{C}$ bond. As noted in Chapter 4, for the hydrogen-appended structure the iodide complex tends towards a bifurcated minima with AVQZ basis sets. The presence of the chloride and bromide minima at this level of theory, coupled with the similarly bound PH_2^- complex,

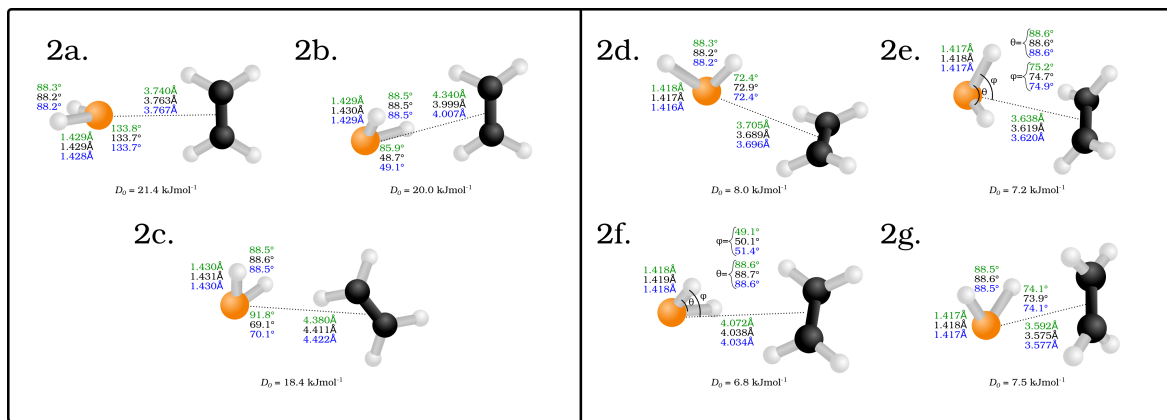


Figure 6.2: Optimised structures of the $\text{PH}_2 \cdots \text{C}_2\text{H}_4$ anion (left) and neutral (right) complexes. Structures are calculated with the DSD-PBEP86-D3BJ functional and def-2QZVP (green), AVTZ (black) and AVQZ (blue) basis sets. Associated D_0 values are included for each structure from W2w methods.

suggests that while the anions are bound by a charge-induced dipole interaction, the polarisability of the anion is also important. Where the anion is more polarisable, the bifurcated structure would appear to be favoured with respect to the hydrogen bound structure.

For the neutral complexes, previous experimental studies of the $\text{H}_2\text{O} \cdots \text{C}_2\text{H}_4$ complex by electric resonance spectroscopy showed a structure of C_s symmetry where the O–H bond was directed towards the C=C bond.⁴²⁸ Later THz absorption spectra showed large OH liberational modes at 255.0 cm^{-1} and 187.5 cm^{-1} corresponding to two weakly bound conformers with OH $\cdots\pi$ interactions.⁴²⁹ Previous calculations utilising a composite CBS extrapolation ($(E(\text{MP2})_{\text{CBS}} + (E(\text{CCSD}(T)) - E(\text{MP2}))_{\text{AVTZ}}$) method¹⁷⁰ determined interaction energies for a number of C_2H_4 dimer conformers.⁴³⁰ The conformer with the highest calculated interaction energy is similar to that of the bifurcated $\text{PH}_2 \cdots \text{C}_2\text{H}_4$ complex, representing two staggered monomers of D_{2d} symmetry. The interaction energy of this structure is $-6.15 \text{ kJ mol}^{-1}$ which agrees well with a previously calculated value at CBS of $-6.44 \text{ kJ mol}^{-1}$.⁴³¹ While not directly comparable to the D_0 values calculated here (as it accounts for perturbation of the monomers when interacting), the interaction energy is similar to the calculated W2w value of the comparable 2f structure (6.8 kJ mol^{-1}). The remaining neutral

structures are slightly more stable with D_0 values of 8.0 kJ mol^{-1} , 7.2 kJ mol^{-1} and 7.5 kJ mol^{-1} for 2d, 2e and 2g respectively. The authors also decompose the interaction energies present in the C_2H_4 dimer using Symmetry-Adapted Perturbation Theory (SAPT2) methods, noting that the interaction energy is determined largely by exchange contributions at intermolecular distances less than $11a_0$.⁴³⁰ It is likely however, given the polarisability of the C=C bond that the induced dipole-dipole interaction is what drives bonding in the neutral $\text{PH}_2\cdots\text{C}_2\text{H}_4$ complexes.

	2a	2b	2c	2a	2b	2c	2a	2b	2c
2d	1.406	1.386	1.391	0.009	0.017	0.013	0.753	0.654	0.638
2e	1.419	1.399	1.404	0.016	0.009	0.009	0.752	0.756	0.616
2f	1.411	1.392	1.396	0.011	0.013	0.010	0.718	0.990	0.491
2g	1.424	1.404	1.409	0.020	0.009	0.010	0.845	0.665	0.661

Table 6.3: Left: Calculated $\text{PH}_2^-\cdots\text{C}_2\text{H}_4$ ADE transitions between pairs of anion and neutral complexes. Middle: Calculated MADs of those ADEs from the set of transition combinations. Right: $|\det(S)|$ values from modelling photodetachment spectra with Duschinsky rotations. Both the middle and right sections of the table are coded independently with red and green representing minimum and maximum values respectively.

Finally, comparing the ADEs for the $\text{PH}_2^-\cdots\text{C}_2\text{H}_4$ complexes, while those presented in Appendix E correspond to transitions between similar geometries, due to the larger conformer space additional transitions are included for completeness (see Figure 6.3). Also in Table 6.3 are the mean absolute deviation (MAD) values for each ADE within the set and the $|\det(S)|$ value of that transition from ezSpectrum. The largest MAD value is that for the $2g\leftarrow 2a$ (0.020 eV), however over the set the average MAD is 0.012 eV. This values do not account for FCFs of individual transitions and as such larger changes in energy also correspond to large conformer changes. The analysis does, however, suggest that from an energy perspective, many of the transitions may not be distinguishable from each other. However within the $|\det(S)|$ values, those transitions from the most stable anion conformer 2a, range between 0.718 and 0.845. While these are significantly higher than that of the $\text{PH}_2\cdots\text{CH}_4$ complexes, these transitions do not produce suitable intensities under restricted vibrational excitation. Due to the strong similarity between the 2b and 2f structures,

the $|det(S)|$ value for this transition is 0.990. These calculations are similarly undertaken at a temperature of 50 K to replicate a molecular beam environment. To filter the calculated vibronic spectrum for clarity, the maximum vibrational quanta included are set to 3 and 8 for the anion and neutral electronic states respectively and only intensities greater than 5×10^{-4} are included. The resulting stick spectrum, convoluted with an energy resolution of 5 meV, is presented in Figure 6.3a and shows an intense peak belonging to the band origin (ADE). Full assignment of the FCFs is provided in Table E117. An additional feature lies at approximately 1.4 eV and forms a shoulder on the main peak with the most intense transition in this region originating from 3_0^2 (1.4094 eV) and corresponding to the twisting mode of the PH_2^- .ⁱ The next comparable transition ($2g \leftarrow 2a$) is shown in Figure 6.3b, however the intensities of vibronic transitions are negligible when compared to those in the $2f \leftarrow 2b$ with the required intensity threshold of 5×10^{-30} to populate the spectrum. Also present in the $2f \leftarrow 2b$ spectrum are a number of combination bands ranging from 1.6923 eV to 1.7219 eV representing combination bands of single quantum of both the symmetric or asymmetric stretches of PH_2 with vibrational quanta of the low frequency intermolecular modes. The spectrum demonstrates that the geometric similarity between the structures 2b and 2f favour photodetachment with $v'', v' = 0$. This is not the case for analogous CH_4 complexes, and combined with the relatively stronger binding of the anion complex and measurable E_{stab} value, suggests that the $\text{PH}_2^- \cdots \text{C}_2\text{H}_4$ represent good candidates for PES experiments.

6.3.3 $\text{PH}_2^- \cdots \text{HCCH}$ Complexes

The $\text{PH}_2 \cdots \text{HCCH}$ complexes contain only a single anion minimum bound axially to one of the hydrogen atom, and three neutral minima (Figure 6.4). Of the three neutral minima (denoted 3b, 3c and 3d) only 3b is appended in a fashion that is

ⁱIn the notation used here ($X_{v''=a}^{v'=b}$); X represents the vibration mode excited (ie ω_X); and a and b represent the number of vibrational quanta in that mode in the ground and excited electronic states respectively

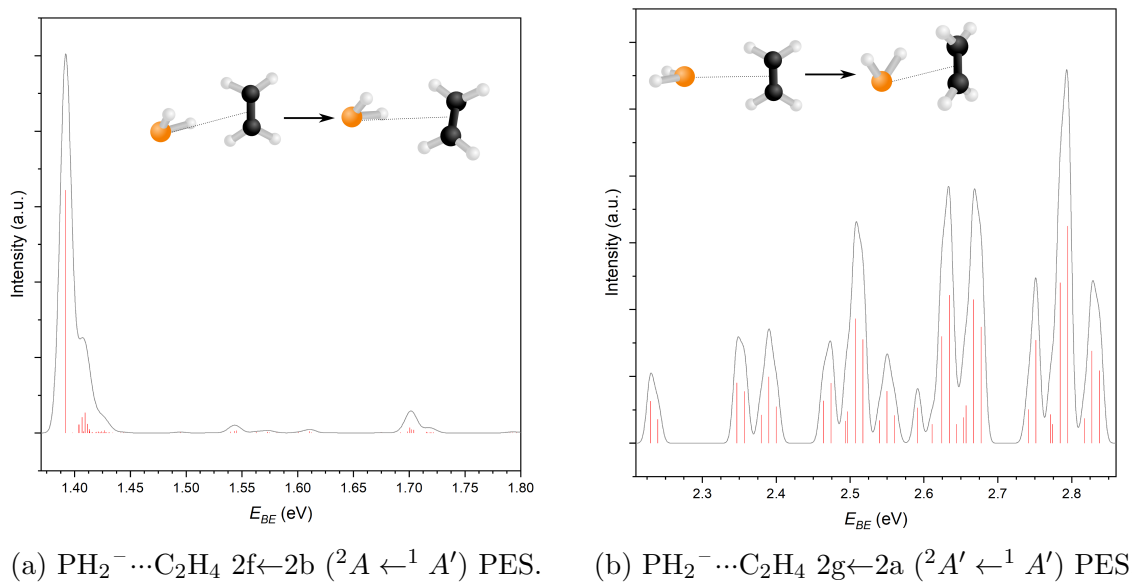


Figure 6.3: Simulated photoelectron spectra for the transitions representing (a) $2\text{f} \leftarrow 2\text{b}$ and (b) $2\text{g} \leftarrow 2\text{a}$ of the $\text{PH}_2^- \cdots \text{C}_2\text{H}_4$ complex. Stick spectra (red) represent the individual FCFs calculated. The black trace is a Gaussian convolution with width, $\omega = 0.005$.

comparable to the anion. For 3b the molecular dipole of PH_2^- interacts with partial charge on the hydrogen and inducing a weak dipole in the $\text{C}\equiv\text{C}$ bond. The two remaining neutral structures interact via an alignment of the dipoles within bonds. In the case of 3c where the hydrogens are out of the $\text{C}-\text{C}-\text{P}$ plane, the dipole-dipole interactions appear to be with the molecular dipole of PH_2 as a whole (0.57 D in the monomer). Conversely, for structure 3d, the dipole-dipole interaction appears to be within the $\text{P}-\text{H}$ bond itself with the bond-parallel dipole component of similar magnitude (0.41 D). All three neutral structures are similarly weakly bound as the $\text{PH}_2 \cdots \text{CH}_4$ complexes discussed previously with the largest D_0 being 6.5 kJ mol^{-1} . In the same THz absorption work described previously, the $\text{H}_2\text{O} \cdots \text{HCCH}$ complex was confirmed to have a C_{2v} symmetry structure where the oxygen is bound via a hydrogen-bonded axially to the acetylene.⁴²⁹ This shows great similarity in structure to 3b in the $\text{PH}_2 \cdots \text{HCCH}$ complexes calculated here. Additionally, CCSD(T)-F12b/AVQZ calculations predict two $\text{H}_2\text{O} \cdots \text{HCCH}$ geometries; the former bound axially is more stable with a comparable D_0 to the analogous PH_2 complex of 9.10 kJ mol^{-1} ; and the latter is bound perpendicularly with a D_0 of

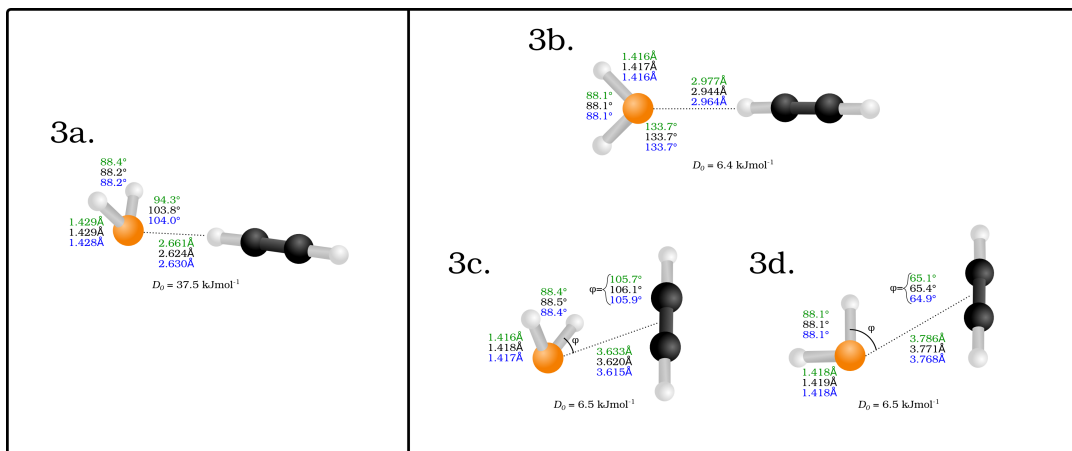


Figure 6.4: Optimised structures of the $\text{PH}_2\cdots\text{HCCH}$ anion (left) and neutral (right) complexes. Structures are calculated with the DSD-PBEP86-D3BJ functional and def-2QZVP (green), AVTZ (black) and AVQZ (blue) basis sets. Associated D_0 values are included for each structure from W2w methods.

6.35 kJ mol^{-1} .

$$V(R, \theta) = \frac{Q\Theta P_2(\cos \theta)}{(4\pi\epsilon_0)R^3} - \frac{1}{2} \frac{Q^2(\alpha_{||} \cos^2 \theta + \alpha_{\perp} \sin^2 \theta)}{(4\pi\epsilon_0)^2 R^4} \quad (6.5)$$

The anion structure is dominated by the charge-induced dipole and charge-quadrupole interaction (Equation 6.5)⁴³² and is a relatively strong vdW bond, with a D_0 of 37.5 kJ mol^{-1} . In Equation 6.5; Q is the charge on the anion, Θ is the quadrupole moment, P_2 is the second-order Legendre polynomial (where θ is the X-|||C angle) and $\alpha_{||}$ and α_{\perp} are the parallel and perpendicular polarisabilities of HCCH. Comparing the bonding interaction with previously studied halide-acetylene complexes,²⁵⁹ the anion corresponds to the $C_{\infty v}$ structure and the halogen-acetylene complexes similarly exhibit bonding both axially and orthogonally. As was demonstrated for the $\text{PH}_2^- \cdots \text{CH}_4$ complexes, the D_0 values of the hydrogen-appended anion is most similar to the corresponding Br^- complex. This suggests that the strength of interaction is similar in both cases and implies that calculation of Br^- complex stability may have some predictive capacity while reducing the dimensionality of the problem. Considering the D_0 values of the C_2H_4 complexes are 22.1 kJ mol^{-1} and 18.4 kJ mol^{-1} respectively, this appears to hold for simple cases.

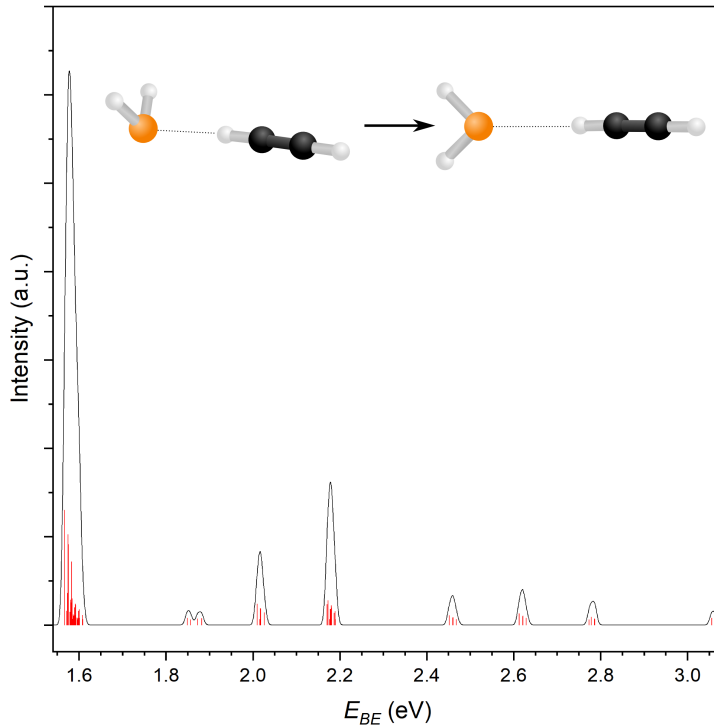


Figure 6.5: Simulated photoelectron spectrum for the transitions representing $3b \leftarrow 3a$ ($^2B_1 \leftarrow ^1A'$) of the $\text{PH}_2^- \cdots \text{HCCH}$ complex. Stick spectra (red) represent the individual FCFs calculated. The black trace is a Gaussian convolution with width, $\omega = 0.005$.

Given that previous vibronic transition calculations have only been appropriate in cases where there is little change in geometry between the initial and final states only the $3b \leftarrow 3a$ transition has been modelled for these complexes. As the E_{stab} of a given complex is determined by the difference in their D_0 values, the E_{stab} of the $\text{PH}_2^- \cdots \text{HCCH}$ complexes is 0.32 eV and should be readily distinguished from bare PH_2^- in experiment.

The simulated spectrum, shown in Figure 6.5 shows comparable intensities to those of the $2f \leftarrow 2b$ transitions detailed in the Figure 6.3. This represents a good candidate for PES spectroscopy, especially given the relevance of acetylene in the formation of polycyclic aromatic hydrocarbons (PAH) species of astrochemical significance.⁴³³ The spectrum consists of an intense transition at the band origin with numerous peaks of similar binding energy to the ADE (~ 1.6 eV). These transitions correspond to detachment to excited vibrational states and combination bands of the low

frequency intermolecular modes. This is likely due to the significant difference in geometry between the anion and neutral states, and that the neutral C_{2v} geometry represents a displacement along the PH_2 wagging mode. Two such modes are assigned in Table E118 (ω_2 and ω_4) as this molecular wag, be that coupled with vibrations within the HCCH. Higher binding energy features at 1.85, 2.0, 2.2, 2.45, 2.6, 2.8 and 3.05 eV then represents combination bands of the ω_{10} , ω_{12} and ω_{13} modes which represent the PH_2 scissor, symmetric and asymmetric stretch respectively. These modes can similarly be accounted for by the equilibrium geometry change upon photodetachment with the length of the P–H reducing from 1.428 Å to 1.416 Å.

6.3.4 $\text{PH}_2^- \cdots \text{CO}_2$ Complexes

Geometry optimisations of the $\text{PH}_2 \cdots \text{CO}_2$ anion and neutral complexes have returned two minima for each state respectively. Most notable of the anion structures is 4b (see Figure 6.6) where a dative bond appears to be formed between the lone pair of the PH_2^- and the CO_2 . The length of this bond is 1.943 Å and is significantly stronger than any interaction in a PH_2 complex discussed thus far ($D_0=108.7 \text{ kJ mol}^{-1}$). The PH_2 group in this case sits out-of-plane from the CO_2 group with a dihedral angle of 100.0°. This interaction also deforms the CO_2 from linearity to an O–C–O angle of 132.7°. This structure is indicative of recently quantitatively synthesised, air-stable phosphinecarboxamide ($\text{PH}_2\text{C(O)NH}_2$).^{434,435} In this case, X-ray diffraction experiments support the bonding motif and orientation of the PH_2 group. This structure agrees well with recent calculations of PH_2COO^- where the P–C bond was determined to be 1.967 Å (PBE1PBE/6-31g++g(d,p)),⁴³⁶ 1.963 Å (M06-2X/AVTZ) and 1.994 Å (B3LYP-D3/AVTZ).⁴¹⁴ The associated D_0 was also determined via G4-T CBS extrapolation as 59.6 kJ mol^{-1} .⁴³⁶ Structure 4a, while still a minimum, does not represent the global minimum of the surface. It is bound, with a D_0 of 27.1 kJ mol^{-1} , however requires the constraint of the CO_2

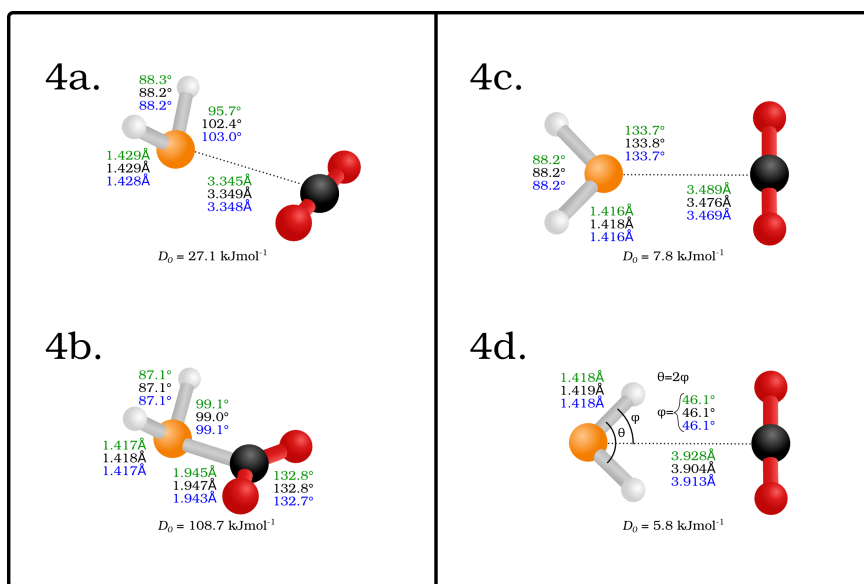


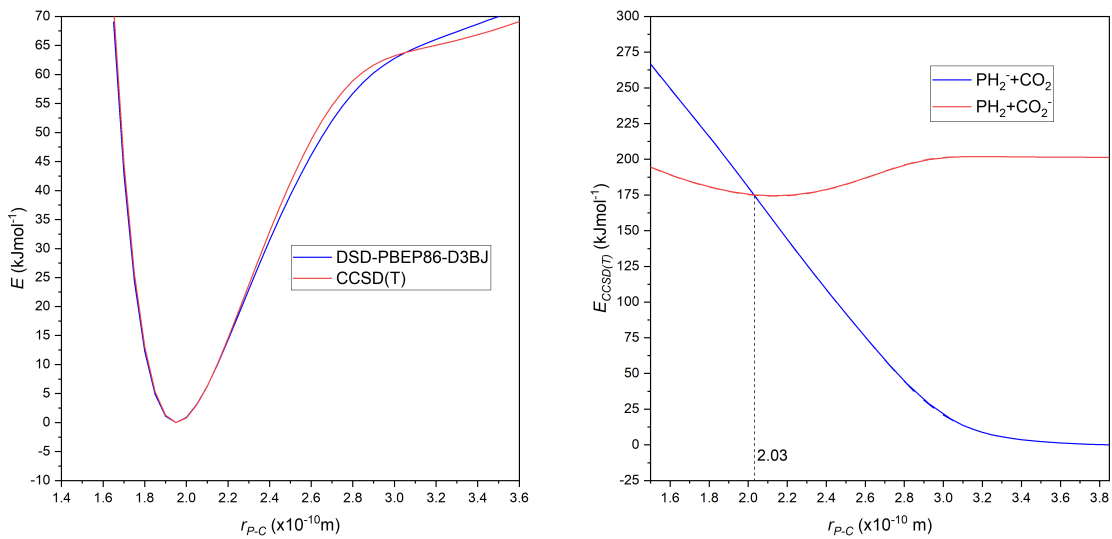
Figure 6.6: Optimised structures of the $\text{PH}_2\cdots\text{CO}_2$ anion (left) and neutral (right) complexes. Structures are calculated with the DSD-PBEP86-D3BJ functional and def-2QZVP (green), AVTZ (black) and AVQZ (blue) basis sets. Associated D_0 values are included for each structure from W2w methods.

being linear. Two C_{2v} structures are determined to be minima for the neutral $\text{PH}_2\cdots\text{CO}_2$ complex, where the hydrogens of PH_2 are pointed away from (4c) and towards (4d) the CO_2 . Both structures exhibit typical vdW dimer D_0 values with stabilities of 7.8 kJ mol^{-1} and 5.8 kJ mol^{-1} respectively. Following the optimisation of the PH_2COO^- anion, as it had not been similarly calculated for the neutral, the anion geometry was used as a starting point to determine whether the corresponding formate radical could be optimised. For all basis sets the optimisation would tend back towards structure 4c suggesting that the formal charge is crucial in PH_2COO^- formation.

To investigate the pathway of PH_2COO^- formation, a relaxed potential energy surface scan was undertaken. DSD-PBEP86-D3BJ/AVTZ optimisations were completed at fixed P–C distances ranging from 1.50 \AA to 3.85 \AA . In addition to the DFT optimisations, upon completion a CCSD(T) energy calculation was performed for the complex. The complex energies determined from the relaxed scan are shown in Figure 6.7a and highlights the similarities in CCSD(T) and DFT energies across the scan. This validation of double-hybrid energies demonstrates the confidence of the

functional in approaching species with long-range interactions. Present in the scan is a minimum in the P–C coordinate that corresponds approximately to the global minimum, the phosphino formate anion (PH_2COO^-). There appears also in the CCSD(T) scan, a reduction in the energy gradient at P–C distances around 3.0\AA to 3.2\AA . This may be a region of meta-stability that leads to the formation of the $\text{PH}_2^- \cdots \text{CO}_2$ vdW complex (4a), however the scan also suggests that the formation of the phosphino formate anion is barrierless. This is particularly pertinent given that previous experimental studies have only recently produced the analogous neutral.⁴³⁷ In previous work, the authors utilised vacuum ultraviolet photoionization reflectron TOF-MS to produce phosphino formic acid (PH_2COOH) from binary mixtures of PH_3 and CO_2 ices alongside B3LYP optimisations and CCSD(T)/CBS energies. They report a vdW pre-reaction complex ($\text{PH}_3 \cdots \text{CO}_2$) with a D_0 of 4 kJ mol^{-1} and a barrier to phosphino formic acid formation of 261 kJ mol^{-1} . Contrary to this work, the potential energy scan presented here and the D_0 of PH_2COO^- coupled with the fact that PH_2^- readily forms via dissociative electron attachment⁴¹⁰ suggests that an alternate pathway to formation is indeed present. This is further supported by the recent syntheses of NaPH_2CO_2 (referred to a phosphine carboxylate in these works) via direct reaction or hydration of NaPCO under basic conditions.^{436,438}

The charge-transfer thermodynamics of the $\text{PH}_2^- + \text{CO}_2$ reaction were similarly investigated by CCSD(T)/AVTZ single point energies of the anion and neutral fragments of the perturbed PH_2COO^- geometry (PH_2 , PH_2^- , CO_2 , CO_2^-). By considering the comparative stability of non-interacting fragments ($\text{PH}_2^- + \text{CO}_2$ or $\text{PH}_2 + \text{CO}_2^-$), the point at which charge-transfer is favoured can be identified. These surfaces are presented in Figure 6.7b where, at longer P–C bond distances, the PH_2^- anion is favoured. When reducing the P–C distance the CO_2^- anion becomes favoured from $\sim 2.03\text{\AA}$ indicating charge-transfer and bond formation. This is likely due to the deformation and breakdown of degeneracy of the $\text{CO}_2 \pi$ orbitals and localisation of charge on the oxygen atoms. This distance also corresponds well to the minimum P–C bond distance but also provides insight into the tolerance to



(a) Relaxed potential energy scan along the r_{P-C} coordinate with both DSD-PBEP86-D3BJ geometries and energies (blue) and CCSD(T) single point energies (red). Energy is relative to that of the minimum geometry.

(b) Potential energy of the perturbed geometry component fragments where formal charge is assigned to either fragment. The lower of the two curves then represent where charge is favoured for a given r_{P-C} distance.

Figure 6.7: Potential energy scans of (a) the energy of the $\text{PH}_2^- \cdots \text{CO}_2$ complex and (b) perturbed geometry component fragments where formal charge is assigned to either fragment. All energies are in kJ mol⁻¹.

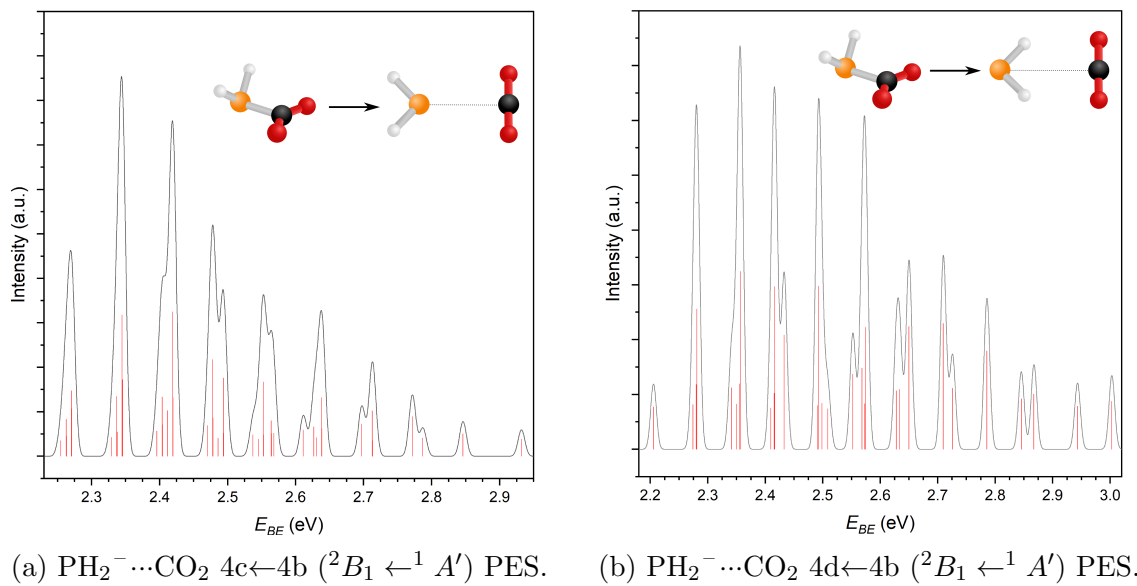


Figure 6.8: Simulated photoelectron spectra for the transitions representing (a) $4\text{c} \leftarrow 4\text{b}$ and (b) $4\text{d} \leftarrow 4\text{b}$ of the $\text{PH}_2^- \cdots \text{CO}_2$ complex. Stick spectra (red) represent the individual FCFs calculated. The black trace is a Gaussian convolution with width, $\omega = 0.005$.

deformation within the bond. Within a PES experiment, the reaction could be readily confirmed as the change in electronic environment results in photodetachment from the COO^- moiety rather than a perturbed PH_2^- . This represents a change in the ADE from 1.462 eV and 1.472 eV for the vdW complex to 2.134 eV and 2.149 eV for the phosphino formate anion.

Comparing the two simulated spectra in Figure 6.8, representing transitions from structure 4b to the two neutral complexes it can be seen that there are similar band structures present. For Figure 6.8a, the spectrum appears structured predominantly around a single vibrational progression with combination bands included. This corresponds to the ω_6 mode, a planar rocking mode of the CO_2 molecule, and appears to be restorative of the linear CO_2 structure of the neutral. The other modes present as combination bands include quanta in the ω_8 and ω_{11} modes which correspond to the PH_2 scissor and asymmetric stretch. As with previous complexes, these are due to the change in geometry of the PH_2 moiety upon photodetachment. In Figure 6.8b, similar vibrational progressions are present, with quanta in the ω_6 , ω_8 and ω_{11} modes contributing to transitions. While vdW modes can contribute to the

combination bands, only the intermolecular P–C stretching mode appears to be included in the spectrum. Experimentally, while both spectra show similarities in spectral features and indeed contain quanta of similar vibrational modes, they can likely be discriminated by their relative intensities. While the intensity threshold for the $4c \leftarrow 4b$ spectrum is set to 1×10^{-7} , in order to populate the $4d \leftarrow 4b$ spectrum this was needed to be reduced to 1×10^{-11} . The relative intensities can be again attributed to conformational similarity between the anion and neutral structures, with the most similar to structure 4b being 4c. As such it is expected that only the $4c \leftarrow 4b$ spectrum would be observed. In extraterrestrial environments such as Venus, the high atmospheric composition of CO₂⁴²⁰ coupled with the high energy environment of electrical activity in the atmosphere,⁴³⁹ suggests that the phosphino formate anion may represent a possible atmospheric sink. Collectively, this with the ability to discriminate between anion structures based on the observed ADE and the ability to determine probably neutral photodetachment based on the band structures and intensities suggest that PH₂⁻…CO₂ is a prime candidate to explore PH₂ gas phase reactivity.

6.3.5 PH₂⁻…H₂S Complexes

As noted in Section 6.2 the proton affinities of PH₃ and H₂S are 1522.0(63) kJ mol⁻¹²⁰ and 1470.42(25) kJ mol⁻¹⁴²⁵ respectively. In the anion, this results in proton transfer within the PH₂⁻…H₂S complex to form PH₃…HS⁻. These structures, denoted 5a-5d are shown in Figure 6.9, along with a number of neutral minima. Some neutral conformers were not optimised with the def-2QZVP basis sets and structures are only reported for calculations with Dunning basis sets (5h-5k). Given that proton transfer is likely, a number of neutral PH₃…HS (5g, 5j) complexes were optimised alongside the PH₂…H₂S complexes (5e, 5f, 5h, 5i, 5k) and it was these that were used for photoelectron spectra simulation. Both the anion and neutral complexes present similar bonding motifs to those discussed previously, where hydrogen bond-

ing interactions appear to dominate structures 5a and 5b while donation from the lone pair of the HS^- to the LUMO orbital of the PH_3 drives the interaction in 5c and 5d. All anion structures are of similar stability with D_0 values ranging from 28.6 kJ mol^{-1} (5c) to 29.1 kJ mol^{-1} (5b). What is noticeable is the breakdown of C_{3v} symmetry typically present in PH_3 during proton transfer and complexation. In cases where the interaction is electrostatic in nature (5a, 5b) there is a lengthening of the P–H bond axially towards the sulfur atom while the remaining P–H bonds are unperturbed with respect to monomer PH_2 . This interaction is also expressed in the destabilisation of the P–H stretching modes. While the calculated modes are harmonic, and the proton transfer would be expected to be significantly anharmonic, the high frequency modes of the PH_3 monomer (2423 cm^{-1} and doubly degenerate 2430 cm^{-1}) are red shifted to 2085 cm^{-1} , 2398 cm^{-1} and 2399 cm^{-1} respectively within 5a with the lowest of these modes corresponding to proton transfer. Where the interaction is one of donation, as is the case for structures 5c and 5d, there is a distinct destabilisation and lengthening of the far-side P–H bond (1.414 \AA to 1.442 \AA in 5c) with a corresponding contraction of the remaining P–H bonds to 1.407 \AA . For the corresponding neutral $\text{PH}_2\cdots\text{H}_2\text{S}$ complexes where the S–H bond is directional to the phosphorus atom, while there is a small red shift present in one of the modes ($5\text{h}:\Delta = 18 \text{ cm}^{-1}$), it is minimal by comparison to the anion.

Of the neutral complexes, the $\text{PH}_2\cdots\text{H}_2\text{S}$ complexes exhibit typical stabilities to those seen for other PH_2 vdW complexes. The SH complexes however, are significantly more stable and 5j is the most stable of structures from either the anion or neutral complexes ($D_0=42.0 \text{ kJ mol}^{-1}$). This stability is also represented by the significant blue shift in the vdW vibrational modes when compared with other complexes, the P–S stretch for example is 224 cm^{-1} compared to 65 cm^{-1} in 5g. This structure has precedent in literature and has been optimised using UMP2/6-311G** and thermodynamics calculated using QCISD(T).⁴⁴⁰ In these calculations and others, PH_3 forms a hyperconjugated trigonal bipyramidal structure where the lone pair electrons extend axially or equatorially from the phosphorus forming mercap-

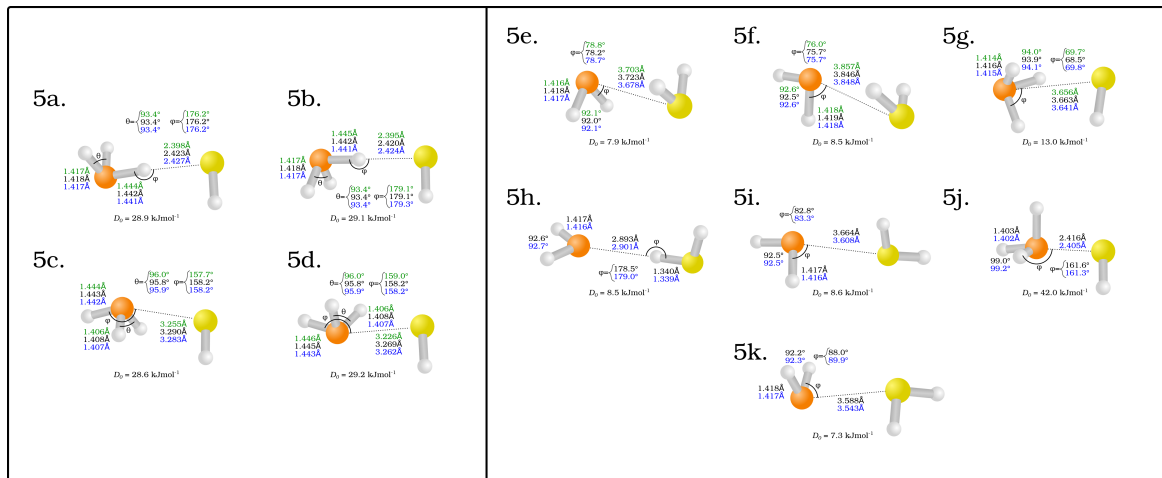


Figure 6.9: Optimised structures of the $\text{HS}^- \cdots \text{PH}_3$ anion (left) and neutral (right) $\text{PH}_2 \cdots \text{H}_2\text{S}$ and $\text{HS} \cdots \text{PH}_3$ complexes. Structures are calculated with the DSD-PBEP86-D3BJ functional and def-2QZVP (green), AVTZ (black) and AVQZ (blue) basis sets. Associated D_0 values are included for each structure from W2w methods.

topophosphoranyl H_3PSH .⁴⁴¹ The orientation of the thiol group in this structure would then likely align with the electron density of the phosphorus lone pair. An analogous axial structure to 5j has been reported as a transition state in previous work⁴⁴⁰ with a relative energy D_e of $-122.2 \text{ kJ mol}^{-1}$. No such equatorial conformer has been reported in literature to the writer's knowledge and photodetachment to such a radical may be of interest in studying hyperconjugation spectroscopically.

The probability of proton transfer in the anion complex required that a number of analogous $\text{HS} \cdots \text{PH}_3$ complexes were also optimised. Of these, the only transition that was amenable to simulated photodetachment spectra with sufficient intensity is that of the $5\text{g} \leftarrow 5\text{b}$ transition and is presented in Figure 6.10. The onset of the spectrum begins with the ADE and has a comparable intensity threshold to the $2\text{f} \leftarrow 2\text{b}$ and $3\text{b} \leftarrow 3\text{a}$ spectra. The spectrum also features two distinct vibrational bands with peak intensities at approximately 4.1 eV and 4.2 eV respectively. The dominant band is made up of combinations of low frequency modes, namely the ω_1 , ω_3 and ω_4 corresponding to the intermolecular stretch and rotations of the PH_3 group, with a progression in the symmetric PH_3 stretch ($\omega_9, v' = 1 - 7$). The secondary band is made up of the same vibration modes with an additional quantum

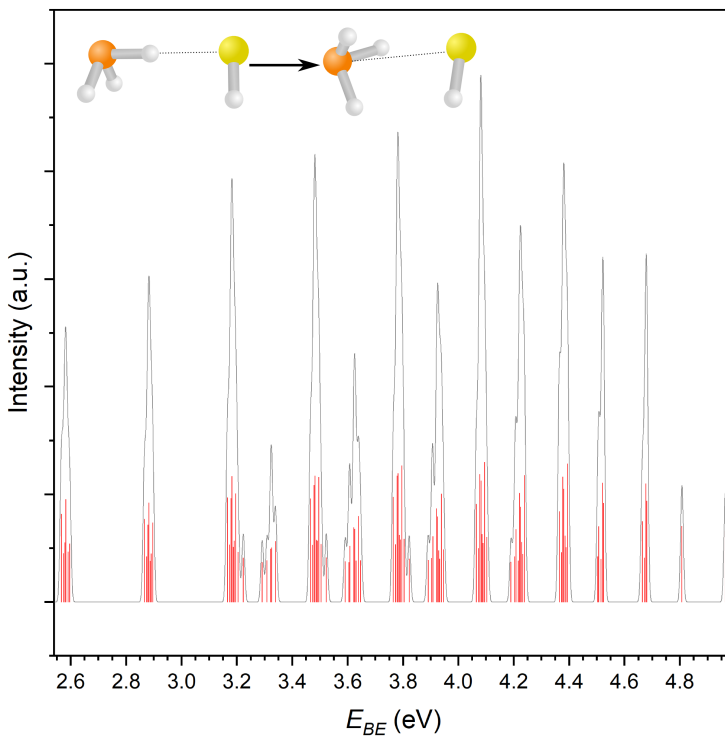


Figure 6.10: Simulated photoelectron spectrum for the transitions representing $5g \leftarrow 5b$ ($^2A \leftarrow ^1A'$) of the $\text{HS}^- \cdots \text{PH}_3$ complex. Stick spectra (red) represent the individual FCFs calculated. The black trace is a Gaussian convolution with width, $\omega = 0.005$.

of PH_3 asymmetric scissor ($\omega_7, v' = 1$).

6.3.6 $\text{PH}_2^- \cdots \text{NH}_3$ Complexes

Lastly, anion and neutral complexes of $\text{PH}_2 \cdots \text{NH}_3$ were optimised with a single anion minimum and three neutral minima determined (Figure 6.11). The structure of the PH_2 in the anion and neutral geometries is relatively unperturbed with respect to monomer PH_2 . For the anion the P–HN distance is comparable to other PH_2^- complexes interacting electrostatically, while in the neutral complexes the P–N are longer ($\sim 3.3 \text{ \AA}$ for 6b, 6d). While the anion structure is similar to the previously calculated isovalent $\text{NH}_2^- \cdots \text{NH}_3$ complex, in that the interaction with the solvent NH_3 is hydrogen bonding, the PH_2^- complex displays C_s symmetry with the two pairs of NH_2 trans to each other.⁴⁴² It might be expected that the hydrogen-bonded proton resides equidistant between the two N atoms, the respective bond lengths are

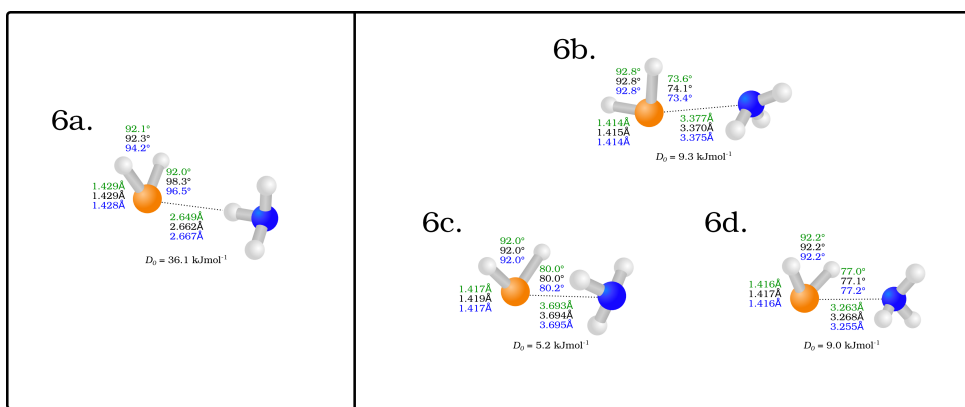


Figure 6.11: Optimised structures of the $\text{PH}_2\cdots\text{NH}_3$ anion (left) and neutral (right) complexes. Structures are calculated with the DSD-PBEP86-D3BJ functional and def-2QZVP (green), AVTZ (black) and AVQZ (blue) basis sets. Associated D_0 values are included for each structure from W2w methods.

1.068 Å and 1.852 Å in the NH_3 and NH_2 groups respectively and the equidistant structure likely representing a reversible proton transfer transition state. Similarly to the formation of PH_2COOH , electronically excited $\text{PH}_3:\text{NH}_3$ ice mixtures have been shown to produce a number of NPH_4 isomers, including structures similar to that of 6a in PH_2NH_2 .⁴⁴³ Comparing the anion structure to another rudimentary anion- NH_3 complexes, $\text{Cl}^-\cdots\text{NH}_3$, calculated MP2/AVTZ geometries a further contracted Cl-HN distance (2.290 Å) compared to that of the PH_2^- complex.⁴⁴⁴ In the corresponding OH^- complex, the bond lengths (~ 2.7 Å) are much more similar to that of the PH_2^- complex, which may be indicative of the strength of interaction present.

This can be confirmed by comparing the electronic stability of a number of complexes via their ADEs. These are presented for NH_3 solvated NH_2^- , Cl^- , OH^- and NO^- in Table 6.4, with the PH_2^- complex ADE representative of the 6d \leftarrow 6a transition. Here the PH_2^- complex presents the least stabilising affect from NH_3 solvation whereas the OH^- is most greatly stabilised upon solvation. The most comparable complex structurally, $\text{NH}_2^- \cdots \text{NH}_3$ is still significantly more stable electronically than the calculated PH_2^- complex, reflective of the higher energy orbitals from which photodetachment occurs on the phosphorus.

Comparing these energies with the simulated photoelectron spectrum we see

Table 6.4: Comparison between literature experimental ADEs for a range of NH_3 solvated anions and those calculated in this work for $\text{PH}_2^- - \text{NH}_3$.

Complex	Ref.	ADE	E_{stab}
$\text{PH}_2^- \cdots \text{NH}_3$	This work [†]	1.537	0.274
$\text{Cl}^- \cdots \text{NH}_3$	Markovich <i>et al.</i> ⁴⁴⁵	4.00	0.39
$\text{NO}^- \cdots \text{NH}_3$	Hendricks <i>et al.</i> ⁴⁴⁶	0.50	0.45
$\text{NH}_2^- \cdots \text{NH}_3$	Snodgrass <i>et al.</i> ⁴⁴⁷	1.311	0.531
$\text{OH}^- \cdots \text{NH}_3$	Schwartz <i>et al.</i> ⁴⁴⁸	2.35	0.75

[†]: This work is reliant only on computational results.

that the ADE is not present, the lowest energy transition representing 4_0^2 . This is again due to the conformational change following photodetachment and the ω_4 mode representing a rotation of the NH_3 . The bands in the presented spectrum represent progressions in the ω_{13} NH_3 symmetric stretching mode ($3492\text{ cm}^{-1} v' = 1 - 3$) combined with progressions in the ω_{10} NH_2 scissor ($1674\text{ cm}^{-1} v' = 1, 2$). As $\omega_{13} \sim 2\omega_{10}$ often transitions to states with vibrational quanta ω_{13} are close in energy to those with two quanta of the NH_2 scissor from the previous peak especially when coupled to vdW modes (ie. $4_0^2 10_0^3 13_0^1 = 2.6190\text{ eV} \sim 4_0^1 10_0^1 13_0^2 = 2.6237\text{ eV}$).

6.4 Summary

In summary, a number of PH_2 anion and neutral vdW complexes have been investigated by DSD-PBEP86-D3BJ optimisations and harmonic frequency calculations, W2w protocol single point energies and vibronic simulations. A number of vdW complexes are reported for the solvating molecules methane, ethene, acetylene, CO_2 , H_2S and NH_3 . These complexes appear nearly universally bound via a hydrogen bonding interaction on their anion potential energy surface, however exhibit a range of electrostatic, dative and hypervalent interactions in the neutrals. Of these complexes, those that are most promising to pursue with PES experiments are the transitions $2\text{f} \leftarrow 2\text{b}$ for $\text{PH}_2^- \cdots \text{C}_2\text{H}_4$, $3\text{b} \leftarrow 3\text{a}$ for $\text{PH}_2^- \cdots \text{HCCH}$, $4\text{c} \leftarrow 4\text{b}$ for $\text{PH}_2^- \cdots \text{CO}_2$ and $5\text{g} \leftarrow 5\text{b}$ for $\text{HS}^- \cdots \text{PH}_3$. In each case the simulated FCFs are suitably intense, and the change in electron binding energy (E_{stab}) is sufficient to differenti-

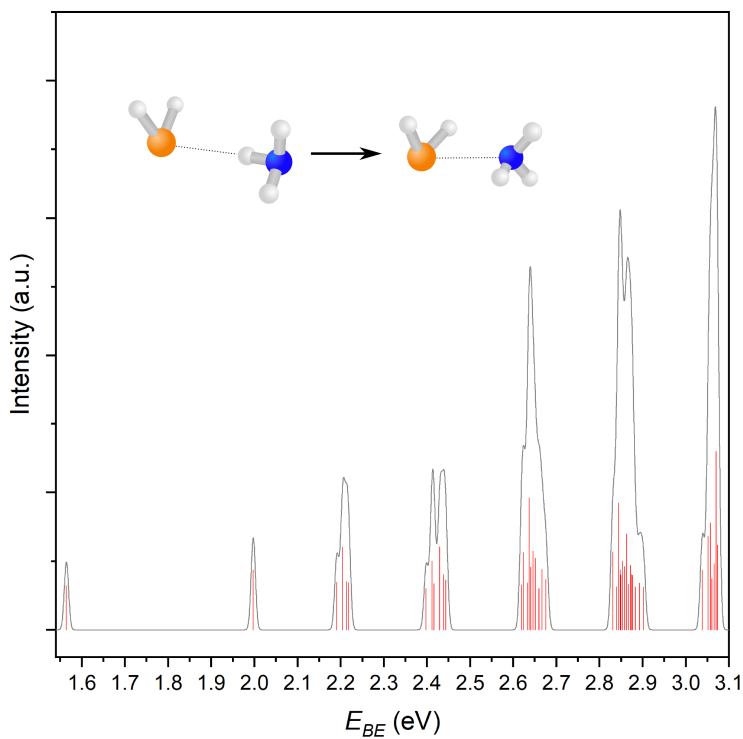


Figure 6.12: Simulated photoelectron spectrum for the transitions representing $6d \leftarrow 6a$ ($^2A \leftarrow ^1A$) of the $\text{PH}_2^- \cdots \text{NH}_3$ complex. Stick spectra (red) represent the individual FCFs calculated. The black trace is a Gaussian convolution with width, $\omega = 0.005$.

ate the complex readily from bare PH_2^- . Of particular astrochemical interest is the barrierless formation of the phosphino formate anion PH_2COO^- as it represents a notable sink for PH_2 and is favourable when compared to the thermodynamically unfavoured neutral formation of the corresponding acid.

Chapter 7

Conclusions

In this thesis, a number of ongoing improvements to the TOF-PES spectrometer at the University of Western Australia have been detailed. Utilising the existing spectrometer, a study of the transient iodide-methyperoxy complex has been performed. This PES spectrum shows evidence of photodetachment from both the superoxide complex ($O_2^- \cdots CH_3I$) and the iodide-methylperoxy complex ($I^- \cdots CH_3OO$, $E_{BE}=3.46\text{ eV}$). The calculated W1w photodetachment of the iodide-methylperoxy complex shows excellent agreement with experiment within the resolution of the spectrometer. The potential energy surfaces of the S_N2 and ET reactions have been modelled using MP2 optimisations and W1w energies to determine which is favourable. The S_N2 mechanism is shown to be favoured, and interestingly, ΔG of the reaction inverts between the anion and neutral potential energy surfaces. This further demonstrates the power of anion PES in performing spectroscopy on typically inaccessible species.

PES spectroscopy was then applied to halide complexes with propene as representative systems of atmospheric and extraterrestrial radical gas-phase chemistry. The experimental E_{BE} values, representing transitions to 2P states of the halogen perturbed by the solvating propene, are 3.89 eV and 4.00 eV, 3.59 eV and 4.01 eV, and 3.26 eV and 4.20 eV. To investigate these complexes computationally, the DSD-PBEP86-D3BJ functional was chosen as an alternative to ab intio methods for its

reduced computational cost with the intention to extend these methods to larger systems. Prior to use, the functional was validated against an existing data set of halide-molecule complexes and showed good performance in predicting both geometric and electronic structure of these complexes. When applied to the halide-propene complexes, the interaction between and the anion and propene is driven by electrostatics and does not favour coordination to the π -system of the propene. For the corresponding halogen complexes however, this interaction is much stronger, and forms a 1-chloropropyl radical in the chlorine.

Extending the DSD-PBEP86-D3BJ functional to complexes of halides and 1,3-butadiene, similar bonding motifs are present in these complexes as there were in the halide and halogen-propene complexes. PES spectra were recorded for a number of $X^- \cdots (C_4H_6)_n$ solvated complexes with $n \leq 3$ for chloride and bromide, while for the iodide complexes $n \leq 7$. For those with each additional solvating 1,3-butadiene molecule, the E_{solv} value decreased. At $n = 5$ and $n = 7$ however the E_{solv} showed increases in stability suggesting that the $n = 4$ complex is a metastable partial solvation shell surrounding the halide and the $n = 6$ complex is a complex solvation shell. DSD-PBEP86-D3BJ optimisations were undertaken on the $I^- \cdots (C_4H_6)_2$ complex to determine whether the trimer complex was forming, or whether the photoelectron signal was the result of a [4+2] cycloaddition of two butadiene molecules and the resulting iodide-4-vinylhexene complex. The VDE of this complex was found to be 3.35 eV whereas the trimer butadiene complex has a VDE of 3.52 eV, much more aligned to the experimental value of 3.47 eV.

Finally, a number of phosphorus-hydride-molecule complexes have been investigated for their relevance in extraterrestrial atmospheric contexts. The molecules chosen were CH_4 , C_2H_4 , $HCCH$, CO_2 , H_2S and NH_3 , with each complexing a PH_2^- anion. As the study did not include experimental photoelectron spectra, W2w energies were calculated from DSD-PBEP86-D3BJ functionals to ensure accurate energy determinations. Of these complexes, those that are most promising to pursue with PES experiments are the transitions $2f \leftarrow 2b$ for $PH_2^- \cdots C_2H_4$, $3b \leftarrow 3a$ for

$\text{PH}_2^- \cdots \text{HCCH}$, $4\text{c} \leftarrow 4\text{b}$ for $\text{PH}_2^- \cdots \text{CO}_2$ and $5\text{g} \leftarrow 5\text{b}$ for $\text{HS}^- \cdots \text{PH}_3$. In each case the simulated FCFs are suitably intense, and the change in electron binding energy (E_{stab}) is sufficient to differentiate the complex readily from bare PH_2^- . Of particular astrochemical interest is the barrierless formation of the phosphino formate anion PH_2COO^- as it represents a notable sink for PH_2 and is favourable when compared to the thermodynamically unfavoured neutral formation of the corresponding acid.

Collectively, the author believes the work presented in this thesis represents a significant collation of established experimental and *ab initio* methods in the application to halide-molecule vdW complexes. The introduction of DFT methods, particularly the double-hybrid functional DSD-PBEP86-D3BJ, introduces one possible route forward in calculating largely solvated systems in the gas-phase. However, these methods are themselves limited by their applicability to large systems and further work benchmarking hybrid and meta-GGA functionals may help to extend them further. A suggested strategy for this work would be to begin with high level *ab initio* methods for monosolvated complexes and then with increasing solvation ensure overlap between computational methods. Regarding the experimental work presented in this thesis, the author notes that Figure 4.4 includes peaks with m/z ratio values corresponding to $\text{I}^- \cdots (\text{C}_3\text{H}_6)_n$ ($n = 1\text{-}3$). To complement the halide-butadiene solvation study presented, further experiments on solvated halide-propene complexes may be undertaken for comparison. Additionally, while development of the SEVI spectrometer in the Wild Group has been ongoing, completion of the instrument would open new possibilities to explore, in detail, the non-covalent interactions presented in this thesis and further potential photodynamics.

References

- [1] Skouteris, D.; Manolopoulos, D. E.; Bian, W.; Werner, H.-J.; Lai, L.-H.; Liu, K. *Science* **1999**, *286*, 1713–1716.
- [2] Li, J.; Wang, Y.; An, L.; Chen, J.; Yao, L. *Journal of the American Chemical Society* **2018**, *140*, 3194–3197.
- [3] Bernstein, E. R. *Annual Review of Physical Chemistry* **1995**, *46*, 197–222.
- [4] Klemperer, W.; Vaida, V. *Proceedings of the National Academy of Sciences* **2006**, *103*, 10584–10588.
- [5] Potapov, A. *Molecular Astrophysics* **2017**, *6*, 16–21.
- [6] Calo, J. M.; Narcisi, R. S. *Geophysical Research Letters* **1980**, *7*, 289–292.
- [7] Sennikov, P. G.; Ignatov, S. K.; Schrems, O. *ChemPhysChem* **2005**, *6*, 392–412.
- [8] Ewing, G. E. *Canadian Journal of Physics* **1976**, *54*, 487–504.
- [9] Dewar, M.; Hafner, K. *Topics in Current Chemistry: Van der Waals Systems*; Springer-Verlag, New York, 1980.
- [10] Eugenia Sanz, M.; Lopez, J. C.; Alonso, J. L.; Melandri, S.; Caminati, W.; Favero, P. G. *Physical Chemistry Chemical Physics* **1999**, *1*, 239–242.
- [11] Dalbouha, S.; Boussessi, R.; Komiha, N.; Jaïdane, N.; Senent, M. *Computational and Theoretical Chemistry* **2017**, *1099*, 8–13.

- [12] Zhang, X.; Liu, G.; Ciborowski, S.; Wang, W.; Gong, C.; Yao, Y.; Bowen, K. *Angewandte Chemie International Edition* **2019**, *58*, 11400–11403.
- [13] Atkins, P.; de Paula, J. *Atkins' Physical Chemistry*, 9th ed.; Oxford University Press, 2010.
- [14] Brehm, B.; Gusinow, M.; Hall, J. *Physical Review Letters* **1967**, *19*, 737–741.
- [15] Wiley, W. C.; McLaren, I. H. *Rev. Sci. Instrum.* **1955**, *26*, 1150–1157.
- [16] Branton, G.; Frost, D.; McDowell, C.; Stenhouse, I. *Chemical Physics Letters* **1970**, *5*, 1–2.
- [17] Wickham-Jones, C. T.; Ervin, K. M.; Ellison, G. B.; Lineberger, W. C. *The Journal of Chemical Physics* **1989**, *91*, 2762–2763.
- [18] Lenzer, T.; Furlanetto, M. R.; Asmis, K. R.; Neumark, D. M. *The Journal of Chemical Physics* **1998**, *109*, 10754–10766.
- [19] Yourshaw, I.; Lenzer, T.; Reiser, G.; Neumark, D. M. *The Journal of Chemical Physics* **1998**, *109*, 5247–5256.
- [20] Ervin, K. M.; Lineberger, W. C. *The Journal of Chemical Physics* **2005**, *122*, 194303.
- [21] Calvi, R. M.; Andrews, D. H.; Lineberger, W. C. *Chemical Physics Letters* **2007**, *442*, 12–16.
- [22] Zhou, J.; Garand, E.; Neumark, D. M. *The Journal of Chemical Physics* **2007**, *127*, 154320.
- [23] Bull, J. N.; West, C. W.; Verlet, J. R. R. *Chem. Sci.* **2015**, *6*, 1578–1589.
- [24] Belogolova, E. F.; Liu, G.; Doronina, E. P.; Ciborowski, S. M.; Sidorkin, V. F.; Bowen, K. H. *The Journal of Physical Chemistry Letters* **2018**, *9*, 1284–1289.

- [25] Ohara, M.; Miyajima, K.; Pramann, A.; Nakajima, A.; Kaya, K. *The Journal of Physical Chemistry A* **2002**, *106*, 3702–3705.
- [26] Li, X.; Wang, L.-S. *The European Physical Journal D* **2005**, *34*, 9–14.
- [27] Kammerath, A.; Verlet, J. R. R.; Griffin, G. B.; Neumark, D. M. *The Journal of Chemical Physics* **2006**, *125*, 1–2.
- [28] Jellinek, J.; Acioli, P.; Garciá-Rodeja, J.; Zheng, W.; Thomas, O.; Bowen, K. *Physical Reviews B* **2006**, *74*, 1–4.
- [29] Li, R.-Z.; Yuan, Q.; Yang, Z.; Aprà, E.; Li, Z.; Azov, V. A.; Kirakci, K.; Warneke, J.; Wang, X.-B. *The Journal of Chemical Physics* **2019**, *151*, 194310.
- [30] Cheung, L. F.; Czekner, J.; Kocheril, G. S.; Wang, L.-S. *The Journal of Chemical Physics* **2020**, *152*, 244306.
- [31] Cheung, L. F.; Kocheril, G. S.; Czekner, J.; Wang, L.-S. *The Journal of Physical Chemistry A* **2020**, *124*, 2820–2825.
- [32] Zhao, Y.; Yourshaw, I.; Reiser, G.; Arnold, C. C.; Neumark, D. M. *The Journal of Chemical Physics* **1994**, *101*, 6538–6551.
- [33] Yourshaw, I.; Zhao, Y.; Neumark, D. M. *The Journal of Chemical Physics* **1996**, *105*, 351–373.
- [34] Distelrath, V.; Boesl, U. *Faraday Discussions* **2000**, *115*, 161–174.
- [35] Lenzer, T.; Yourshaw, I.; Furlanetto, M. R.; Pivonka, N. L.; Neumark, D. M. *The Journal of Chemical Physics* **2002**, *116*, 4170–4175.
- [36] Verlet, J. R. R.; Kammerath, A.; Griffin, G. B.; Neumark, D. M. *The Journal of Chemical Physics* **2005**, *123*, 1–4.
- [37] Elliott, B. M.; McCunn, L. R.; Johnson, M. A. *Chemical Physics Letters* **2008**, *467*, 32–36.

- [38] Wang, X.-B.; Jagoda-Cwiklik, B.; Chi, C.; Xing, X.-P.; Zhou, M.; Jungwirth, P.; Wang, L.-S. *Chemical Physics Letters* **2009**, *477*, 41–44.
- [39] Wang, X.-B.; Kowalski, K.; Wang, L.-S.; Xantheas, S. S. *The Journal of Chemical Physics* **2010**, *132*, 1–10.
- [40] Kunin, A.; McGraw, V. S.; Lunny, K. G.; Neumark, D. M. *The Journal of Chemical Physics* **2019**, *151*, 154304.
- [41] Dobulis, M. A.; Thompson, M. C.; Patros, K. M.; Sommerfeld, T.; Jarrold, C. C. *The Journal of Physical Chemistry A* **2020**, *124*, 2279–2287.
- [42] Henley, A.; Fielding, H. H. *International Reviews in Physical Chemistry* **2019**, *38*, 1–34.
- [43] Verlet, J. R. R.; Anstöter, C. S.; Bull, J. N.; Rogers, J. P. *The Journal of Physical Chemistry A* **2020**, *124*, 3507–3519.
- [44] Jiao, C.; Qin, Z.; Cong, R.; Zheng, X.; Cui, Z.; Xie, H.; Tang, Z. *The Journal of Chemical Physics* **2018**, *149*, 224302.
- [45] Liu, G.; Ciborowski, S. M.; Graham, J. D.; Buytendyk, A. M.; Bowen, K. H. *The Journal of Chemical Physics* **2019**, *151*, 101101.
- [46] Neumark, D. M. *The Journal of Physical Chemistry A* **2008**, *112*, 13287–13301.
- [47] Yacovitch, T. I.; Garand, E.; Kim, J. B.; Hock, C.; Theis, T.; Neumark, D. M. *Faraday Discussions* **2012**, *157*, 399.
- [48] Kim, J. B.; Weichman, M. L.; Sjolander, T. F.; Neumark, D. M.; Kos, J.; Alexander, M. H.; Manolopoulos, D. E. *Science* **2015**, *349*, 510–513.
- [49] Posey, L. A.; Deluca, M. J.; Johnson, M. A. *Chemical Physics Letters* **1986**, *131*, 170–174.

- [50] Weichman, M. L.; Kim, J. B.; Neumark, D. M. *The Journal of Chemical Physics* **2014**, *140*, 104305.
- [51] Skoog, D. A.; Holler, F. J.; Crouch, S. R. *Principles of Instrumental Analysis*, 6th ed.; Thomson, 2007.
- [52] Samson, J. A. R. *Review of Scientific Instruments* **1969**, *40*, 1174–1177.
- [53] Ervin, K. M.; Lineberger, W. C. *The Journal of Physical Chemistry* **1991**, *95*, 1167–1177.
- [54] Metz, R. B.; Weaver, A.; Bradforth, S. E.; Kitsopoulos, T. N.; Neumark, D. M. *The Journal of Physical Chemistry* **1990**, *94*, 1377–1388.
- [55] Wang, L.; Cheng, H.; Fan, J. *The Journal of Chemical Physics* **1995**, *102*, 9480–9493.
- [56] Cheshnovsky, O.; Yang, S. H.; Pettiette, C. L.; Craycraft, M. J.; Smalley, R. E. *Review of Scientific Instruments* **1987**, *58*, 2131–2137.
- [57] Watson, P. D.; Yong, H.-w.; Lapere, K. M.; Kettner, M.; McKinley, A. J.; Wild, D. A. *Chemical Physics Letters* **2016**, *654*, 119–124.
- [58] Schlag, E. *ZEKE Spectroscopy*; Cambridge University Press (CUP), 2005.
- [59] Ellis, A. M.; Feher, M.; Wright, T. G. *Electronic and Photoelectron Spectroscopy*; Cambridge University Press (CUP), 2005.
- [60] Osterwalder, A.; Nee, M. J.; Zhou, J.; Neumark, D. M. *J. Chem. Phys.* **2004**, *121*, 6317.
- [61] Chupka, W. A. *The Journal of Chemical Physics* **1993**, *98*, 4520–4530.
- [62] Müller-Dethlefs, K. In *High Resolution Laser Photoionization and Photoelectron Studies*; Powis, T., I.; Baer, Ng, C., Eds.; John Wiley & Sons Ltd., 1995; Chapter 2, pp 21–78.

- [63] Lindner, R.; Dietrich, H.-J.; Müller-Dethlefs, K. *Chemical Physics Letters* **1994**, *228*, 417–425.
- [64] Åsbrink, L.; Lindholm, E.; Edqvist, O. *Chemical Physics Letters* **1970**, *5*, 609–612.
- [65] Dietrich, H.-J.; Müller-Dethlefs, K.; Baranov, L. Y. *Physical Review Letters* **1996**, *76*, 3530–3533.
- [66] Wigner, E. P. *Physical Review* **1948**, *73*, 1002–1009.
- [67] Kitsopoulos, T. N.; Chick, C. J.; Zhao, Y.; Neumark, D. M. *The Journal of Chemical Physics* **1991**, *95*, 1441–1448.
- [68] Arnold, C. C.; Neumark, D. M. *The Journal of Chemical Physics* **1993**, *99*, 3353–3362.
- [69] Wolf, I.; Ronen, S.; Giniger, R.; Cheshnovsky, O. *The Journal of Chemical Physics* **2005**, *122*, 141101.
- [70] Pinaré, J. C.; Baguenard, B.; Bordas, C.; Broyer, M. *Physical Review Letters* **1998**, *81*, 2225–2228.
- [71] Eppink, A. T. J. B.; Parker, D. H. *Review of Scientific Instruments* **1997**, *68*, 3477–3484.
- [72] Reid, K. L. *Annual Review of Physical Chemistry* **2003**, *54*, 397–424.
- [73] Hart, C. A.; Lyle, J.; Spellberg, J.; Krylov, A. I.; Mabbs, R. *The Journal of Physical Chemistry Letters* **2021**, *12*, 10086–10092.
- [74] Cooper, J.; Zare, R. N. *The Journal of Chemical Physics* **1968**, *48*, 942–943.
- [75] Culberson, L. M.; Blackstone, C. C.; Sanov, A. *The Journal of Physical Chemistry A* **2013**, *117*, 11760–11765.

- [76] Weichman, M. L.; Kim, J. B.; DeVine, J. A.; Levine, D. S.; Neumark, D. M. *Journal of the American Chemical Society* **2015**, *137*, 1420–1423.
- [77] Weichman, M. L.; DeVine, J. A.; Levine, D. S.; Kim, J. B.; Neumark, D. M. *Proceedings of the National Academy of Sciences* **2016**, *113*, 1698–1705.
- [78] Grumbling, E. R.; Sanov, A. *The Journal of Chemical Physics* **2011**, *135*, 164302.
- [79] Blackstone, C. C.; Wallace, A. A.; Sanov, A. *Molecular Physics* **2020**, *119*, e1831636.
- [80] Mabbs, R.; Surber, E.; Sanov, A. *The Analyst* **2003**, *128*, 765.
- [81] Surber, E.; Mabbs, R.; Sanov, A. *The Journal of Physical Chemistry A* **2003**, *107*, 8215–8224.
- [82] Dauletyarov, Y.; Wallace, A. A.; Blackstone, C. C.; Sanov, A. *The Journal of Physical Chemistry A* **2019**, *123*, 4158–4167.
- [83] Sanov, A.; Mabbs, R. *International Reviews in Physical Chemistry* **2008**, *27*, 53–85.
- [84] Peterka, D. S.; Lindinger, A.; Poisson, L.; Ahmed, M.; Neumark, D. M. *Physical Review Letters* **2003**, *91*.
- [85] Hock, C.; Kim, J. B.; Weichman, M. L.; Yacovitch, T. I.; Neumark, D. M. *The Journal of Chemical Physics* **2012**, *137*, 244201.
- [86] Yandell, M. A.; King, S. B.; Neumark, D. M. *Journal of the American Chemical Society* **2013**, *135*, 2128–2131.
- [87] King, S. B.; Yandell, M. A.; Neumark, D. M. *Faraday Discussions* **2013**, *163*, 59.

- [88] Boudaïffa, B.; Cloutier, P.; Hunting, D.; Huels, M. A.; Sanche, L. *Science* **2000**, *287*, 1658–1660.
- [89] Schiedt, J.; Weinkauf, R.; Neumark, D.; Schlag, E. *Chemical Physics* **1998**, *239*, 511–524.
- [90] Jordan, K. D.; Wang, F. *Annual Review of Physical Chemistry* **2003**, *54*, 367–396.
- [91] Long, F. H.; Lu, H.; Shi, X.; Eisenthal, K. B. *Chemical Physics Letters* **1990**, *169*, 165–171.
- [92] Castellani, M. E.; Anstöter, C. S.; Verlet, J. R. R. *Physical Chemistry Chemical Physics* **2019**, *21*, 24286–24290.
- [93] Hendricks, J. H.; Lyapustina, S. A.; de Clercq, H. L.; Snodgrass, J. T.; Bowen, K. H. *The Journal of Chemical Physics* **1996**, *104*, 7788–7791.
- [94] Li, W.-L.; Kunin, A.; Matthews, E.; Yoshikawa, N.; Dessent, C. E. H.; Neumark, D. M. *The Journal of Chemical Physics* **2016**, *145*, 044319.
- [95] Kunin, A.; Li, W.-L.; Neumark, D. M. *The Journal of Chemical Physics* **2018**, *149*, 084301.
- [96] Matthews, E.; Cercola, R.; Mensa-Bonsu, G.; Neumark, D. M.; Dessent, C. E. H. *The Journal of Chemical Physics* **2018**, *148*, 084304.
- [97] Cavanagh, S. J.; Gibson, S. T.; Gale, M. N.; Dedman, C. J.; Roberts, E. H.; Lewis, B. R. *Physical Review A* **2007**, *76*.
- [98] Dedman, C. J.; Roberts, E. H.; Gibson, S. T.; Lewis, B. R. *Review of Scientific Instruments* **2001**, *72*, 2915–2922.
- [99] Laws, B. A.; Cavanagh, S. J.; Lewis, B. R.; Gibson, S. T. *The Journal of Physical Chemistry A* **2019**, *123*, 10418–10425.

- [100] Laws, B. A.; Gibson, S. T.; Lewis, B. R.; Field, R. W. *Nature Communications* **2019**, *10*.
- [101] Laws, B. A.; Cavanagh, S. J.; Lewis, B. R.; Gibson, S. T. *The Journal of Physical Chemistry Letters* **2017**, *8*, 4397–4401.
- [102] DeVine, J. A.; Babin, M. C.; Blackford, K.; Neumark, D. M. *The Journal of Chemical Physics* **2019**, *151*, 064302.
- [103] Kim, J. B.; Weichman, M. L.; Neumark, D. M. *Journal of the American Chemical Society* **2014**, *136*, 7159–7168.
- [104] DeVine, J. A.; Babin, M. C.; Neumark, D. M. *Faraday Discussions* **2019**, *217*, 235–255.
- [105] Laws, B. A.; Levey, Z. D.; Schmidt, T. W.; Gibson, S. T. *Journal of the American Chemical Society* **2021**, *143*, 18684–18692.
- [106] León, I.; Yang, Z.; Liu, H.-T.; Wang, L.-S. *Review of Scientific Instruments* **2014**, *85*, 083106.
- [107] Qin, Z.; Wu, X.; Tang, Z. *Review of Scientific Instruments* **2013**, *84*, 066108.
- [108] Sheps, L.; Miller, E. M.; Lineberger, W. C. *The Journal of Chemical Physics* **2009**, *131*, 064304.
- [109] Oliveira, A. M.; Lu, Y.-J.; Lehman, J. H.; Changala, P. B.; Baraban, J. H.; Stanton, J. F.; Lineberger, W. C. *Journal of the American Chemical Society* **2015**, *137*, 12939–12945.
- [110] Worth, G.; Carley, R.; Fielding, H. *Chemical Physics* **2007**, *338*, 220–227.
- [111] Horke, D. A.; Roberts, G. M.; Lecointre, J.; Verlet, J. R. R. *Review of Scientific Instruments* **2012**, *83*, 063101.

- [112] McKay, A. R.; Sanz, M. E.; Mooney, C. R. S.; Minns, R. S.; Gill, E. M.; Fielding, H. H. *Review of Scientific Instruments* **2010**, *81*, 123101.
- [113] Mooney, C. R. S.; Sanz, M. E.; McKay, A. R.; Fitzmaurice, R. J.; Aliev, A. E.; Caddick, S.; Fielding, H. H. *The Journal of Physical Chemistry A* **2012**, *116*, 7943–7949.
- [114] Mooney, C. R. S.; Parkes, M. A.; Zhang, L.; Hailes, H. C.; Simperler, A.; Bearpark, M. J.; Fielding, H. H. *The Journal of Chemical Physics* **2014**, *140*, 205103.
- [115] Lecointre, J.; Roberts, G. M.; Horke, D. A.; Verlet, J. R. R. *The Journal of Physical Chemistry A* **2010**, *114*, 11216–11224.
- [116] Mensa-Bonsu, G.; Tozer, D. J.; Verlet, J. R. R. *Physical Chemistry Chemical Physics* **2019**, *21*, 13977–13985.
- [117] Anstöter, C. S.; Verlet, J. R. R. *The Journal of Physical Chemistry Letters* **2020**, *11*, 6456–6462.
- [118] Bull, J. N.; Anstöter, C. S.; Stockett, M. H.; Clarke, C. J.; Gibbard, J. A.; Bieske, E. J.; Verlet, J. R. R. *The Journal of Physical Chemistry Letters* **2021**, *12*, 11811–11816.
- [119] Bull, J. N.; Verlet, J. R. R. *Phys. Chem. Chem. Phys.* **2017**, *19*, 26589–26595.
- [120] Anstöter, C. S.; Rogers, J. P.; Verlet, J. R. R. *Journal of the American Chemical Society* **2019**, *141*, 6132–6135.
- [121] Kregel, S. J.; Thurston, G. K.; Zhou, J.; Garand, E. *The Journal of Chemical Physics* **2017**, *147*, 094201.
- [122] Bracewell, R. *The Fourier Transform and Its Applications*, 2nd ed.; McGraw-Hill, 1978.

- [123] Roberts, G. M.; Nixon, J. L.; Lecointre, J.; Wrede, E.; Verlet, J. R. R. *Review of Scientific Instruments* **2009**, *80*, 053104.
- [124] Manzhos, S.; Loock, H.-P. *Computer Physics Communications* **2003**, *154*, 76–87.
- [125] Dribinski, V.; Ossadtchi, A.; Mandelshtam, V. A.; Reisler, H. *Review of Scientific Instruments* **2002**, *73*, 2634.
- [126] Garcia, G. A.; Nahon, L.; Powis, I. *Review of Scientific Instruments* **2004**, *75*, 4989.
- [127] Hickstein, D. D.; Gibson, S. T.; Yurchak, R.; Das, D. D.; Ryazanov, M. *Review of Scientific Instruments* **2019**, *90*, 065115.
- [128] Dick, B. *Phys. Chem. Chem. Phys.* **2014**, *16*, 570–580.
- [129] Hansen, E. W.; Law, P.-L. *Journal of the Optical Society of America A* **1985**, *2*, 510.
- [130] Hansen, E. *IEEE Transactions on Acoustics, Speech, and Signal Processing* **1985**, *33*, 666–671.
- [131] Lowe, J.; Peterson, K. *Quantum Chemistry*, 3rd ed.; Academic Press, 2005.
- [132] Foresman, J.; Frisch, ÅE. *Exploring Chemistry with Electronic Structure Methods*, 3rd ed.; Gaussian Inc., 2015.
- [133] Bartlett, R. J.; Musiał, M. *Reviews of Modern Physics* **2007**, *79*, 291–352.
- [134] Roos, B. O.; Lindh, R.; Malmqvist, P. A. k.; Veryazov, V.; Widmark, P.-O. **2016**,
- [135] Parr, R.; Yang, W. *Density-Functional Theory of Atoms and Molecules*; International Series of Monographs on Chemistry; Oxford University Press, 1989.
- [136] Schrödinger, E. *Annalen der Physik* **1926**, *385*, 437–490.

- [137] Born, M.; Oppenheimer, R. *Annalen der Physik* **1927**, *389*, 457–484.
- [138] Dirac, P. A. M.; Fowler, R. H. *Proceedings of the Royal Society of London. Series A, Containing Papers of a Mathematical and Physical Character* **1928**, *117*, 610–624.
- [139] Zeeman, P. *Verslagen en Mededeelingen der Kon. Academie van Wetenschappen, Afd. Natuurkunde* **1896**, *5*, 181.
- [140] Pauli, W. *Zeitschrift für Physik* **1925**, *31*, 765–783.
- [141] Slater, J. C. *Phys. Rev.* **1929**, *34*, 1293–1322.
- [142] Hartree, D. R. *Mathematical Proceedings of the Cambridge Philosophical Society* **1928**, *24*, 111–132.
- [143] Fock, V. *Zeitschrift für Physik* **1930**, *61*, 126–148.
- [144] Hartree, D. R.; Hartree, W. *Proceedings of the Royal Society of London. Series A - Mathematical and Physical Sciences* **1935**, *150*, 9–33.
- [145] Roothaan, C. C. J. *Reviews of Modern Physics* **1951**, *23*, 69–89.
- [146] Roothaan, C. C. J. *Reviews of Modern Physics* **1960**, *32*, 179–185.
- [147] Pople, J. A.; Nesbet, R. K. *The Journal of Chemical Physics* **1954**, *22*, 571–572.
- [148] Löwdin, P.-O. *Advances in Chemical Physics* **1958**, 207–322.
- [149] Lowdin, P. O. *Annual Review of Physical Chemistry* **1960**, *11*, 107–132.
- [150] Knowles, P.; Handy, N. *Chemical Physics Letters* **1984**, *111*, 315–321.
- [151] Hofmann, M.; Schaefer, H. F. In *Encyclopedia of Physical Science and Technology (Third Edition)*, third edition ed.; Meyers, R. A., Ed.; Academic Press: New York, 2003; pp 487–506.

- [152] Pople, J. A. Theoretical Models for Chemistry. Proceedings of the Summer Research Conference on Theoretical Chemistry, Energy Structure and Reactivity. 1973.
- [153] Møller, C.; Plesset, M. S. *Phys. Rev.* **1934**, *46*, 618–622.
- [154] Pople, J. A.; Binkley, J. S.; Seeger, R. *International Journal of Quantum Chemistry* **1976**, *10*, 1–19.
- [155] Pople, J. A.; Seeger, R.; Krishnan, R. *International Journal of Quantum Chemistry* **1977**, *12*, 149–163.
- [156] Krishnan, R.; Frisch, M. J.; Pople, J. A. *The Journal of Chemical Physics* **1980**, *72*, 4244–4245.
- [157] Raghavachari, K.; Pople, J. A.; Replogle, E. S.; Head-Gordon, M. *The Journal of Physical Chemistry* **1990**, *94*, 5579–5586.
- [158] Cremer, D. *WIREs Computational Molecular Science* **2011**, *1*, 509–530.
- [159] Gill, P. M.; Radom, L. *Chemical Physics Letters* **1986**, *132*, 16–22.
- [160] Lawley, K. *Ab initio Methods in Quantum Chemistry: Part I*; John Wiley & Sons, 1977.
- [161] Handy, N. C.; Knowles, P. J.; Somasundram, K. *Theoretica Chimica Acta* **1985**, *68*, 87–100.
- [162] Jung, Y.; Lochan, R. C.; Dutoi, A. D.; Head-Gordon, M. *The Journal of Chemical Physics* **2004**, *121*, 9793–9802.
- [163] Ma, N. L.; Smith, B. J.; Radom, L. *Chemical Physics Letters* **1992**, *193*, 386–394.
- [164] Riley, K. E.; Platts, J. A.; Řezáč, J.; Hobza, P.; Hill, J. G. *The Journal of Physical Chemistry A* **2012**, *116*, 4159–4169.

- [165] Christiansen, O.; Olsen, J.; Jørgensen, P.; Koch, H.; Malmqvist, P.-A. k. *Chemical Physics Letters* **1996**, *261*, 369–378.
- [166] Condon, E. U. *Phys. Rev.* **1930**, *36*, 1121–1133.
- [167] Pople, J. A.; Krishnan, R.; Schlegel, H. B.; Binkley, J. S. *International Journal of Quantum Chemistry* **1978**, *14*, 545–560.
- [168] Scuseria, G. E.; Schaefer, H. F. *Chemical Physics Letters* **1988**, *152*, 382–386.
- [169] Raghavachari, K.; Trucks, G. W.; Pople, J. A.; Head-Gordon, M. *Chemical Physics Letters* **1989**, *157*, 479–483.
- [170] Jurečka, P.; Šponer, J.; Černý, J.; Hobza, P. *Phys. Chem. Chem. Phys.* **2006**, *8*, 1985–1993.
- [171] Řezáč, J.; Riley, K. E.; Hobza, P. *Journal of Chemical Theory and Computation* **2011**, *7*, 2427–2438, PMID: 21836824.
- [172] Řezáč, J.; Hobza, P. *Journal of Chemical Theory and Computation* **2013**, *9*, 2151–2155, PMID: 26583708.
- [173] Haakansson, C. T.; Corkish, T. R.; Watson, P. D.; McKinley, A. J.; Wild, D. A. *Chemical Physics Letters* **2020**, *761*, 138060.
- [174] Neogrády, P.; Medved, M.; Černušák, I.; Urban, M. *Molecular Physics* **2002**, *100*, 541–560.
- [175] Stanton, J. F.; Bartlett, R. J. *The Journal of Chemical Physics* **1993**, *98*, 7029–7039.
- [176] Szalay, P. G.; Müller, T.; Gidofalvi, G.; Lischka, H.; Shepard, R. *Chemical Reviews* **2011**, *112*, 108–181.
- [177] Vogiatzis, K. D.; Ma, D.; Olsen, J.; Gagliardi, L.; de Jong, W. A. *The Journal of Chemical Physics* **2017**, *147*, 184111.

- [178] Sinanoğlu, O. *Advances in Chemical Physics* **1964**, 315–412.
- [179] Mok, D. K. W.; Neumann, R.; Handy, N. C. *The Journal of Physical Chemistry* **1996**, *100*, 6225–6230.
- [180] Page, C. S.; Olivucci, M. *Journal of Computational Chemistry* **2003**, *24*, 298–309.
- [181] Tran, V. T.; Tran, X. M. T.; Nguyen, M. T.; Nguyen, H. T.; Tran, Q. T. *Chemical Physics Letters* **2017**, *690*, 140–146.
- [182] Ivanov, A. S.; Zhang, X.; Wang, H.; Boldyrev, A. I.; Gantefoer, G.; Bowen, K. H.; Černušák, I. *The Journal of Physical Chemistry A* **2015**, *119*, 11293–11303.
- [183] Weichman, M. L.; Vlaisavljevich, B.; DeVine, J. A.; Shuman, N. S.; Ard, S. G.; Shiozaki, T.; Neumark, D. M.; Viggiano, A. A. *The Journal of Chemical Physics* **2017**, *147*, 234311.
- [184] Pulay, P. *International Journal of Quantum Chemistry* **2011**, *111*, 3273–3279.
- [185] Kollmar, C.; Sivalingam, K.; Neese, F. *The Journal of Chemical Physics* **2020**, *152*, 214110.
- [186] Camacho, C.; Witek, H. A.; Yamamoto, S. *Journal of Computational Chemistry* **2009**, *30*, 468–478.
- [187] Angeli, C.; Cimiraglia, R.; Evangelisti, S.; Leininger, T.; Malrieu, J.-P. *The Journal of Chemical Physics* **2001**, *114*, 10252–10264.
- [188] Angeli, C.; Cimiraglia, R.; Malrieu, J.-P. *The Journal of Chemical Physics* **2002**, *117*, 9138–9153.
- [189] Angeli, C.; Pastore, M.; Cimiraglia, R. *Theoretical Chemistry Accounts* **2006**, *117*, 743–754.

- [190] Dyall, K. G. *The Journal of Chemical Physics* **1995**, *102*, 4909–4918.
- [191] Havenith, R. W. A.; Taylor, P. R.; Angeli, C.; Cimiraglia, R.; Ruud, K. *The Journal of Chemical Physics* **2004**, *120*, 4619–4625.
- [192] Guo, Y.; Sivalingam, K.; Neese, F. *The Journal of Chemical Physics* **2021**, *154*, 214111.
- [193] Pham, L. N.; Nguyen, M. T. *The Journal of Physical Chemistry A* **2017**, *121*, 1940–1949.
- [194] Tran, V. T.; Tran, Q. T.; Hendrickx, M. F. *Chemical Physics Letters* **2015**, *627*, 121–125.
- [195] Thomas, L. H. *Mathematical Proceedings of the Cambridge Philosophical Society* **1927**, *23*, 542–548.
- [196] Hohenberg, P.; Kohn, W. *Physical Review* **1964**, *136*, B864–B871.
- [197] Kohn, W.; Sham, L. J. *Physical Review* **1965**, *140*, A1133–A1138.
- [198] Becke, A. D. *The Journal of Chemical Physics* **2014**, *140*, 18A301.
- [199] Goerigk, L.; Mehta, N. *Australian Journal of Chemistry* **2019**, *72*, 563.
- [200] Zhao, Y.; Truhlar, D. G. *Theoretical Chemistry Accounts* **2007**, *120*, 215–241.
- [201] Perdew, J. P. *AIP Conference Proceedings* **2001**,
- [202] Mardirossian, N.; Head-Gordon, M. *Molecular Physics* **2017**, *115*, 2315–2372.
- [203] Peng, Q.; Duarte, F.; Paton, R. S. *Chemical Society Reviews* **2016**, *45*, 6093–6107.
- [204] Vosko, S. H.; Wilk, L.; Nusair, M. *Canadian Journal of Physics* **1980**, *58*, 1200–1211.
- [205] Becke, A. D. *The Journal of Chemical Physics* **1997**, *107*, 8554–8560.

- [206] Perdew, J. P.; Chevary, J. A.; Vosko, S. H.; Jackson, K. A.; Pederson, M. R.; Singh, D. J.; Fiolhais, C. *Physical Review B* **1992**, *46*, 6671–6687.
- [207] Perdew, J. P.; Burke, K.; Ernzerhof, M. *Physical Review Letters* **1996**, *77*, 3865–3868.
- [208] Becke, A. D. *Physical Review A* **1988**, *38*, 3098–3100.
- [209] Lee, C.; Yang, W.; Parr, R. G. *Physical Review B* **1988**, *37*, 785–789.
- [210] Perdew, J. P. *Physical Review B* **1986**, *33*, 8822–8824.
- [211] Perdew, J. P.; Kurth, S.; Zupan, A.; Blaha, P. *Physical Review Letters* **1999**, *82*, 2544–2547.
- [212] Tao, J.; Perdew, J. P.; Staroverov, V. N.; Scuseria, G. E. *Physical Review Letters* **2003**, *91*.
- [213] Zhao, Y.; Truhlar, D. G. *The Journal of Chemical Physics* **2006**, *125*, 194101.
- [214] Goerigk, L.; Grimme, S. *Journal of Chemical Theory and Computation* **2009**, *6*, 107–126.
- [215] Becke, A. D. *The Journal of Chemical Physics* **1993**, *98*, 5648–5652.
- [216] Curtiss, L. A.; Raghavachari, K.; Redfern, P. C.; Pople, J. A. *The Journal of Chemical Physics* **1997**, *106*, 1063–1079.
- [217] Tirado-Rives, J.; Jorgensen, W. L. *Journal of Chemical Theory and Computation* **2008**, *4*, 297–306.
- [218] Grimme, S.; Steinmetz, M.; Korth, M. *The Journal of Organic Chemistry* **2007**, *72*, 2118–2126.
- [219] Holroyd, L. F.; van Mourik, T. *Chemical Physics Letters* **2007**, *442*, 42–46.
- [220] Tsuzuki, S.; Lüthi, H. P. *The Journal of Chemical Physics* **2001**, *114*, 3949–3957.

- [221] Zhao, Y.; Truhlar, D. G. *The Journal of Physical Chemistry A* **2006**, *110*, 13126–13130.
- [222] Medvedev, M. G.; Bushmarinov, I. S.; Sun, J.; Perdew, J. P.; Lyssenko, K. A. *Science* **2017**, *355*, 49–52.
- [223] Martin, J. M. L.; Santra, G. *Israel Journal of Chemistry* **2019**, *60*, 787–804.
- [224] Görling, A.; Levy, M. *Physical Review B* **1993**, *47*, 13105–13113.
- [225] Grimme, S. *The Journal of Chemical Physics* **2006**, *124*, 034108.
- [226] Grimme, S. *The Journal of Chemical Physics* **2003**, *118*, 9095–9102.
- [227] Kozuch, S.; Martin, J. M. L. *Physical Chemistry Chemical Physics* **2011**, *13*, 20104.
- [228] Goerigk, L.; Hansen, A.; Bauer, C.; Ehrlich, S.; Najibi, A.; Grimme, S. *Physical Chemistry Chemical Physics* **2017**, *19*, 32184–32215.
- [229] Casimir, H. B. G.; Polder, D. *Physical Review* **1948**, *73*, 360–372.
- [230] Grimme, S. *Journal of Computational Chemistry* **2006**, *27*, 1787–1799.
- [231] Becke, A. D.; Johnson, E. R. *The Journal of Chemical Physics* **2005**, *123*, 154101.
- [232] Caldeweyher, E.; Bannwarth, C.; Grimme, S. *The Journal of Chemical Physics* **2017**, *147*, 034112.
- [233] Caldeweyher, E.; Ehlert, S.; Hansen, A.; Neugebauer, H.; Spicher, S.; Bannwarth, C.; Grimme, S. *The Journal of Chemical Physics* **2019**, *150*, 154122.
- [234] Chai, J.-D.; Head-Gordon, M. *Physical Chemistry Chemical Physics* **2008**, *10*, 6615.
- [235] Slater, J. C. *Physical Review* **1930**, *36*, 57–64.

- [236] Boys, S. F. *Proceedings of the Royal Society of London. Series A. Mathematical and Physical Sciences* **1950**, *200*, 542–554.
- [237] Pritchard, B. P.; Altarawy, D.; Didier, B.; Gibson, T. D.; Windus, T. L. *Journal of Chemical Information and Modeling* **2019**, *59*, 4814–4820.
- [238] Peterson, K. A.; Figgen, D.; Goll, E.; Stoll, H.; Dolg, M. *J. Chem. Phys.* **2003**, *119*, 11113–11123.
- [239] Halkier, A.; Helgaker, T.; Jørgensen, P.; Klopper, W.; Koch, H.; Olsen, J.; Wilson, A. K. *Chemical Physics Letters* **1998**, *286*, 243–252.
- [240] Martin, J. M. L.; de Oliveira, G. *The Journal of Chemical Physics* **1999**, *111*, 1843–1856.
- [241] Parthiban, S.; Martin, J. M. L. *The Journal of Chemical Physics* **2001**, *114*, 6014–6029.
- [242] Boese, A. D.; Oren, M.; Atasoylu, O.; Martin, J. M. L.; Kállay, M.; Gauss, J. *The Journal of Chemical Physics* **2004**, *120*, 4129–4141.
- [243] Karton, A.; Rabinovich, E.; Martin, J. M. L.; Ruscic, B. *The Journal of Chemical Physics* **2006**, *125*, 144108.
- [244] Tajti, A.; Szalay, P. G.; Császár, A. G.; Kállay, M.; Gauss, J.; Valeev, E. F.; Flowers, B. A.; Vázquez, J.; Stanton, J. F. *The Journal of Chemical Physics* **2004**, *121*, 11599–11613.
- [245] Karton, A. *The Journal of Chemical Physics* **2020**, *153*, 024102.
- [246] Karton, A.; Sylvetsky, N.; Martin, J. M. L. *Journal of Computational Chemistry* **2017**, *38*, 2063–2075.
- [247] Raffenetti, R. C. *The Journal of Chemical Physics* **1973**, *58*, 4452–4458.
- [248] Weigend, F.; Ahlrichs, R. *Physical Chemistry Chemical Physics* **2005**, *7*, 3297.

- [249] Weigend, F.; Furche, F.; Ahlrichs, R. *The Journal of Chemical Physics* **2003**, *119*, 12753–12762.
- [250] Jensen, F. *The Journal of Chemical Physics* **2005**, *122*, 074111.
- [251] Franck, J.; Dymond, E. G. *Transactions of the Faraday Society* **1926**, *21*, 536.
- [252] Condon, E. *Physical Review* **1926**, *28*, 1182–1201.
- [253] Koziol, L.; Mozhayskiy, V. A.; Braams, B. J.; Bowman, J. M.; Krylov, A. I. *The Journal of Physical Chemistry A* **2009**, *113*, 7802–7809.
- [254] Duschinsky, F. *Acta Physicochim. USSR* **1937**, *7*.
- [255] *Reviews in computational chemistry. Volume 30*; Reviews in Computational Chemistry; Wiley: Hoboken, NJ, 2017.
- [256] Mozhayskiy, V. A.; Krylov, A. I. ezSpectrum 3.0. 2009.
- [257] Gozem, S.; Krylov, A. I. *WIREs Computational Molecular Science* **2021**,
- [258] Gozem, S.; Gunina, A. O.; Ichino, T.; Osborn, D. L.; Stanton, J. F.; Krylov, A. I. *The Journal of Physical Chemistry Letters* **2015**, *6*, 4532–4540.
- [259] Beckham, D.; Conran, S.; Lapere, K.; Kettner, M.; McKinley, A.; Wild, D. *Chemical Physics Letters* **2015**, *619*, 241–246.
- [260] Kettner, M.; Karton, A.; McKinley, A.; Wild, D. *Chemical Physics Letters* **2015**, *621*, 193–198.
- [261] Lapere, K.; LaMacchia, R.; Quak, L.; McKinley, A.; Wild, D. *Chemical Physics Letters* **2011**, *504*, 13–19.
- [262] Lapere, K. M.; LaMacchia, R. J.; Quak, L. H.; Kettner, M.; Dale, S. G.; McKinley, A. J.; Wild, D. A. *Australian Journal of Chemistry* **2012**, *65*, 457–462.

- [263] Lapere, K. M.; LaMacchia, R. J.; Quak, L. H.; Kettner, M.; Dale, S. G.; McKinley, A. J.; Wild, D. A. *The Journal of Physical Chemistry A* **2012**, *116*, 3577–3584.
- [264] Dunning, T. H. *The Journal of Chemical Physics* **1989**, *90*, 1007–1023.
- [265] Dunning, T. H.; Peterson, K. A.; Wilson, A. K. *The Journal of Chemical Physics* **2001**, *114*, 9244–9253.
- [266] Peterson, K. A.; Shepler, B. C.; Figgen, D.; Stoll, H. *J. Phys. Chem. A* **2006**, *110*, 13877–13883.
- [267] Frisch, M. J. et al. Gaussian 09 Revision D.01. Gaussian Inc. Wallingford CT 2009.
- [268] Pople, J. A. *The Journal of Chemical Physics* **1965**, *43*, S229–S230.
- [269] Karplus, M. *The Journal of Physical Chemistry* **1990**, *94*, 5435–5436.
- [270] Kozuch, S.; Martin, J. M. L. *Journal of Computational Chemistry* **2013**, *34*, 2327–2344.
- [271] Grimme, S.; Ehrlich, S.; Goerigk, L. *Journal of Computational Chemistry* **2011**, *32*, 1456–1465.
- [272] Weigend, F. *Physical Chemistry Chemical Physics* **2006**, *8*, 1057.
- [273] CFOUR, a quantum chemical program package written by J.F. Stanton, J. Gauss, M.E. Harding, P.G. Szalay with contributions from A.A. Auer, R.J. Bartlett, U. Benedikt, C. Berger, D.E. Bernholdt, Y.J. Bomble, O. Christiansen, M. Heckert, O. Heun, C. Huber, T.-C. Jagau, D. Jonsson, J. Jusélius, K. Klein, W.J. Lauderdale, D.A. Matthews, T. Metzroth, D.P. O'Neill, D.R. Price, E. Prochnow, K. Ruud, F. Schiffmann, S. Stopkowicz, A. Tajti, J. Vázquez, F. Wang, J.D. Watts and the integral packages MOLECULE (J. Almlöf and P.R. Taylor), PROPS (P.R. Taylor), ABACUS (T. Helgaker, H.J.

- Aa. Jensen, P. Jørgensen, and J. Olsen), and ECP routines by A. V. Mitin and C. van Wüllen. For the current version, see <http://www.cfour.de>.
- [274] Neese, F. *WIREs Computational Molecular Science* **2011**, *2*, 73–78.
- [275] Neese, F. *WIREs Computational Molecular Science* **2017**, *8*.
- [276] Roizard, D. *Encyclopedia of Membranes* **2016**, 97–99.
- [277] Stull, D. R. *Industrial & Engineering Chemistry* **1947**, *39*, 517–540.
- [278] Heisig, G. B. *Journal of the American Chemical Society* **1933**, *55*, 2304–2311.
- [279] Hull, H.; Reid, A.; Turnbull, A. *Australian Journal of Chemistry* **1965**, *18*, 249.
- [280] de Nevers, N. *Physical and Chemical Equilibrium for Chemical Engineers*; John Wiley & Sons, Inc., 2012.
- [281] Waddington, G.; Smith, J. C.; Williamson, K. D.; Scott, D. W. *The Journal of Physical Chemistry* **1962**, *66*, 1074–1077.
- [282] LaMacchia, R. Towards Anion Photoelectron Spectroscopy of Complexes and Clusters. Honours Thesis, University of Western Australia: School of Chemistry and Biochemistry, 2008.
- [283] Quak, H. Towards Anion Photoelectron Spectroscopy - Optimisation of the Time-of-Flight Mass Spectrometer with Photoelectron Spectrometer in Tandem. Honours Thesis, University of Western Australia: School of Chemistry and Biochemistry, 2009.
- [284] Dale, S. G. The preliminary investigation the amidogen anion using Anion Photoelectron Spectroscopy and investigation of amidogen anion complexes through ab initio calculations. Honours Thesis, University of Western Australia: School of Chemistry and Biochemistry, 2012.

- [285] Conran, S. E. Investigating $\text{Br}^- \cdots (\text{HCCH})_n$, $\text{Cl}^- \cdots (\text{HCCH})_n$ and $\text{I}^- \cdots (\text{HCCH})_n$ using Anion Photoelectron Spectroscopy and ab initio Calculations. Honours Thesis, University of Western Australia: School of Chemistry and Biochemistry, 2013.
- [286] Lapere, K. An Investigation of the $\text{Cl}^- \cdots \text{CO}$ and $\text{Br}^- \cdots \text{CO}$ van der Waals Clusters with Anion Photoelectron Spectroscopy and ab initio Calculations. Honours Thesis, University of Western Australia: School of Chemistry and Biochemistry, 2009.
- [287] Lapere, K. Anion Photoelectron Spectroscopy of Halide Complexes and Clusters. Ph.D. thesis, University of Western Australia: School of Chemistry and Biochemistry, 2015.
- [288] Beckham, D. Gas Phase Anion Photoelectron Spectroscopy. Masters Thesis, University of Western Australia: School of Chemistry and Biochemistry, 2014.
- [289] Kettner, M. Anion Photoelectron Spectroscopy of Halide Complexes and Clusters. Ph.D. thesis, University of Western Australia: School of Chemistry and Biochemistry, 2015.
- [290] Havenith, M. *Infrared Spectroscopy of Molecular Clusters: An Introduction to Molecular Forces*; Springer, New York, 2002; Vol. 176.
- [291] Christen, W.; Rademann, K. *Physical Reviews A* **2008**, *77*, 1–5.
- [292] Hagen, O. F.; Obert, W. *The Journal of Chemical Physics* **1972**, *56*, 1793–1802.
- [293] Christophorou, L.; McCorkle, D.; Christodoulides, A. In *Electron–Molecule Interactions and their Applications*; Christophorou, L., Ed.; Academic Press, 1984; pp 477–617.
- [294] Chen, E. C. M.; Albyn, K.; Dussack, L.; Wentworth, W. E. *The Journal of Physical Chemistry* **1989**, *93*, 6827–6832.

- [295] Wnorowska, J.; Kočíšek, J.; Matejčík, v. *International Journal of Mass Spectrometry* **2014**, *365-366*, 177–180.
- [296] Aberth, W. H.; Schnitzer, R.; Engesser, F. C. *Review of Scientific Instruments* **1974**, *45*, 1289–1290.
- [297] Adams, A.; Read, F. H. *Journal of Physics E: Scientific Instruments* **1972**, *5*, 150–155.
- [298] Murphy, D.; Speirs, R. W.; Sheludko, D. V.; Putkunz, C. T.; McCulloch, A. J.; Sparkes, B. M.; Scholten, R. E. *Nature Communications* **2014**, *5*.
- [299] Kopczynski, M. Femtosekunden Photodetachment-Photoelektronenspektroskopie an isolierten und massenselektierten Halogen-Edelgas-Clustern. Ph.D. thesis, Georg-August-Universität Göttingen, 2010.
- [300] Watson, P. D.; McKinley, A. J.; Wild, D. A. *Journal of Molecular Spectroscopy* **2020**, *372*, 111320.
- [301] Radziemski, L. J.; Kaufman, V. *Journal of the Optical Society of America* **1969**, *59*, 424.
- [302] D.C., M.; D.A., D. Simion 8.1.1.1. 2012.
- [303] Vogel, M.; Winters, D.; Ernst, H.; Zimmermann, H.; Kester, O. *Nuclear Instruments and Methods in Physics Research Section B: Beam Interactions with Materials and Atoms* **2007**, *263*, 518–522.
- [304] Proch, D.; Trickl, T. *Review of Scientific Instruments* **1989**, *60*, 713–716.
- [305] Schießer, A.; Schäfer, R. *Review of Scientific Instruments* **2009**, *80*, 086103.
- [306] Corkish, T. R.; Haakansson, C. T.; Watson, P. D.; McKinley, A. J.; Wild, D. A. *ChemPhysChem* **2020**, *22*, 69–75.
- [307] Wang, L.-S. *The Journal of Chemical Physics* **2015**, *143*, 040901.

- [308] Müller, J.-F.; Liu, Z.; Nguyen, V. S.; Stavrakou, T.; Harvey, J. N.; Peeters, J. *Nature Communications* **2016**, *7*.
- [309] Caravan, R. L.; Khan, M. A. H.; Zádor, J.; Sheps, L.; Antonov, I. O.; Rotavera, B.; Ramasesha, K.; Au, K.; Chen, M.-W.; Rösch, D.; et al., *Nature Communications* **2018**, *9*.
- [310] Chhantyal-Pun, R.; Khan, M. A. H.; Zachhuber, N.; Percival, C. J.; Shallcross, D. E.; Orr-Ewing, A. J. *ACS Earth and Space Chemistry* **2020**, *4*, 1743–1755.
- [311] Lightfoot, P.; Cox, R.; Crowley, J.; Destriau, M.; Hayman, G.; Jenkin, M.; Moortgat, G.; Zabel, F. *Atmospheric Environment. Part A. General Topics* **1992**, *26*, 1805–1961.
- [312] Maricq, M. M.; Wallington, T. J. *The Journal of Physical Chemistry* **1992**, *96*, 986–992.
- [313] Maricq, M. M.; Szente, J. J. *The Journal of Physical Chemistry* **1994**, *98*, 2078–2082.
- [314] Dillon, T. J.; Tucceri, M. E.; Crowley, J. N. *Physical Chemistry Chemical Physics* **2006**, *8*, 5185.
- [315] Hunziker, H. E.; Wendt, H. R. *The Journal of Chemical Physics* **1974**, *60*, 4622–4623.
- [316] Hunziker, H. E. *The Journal of Chemical Physics* **1976**, *64*, 3488.
- [317] Pushkarsky, M. B.; Zalyubovsky, S. J.; Miller, T. A. *The Journal of Chemical Physics* **2000**, *112*, 10695–10698.
- [318] Chung, C.-Y.; Cheng, C.-W.; Lee, Y.-P.; Liao, H.-Y.; Sharp, E. N.; Rupper, P.; Miller, T. A. *The Journal of Chemical Physics* **2007**, *127*, 1–14.

- [319] Blanksby, S. J.; Ramond, T. M.; Davico, G. E.; Nimlos, M. R.; Kato, S.; Bierbaum, V. M.; Lineberger, W. C.; Ellison, G. B.; Okumura, M. *Journal of the American Chemical Society* **2001**, *123*, 9585–9596.
- [320] Sullivan, E. N.; Nichols, B.; Neumark, D. M. *The Journal of Chemical Physics* **2018**, *148*, 044309.
- [321] Ase, P.; Bock, W.; Snelson, A. *The Journal of Physical Chemistry* **1986**, *90*, 2099–2109.
- [322] Nandi, S.; Blanksby, S. J.; Zhang, X.; Nimlos, M. R.; Dayton, D. C.; Ellison, G. B. *The Journal of Physical Chemistry A* **2001**, *106*, 7547–7556.
- [323] Huang, D.-R.; Chu, L.-K.; Lee, Y.-P. *The Journal of Chemical Physics* **2007**, *127*, 234318.
- [324] Xu, W.; Lu, G. *The Journal of Physical Chemistry A* **2008**, *112*, 6999–7014.
- [325] Gao, A.; Sun, X.; Liang, X.; Fang, X.; Zhu, Z.; Xie, Y. *Journal of Molecular Structure: THEOCHEM* **2008**, *862*, 105–111.
- [326] Li, R.; Liu, C.; Wang, C.; Ning, L.; Liang, J.; Cui, Z. *Journal of Molecular Structure: THEOCHEM* **2009**, *897*, 17–21.
- [327] Zhao, Z.; Song, J.; Su, B.; Wang, X.; Li, Z. *The Journal of Physical Chemistry A* **2018**, *122*, 5078–5088.
- [328] Zhang, Y.; Song, R.; Sun, Y.; Sun, J.; Wang, R. *Journal of Molecular Graphics and Modelling* **2017**, *76*, 512–520.
- [329] Metz, R. B.; Kitsopoulos, T.; Weaver, A.; Neumark, D. M. *The Journal of Chemical Physics* **1988**, *88*, 1463–1465.
- [330] Fu, H. B.; Hu, Y. J.; Bernstein, E. R. *The Journal of Chemical Physics* **2006**, *125*, 014310.

- [331] Kendall, R. A.; Dunning, T. H.; Harrison, R. J. *The Journal of Chemical Physics* **1992**, *96*, 6796–6806.
- [332] Roos, B. O.; Taylor, P. R.; Sigbahn, P. E. *Chemical Physics* **1980**, *48*, 157–173.
- [333] Neese, F. *WIREs Computational Molecular Science* **2012**, *2*, 73–78.
- [334] Irikura, K. K. *International Journal of Mass Spectrometry* **2003**, *228*, 667–676.
- [335] Ervin, K. M.; Anusiewicz, I.; Skurski, P.; Simons, J.; Lineberger, W. C. *The Journal of Physical Chemistry A* **2003**, *107*, 8521–8529.
- [336] Lee, S. H.; Kim, N.; Kim, T.-R.; Shin, S.; Kim, S. K. *The Journal of Physical Chemistry A* **2021**, *125*, 5794–5799.
- [337] Dobulis, M. A.; Thompson, M. C.; Jarrold, C. C. *The Journal of Physical Chemistry A* **2021**, *125*, 10089–10102.
- [338] Dobulis, M. A.; McGee, C. J.; Sommerfeld, T.; Jarrold, C. C. *The Journal of Physical Chemistry A* **2021**, *125*, 9128–9142.
- [339] Corkish, T. R.; ’t Hart, D. B.; Watson, P. D.; McKinley, A. J.; Wild, D. A. *Journal of Molecular Spectroscopy* **2019**, *364*, 111178.
- [340] Montaña, A. M. *ChemistrySelect* **2017**, *2*, 9094–9112.
- [341] Peláez, R. J.; Blondel, C.; Delsart, C.; Drag, C. *Journal of Physics B: Atomic, Molecular and Optical Physics* **2009**, *42*, 1–7.
- [342] Corkish, T. R.; Haakansson, C. T.; Watson, P. D.; Robinson, H. T.; McKinley, A. J.; Wild, D. A. *ChemPhysChem* **2021**, *22*, 1316–1320.
- [343] Corkish, T. R.; Haakansson, C. T.; McKinley, A. J.; Wild, D. A. *Australian Journal of Chemistry* **2020**, *73*, 693.
- [344] Dessent, C. E. H.; Bailey, C. G.; Johnson, M. A. *The Journal of Chemical Physics* **1995**, *102*, 6335–6338.

- [345] Davico, G. E.; Bierbaum, V. M. *Journal of the American Chemical Society* **2000**, *122*, 1740–1748.
- [346] Samson, J. J. C.; van Middelkoop, B.; Weickert, G.; Westerterp, K. R. *AICHE J.* **1999**, *45*, 1548–1558.
- [347] Cancelas, A. J.; Monteil, V.; McKenna, T. F. L. *Macromolecular Symposia* **2016**, *360*, 133–141.
- [348] Marcelino, N.; Cernicharo, J.; Agúndez, M.; Roueff, E.; Gerin, M.; Martín-Pintado, J.; Mauersberger, R.; Thum, C. *The Astrophysical Journal* **2007**, *665*, L127–L130.
- [349] Nixon, C. A.; Jennings, D. E.; Bézard, B.; Vinatier, S.; Teanby, N. A.; Sung, K.; Ansty, T. M.; Irwin, P. G. J.; Gorius, N.; Cottini, V.; et al., *The Astrophysical Journal* **2013**, *776*, L14.
- [350] Jones, B. M.; Zhang, F.; Kaiser, R. I.; Jamal, A.; Mebel, A. M.; Cordiner, M. A.; Charnley, S. B. *Proceedings of the National Academy of Sciences* **2010**, *108*, 452–457.
- [351] Bouwman, J.; Goulay, F.; Leone, S. R.; Wilson, K. R. *The Journal of Physical Chemistry A* **2012**, *116*, 3907–3917.
- [352] Chastaing, D.; James, P. L.; Sims, I. R.; Smith, I. W. M. *Faraday Discussions* **1998**, *109*, 165–181.
- [353] Vakhtin, A. B.; Heard, D. E.; Smith, I. W.; Leone, S. R. *Chemical Physics Letters* **2001**, *348*, 21–26.
- [354] Carter, W. P. L.; Lloyd, A. C.; Sprung, J. L.; Pitts, J. N. *Int. J. Chem. Kinet.* **1979**, *11*, 45–101.
- [355] Wayne, R. *Chemistry of Atmospheres*, 3rd ed.; Oxford University Press: New York, 2000.

- [356] von Glasow, R.; von Kuhlmann, R.; Lawrence, M. G.; Platt, U.; Crutzen, P. J. *Atmos. Chem. Phys.* **2004**, *4*, 2481–2497.
- [357] Warneck, P. *Chemistry of the Natural Atmosphere*, 2nd ed.; Academic Press, 2000.
- [358] Brynteson, M. D.; Womack, C. C.; Booth, R. S.; Lee, S. H.; Lin, J. J.; Butler, L. J. *The Journal of Physical Chemistry A* **2014**, *118*, 3211–3229.
- [359] Xu, L.; Kuczkowski, R. L. *The Journal of Chemical Physics* **1994**, *100*, 15–22.
- [360] Peebles, S. A.; Kuczkowski, R. L. *Journal of Molecular Structure* **1997**, *436-437*, 59–67.
- [361] Peebles, S. A.; Kuczkowski, R. L. *Journal of Molecular Structure* **1998**, *447*, 151–158.
- [362] Lapere, K. M. L.; Kettner, M.; Watson, P. D.; McKinley, A. J.; Wild, D. A. *The Journal of Physical Chemistry A* **2015**, *119*, 9722–9728.
- [363] Haakansson, T. R., Christian T. Corkish; D., W. P.; McKinley, A. J.; Wild, D. A. In Preparation.
- [364] Haakansson, T. R., Christian T. Corkish; D., W. P.; McKinley, A. J.; Wild, D. A. In Preparation.
- [365] Suits, A. G. *Annual Review of Physical Chemistry* **2020**, *71*, 77–100.
- [366] Rappoport, D.; Furche, F. *The Journal of Chemical Physics* **2010**, *133*, 134105.
- [367] Woon, D. E.; Dunning, T. H. *The Journal of Chemical Physics* **1994**, *100*, 2975–2988.
- [368] Jeziorski, B.; Moszynski, R.; Szalewicz, K. *Chemical Reviews* **1994**, *94*, 1887–1930.

- [369] Chuang, Y.-Y.; Chen, S.-M. *Journal of Computational Chemistry* **2011**, *32*, 1671–1679.
- [370] Chuang, Y.-Y.; Chen, S.-M. *Journal of the Chinese Chemical Society* **2012**, *59*, 1094–1103.
- [371] Feller, D.; Dixon, D. A. *The Journal of Physical Chemistry A* **2018**, *122*, 2598–2603.
- [372] Kraus, P. *Journal of Chemical Theory and Computation* **2020**, *16*, 5712–5722.
- [373] Kraus, P. *Journal of Chemical Theory and Computation* **2021**, *17*, 5651–5660.
- [374] Amicangelo, J. C.; Lee, Y.-P. *The Journal of Physical Chemistry Letters* **2010**, *1*, 2956–2961.
- [375] Lee, F. S. C.; Rowland, F. S. *The Journal of Physical Chemistry* **1977**, *81*, 1222–1229.
- [376] Braña, P.; Sordo, J. A. *Journal of Computational Chemistry* **2003**, *24*, 2044–2062.
- [377] Hiraoka, K.; Fujita, K.; Ishida, M.; Ichikawa, T.; Okada, H.; Hiizumi, K.; Wada, A.; Takao, K.; Yamabe, S.; Tsuchida, N. *The Journal of Physical Chemistry A* **2005**, *109*, 1049–1056.
- [378] Abplanalp, M. J.; Góbi, S.; Kaiser, R. I. *Physical Chemistry Chemical Physics* **2019**, *21*, 5378–5393.
- [379] Morales, S. B.; Bennett, C. J.; Le Picard, S. D.; Canosa, A.; Sims, I. R.; Sun, B. J.; Chen, P. H.; Chang, A. H. H.; Kislov, V. V.; Mebel, A. M.; et al., *The Astrophysical Journal* **2011**, *742*, 26.
- [380] Muzangwa, L. G.; Yang, T.; Parker, D. S. N.; Kaiser, R. I.; Mebel, A. M.; Jamal, A.; Ryazantsev, M.; Morokuma, K. *Physical Chemistry Chemical Physics* **2015**, *17*, 7699–7706.

- [381] Kaiser, R. I.; Parker, D. S. N.; Zhang, F.; Landera, A.; Kislov, V. V.; Mebel, A. M. *The Journal of Physical Chemistry A* **2012**, *116*, 4248–4258.
- [382] Chenoweth, K.; van Duin, A. C. T.; Dasgupta, S.; Goddard III, W. A. *The Journal of Physical Chemistry A* **2009**, *113*, 1740–1746.
- [383] Vijayakumar, S.; Rajakumar, B. *The Journal of Physical Chemistry A* **2017**, *121*, 1976–1984.
- [384] Hansen, N.; Miller, J. A.; Kasper, T.; Kohse-Höinghaus, K.; Westmoreland, P. R.; Wang, J.; Cool, T. A. *Proceedings of the Combustion Institute* **2009**, *32*, 623–630.
- [385] Laine, P. L.; Sohn, Y. S.; Nicovich, J. M.; McKee, M. L.; Wine, P. H. *The Journal of Physical Chemistry A* **2012**, *116*, 6341–6357.
- [386] Hiraoka, K.; Mizuse, S.; Yamabe, S. *The Journal of Physical Chemistry* **1988**, *92*, 3943–3952.
- [387] Doering, W. v. E.; Franck-Neumann, M.; Hasselmann, D.; Kaye, R. L. *Journal of the American Chemical Society* **1972**, *94*, 3833–3844.
- [388] Lording, W. J.; Fallon, T.; Sherburn, M. S.; Paddon-Row, M. N. *Chemical Science* **2020**, *11*, 11915–11926.
- [389] Arnold, D. W.; Bradforth, S. E.; Kim, E. H.; Neumark, D. M. *The Journal of Chemical Physics* **1995**, *102*, 3510–3518.
- [390] Markovich, G.; Pollack, S.; Giniger, R.; Cheshnovsky, O. *The Journal of Chemical Physics* **1994**, *101*, 9344–9353.
- [391] Hanwell, M. D.; Curtis, D. E.; Lonie, D. C.; Vandermeersch, T.; Zurek, E.; Hutchison, G. R. *Journal of Cheminformatics* **2012**, *4*.
- [392] Masseron, T.; García-Hernández, D. A.; Santoveña, R.; Manchado, A.; Zamora, O.; Manteiga, M.; Dafonte, C. *Nature Communications* **2020**, *11*.

- [393] Tenenbaum, E. D.; Ziurys, L. M. *The Astrophysical Journal* **2008**, *680*, L121–L124.
- [394] Agúndez, M.; Cernicharo, J.; Decin, L.; Encrénaz, P.; Teyssier, D. *The Astrophysical Journal* **2014**, *790*, L27.
- [395] Müller, H. S. P.; Woon, D. E. *The Journal of Physical Chemistry A* **2013**, *117*, 13868–13877.
- [396] Langleben, J.; Tennyson, J.; Yurchenko, S. N.; Bernath, P. *Monthly Notices of the Royal Astronomical Society* **2019**, *488*, 2332–2342.
- [397] Kleiner, I.; Tarrago, G.; Cottaz, C.; Sagui, L.; Brown, L.; Poynter, R.; Pickett, H.; Chen, P.; Pearson, J.; Sams, R.; et al., *Journal of Quantitative Spectroscopy and Radiative Transfer* **2003**, *82*, 293–312.
- [398] Larson, H. P.; Fink, U.; Treffers, R. R. *The Astrophysical Journal* **1977**, *211*, 972.
- [399] Bregman, J. D.; Lester, D. F.; Rank, D. M. *The Astrophysical Journal* **1975**, *202*, L55.
- [400] Weisstein, E. W.; Serabyn, E. *Icarus* **1996**, *123*, 23–36.
- [401] Moreno, R.; Marten, A.; Lellouch, E. Search for PH₃ in the Atmospheres of Uranus and Neptune at Millimeter Wavelength. AAS/Division for Planetary Sciences Meeting Abstracts #41. 2009; p 28.02.
- [402] Crovisier, J.; Bockelée-Morvan, D.; Colom, P.; Biver, N.; Despois, D.; Lis, D. C. *Astronomy & Astrophysics* **2004**, *418*, 1141–1157.
- [403] Greaves, J. S.; Richards, A. M. S.; Bains, W.; Rimmer, P. B.; Sagawa, H.; Clements, D. L.; Seager, S.; Petkowski, J. J.; Sousa-Silva, C.; Ranjan, S.; et al., *Nature Astronomy* **2021**, *5*, 726–728.

- [404] Villanueva, G. L.; Cordiner, M.; Irwin, P. G. J.; de Pater, I.; Butler, B.; Gurwell, M.; Milam, S. N.; Nixon, C. A.; Luszcz-Cook, S. H.; Wilson, C. F.; et al., *Nature Astronomy* **2021**, *5*, 631–635.
- [405] Bains, W.; Petkowski, J. J.; Seager, S.; Ranjan, S.; Sousa-Silva, C.; Rimmer, P. B.; Zhan, Z.; Greaves, J. S.; Richards, A. M. *Astrobiology* **2021**, *21*, 1277–1304.
- [406] Arthur, N. L.; Cooper, I. A. *Journal of the Chemical Society, Faraday Transactions* **1997**, *93*, 521–524.
- [407] Kaye, J. A.; Strobel, D. F. *Icarus* **1984**, *59*, 314–335.
- [408] Norrish, R. G. W.; Oldershaw, G. A. *Proceedings of the Royal Society of London. Series A, Mathematical and Physical Sciences* **1961**, *262*, 10–18.
- [409] Pätzold, M.; Häusler, B.; Bird, M. K.; Tellmann, S.; Mattei, R.; Asmar, S. W.; Dehant, V.; Eidel, W.; Imamura, T.; Simpson, R. A.; et al., *Nature* **2007**, *450*, 657–660.
- [410] Halmann, M.; Platzner, I. *The Journal of Physical Chemistry* **1969**, *73*, 4376–4378.
- [411] Zittel, P. F.; Lineberger, W. C. *The Journal of Chemical Physics* **1976**, *65*, 1236–1243.
- [412] Ricca, A.; Bauschlicher Jr, C. W. *Chemical Physics Letters* **1998**, *285*, 455–458.
- [413] Vermeeren, P.; Hansen, T.; Grasser, M.; Silva, D. R.; Hamlin, T. A.; Bickelhaupt, F. M. *The Journal of Organic Chemistry* **2020**, *85*, 14087–14093.
- [414] Torrent-Sucarrat, M.; Varandas, A. J. C. *Chemistry - A European Journal* **2016**, *22*, 14056–14063.

- [415] Phosphine Safety Data Sheet P-4643. Linde, 2021; Version 1.1.
- [416] Sandel, B. R.; Shemansky, D. E.; Broadfoot, A. L.; Holberg, J. B.; Smith, G. R.; McConnell, J. C.; Strobel, D. F.; Atreya, S. K.; Donahue, T. M.; Moos, H. W.; et al., *Science* **1982**, *215*, 548–553.
- [417] Barman, T. S.; Konopacky, Q. M.; Macintosh, B.; Marois, C. *The Astrophysical Journal* **2015**, *804*, 61.
- [418] Sada, P. V.; Romani, P. N.; Jennings, D. E.; Bjoraker, G. L.; Boyle, R.; McCabe, G. Mid-IR Observations of Ethylene on Jupiter. AAS/Division for Planetary Sciences Meeting Abstracts #32. 2000; p 12.14.
- [419] Fonfria, J. P.; Cernicharo, J.; Richter, M. J.; Lacy, J. H. *The Astrophysical Journal* **2008**, *673*, 445–469.
- [420] Reese, D. E.; Swan, P. R. *Science* **1968**, *159*, 1228–1230.
- [421] Krasnopol'sky, V. Sulfur chemistry and clouds on Venus. 42nd COSPAR Scientific Assembly. 2018; pp C3.1–6–18.
- [422] de Pater, I.; Romani, P. N.; Atreya, S. K. *Icarus* **1991**, *91*, 220–233.
- [423] Guillot, T.; Li, C.; Bolton, S. J.; Brown, S. T.; Ingersoll, A. P.; Janssen, M. A.; Levin, S. M.; Lunine, J. I.; Orton, G. S.; Steffes, P. G.; et al., *Journal of Geophysical Research: Planets* **2020**, *125*.
- [424] Hättig, C. *Phys. Chem. Chem. Phys.* **2005**, *7*, 59–66.
- [425] Chaibi, W.; Delsart, C.; Drag, C.; Blondel, C. *Journal of Molecular Spectroscopy* **2006**, *239*, 11–15.
- [426] Veseth, L. *Journal of Molecular Spectroscopy* **1971**, *38*, 228–242.
- [427] Novoa, J. J.; Whangbo, M.-H.; Williams, J. M. *Chemical Physics Letters* **1991**, *180*, 241–248.

- [428] Peterson, K. I.; Klemperer, W. *The Journal of Chemical Physics* **1986**, *85*, 725–732.
- [429] Andersen, J.; Heimdal, J.; Nelander, B.; Wugt Larsen, R. *The Journal of Chemical Physics* **2017**, *146*, 194302.
- [430] Kalugina, Y. N.; Cherepanov, V. N.; Buldakov, M. A.; Zvereva-Loëte, N.; Boudon, V. *Journal of Computational Chemistry* **2011**, *33*, 319–330.
- [431] Tsuzuki, S.; Uchimaru, T.; Mikami, M.; Tanabe, K. *The Journal of Physical Chemistry A* **1998**, *102*, 2091–2094.
- [432] Buckingham, A. D. *Advances in Chemical Physics* **2007**, 107–142.
- [433] Frenklach, M.; Feigelson, E. D. *The Astrophysical Journal* **1989**, *341*, 372.
- [434] Jupp, A. R.; Goicoechea, J. M. *Journal of the American Chemical Society* **2013**, *135*, 19131–19134.
- [435] Gudat, D. *Angewandte Chemie International Edition* **2014**, *53*, 4753–4754.
- [436] Schreiber, R. E.; Goicoechea, J. M. *Angewandte Chemie International Edition* **2020**, *60*, 3759–3767.
- [437] Zhu, C.; Frigge, R.; Turner, A. M.; Kaiser, R. I.; Sun, B.-J.; Chen, S.-Y.; Chang, A. H. H. *Chemical Communications* **2018**, *54*, 5716–5719.
- [438] Puschmann, F. F.; Stein, D.; Heift, D.; Hendriksen, C.; Gal, Z. A.; Grützmacher, H.-F.; Grützmacher, H. *Angewandte Chemie International Edition* **2011**, *50*, 8420–8423.
- [439] Russell, C. T.; Leinweber, H.; Zhang, T. L.; Daniels, J. T. M.; Strange-way, R. J.; Wei, H. *Geophysical Research Letters* **2013**, *40*, 216–220.
- [440] Cramer, C. J. *Chemical Physics Letters* **1993**, *202*, 297–302.

- [441] Cramer, C. J. *Journal of Molecular Structure: THEOCHEM* **1996**, *370*, 135–146.
- [442] Roszak, S. *The Journal of Chemical Physics* **1996**, *105*, 7569–7572.
- [443] Zhu, C.; Bergantini, A.; Singh, S. K.; Kaiser, R. I.; Eckhardt, A. K.; Schreiner, P. R.; Huang, Y.-S.; Sun, B.-J.; Chang, A. H. H. *Chemical Communications* **2021**, *57*, 4958–4961.
- [444] Weiser, P. S.; Wild, D. A.; Wolynec, P. P.; Bieske, E. J. *The Journal of Physical Chemistry A* **2000**, *104*, 2562–2566.
- [445] Markovich, G.; Cheshnovsky, O.; Kaldor, U. *The Journal of Chemical Physics* **1993**, *99*, 6201–6204.
- [446] Hendricks, J. H.; de Clercq, H. L.; Freidhoff, C. B.; Arnold, S. T.; Eaton, J. G.; Fancher, C.; Lyapustina, S. A.; Snodgrass, J. T.; Bowen, K. H. *The Journal of Chemical Physics* **2002**, *116*, 7926–7938.
- [447] Snodgrass, J. T.; Coe, J. V.; Freidhoff, C. B.; McHugh, K. M.; Arnold, S. T.; Bowen, K. H. *The Journal of Physical Chemistry* **1995**, *99*, 9675–9680.
- [448] Schwartz, R. L.; Davico, G. E.; Kim, J. B.; Carl Lineberger, W. *The Journal of Chemical Physics* **2000**, *112*, 4966–4973.

Appendix A

Tables and Data: Methylperoxy Radical Complexes

Table A1: Peak positions and assignments of 100 kPa O₂:CH₃I:CH₂Br₂:argon gas mix at low *m/z*.

Position (<i>m/z</i>)	Assignment
32.3	O ₂ ⁻
46.3	CH ₂ O ₂ ⁻
48.4	O ₃ ⁻
50.4	O ₂ ⁻ ...H ₂ O
64.4	O ₂ ⁻ ...O ₂
68.5	O ₂ ⁻ ...(H ₂ O) ₂
72.4	O ₂ ⁻ ...Ar

Table A2: Peak positions and assignments of 100 kPa O₂:CH₃I:CH₂Br₂:argon gas mix at high *m/z*.

Position (<i>m/z</i>)	Assignment
78.9	⁷⁹ Br ⁻
80.9	⁸¹ Br ⁻
97.0	⁷⁹ Br ⁻ ...H ₂ O
98.9	⁸¹ Br ⁻ ...H ₂ O
107.0	⁷⁹ Br ⁻ ...N ₂
108.8	⁸¹ Br ⁻ ...N ₂
118.9	⁷⁹ Br ⁻ ...Ar
120.8	⁸¹ Br ⁻ ...Ar
126.7	I ⁻
145.1	I ⁻ ...H ₂ O
155.0	I ⁻ ...N ₂
158.9	I ⁻ ...O ₂
162.9	I ⁻ ...(H ₂ O) ₂
167.0	I ⁻ ...Ar
174.0	O ₂ CH ₃ I
181.1	I ⁻ ...(H ₂ O) ₃
183.1	I ⁻ ...(N ₂) ₂
195.1	I ⁻ ...N ₂ ·Ar
199.2	I ⁻ ...O ₂ ·Ar
221.0	⁷⁹ Br ⁻ ...CH ₃ I
222.9	⁸¹ Br ⁻ ...CH ₃ I
268.9	I ⁻ ...CH ₃ I

Table A3: Cartesian coordinates of the component species optimised at MP2/aug-cc-pvnZ ($n = T, Q$) in Å.

		$O_2^- ({}^2\Pi_g)$			$O_2 ({}^3\Sigma_g)$		
		x	y	z	x	y	z
pVTZ	O	0.000000	0.000000	0.678580	O	0.000000	0.000000
	O	0.000000	0.000000	-0.678580	O	0.000000	0.000000
pVQZ	O	0.000000	0.000000	0.675084	O	0.000000	0.000000
	O	0.000000	0.000000	-0.675084	O	0.000000	-0.609451
		$CH_3I ({}^1A_1)$			$CH_3OO ({}^2A'')$		
		x	y	z	x	y	z
pVTZ	C	0.000000	-1.798770	0.000000	C	0.987097	-0.491358
	I	0.000000	0.324107	0.000000	H	1.948962	0.011290
	H	1.031744	-2.128352	0.000000	H	0.854804	-1.090383
	H	-0.515865	-2.128359	0.893517	H	0.854804	-1.090383
	H	-0.515865	-2.128359	-0.893517	O	0.000000	0.567805
		x	y	z	x	y	z
pVQZ	C	-1.784162	0.000000	0.000000	C	0.984168	-0.491772
	I	0.321851	0.000000	0.000000	H	1.945471	0.008585
	H	-2.117703	0.768764	0.684014	H	0.850926	-1.090049
	H	-2.117702	0.207992	-1.007776	H	0.850926	-1.090049
	H	-2.117703	-0.976755	0.323762	O	0.000000	0.565483
		$CH_3 ({}^2A''_2)$					
pVTZ	C	0.000000	0.000000	0.000000			
	H	0.000000	1.074914	0.000000			
	H	0.930903	-0.537457	0.000000			
	H	-0.930903	-0.537457	0.000000			
		x	y	z			
pVQZ	C	0.000000	0.000000	0.000000			
	H	0.000000	1.073436	0.000000			
	H	0.929623	-0.536718	0.000000			
	H	-0.929623	-0.536718	0.000000			

Table A4: MP2 harmonic frequencies of O_2 anion and neutral.

$O_2^- ({}^2\Pi_g)$					
	Mode	Symmetry	Frequency (cm $^{-1}$)	zpe (kJ mol $^{-1}$)	Description
pVTZ	ω_1	σ_g	1095	6.6	O=O stretch
pVQZ	ω_1	σ_g	1111	6.6	O=O stretch
$O_2 ({}^3\Sigma_g)$					
	Mode	Symmetry	Frequency (cm $^{-1}$)	zpe (kJ mol $^{-1}$)	Description
pVTZ	ω_1	σ_g	1455	8.7	O=O stretch
pVQZ	ω_1	σ_g	1480	8.9	O=O stretch

Table A5: MP2 harmonic frequencies of CH₃ radical.

CH ₃ (² A'' ₂)					
	Mode	Symmetry	Frequency (cm ⁻¹)	Intensity (km mol ⁻¹)	Description
pVTZ	ω_1	a'_2	489	75.8451	CH ₃ planar bend
	ω_2	e'	1439	2.0146	CH asymmetric bend
	ω_3	e'	1439	2.0146	CH ₂ symmetric bend
	ω_4	a'_1	3174	0.0000	CH ₃ symmetric stretch
	ω_5	e'	3364	1.7866	CH ₃ asymmetric stretch
	ω_6	e'	3364	1.7866	CH ₂ asymmetric stretch
	zpe		79.4		
pVQZ	Mode	Symmetry	Frequency (cm ⁻¹)	Intensity (km mol ⁻¹)	Description
	ω_1	a'_2	505	76.4691	CH ₃ planar bend
	ω_2	e'	1441	2.1939	CH asymmetric bend
	ω_3	e'	1441	2.1939	CH ₂ symmetric bend
	ω_4	a'_1	3178	0.0000	CH ₃ symmetric stretch
	ω_5	e'	3371	1.5176	CH ₃ asymmetric stretch
	ω_6	e'	3371	1.5176	CH ₂ asymmetric stretch
	zpe		79.6		

Table A6: MP2 harmonic frequencies of CH₃I.

CH ₃ I (¹ A ₁)					
	Mode	Symmetry	Frequency (cm ⁻¹)	Intensity (km mol ⁻¹)	Description
pVTZ	ω_1	a_1	580	1.2118	C—I stretch
	ω_2	e	908	4.9094	CH ₃ asymmetric wag
	ω_3	e	908	4.9094	CH ₃ asymmetric wag
	ω_4	a_1	1301	22.0907	CH ₃ symmetric wag
	ω_5	e	1490	4.8363	CH ₃ rock
	ω_6	e	1490	4.8363	CH ₃ scissor
	ω_7	a_1	3116	9.088	CH ₃ symmetric stretch
	ω_8	e	3236	0.0333	CH ₃ asymmetric stretch
	ω_9	e	3236	0.0333	H—CH ₂ asymmetric stretch
	zpe		97.3		
pVQZ	Mode	Symmetry	Frequency (cm ⁻¹)	Intensity (km mol ⁻¹)	Description
	ω_1	a_1	585	1.3607	C—I stretch
	ω_2	e	918	5.2682	CH ₃ asymmetric wag
	ω_3	e	918	5.2682	CH ₃ asymmetric wag
	ω_4	a_1	1304	21.1936	CH ₃ symmetric wag
	ω_5	e	1486	5.0599	CH ₃ rock
	ω_6	e	1486	5.0599	CH ₃ scissor
	ω_7	a_1	3120	8.969	CH ₃ symmetric stretch
	ω_8	e	3241	0.0133	CH ₃ asymmetric stretch
	ω_9	e	3241	0.0133	H—CH ₂ asymmetric stretch
	zpe		97.5		

Table A7: MP2 harmonic frequencies of CH₃OO radical.

CH ₃ OO (² A'')					
	Mode	Symmetry	Frequency (cm ⁻¹)	Intensity (km mol ⁻¹)	Description
pVTZ	Mode	Symmetry	Frequency	Intensity	Description
	ω_1	a''	126	0.0904	CH ₃ rotation
	ω_2	a'	502	7.4281	C–O–O bend
	ω_3	a'	949	17.7493	C–O stretch
	ω_4	a''	1148	0.9289	CH ₃ twist
	ω_5	a'	1202	1.4325	CH ₃ asymmetric wag
	ω_6	a'	1278	93.3186	O–O stretch
	ω_7	a'	1466	0.1257	CH ₃ symmetric wag
	ω_8	a''	1503	9.6056	CH ₃ rock
	ω_9	a'	1513	14.8506	CH ₃ scissor
	ω_{10}	a'	3101	18.4906	CH ₃ symmetric stretch
	ω_{11}	a''	3216	6.2192	H–CH ₂ asymmetric stretch
	ω_{12}	a'	3223	3.4961	CH ₃ asymmetric stretch
pVQZ	zpe		115.0		
	Mode	Symmetry	Frequency (cm ⁻¹)	Intensity (km mol ⁻¹)	Description
	ω_1	a''	130	0.0807	CH ₃ rotation
	ω_2	a'	505	7.5106	C–O–O bend
	ω_3	a'	952	17.8504	C–O stretch
	ω_4	a''	1150	0.8564	CH ₃ twist
	ω_5	a'	1205	1.6241	CH ₃ asymmetric wag
	ω_6	a'	1293	87.4152	O–O stretch
	ω_7	a'	1464	0.271	CH ₃ symmetric wag
	ω_8	a''	1499	10.0591	CH ₃ rock
	ω_9	a'	1511	15.8745	CH ₃ scissor
	ω_{10}	a'	3105	17.9768	CH ₃ symmetric stretch
	ω_{11}	a''	3222	5.7179	H–CH ₂ asymmetric stretch
	ω_{12}	a'	3230	3.1502	CH ₃ asymmetric stretch
	zpe		115.2		

Table A8: Energies associated with the bare oxygen anion, vertical detachment energies and neutral (all in E_h).

	O_2^- ($^2\Pi_g$)						
	E_{MP2}	E_{SCF}	E_{CCSD}	E_{corr}	$E_{CCSD(T)}$	$E_{(T)}$	E_{W1w}
pVDZ		-149.6119114	-150.0155985	-0.4036871	-150.0302745	-0.014676	
pVTZ	-150.1317771	-149.6456353	-150.1317199	-0.4860846	-150.1540225	-0.0223027	
pVQZ	-150.1728254	-149.6548341	-150.1686168	-0.5137826			
CBS		-149.6576963		-0.5319424		-0.0251379	-150.2147766
	O_2^- ($^3\Sigma_g$ VDE)						
pVDZ		-149.5967483	-149.9881501	-0.3914018	-150.0048253	-0.0166752	
pVTZ	-150.1067475	-149.6319499	-150.0985082	-0.4665582	-150.1226776	-0.0241694	
pVQZ	-150.1460183	-149.6414228	-150.1327701	-0.4913473			
CBS		-149.6443702		-0.5075998		-0.0269555	-150.1789255
	O_2^- ($^1\Delta_g$ VDE)						
pVDZ		-149.5091979	-149.941992	-0.4327941	-149.9644722	-0.0224803	
pVTZ	-150.0747198	-149.5440181	-150.0759538	-0.5319357	-150.1066902	-0.0307363	
pVQZ	-150.1151552	-149.5533448	-150.1442933	-0.5909486			
CBS		-149.5562467		-0.6296394		-0.0338056	-150.2196917
	O_2 ($^3\Sigma_g$)						
pVDZ		-149.6403938	-150.008539	-0.3681453	-150.021076	-0.0125369	
pVTZ	-150.1209379	-149.6760792	-150.1216127	-0.4455334	-150.140977	-0.0193644	
pVQZ	-150.1604304	-149.6862889	-150.1575701	-0.4712812			
CBS		-149.6894655		-0.4881623		-0.0219025	-150.1995304
	O_2 ($^3\Sigma_g$) Experimental Geometry						
pVDZ		-149.6424474	-150.0086264	-0.3661790	-150.0208501	-0.0122237	
pVTZ	-150.1209379	-149.6781984	-150.1219859	-0.4437875	-150.1409759	-0.0189900	
pVQZ	-150.1604304	-149.6884795	-150.1581097	-0.4696302			
CBS		-149.6916784		-0.4865736		-0.0215055	-150.1997574

Table A9: Energies associated with the methliodide, CH_3OO radical, bare iodide and iodine and CH_3 radical (all in E_h).

	$\text{CH}_3\text{I} (^1A_1)$						
	E_{MP2}	E_{SCF}	E_{CCSD}	E_{corr}	$E_{CCSD(T)}$	$E_{(T)}$	E_{W1w}
pVDZ		-334.269872	-334.5808649	-0.3109928	-334.5904053	-0.0095404	
pVTZ	-334.696672	-334.29133	-334.7181229	-0.4267929	-334.7345474	-0.0164244	
pVQZ	-334.7889329	-334.2946148	-334.8024011	-0.5077862			
CBS		-334.2956369		-0.5608882		-0.0189836	-334.8755087
	$\text{CH}_3\text{OO} (^2A'')$						
pVDZ		-189.2332705	-189.77807	-0.5447995	-189.7957528	-0.0176829	
pVTZ	-189.9071182	-189.2812996	-189.9339336	-0.652634	-189.9602433	-0.0263097	
pVQZ	-189.9596779	-189.2935016	-189.9803606	-0.686859			
CBS		-189.2972981		-0.709298		-0.0295168	-190.0361129
	$\text{I}^- (^1S)$						
pVDZ		-294.7418251	-294.8800073	-0.1381822	-294.883258	-0.0032507	
pVTZ	-294.9658304	-294.7464575	-294.9736832	-0.2272257	-294.9822875	-0.0086044	
pVQZ	-295.0462742	-294.7468485	-295.0497698	-0.3029213			
CBS		-294.7469702		-0.3525499		-0.0105947	-295.1101148
	$\text{I} (^2P)$						
pVDZ		-294.6537254	-294.767068	-0.1133426	-294.7690621	-0.0019941	
pVTZ	-294.845897	-294.6618826	-294.8593685	-0.1974859	-294.8654129	-0.0060444	
pVQZ	-294.9223506	-294.6624938	-294.9313926	-0.2688988			
CBS		-294.6626839		-0.3157196		-0.0075501	-294.9859536
	$\text{CH}_3 (^2A''_2)$						
pVDZ		-39.5657383	-39.7206638	-0.1549255	-39.7239147	-0.0032509	
pVTZ	-39.7383177	-39.5780794	-39.7586343	-0.1805549	-39.7635872	-0.0049529	
pVQZ	-39.7497912	-39.5805154	-39.7679513	-0.1874359			
CBS		-39.5812733		-0.1919473		-0.0055856	-39.7788063

Table A10: Geometric parameters of the component species optimised at MP2/aug-cc-pvnZ ($n = T, Q$) in Å.

	R_{O-O}				
O_2^-	pVTZ	1.357			
	pVQZ	1.350			
O_2	pVTZ	1.224			
	pVQZ	1.219			
	R_{O-O}	R_{C-O}	R_{C-H}	\angle_{H-C-O}	\angle_{C-O-O}
CH_3OO	pVTZ	1.296	1.448	1.085	105.4
	pVQZ	1.291	1.444	1.084	105.7
		R_{C-I}	R_{C-H}	\angle_{H-C-I}	
CH_3I	pVTZ		2.123	1.083	107.7
	pVQZ		2.106	1.082	108.0

Table A11: Vertical detachment energies (VDE) and electron affinities (ADE) of the bare oxygen anion and iodide. W1w energies are in E_h , zero point corrections are in kJ mol⁻¹ and detachments are in eV.

Geometry	State	E_{W1w}	zpe	VDE	Exp	Shift
O_2^-	$^2\Pi_g$	-150.2147766	6.6			
	$^3\Sigma_g$	-150.1789255		0.907		
Geometry	State	E_{W1w}	zpe	ADE		
O_2	$^3\Sigma_g$	-150.1995304	8.9	0.438	0.451	0.013
Geometry	State	E_{W1w}	zpe	ADE		
I^-	1S	-295.1101148				
I	$^2P_{3/2}$	-294.9859536		3.065	3.059	-0.006
	$^2P_{1/2}$			4.007		

Table A12: Geometric parameters of MP2 optimised CH_3OOI^- complexes.

vdW1: $\text{O}_2^- \cdots \text{H}_3\text{Cl}$ ($^2A''$)									
Method	$R_{\text{I}-\text{C}}$ Å	$R_{\text{C}-\text{O}}$ Å	$R_{\text{O}-\text{O}}$ Å	$\angle_{\text{C}-\text{O}-\text{O}}$ °	$\angle_{\text{I}-\text{C}-\text{O}}$ °	E_h	zpe kJ mol ⁻¹	D_e kJ mol ⁻¹	D_o kJ mol ⁻¹
MP2/Tz	2.159	2.731	1.352	85.0	160.3	-484.8538677	108.0	66.7	62.9
MP2/Qz	2.139	2.743	1.345	84.3	160.0	-484.9871263	108.1	66.6	62.6
CCSD(T)/Dz						-484.6478286		71.3	67.3
CCSD(T)/Tz						-484.9143903		67.8	63.8
CCSD/Qz						-484.9951322		63.3	59.3
W1w						-485.1158986		67.2	63.3
TS1: $[\text{O}_2 \cdots \text{CH}_3 \cdots \text{I}]^-$ TS ($^2A'$)									
Method	$R_{\text{I}-\text{C}}$ Å	$R_{\text{C}-\text{O}}$ Å	$R_{\text{O}-\text{O}}$ Å	$\angle_{\text{C}-\text{O}-\text{O}}$ °	$\angle_{\text{I}-\text{C}-\text{O}}$ °	E_h	zpe kJ mol ⁻¹	$\ddagger_{\text{Forward}}$ kJ mol ⁻¹	$\ddagger_{\text{Reverse}}$ kJ mol ⁻¹
MP2/Tz	2.594	1.935	1.315	105.9	176.4	-484.8258091	108.5	74.2	164.2
MP2/Qz	2.586	1.931	1.310	106.2	176.4	-484.9590084	108.7	74.4	164.7
CCSD(T)/Dz						-484.6320611		41.9	160.6
CCSD(T)/Tz						-484.8960536		48.7	160.1
CCSD/Qz						-484.9761656		50.3	177.6
W1w						-485.0981189		47.2	165.3

Table A13: Geometric parameters of MP2 optimised CH_3OOI^- complexes.

Method	vdW2: $\text{I}^- \cdots \text{H}_3\text{COO}$ ($^2\text{A}''$)						zpe kJ mol $^{-1}$	D_e kJ mol $^{-1}$	D_o kJ mol $^{-1}$
	$R_{\text{I}-\text{C}}$ Å	$R_{\text{C}-\text{O}}$ Å	$R_{\text{O}-\text{O}}$ Å	$\angle_{\text{C}-\text{O}-\text{O}}$ °	$\angle_{\text{I}-\text{C}-\text{O}}$ °	E_h			
MP2/Tz	3.513	1.465	1.291	111.5	164.9	-484.8910751	115.6	47.6	47.2
MP2/Qz	3.485	1.462	1.286	111.8	168.2	-485.0245290	116.0	48.8	48.0
CCSD(T)/Dz						-484.6960336		44.7	43.9
CCSD(T)/Tz						-484.9598295		45.4	44.6
CCSD/Qz						-485.0466225		43.3	42.5
W1w						-485.1638659		46.3	45.5
vdW3: $\text{O}_2^- \cdots \text{ICH}_3$ ($^2\text{A}''$)									
Method	$R_{\text{I}-\text{C}}$ Å	$R_{\text{I}-\text{O}}$ Å	$R_{\text{O}-\text{O}}$ Å	$\angle_{\text{I}-\text{O}-\text{O}}$ °	$\angle_{\text{C}-\text{I}-\text{O}}$ °	E_h	zpe kJ mol $^{-1}$	D_e kJ mol $^{-1}$	D_o kJ mol $^{-1}$
MP2/Tz	2.179	2.535	1.314	109.3	179.7	-484.8508447	107.9	58.8	55.1
MP2/Qz	2.162	2.53	1.31	109.2	179.9	-484.9843567	108.2	59.3	55.2
CCSD(T)/Dz						-484.6448346		63.4	59.3
CCSD(T)/Tz						-484.9126845		63.3	59.2
CCSD/Qz						-484.9929251		57.5	53.4
W1w						-485.1147113		64.1	60.0

Table A14: Geometric parameters of MP2 optimised CH_3OOI^- complexes.

Method	TS2: $\text{O}_2 \cdots \text{CH}_3\text{I}$ TS (${}^2\text{A}'$)						zpe kJ mol $^{-1}$	$\ddagger_{Forward}$ kJ mol $^{-1}$	$\ddagger_{Reverse}$ kJ mol $^{-1}$
	$R_{\text{I}-\text{C}}$ Å	$R_{\text{C}-\text{O}}$ Å	$R_{\text{O}-\text{O}}$ Å	$\angle_{\text{C}-\text{O}-\text{O}}$ °	$\angle_{\text{I}-\text{C}-\text{O}}$ °	E_h			
MP2/Tz	2.121	3.846	1.349	110.7	55.2	-484.8351560	106.3	47.5	39.7
MP2/Qz	2.105	3.830	1.343	110.4	54.7	-484.9687317	106.4	46.5	39.1
CCSD(T)/Dz						-484.6262749		54.8	46.8
CCSD(T)/Tz						-484.8955729		47.7	43.0
CCSD/Qz						-484.9761206		48.2	42.2
W1w						-485.0972345		47.3	44.0
TS3: $\text{O}_2 \cdots \text{I}^- \cdots \text{H}_3\text{C}$ ET-TS (${}^4\text{A}$)									
Method	$R_{\text{I}-\text{O}}$ Å	$R_{\text{I}-\text{H}}$ Å	$R_{\text{O}-\text{O}}$ Å	$\angle_{\text{I}-\text{O}-\text{O}}$ °	$\angle_{\text{H}-\text{I}-\text{O}}$ °	E_h	zpe kJ mol $^{-1}$	$\ddagger_{Forward}$ kJ mol $^{-1}$	$\ddagger_{Reverse}$ kJ mol $^{-1}$
	3.786	2.950	1.226	176.0	179.4	-484.8326033	90.8	30.9	-17.0
MP2/Qz	3.767	2.935	1.221	164.3	177.8	-484.9641586	91.4	36.2	-17.1
CCSD(T)/Dz						-484.6357432		7.1	-16.7
CCSD(T)/Tz						-484.8944814		31.0	-17.0
CCSD/Qz						-484.9818548		12.3	-14.3
W1w						-485.0958745		32.6	-16.5

Table A15: Geometric parameters of MP2 optimised CH_3OOI^- complexes.

Method	vdW4: $\text{I}^- \cdots \text{OOCH}_3$ (${}^2A'$)					E_h
	$R_{\text{I}-\text{O}}$	$R_{\text{C}-\text{O}}$	$R_{\text{O}-\text{O}}$	$\angle_{\text{C}-\text{O}-\text{O}}$	$\angle_{\text{O}-\text{O}-\text{I}}$	
	Å	Å	Å	°	°	
MP2/Tz	2.492	1.403	1.440	105.7	126.3	-484.8641368
vdw5: $\text{I}^- \cdots \text{OOCH}_3$ (${}^2A'$)						
Method	O-O-I appended					E_h
	$R_{\text{I}-\text{O}}$	$R_{\text{C}-\text{O}}$	$R_{\text{O}-\text{O}}$	$\angle_{\text{C}-\text{O}-\text{O}}$	$\angle_{\text{C}-\text{O}-\text{I}}$	
	Å	Å	Å	°	°	
MP2/Tz	2.329	1.394	1.493	108.3	118.6	-484.8348871

Table A16: Geometric parameters of MP2 optimised CH₃OOI complexes.

Method	vdW1: O ₂ ... H ₃ Cl (³ A'')					E_h kJ mol ⁻¹	zpe kJ mol ⁻¹	D_e kJ mol ⁻¹	D_o kJ mol ⁻¹
	$R_{\text{I-C}}$ Å	$R_{\text{C-O}}$ Å	$R_{\text{O-O}}$ Å	$\angle_{\text{C-O-O}}$ °	$\angle_{\text{I-C-O}}$ °				
MP2/Tz	2.123	3.276	1.225	83.0	175.6	-484.8192098	106.9	4.2	1.4
MP2/Qz	2.105	3.301	1.220	81.4	172.0	-484.9508705	107.3	4.0	0.8
CCSD(T)/Dz						-484.6133436		4.9	1.7
CCSD(T)/Tz						-484.8769942		3.9	0.7
CCSD/Qz						-484.9608965		2.4	-0.8
W1w						-485.0762692		3.2	0.0
TS1: O ₂ ... CH ₃ ... I TS (³ A'')									
Method	$R_{\text{I-C}}$ Å	$R_{\text{C-O}}$ Å	$R_{\text{O-O}}$ Å	$\angle_{\text{C-O-O}}$ °	$\angle_{\text{I-C-O}}$ °	E_h kJ mol ⁻¹	zpe kJ mol ⁻¹	$\ddagger_{\text{Forward}}$ kJ mol ⁻¹	$\ddagger_{\text{Reverse}}$ kJ mol ⁻¹
	2.605	1.749	1.218	114.6	179.2			271.4	96.2
MP2/Qz	2.592	1.741	1.214	114.7	179.2	-484.8475957	110.9	274.7	93.5
CCSD(T)/Dz						-484.5370801		203.8	74.9
CCSD(T)/Tz						-484.7978193		211.5	75.0
CCSD/Qz						-484.8769360		224.0	92.6
W1w						-484.9958887		214.6	71.3

Table A17: Geometric parameters of MP2 optimised CH₃OOI complexes.

vdW2: I...H ₃ COO (³ A'')									
Method	$R_{\text{I-C}}$ Å	$R_{\text{C-O}}$ Å	$R_{\text{O-O}}$ Å	$\angle_{\text{C-O-O}}$ °	$\angle_{\text{I-C-O}}$ °	E_h	zpe kJ mol ⁻¹	D_e kJ mol ⁻¹	D_o kJ mol ⁻¹
MP2/Tz	3.786	1.448	1.296	110.5	176.2	-484.7557311	115.6	7.1	6.6
MP2/Qz	3.736	1.445	1.291	110.6	179.2	-484.8850279	115.7	7.9	7.4
CCSD(T)/Dz						-484.5674473		6.9	6.4
CCSD(T)/Tz						-484.8282280		6.8	6.2
CCSD/Qz						-484.9140313		6.0	5.5
W1w						-485.0248884		7.4	6.9
vdW3: O ₂ ...ICH ₃ (³ A'')									
Method	$R_{\text{I-C}}$ Å	$R_{\text{C-O}}$ Å	$R_{\text{O-O}}$ Å	$\angle_{\text{C-O-O}}$ °	$\angle_{\text{I-C-O}}$ °	E_h	zpe kJ mol ⁻¹	D_e kJ mol ⁻¹	D_o kJ mol ⁻¹
MP2/Tz	2.123	3.322	1.224	128.6	177.5	-484.8195115	107.8	5.0	1.0
MP2/Qz	2.107	3.325	1.219	130.9	178.0	-484.9514930	107.8	5.6	1.9
CCSD(T)/Dz						-484.6130872		4.2	0.6
CCSD(T)/Tz						-484.8770593		4.0	0.4
CCSD/Qz						-484.9612321		3.3	-0.3
W1w						-485.0768198		4.7	1.0

Table A18: Geometric parameters of MP2 optimised CH₃OOI complexes.

vdW4: I...OOCH ₃ (³ A'')									
Method	C–O–I appended					E_h	zpe kJ mol ⁻¹	D_e kJ mol ⁻¹	D_o kJ mol ⁻¹
	$R_{\text{I}-\text{O}}$ Å	$R_{\text{C}-\text{O}}$ Å	$R_{\text{O}-\text{O}}$ Å	$\angle_{\text{C}-\text{O}-\text{O}}$ °	$\angle_{\text{O}-\text{O}-\text{I}}$ °				
MP2/Tz	3.041	1.451	1.297	111.6	125.7	-484.7584731	106.4	14.3	22.9
MP2/Qz	2.976	1.448	1.291	111.8	126.0	-484.8879630	116.1	15.6	14.7
CCSD(T)/Dz						-484.5694759		12.2	11.4
CCSD(T)/Tz						-484.8307216		13.3	12.4
CCSD/Qz						-484.9161530		11.6	10.7
W1w						-485.0277224		14.8	14.0

vdW5: I...OOCH ₃ (³ A'')									
Method	O–O–I appended					E_h	zpe kJ mol ⁻¹	D_e kJ mol ⁻¹	D_o kJ mol ⁻¹
	$R_{\text{I}-\text{O}}$ Å	$R_{\text{C}-\text{O}}$ Å	$R_{\text{O}-\text{O}}$ Å	$\angle_{\text{C}-\text{O}-\text{O}}$ °	$\angle_{\text{C}-\text{O}-\text{I}}$ °				
MP2/Tz	2.872	1.454	1.290	111.1	112.4	-484.7607190	117.1	20.2	18.1
MP2/Qz	2.815	1.451	1.284	111.3	113.1	-484.8905771	117.5	22.4	20.2
CCSD(T)/Dz						-484.5693004		11.8	9.5
CCSD(T)/Tz						-484.8306058		13.0	10.7
CCSD/Qz						-484.9157145		10.4	8.1
W1w						-485.0273747		13.9	11.7

Table A19: Geometric parameters of MP2 optimised CH_3OOI complexes.

Method	vdW6: I... OOCH_3 (3A)						E_h kJ mol $^{-1}$	zpe kJ mol $^{-1}$	D_e kJ mol $^{-1}$	D_o
	$R_{\text{I}-\text{O}}$ Å	$R_{\text{C}-\text{O}}$ Å	$R_{\text{O}-\text{O}}$ Å	$\angle_{\text{C}-\text{O}-\text{O}}$ °	$\angle_{\text{C}-\text{O}-\text{I}}$ °	\angle_{IOCO}				
MP2/Tz	3.755	1.451	1.300	110.6	102.8	88.1	-484.7586408	116.3	14.8	13.5
MP2/Qz	3.730	1.448	1.295	110.7	103.3	88.2	-484.8880204	116.4	15.7	14.5
CCSD(T)/Dz							-484.5693004		11.8	10.6
CCSD(T)/Tz							-484.8306058		13.0	11.8
CCSD/Qz							-484.9157145		10.4	9.2
W1w							-485.0273747		13.9	12.7
vdW7: O-O... H_3Cl (3A)										
Method	$R_{\text{I}-\text{C}}$ Å	$R_{\text{C}-\text{O}}$ Å	$R_{\text{O}-\text{O}}$ Å	$\angle_{\text{C}-\text{O}-\text{O}}$ °	$\angle_{\text{I}-\text{C}-\text{O}}$ °		E_h kJ mol $^{-1}$	zpe kJ mol $^{-1}$	D_e kJ mol $^{-1}$	D_o
MP2/Tz	2.123	3.147	1.225	180.0	180.0		-484.8190267	106.6	3.7	1.0
MP2/Qz	2.106	3.146	1.219	180.0	180.0		-484.9507827	107.0	3.7	0.9
CCSD(T)/Dz							-484.6132494		4.6	1.8
CCSD(T)/Tz							-484.8768105		3.4	0.5
CCSD/Qz							-484.9608909		2.4	-0.4
W1w							-485.0762255		3.1	0.3

Table A20: Calculated complex dissociation energies, electron affinities and vertical detachment energies of CH_3OOI complexes. For CCSD(T) and W1w methods, vibrational contributions are included from MP2/aus-cc-pVQZ harmonic frequencies.

vdW1: $\text{O}_2^- \cdots \text{H}_3\text{Cl}$ ($^2\text{A}''$)								
Method	E_h	zpe kJ mol ⁻¹	D_e kJ mol ⁻¹	D_o kJ mol ⁻¹	$VDE_{^3\text{A}''}$ eV	$VDE_{^1\text{A}'}$ eV	$ADE_{^3\text{A}''}$ eV	
MP2/Tz	-484.8538677	108.0	66.7	62.9				
MP2/Qz	-484.9871263	108.1	66.6	62.6				
CCSD(T)/Dz	-484.6478286		71.3	67.3	1.444	2.749	0.930	
CCSD(T)/Tz	-484.9143903		67.8	63.8	1.503	2.569	1.010	
CCSD/Qz	-484.9951322		63.3	59.3	1.384	2.632	0.924	
W1w	-485.1158986		67.2	63.3	1.187	2.337	1.070	
vdW2: $\text{I}^- \cdots \text{H}_3\text{COO}$ ($^2\text{A}''$)								
Method	E_h	zpe kJ mol ⁻¹	D_e kJ mol ⁻¹	D_o kJ mol ⁻¹	$VDE_{^2\text{P}_{3/2}}$ eV	$VDE_{^2\text{P}_{1/2}}$ eV	$ADE_{^2\text{P}_{3/2}}$ eV	$ADE_{^2\text{P}_{1/2}}$ eV
MP2/Tz	-484.8910751	115.6	47.6	47.2				
MP2/Qz	-485.024529	116.0	48.8	48.0				
CCSD(T)/Dz	-484.6960336		44.7	43.9	3.442	4.384	3.448	4.390
CCSD(T)/Tz	-484.9598295		45.4	44.6	3.445	4.387	3.457	4.399
CCSD/Qz	-485.0466225		43.3	42.5	3.440	4.382	3.443	4.385
W1w	-485.1638659		46.3	45.5	3.449	4.391	3.459	4.401

Table A21: Calculated complex dissociation energies, electron affinities and vertical detachment energies of CH_3OOI complexes. For CCSD(T) and W1w methods, vibrational contributions are included from MP2/aus-cc-pVQZ harmonic frequencies.

Method	vdW3: $\text{O}_2^- \cdots \text{ICH}_3$ (${}^2A''$)						
	E_h	zpe kJ mol $^{-1}$	D_e kJ mol $^{-1}$	D_o kJ mol $^{-1}$	$VDE_{{}^3A''}$ eV	$VDE_{{}^1A'}$ eV	$ADE_{{}^3A''}$ eV
MP2/Tz	-484.8508447	107.9	58.8	55.1			
MP2/Qz	-484.9843567	108.2	59.3	55.2			
CCSD(T)/Dz	-484.6448346		63.4	59.3	1.397	2.694	0.859
CCSD(T)/Tz	-484.9126845		63.3	59.2	1.405	2.587	0.965
CCSD/Qz	-484.9929251		57.5	53.4	1.259	2.545	0.858
W1w	-485.1147113		64.1	60.0	1.163	2.256	1.026

Table A22: MP2 harmonic frequencies of $\text{O}_2^- \cdots \text{H}_3\text{Cl}$ ($^2\text{A}''$) complex.

vdW1: $\text{O}_2^- \cdots \text{H}_3\text{Cl}$ ($^2\text{A}''$)					
	Mode	Symmetry	Frequency (cm $^{-1}$)	Intensity (km mol $^{-1}$)	Description
pVTZ	ω_1	a'	67	0.6574	Intermolecular bend
	ω_2	a''	83	5.3869	Intermolecular rock
	ω_3	a'	136	67.8718	C- stretch
	ω_4	a''	169	0.2684	CH_3 rotation
	ω_5	a'	250	64.0967	O_2 planar rotation
	ω_6	a'	512	91.8539	I- CH_3 stretch
	ω_7	a''	912	3.2416	CH_3 twist
	ω_8	a'	917	29.2807	CH_3 asymmetric wag
	ω_9	a'	1226	1847.5167	$\text{O}=\text{O}$ stretch
	ω_{10}	a'	1274	137.7106	CH_3 symmetric wag
	ω_{11}	a'	1466	10.6656	CH_3 scissor
	ω_{12}	a''	1484	3.8487	H- CH_2 scissor
	ω_{13}	a'	3081	1318.5635	CH_3 symmetric stretch
	ω_{14}	a'	3214	233.035	CH_3 asymmetric stretch
	ω_{15}	a''	3263	0.3855	H- CH_2 asymmetric stretch
		zpe	108.0		
pVQZ	Mode	Symmetry	Frequency (cm $^{-1}$)	Intensity (km mol $^{-1}$)	Description
	ω_1	a'	56	3.5339	Intermolecular C- $\text{O}=\text{O}$ bend
	ω_2	a''	92	4.8846	Intermolecular rock
	ω_3	a'	137	63.8553	C- stretch
	ω_4	a''	190	0.1247	CH_3 rotation
	ω_5	a'	251	72.0667	O_2 planar rotation
	ω_6	a'	519	79.973	I- CH_3 stretch
	ω_7	a'	917	28.2569	CH_3 twist
	ω_8	a''	920	3.4788	CH_3 asymmetric wag
	ω_9	a'	1224	1218.928	$\text{O}=\text{O}$ stretch
	ω_{10}	a'	1280	17.3092	CH_3 symmetric wag
	ω_{11}	a'	1462	10.004	CH_3 scissor
	ω_{12}	a''	1486	3.1549	H- CH_2 scissor
	ω_{13}	a'	3062	746.3699	CH_3 symmetric stretch
	ω_{14}	a'	3214	195.9201	CH_3 asymmetric stretch
	ω_{15}	a''	3265	0.2836	H- CH_2 asymmetric stretch
		zpe	108.1		

Table A23: MP2 harmonic frequencies of $[\text{O}_2\cdots\text{CH}_3\cdots\text{I}]^- \text{ TS } (^2\text{A}')$ complex.

TS1: $[\text{O}_2\cdots\text{CH}_3\cdots\text{I}]^- \text{ TS } (^2\text{A}')$					
	Mode	Symmetry	Frequency (cm $^{-1}$)	Intensity (km mol $^{-1}$)	Description
pVTZ	ω_1	a'	609 <i>i</i>	3174.3031	O–C–I asymmetric stretch
	ω_2	a'	123	10.4858	C–O=O bend
	ω_3	a''	141	1.4598	CH ₃ rotation
	ω_4	a'	213	21.7506	O–C–I bend
	ω_5	a''	225	7.3427	Intermolecular rock
	ω_6	a'	301	7.8486	O ₂ planar rotation
	ω_7	a''	964	0.5883	CH ₃ twist
	ω_8	a'	987	12.0049	CH ₃ asymmetric wag
	ω_9	a'	1028	286.5871	CH ₃ symmetric wag
	ω_{10}	a'	1322	140.3345	O=O stretch
	ω_{11}	a''	1407	3.046	H–CH ₂ scissor
	ω_{12}	a'	1421	5.0531	CH ₃ scissor
	ω_{13}	a'	3197	2.8702	CH ₃ symmetric stretch
	ω_{14}	a'	3401	6.8154	CH ₃ asymmetric stretch
	ω_{15}	a''	3404	5.4205	H–CH ₂ asymmetric stretch
		zpe	108.5		
pVQZ	Mode	Symmetry	Frequency (cm $^{-1}$)	Intensity (km mol $^{-1}$)	Description
	ω_1	a'	604 <i>i</i>	3101.8401	O–C–I asymmetric stretch
	ω_2	a'	124	11.0908	C–O=O bend
	ω_3	a''	142	1.5056	CH ₃ rotation
	ω_4	a'	213	22.4718	O–C–I bend
	ω_5	a''	228	7.2769	Intermolecular rock
	ω_6	a'	302	8.2865	O ₂ planar rotation
	ω_7	a''	962	0.6347	CH ₃ twist
	ω_8	a'	982	8.4509	CH ₃ asymmetric wag
	ω_9	a'	1035	288.2349	CH ₃ symmetric wag
	ω_{10}	a'	1335	131.9503	O=O stretch
	ω_{11}	a''	1408	3.1291	H–CH ₂ scissor
	ω_{12}	a'	1420	5.6731	CH ₃ scissor
	ω_{13}	a'	3199	2.5883	CH ₃ symmetric stretch
	ω_{14}	a'	3407	6.5834	CH ₃ asymmetric stretch
	ω_{15}	a''	3410	5.5299	H–CH ₂ asymmetric stretch
		zpe	108.7		

Table A24: MP2 harmonic frequencies of $\text{I}^- \cdots \text{H}_3\text{COO}$ ($^2A''$) complex.

vdW2: $\text{I}^- \cdots \text{H}_3\text{COO}$ ($^2A''$)					
	Mode	Symmetry	Frequency (cm $^{-1}$)	Intensity (km mol $^{-1}$)	Description
pVTZ	ω_1	a'	46	4.6875	Intermolecular bend
	ω_2	a''	67	6.8517	Intermolecular rock
	ω_3	a'	89	5.1493	Intermolecular stretch
	ω_4	a''	109	0.1188	CH_3 rotation
	ω_5	a'	492	17.2581	$\text{C}-\text{O}-\text{O}$ bend
	ω_6	a'	894	67.1442	$\text{C}-\text{O}$ stretch
	ω_7	a''	1114	0.7473	CH_3 twist
	ω_8	a'	1157	2.373	CH_3 asymmetric wag
	ω_9	a'	1328	75.409	$\text{O}=\text{O}$ stretch
	ω_{10}	a'	1432	17.5669	CH_3 symmetric wag
	ω_{11}	a''	1484	3.467	$\text{H}-\text{CH}_2$ scissor
	ω_{12}	a'	1494	19.2866	CH_3 scissor
	ω_{13}	a'	3123	7.9458	CH_3 symmetric stretch
	ω_{14}	a''	3246	1.3469	$\text{H}-\text{CH}_2$ asymmetric stretch
	ω_{15}	a'	3255	1.3124	CH_3 asymmetric stretch
zpe			115.6		
pVQZ	Mode	Symmetry	Frequency (cm $^{-1}$)	Intensity (km mol $^{-1}$)	Description
	ω_1	a'	51	4.7779	Intermolecular bend
	ω_2	a''	61	6.6923	Intermolecular rock
	ω_3	a'	90	5.3529	Intermolecular stretch
	ω_4	a''	129	0.0995	CH_3 rotation
	ω_5	a'	495	19.4932	$\text{C}-\text{O}-\text{O}$ bend
	ω_6	a'	897	66.8674	$\text{C}-\text{O}$ stretch
	ω_7	a''	1123	0.6158	CH_3 twist
	ω_8	a'	1162	1.0068	CH_3 asymmetric wag
	ω_9	a'	1340	59.9975	$\text{O}=\text{O}$ stretch
	ω_{10}	a'	1436	22.1784	CH_3 symmetric wag
	ω_{11}	a''	1481	3.6717	$\text{H}-\text{CH}_2$ scissor
	ω_{12}	a'	1491	21.3461	CH_3 scissor
	ω_{13}	a'	3127	5.9636	CH_3 symmetric stretch
	ω_{14}	a''	3252	1.1759	$\text{H}-\text{CH}_2$ asymmetric stretch
	ω_{15}	a'	3261	0.9536	CH_3 asymmetric stretch
zpe			116.0		

Table A25: MP2 harmonic frequencies of $\text{O}_2^- \cdots \text{ICH}_3$ ($^2\text{A}''$) complex.

vdW3: $\text{O}_2^- \cdots \text{ICH}_3$ ($^2\text{A}''$)					
	Mode	Symmetry	Frequency (cm $^{-1}$)	Intensity (km mol $^{-1}$)	Description
pVTZ	ω_1	a''	16	0.4107	CH_3 rotation
	ω_2	a'	89	8.1446	Intermolecular planar bend
	ω_3	a''	126	0.9659	Intermolecular out of plane bend
	ω_4	a'	155	64.2748	Intermolecular stretch
	ω_5	a'	249	97.8966	I–O stretch
	ω_6	a'	510	66.6029	I–C stretch
	ω_7	a''	825	4.37	CH_3 twist
	ω_8	a'	828	4.1236	CH_3 asymmetric wag
	ω_9	a'	1228	3.7494	CH_3 symmetric wag
	ω_{10}	a'	1483	2.7982	CH_3 scissor
	ω_{11}	a''	1483	2.4467	H– CH_2 scissor
	ω_{12}	a'	1607	608.82	O=O stretch
	ω_{13}	a'	3074	77.8514	CH_3 symmetric stretch
	ω_{14}	a'	3181	13.4091	CH_3 asymmetric stretch
	ω_{15}	a''	3181	13.8853	H– CH_2 asymmetric stretch
			zpe	107.9	
pVQZ	Mode	Symmetry	Frequency (cm $^{-1}$)	Intensity (km mol $^{-1}$)	Description
	ω_1	a''	43	0.7435	CH_3 rotation
	ω_2	a'	89	8.1631	Intermolecular planar bend
	ω_3	a''	132	0.6631	Intermolecular out of plane bend
	ω_4	a'	156	58.9558	Intermolecular stretch
	ω_5	a'	253	98.9845	I–O stretch
	ω_6	a'	516	61.1167	I–C stretch
	ω_7	a''	837	4.4271	CH_3 twist
	ω_8	a'	839	4.5391	CH_3 asymmetric wag
	ω_9	a'	1233	2.8989	CH_3 symmetric wag
	ω_{10}	? a	1480	2.8828	CH_3 scissor
	ω_{11}	? a	1480	2.7908	H– CH_2 scissor
	ω_{12}	a'	1590	590.0093	O=O stretch
	ω_{13}	? a	3078	73.4755	CH_3 symmetric stretch
	ω_{14}	? a	3187	12.9871	CH_3 asymmetric stretch
	ω_{15}	a''	3187	13.0747	H– CH_2 asymmetric stretch
			zpe	108.2	

Table A26: MP2 harmonic frequencies of $\text{O}_2^- \cdots \text{CH}_3\text{I}$ TS (${}^2\text{A}'$) complex.

TS2: $\text{O}_2^- \cdots \text{CH}_3\text{I}$ TS (${}^2\text{A}'$)					
	Mode	Symmetry	Frequency (cm $^{-1}$)	Intensity (km mol $^{-1}$)	Description
pVTZ	ω_1	a'	79i	2.2149	Intermolecular planar bend
	ω_2	a''	79	0.198	Intermolecular out of plane bend
	ω_3	a''	91	0.0596	CH_3 rotation
	ω_4	a'	103	57.3705	Intermolecular stretch
	ω_5	a'	198	9.8183	O_2 planar rotation
	ω_6	a'	582	4.0795	I–C stretch
	ω_7	a''	883	4.0408	CH_3 twist
	ω_8	a'	892	13.4395	CH_3 asymmetric wag
	ω_9	a'	1196	1146.1072	$\text{O}=\text{O}$ stretch
	ω_{10}	a'	1278	257.3134	CH_3 symmetric wag
	ω_{11}	a'	1482	2.5585	CH_3 scissor
	ω_{12}	a''	1494	2.8832	H– CH_2 scissor
	ω_{13}	a'	3091	41.7876	CH_3 symmetric stretch
	ω_{14}	a''	3204	6.5679	CH_3 asymmetric stretch
	ω_{15}	a'	3206	2.0978	H– CH_2 asymmetric stretch
		zpe	106.3		
pVQZ	Mode	Symmetry	Frequency (cm $^{-1}$)	Intensity (km mol $^{-1}$)	Description
	ω_1	a'	80i	1.8146	Intermolecular planar bend
	ω_2	a''	80	0.1408	Intermolecular out of plane bend
	ω_3	a''	90	0.044	CH_3 rotation
	ω_4	a'	103	58.8702	Intermolecular stretch
	ω_5	a'	203	10.4056	O_2 planar rotation
	ω_6	a'	587	3.8522	I–C stretch
	ω_7	a''	894	4.2479	CH_3 twist
	ω_8	a'	899	13.873	CH_3 asymmetric wag
	ω_9	a'	1168	560.8826	$\text{O}=\text{O}$ stretch
	ω_{10}	a'	1277	94.9987	CH_3 symmetric wag
	ω_{11}	a'	1479	1.4082	CH_3 scissor
	ω_{12}	a''	1490	3.0413	H– CH_2 scissor
	ω_{13}	a'	3094	44.0807	CH_3 symmetric stretch
	ω_{14}	a''	3209	6.3929	CH_3 asymmetric stretch
	ω_{15}	a'	3210	2.1615	H– CH_2 asymmetric stretch
		zpe	106.4		

Table A27: MP2 harmonic frequencies of $\text{O}_2\cdots\text{I}^-\cdots\text{H}_3\text{C}$ ET-TS (4A) complex.

TS3: $\text{O}_2\cdots\text{I}^-\cdots\text{H}_3\text{C}$ ET-TS (4A)					
	Mode	Symmetry	Frequency (cm $^{-1}$)	Intensity (km mol $^{-1}$)	Description
pVTZ	ω_1	<i>a</i>	10 <i>i</i>	0.9588	Intermolecular out of plane bend
	ω_2	<i>a</i>	2	0.9408	Intermolecular planar bend
	ω_3	<i>a</i>	5	0.111	O_2 planar rotation
	ω_4	<i>a</i>	17	0.0762	O_2 out of plane rotation
	ω_5	<i>a</i>	37	1.193	I–O stretch
	ω_6	<i>a</i>	95	2.2614	I–CH ₃ stretch
	ω_7	<i>a</i>	141	0.0401	CH ₃ planar rotation
	ω_8	<i>a</i>	212	6.9294	CH ₃ out of plane rotation
	ω_9	<i>a</i>	570	48.309	CH ₃ symmetric wag
	ω_{10}	<i>a</i>	1429	0.1369	CH ₃ scissor
	ω_{11}	<i>a</i>	1456	0.3409	CH ₃ rock
	ω_{12}	<i>a</i>	1462	2.3232	O=O stretch
	ω_{13}	<i>a</i>	3122	118.8939	CH ₃ symmetric stretch
	ω_{14}	<i>a</i>	3319	11.8686	CH ₃ asymmetric stretch
	ω_{15}	<i>a</i>	3323	37.3095	H–CH ₂ asymmetric stretch
zpe			90.8		
pVQZ	Mode	Symmetry	Frequency (cm $^{-1}$)	Intensity (km mol $^{-1}$)	Description
	ω_1	<i>a</i>	7 <i>i</i>	0.8132	Intermolecular out of plane bend
	ω_2	<i>a</i>	7	0.933	Intermolecular planar bend
	ω_3	<i>a</i>	14	0.3623	O_2 planar rotation
	ω_4	<i>a</i>	42	1.0347	I–O stretch
	ω_5	<i>a</i>	60	0.0705	O_2 out of plane rotation
	ω_6	<i>a</i>	94	2.3659	I–CH ₃ stretch
	ω_7	<i>a</i>	140	0.0381	CH ₃ planar rotation
	ω_8	<i>a</i>	202	5.6544	CH ₃ out of plane rotation
	ω_9	<i>a</i>	573	50.0214	CH ₃ symmetric wag
	ω_{10}	<i>a</i>	1430	0.0892	CH ₃ scissor
	ω_{11}	<i>a</i>	1453	0.2715	CH ₃ rock
	ω_{12}	<i>a</i>	1497	1.8258	O=O stretch
	ω_{13}	<i>a</i>	3124	120.9096	CH ₃ symmetric stretch
	ω_{14}	<i>a</i>	3325	11.0113	CH ₃ asymmetric stretch
	ω_{15}	<i>a</i>	3326	38.4988	H–CH ₂ asymmetric stretch
zpe			91.4		

Table A28: MP2 harmonic frequencies of $\text{I}^- \cdots \text{OOCH}_3$ ($^2\text{A}'$) complex.

vdW4: $\text{I}^- \cdots \text{OOCH}_3$ ($^2\text{A}'$) C–O–I appended					
	Mode	Symmetry	Frequency (cm $^{-1}$)	Intensity (km mol $^{-1}$)	Description
pVTZ	ω_1	a''	288 <i>i</i>	1.1999	Intermolecular out of plane bend
	ω_2	a'	128	11.4625	Intermolecular planar bend
	ω_3	a'	170	37.182	Intermolecular stretch
	ω_4	a''	253	0.0038	CH_3 rotation
	ω_5	a'	445	10.5339	C–O–O bend
	ω_6	a'	865	61.5986	O–O stretch
	ω_7	a'	1088	245.3649	C–O stretch
	ω_8	a''	1146	1.3388	CH_3 twist
	ω_9	a'	1201	16.2358	CH_3 asymmetric wag
	ω_{10}	a'	1425	24.7103	CH_3 symmetric wag
	ω_{11}	a''	1467	1.5675	H– CH_2 scissor
	ω_{12}	a'	1518	7.6715	CH_3 scissor
	ω_{13}	a'	3007	205.9018	CH_3 symmetric stretch
	ω_{14}	a''	3079	77.5282	H– CH_2 asymmetric stretch
	ω_{15}	a'	3121	15.8018	CH_3 asymmetric stretch
zpe			113.1		

Table A29: MP2 harmonic frequencies of $\text{I}^- \cdots \text{OOCH}_3$ ($^2\text{A}'$) complex.

vdW5: $\text{I}^- \cdots \text{OOCH}_3$ ($^2\text{A}'$) O–O–I appended					
	Mode	Symmetry	Frequency (cm $^{-1}$)	Intensity (km mol $^{-1}$)	Description
pVTZ	ω_1	a''	182 <i>i</i>	0.0037	Intermolecular out of plane bend
	ω_2	a'	167	12.5783	Intermolecular planar bend
	ω_3	a''	289	0.596	CH_3 rotation
	ω_4	a'	371	386.6988	Intermolecular stretch
	ω_5	a'	532	920.3592	C–O–O bend
	ω_6	a'	1043	150.1618	C–O stretch
	ω_7	a''	1163	0.8743	CH_3 twist
	ω_8	a'	1214	68.0183	CH_3 asymmetric wag
	ω_9	a'	1445	60.9096	CH_3 symmetric wag
	ω_{10}	a''	1472	4.928	H– CH_2 scissor
	ω_{11}	a'	1520	42.292	CH_3 scissor
	ω_{12}	a'	1996	41911.0927	O–O stretch
	ω_{13}	a'	3011	3111.8001	CH_3 symmetric stretch
	ω_{14}	a''	3052	55.1215	H– CH_2 asymmetric stretch
	ω_{15}	a'	3080	1649.6425	CH_3 asymmetric stretch
zpe			121.8		

Table A30: MP2 harmonic frequencies of O₂ ··· H₃Cl (³A'') complex.

vdW1: O ₂ ··· H ₃ Cl (³ A'')					
	Mode	Symmetry	Frequency (cm ⁻¹)	Intensity (km mol ⁻¹)	Description
pVTZ	ω_1	a'	17	1.5873	Intermolecular bend
	ω_2	a''	18	0.3988	Intermolecular rock
	ω_3	a''	27	1.1159	Intermolecular twist
	ω_4	a'	47	0.0061	C–O=O bend
	ω_5	a'	48	0.0141	C–O=O bend
	ω_6	a'	583	1.946	C–I stretch
	ω_7	a''	909	5.6089	CH ₃ twist
	ω_8	a'	910	6.0021	CH ₃ asymmetric wag
	ω_9	a'	1296	20.8507	CH ₃ symmetric wag
	ω_{10}	a'	1458	0.3429	O=O stretch
	ω_{11}	a'	1487	3.557	CH ₃ scissor
	ω_{12}	a''	1489	3.6588	H–CH ₂ scissor
	ω_{13}	a'	3115	10.7708	CH ₃ symmetric stretch
	ω_{14}	a''	3235	0	H–CH ₂ asymmetric stretch
	ω_{15}	a'	3237	0.0308	CH ₃ asymmetric stretch
zpe			106.9		
	Mode	Symmetry	Frequency (cm ⁻¹)	Intensity (km mol ⁻¹)	Description
pVQZ	ω_1	a'	15	1.6267	Intermolecular bend
	ω_2	a''	26	1.5634	Intermolecular rock
	ω_3	a''	45	0.0393	Intermolecular twist
	ω_4	? a	48	0.0159	C–O=O bend
	ω_5	? a	52	0.0249	C–O=O bend
	ω_6	a'	588	2.0881	C–I stretch
	ω_7	a''	914	5.9759	CH ₃ twist
	ω_8	a'	915	6.2766	CH ₃ asymmetric wag
	ω_9	a'	1299	20.0606	CH ₃ symmetric wag
	ω_{10}	a'	1475	0.1361	O=O stretch
	ω_{11}	a'	1485	3.9105	CH ₃ scissor
	ω_{12}	a''	1486	3.956	H–CH ₂ scissor
	ω_{13}	a'	3118	10.6733	CH ₃ symmetric stretch
	ω_{14}	? a	3239	0.0005	H–CH ₂ asymmetric stretch
	ω_{15}	? a	3240	0.0163	CH ₃ asymmetric stretch
zpe			107.3		

Table A31: MP2 harmonic frequencies of $\text{O}_2 \cdots \text{CH}_3 \cdots \text{I}$ TS (${}^3\text{A}''$) complex.

TS1: $\text{O}_2 \cdots \text{CH}_3 \cdots \text{I}$ TS (${}^3\text{A}''$)					
	Mode	Symmetry	Frequency (cm $^{-1}$)	Intensity (km mol $^{-1}$)	Description
pVTZ	ω_1	a'	1985i	38087.6154	O–C–I asymmetric stretch
	ω_2	a''	96	0.6031	CH_3 rotation
	ω_3	a'	123	4.5078	Intermolecular bend
	ω_4	a''	191	5.3861	Intermolecular rock
	ω_5	a'	199	6.5393	O–C–I bend
	ω_6	a'	459	18.9642	C–O=O bend
	ω_7	a'	1048	1104.3109	CH_3 symmetric wag
	ω_8	a''	1092	0.5112	CH_3 twist
	ω_9	a'	1128	243.0868	CH_3 asymmetric wag
	ω_{10}	a'	1423	26.4314	CH_3 scissor
	ω_{11}	a''	1425	5.045	H–CH $_2$ scissor
	ω_{12}	a'	1462	2447.5993	O=O stretch
	ω_{13}	a'	3156	100.2018	CH_3 symmetric stretch
	ω_{14}	a'	3351	8.7844	CH_3 asymmetric stretch
	ω_{15}	a''	3355	10.8233	H–CH $_2$ asymmetric stretch
zpe			110.7		
pVQZ	Mode	Symmetry	Frequency (cm $^{-1}$)	Intensity (km mol $^{-1}$)	Description
	ω_1	a'	2016i	39976.4697	O–C–I asymmetric stretch
	ω_2	a''	99	0.6014	CH_3 rotation
	ω_3	a'	124	4.6016	Intermolecular bend
	ω_4	a''	191	5.4262	Intermolecular rock
	ω_5	a'	200	7.7534	O–C–I bend
	ω_6	a'	461	20.7826	C–O=O bend
	ω_7	a'	1052	1114.7714	CH_3 symmetric wag
	ω_8	a''	1098	0.5362	CH_3 twist
	ω_9	a'	1133	246.9184	CH_3 asymmetric wag
	ω_{10}	a'	1420	15.4416	CH_3 scissor
	ω_{11}	a''	1424	5.1777	H–CH $_2$ scissor
	ω_{12}	a'	1471	2508.7568	O=O stretch
	ω_{13}	a'	3158	106.6054	CH_3 symmetric stretch
	ω_{14}	a'	3355	9.2295	CH_3 asymmetric stretch
	ω_{15}	a''	3359	11.2888	H–CH $_2$ asymmetric stretch
zpe			110.9		

Table A32: MP2 harmonic frequencies of I \cdots H₃COO ($^3A''$) complex.

vdW2: I \cdots H ₃ COO ($^3A''$)					
	Mode	Symmetry	Frequency (cm $^{-1}$)	Intensity (km mol $^{-1}$)	Description
pVTZ	ω_1	a''	27	5.0482	Intermolecular bend
	ω_2	a''	47	0.7593	Intermolecular stretch
	ω_3	a''	50	4.6452	Intermolecular rock
	ω_4	a''	128	0.0593	CH ₃ rotation
	ω_5	a'	504	8.6369	C–O–O bend
	ω_6	a'	946	24.4795	C–O stretch
	ω_7	a''	1141	0.1321	CH ₃ twist
	ω_8	a'	1197	1.7137	CH ₃ asymmetric wag
	ω_9	a'	1279	96.0478	O=O stretch
	ω_{10}	a'	1454	1.263	CH ₃ symmetric wag
	ω_{11}	a''	1491	5.7748	H–CH ₂ scissor
	ω_{12}	a'	1505	11.6045	CH ₃ scissor
	ω_{13}	a'	3102	27.9656	CH ₃ symmetric stretch
	ω_{14}	a''	3224	2.5565	CH ₃ asymmetric stretch
	ω_{15}	a'	3225	1.0776	H–CH ₂ asymmetric stretch
zpe			115.6		
pVQZ	Mode	Symmetry	Frequency (cm $^{-1}$)	Intensity (km mol $^{-1}$)	Description
	ω_1	a''	38	4.7467	Intermolecular bend
	ω_2	a''	44	1.6296	Intermolecular stretch
	ω_3	a''	50	1.0488	Intermolecular rock
	ω_4	a''	127	3.9427	CH ₃ rotation
	ω_5	a'	508	9.8296	C–O–O bend
	ω_6	a'	950	24.8839	C–O stretch
	ω_7	a''	1119	0.4225	CH ₃ twist
	ω_8	a'	1203	1.1818	CH ₃ asymmetric wag
	ω_9	a'	1295	89.4101	O=O stretch
	ω_{10}	a'	1453	2.0661	CH ₃ symmetric wag
	ω_{11}	a''	1500	7.2532	H–CH ₂ scissor
	ω_{12}	a'	1504	12.1383	CH ₃ scissor
	ω_{13}	a'	3105	24.9057	CH ₃ symmetric stretch
	ω_{14}	a''	3225	2.6661	CH ₃ asymmetric stretch
	ω_{15}	a'	3231	1.7009	H–CH ₂ asymmetric stretch
zpe			115.7		

Table A33: MP2 harmonic frequencies of O₂ ··· ICH₃ (³A'') complex.

vdW3: O ₂ ··· ICH ₃ (³ A'')					
	Mode	Symmetry	Frequency (cm ⁻¹)	Intensity (km mol ⁻¹)	Description
pVTZ	ω_1	a''	3	0.0978	CH ₃ rotation
	ω_2	a'	15	0.5931	Intermolecular planar bend
	ω_3	a'	34	1.0767	Intermolecular stretch
	ω_4	a''	36	1.4675	Intermolecular out of plane bend
	ω_5	a'	69	0.247	I–O stretch
	ω_6	a'	579	0.7569	I–C stretch
	ω_7	a'	908	4.2438	CH ₃ asymmetric wag
	ω_8	a''	909	3.8987	CH ₃ twist
	ω_9	a'	1300	24.3109	CH ₃ symmetric wag
	ω_{10}	a'	1489	4.9377	CH ₃ scissor
	ω_{11}	a''	1489	5.0117	H–CH ₂ scissor
	ω_{12}	a'	1606	18.4305	O=O stretch
	ω_{13}	a'	3116	9.1234	CH ₃ symmetric stretch
	ω_{14}	a'	3235	0.0554	CH ₃ asymmetric stretch
	ω_{15}	a''	3236	0.061	H–CH ₂ asymmetric stretch
		zpe	107.8		
	Mode	Symmetry	Frequency (cm ⁻¹)	Intensity (km mol ⁻¹)	Description
pVQZ	ω_1	?a	16	0.1734	CH ₃ rotation
	ω_2	?a	21	1.4401	Intermolecular planar bend
	ω_3	a'	32	1.5799	Intermolecular stretch
	ω_4	a''	57	0.0673	Intermolecular out of plane bend
	ω_5	a'	68	0.1771	I–O stretch
	ω_6	a'	584	0.8952	I–C stretch
	ω_7	?a	919	4.5595	CH ₃ asymmetric wag
	ω_8	?a	919	4.7422	CH ₃ twist
	ω_9	a'	1302	23.8312	CH ₃ symmetric wag
	ω_{10}	?a	1486	5.2403	CH ₃ scissor
	ω_{11}	?a	1486	5.1744	H–CH ₂ scissor
	ω_{12}	a'	1531	4.4079	O=O stretch
	ω_{13}	a'	3120	8.6669	CH ₃ symmetric stretch
	ω_{14}	?a	3241	0.0391	CH ₃ asymmetric stretch
	ω_{15}	?a	3241	0.0375	H–CH ₂ asymmetric stretch
		zpe	107.8		

Table A34: MP2 harmonic frequencies of I ...OOCH₃ (³A'') complex.

vdW4: I ...OOCH ₃ (³ A'') C–O–I appended					
	Mode	Symmetry	Frequency (cm ⁻¹)	Intensity (km mol ⁻¹)	Description
pVTZ	ω_1	a''	51	0.429	Intermolecular out of plane bend
	ω_2	a'	53	10.7167	Intermolecular planar bend
	ω_3	a'	70	0.1034	Intermolecular stretch
	ω_4	a''	132	0.0983	CH ₃ rotation
	ω_5	a'	500	6.7524	C–O–O bend
	ω_6	a'	942	22.3095	C–O stretch
	ω_7	a''	1149	1.0932	CH ₃ twist
	ω_8	a'	1201	1.2232	CH ₃ asymmetric wag
	ω_9	a'	1268	96.8033	O–O stretch
	ω_{10}	a'	1463	1.3676	CH ₃ symmetric wag
	ω_{11}	a''	1501	7.0148	H–CH ₂ scissor
	ω_{12}	a'	1510	14.128	CH ₃ scissor
	ω_{13}	a'	1510	14.0147	CH ₃ symmetric stretch
	ω_{14}	a''	3220	3.9106	H–CH ₂ asymmetric stretch
	ω_{15}	a'	3224	2.6103	CH ₃ asymmetric stretch
		zpe	106.4		
pVQZ	Mode	Symmetry	Frequency (cm ⁻¹)	Intensity (km mol ⁻¹)	Description
	ω_1	a''	26	0.4052	Intermolecular out of plane bend
	ω_2	a'	55	11.2637	Intermolecular planar bend
	ω_3	a'	73	0.0553	Intermolecular stretch
	ω_4	a''	140	0.0874	CH ₃ rotation
	ω_5	a'	503	7.4128	C–O–O bend
	ω_6	a'	944	23.2352	C–O stretch
	ω_7	a''	1157	0.9849	CH ₃ twist
	ω_8	a'	1205	1.2801	CH ₃ asymmetric wag
	ω_9	a'	1282	88.1858	O–O stretch
	ω_{10}	a'	1461	2.3271	CH ₃ symmetric wag
	ω_{11}	a''	1498	7.1961	H–CH ₂ scissor
	ω_{12}	a'	1507	15.051	CH ₃ scissor
	ω_{13}	a'	3105	11.6767	CH ₃ symmetric stretch
	ω_{14}	a''	3227	3.2978	H–CH ₂ asymmetric stretch
	ω_{15}	a'	3227	2.3329	CH ₃ asymmetric stretch
		zpe	116.1		

Table A35: MP2 harmonic frequencies of I ...OOCH₃ (³A'') complex.

vdW5: I ...OOCH ₃ (³ A'') O–O–I appended					
	Mode	Symmetry	Frequency (cm ⁻¹)	Intensity (km mol ⁻¹)	Description
pVTZ	ω_1	a'	76	1.6515	Intermolecular stretch
	ω_2	a''	108	0.3201	Intermolecular out of plane bend
	ω_3	a'	123	20.3432	Intermolecular planar bend
	ω_4	a''	161	0.1236	CH ₃ rotation
	ω_5	a'	503	5.8105	C–O–O bend
	ω_6	a'	933	15.5692	C–O stretch
	ω_7	a''	1144	0.5285	CH ₃ twist
	ω_8	a'	1199	3.3971	CH ₃ asymmetric wag
	ω_9	a'	1311	112.8478	O–O stretch
	ω_{10}	a'	1467	0.7614	CH ₃ symmetric wag
	ω_{11}	a''	1500	15.8273	H–CH ₂ scissor
	ω_{12}	a'	1504	38.3521	CH ₃ scissor
	ω_{13}	a'	3102	9.5947	CH ₃ symmetric stretch
	ω_{14}	a''	3221	1.884	H–CH ₂ asymmetric stretch
	ω_{15}	a'	3229	3.4785	CH ₃ asymmetric stretch
		zpe	117.1		
pVQZ	Mode	Symmetry	Frequency (cm ⁻¹)	Intensity (km mol ⁻¹)	Description
	ω_1	a'	80	1.3572	Intermolecular stretch
	ω_2	a''	106	0.3498	Intermolecular out of plane bend
	ω_3	a'	133	22.6304	Intermolecular planar bend
	ω_4	a''	176	0.0975	CH ₃ rotation
	ω_5	a'	506	5.8906	C–O–O bend
	ω_6	a'	935	15.8224	C–O stretch
	ω_7	a''	1151	0.4168	CH ₃ twist
	ω_8	a'	1201	3.19	CH ₃ asymmetric wag
	ω_9	a'	1328	107.9148	O–O stretch
	ω_{10}	a'	1467	0.7956	CH ₃ symmetric wag
	ω_{11}	a''	1495	16.8973	H–CH ₂ scissor
	ω_{12}	a'	1500	41.4221	CH ₃ scissor
	ω_{13}	a'	3106	6.9592	CH ₃ symmetric stretch
	ω_{14}	a''	3227	1.4031	H–CH ₂ asymmetric stretch
	ω_{15}	a'	3236	3.5364	CH ₃ asymmetric stretch
		zpe	117.5		

Table A36: MP2 harmonic frequencies of I...OOCH₃ (³A) complex.

vdW6: I...OOCH ₃ (³ A)					
	Mode	Symmetry	Frequency (cm ⁻¹)	Intensity (km mol ⁻¹)	Description
pVTZ	ω_1	<i>a</i>	64	1.397	Intermolecular CO-I stretch
	ω_2	<i>a</i>	71	7.2833	Intermolecular OO-I stretch
	ω_3	<i>a</i>	93	5.6415	Intermolecular rotation
	ω_4	<i>a</i>	139	1.0214	CH ₃ rotation
	ω_5	<i>a</i>	498	7.409	C-O-O bend
	ω_6	<i>a</i>	939	19.1289	C-O stretch
	ω_7	<i>a</i>	1147	0.724	CH ₃ twist
	ω_8	<i>a</i>	1199	1.0552	CH ₃ asymmetric wag
	ω_9	<i>a</i>	1270	78.3434	O=O stretch
	ω_{10}	<i>a</i>	1462	1.1807	CH ₃ symmetric wag
	ω_{11}	<i>a</i>	1500	10.317	H-CH ₂ scissor
	ω_{12}	<i>a</i>	1508	14.7053	CH ₃ scissor
	ω_{13}	<i>a</i>	3102	14.236	CH ₃ symmetric stretch
	ω_{14}	<i>a</i>	3220	4.2497	H-CH ₂ asymmetric stretch
	ω_{15}	<i>a</i>	3226	1.8349	CH ₃ asymmetric stretch
		zpe	116.3		
pVQZ	Mode	Symmetry	Frequency (cm ⁻¹)	Intensity (km mol ⁻¹)	Description
	ω_1	<i>a</i>	60	4.0844	Intermolecular CO-I stretch
	ω_2	<i>a</i>	68	0.9354	Intermolecular OO-I stretch
	ω_3	<i>a</i>	76	10.0452	Intermolecular rotation
	ω_4	<i>a</i>	148	0.5601	CH ₃ rotation
	ω_5	<i>a</i>	501	8.0319	C-O-O bend
	ω_6	<i>a</i>	942	19.5943	C-O stretch
	ω_7	<i>a</i>	1155	0.5975	CH ₃ twist
	ω_8	<i>a</i>	1203	1.0497	CH ₃ asymmetric wag
	ω_9	<i>a</i>	1284	71.4586	O=O stretch
	ω_{10}	<i>a</i>	1461	1.7245	CH ₃ symmetric wag
	ω_{11}	<i>a</i>	1497	10.9544	H-CH ₂ scissor
	ω_{12}	<i>a</i>	1506	14.867	CH ₃ scissor
	ω_{13}	<i>a</i>	3105	11.4425	CH ₃ symmetric stretch
	ω_{14}	<i>a</i>	3226	3.5552	H-CH ₂ asymmetric stretch
	ω_{15}	<i>a</i>	3233	1.8161	CH ₃ asymmetric stretch
		zpe	116.4		

Table A37: MP2 harmonic frequencies of O–O···H₃Cl (³A) complex.

vdW7: O–O···H ₃ Cl (³ A)					
	Mode	Symmetry	Frequency (cm ⁻¹)	Intensity (km mol ⁻¹)	Description
pVTZ	ω_1	<i>a</i>	11	0.0402	Intermolecular O ₂ rotation
	ω_2	<i>a</i>	11	0.041	Intermolecular O ₂ rotation
	ω_3	<i>a</i>	21	1.5476	Intermolecular bend
	ω_4	<i>a</i>	21	1.5484	Intermolecular bend
	ω_5	<i>a</i>	44	0.0199	Intermolecular stretch
	ω_6	<i>a</i>	582	2.0107	C–I stretch
	ω_7	<i>a</i>	908	5.4646	CH ₃ twist
	ω_8	<i>a</i>	908	5.4651	CH ₃ twist
	ω_9	<i>a</i>	1296	20.2401	CH ₃ symmetric wag
	ω_{10}	<i>a</i>	1451	1.0495	O=O stretch
	ω_{11}	<i>a</i>	1488	4.037	H–CH ₂ scissor
	ω_{12}	<i>a</i>	1488	4.0363	H–CH ₂ scissor
	ω_{13}	<i>a</i>	3116	11.2973	CH ₃ symmetric stretch
	ω_{14}	<i>a</i>	3237	0.0004	H–CH ₂ asymmetric stretch
	ω_{15}	<i>a</i>	3237	0.0004	CH ₃ asymmetric stretch
		zpe	106.6		
pVQZ	Mode	Symmetry	Frequency (cm ⁻¹)	Intensity (km mol ⁻¹)	Description
	ω_1	<i>a</i>	19	0.5394	Intermolecular O ₂ rotation
	ω_2	<i>a</i>	20	0.2983	Intermolecular O ₂ rotation
	ω_3	<i>a</i>	23	1.0476	Intermolecular bend
	ω_4	<i>a</i>	24	1.334	Intermolecular bend
	ω_5	<i>a</i>	44	0.0198	Intermolecular stretch
	ω_6	<i>a</i>	587	2.2618	C–I stretch
	ω_7	<i>a</i>	913	5.8194	CH ₃ twist
	ω_8	<i>a</i>	913	5.7629	CH ₃ twist
	ω_9	<i>a</i>	1297	19.5695	CH ₃ symmetric wag
	ω_{10}	<i>a</i>	1476	0.8816	O=O stretch
	ω_{11}	<i>a</i>	1485	4.2875	H–CH ₂ scissor
	ω_{12}	<i>a</i>	1485	4.2857	H–CH ₂ scissor
	ω_{13}	<i>a</i>	3120	10.4634	CH ₃ symmetric stretch
	ω_{14}	<i>a</i>	3241	0.0001	H–CH ₂ asymmetric stretch
	ω_{15}	<i>a</i>	3241	0.0003	CH ₃ asymmetric stretch
		zpe	107		

Table A38: Energies of the conformers of CH_3OOI^- complexes from optimised MP2/aug-cc-pvQZ geometries in E_h .

	vdW1: $\text{O}_2^- \cdots \text{H}_3\text{Cl}$ (${}^2\text{A}''$)					
	E_{SCF}	E_{CCSD}	E_{corr}	$E_{CCSD(T)}$	$E_{(T)}$	E_{W1w}
pVDZ	-483.9028681	-484.6220592	-0.7191911	-484.6478286	-0.0257694	
pVTZ	-483.9562134	-484.8741153	-0.9179019	-484.9143903	-0.0402750	
pVQZ	-483.9685331	-484.9951322	-1.0265991			
CBS	-483.9723663		-1.0978647		-0.0456676	-485.1158986
	TS1: $[\text{O}_2 \cdots \text{CH}_3 \cdots \text{I}]^-$ (${}^2\text{A}'$)					
pVDZ	-483.8992668	-484.6052882	-0.7060214	-484.6320611	-0.0267729	
pVTZ	-483.9506906	-484.8548372	-0.9041466	-484.8960536	-0.0412164	
pVQZ	-483.9628236	-484.9761656	-1.0133420			
CBS	-483.9665986		-1.0849343		-0.0465860	-485.0981189
	vdW2: $\text{I}^- \cdots \text{H}_3\text{COO}$ (${}^2\text{A}'$)					
pVDZ	-483.9840131	-484.6741477	-0.6901346	-484.6960336	-0.0218859	
pVTZ	-484.0362717	-484.9239217	-0.8876501	-484.9598295	-0.0359078	
pVQZ	-484.0488236	-485.0466225	-0.9977989			
CBS	-484.0527290		-1.0700163		-0.0411206	-485.1638659

Table A39: Energies of the conformers of CH_3OOI^- complexes from optimised MP2/aug-cc-pvQZ geometries in E_h .

	vdW1: $\text{O}_2^- \cdots \text{H}_3\text{Cl}$ (${}^2\text{A}''$)					
	E_{SCF}	E_{CCSD}	E_{corr}	$E_{CCSD(T)}$	$E_{(T)}$	E_{W1w}
	vdW3: $\text{O}_2^- \cdots \text{ICH}_3$ (${}^2\text{A}''$)					
pVDZ	-483.8963704	-484.6184462	-0.7220758	-484.6448346	-0.0263883	
pVTZ	-483.9501145	-484.8715430	-0.9214286	-484.9126845	-0.0411415	
pVQZ	-483.9629512	-484.9929251	-1.0299739			
CBS	-483.9669452		-1.1011400		-0.0466261	-485.1147113
	TS2: $\text{O}_2^- \cdots \text{CH}_3\text{I}$ TS (${}^2\text{A}'$)					
pVDZ	-483.8782035	-484.6005340	-0.7223305	-484.6262749	-0.0257409	
pVTZ	-483.9334624	-484.8550392	-0.9215768	-484.8955729	-0.0405337	
pVQZ	-483.9459568	-484.9761206	-1.0301638			
CBS	-483.9498443		-1.1013572		-0.0460331	-485.0972345
	TS3: $\text{O}_2 \cdots \text{I}^- \cdots \text{H}_3\text{C}$ ET-TS (${}^4\text{A}$)					
pVDZ	-483.9482867	-484.6157913	-0.6675047	-484.6357432	-0.0199519	
pVTZ	-484.0006161	-484.8606367	-0.8600205	-484.8944814	-0.0338447	
pVQZ	-484.0135757	-484.9818548	-0.9682790			
CBS	-484.0176079		-1.0392570		-0.0390095	-485.0958745

Table A40: Energies of the conformers of CH_3OOI^- complexes from optimised MP2/aug-cc-pvQZ geometries in E_h .

	vdW1: $\text{O}_2^- \cdots \text{H}_3\text{Cl}$ ($^3A''$) VDE					
	E_{SCF}	E_{CCSD}	E_{corr}	$E_{CCSD(T)}$	$E_{(T)}$	E_{W1w}
pVDZ	-483.8555891	-484.5657333	-0.7101442	-484.5931008	-0.0273675	
pVTZ	-483.9212823	-484.8165034	-0.8952211	-484.8575035	-0.0410000	
pVQZ	-483.9234229	-484.9426069	-1.0191841			
CBS	-483.9240889		-1.1004585		-0.0460681	-485.0706155
	vdW1: $\text{O}_2^- \cdots \text{H}_3\text{Cl}$ ($^1A'$) VDE					
pVDZ	-483.7654828	-484.5119201	-0.7464373	-484.5451665	-0.0332464	
pVTZ	-483.8264675	-484.7705915	-0.9441240	-484.8183380	-0.0477464	
pVQZ	-483.8388056	-484.8967627	-1.0579571			
CBS	-483.8426445		-1.1325900		-0.0531370	-485.0283714
	vdW2: $\text{I}^- \cdots \text{H}_3\text{COO}$ ($^3A'$) VDE					
pVDZ	-483.8825706	-484.5456269	-0.6630563	-484.5658769	-0.0202500	
pVTZ	-483.9382247	-484.7938406	-0.8556160	-484.8268770	-0.0330364	
pVQZ	-483.9509012	-484.9123707	-0.9614695			
CBS	-483.9548454		-1.0308707		-0.0377899	-485.0235060
	vdW3: $\text{O}_2^- \cdots \text{ICH}_3$ ($^3A''$) VDE					
pVDZ	-483.8593439	-484.5653669	-0.7060231	-484.5919793	-0.0266124	
pVTZ	-483.9149738	-484.8183312	-0.9033574	-484.8595367	-0.0412055	
pVQZ	-483.9278490	-484.9451285	-1.0172795			
CBS	-483.9318550		-1.0919707		-0.0466307	-485.0704565
	vdW3: $\text{O}_2^- \cdots \text{ICH}_3$ ($^1A'$) VDE					
pVDZ	-483.7726267	-484.5121989	-0.7395722	-484.5443025	-0.0321036	
pVTZ	-483.8283352	-484.7688963	-0.9405611	-484.8160754	-0.0471791	
pVQZ	-483.8427069	-484.8978656	-1.0551587			
CBS	-483.8471786		-1.1302927		-0.0527836	-485.0302549

Table A41: Energies of the conformers of CH_3OOI complexes from optimised MP2/aug-cc-pvQZ geometries in E_h .

	vdW1: $\text{O}_2\cdots\text{H}_3\text{Cl}$ (${}^3A''$)					
	E_{SCF}	E_{CCSD}	E_{corr}	$E_{CCSD(T)}$	$E_{(T)}$	E_{W1w}
pVDZ	-483.9093055	-484.5908815	-0.6815759	-484.6133436	-0.0224622	
pVTZ	-483.9661346	-484.8408301	-0.8746955	-484.8769942	-0.0361641	
pVQZ	-483.9795019	-484.9608965	-0.9813947			
CBS	-483.9836609		-1.0513503		-0.0412579	-485.0762692
	TS1: $[\text{O}_2\cdots\text{CH}_3\cdots\text{I}]$ (${}^3A''$)					
pVDZ	-483.8254716	-484.5107749	-0.6853032	-484.5370801	-0.0263052	
pVTZ	-483.8799766	-484.7577084	-0.8777319	-484.7978193	-0.0401108	
pVQZ	-483.8929236	-484.8769360	-0.9840124			
CBS	-483.8969519		-1.0536936		-0.0452432	-484.9958887
	vdW2: $\text{I}\cdots\text{H}_3\text{COO}$ (${}^3A''$)					
pVDZ	-483.8858525	-484.5473762	-0.6615237	-484.5674474	-0.0200712	
pVTZ	-483.9416236	-484.7954429	-0.8538193	-484.8282281	-0.0327852	
pVQZ	-483.9544115	-484.9140313	-0.9596198			
CBS	-483.9583904		-1.0289863		-0.0375118	-485.0248884
	vdW3: $\text{O}_2\cdots\text{ICH}_3$ (${}^3A''$) in CFOUR					
pVDZ	-483.8639607	-484.5633596	-0.6993989	-484.5891459	-0.0257863	
pVTZ	-483.9149738	-484.8116587	-0.8966849	-484.8526484	-0.0409897	
pVQZ	-483.9278490	-484.9307747	-1.0029257			
CBS	-483.9318550		-1.0725808		-0.0466418	-485.0510776
	vdW3: $\text{O}_2\cdots\text{ICH}_3$ (${}^3A''$) in G09					
pVDZ	-483.9091474	-484.5906641	-0.6815167	-484.6130872	-0.0224231	
pVTZ	-483.9659440	-484.8408741	-0.8749301	-484.8770593	-0.0361852	
pVQZ	-483.9793683	-484.9612321	-0.9818638			
CBS	-483.9835451		-1.0519732		-0.0413014	-485.0768198

Table A42: Energies of the conformers of CH_3OOI complexes from optimised MP2/aug-cc-pvQZ geometries in E_h .

	vdW4: I...OOCH ₃ (³ A'')					
	E_{SCF}	E_{CCSD}	E_{corr}	$E_{CCSD(T)}$	$E_{(T)}$	E_{W1w}
pVDZ	-483.8857725	-484.5490113	-0.6632388	-484.5694759	-0.0204646	
pVTZ	-483.9412312	-484.7973972	-0.8561660	-484.8307216	-0.0333244	
pVQZ	-483.9539925	-484.9161530	-0.9621605			
CBS	-483.9579631		-1.0316541		-0.0381052	-485.0277224
	vdW5: I...OOCH ₃ (³ A'')					
pVDZ	-483.8822141	-484.5510460	-0.6688319	-484.5724839	-0.0214379	
pVTZ	-483.9372319	-484.7990966	-0.8618648	-484.8335558	-0.0344592	
pVQZ	-483.9499874	-484.9181264	-0.9681391			
CBS	-483.9539561		-1.0378162		-0.0393001	-485.0310723
	vdW6: I...OOCH ₃ (³ A)					
pVDZ	-483.8844700	-484.5486926	-0.6642226	-484.5693004	-0.0206078	
pVTZ	-483.9397588	-484.7971191	-0.8573603	-484.8306058	-0.0334867	
pVQZ	-483.9524431	-484.9157145	-0.9632715			
CBS	-483.9563896		-1.0327105		-0.0382745	-485.0273747
	vdW7: O—O...ICH ₃ (³ A)					
pVDZ	-483.9096281	-484.5908542	-0.6812261	-484.6132494	-0.0223952	
pVTZ	-483.9664942	-484.8407249	-0.8742307	-484.8768105	-0.0360856	
pVQZ	-483.9799209	-484.9608909	-0.9809700			
CBS	-483.9840984		-1.0509519		-0.0411751	-485.0762255

Table A43: Cartesian coordinates of the conformers of CH_3OOI^- complexes optimised at MP2/aug-cc-pvnZ ($n = T, Q$) in Å.

	vdW1: $\text{O}_2^- \cdots \text{H}_3\text{Cl}$ ($^2A''$)			TS1: $[\text{O}_2 \cdots \text{CH}_3 \cdots \text{I}]^- \text{ TS}$ ($^2A'$)			vdW2: $\text{I}^- \cdots \text{H}_3\text{COO}$ ($^2A''$)			
	x	y	z	x	y	z	x	y	z	
pVTZ	C	0.000000	1.034364	0.000000	0.207533	-1.309031	0.000000	-0.103825	-2.029252	0.000000
	I	0.656964	-1.021794	0.000000	0.000000	1.276487	0.000000	0.000000	1.482073	0.000000
	H	-1.089559	1.056301	0.000000	1.274918	-1.209106	0.000000	-1.032669	-1.472572	0.000000
	H	0.412813	1.478760	0.895037	-0.328043	-1.355590	0.926975	0.471397	-1.819951	0.894014
	H	0.412813	1.478760	-0.895037	-0.328043	-1.355590	-0.926975	0.471397	-1.819951	-0.894014
	O	-2.658428	2.289555	0.000000	0.483725	-3.224017	0.000000	-0.475381	-3.446223	0.000000
	O	-1.660969	3.202330	0.000000	-0.716729	-3.760900	0.000000	0.564484	-4.211513	0.000000
	x	y	z	x	y	z	x	y	z	
pVQZ	C	0.000000	1.022591	0.000000	0.206639	-1.303773	0.000000	-0.120681	-2.011299	0.000000
	I	0.662504	-1.011274	0.000000	0.000000	1.273518	0.000000	0.000000	1.471662	0.000000
	H	-1.089277	1.048410	0.000000	1.272627	-1.202767	0.000000	-1.057422	-1.470896	0.000000
	H	0.407557	1.474737	0.892207	-0.328540	-1.349302	0.925820	0.450357	-1.792407	0.892610
	H	0.407557	1.474737	-0.892207	-0.328540	-1.349302	-0.925820	0.450357	-1.792407	-0.892610
	O	-2.663297	2.251316	0.000000	0.480439	-3.215349	0.000000	-0.468286	-3.430928	0.000000
	O	-1.691522	3.181692	0.000000	-0.712362	-3.756205	0.000000	0.578385	-4.178393	0.000000

Table A44: Cartesian coordinates of the conformers of CH_3OOI^- complexes optimised at MP2/aug-cc-pvnZ ($n = T, Q$) in Å.

	vdW3: $\text{O}_2^- \cdots \text{H}_3\text{Cl}$ ($^2A''$)			TS2: $\text{O}_2^- \cdots \text{CH}_3\text{I}$ TS ($^2A''$)			TS3: $\text{O}_2^- \cdots \text{I}^- \cdots \text{H}_3\text{C}$ (4A)			
	x	y	z	x	y	z	x	y	z	
pVTZ	C	-0.840343	2.335481	0.000000	-2.089336	0.255873	0.000000	-4.465902	0.003598	0.000173
	I	0.000000	0.324955	0.000000	0.000000	0.623759	0.000000	-0.437090	0.000352	0.000017
	H	-1.925020	2.261960	0.000000	-2.188244	-0.825092	0.000000	-3.387431	0.002729	0.000131
	H	-0.504186	2.861241	0.890130	-2.529618	0.688819	0.892189	-5.014443	0.932147	-0.000360
	H	-0.504186	2.861241	-0.890130	-2.529618	0.688819	-0.892189	-5.015922	-0.924076	0.000748
	O	0.985485	-2.010252	0.000000	1.851704	-1.920711	0.000000	3.349060	-0.039458	-0.001901
	O	0.011446	-2.892241	0.000000	0.621232	-2.472666	0.000000	4.573310	0.033075	0.001595
	x	y	z	x	y	z	x	y	z	
pVQZ	C	-0.835384	2.319296	0.000000	-2.076598	0.268885	0.000000	4.443120	0.004387	-0.012942
	I	0.000000	0.325472	0.000000	0.000000	0.615067	0.000000	0.430612	0.000425	-0.001254
	H	-1.918885	2.248801	0.000000	-2.189532	-0.809463	0.000000	3.366027	0.003324	-0.009805
	H	-0.501992	2.847697	0.887907	-2.516344	0.703438	0.890006	4.990992	0.930315	0.038380
	H	-0.501992	2.847697	-0.887907	-2.516344	0.703438	-0.890006	4.992520	-0.920452	-0.067460
	O	0.982760	-2.005832	0.000000	1.841780	-1.899005	0.000000	-3.333111	-0.049065	0.145171
	O	0.009136	-2.882915	0.000000	0.618446	-2.452154	0.000000	-4.520729	0.041310	-0.122294

Table A45: Cartesian coordinates of the conformers of CH_3OOI^- complexes optimised at MP2/aug-cc-pvTZ in Å.

		vdW4: $\text{I}^- \cdots \text{H}_3\text{COO}$ ($^2\text{A}''$)			vdW5: $\text{I}^- \cdots \text{H}_3\text{COO}$ ($^2\text{A}''$)		
		C–O–I appended			O–O–I appended		
		x	y	z	x	y	z
pVTZ	C	1.081230	-2.232710	0.000000	1.058531	-2.240860	0.000000
	I	0.000000	0.984533	0.000000	0.000000	0.928870	0.000000
	H	1.895937	-1.505000	0.000000	1.542548	-3.224226	0.000000
	H	1.131016	-2.866868	0.890659	1.377960	-1.679918	0.886556
	H	1.131016	-2.866868	-0.890659	1.377960	-1.679918	-0.886556
	O	-0.117756	-1.504408	0.000000	-1.016676	-1.166369	0.000000
	O	-1.212912	-2.438751	0.000000	-0.314530	-2.483744	0.000000

Table A46: Cartesian coordinates of the conformers of CH₃OOI complexes optimised at MP2/aug-cc-pvnZ ($n = T, Q$) in Å.

	vdW1: O ₂ …H ₃ Cl (³ A'')			TS1: O ₂ …CH ₃ …I TS (³ A'')			vdW2: I…H ₃ COO (³ A'')			
	x	y	z	x	y	z	x	y	z	
pVTZ	C	0.000000	0.768778	0.000000	0.249138	-1.346885	0.000000	-0.358212	-2.226484	0.000000
	I	0.204209	-1.343896	0.000000	0.000000	1.245691	0.000000	0.000000	1.542105	0.000000
	H	-1.058632	0.998172	0.000000	1.308715	-1.154145	0.000000	-1.395626	-1.907209	0.000000
	H	0.481786	1.147250	0.893363	-0.291733	-1.290087	0.928789	0.155188	-1.890585	0.895198
	H	0.481786	1.147250	-0.893363	-0.291733	-1.290087	-0.928789	0.155188	-1.890585	-0.895198
	O	-1.276805	3.870715	0.000000	0.392023	-3.089564	0.000000	-0.398476	-3.674375	0.000000
	O	-0.064197	4.044430	0.000000	-0.669532	-3.686188	0.000000	0.802791	-4.161161	0.000000
	x	y	z	x	y	z	x	y	z	
pVQZ	C	0.000000	0.749101	0.000000	0.248824	-1.339945	0.000000	0.312754	-2.191577	0.000000
	I	-0.087815	-1.354310	0.000000	0.000000	1.240013	0.000000	0.000000	1.531320	0.000000
	H	1.041870	1.040840	0.000000	1.306965	-1.146751	0.000000	1.334030	-1.828614	0.000000
	H	-0.500253	1.105271	-0.890796	-0.291495	-1.281383	0.927575	-0.213831	-1.878105	-0.893963
	H	-0.500253	1.105271	0.890796	-0.291495	-1.281383	-0.927575	-0.213831	-1.878105	0.893963
	O	0.897248	3.969894	0.000000	0.390361	-3.075118	0.000000	0.413012	-3.633148	0.000000
	O	-0.320644	4.034162	0.000000	-0.667476	-3.671319	0.000000	-0.760874	-4.170058	0.000000

Table A47: Cartesian coordinates of the conformers of CH₃OOI complexes optimised at MP2/aug-cc-pvnZ ($n = T, Q$) in Å.

	vdW3: O ₂ ···ICH ₃ (³ A'')			vdW4: I···OOCH ₃ (³ A'')			vdW5: I···OOCH ₃ (³ A'')			
	C–O–I appended			O–O–I appended			x	y	z	
	x	y	z	x	y	z	x	y	z	
pVTZ	C	-0.543096	2.566541	0.000000	1.102684	-2.531380	0.000000	1.099095	-2.408382	0.000000
	I	0.000000	0.514175	0.000000	0.000000	1.141514	0.000000	0.000000	1.058519	0.000000
	H	-1.624829	2.621726	0.000000	1.817477	-1.714479	0.000000	1.584612	-3.378548	0.000000
	H	-0.128897	3.017612	0.893402	1.189821	-3.136577	-0.896507	1.333221	-1.841445	0.895289
	H	-0.128897	3.017612	-0.893402	1.189821	-3.136577	0.896507	1.333221	-1.841445	-0.895289
	O	0.707519	-2.732103	0.000000	-0.199693	-1.892601	0.000000	-0.324560	-2.701480	0.000000
	O	-0.064869	-3.681330	0.000000	-1.151960	-2.772943	0.000000	-1.031143	-1.622242	0.000000
	x	y	z	x	y	z	x	y	z	
pVQZ	C	0.489466	2.567781	0.000000	-1.099123	2.502664	0.000000	-1.095457	-2.387952	0.000000
	I	0.000000	0.518669	0.000000	0.000000	-1.120844	0.000000	0.000000	1.042719	0.000000
	H	1.567854	2.653345	0.000000	-1.824110	1.696881	0.000000	-1.566834	-3.363281	0.000000
	H	0.066582	3.011934	-0.891144	-1.177052	3.108364	-0.895173	-1.336370	-1.824302	-0.893868
	H	0.066582	3.011934	0.891144	-1.177052	3.108364	0.895173	-1.336370	-1.824302	0.893868
	O	-0.661567	-2.740307	0.000000	0.192412	1.848785	0.000000	0.329222	-2.660940	0.000000
	O	0.081840	-3.706361	0.000000	1.154206	2.710610	0.000000	1.022317	-1.579627	0.000000

Table A48: Cartesian coordinates of the conformers of CH₃OOI complexes optimised at MP2/aug-cc-pvnZ ($n = T, Q$) in Å.

		vdW6: I···OOC ₃ (³ A)			vdW7: O–O···H ₃ Cl (³ A)		
		x	y	z	x	y	z
pVTZ	C	2.583853	-0.957036	-0.177791	0.658755	-0.000023	0.000450
	I	-1.051863	-0.035097	-0.004740	-1.464227	0.000031	-0.000433
	H	2.578444	-1.769672	0.541321	0.989136	0.038343	-1.030343
	H	3.591651	-0.718055	-0.501881	0.988500	0.873594	0.549287
	H	1.934235	-1.169917	-1.020681	0.988482	-0.912032	0.482820
	O	2.049301	0.187703	0.536630	3.805411	-0.000081	0.001138
	O	1.968364	1.219797	-0.249230	5.030265	-0.000095	0.001176
		x	y	z	x	y	z
pVQZ	C	2.570782	-0.949200	-0.176586	0.108150	-0.231565	-0.595022
	I	-1.041334	-0.036228	-0.004864	-0.243774	0.521391	1.339696
	H	2.575702	-1.759474	0.542823	1.173345	-0.384156	-0.706175
	H	3.574043	-0.697626	-0.500185	-0.427531	-1.166299	-0.692979
	H	1.925305	-1.171339	-1.018511	-0.253537	0.496693	-1.308535
	O	2.022947	0.187782	0.533342	0.634122	-1.356400	-3.485242
	O	1.938421	1.217685	-0.246692	0.838236	-1.792422	-4.605516

Table A49: Energies, Intensities and Franck-Condon factors calculated from ezSpectrum 3.0 for the vdW2 $^3A'' \leftarrow ^2A''$ transition. Notation for the transition, 2_0^1 indicates the transition in ω_2 from $v'' = 0$ to $v' = 1$ with modes numbered according to Table A32. The band origin is the ADE from Table A21.

E eV	Intensity	FCF	Assignment
3.4590	3.3902E-01	5.8226E-01	ADE
3.4638	4.1590E-02	-2.0394E-01	1_0^1
3.4652	2.6112E-01	5.1100E-01	2_0^1
3.4698	4.3894E-02	-2.0951E-01	3_0^2
3.4699	1.8697E-02	-1.3674E-01	$1_0^1 2_0^1$
3.4714	4.0084E-02	2.0021E-01	2_0^2
3.4746	5.3849E-03	7.3382E-02	$1_0^1 3_0^2$
3.4760	3.3808E-02	-1.8387E-01	$2_0^1 3_0^2$
3.4904	1.5246E-02	1.2347E-01	4_0^2
3.4966	1.1743E-02	1.0836E-01	$2_0^1 4_0^2$
3.5815	8.7680E-03	9.3638E-02	$1_0^1 6_0^1$
3.5877	8.6101E-03	9.2791E-02	$1_0^1 2_0^1 6_0^1$
3.6243	1.3174E-02	1.1478E-01	$1_0^1 9_0^1$
3.6305	1.0896E-02	1.0438E-01	$1_0^1 2_0^1 9_0^1$

Table A50: Parameters of the three Gaussians fitted to experimental spectra. These include for the iodide calibration spectrum as well as two features within the O_2MeI^- spectrum.

	A (a.u.)	dA	E_{BE} eV	dE_{BE}	ω	$d\omega$	R^2
Iodide Spectrum							
1	3.26E-16	2.94E-18	3.029	5.80E-04			
2	2.53E-16	3.80E-18	3.126	1.23E-03	3.22E-01	2.93E-04	0.99127
3	2.09E-16	3.61E-18	3.215	9.19E-04			
O_2MeI^- : vdW2 Complex Peak							
1	2.51E-16	1.01E-17	3.060	1.59E-03			
2	2.74E-16	9.14E-18	3.124	1.87E-03	2.65E-02	4.97E-04	0.98448
3	2.53E-16	4.04E-18	3.211	9.41E-04			
O_2MeI^- : “Bare” Iodide							
1	7.12E-15	7.49E-17	3.457	4.34E-04			
2	7.30E-15	8.10E-17	3.522	5.76E-04	2.36E-02	1.53E-04	0.99744
3	6.16E-15	5.32E-17	3.591	3.52E-04			

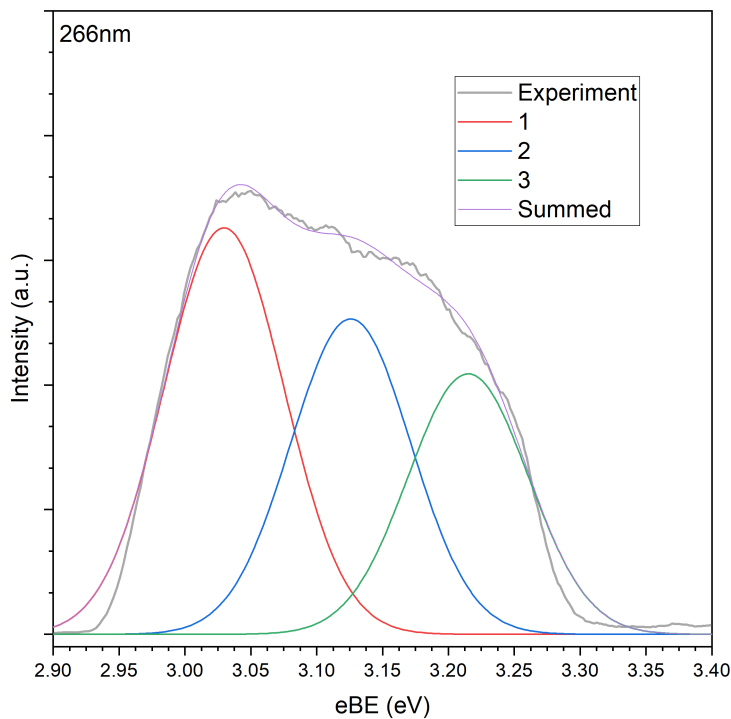


Figure A.1: Representative photoelectron spectrum of bare I^- centred on the $^2P_{3/2} \leftarrow ^1S$ transition. The spectrum is deconvoluted into 3 contributing gaussians representing photoelectrons ejected towards (red), perpendicularly to (blue), and away from (green) the detector.

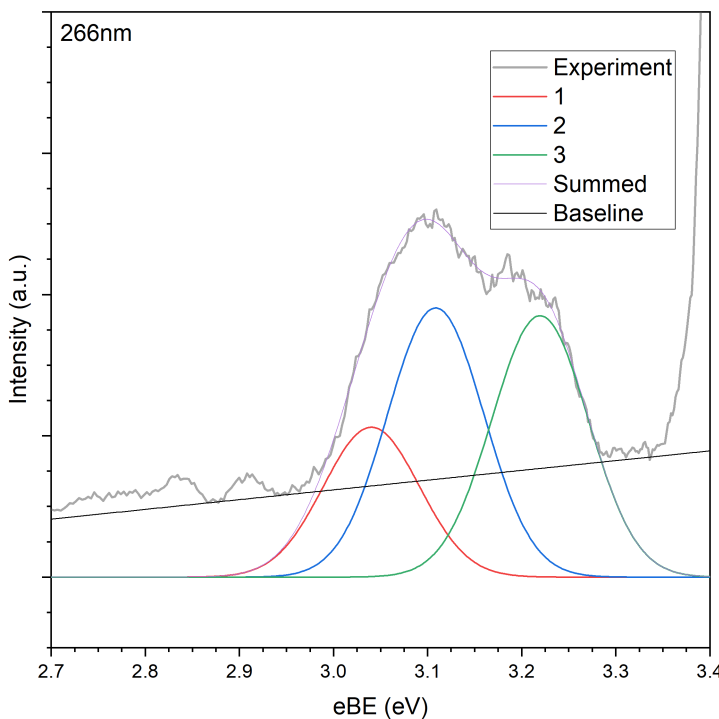


Figure A.2: Representative $173.9\text{ }m/z$ photoelectron spectrum of the assigned I^- $^2P_{3/2} \leftarrow ^1S$ transition. The spectrum is deconvoluted into 3 contributing gaussians representing photoelectrons ejected towards (red), perpendicularly to (blue), and away from (green) the detector. The difference in relative intensities of these peaks lead to the subtraction of a baseline (black) prior to refitting the peaks presented in text.

Appendix B

Tables and Data: Double-Hybrid Benchmarking

Table B1: Gaussian format of the d-aug-cc-pV(T+d)Z basis set for chlorine. Generated using the Basis Set Exchange Python API module.^{237,367}

Cl	0	<i>Continued</i>	P	9	<i>Continued</i>
S	15	1	S	15	1
	4.561000D+05	4.929700D-05		4.561000D+05	4.185460D-06
	6.833000D+04	3.830290D-04		6.833000D+04	3.243950D-05
	1.555000D+04	2.008540D-03		1.555000D+04	1.711050D-04
	4.405000D+03	8.385580D-03		4.405000D+03	7.141760D-04
	1.439000D+03	2.947030D-02		1.439000D+03	2.567050D-03
	5.204000D+02	8.783250D-02		5.204000D+02	7.885520D-03
	2.031000D+02	2.114730D-01		2.031000D+02	2.108670D-02
	8.396000D+01	3.653640D-01		8.396000D+01	4.422640D-02
	3.620000D+01	3.408840D-01		3.620000D+01	6.516700D-02
	1.583000D+01	1.021330D-01		1.583000D+01	6.030120D-03
	6.334000D+00	3.116750D-03		6.334000D+00	-2.064950D-01
	2.694000D+00	1.057510D-03		2.694000D+00	-4.058710D-01
	9.768000D-01	-3.780000D-04		9.768000D-01	7.595580D-02
	4.313000D-01	1.561360D-04		4.313000D-01	7.256610D-01
	1.625000D-01	-5.141260D-05		1.625000D-01	3.944230D-01
S	15	1	S	1	1
	4.561000D+05	-1.383040D-05		1.625000D-01	1.000000D+00
	6.833000D+04	-1.072790D-04	S	1	1
	1.555000D+04	-5.650830D-04		0.0591	1
	4.405000D+03	-2.361350D-03	S	1	1
	1.439000D+03	-8.458860D-03		2.149422D-02	1
	5.204000D+02	-2.596380D-02	P	9	1
	2.031000D+02	-6.863620D-02		6.633000D+02	2.404480D-03
	8.396000D+01	-1.418740D-01		1.568000D+02	1.921480D-02
	3.620000D+01	-1.993190D-01		4.998000D+01	8.850970D-02
	1.583000D+01	-1.956620D-02		1.842000D+01	2.560200D-01
	6.334000D+00	4.997410D-01		7.240000D+00	4.369270D-01
	2.694000D+00	5.637360D-01		2.922000D+00	3.503340D-01
	9.768000D-01	7.903250D-02		1.022000D+00	5.854950D-02
	4.313000D-01	-8.350910D-03		3.818000D-01	-4.584230D-03
	1.625000D-01	2.324560D-03	P	1	1
S	1	1		1.301000D-01	2.269700D-03
	9.768000D-01	1.000000D+00	P	1	1
				1.022000D+00	1.000000D+00

Table B2: X⁻ VDE values from DSD-PBEP86-D3BJ calculations.

	E_{DFT}	VDE	$VDE_{2P_{3/2}}$	$VDE_{2P_{1/2}}$	VDE_{exp}	Shift
Cl^-	def2QZVP	-459.9780761	3.498	3.462	3.571	0.151
	AVTZ	-459.9695313	3.566	3.530	3.639	0.083
	AVQZ	-459.9821509	3.609	3.573	3.682	0.040
Cl	def2QZVP	-459.8495275				
	AVTZ	-459.8384744				
	AVQZ	-459.8495294				
Br^-	def2QZVP	-2573.4537545	3.384	3.232	3.689	0.132
	AVTZ	-416.3037678	3.396	3.244	3.701	3.364
	AVQZ	-416.3403815	3.443	3.291	3.748	0.073
Br	def2QZVP	-2573.3294072				
	AVTZ	-416.1789782				
	AVQZ	-416.2138432				
I^-	def2TZVPD	-297.4673082	3.222	2.908	3.850	0.151
	def2QZVP	-297.5439463	3.232	2.918	3.860	0.141
	AVTZ	-295.3511569	3.235	2.921	3.863	3.059
I	AVQZ	-295.3884861	3.290	2.976	3.918	0.138
	def2TZVPD	-297.3488981				
	def2QZVP	-297.4251586				
I	AVTZ	-295.2322600				
	AVQZ	-295.2675757				

Table B3: DSD-PBEP86-D3BJ calculated energies for N₂, O₂, HCCH, C₂H₄, HCOOH, C₃H₆, C₄H₆ and C₈H₁₂.

		E_{DFT}
N ₂	def2QZVP	-109.4134226
	AVTZ	-109.3966059
	AVQZ	-109.4146999
O ₂	def2QZVP	-150.1826986
	AVTZ	-150.1591013
	AVQZ	-150.1841387
HCCH	def2QZVP	-77.2198341
	AVTZ	-77.2071669
	AVQZ	-77.2204955
C ₂ H ₄	def2QZVP	-78.4700163
	AVTZ	-78.4564437
	AVQZ	-78.4707010
<i>syn</i> -HCOOH	def2QZVP	-189.5772139
	AVTZ	-189.5455173
	AVQZ	-189.5789606
<i>anti</i> -HCOOH	def2QZVP	-189.5704712
	AVTZ	-189.5388110
	AVQZ	-189.5722829
C ₃ H ₆	def2QZVP	-117.7315112
	AVTZ	-117.7113490
<i>cis</i> -C ₄ H ₆	def2QZVP	-155.7567405
	AVTZ	-155.7308206
<i>trans</i> -C ₄ H ₆	def2TZVPD	-155.7263809
	def2QZVP	-155.7627866
	AVTZ	-155.7368643
C ₈ H ₁₂	def2TZVPD	-311.5222167

Table B4: Cartesian coordinates of the geometries of N₂, O₂, HCCH and C₂H₄ optimised with the DSD-PBEP86-D3BJ functional, in Å.

		N ₂			
		x	y	z	
def2QZVP	N	0.000000	0.000000	0.549874	
	N	0.000000	0.000000	-0.549874	
	AVTZ	0.000000	0.000000	0.551020	
		0.000000	0.000000	-0.551020	
	AVQZ	0.000000	0.000000	0.549977	
		0.000000	0.000000	-0.549977	
		O ₂			
		x	y	z	
def2QZVP	O	0.000000	0.000000	0.602257	
	O	0.000000	0.000000	-0.602257	
	AVTZ	0.000000	0.000000	0.551020	
		0.000000	0.000000	-0.551020	
	AVQZ	0.000000	0.000000	0.549977	
		0.000000	0.000000	-0.549977	
		HCCH			
		x	y	z	
def2QZVP	H	0.000000	0.000000	1.664640	
	C	0.000000	0.000000	0.601800	
	C	0.000000	0.000000	-0.601800	
	H	0.000000	0.000000	-1.664640	
	H	0.000000	0.000000	1.6666097	
	AVTZ	C	0.000000	0.000000	
		C	0.000000	0.602865	
	AVQZ	H	0.000000	0.000000	
		H	0.000000	-0.602865	
	AVQZ	H	0.000000	0.000000	
		H	0.000000	-1.6666097	
		H	0.000000	0.000000	
		C	0.000000	1.664982	
		C	0.000000	0.601954	
		C	0.000000	-0.601954	
		H	0.000000	-1.664982	
		C ₂ H ₄			
		x	y	z	
def2QZVP	C	0.000000	0.000000	0.664363	
	C	0.000000	0.000000	-0.664363	
	AVTZ	H	0.000000	0.922830	
		H	0.000000	-0.922830	
	AVQZ	H	0.000000	0.922830	
		H	0.000000	-1.229687	
	AVQZ	H	0.000000	-0.922830	
		C	0.000000	-1.229687	
		C	0.000000	0.665374	
		C	0.000000	0.000000	
		H	0.000000	-0.665374	
		H	0.000000	0.923801	
	AVTZ	H	0.000000	1.231011	
		H	0.000000	-0.923801	
	AVQZ	H	0.000000	0.923801	
		H	0.000000	-1.231011	
	AVQZ	H	0.000000	-0.923801	
		C	0.000000	0.664527	
		C	0.000000	0.000000	
		H	0.000000	-0.664527	
		H	0.000000	0.923119	
		H	0.000000	1.229862	

Table B5: Cartesian coordinates of the geometries of HCOOH optimised with the DSD-PBEP86-D3BJ functional, in Å.

		<i>syn</i> -HCOOH		
		x	y	z
def2QZVP	C	0.000000	0.420861	0.000000
	O	-1.029128	-0.439674	0.000000
	H	-0.652638	-1.330813	0.000000
	O	1.157655	0.109274	0.000000
	H	-0.375575	1.448852	0.000000
	C	0.000000	0.421667	0.000000
AVTZ	O	-1.031572	-0.439849	0.000000
	H	-0.653735	-1.332777	0.000000
	O	1.160220	0.108900	0.000000
	H	-0.375451	1.450370	0.000000
	C	0.000000	0.421103	0.000000
	O	-1.029438	-0.439440	0.000000
AVQZ	H	-0.653250	-1.331125	0.000000
	O	1.157942	0.108805	0.000000
	H	-0.374783	1.449590	0.000000
		<i>anti</i> -HCOOH		
		x	y	z
def2QZVP	C	0.000000	0.384423	0.000000
	O	-0.895847	-0.623262	0.000000
	H	-1.786619	-0.259457	0.000000
	O	1.176923	0.194405	0.000000
	H	-0.461992	1.383774	0.000000
	C	0.000000	0.385682	0.000000
AVTZ	O	-0.897988	-0.623662	0.000000
	H	-1.790361	-0.257933	0.000000
	O	1.179387	0.193382	0.000000
	H	-0.460834	1.386081	0.000000
	C	0.000000	0.384982	0.000000
	O	-0.896086	-0.623021	0.000000
AVQZ	H	-1.787680	-0.260102	0.000000
	O	1.177187	0.193691	0.000000
	H	-0.461123	1.384852	0.000000

Table B6: Cartesian coordinates of the geometries of C₃H₆ and *cis*-C₄H₆ optimised with the DSD-PBEP86-D3BJ functional, in Å.

		C ₃ H ₆		
		x	y	z
def2QZVP	H	0.000000	1.553187	0.000000
	C	0.081182	0.470159	0.000000
	C	1.291857	-0.081703	0.000000
	H	2.188451	0.523436	0.000000
	H	1.418361	-1.158049	0.000000
	C	-1.202680	-0.296420	0.000000
	H	-1.019482	-1.370853	0.000000
	H	-1.804758	-0.049943	-0.877274
	H	-1.804758	-0.049943	0.877274
	H	1.551265	0.098326	0.000000
AVTZ	C	0.474521	-0.051169	0.000000
	C	0.000000	-1.296202	0.000000
	H	0.661801	-2.153115	0.000000
	H	-1.067163	-1.490843	0.000000
	C	-0.372063	1.183073	0.000000
	H	-1.433972	0.932017	0.000000
	H	-0.163322	1.799712	-0.878462
	H	-0.163322	1.799712	0.878462
	<i>cis</i> -C ₄ H ₆			
		x	y	z
def2QZVP	C	0.000000	1.527516	0.506118
	C	0.000000	0.734436	-0.568462
	H	0.000000	2.605404	0.413170
	H	0.000000	1.120990	1.508723
	H	0.000000	1.200589	-1.547822
	C	0.000000	-0.734436	-0.568462
	H	0.000000	-1.200589	-1.547822
	C	0.000000	-1.527516	0.506118
	H	0.000000	-2.605404	0.413170
	H	0.000000	-1.120990	1.508723
AVTZ	C	1.337097	0.899849	0.000000
	C	0.000000	0.929308	0.000000
	H	1.922908	1.810640	0.000000
	H	1.882227	-0.035857	0.000000
	H	-0.489969	1.898061	0.000000
	C	-0.899650	-0.232974	0.000000
	H	-1.960297	-0.001511	0.000000
	C	-0.535902	-1.519983	0.000000
	H	-1.270734	-2.315429	0.000000
	H	0.506591	-1.813103	0.000000

Table B7: Cartesian coordinates of the geometries of *trans*-C₄H₆ and C₈H₁₂ optimised with the DSD-PBEP86-D3BJ functional, in Å.

		<i>trans</i> -C ₄ H ₆		
		x	y	z
def2TZVPD	C	1.112847	1.470773	0.000000
	C	-0.000021	0.727654	0.000000
	H	2.096516	1.013249	0.000000
	H	1.067226	2.554678	0.000000
	H	-0.972773	1.215892	0.000000
	C	0.000000	-0.727622	0.000000
	H	0.972754	-1.215858	0.000000
	C	-1.112833	-1.470795	0.000000
	H	-1.067160	-2.554698	0.000000
	H	-2.096524	-1.013319	0.000000
def2QZVP	C	-1.111673	1.469159	0.000000
	C	0.000000	0.727047	0.000000
	H	-2.092729	1.012140	0.000000
	H	-1.065796	2.550469	0.000000
	H	0.970426	1.214153	0.000000
	C	0.000000	-0.727047	0.000000
	H	-0.970426	-1.214153	0.000000
	C	1.111673	-1.469159	0.000000
	H	1.065796	-2.550469	0.000000
	H	2.092729	-1.012140	0.000000
AVTZ	C	1.337097	0.899849	0.000000
	C	0.000000	0.929308	0.000000
	H	1.922908	1.810640	0.000000
	H	1.882227	-0.035857	0.000000
	H	-0.489969	1.898061	0.000000
	C	-0.899650	-0.232974	0.000000
	H	-1.960297	-0.001511	0.000000
	C	-0.535902	-1.519983	0.000000
	H	-1.270734	-2.315429	0.000000
	H	0.506591	-1.813103	0.000000
		C ₈ H ₁₂		
		x	y	z
def2TZVPD	C	-1.610322	1.238566	-0.036604
	C	-2.268346	0.091183	-0.219765
	H	-2.155668	2.178275	-0.082910
	H	-3.338385	0.115996	-0.412120
	C	-1.601718	-1.254571	-0.174156
	H	-1.539663	-1.665011	-1.191697
	H	-2.224998	-1.956121	0.392283
	C	-0.206632	-1.175494	0.441320
	H	-0.292134	-1.033955	1.527037
	H	0.337147	-2.111820	0.280355
	C	0.583734	-0.000431	-0.144740
	H	0.595382	-0.107397	-1.238601
	C	-0.128266	1.313084	0.201705
	C	1.996300	0.011757	0.348649
	H	0.065387	1.567534	1.254331
	H	0.304277	2.130804	-0.386186
	C	3.078296	-0.061062	-0.426041
	H	2.120048	0.087415	1.429964
	H	4.078968	-0.048162	-0.008182
	H	2.991368	-0.135754	-1.506487

Table B8: Calculated harmonic frequencies and mode assignments for the N₂ and O₂. All frequencies and intensities are in cm⁻¹ and km mol⁻¹ and zero-point energies are in kJ mol⁻¹.

		N ₂		O ₂				
	Mode	Symmetry	Frequency (cm ⁻¹)	Intensity (km mol ⁻¹)	Mode	Symmetry	Frequency (cm ⁻¹)	Intensity (km mol ⁻¹)
def2QZVP	ω_1	σ_g	2329	0	ω_1	σ_g	1590	0
		zpe	13.9			zpe	9.5	
AVTZ	ω_1	σ_g	2319	0	ω_1	σ_g	1573	0
		zpe	13.9			zpe	9.4	
AVQZ	ω_1	σ_g	2327	0	ω_1	σ_g	1591	0
		zpe	13.9			zpe	9.5	

Table B9: Calculated harmonic frequencies and mode assignments for the HCCH. All frequencies and intensities are in cm⁻¹ and km mol⁻¹ and zero-point energies are in kJ mol⁻¹.

HCCH				
	Mode	Symmetry	Frequency (cm ⁻¹)	Intensity (km mol ⁻¹)
def2QZVP	ω_1	π_g	637	0
	ω_2	π_g	637	0
	ω_3	π_u	762	96.1584
	ω_4	π_u	762	96.1584
	ω_5	σ_g	2018	0
	ω_6	σ_u	3430	89.6562
	ω_7	σ_g	3521	0
		zpe	70.4	
AVTZ	ω_1	π_g	637	0
	ω_2	π_g	637	0
	ω_3	π_u	760	94.2912
	ω_4	π_u	760	94.2912
	ω_5	σ_g	2017	0
	ω_6	σ_u	3427	89.3858
	ω_7	σ_g	3519	0
		zpe	70.3	
AVQZ	ω_1	π_g	631	0
	ω_2	π_g	631	0
	ω_3	π_u	764	95.0086
	ω_4	π_u	764	95.0086
	ω_5	σ_g	2014	0
	ω_6	σ_u	3421	90.0289
	ω_7	σ_g	3524	0
		zpe	70.3	

Table B10: Calculated harmonic frequencies and mode assignments for the C₂H₄. All frequencies and intensities are in cm⁻¹ and km mol⁻¹ and zero-point energies are in kJ mol⁻¹.

C ₂ H ₄				
	Mode	Symmetry	Frequency (cm ⁻¹)	Intensity (km mol ⁻¹)
def2QZVP	ω_1	b_{2u}	847	0.0559
	ω_2	b_{2g}	987	0
	ω_3	b_{3u}	991	96.7265
	ω_4	a_u	1077	0
	ω_5	b_{3g}	1259	0
	ω_6	a_g	1383	0
	ω_7	b_{1u}	1490	9.2607
	ω_8	a_g	1682	0
	ω_9	b_{1u}	3134	14.3934
	ω_{10}	a_g	3148	0
	ω_{11}	b_{3g}	3211	0
	ω_{12}	b_{2u}	3238	18.2044
		zpe	134.3	
AVTZ	ω_1	b_{2u}	845	0.0112
	ω_2	b_{2g}	982	0
	ω_3	b_{3u}	990	95.605
	ω_4	a_u	1066	0
	ω_5	b_{3g}	1256	0
	ω_6	a_g	1381	0
	ω_7	b_{1u}	1488	9.121
	ω_8	a_g	1679	0
	ω_9	b_{1u}	3130	14.3582
	ω_{10}	a_g	3146	0
	ω_{11}	b_{3g}	3206	0
	ω_{12}	b_{2u}	3234	18.087
		zpe	134.0	
AVQZ	ω_1	b_{2u}	847	0.0147
	ω_2	b_{2g}	989	0
	ω_3	b_{3u}	992	95.0699
	ω_4	a_u	1076	0
	ω_5	b_{3g}	1259	0
	ω_6	a_g	1382	0
	ω_7	b_{1u}	1490	9.236
	ω_8	a_g	1681	0
	ω_9	b_{1u}	3132	14.3126
	ω_{10}	a_g	3146	0
	ω_{11}	b_{3g}	3208	0
	ω_{12}	b_{2u}	3236	17.7833
		zpe	134.2	

Table B11: Calculated harmonic frequencies and mode assignments for the *syn*-HCOOH. All frequencies and intensities are in cm^{-1} and km mol^{-1} and zero-point energies are in kJ mol^{-1} .

<i>syn</i> -HCOOH				
	Mode	Symmetry	Frequency (cm^{-1})	Intensity (km mol^{-1})
def2QZVP	ω_1	a'	631	42.8576
	ω_2	a''	680	139.6173
	ω_3	a''	1064	2.2978
	ω_4	a'	1131	258.6051
	ω_5	a'	1311	10.7484
	ω_6	a'	1414	2.1165
	ω_7	a'	1801	349.9734
	ω_8	a'	3074	38.6537
	ω_9	a'	3752	67.9389
	zpe		88.9	
AVTZ	ω_1	a'	628	41.8438
	ω_2	a''	678	135.9755
	ω_3	a''	1061	2.5649
	ω_4	a'	1129	259.2305
	ω_5	a'	1308	10.1887
	ω_6	a'	1410	2.1837
	ω_7	a'	1793	353.6612
	ω_8	a'	3073	36.5412
	ω_9	a'	3733	67.0135
	zpe		88.6	
AVQZ	ω_1	a'	632	42.7646
	ω_2	a''	679	136.403
	ω_3	a''	1062	2.6452
	ω_4	a'	1138	260.9
	ω_5	a'	1312	13.475
	ω_6	a'	1412	2.1979
	ω_7	a'	1810	352.4324
	ω_8	a'	3097	36.1147
	ω_9	a'	3761	71.7799
	zpe		89.1	

Table B12: Calculated harmonic frequencies and mode assignments for the *anti*-HCOOH. All frequencies and intensities are in cm^{-1} and km mol^{-1} and zero-point energies are in kJ mol^{-1} .

<i>anti</i> -HCOOH				
	Mode	Symmetry	Frequency (cm^{-1})	Intensity (km mol^{-1})
def2QZVP	ω_1	a''	531	84.8941
	ω_2	a'	663	9.9889
	ω_3	a''	1044	0.0004
	ω_4	a'	1117	53.8717
	ω_5	a'	1281	309.5716
	ω_6	a'	1428	0.2462
	ω_7	a'	1845	286.9204
	ω_8	a'	2986	72.9278
	ω_9	a'	3819	66.3408
	zpe		88.0	
AVTZ	ω_1	a''	531	82.4527
	ω_2	a'	658	9.841
	ω_3	a''	1040	0.0276
	ω_4	a'	1114	55.7165
	ω_5	a'	1278	307.9854
	ω_6	a'	1422	0.3037
	ω_7	a'	1836	289.8965
	ω_8	a'	2986	68.5814
	ω_9	a'	3799	64.7155
	zpe		87.7	
AVQZ	ω_1	a''	532	83.8795
	ω_2	a'	663	10.0384
	ω_3	a''	1041	0.0379
	ω_4	a'	1122	51.3566
	ω_5	a'	1287	315.6214
	ω_6	a'	1424	0.2124
	ω_7	a'	1852	291.3314
	ω_8	a'	3011	67.0324
	ω_9	a'	3828	71.5515
	zpe		88.3	

Table B13: Calculated harmonic frequencies and mode assignments for the C₃H₆. All frequencies and intensities are in cm⁻¹ and km mol⁻¹ and zero-point energies are in kJ mol⁻¹.

C ₃ H ₆				
	Mode	Symmetry	Frequency (cm ⁻¹)	Intensity (km mol ⁻¹)
def2QZVP	ω_1	a''	240	0.4944
	ω_2	a'	436	0.989
	ω_3	a''	608	12.1755
	ω_4	a'	936	3.1317
	ω_5	a''	956	45.1356
	ω_6	a'	962	2.8641
	ω_7	a''	1040	11.6772
	ω_8	a''	1085	3.188
	ω_9	a'	1203	0.2129
	ω_{10}	a'	1336	0.0264
	ω_{11}	a'	1422	1.6779
	ω_{12}	a'	1464	1.0468
	ω_{13}	a''	1495	6.4543
	ω_{14}	a'	1509	14.6895
	ω_{15}	a'	1702	13.9876
	ω_{16}	a'	3024	22.8269
	ω_{17}	a''	3077	16.5321
	ω_{18}	a'	3105	9.8699
	ω_{19}	a'	3131	18.4572
	ω_{20}	a'	3139	10.5356
	ω_{21}	a'	3222	14.9995
		zpe	209.9	
AVTZ	ω_1	a''	243	0.5103
	ω_2	a'	435	0.9905
	ω_3	a''	608	12.0366
	ω_4	a'	934	2.9633
	ω_5	a''	955	44.3972
	ω_6	a'	961	2.9805
	ω_7	a''	1038	12.3244
	ω_8	a''	1085	3.2642
	ω_9	a'	1202	0.1988
	ω_{10}	a'	1334	0.0231
	ω_{11}	a'	1421	1.5594
	ω_{12}	a'	1463	1.1066
	ω_{13}	a''	1496	6.4428
	ω_{14}	a'	1510	14.5494
	ω_{15}	a'	1698	14.3762
	ω_{16}	a'	3021	23.1078
	ω_{17}	a''	3073	16.3951
	ω_{18}	a'	3100	10.0625
	ω_{19}	a'	3127	19.4893
	ω_{20}	a'	3136	9.2531
	ω_{21}	a'	3217	15.2241
		zpe	209.7	

Table B14: Calculated harmonic frequencies and mode assignments for the *cis*-C₄H₆. All frequencies and intensities are in cm⁻¹ and km mol⁻¹ and zero-point energies are in kJ mol⁻¹.

<i>cis</i> -C ₄ H ₆				
	Mode	Symmetry	Frequency (cm ⁻¹)	Intensity (km mol ⁻¹)
def2QZVP	ω_1	a_2	172 <i>i</i>	0
	ω_2	a_1	303	0.0443
	ω_3	b_1	523	19.7765
	ω_4	b_2	562	5.2527
	ω_5	a_2	747	0
	ω_6	a_1	888	0.0252
	ω_7	a_2	934	0
	ω_8	b_1	946	74.8041
	ω_9	a_2	1029	0
	ω_{10}	b_1	1039	31.4164
	ω_{11}	a_1	1064	0.2554
	ω_{12}	b_2	1115	7.365
	ω_{13}	b_2	1321	0.2312
	ω_{14}	a_1	1362	0.187
	ω_{15}	b_2	1445	3.9251
	ω_{16}	a_1	1476	11.8902
	ω_{17}	a_1	1678	2.2656
	ω_{18}	b_2	1698	2.695
	ω_{19}	b_2	3161	1.4643
	ω_{20}	a_1	3166	16.4279
	ω_{21}	b_2	3169	10.1754
	ω_{22}	a_1	3184	8.8174
	ω_{23}	b_2	3253	9.7057
	ω_{24}	a_1	3256	7.6674
		zpe	223.2	
AVTZ	ω_1	a''	182 <i>i</i>	0
	ω_2	a'	301	0.0522
	ω_3	a''	522	19.9613
	ω_4	a'	559	5.4694
	ω_5	a''	726	0
	ω_6	a'	886	0.02
	ω_7	a''	927	0.0001
	ω_8	a''	943	72.4491
	ω_9	a''	995	0
	ω_{10}	a''	1034	33.4351
	ω_{11}	a'	1061	0.2892
	ω_{12}	a'	1111	6.997
	ω_{13}	a'	1318	0.2237
	ω_{14}	a'	1360	0.1742
	ω_{15}	a'	1443	3.7391
	ω_{16}	a'	1475	11.7106
	ω_{17}	a'	1676	2.137
	ω_{18}	a'	1694	3.1515
	ω_{19}	a'	3156	2.1048
	ω_{20}	a'	3162	17.312
	ω_{21}	a'	3165	9.5019
	ω_{22}	a'	3180	8.1474
	ω_{23}	a'	3248	10.1274
	ω_{24}	a'	3252	7.9556
		zpe	222.5	

Table B15: Calculated harmonic frequencies and mode assignments for the *trans*-C₄H₆. All frequencies and intensities are in cm⁻¹ and km mol⁻¹ and zero-point energies are in kJ mol⁻¹.

<i>trans</i> -C ₄ H ₆				
	Mode	Symmetry	Frequency (cm ⁻¹)	Intensity (km mol ⁻¹)
def2TZVPD	ω_1	a''	168	0.7023
	ω_2	a'	294	2.5783
	ω_3	a'	515	0
	ω_4	a''	541	11.693
	ω_5	a''	780	0
	ω_6	a'	906	0
	ω_7	a''	937	0.0002
	ω_8	a''	937	80.9002
	ω_9	a''	1000	0
	ω_{10}	a'	1002	1.561
	ω_{11}	a''	1057	35.2513
	ω_{12}	a'	1235	0
	ω_{13}	a'	1317	0
	ω_{14}	a'	1322	2.1406
	ω_{15}	a'	1417	4.0463
	ω_{16}	a'	1479	0
	ω_{17}	a'	1649	18.7352
	ω_{18}	a'	1711	0
	ω_{19}	a'	3149	0
	ω_{20}	a'	3153	13.3662
	ω_{21}	a'	3161	0
	ω_{22}	a'	3165	9.2534
	ω_{23}	a'	3246	0.0003
	ω_{24}	a'	3246	19.0526
		zpe	223.6	
def2QZVP	ω_1	a_u	168	0.6755
	ω_2	b_u	294	2.6303
	ω_3	a_g	516	0
	ω_4	a_u	541	11.6941
	ω_5	b_g	783	0
	ω_6	a_g	907	0
	ω_7	b_g	939	0
	ω_8	a_u	940	82.5885
	ω_9	b_u	1003	1.6333
	ω_{10}	b_g	1003	0
	ω_{11}	a_u	1058	34.0289
	ω_{12}	a_g	1234	0
	ω_{13}	a_g	1317	0
	ω_{14}	b_u	1321	2.1667
	ω_{15}	b_u	1420	4.0515
	ω_{16}	a_g	1483	0
	ω_{17}	b_u	1651	19.4412
	ω_{18}	a_g	1713	0
	ω_{19}	a_g	3156	0
	ω_{20}	b_u	3160	13.5537
	ω_{21}	a_g	3168	0
	ω_{22}	b_u	3172	9.8905
	ω_{23}	a_g	3253	0
	ω_{24}	b_u	3253	19.2025
		zpe	224.0	

Table B16: (*Continued.*) Calculated harmonic frequencies and mode assignments for the *trans*-C₄H₆. All frequencies and intensities are in cm⁻¹ and km mol⁻¹ and zero-point energies are in kJ mol⁻¹.

<i>trans</i> -C ₄ H ₆				
	Mode	Symmetry	Frequency (cm ⁻¹)	Intensity (km mol ⁻¹)
AVTZ	ω_1	a_u	165	0.6743
	ω_2	b_u	292	2.6156
	ω_3	a_g	513	0
	ω_4	a_u	537	11.6759
	ω_5	b_g	776	0
	ω_6	a_g	905	0
	ω_7	b_g	936	0
	ω_8	a_u	938	80.1523
	ω_9	b_g	992	0
	ω_{10}	b_u	999	1.5364
	ω_{11}	a_u	1052	35.6267
	ω_{12}	a_g	1231	0
	ω_{13}	a_g	1315	0
	ω_{14}	b_u	1318	2.133
	ω_{15}	b_u	1418	3.8003
	ω_{16}	a_g	1481	0
	ω_{17}	b_u	1648	19.8993
	ω_{18}	a_g	1710	0
	ω_{19}	a_g	3151	0
	ω_{20}	b_u	3155	14.3151
	ω_{21}	a_g	3164	0
	ω_{22}	b_u	3167	9.2201
	ω_{23}	a_g	3248	0
	ω_{24}	b_u	3248	19.8273
			zpe	223.5

Table B17: Calculated harmonic frequencies and mode assignments for the C₈H₁₂. All frequencies and intensities are in cm⁻¹ and km mol⁻¹ and zero-point energies are in kJ mol⁻¹.

C ₈ H ₁₂								
	Mode	Symmetry	Frequency (cm ⁻¹)	Intensity (km mol ⁻¹)	Mode	Symmetry	Frequency (cm ⁻¹)	Intensity (km mol ⁻¹)
AVTZ	ω_1	<i>a</i>	83	0.0156	ω_{28}	<i>a</i>	1253	0.4874
	ω_2	<i>a</i>	115	0.1053	ω_{29}	<i>a</i>	1285	2.804
	ω_3	<i>a</i>	190	0.2465	ω_{30}	<i>a</i>	1306	0.8284
	ω_4	<i>a</i>	274	0.2116	ω_{31}	<i>a</i>	1324	1.3563
	ω_5	<i>a</i>	324	0.4843	ω_{32}	<i>a</i>	1331	0.6389
	ω_6	<i>a</i>	387	0.3289	ω_{33}	<i>a</i>	1372	2.2343
	ω_7	<i>a</i>	419	0.522	ω_{34}	<i>a</i>	1379	0.6718
	ω_8	<i>a</i>	483	1.3075	ω_{35}	<i>a</i>	1395	0.3428
	ω_9	<i>a</i>	521	0.5156	ω_{36}	<i>a</i>	1425	0.4965
	ω_{10}	<i>a</i>	665	26.7795	ω_{37}	<i>a</i>	1464	2.7285
	ω_{11}	<i>a</i>	685	8.5577	ω_{38}	<i>a</i>	1480	1.4161
	ω_{12}	<i>a</i>	745	8.4698	ω_{39}	<i>a</i>	1486	8.2538
	ω_{13}	<i>a</i>	824	0.7391	ω_{40}	<i>a</i>	1501	3.7785
	ω_{14}	<i>a</i>	890	2.0742	ω_{41}	<i>a</i>	1702	14.2261
	ω_{15}	<i>a</i>	930	6.1337	ω_{42}	<i>a</i>	1715	5.5026
	ω_{16}	<i>a</i>	944	43.4723	ω_{43}	<i>a</i>	3008	14.8613
	ω_{17}	<i>a</i>	950	2.5868	ω_{44}	<i>a</i>	3018	31.6605
	ω_{18}	<i>a</i>	971	0.9113	ω_{45}	<i>a</i>	3020	0.8768
	ω_{19}	<i>a</i>	989	1.728	ω_{46}	<i>a</i>	3031	37.7378
	ω_{20}	<i>a</i>	1001	0.1302	ω_{47}	<i>a</i>	3064	23.097
	ω_{21}	<i>a</i>	1033	15.4859	ω_{48}	<i>a</i>	3066	30.4116
	ω_{22}	<i>a</i>	1068	3.3257	ω_{49}	<i>a</i>	3087	32.0515
	ω_{23}	<i>a</i>	1093	0.0647	ω_{50}	<i>a</i>	3129	17.8128
	ω_{24}	<i>a</i>	1112	0.8274	ω_{51}	<i>a</i>	3148	5.1294
	ω_{25}	<i>a</i>	1163	1.9439	ω_{52}	<i>a</i>	3152	7.0359
	ω_{26}	<i>a</i>	1167	3.4029	ω_{53}	<i>a</i>	3176	37.7654
	ω_{27}	<i>a</i>	1213	0.8008	ω_{54}	<i>a</i>	3237	13.1711
						zpe		471.3

Table B18: $\text{X}^- \cdots \text{N}_2$ complex geometric parameters and D_0 values from DSD-PBEP86-D3BJ optimisations. zpe values are drawn from relevant harmonic frequency calculations.

		$R_{\text{X} \cdots \text{N}}$	$R_{\text{X} \cdots \parallel \parallel}$	$R_{\text{N} \equiv \text{N}}$	$\angle_{\text{X} \cdots \parallel \parallel - \text{N}}$	E_{DFT}	zpe	D_e	D_o
		\AA	\AA	\AA	$^\circ$	E_h	kJ mol^{-1}	kJ mol^{-1}	kJ mol^{-1}
$\text{Cl}^- \cdots \text{N}_2$	$C_{2v} (^1A_1)$	def2QZVP	3.550	3.507	1.100	90.0	-569.3954404	15.0	10.3
		pVTZ	3.562	3.519	1.102	90.0	-569.3697830	15.0	9.6
		pVQZ	3.567	3.524	1.100	90.0	-569.4004761	15.0	9.5
	$C_{2v} (^1A_1)$	def2QZVP	1.784	1.625	1.473	90.0	-569.0662056	11.8	-854.1
		pVTZ	1.789	1.632	1.465	90.0	-569.044673	11.7	-844.0
		pVQZ	1.781	1.625	1.460	90.0	-569.0754805	11.8	-843.8
$\text{Br}^- \cdots \text{N}_2$	$C_{2v} (^1A_1)$	def2QZVP	3.751	3.710	1.100	90.0	-2682.870589	14.9	9.0
		pVTZ	3.755	3.714	1.102	90.0	-525.7036079	14.9	8.5
		pVQZ	3.753	3.712	1.100	90.0	-525.7583353	14.9	8.5
	$C_{2v} (^1A_1)$	def2QZVP	1.928	1.786	1.455	90.0	-2682.542289	11.3	-853.0
		pVTZ	1.934	1.794	1.446	90.0	-525.3807198	11.2	-839.3
		pVQZ	1.926	1.786	1.441	90.0	-525.4359308	11.3	-837.9
$\text{I}^- \cdots \text{N}_2$	$C_{2v} (^1A_1)$	def2QZVP	4.053	4.015	1.100	90.0	-406.9600737	14.9	7.1
		pVTZ	4.041	4.003	1.102	90.0	-404.7504327	14.8	7.0
		pVQZ	4.048	4.010	1.100	90.0	-404.8059345	14.9	7.2
	$C_{2v} (^1A_1)$	def2QZVP	2.065	1.936	1.435	90.0	-406.6462360	11.2	-816.9
		pVTZ	2.087	1.962	1.421	90.0	-404.4398739	11.0	-808.4
		pVQZ	2.075	1.950	1.417	90.0	-404.4962983	11.1	-805.7

Table B19: X···N₂ complex geometric parameters and D_0 values from DSD-PBEP86-D3BJ optimisations. zpe values are drawn from relevant harmonic frequency calculations.

		$R_{X\cdots N}$	$R_{X\cdots }$	$R_{N\equiv N}$	$\angle_{X\cdots - N}$	E_{DFT}	zpe	D_e	D_o	
		Å	Å	Å	°	E_h	kJ mol ⁻¹	kJ mol ⁻¹	kJ mol ⁻¹	
Cl···N ₂	C_{2v} (² A ₁)	def2QZVP	3.452	3.408	1.100	90.0	-569.2636164	14.7	1.7	2.5
		pVTZ	3.440	3.396	1.102	90.0	-569.2358274	14.7	2.0	2.8
		pVQZ	3.438	3.394	1.100	90.0	-569.2649119	14.7	1.8	2.6
	C_∞ (² Σ)	def2QZVP	3.090	3.640	1.100	180.0	-569.2645367	15.5	4.2	5.8
		pVTZ	3.090	3.641	1.102	180.0	-569.2368121	15.6	4.5	6.3
		pVQZ	3.080	3.630	1.100	180.0	-569.2659032	15.6	4.4	6.0
Br···N ₂	C_{2v} (² A ₂)	def2QZVP	1.826	1.710	1.284	90.0	-569.0855604	14.7	-465.7	-465.0
		pVTZ	1.832	1.715	1.286	90.0	-569.0580805	14.6	-464.7	-464.0
		pVQZ	1.826	1.709	1.284	90.0	-569.0878104	14.7	-463.2	-462.4
	C_{2v} (² A ₁)	def2QZVP	3.578	3.536	1.100	90.0	-2682.743574	14.7	2.0	2.7
		pVTZ	3.541	3.498	1.102	90.0	-525.5765349	14.7	2.5	3.3
		pVQZ	3.521	3.477	1.100	90.0	-525.6294864	14.7	2.5	3.2
I···N ₂	C_∞ (² Σ)	def2QZVP	3.213	3.763	1.100	180.0	-2682.744566	15.5	4.6	6.1
		pVTZ	3.178	3.729	1.102	180.0	-525.5776332	15.6	5.4	7.1
		pVQZ	3.163	3.713	1.100	180.0	-525.6306504	15.5	5.5	7.2
	C_{2v} (² A ₂)	def2QZVP	1.972	1.867	1.271	90.0	-2682.566674	14.1	-462.5	-462.3
		pVTZ	1.979	1.874	1.272	90.0	-525.4002369	14.0	-460.4	-460.2
		pVQZ	1.972	1.866	1.271	90.0	-525.4542589	14.1	-457.6	-457.4

Table B20: $X^- \cdots N_2$ complex VDEs from DSD-PBEP86-D3BJ optimisations. zpe values are drawn from relevant harmonic frequency calculations.

			E_{VDE}	$VDE_{2P_{3/2}}$	$VDE_{2P_{1/2}}$	$ADE_{2P_{3/2}}$	$ADE_{2P_{1/2}}$
			E_h	eV	eV	eV	eV
$Cl^- \cdots N_2$	$C_{2v} (^1A_1)$	def2QZVP	-569.2635983	3.692	3.801	3.699	3.808
		pVTZ	-569.2357978	3.681	3.790	3.689	3.798
		pVQZ	-569.2648817	3.683	3.792	3.690	3.799
$Br^- \cdots N_2$	$C_{2v} (^1A_1)$	def2QZVP	-2682.743523	3.428	3.885	3.434	3.891
		pVTZ	-525.5764473	3.418	3.875	3.424	3.881
		pVQZ	-525.6293851	3.419	3.876	3.425	3.882
$I^- \cdots N_2$	$C_{2v} (^1A_1)$	def2QZVP	-406.8393688	3.101	4.043	3.106	4.048
		pVTZ	-404.6297293	3.098	4.040	3.103	4.045
		pVQZ	-404.6831711	3.100	4.042	3.104	4.046

Table B21: Calculated harmonic frequencies and mode assignments for the $\text{Cl}^- \cdots \text{N}_2$ complex. All frequencies and intensities are in cm^{-1} and km mol^{-1} respectively.

$\text{Cl}^- \cdots \text{N}_2$ $C_{2v} (^1A_1)$ vdW Complex					
	Mode	Symmetry	Frequency (cm^{-1})	Intensity (km mol^{-1})	Description
def2QZVP	ω_1	a_1	72	15.0073	Intermolecular stretch
	ω_2	b_2	108	0.0045	Intermolecular bend
	ω_3	a_1	2329	0.9975	N_2 stretch
		zpe	15		
pVTZ	ω_1	a_1	71	14.0865	Intermolecular stretch
	ω_2	b_2	116	0.002	Intermolecular bend
	ω_3	a_1	2319	1.7023	N_2 stretch
		zpe	15		
pVQZ	ω_1	a_1	70	14.0712	Intermolecular stretch
	ω_2	b_2	109	0.0012	Intermolecular bend
	ω_3	a_1	2327	1.6745	N_2 stretch
		zpe	15		
$\text{Cl}^- \cdots \text{N}_2$ $C_{2v} (^1A_1)$ Molecular Anion					
	Mode	Symmetry	Frequency (cm^{-1})	Intensity (km mol^{-1})	Description
def2QZVP	ω_1	a_1	504	1.6905	$\text{Cl}-\text{N}$ symmetric stretch
	ω_2	b_2	559	4.8361	$\text{Cl}-\text{N}$ asymmetric stretch
	ω_3	a_1	907	0.3536	N_2 stretch
		zpe	11.8		
pVTZ	ω_1	a_1	507	0.1693	$\text{Cl}-\text{N}$ symmetric stretch
	ω_2	b_2	553	17.445	$\text{Cl}-\text{N}$ asymmetric stretch
	ω_3	a_1	895	1.2473	N_2 stretch
		zpe	11.7		
pVQZ	ω_1	a_1	511	0.029	$\text{Cl}-\text{N}$ symmetric stretch
	ω_2	b_2	559	22.1362	$\text{Cl}-\text{N}$ asymmetric stretch
	ω_3	a_1	902	0.936	N_2 stretch
		zpe	11.8		

Table B22: Calculated harmonic frequencies and mode assignments for the $\text{Br}^- \cdots \text{N}_2$ complex. All frequencies and intensities are in cm^{-1} and km mol^{-1} respectively.

$\text{Br}^- \cdots \text{N}_2$ $C_{2v} (^1A_1)$ vdW Complex					
	Mode	Symmetry	Frequency (cm^{-1})	Intensity (km mol^{-1})	Description
def2QZVP	ω_1	a_1	57	4.0559	Intermolecular stretch
	ω_2	b_2	109	0.0877	Intermolecular bend
	ω_3	a_1	2329	0.7423	N_2 stretch
		zpe	14.9		
pVTZ	ω_1	a_1	56	3.6149	Intermolecular stretch
	ω_2	b_2	116	0.1073	Intermolecular bend
	ω_3	a_1	2319	1.4442	N_2 stretch
		zpe	14.9		
pVQZ	ω_1	a'	56	3.6124	Intermolecular stretch
	ω_2	a'	109	0.1133	Intermolecular bend
	ω_3	a'	2326	1.4457	N_2 stretch
		zpe	14.9		
$\text{Br}^- \cdots \text{N}_2$ $C_{2v} (^1A_1)$ Molecular Anion					
	Mode	Symmetry	Frequency (cm^{-1})	Intensity (km mol^{-1})	Description
def2QZVP	ω_1	a_1	463	1.0411	Cl–N symmetric stretch
	ω_2	b_2	513	8.9023	Cl–N asymmetric stretch
	ω_3	a_1	910	0.2415	N_2 stretch
		zpe	11.3		
pVTZ	ω_1	a_1	464	3.812	Cl–N symmetric stretch
	ω_2	b_2	509	27.7077	Cl–N asymmetric stretch
	ω_3	a_1	893	2.2495	N_2 stretch
		zpe	11.2		
pVQZ	ω_1	a_1	469	4.589	Cl–N symmetric stretch
	ω_2	b_2	516	38.4954	Cl–N asymmetric stretch
	ω_3	a_1	899	2.1305	N_2 stretch
		zpe	11.3		

Table B23: Calculated harmonic frequencies and mode assignments for the $\text{I}^- \cdots \text{N}_2$ complex. All frequencies and intensities are in cm^{-1} and km mol^{-1} respectively.

$\text{I}^- \cdots \text{N}_2$ $C_{2v} ({}^1A_1)$ vdW Complex					
	Mode	Symmetry	Frequency (cm^{-1})	Intensity (km mol^{-1})	Description
def2QZVP	ω_1	a_1	46	1.6224	Intermolecular stretch
	ω_2	b_2	110	0.1865	Intermolecular bend
	ω_3	a_1	2329	0.5022	N_2 stretch
		zpe	14.9		
pVTZ	ω_1	a_1	46	1.4147	Intermolecular stretch
	ω_2	b_2	117	0.1717	Intermolecular bend
	ω_3	a_1	2319	1.0515	N_2 stretch
		zpe	14.8		
pVQZ	ω_1	a_1	46	1.4231	Intermolecular stretch
	ω_2	b_2	110	0.1744	Intermolecular bend
	ω_3	a_1	2326	1.0342	N_2 stretch
		zpe	14.9		
$\text{I}^- \cdots \text{N}_2$ $C_{2v} ({}^1A_1)$ Molecular Anion					
	Mode	Symmetry	Frequency (cm^{-1})	Intensity (km mol^{-1})	Description
def2QZVP	ω_1	a_1	454	10.9117	Cl–N symmetric stretch
	ω_2	b_2	495	24.3173	Cl–N asymmetric stretch
	ω_3	a_1	916	0.7516	N_2 stretch
		zpe	11.2		
pVTZ	ω_1	a_1	453	17.4854	Cl–N symmetric stretch
	ω_2	b_2	481	48.1854	Cl–N asymmetric stretch
	ω_3	a_1	905	0.4241	N_2 stretch
		zpe	11		
pVQZ	ω_1	a_1	456	18.5728	Cl–N symmetric stretch
	ω_2	b_2	488	65.1373	Cl–N asymmetric stretch
	ω_3	a_1	910	0.3125	N_2 stretch
		zpe	11.1		

Table B24: Calculated harmonic frequencies and mode assignments for the Cl···N₂ complex. All frequencies and intensities are in cm⁻¹ and km mol⁻¹ respectively.

Cl ··· N ₂ <i>C</i> _{2v} (² A ₁) vdW Complex					
	Mode	Symmetry	Frequency (cm ⁻¹)	Intensity (km mol ⁻¹)	Description
def2QZVP	ω_1	<i>a</i> ₁	44	0.0637	Intermolecular stretch
	ω_2	<i>b</i> ₂	85	0.0559	Intermolecular bend
	ω_3	<i>a</i> ₁	2326	0.1393	N ₂ stretch
	zpe		14.7		
pVTZ	ω_1	<i>a</i> ₁	47	0.0655	Intermolecular stretch
	ω_2	<i>b</i> ₂	97	0.0438	Intermolecular bend
	ω_3	<i>a</i> ₁	2316	0.1371	N ₂ stretch
	zpe		14.7		
pVQZ	ω_1	<i>a</i> ₁	46	0.0673	Intermolecular stretch
	ω_2	<i>b</i> ₂	86	0.0462	Intermolecular bend
	ω_3	<i>a</i> ₁	2324	0.1368	N ₂ stretch
	zpe		14.7		
Cl ··· N ₂ <i>C</i> _∞ (² Σ) vdW Complex					
	Mode	Symmetry	Frequency (cm ⁻¹)	Intensity (km mol ⁻¹)	Description
def2QZVP	ω_1	σ	59	0.4721	Intermolecular bend
	ω_2	π	105	0.0115	Degenerate intermolecular bend
	ω_3	π	105	0.0115	Degenerate intermolecular bend
	ω_4	σ	2330	0.2437	N ₂ stretch
	zpe		15.5		
pVTZ	ω_1	σ	59	0.459	Intermolecular bend
	ω_2	π	115	0.012	Degenerate intermolecular bend
	ω_3	π	115	0.012	Degenerate intermolecular bend
	ω_4	σ	2320	0.2338	N ₂ stretch
	zpe		15.6		
pVQZ	ω_1	σ	60	0.4866	Intermolecular bend
	ω_2	π	107	0.0133	Degenerate intermolecular bend
	ω_3	π	107	0.0133	Degenerate intermolecular bend
	ω_4	σ	2328	0.2419	N ₂ stretch
	zpe		15.6		
Cl ··· N ₂ <i>C</i> _{2v} (¹ A ₁) Neutral Molecule					
	Mode	Symmetry	Frequency (cm ⁻¹)	Intensity (km mol ⁻¹)	Description
def2QZVP	ω_1	<i>b</i> ₂	496	0.3686	Cl–N asymmetric stretch
	ω_2	<i>a</i> ₁	577	2.9976	Cl–N symmetric stretch
	ω_3	<i>a</i> ₁	1387	1.541	N ₂ stretch
	zpe		14.7		
pVTZ	ω_1	<i>b</i> ₂	494	0.5564	Cl–N asymmetric stretch
	ω_2	<i>a</i> ₁	575	2.6304	Cl–N symmetric stretch
	ω_3	<i>a</i> ₁	1376	1.7213	N ₂ stretch
	zpe		14.6		
pVQZ	ω_1	<i>b</i> ₂	498	0.6094	Cl–N asymmetric stretch
	ω_2	<i>a</i> ₁	578	2.6496	Cl–N symmetric stretch
	ω_3	<i>a</i> ₁	1384	1.4423	N ₂ stretch
	zpe		14.7		

Table B25: Calculated harmonic frequencies and mode assignments for the Br \cdots N₂ complex. All frequencies and intensities are in cm⁻¹ and km mol⁻¹ respectively.

Br \cdots N ₂ C_{2v} (² A ₁) vdW Complex					
	Mode	Symmetry	Frequency (cm ⁻¹)	Intensity (km mol ⁻¹)	Description
def2QZVP	ω_1	a_1	39	0.0543	Intermolecular stretch
	ω_2	b_2	86	0.0412	Intermolecular bend
	ω_3	a_1	2326	0.1255	N ₂ stretch
	zpe		14.7		
pVTZ	ω_1	a_1	43	0.0628	Intermolecular stretch
	ω_2	b_2	97	0.0208	Intermolecular bend
	ω_3	a_1	2315	0.129	N ₂ stretch
	zpe		14.7		
pVQZ	ω_1	a_1	44	0.0712	Intermolecular stretch
	ω_2	b_2	87	0.0199	Intermolecular bend
	ω_3	a_1	2323	0.1363	N ₂ stretch
	zpe		14.7		
Br \cdots N ₂ C_∞ (² Σ) vdW Complex					
	Mode	Symmetry	Frequency (cm ⁻¹)	Intensity (km mol ⁻¹)	Description
def2QZVP	ω_1	σ	52	0.3871	Intermolecular bend
	ω_2	π	105	0.0148	Degenerate intermolecular bend
	ω_3	π	105	0.0148	Degenerate intermolecular bend
	ω_4	σ	2330	0.208	N ₂ stretch
	zpe		15.5		
pVTZ	ω_1	σ	55	0.4193	Intermolecular bend
	ω_2	π	115	0.02	Degenerate intermolecular bend
	ω_3	π	115	0.02	Degenerate intermolecular bend
	ω_4	σ	2320	0.2146	N ₂ stretch
	zpe		15.6		
pVQZ	ω_1	σ	58	0.449	Intermolecular bend
	ω_2	π	107	0.0219	Degenerate intermolecular bend
	ω_3	π	107	0.0219	Degenerate intermolecular bend
	ω_4	σ	2328	0.2254	N ₂ stretch
	zpe		15.5		
Br \cdots N ₂ C_{2v} (¹ A ₁) Neutral Molecule					
	Mode	Symmetry	Frequency (cm ⁻¹)	Intensity (km mol ⁻¹)	Description
def2QZVP	ω_1	b_2	452	1.1287	Br–N asymmetric stretch
	ω_2	a_1	486	0.0349	Br–N symmetric stretch
	ω_3	a_1	1416	1.1292	N ₂ stretch
	zpe		14.1		
pVTZ	ω_1	b_2	453	1.4864	Br–N asymmetric stretch
	ω_2	a_1	483	0.0058	Br–N symmetric stretch
	ω_3	a_1	1407	1.634	N ₂ stretch
	zpe		14		
pVQZ	ω_1	b_2	459	1.5664	Br–N asymmetric stretch
	ω_2	a_1	487	0.0099	Br–N symmetric stretch
	ω_3	a_1	1413	1.2875	N ₂ stretch
	zpe		14.1		

Table B26: Calculated harmonic frequencies and mode assignments for the I...N₂ complex. All frequencies and intensities are in cm⁻¹ and km mol⁻¹ respectively.

I...N ₂ <i>C</i> _{2v} (² A ₁) vdW Complex					
	Mode	Symmetry	Frequency (cm ⁻¹)	Intensity (km mol ⁻¹)	Description
def2QZVP	ω_1	<i>a</i> ₁	40	0.0592	Intermolecular stretch
	ω_2	<i>b</i> ₂	89	0.0098	Intermolecular bend
	ω_3	<i>a</i> ₁	2326	0.111	N ₂ stretch
	zpe		14.7		
pVTZ	ω_1	<i>a</i> ₁	42	0.0636	Intermolecular stretch
	ω_2	<i>b</i> ₂	99	0.0062	Intermolecular bend
	ω_3	<i>a</i> ₁	2315	0.1028	N ₂ stretch
	zpe		14.7		
pVQZ	ω_1	<i>a</i> ₁	41	0.0621	Intermolecular stretch
	ω_2	<i>b</i> ₂	89	0.0078	Intermolecular bend
	ω_3	<i>a</i> ₁	2323	0.1006	N ₂ stretch
	zpe		14.7		
I...N ₂ <i>C</i> _∞ (² Σ) vdW Complex					
	Mode	Symmetry	Frequency (cm ⁻¹)	Intensity (km mol ⁻¹)	Description
def2QZVP	ω_1	σ	50	0.363	Intermolecular bend
	ω_2	π	104	0.0373	Degenerate intermolecular bend
	ω_3	π	104	0.0373	Degenerate intermolecular bend
	ω_4	σ	2329	0.1224	N ₂ stretch
	zpe		15.5		
pVTZ	ω_1	σ	52	0.3667	Intermolecular bend
	ω_2	π	114	0.0291	Degenerate intermolecular bend
	ω_3	π	114	0.0291	Degenerate intermolecular bend
	ω_4	σ	2320	0.1219	N ₂ stretch
	zpe		15.6		
pVQZ	ω_1	σ	52	0.4089	Intermolecular bend
	ω_2	π	106	0.0329	Degenerate intermolecular bend
	ω_3	π	106	0.0329	Degenerate intermolecular bend
	ω_4	σ	2327	0.1341	N ₂ stretch
	zpe		15.5		
I...N ₂ <i>C</i> _{2v} (¹ A ₁) Neutral Molecule					
	Mode	Symmetry	Frequency (cm ⁻¹)	Intensity (km mol ⁻¹)	Description
def2QZVP	ω_1	<i>b</i> ₂	407	3.6661	I–N asymmetric stretch
	ω_2	<i>a</i> ₁	435	2.3388	I–N symmetric stretch
	ω_3	<i>a</i> ₁	1458	0.0268	N ₂ stretch
	zpe		13.8		
pVTZ	ω_1	<i>b</i> ₂	400	3.7069	I–N asymmetric stretch
	ω_2	<i>a</i> ₁	433	2.7182	I–N symmetric stretch
	ω_3	<i>a</i> ₁	1452	0.0488	N ₂ stretch
	zpe		13.7		
pVQZ	ω_1	<i>b</i> ₂	407	3.8895	I–N asymmetric stretch
	ω_2	<i>a</i> ₁	436	2.5425	I–N symmetric stretch
	ω_3	<i>a</i> ₁	1457	0.0017	N ₂ stretch
	zpe		13.8		

Table B27: Cartesian coordinates of the geometries of halide-nitrogen complexes optimised with the DSD-PBEP86-D3BJ functional, in Å.

		$\text{Cl}^- \cdots \text{N}_2$			$\text{Br}^- \cdots \text{N}_2$			$\text{I}^- \cdots \text{N}_2$			
		x	y	z	x	y	z	x	y	z	
C_{2v} (1A_1)	def2QZVP	X	0.000000	0.000000	-1.583880	0.000000	0.000000	-1.060026	0.000000	0.000000	0.839020
		N	0.000000	-0.549796	1.923282	0.000000	-0.549808	2.650065	0.000000	-0.549838	-3.176289
		N	0.000000	0.549796	1.923282	0.000000	0.549808	2.650065	0.000000	0.549838	-3.176289
	pVTZ	X	0.000000	0.000000	1.589098	0.000000	0.000000	-1.061265	0.000000	0.000000	-0.836491
		N	0.000000	0.550974	-1.929619	0.000000	-0.550989	2.653163	0.000000	-0.551001	3.166717
		N	0.000000	-0.550974	-1.929619	0.000000	0.550989	2.653163	0.000000	0.551001	3.166717
	pVQZ	X	0.000000	0.000000	1.591687	0.000000	0.000000	-1.060653	0.000000	0.000000	0.838004
		N	0.000000	0.549948	-1.932763	0.000000	-0.549963	2.651567	0.000000	-0.549974	-3.172444
		N	0.000000	-0.549948	-1.932763	0.000000	0.549963	2.651697	0.000000	0.549974	-3.172444
		x	y	z	x	y	z	x	y	z	
C_{2v} (1A_1)	def2QZVP	X	0.000000	0.000000	0.733734	0.000000	0.000000	0.510172	0.000000	0.000000	0.404622
		N	0.000000	-0.736692	-0.890963	0.000000	-0.727693	-1.275431	0.000000	-0.717268	-1.531782
		N	0.000000	0.736692	-0.890963	0.000000	0.727693	-1.275431	0.000000	0.717268	-1.531782
	pVTZ	X	0.000000	0.000000	0.737106	0.000000	0.000000	0.512599	0.000000	0.000000	0.410056
		N	0.000000	-0.732619	-0.895058	0.000000	0.722812	-1.281497	0.000000	-0.710523	-1.552356
		N	0.000000	0.732619	-0.895058	0.000000	-0.722812	-1.281497	0.000000	0.710523	-1.552356
	pVQZ	X	0.000000	0.000000	0.733819	0.000000	0.000000	0.510399	0.000000	0.000000	0.407469
		N	0.000000	-0.730168	-0.891066	0.000000	-0.720416	-1.275998	0.000000	-0.708427	-1.542560
		N	0.000000	0.730168	-0.891066	0.000000	0.720416	-1.275998	0.000000	0.708427	-1.542560

Table B28: Cartesian coordinates of the geometries of halogen-nitrogen complexes optimised with the DSD-PBEP86-D3BJ functional, in Å.

		Cl … N ₂			Br … N ₂			I … N ₂				
		x	y	z	x	y	z	x	y	z		
<i>C_{2v}</i> (² A ₁)	def2QZVP	X	0.000000	0.000000	1.539002	0.000000	0.000000	1.010210	0.000000	0.000000	0.781461	
		N	0.000000	0.550032	-1.868788	0.000000	0.550040	-2.525524	0.000000	0.550049	-2.958388	
		N	0.000000	-0.550032	-1.868788	0.000000	-0.550040	-2.525524	0.000000	-0.550049	-2.958388	
	pVTZ	X	0.000000	0.000000	1.533680	0.000000	0.000000	0.999523	0.000000	0.000000	0.775841	
		N	0.000000	0.551182	-1.862326	0.000000	0.551202	-2.498806	0.000000	0.551201	-2.937114	
		N	0.000000	-0.551182	-1.862326	0.000000	-0.551202	-2.498806	0.000000	-0.551201	-2.937114	
	pVQZ	X	0.000000	0.000000	1.532795	0.000000	0.000000	0.993570	0.000000	0.000000	0.777890	
		N	0.000000	0.550149	-1.861252	0.000000	0.550176	-2.483925	0.000000	0.550167	-2.944868	
		N	0.000000	-0.550149	-1.861252	0.000000	-0.550176	-2.483925	0.000000	-0.550167	-2.944868	
<i>C_∞</i> (² Σ)				x	y	z	x	y	z	x	y	z
	def2QZVP	X	0.000000	0.000000	1.643833	0.000000	0.000000	1.075012	0.000000	0.000000	0.827244	
		N	0.000000	0.000000	-1.446279	0.000000	0.000000	-2.137722	0.000000	0.000000	-2.581886	
		N	0.000000	0.000000	-2.545888	0.000000	0.000000	-3.237336	0.000000	0.000000	-3.681537	
	pVTZ	X	0.000000	0.000000	1.644099	0.000000	0.000000	1.065363	0.000000	0.000000	0.826239	
		N	0.000000	0.000000	-1.445472	0.000000	0.000000	-2.112473	0.000000	0.000000	-2.576955	
		N	0.000000	0.000000	-2.547339	0.000000	0.000000	-3.214340	0.000000	0.000000	-3.678854	
	pVQZ	X	0.000000	0.000000	1.639142	0.000000	0.000000	1.060841	0.000000	0.000000	0.820245	
		N	0.000000	0.000000	-1.440475	0.000000	0.000000	-2.102192	0.000000	0.000000	-2.555285	
		N	0.000000	0.000000	-2.540297	0.000000	0.000000	-3.202014	0.000000	0.000000	-3.655138	
<i>C_{2v}</i> (² A ₂)				x	y	z	x	y	z	x	y	z
	def2QZVP	X	0.000000	0.000000	0.772132	0.000000	0.000000	0.533520	0.000000	0.000000	0.427634	
		N	0.000000	0.641839	-0.937589	0.000000	0.635333	-1.333799	0.000000	0.627633	-1.618901	
		N	0.000000	-0.641839	-0.937589	0.000000	-0.635333	-1.333799	0.000000	-0.627633	-1.618901	
	pVTZ	X	0.000000	0.000000	0.774634	0.000000	0.000000	0.535362	0.000000	0.000000	0.431369	
		N	0.000000	0.643051	-0.940627	0.000000	0.636249	-1.338406	0.000000	0.628272	-1.633038	
		N	0.000000	-0.643051	-0.940627	0.000000	-0.636249	-1.338406	0.000000	-0.628272	-1.633038	
	pVQZ	X	0.000000	0.000000	0.771904	0.000000	0.000000	0.533253	0.000000	0.000000	0.428999	
		N	0.000000	0.642039	-0.937312	0.000000	-0.635355	-1.333132	0.000000	0.627461	-1.624068	
		N	0.000000	-0.642039	-0.937312	0.000000	0.635355	-1.333132	0.000000	-0.627461	-1.624068	

Table B29: $\text{X}^- \cdots \text{HCCH}$ complex geometric parameters and D_0 values from DSD-PBEP86-D3BJ optimisations. zpe values are drawn from relevant harmonic frequency calculations.

			$R_{\text{X} \cdots \text{H}}$	$R_{\text{H}-\text{C}}$	$R_{\text{C}\equiv\text{C}}$	$\angle_{\text{X} \cdots \text{ }-\text{C}}$	E_{DFT}	zpe	D_e	D_o
			Å	Å	Å	°	E_h	kJ mol ⁻¹	kJ mol ⁻¹	kJ mol ⁻¹
$\text{Cl}^- \cdots \text{HCCH}$	C_∞ ($^1\Sigma$)	def2QZVP	2.227	1.095	1.210	180.0	-537.2167692	72.4	49.5	51.6
		pVTZ	2.234	1.094	1.212	180.0	-537.1947703	72.6	47.4	49.7
		pVQZ	2.238	1.094	1.210	180.0	-537.2204020	72.4	46.6	48.8
$\text{Br}^- \cdots \text{HCCH}$	C_∞ ($^1\Sigma$)	def2QZVP	2.444	1.088	1.209	180.0	-2650.6896270	72.4	42.1	44.1
		pVTZ	2.429	1.088	1.211	180.0	-493.5268837	72.8	41.9	44.3
		pVQZ	2.417	1.089	1.209	180.0	-493.5765940	72.6	41.3	43.6
$\text{I}^- \cdots \text{HCCH}$	C_∞ ($^1\Sigma$)	def2QZVP	2.748	1.082	1.208	180.0	-374.7762103	72.4	32.6	34.6
		pVTZ	2.723	1.082	1.210	180.0	-372.5712921	72.4	34.0	36.2
		pVQZ	2.726	1.082	1.208	180.0	-372.6217568	72.4	33.5	35.7

Table B30: X...HCCH complex geometric parameters and D_0 values from DSD-PBEP86-D3BJ optimisations. zpe values are drawn from relevant harmonic frequency calculations.

			$R_{\text{X}-\text{H}}$	$R_{\text{H}-\text{C}}$	$R_{\text{C}\equiv\text{C}}$	$\angle_{\text{X} \cdots \text{ }-\text{C}}$	E_{DFT}	zpe	D_e	D_o
			Å	Å	Å	°	E_h	kJ mol ⁻¹	kJ mol ⁻¹	kJ mol ⁻¹
Cl ... HCCH	C_∞ ($^2\Sigma$)	def2QZVP	2.862	1.064	1.204	180.0	-537.0706373	72.1	3.3	5.0
		pVTZ	2.808	1.064	1.206	180.0	-537.0472343	72.0	4.2	5.9
		pVQZ	2.839	1.064	1.204	180.0	-537.0714364	72.1	3.7	5.5
	C_{2v} (2A_1)	$R_{\text{X}-\parallel}$	2.599	1.064	1.211	90.0	-537.0784914	72.2	24.0	25.8
		def2QZVP	2.598	1.064	1.213	90.0	-537.0550247	72.4	24.6	26.7
		pVTZ	2.590	1.064	1.211	90.0	-537.0796033	72.2	25.1	27.1
Br ... HCCH	C_∞ ($^2\Sigma$)	$R_{\text{X}-\text{H}}$	2.974	1.064	1.204	180.0	-2650.550701	72.0	3.8	5.4
		def2QZVP	2.873	1.065	1.206	180.0	-493.388187	71.9	5.4	6.9
		pVTZ	2.921	1.064	1.204	180.0	-493.4362775	71.9	5.1	6.8
	C_{2v} (2A_1)	$R_{\text{X}-\parallel}$	2.804	1.064	1.209	90.0	-2650.557247	72.1	21.0	22.8
		def2QZVP	2.792	1.064	1.211	90.0	-493.3946638	72.4	22.4	24.5
		pVTZ	2.782	1.064	1.209	90.0	-493.4432061	72.3	23.3	25.3
I ... HCCH	C_∞ ($^2\Sigma$)	$R_{\text{X}-\text{H}}$	3.170	1.064	1.204	180.0	-374.6465738	71.8	4.2	5.6
		def2QZVP	3.082	1.065	1.206	180.0	-372.4416306	71.8	5.8	7.2
		pVTZ	3.101	1.065	1.204	180.0	-372.49021	71.9	5.6	7.2
	C_{2v} (2A_1)	$R_{\text{X}-\parallel}$	3.079	1.064	1.207	90.0	-374.6517729	72.1	17.8	19.5
		def2QZVP	3.088	1.064	1.209	90.0	-372.4465497	72.3	18.7	20.6
		pVTZ	3.062	1.064	1.208	90.0	-372.4956211	72.2	19.8	21.8

Table B31: $X^- \cdots \text{HCCH}$ complex VDEs from DSD-PBEP86-D3BJ optimisations. zpe values are drawn from relevant harmonic frequency calculations.

		E_{VDE}	$VDE_{2P_{3/2}}$	$VDE_{2P_{1/2}}$	$ADE_{2P_{3/2}}$	$ADE_{2P_{1/2}}$	
		E_h	eV	eV	eV	eV	
$\text{Cl}^- \cdots \text{HCCH}$	$C_\infty ({}^1\Sigma)$	def2QZVP	-537.0663205	4.177	4.286	4.088	4.197
		pVTZ	-537.0433570	4.135	4.244	4.056	4.165
		pVQZ	-537.0675151	4.133	4.242	4.054	4.163
$\text{Br}^- \cdots \text{HCCH}$	$C_\infty ({}^1\Sigma)$	def2QZVP	-2650.548089	3.804	4.261	3.756	4.213
		pVTZ	-493.3859097	3.775	4.232	3.733	4.190
		pVQZ	-493.4337816	3.778	4.235	3.732	4.189
$\text{I}^- \cdots \text{HCCH}$	$C_\infty ({}^1\Sigma)$	def2QZVP	-374.6452678	3.365	4.307	3.349	4.291
		pVTZ	-372.4404508	3.358	4.300	3.345	4.287
		pVQZ	-372.4890118	3.356	4.298	3.342	4.284

Table B32: Calculated harmonic frequencies and mode assignments for the $\text{Cl}^- \cdots \text{HCCH}$ complex. All frequencies and intensities are in cm^{-1} and km mol^{-1} respectively.

$\text{Cl}^- \cdots \text{HCCH}$ $C_\infty ({}^1\Sigma)$ vdW Complex					
	Mode	Symmetry	Frequency (cm^{-1})	Intensity (km mol^{-1})	Description
def2QZVP	ω_1	σ	158	36.2239	Intermolecular stretch
	ω_2	π	175	0.0072	Intermolecular bend
	ω_3	π	175	0.0072	Intermolecular bend
	ω_4	π	646	40.1775	HCCH asymmetric bend
	ω_5	π	646	40.1775	HCCH asymmetric bend
	ω_6	π	951	41.1917	HCCH symmetric bend
	ω_7	π	951	41.1917	HCCH symmetric bend
	ω_8	σ	1942	200.0991	C=C stretch
	ω_9	σ	3004	1036.1935	X–HC stretch
	ω_{10}	σ	3463	3.4646	CH stretch
	zpe		72.4		
pVTZ	ω_1	σ	157	35.6147	Intermolecular stretch
	ω_2	π	180	0.0139	Intermolecular bend
	ω_3	π	180	0.0139	Intermolecular bend
	ω_4	π	647	39.3462	HCCH asymmetric bend
	ω_5	π	647	39.3462	HCCH asymmetric bend
	ω_6	π	954	34.5997	HCCH symmetric bend
	ω_7	π	954	34.5997	HCCH symmetric bend
	ω_8	σ	1939	201.5187	C=C stretch
	ω_9	σ	3021	1057.398	X–HC stretch
	ω_{10}	σ	3459	2.0068	CH stretch
	zpe		72.6		
pVQZ	ω_1	σ	155	35.494	Intermolecular stretch
	ω_2	π	174	0.0191	Intermolecular bend
	ω_3	π	174	0.0191	Intermolecular bend
	ω_4	π	648	39.084	HCCH asymmetric bend
	ω_5	π	648	39.084	HCCH asymmetric bend
	ω_6	π	944	33.1817	HCCH symmetric bend
	ω_7	π	944	33.1816	HCCH symmetric bend
	ω_8	σ	1943	198.6608	C=C stretch
	ω_9	σ	3020	1044.7302	X–HC stretch
	ω_{10}	σ	3460	3.2184	CH stretch
	zpe		72.4		

Table B33: Calculated harmonic frequencies and mode assignments for the $\text{Br}^- \cdots \text{HCCH}$ complex. All frequencies and intensities are in cm^{-1} and km mol^{-1} respectively.

Br ⁻ ... HCCH $C_\infty ({}^1\Sigma)$ vdW Complex					
	Mode	Symmetry	Frequency (cm^{-1})	Intensity (km mol^{-1})	Description
def2QZVP	ω_1	σ	122	11.9635	Intermolecular stretch
	ω_2	π	165	0.0683	Intermolecular bend
	ω_3	π	165	0.0683	Intermolecular bend
	ω_4	π	650	36.2362	HCCH asymmetric bend
	ω_5	π	650	36.2362	HCCH asymmetric bend
	ω_6	π	916	42.5262	HCCH symmetric bend
	ω_7	π	916	42.5262	HCCH symmetric bend
	ω_8	σ	1956	147.0963	C=C stretch
	ω_9	σ	3095	897.1692	X-HC stretch
	ω_{10}	σ	3465	2.5913	CH stretch
	zpe		72.4		
pVTZ	ω_1	σ	126	11.6269	Intermolecular stretch
	ω_2	π	174	0.3301	Intermolecular bend
	ω_3	π	174	0.3301	Intermolecular bend
	ω_4	π	651	38.1887	HCCH asymmetric bend
	ω_5	π	651	38.1887	HCCH asymmetric bend
	ω_6	π	939	29.9404	HCCH symmetric bend
	ω_7	π	939	29.9404	HCCH symmetric bend
	ω_8	σ	1952	157.2776	C=C stretch
	ω_9	σ	3098	949.7586	X-HC stretch
	ω_{10}	σ	3462	1.4997	CH stretch
	zpe		72.8		
pVQZ	ω_1	σ	126	11.8294	Intermolecular stretch
	ω_2	π	166	0.3284	Intermolecular bend
	ω_3	π	166	0.3284	Intermolecular bend
	ω_4	π	659	38.4296	HCCH asymmetric bend
	ω_5	π	659	38.4296	HCCH asymmetric bend
	ω_6	π	929	28.5729	HCCH symmetric bend
	ω_7	π	929	28.5729	HCCH symmetric bend
	ω_8	σ	1954	161.8224	HCCH stretch
	ω_9	σ	3087	961.8901	X-HC stretch
	ω_{10}	σ	3463	2.5801	CH stretch
	zpe		72.6		

Table B34: Calculated harmonic frequencies and mode assignments for the $\text{I}^- \cdots \text{HCCH}$ complex. All frequencies and intensities are in cm^{-1} and km mol^{-1} respectively.

I ⁻ ... HCCH $C_{\infty} ({}^1\Sigma)$ vdW Complex					
	Mode	Symmetry	Frequency (cm^{-1})	Intensity (km mol^{-1})	Description
def2QZVP	ω_1	σ	96	5.1021	Intermolecular stretch
	ω_2	π	155	0.2184	Intermolecular bend
	ω_3	π	155	0.2184	Intermolecular bend
	ω_4	π	654	33.2069	HCCH asymmetric bend
	ω_5	π	654	33.2069	HCCH asymmetric bend
	ω_6	π	882	37.6393	HCCH symmetric bend
	ω_7	π	882	37.6393	HCCH symmetric bend
	ω_8	σ	1970	105.0683	C=C stretch
	ω_9	σ	3183	756.1346	X-HC stretch
	ω_{10}	σ	3469	1.6545	CH stretch
	zpe		72.4		
pVTZ	ω_1	σ	101	4.9837	Intermolecular stretch
	ω_2	π	160	0.4863	Intermolecular bend
	ω_3	π	160	0.4863	Intermolecular bend
	ω_4	π	652	32.4392	HCCH asymmetric bend
	ω_5	π	652	32.4392	HCCH asymmetric bend
	ω_6	π	890	31.425	HCCH symmetric bend
	ω_7	π	890	31.425	HCCH symmetric bend
	ω_8	σ	1964	113.7152	C=C stretch
	ω_9	σ	3176	794.6119	X-HC stretch
	ω_{10}	σ	3466	0.8813	CH stretch
	zpe		72.4		
pVQZ	ω_1	σ	100	5.0038	Intermolecular stretch
	ω_2	π	155	0.4579	Intermolecular bend
	ω_3	π	155	0.4579	Intermolecular bend
	ω_4	π	658	33.4378	HCCH asymmetric bend
	ω_5	π	658	33.4378	HCCH asymmetric bend
	ω_6	π	888	29.8602	HCCH symmetric bend
	ω_7	π	888	29.8602	HCCH symmetric bend
	ω_8	σ	1968	112.3375	C=C stretch
	ω_9	σ	3176	784.8093	X-HC stretch
	ω_{10}	σ	3465	1.6412	CH stretch
	zpe		72.4		

Table B35: Calculated harmonic frequencies and mode assignments for the Cl \cdots HCCH complex. All frequencies and intensities are in cm^{-1} and km mol^{-1} respectively.

Cl \cdots HCCH C_∞ ($^2\Sigma$) vdW Complex					
	Mode	Symmetry	Frequency (cm^{-1})	Intensity (km mol^{-1})	Description
def2QZVP	ω_1	σ	57	0.1258	Intermolecular stretch
	ω_2	π	104	0.0377	Intermolecular bend
	ω_3	π	109	0.1129	Intermolecular bend
	ω_4	π	664	0.5109	HCCH asymmetric bend
	ω_5	π	666	1.2491	HCCH asymmetric bend
	ω_6	π	781	90.1171	HCCH symmetric bend
	ω_7	π	785	85.1233	HCCH symmetric bend
	ω_8	σ	2007	1.2608	C=C stretch
	ω_9	σ	3401	152.3152	X–HC stretch
	ω_{10}	σ	3494	1.867	CH stretch
	zpe		72.2		
pVTZ	ω_1	σ	64	0.1327	Intermolecular stretch
	ω_2	π	114	0.0532	Intermolecular bend
	ω_3	π	119	0.1607	Intermolecular bend
	ω_4	π	665	0.8408	HCCH asymmetric bend
	ω_5	π	666	1.9224	HCCH asymmetric bend
	ω_6	π	788	88.293	HCCH symmetric bend
	ω_7	π	792	82.0002	HCCH symmetric bend
	ω_8	σ	2002	1.4636	C=C stretch
	ω_9	σ	3396	159.283	X–HC stretch
	ω_{10}	σ	3497	3.7276	CH stretch
	zpe		72.4		
pVQZ	ω_1	σ	59	0.1266	Intermolecular stretch
	ω_2	π	105	0.0482	Intermolecular bend
	ω_3	π	111	0.1421	Intermolecular bend
	ω_4	π	667	0.6021	HCCH asymmetric bend
	ω_5	π	668	1.4777	HCCH asymmetric bend
	ω_6	π	781	87.3219	HCCH symmetric bend
	ω_7	π	785	81.6343	HCCH symmetric bend
	ω_8	σ	2006	1.3698	C=C stretch
	ω_9	σ	3398	155.8578	X–HC stretch
	ω_{10}	σ	3491	2.0886	CH stretch
	zpe		72.2		

Table B36: Calculated harmonic frequencies and mode assignments for the Br \cdots HCCH complex. All frequencies and intensities are in cm^{-1} and km mol^{-1} respectively.

Br \cdots HCCH C_∞ ($^2\Sigma$) vdW Complex					
	Mode	Symmetry	Frequency (cm^{-1})	Intensity (km mol^{-1})	Description
def2QZVP	ω_1	σ	51	0.104	Intermolecular stretch
	ω_2	π	104	0.0528	Intermolecular bend
	ω_3	π	109	0.1494	Intermolecular bend
	ω_4	π	665	0.6803	HCCH asymmetric bend
	ω_5	π	666	1.5808	HCCH asymmetric bend
	ω_6	π	781	88.2055	HCCH symmetric bend
	ω_7	π	785	82.5714	HCCH symmetric bend
	ω_8	σ	2007	1.8296	C=C stretch
	ω_9	σ	3399	166.6195	X–HC stretch
	ω_{10}	σ	3492	2.0565	CH stretch
	zpe		72.1		
pVTZ	ω_1	σ	62	0.1127	Intermolecular stretch
	ω_2	π	116	0.099	Intermolecular bend
	ω_3	π	122	0.2683	Intermolecular bend
	ω_4	π	668	1.7655	HCCH asymmetric bend
	ω_5	π	669	3.4562	HCCH asymmetric bend
	ω_6	π	791	84.5822	HCCH symmetric bend
	ω_7	π	797	76.5271	HCCH symmetric bend
	ω_8	σ	2001	2.4292	C=C stretch
	ω_9	σ	3391	184.4347	X–HC stretch
	ω_{10}	σ	3493	4.0307	CH stretch
	zpe		72.4		
pVQZ	ω_1	σ	56	0.1053	Intermolecular stretch
	ω_2	π	108	0.0877	Intermolecular bend
	ω_3	π	114	0.2292	Intermolecular bend
	ω_4	π	671	1.4347	HCCH asymmetric bend
	ω_5	π	672	2.8585	HCCH asymmetric bend
	ω_6	π	784	83.9909	HCCH symmetric bend
	ω_7	π	789	76.8878	HCCH symmetric bend
	ω_8	σ	2005	2.1632	C=C stretch
	ω_9	σ	3395	176.3143	X–HC stretch
	ω_{10}	σ	3489	2.4602	CH stretch
	zpe		72.3		

Table B37: Calculated harmonic frequencies and mode assignments for the I...HCCH complex. All frequencies and intensities are in cm^{-1} and km mol^{-1} respectively.

I...HCCH $C_\infty ({}^2\Sigma)$ vdW Complex					
	Mode	Symmetry	Frequency (cm^{-1})	Intensity (km mol^{-1})	Description
def2QZVP	ω_1	σ	50	0.0797	Intermolecular stretch
	ω_2	π	104	0.1133	Intermolecular bend
	ω_3	π	109	0.2532	Intermolecular bend
	ω_4	π	665	1.0309	HCCH asymmetric bend
	ω_5	π	666	2.1477	HCCH asymmetric bend
	ω_6	π	781	83.2566	HCCH symmetric bend
	ω_7	π	786	77.0709	HCCH symmetric bend
	ω_8	σ	2006	2.6096	C=C stretch
	ω_9	σ	3396	184.7604	X-HC stretch
	ω_{10}	σ	3491	2.2965	CH stretch
	zpe		72.1		
pVTZ	ω_1	σ	59	0.0833	Intermolecular stretch
	ω_2	π	113	0.1418	Intermolecular bend
	ω_3	π	119	0.3402	Intermolecular bend
	ω_4	π	664	1.5656	HCCH asymmetric bend
	ω_5	π	666	3.1478	HCCH asymmetric bend
	ω_6	π	788	81.0712	HCCH symmetric bend
	ω_7	π	793	73.0896	HCCH symmetric bend
	ω_8	σ	2001	3.2749	C=C stretch
	ω_9	σ	3388	201.675	X-HC stretch
	ω_{10}	σ	3491	3.7948	CH stretch
	zpe		72.3		
pVQZ	ω_1	σ	57	0.0812	Intermolecular stretch
	ω_2	π	107	0.14	Intermolecular bend
	ω_3	π	113	0.3231	Intermolecular bend
	ω_4	π	668	1.7621	HCCH asymmetric bend
	ω_5	π	670	3.3666	HCCH asymmetric bend
	ω_6	π	784	80.1203	HCCH symmetric bend
	ω_7	π	790	72.5081	HCCH symmetric bend
	ω_8	σ	2004	3.0965	C=C stretch
	ω_9	σ	3391	196.8645	X-HC stretch
	ω_{10}	σ	3487	2.7528	CH stretch
	zpe		72.2		

Table B38: Calculated harmonic frequencies and mode assignments for the Cl···HCCH complex. All frequencies and intensities are in cm^{-1} and km mol^{-1} respectively.

Cl···HCCH C_{2v} (2A_1) vdW Complex					
	Mode	Symmetry	Frequency (cm^{-1})	Intensity (km mol^{-1})	Description
def2QZVP	ω_1	b_2	106	0.4344	Intermolecular bend
	ω_2	a_1	190	8.2528	Intermolecular stretch
	ω_3	a_2	653	0	HCCH \perp asymmetric stretch
	ω_4	b_2	669	0.0155	HCCH \parallel asymmetric stretch
	ω_5	b_1	773	87.9909	HCCH \perp symmetric stretch
	ω_6	a_1	791	98.6903	HCCH \parallel symmetric stretch
	ω_7	a_1	1974	45.0413	C=C stretch
	ω_8	b_2	3402	133.8134	HCCH asymmetric stretch
	ω_9	a_1	3491	0.9595	HCCH symmetric stretch
	zpe		72.1		
pVTZ	ω_1	b_2	109	0.4881	Intermolecular bend
	ω_2	a_1	191	8.0043	Intermolecular stretch
	ω_3	a_2	650	0	HCCH \perp asymmetric stretch
	ω_4	b_2	665	0.0008	HCCH \parallel asymmetric stretch
	ω_5	b_1	776	86.3087	HCCH \perp symmetric stretch
	ω_6	a_1	793	98.4618	HCCH \parallel symmetric stretch
	ω_7	a_1	1970	43.9158	C=C stretch
	ω_8	b_2	3396	133.261	HCCH asymmetric stretch
	ω_9	a_1	3491	0.894	HCCH symmetric stretch
	zpe		72		
pVQZ	ω_1	b_2	106	0.4888	Intermolecular bend
	ω_2	a_1	194	7.803	Intermolecular stretch
	ω_3	a_2	656	0	HCCH \perp asymmetric stretch
	ω_4	b_2	670	0.0017	HCCH \parallel asymmetric stretch
	ω_5	b_1	773	85.7775	HCCH \perp symmetric stretch
	ω_6	a_1	791	97.5035	HCCH \parallel symmetric stretch
	ω_7	a_1	1972	43.9868	C=C stretch
	ω_8	b_2	3399	132.8153	HCCH asymmetric stretch
	ω_9	a_1	3488	0.8801	HCCH symmetric stretch
	zpe		72.1		

Table B39: Calculated harmonic frequencies and mode assignments for the Br...HCCH complex. All frequencies and intensities are in cm^{-1} and km mol^{-1} respectively.

Br...HCCH C_{2v} (2A_1) vdW Complex					
	Mode	Symmetry	Frequency (cm^{-1})	Intensity (km mol^{-1})	Description
def2QZVP	ω_1	b_2	129	0.3115	Intermolecular bend
	ω_2	a_1	142	7.5928	Intermolecular stretch
	ω_3	a_2	655	0	HCCH \perp asymmetric stretch
	ω_4	b_2	667	0.021	HCCH \parallel asymmetric stretch
	ω_5	b_1	774	87.0683	HCCH \perp symmetric stretch
	ω_6	a_1	790	108.6275	HCCH \parallel symmetric stretch
	ω_7	a_1	1982	38.9597	C=C stretch
	ω_8	b_2	3402	127.4093	HCCH asymmetric stretch
	ω_9	a_1	3491	0.3827	HCCH symmetric stretch
	zpe		72		
pVTZ	ω_1	b_2	133	0.3771	Intermolecular bend
	ω_2	a_1	143	7.0278	Intermolecular stretch
	ω_3	a_2	651	0	HCCH \perp asymmetric stretch
	ω_4	b_2	661	0.001	HCCH \parallel asymmetric stretch
	ω_5	b_1	777	84.5057	HCCH \perp symmetric stretch
	ω_6	a_1	792	107.8652	HCCH \parallel symmetric stretch
	ω_7	a_1	1977	35.0775	C=C stretch
	ω_8	b_2	3395	125.8284	HCCH asymmetric stretch
	ω_9	a_1	3492	0.2501	HCCH symmetric stretch
	zpe		71.9		
pVQZ	ω_1	b_2	130	0.3789	Intermolecular bend
	ω_2	a_1	146	6.9612	Intermolecular stretch
	ω_3	a_2	658	0	HCCH \perp asymmetric stretch
	ω_4	b_2	667	0.0018	HCCH \parallel asymmetric stretch
	ω_5	b_1	774	83.9539	HCCH \perp symmetric stretch
	ω_6	a_1	788	107.0564	HCCH \parallel symmetric stretch
	ω_7	a_1	1979	35.4508	C=C stretch
	ω_8	b_2	3399	125.5024	HCCH asymmetric stretch
	ω_9	a_1	3488	0.2567	HCCH symmetric stretch
	zpe		71.9		

Table B40: Calculated harmonic frequencies and mode assignments for the I...HCCH complex. All frequencies and intensities are in cm^{-1} and km mol^{-1} respectively.

I...HCCH C_{2v} (2A_1) vdW Complex					
	Mode	Symmetry	Frequency (cm^{-1})	Intensity (km mol^{-1})	Description
def2QZVP	ω_1	a_1	109	6.3793	Intermolecular stretch
	ω_2	b_2	136	0.3997	Intermolecular bend
	ω_3	a_2	656	0	HCCH \perp asymmetric stretch
	ω_4	b_2	664	0.0224	HCCH \parallel asymmetric stretch
	ω_5	b_1	776	82.4624	HCCH \perp symmetric stretch
	ω_6	a_1	789	119.8728	HCCH \parallel symmetric stretch
	ω_7	a_1	1989	25.2862	C=C stretch
	ω_8	b_2	3401	117.3399	HCCH asymmetric stretch
	ω_9	a_1	3491	0.0005	HCCH symmetric stretch
	zpe		71.8		
pVTZ	ω_1	a_1	109	6.2255	Intermolecular stretch
	ω_2	b_2	139	0.4278	Intermolecular bend
	ω_3	a_2	653	0	HCCH \perp asymmetric stretch
	ω_4	b_2	657	0.0453	HCCH \parallel asymmetric stretch
	ω_5	b_1	779	81.6111	HCCH \perp symmetric stretch
	ω_6	a_1	790	120.39	HCCH \parallel symmetric stretch
	ω_7	a_1	1985	24.072	C=C stretch
	ω_8	b_2	3395	116.3059	HCCH asymmetric stretch
	ω_9	a_1	3493	0.0031	HCCH symmetric stretch
	zpe		71.8		
pVQZ	ω_1	a_1	114	6.3293	Intermolecular stretch
	ω_2	b_2	139	0.4385	Intermolecular bend
	ω_3	a_2	659	0	HCCH \perp asymmetric stretch
	ω_4	b_2	665	0.0508	HCCH \parallel asymmetric stretch
	ω_5	b_1	776	80.8719	HCCH \perp symmetric stretch
	ω_6	a_1	788	119.0957	HCCH \parallel symmetric stretch
	ω_7	a_1	1987	24.7003	C=C stretch
	ω_8	b_2	3398	116.6343	HCCH asymmetric stretch
	ω_9	a_1	3488	0.0031	HCCH symmetric stretch
	zpe		71.9		

Table B41: Cartesian coordinates of the geometries of halide-acetylene complexes optimised with the DSD-PBEP86-D3BJ functional, in Å.

		Cl ⁻ ... HCCH			Br ⁻ ... HCCH			I ⁻ ... HCCH			
		x	y	z	x	y	z	x	y	z	
C_{∞} (¹ Σ)	def2QZVP	X	0.000000	0.000000	1.772137	0.000000	0.000000	1.181204	0.000000	0.000000	0.926032
		H	0.000000	0.000000	-3.821020	0.000000	0.000000	-4.621083	0.000000	0.000000	-5.172717
		C	0.000000	0.000000	-2.759224	0.000000	0.000000	-3.559348	0.000000	0.000000	-4.110998
		C	0.000000	0.000000	-1.549258	0.000000	0.000000	-2.350434	0.000000	0.000000	-2.903213
		H	0.000000	0.000000	-0.454408	0.000000	0.000000	-1.262354	0.000000	0.000000	-1.821695
	pVTZ	X	0.000000	0.000000	1.775545	0.000000	0.000000	1.177498	0.000000	0.000000	0.921173
		H	0.000000	0.000000	-3.826651	0.000000	0.000000	-4.613483	0.000000	0.000000	-5.156006
		C	0.000000	0.000000	-2.764221	0.000000	0.000000	-3.551086	0.000000	0.000000	-4.093709
		C	0.000000	0.000000	-1.552292	0.000000	0.000000	-2.340092	0.000000	0.000000	-2.883738
		H	0.000000	0.000000	-0.458536	0.000000	0.000000	-1.251886	0.000000	0.000000	-1.801481
	pVQZ	X	0.000000	0.000000	1.776998	0.000000	0.000000	1.173942	0.000000	0.000000	0.921544
		H	0.000000	0.000000	-3.827124	0.000000	0.000000	-4.603369	0.000000	0.000000	-5.156171
		C	0.000000	0.000000	-2.765103	0.000000	0.000000	-3.541402	0.000000	0.000000	-4.094212
		C	0.000000	0.000000	-1.554977	0.000000	0.000000	-2.332105	0.000000	0.000000	-2.886054
		H	0.000000	0.000000	-0.461362	0.000000	0.000000	-1.243555	0.000000	0.000000	-1.804063

Table B42: Cartesian coordinates of the geometries of halogen-acetylene complexes optimised with the DSD-PBEP86-D3BJ functional, in Å.

		Cl ... HCCH			Br ... HCCH			I ... HCCH				
		x	y	z	x	y	z	x	y	z		
C_∞ ($^2\Sigma$)	def2QZVP	X	0.000000	0.000000	2.044900	0.000000	0.000000	1.325767	0.000000	0.000000	1.010603	
		H	0.000000	0.000000	-4.147965	0.000000	0.000000	-4.979329	0.000000	0.000000	-5.490805	
		C	0.000000	0.000000	-3.085148	0.000000	0.000000	-3.916514	0.000000	0.000000	-4.427991	
		C	0.000000	0.000000	-1.881197	0.000000	0.000000	-2.712510	0.000000	0.000000	-3.223937	
		H	0.000000	0.000000	-0.817274	0.000000	0.000000	-1.648381	0.000000	0.000000	-2.159571	
	pVTZ	X	0.000000	0.000000	2.020921	0.000000	0.000000	1.297396	0.000000	0.000000	0.992622	
		H	0.000000	0.000000	-4.120454	0.000000	0.000000	-4.910034	0.000000	0.000000	-5.424340	
		C	0.000000	0.000000	-3.057086	0.000000	0.000000	-3.846692	0.000000	0.000000	-4.361032	
		C	0.000000	0.000000	-1.850997	0.000000	0.000000	-2.640504	0.000000	0.000000	-3.154784	
		H	0.000000	0.000000	-0.786703	0.000000	0.000000	-1.575664	0.000000	0.000000	-2.089727	
C_{2v} (2A_1)	pVQZ	X	0.000000	0.000000	2.034593	0.000000	0.000000	1.310697	0.000000	0.000000	0.996341	
		H	0.000000	0.000000	-4.135819	0.000000	0.000000	-4.942038	0.000000	0.000000	-5.437207	
		C	0.000000	0.000000	-3.072802	0.000000	0.000000	-3.879023	0.000000	0.000000	-4.374198	
		C	0.000000	0.000000	-1.868520	0.000000	0.000000	-2.674669	0.000000	0.000000	-3.169778	
		H	0.000000	0.000000	-0.804339	0.000000	0.000000	-1.610189	0.000000	0.000000	-2.105017	
	pVTZ	x	0.000000	0.000000	1.174600	0.000000	0.000000	0.801656	0.000000	0.000000	0.643655	
		H	0.000000	1.669150	-1.440469	0.000000	1.668263	-2.016796	0.000000	1.667449	-2.447200	
		def2QZVP	C	0.000000	0.605352	-1.423938	0.000000	0.604488	-2.002032	0.000000	0.603692	-2.434943
		C	0.000000	-0.605352	-1.423938	0.000000	-0.604488	-2.002032	0.000000	-0.603692	-2.434943	
		H	0.000000	-1.669150	-1.440469	0.000000	-1.668263	-2.016796	0.000000	-1.667449	-2.447200	
C_{2v} (2A_1)	pVQZ	X	0.000000	0.000000	1.174505	0.000000	0.000000	0.798215	0.000000	0.000000	0.645666	
		H	0.000000	1.670708	-1.439935	0.000000	1.669782	-2.008416	0.000000	1.668865	-2.454292	
		pVTZ	C	0.000000	0.606393	-1.423893	0.000000	0.605533	-1.993390	0.000000	0.604679	-2.442645
		C	0.000000	-0.606393	-1.423893	0.000000	-0.605533	-1.993390	0.000000	-0.604679	-2.442645	
		H	0.000000	-1.670708	-1.439935	0.000000	-1.669782	-2.008416	0.000000	-1.668865	-2.454292	
	pVQZ	X	0.000000	0.000000	1.170925	0.000000	0.000000	0.795512	0.000000	0.000000	0.640116	
		H	0.000000	1.669621	-1.435889	0.000000	1.668712	-2.001656	0.000000	1.667872	-2.433191	
		C	0.000000	0.605595	-1.419495	0.000000	0.604729	-1.986634	0.000000	0.603903	-2.421646	
		C	0.000000	-0.605595	-1.419495	0.000000	-0.604729	-1.986634	0.000000	-0.603903	-2.421646	
		H	0.000000	-1.669621	-1.435889	0.000000	-1.668712	-2.001656	0.000000	-1.667872	-2.433191	

Table B43: $\text{X}^- \cdots \text{O}_2$ complex geometric parameters and D_0 values from DSD-PBEP86-D3BJ optimisations. zpe values are drawn from relevant harmonic frequency calculations.

			$R_{\text{X} \cdots \text{O}}$ Å	$R_{\text{X} \cdots \parallel}$ Å	$R_{\text{O}=\text{O}}$ Å	$\angle_{\text{X} \cdots \parallel - \text{O}}$ °	E_{DFT} E_h	zpe kJ mol ⁻¹	D_e kJ mol ⁻¹	D_o kJ mol ⁻¹
$\text{Cl}^- \cdots \text{O}_2$	C_s ($^3A''$)	def2QZVP	3.376	3.519	1.204	73.3	-610.1632503	9.8	6.5	6.8
		pVTZ	3.356	3.541	1.208	71.3	-610.1309845	9.7	6.2	6.5
		pVQZ	3.456	3.513	1.204	77.4	-610.1686802	9.9	6.3	6.6
	C_{2v} (3B_1)	def2QZVP	3.544	3.493	1.203	90.0	-610.1632375	9.9	6.5	6.9
		pVTZ	3.547	3.496	1.207	90.0	-610.1309601	9.8	6.1	6.5
		pVQZ	3.555	3.504	1.204	90.0	-610.1686792	9.9	6.3	6.6
	C_∞ ($^3\Sigma$)	def2QZVP	3.413	4.017	1.209	180.0	-610.1627115	9.6	5.1	5.2
		pVTZ	3.403	4.009	1.212	180.0	-610.1306244	9.6	5.2	5.4
		pVQZ	3.414	4.018	1.209	180.0	-610.1682058	9.7	5.0	5.2
$\text{Br}^- \cdots \text{O}_2$	C_s ($^3A''$)	def2QZVP	3.535	3.719	1.205	71.9	-2723.6386170	9.7	5.7	5.9
		pVTZ	3.501	3.740	1.209	69.3	-566.4650186	9.6	5.6	5.8
		pVQZ	3.529	3.714	1.205	71.8	-566.5267298	9.7	5.8	6.0
	C_{2v} (3B_1)	def2QZVP	3.732	3.684	1.203	90.0	-2723.6385920	9.8	5.6	5.9
		pVTZ	3.734	3.685	1.207	90.0	-566.4649620	9.7	5.5	5.8
		pVQZ	3.725	3.676	1.204	90.0	-566.5267067	9.8	5.7	6.0
	C_∞ ($^3\Sigma$)	def2QZVP	3.600	4.204	1.208	180.0	-2723.6381500	9.6	4.5	4.5
		pVTZ	3.585	4.190	1.212	180.0	-566.4646799	9.5	4.8	4.8
		pVQZ	3.575	4.179	1.208	180.0	-566.5263040	9.6	4.7	4.8
$\text{I}^- \cdots \text{O}_2$	C_s ($^3A''$)	def2QZVP	3.797	3.994	1.205	72.0	-447.7284107	9.7	4.6	4.8
		pVTZ	3.742	4.019	1.209	68.2	-445.5120777	9.5	4.8	4.9
		pVQZ	3.787	3.986	1.205	71.8	-445.5745371	9.7	5.0	5.2
	C_{2v} (3B_1)	def2QZVP	4.013	3.968	1.204	90.0	-447.7283860	9.8	4.6	4.8
		pVTZ	4.010	3.965	1.207	90.0	-445.5120046	9.6	4.6	4.8
		pVQZ	4.001	3.955	1.204	90.0	-445.5745118	9.8	5.0	5.2
	C_∞ ($^3\Sigma$)	def2QZVP	3.881	4.485	1.207	180.0	-447.7279550	9.6	3.4	3.5
		pVTZ	3.846	4.452	1.211	180.0	-445.5117800	9.5	4.0	4.1
		pVQZ	3.857	4.460	1.208	180.0	-445.5741556	9.6	4.0	4.1

Table B44: X···O₂ complex geometric parameters and D_0 values from DSD-PBEP86-D3BJ optimisations. zpe values are drawn from relevant harmonic frequency calculations.

			$R_{X \cdots O}$ Å	$R_{X \cdots }$ Å	$R_{O=O}$ Å	$\angle_{X \cdots - O}$ °	E_{DFT} E_h	zpe kJ mol ⁻¹	D_e kJ mol ⁻¹	D_o kJ mol ⁻¹
Cl ··· O ₂	C_{2v} ($^4A''$)	def2QZVP	3.232	3.175	1.206	90.0	-610.0332420	9.8	2.7	3.0
		pVTZ	3.211	3.153	1.209	90.0	-609.9986846	9.7	2.9	3.2
		pVQZ	3.224	3.168	1.206	90.0	-610.0347063	9.8	2.7	3.0
	C_∞ ($^4\Sigma$)	def2QZVP	3.122	3.724	1.204	180.0	-610.0330545	9.8	2.2	2.5
		pVTZ	3.119	3.722	1.208	180.0	-609.9984977	9.7	2.4	2.7
		pVQZ	3.113	3.715	1.204	180.0	-610.0345567	9.8	2.3	2.6
Br ··· O ₂	C_{2v} ($^4A''$)	def2QZVP	3.352	3.298	1.206	90.0	-2723.5132140	9.8	2.9	3.2
		pVTZ	3.311	3.256	1.209	90.0	-566.3394182	9.7	3.5	3.8
		pVQZ	3.313	3.258	1.206	90.0	-566.3993241	9.8	3.5	3.8
	C_∞ ($^4\Sigma$)	def2QZVP	3.235	3.837	1.204	180.0	-2723.5130620	9.8	2.5	2.8
		pVTZ	3.200	3.804	1.208	180.0	-566.3392407	9.7	3.0	3.3
		pVQZ	3.183	3.786	1.204	180.0	-566.3992000	9.8	3.2	3.5
I ··· O ₂	C_{2v} ($^4A''$)	def2QZVP	3.549	3.497	1.206	90.0	-447.6091613	9.7	3.4	3.7
		pVTZ	3.520	3.467	1.209	90.0	-445.3927653	9.6	3.7	3.9
		pVQZ	3.533	3.481	1.206	90.0	-445.4531433	9.7	3.8	4.0
	C_∞ ($^4\Sigma$)	def2QZVP	3.397	3.999	1.204	180.0	-447.6090005	9.8	3.0	3.3
		pVTZ	3.389	3.993	1.208	180.0	-445.3926351	9.7	3.3	3.6
		pVQZ	3.372	3.974	1.204	180.0	-445.4530378	9.8	3.5	3.7

Table B45: $\text{X}^- \cdots \text{O}_2$ complex VDEs from DSD-PBEP86-D3BJ optimisations. zpe values are drawn from relevant harmonic frequency calculations.

			E_{VDE} E_h	$VDE_{2P_{3/2}}$ eV	$VDE_{2P_{1/2}}$ eV	$ADE_{2P_{3/2}}$ eV	$ADE_{2P_{1/2}}$ eV
$\text{Cl}^- \cdots \text{O}_2$	$C_s ({}^3A'')$	def2QZVP	-610.0330130	3.656	3.765	3.653	3.762
		pVTZ	-609.9979436	3.664	3.773	3.647	3.756
		pVQZ	-610.0344759	3.653	3.762	3.649	3.758
	$C_{2v} ({}^3B_1)$	def2QZVP	-610.0330359	3.654	3.763	3.651	3.766
		pVTZ	-609.9984333	3.650	3.759	3.646	3.760
		pVQZ	-610.0344807	3.652	3.761	3.649	3.762
$\text{Br}^- \cdots \text{O}_2$	$C_s ({}^3A'')$	def2QZVP	-2723.5129260	3.398	3.855	3.393	3.850
		pVTZ	-566.3390289	3.394	3.851	3.387	3.844
		pVQZ	-566.3989522	3.395	3.852	3.388	3.845
	$C_{2v} ({}^3B_1)$	def2QZVP	-2723.5129330	3.397	3.854	3.392	3.849
		pVTZ	-566.3390458	3.392	3.849	3.384	3.841
		pVQZ	-566.3989575	3.394	3.851	3.387	3.844
$\text{I}^- \cdots \text{O}_2$	$C_s ({}^3A'')$	def2QZVP	-447.6084858	3.088	4.030	3.072	4.014
		pVTZ	-445.3919629	3.090	4.032	3.071	4.013
		pVQZ	-445.4524412	3.089	4.031	3.073	4.015
	$C_{2v} ({}^3B_1)$	def2QZVP	-447.6087767	3.079	4.021	3.071	4.013
		pVTZ	-445.3923135	3.078	4.020	3.068	4.010
		pVQZ	-445.4527358	3.080	4.022	3.071	4.013
$C_\infty ({}^3\Sigma)$	$C_s ({}^3A'')$	def2QZVP	-447.6086445	3.071	4.013	3.066	4.008
		pVTZ	-445.3922748	3.073	4.015	3.068	4.010
	$C_\infty ({}^3\Sigma)$	pVQZ	-445.4526560	3.073	4.015	3.067	4.009

Table B46: Calculated harmonic frequencies and mode assignments for the $\text{Cl}^- \cdots \text{O}_2$ complex. All frequencies and intensities are in cm^{-1} and km mol^{-1} respectively.

$\text{Cl}^- \cdots \text{O}_2$ $C_s ({}^3A'')$ vdW Complex					
	Mode	Symmetry	Frequency (cm^{-1})	Intensity (km mol^{-1})	Description
def2QZVP	ω_1	a'	126 <i>i</i>	2.2704	Intermolecular bend
	ω_2	a'	57	18.1061	Intermolecular stretch
	ω_3	a'	1587	8.748	O_2 stretch
		zpe	9.8		
pVTZ	ω_1	a'	119 <i>i</i>	1.8797	Intermolecular bend
	ω_2	a'	55	18.2687	Intermolecular stretch
	ω_3	a'	1566	12.1418	O_2 stretch
		zpe	9.7		
pVQZ	ω_1	a'	127 <i>i</i>	0.6456	Intermolecular bend
	ω_2	a'	58	15.6093	Intermolecular stretch
	ω_3	a'	1592	2.5507	O_2 stretch
		zpe	9.9		
$\text{Cl}^- \cdots \text{O}_2$ $C_{2v} ({}^3B_1)$ vdW Complex					
	Mode	Symmetry	Frequency (cm^{-1})	Intensity (km mol^{-1})	Description
def2QZVP	ω_1	b_2	131 <i>i</i>	0.0002	Intermolecular bend
	ω_2	a_1	59	15.716	Intermolecular stretch
	ω_3	a_1	1596	0.833	O_2 stretch
		zpe	9.9		
pVTZ	ω_1	b_2	126 <i>i</i>	0.0064	Intermolecular bend
	ω_2	a_1	58	15.0582	Intermolecular stretch
	ω_3	a_1	1577	1.1278	O_2 stretch
		zpe	9.8		
pVQZ	ω_1	b_2	129 <i>i</i>	0.0065	Intermolecular bend
	ω_2	a_1	58	14.9281	Intermolecular stretch
	ω_3	a_1	1594	1.0538	O_2 stretch
		zpe	9.9		
$\text{Cl}^- \cdots \text{O}_2$ $C_\infty ({}^3\Sigma)$ vdW Complex					
	Mode	Symmetry	Frequency (cm^{-1})	Intensity (km mol^{-1})	Description
def2QZVP	ω_1	π	133 <i>i</i>	1.6726	Degenerate intermolecular bend
	ω_2	π	133 <i>i</i>	1.6726	Degenerate intermolecular bend
	ω_3	σ	52	17.2142	Intermolecular stretch
	ω_4	σ	1560	15.0525	O_2 stretch
		zpe	9.6		
pVTZ	ω_1	π	126 <i>i</i>	1.5404	Degenerate intermolecular bend
	ω_2	π	126 <i>i</i>	1.5404	Degenerate intermolecular bend
	ω_3	σ	53	16.8356	Intermolecular stretch
	ω_4	σ	1543	14.5207	O_2 stretch
		zpe	9.6		
pVQZ	ω_1	π	130 <i>i</i>	1.5146	Degenerate intermolecular bend
	ω_2	π	130 <i>i</i>	1.5146	Degenerate intermolecular bend
	ω_3	σ	53	16.6934	Intermolecular stretch
	ω_4	σ	1562	13.651	O_2 stretch
		zpe	9.7		

Table B47: Calculated harmonic frequencies and mode assignments for the $\text{Br}^- \cdots \text{O}_2$ complex. All frequencies and intensities are in cm^{-1} and km mol^{-1} respectively.

$\text{Br}^- \cdots \text{O}_2$ $C_s ({}^3A'')$ vdW Complex					
	Mode	Symmetry	Frequency (cm^{-1})	Intensity (km mol^{-1})	Description
def2QZVP	ω_1	a'	125 <i>i</i>	2.3925	Intermolecular bend
	ω_2	a'	45	5.8516	Intermolecular stretch
	ω_3	a'	1583	14.4937	O_2 stretch
		zpe	9.7		
pVTZ	ω_1	a'	118 <i>i</i>	1.9085	Intermolecular bend
	ω_2	a'	43	6.0956	Intermolecular stretch
	ω_3	a'	1560	22.9537	O_2 stretch
		zpe	9.6		
pVQZ	ω_1	a'	124 <i>i</i>	1.7656	Intermolecular bend
	ω_2	a'	45	5.3901	Intermolecular stretch
	ω_3	a'	1582	13.5477	O_2 stretch
		zpe	9.7		
$\text{Br}^- \cdots \text{O}_2$ $C_{2v} ({}^3B_1)$ vdW Complex					
	Mode	Symmetry	Frequency (cm^{-1})	Intensity (km mol^{-1})	Description
def2QZVP	ω_1	a'	133 <i>i</i>	0.146	Intermolecular bend
	ω_2	a'	45	4.347	Intermolecular stretch
	ω_3	a'	1595	0.7625	O_2 stretch
		zpe	9.8		
pVTZ	ω_1	b_2	128 <i>i</i>	0.0962	Intermolecular bend
	ω_2	a_1	44	4.0585	Intermolecular stretch
	ω_3	a_1	1576	1.1703	O_2 stretch
		zpe	9.7		
pVQZ	ω_1	b_2	131 <i>i</i>	0.0976	Intermolecular bend
	ω_2	a_1	46	4.014	Intermolecular stretch
	ω_3	a_1	1593	1.1484	O_2 stretch
		zpe	9.8		
$\text{Br}^- \cdots \text{O}_2$ $C_\infty ({}^3\Sigma)$ vdW Complex					
	Mode	Symmetry	Frequency (cm^{-1})	Intensity (km mol^{-1})	Description
def2QZVP	ω_1	π	133 <i>i</i>	0.7148	Degenerate intermolecular bend
	ω_2	π	133 <i>i</i>	0.7148	Degenerate intermolecular bend
	ω_3	σ	42	4.9697	Intermolecular stretch
	ω_4	σ	1564	14.0934	O_2 stretch
		zpe	9.6		
pVTZ	ω_1	π	127 <i>i</i>	0.6337	Degenerate intermolecular bend
	ω_2	π	127 <i>i</i>	0.6337	Degenerate intermolecular bend
	ω_3	σ	42	4.7888	Intermolecular stretch
	ω_4	σ	1546	14.6204	O_2 stretch
		zpe	9.5		
pVQZ	ω_1	π	131 <i>i</i>	0.6297	Degenerate intermolecular bend
	ω_2	π	131 <i>i</i>	0.6297	Degenerate intermolecular bend
	ω_3	σ	43	4.7369	Intermolecular stretch
	ω_4	σ	1564	14.2596	O_2 stretch
		zpe	9.6		

Table B48: Calculated harmonic frequencies and mode assignments for the $\text{I}^- \cdots \text{O}_2$ complex. All frequencies and intensities are in cm^{-1} and km mol^{-1} respectively.

$\text{I}^- \cdots \text{O}_2$ $C_s ({}^3A'')$ vdW Complex					
	Mode	Symmetry	Frequency (cm^{-1})	Intensity (km mol^{-1})	Description
def2QZVP	ω_1	a'	126 <i>i</i>	2.0377	Intermolecular bend
	ω_2	a'	36	2.6365	Intermolecular stretch
	ω_3	a'	1582	15.4625	O_2 stretch
		zpe	9.7		
pVTZ	ω_1	a'	117 <i>i</i>	1.5352	Intermolecular bend
	ω_2	a'	37	3.0812	Intermolecular stretch
	ω_3	a'	1557	32.0728	O_2 stretch
		zpe	9.5		
pVQZ	ω_1	a'	124 <i>i</i>	1.6024	Intermolecular bend
	ω_2	a'	37	2.4528	Intermolecular stretch
	ω_3	a'	1581	15.6469	O_2 stretch
		zpe	9.7		
$\text{I}^- \cdots \text{O}_2$ $C_{2v} ({}^3B_1)$ vdW Complex					
	Mode	Symmetry	Frequency (cm^{-1})	Intensity (km mol^{-1})	Description
def2QZVP	ω_1	a'	131 <i>i</i>	0.188	Intermolecular bend
	ω_2	a'	39	1.8068	Intermolecular stretch
	ω_3	a'	1594	0.5861	O_2 stretch
		zpe	9.8		
pVTZ	ω_1	b_2	127 <i>i</i>	0.1321	Intermolecular bend
	ω_2	a_1	39	1.6658	Intermolecular stretch
	ω_3	a_1	1575	1.0028	O_2 stretch
		zpe	9.6		
pVQZ	ω_1	b_2	130 <i>i</i>	0.1328	Intermolecular bend
	ω_2	a_1	40	1.6463	Intermolecular stretch
	ω_3	a_1	1592	0.9749	O_2 stretch
		zpe	9.8		
$\text{I}^- \cdots \text{O}_2$ $C_\infty ({}^3\Sigma)$ vdW Complex					
	Mode	Symmetry	Frequency (cm^{-1})	Intensity (km mol^{-1})	Description
def2QZVP	ω_1	π	132 <i>i</i>	0.4691	Degenerate intermolecular bend
	ω_2	π	132 <i>i</i>	0.4691	Degenerate intermolecular bend
	ω_3	σ	32	2.1958	Intermolecular stretch
	ω_4	σ	1569	12.8008	O_2 stretch
		zpe	9.6		
pVTZ	ω_1	π	127 <i>i</i>	0.393	Degenerate intermolecular bend
	ω_2	π	127 <i>i</i>	0.393	Degenerate intermolecular bend
	ω_3	σ	34	2.0674	Intermolecular stretch
	ω_4	σ	1550	13.6736	O_2 stretch
		zpe	9.5		
pVQZ	ω_1	π	131 <i>i</i>	0.3842	Degenerate intermolecular bend
	ω_2	π	131 <i>i</i>	0.3842	Degenerate intermolecular bend
	ω_3	σ	34	2.0388	Intermolecular stretch
	ω_4	σ	1568	12.699	O_2 stretch
		zpe	9.6		

Table B49: Calculated harmonic frequencies and mode assignments for the Cl...O₂ complex. All frequencies and intensities are in cm⁻¹ and km mol⁻¹ respectively.

Cl...O ₂ <i>C</i> _{2v} (⁴ B ₁) vdW Complex					
	Mode	Symmetry	Frequency (cm ⁻¹)	Intensity (km mol ⁻¹)	Description
def2QZVP	ω_1	<i>b</i> ₂	102 <i>i</i>	0.004	Intermolecular bend
	ω_2	<i>a</i> ₁	54	0.1462	Intermolecular stretch
	ω_3	<i>a</i> ₁	1585	0.3425	O ₂ stretch
		zpe	9.8		
pVTZ	ω_1	<i>b</i> ₂	95 <i>i</i>	0.002	Intermolecular bend
	ω_2	<i>a</i> ₁	57	0.1532	Intermolecular stretch
	ω_3	<i>a</i> ₁	1566	0.3571	O ₂ stretch
		zpe	9.7		
pVQZ	ω_1	<i>b</i> ₂	101 <i>i</i>	0.0027	Intermolecular bend
	ω_2	<i>a</i> ₁	54	0.1454	Intermolecular stretch
	ω_3	<i>a</i> ₁	1584	0.3341	O ₂ stretch
		zpe	9.8		
Cl...O ₂ <i>C</i> _∞ (⁴ Σ) vdW Complex					
	Mode	Symmetry	Frequency (cm ⁻¹)	Intensity (km mol ⁻¹)	Description
def2QZVP	ω_1	π	119 <i>i</i>	0.0031	Degenerate intermolecular bend
	ω_2	π	119 <i>i</i>	0.0031	Degenerate intermolecular bend
	ω_3	σ	46	0.0997	Intermolecular stretch
	ω_4	σ	1592	0.0039	O ₂ stretch
		zpe	9.8		
pVTZ	ω_1	σ	113 <i>i</i>	0.004	Degenerate intermolecular bend
	ω_2	π	113 <i>i</i>	0.004	Degenerate intermolecular bend
	ω_3	π	48	0.1014	Intermolecular stretch
	ω_4	σ	1575	0.004	O ₂ stretch
		zpe	9.7		
pVQZ	ω_1	π	118 <i>i</i>	0.0037	Degenerate intermolecular bend
	ω_2	π	118 <i>i</i>	0.0037	Degenerate intermolecular bend
	ω_3	σ	48	0.1052	Intermolecular stretch
	ω_4	σ	1592	0.0031	O ₂ stretch
		zpe	9.8		

Table B50: Calculated harmonic frequencies and mode assignments for the Br...O₂ complex. All frequencies and intensities are in cm⁻¹ and km mol⁻¹ respectively.

Br ... O ₂ <i>C</i> _{2v} (⁴ B ₁) vdW Complex					
	Mode	Symmetry	Frequency (cm ⁻¹)	Intensity (km mol ⁻¹)	Description
def2QZVP	ω_1	<i>b</i> ₂	103 <i>i</i>	0.001	Intermolecular bend
	ω_2	<i>a</i> ₁	49	0.1173	Intermolecular stretch
	ω_3	<i>a</i> ₁	1584	0.2877	O ₂ stretch
		zpe	9.8		
pVTZ	ω_1	<i>b</i> ₂	94 <i>i</i>	0	Intermolecular bend
	ω_2	<i>a</i> ₁	53	0.1299	Intermolecular stretch
	ω_3	<i>a</i> ₁	1566	0.2927	O ₂ stretch
		zpe	9.7		
pVQZ	ω_1	<i>b</i> ₂	99 <i>i</i>	0	Intermolecular bend
	ω_2	<i>a</i> ₁	53	0.1314	Intermolecular stretch
	ω_3	<i>a</i> ₁	1583	0.2879	O ₂ stretch
		zpe	9.8		
Br ... O ₂ <i>C</i> _∞ (⁴ Σ) vdW Complex					
	Mode	Symmetry	Frequency (cm ⁻¹)	Intensity (km mol ⁻¹)	Description
def2QZVP	ω_1	π	120 <i>i</i>	0.005	Degenerate intermolecular bend
	ω_2	π	120 <i>i</i>	0.005	Degenerate intermolecular bend
	ω_3	σ	43	0.0924	Intermolecular stretch
	ω_4	σ	1592	0	O ₂ stretch
		zpe	9.8		
pVTZ	ω_1	π	114 <i>i</i>	0.0062	Degenerate intermolecular bend
	ω_2	π	114 <i>i</i>	0.0062	Degenerate intermolecular bend
	ω_3	σ	45	0.1063	Intermolecular stretch
	ω_4	σ	1574	0.0003	O ₂ stretch
		zpe	9.7		
pVQZ	ω_1	π	117 <i>i</i>	0.0059	Degenerate intermolecular bend
	ω_2	π	117 <i>i</i>	0.0059	Degenerate intermolecular bend
	ω_3	σ	47	0.1147	Intermolecular stretch
	ω_4	σ	1592	0.0006	O ₂ stretch
		zpe	9.8		

Table B51: Calculated harmonic frequencies and mode assignments for the I...O₂ complex. All frequencies and intensities are in cm⁻¹ and km mol⁻¹ respectively.

I...O ₂ <i>C</i> _{2v} (⁴ B ₁) vdW Complex					
	Mode	Symmetry	Frequency (cm ⁻¹)	Intensity (km mol ⁻¹)	Description
def2QZVP	ω_1	<i>b</i> ₂	105 <i>i</i>	0.0015	Intermolecular bend
	ω_2	<i>a</i> ₁	44	0.1105	Intermolecular stretch
	ω_3	<i>a</i> ₁	1584	0.1934	O ₂ stretch
		zpe	9.7		
pVTZ	ω_1	<i>b</i> ₂	97 <i>i</i>	0.0029	Intermolecular bend
	ω_2	<i>a</i> ₁	46	0.1192	Intermolecular stretch
	ω_3	<i>a</i> ₁	1566	0.1803	O ₂ stretch
		zpe	9.6		
pVQZ	ω_1	<i>b</i> ₂	103 <i>i</i>	0.0023	Intermolecular bend
	ω_2	<i>a</i> ₁	45	0.1163	Intermolecular stretch
	ω_3	<i>a</i> ₁	1583	0.1776	O ₂ stretch
		zpe	9.7		
I...O ₂ <i>C</i> _∞ (⁴ Σ) vdW Complex					
	Mode	Symmetry	Frequency (cm ⁻¹)	Intensity (km mol ⁻¹)	Description
def2QZVP	ω_1	π	120 <i>i</i>	0.0042	Degenerate intermolecular bend
	ω_2	π	120 <i>i</i>	0.0042	Degenerate intermolecular bend
	ω_3	σ	43	0.119	Intermolecular stretch
	ω_4	σ	1591	0.0295	O ₂ stretch
		zpe	9.8		
pVTZ	ω_1	π	114 <i>i</i>	0.0074	Degenerate intermolecular bend
	ω_2	π	114 <i>i</i>	0.0074	Degenerate intermolecular bend
	ω_3	σ	46	0.1222	Intermolecular stretch
	ω_4	σ	1573	0.026	O ₂ stretch
		zpe	9.7		
pVQZ	ω_1	π	118 <i>i</i>	0.0071	Degenerate intermolecular bend
	ω_2	π	118 <i>i</i>	0.0071	Degenerate intermolecular bend
	ω_3	σ	46	0.1333	Intermolecular stretch
	ω_4	σ	1591	0.0299	O ₂ stretch
		zpe	9.8		

Table B52: Cartesian coordinates of the geometries of halide-oxygen complexes optimised with the DSD-PBEP86-D3BJ functional, in Å.

		$\text{Cl}^- \cdots \text{O}_2$			$\text{Br}^- \cdots \text{O}_2$			$\text{I}^- \cdots \text{O}_2$			
		x	y	z	x	y	z	x	y	z	
C_s ($^3A''$)	def2QZVP	X	0.000000	1.705990	0.000000	0.000000	1.166757	0.000000	0.000000	0.926068	0.000000
		O	0.570740	-1.620952	0.000000	0.557186	-2.323602	0.000000	0.553859	-2.830807	0.000000
		O	-0.570740	-2.004278	0.000000	-0.557186	-2.780960	0.000000	-0.553859	-3.304393	0.000000
	pVTZ	X	0.567587	1.620439	0.000000	0.000000	1.173312	0.000000	0.000000	0.931961	0.000000
		O	0.000000	-1.686918	0.000000	0.535460	-2.286370	0.000000	0.517259	-2.774258	0.000000
		O	-1.206123	-1.756516	0.000000	-0.535460	-2.846871	0.000000	-0.517259	-3.399986	0.000000
	pVQZ	X	0.000000	1.703108	0.000000	0.000000	1.165178	0.000000	0.000000	0.924255	0.000000
		O	0.592273	-1.702233	0.000000	0.557254	-2.319914	0.000000	0.553035	-2.822505	0.000000
		O	-0.592273	-1.916871	0.000000	-0.557254	-2.777740	0.000000	-0.553035	-3.300687	0.000000
		x	y	z	x	y	z	x	y	z	
C_{2v} (3B_1)	def2QZVP	X	0.000000	0.000000	-1.693497	0.000000	1.155675	0.000000	0.000000	0.919965	0.000000
		O	0.000000	-0.601593	1.799287	0.601682	-2.527918	0.000000	0.601815	-3.048000	0.000000
		O	0.000000	0.601593	1.799287	-0.601682	-2.528159	0.000000	-0.601815	-3.046768	0.000000
	pVTZ	X	0.000000	0.000000	1.694845	0.000000	1.156168	0.000000	0.000000	0.919357	0.000000
		O	0.000000	0.603420	-1.800710	0.603526	-2.529031	0.000000	0.603633	-3.045369	0.000000
		O	0.000000	-0.603420	-1.800836	-0.603526	-2.529204	0.000000	-0.603633	-3.045369	0.000000
	pVQZ	X	0.000000	0.000000	1.698689	0.000000	1.153366	0.000000	0.000000	0.917077	0.000000
		O	0.000000	0.601780	-1.804857	0.601876	-2.522989	0.000000	0.601979	-3.038406	0.000000
		O	0.000000	-0.601780	-1.804857	-0.601876	-2.522989	0.000000	-0.601979	-3.037227	0.000000
		x	y	z	x	y	z	x	y	z	
C_∞ ($^3\Sigma$)	def2QZVP	X	0.000000	0.000000	1.947587	0.000000	0.000000	1.318907	0.000000	0.000000	1.040041
		O	0.000000	0.000000	-1.464987	0.000000	0.000000	-2.281055	0.000000	0.000000	-2.841417
		O	0.000000	0.000000	-2.673635	0.000000	0.000000	-3.489163	0.000000	0.000000	-4.048852
	pVTZ	X	0.000000	0.000000	1.943783	0.000000	0.000000	1.314630	0.000000	0.000000	1.032295
		O	0.000000	0.000000	-1.459225	0.000000	0.000000	-2.269952	0.000000	0.000000	-2.813969
		O	0.000000	0.000000	-2.671314	0.000000	0.000000	-3.481555	0.000000	0.000000	-4.024989
	pVQZ	X	0.000000	0.000000	1.948333	0.000000	0.000000	1.310994	0.000000	0.000000	1.034300
		O	0.000000	0.000000	-1.465801	0.000000	0.000000	-2.263699	0.000000	0.000000	-2.822335
		O	0.000000	0.000000	-2.674407	0.000000	0.000000	-3.471898	0.000000	0.000000	-4.029901

Table B53: Cartesian coordinates of the geometries of halogen-oxygen complexes optimised with the DSD-PBEP86-D3BJ functional, in Å.

		Cl ... O ₂			Br ... O ₂			I ... O ₂			
		x	y	z	x	y	z	x	y	z	
<i>C_{2v}</i> (⁴ A'')	def2QZVP	X	0.000000	0.000000	-1.539395	0.000000	0.000000	1.034536	0.000000	0.000000	0.810970
		O	0.000000	0.602756	1.635637	0.000000	0.602776	-2.263048	0.000000	0.602757	-2.686338
		O	0.000000	-0.602756	1.635637	0.000000	-0.602776	-2.263048	0.000000	-0.602757	-2.686338
	pVTZ	X	0.000000	0.000000	1.528942	0.000000	0.000000	1.021337	0.000000	0.000000	0.804053
		O	0.000000	0.604589	-1.624499	0.000000	0.604635	-2.234174	0.000000	0.604608	-2.663425
		O	0.000000	-0.604589	-1.624499	0.000000	-0.604635	-2.234174	0.000000	-0.604608	-2.663425
	pVQZ	X	0.000000	0.000000	1.535819	0.000000	0.000000	1.021989	0.000000	0.000000	0.807222
		O	0.000000	0.602900	-1.631807	0.000000	0.602964	-2.235602	0.000000	0.602923	-2.673924
		O	0.000000	-0.602900	-1.631807	0.000000	-0.602964	-2.235602	0.000000	-0.602923	-2.673924
		x	y	z	x	y	z	x	y	z	
<i>C_∞</i> (⁴ Σ)	def2QZVP	X	0.000000	0.000000	1.805653	0.000000	0.000000	1.203833	0.000000	0.000000	0.927252
		O	0.000000	0.000000	-1.316424	0.000000	0.000000	-2.031303	0.000000	0.000000	-2.469420
		O	0.000000	0.000000	-2.520589	0.000000	0.000000	-3.235466	0.000000	0.000000	-3.673626
	pVTZ	X	0.000000	0.000000	1.804848	0.000000	0.000000	1.193509	0.000000	0.000000	0.925979
		O	0.000000	0.000000	-1.313819	0.000000	0.000000	-2.006965	0.000000	0.000000	-2.463440
		O	0.000000	0.000000	-2.521483	0.000000	0.000000	-3.214635	0.000000	0.000000	-3.671168
	pVQZ	X	0.000000	0.000000	1.801359	0.000000	0.000000	1.187644	0.000000	0.000000	0.921444
		O	0.000000	0.000000	-1.311780	0.000000	0.000000	-1.995808	0.000000	0.000000	-2.450092
		O	0.000000	0.000000	-2.516107	0.000000	0.000000	-3.200136	0.000000	0.000000	-3.654476

Table B54: $\text{X}^- \cdots \text{C}_2\text{H}_4$ complex geometric parameters and D_0 values from DSD-PBEP86-D3BJ optimisations. zpe values are drawn from relevant harmonic frequency calculations.

		$R_{\text{X} \cdots \parallel}$	$R_{\text{C}-\text{H}}$	$R_{\text{C}=\text{C}}$	$\angle_{\text{X} \cdots \parallel - \text{C}}$	Dihedral	E_{DFT}	zpe	D_e	D_o	
		Å	Å	Å	°	°	E_h	kJ mol ⁻¹	kJ mol ⁻¹	kJ mol ⁻¹	
$\text{Cl}^- \cdots \text{C}_2\text{H}_4$	BifOut	def2QZVP	4.055	1.082	1.327	90.0	87.9	-538.4475557	133.9	-1.4	-1.8
	C_{2v} (1A_1)	pVTZ	4.088	1.083	1.329	90.0	88.0	-538.4252773	133.9	-1.8	-2.0
		pVQZ	4.147	1.082	1.328	90.0	88.0	-538.4521355	134.1	-1.9	-1.9
	BifPl	def2QZVP	3.521	1.085	1.330	90.0	0.0	-538.4570413	135.8	23.5	25.0
	C_{2v} (1A_1)	pVTZ	3.529	1.085	1.332	90.0	0.0	-538.4343507	135.4	22.0	23.4
		pVQZ	3.531	1.085	1.331	90.0	0.0	-538.4611063	135.6	21.7	23.1
	End	def2QZVP	4.134	1.082	1.331	0.0	NA	-538.4555920	134.9	19.7	20.3
	C_{2v} (1A_1)	pVTZ	4.149	1.083	1.333	0.0	NA	-538.4328090	134.3	17.9	18.3
		pVQZ	4.152	1.082	1.332	0.0	NA	-538.4595891	134.6	17.7	18.1
	HApp	def2QZVP	3.970	1.091	1.331	48.5	0.0	-538.4575113	135.8	24.7	26.3
	C_s ($^1A'$)	pVTZ	3.974	1.092	1.334	48.7	0.0	-538.4348550	135.5	23.3	24.8
		pVQZ	3.976	1.091	1.332	49.0	0.0	-538.4615400	135.7	22.8	24.3
$\text{Br}^- \cdots \text{C}_2\text{H}_4$	BifOut	def2QZVP	4.202	1.082	1.327	90.0	88.0	-2651.9233306	133.9	-1.2	-1.5
	C_{2v} (1A_1)	pVTZ	4.192	1.083	1.329	90.0	88.1	-494.7597711	133.9	-1.2	-1.3
		pVQZ	4.195	1.082	1.328	90.0	88.1	-494.8106543	134.1	-1.1	-1.2
	BifPl	def2QZVP	3.703	1.084	1.330	90.0	0.0	-2651.9317804	135.8	21.0	22.6
	C_{2v} (1A_1)	pVTZ	3.683	1.085	1.332	90.0	0.0	-494.7680598	135.4	20.6	22.0
		pVQZ	3.690	1.084	1.330	90.0	0.0	-494.8189530	135.8	20.7	22.2
	End	def2QZVP	4.319	1.083	1.331	0.0	NA	-2651.9303242	135.0	17.2	17.9
	C_{2v} (1A_1)	pVTZ	4.311	1.083	1.333	0.0	NA	-494.7665089	134.3	16.5	16.8
		pVQZ	4.309	1.082	1.331	0.0	NA	-494.8174215	134.6	16.6	17.0
	HApp	def2QZVP	4.156	1.085	1.331	50.1	0.0	-2651.9318574	135.8	21.2	22.7
	C_s ($^1A'$)	pVTZ	4.122	1.086	1.333	50.9	0.0	-494.7682645	135.8	21.1	22.9
		pVQZ	4.132	1.085	1.331	50.9	0.0	-494.8189657	135.6	20.7	22.1

Table B55: $\text{X}^- \cdots \text{C}_2\text{H}_4$ complex geometric parameters from DSD-PBEP86-D3BJ optimisations. zpe values are drawn from relevant harmonic frequency calculations.

		$R_{\text{X}\cdots }$	$R_{\text{C}-\text{H}}$	$R_{\text{C}=\text{C}}$	$\angle_{\text{X}\cdots -\text{C}}$	Dihedral	E_{DFT}	zpe	D_e	D_o	
		\AA	\AA	\AA	$^\circ$	$^\circ$	E_h	kJ mol^{-1}	kJ mol^{-1}	kJ mol^{-1}	
$\text{I}^- \cdots \text{C}_2\text{H}_4$	BifOut	def2QZVP	4.508	1.082	1.327	90.0	88.2	-376.0134851	134.3	-1.3	-1.2
	$C_{2v} ({}^1A_1)$	pVTZ	4.462	1.083	1.329	90.0	90.0	-373.8071514	133.9	-1.2	-1.3
		pVQZ	4.408	1.082	1.328	90.0	88.2	-373.8589989	134.2	-0.5	-0.5
		BifPl	def2QZVP	4.023	1.084	1.330	90.0	0.0	-376.0203758	135.9	16.8
	$C_{2v} ({}^1A_1)$	pVTZ	3.934	1.085	1.332	90.0	0.0	-373.8145314	135.4	18.2	19.6
		pVQZ	3.936	1.084	1.330	90.0	0.0	-373.8660877	135.6	18.1	19.6
	End	def2QZVP	4.594	1.082	1.331	0.0	NA	-376.0192264	135.1	13.8	14.7
	$C_{2v} ({}^1A_1)$	pVTZ	4.572	1.083	1.333	0.0	NA	-373.8131132	134.4	14.5	14.8
		pVQZ	4.575	1.082	1.331	0.0	NA	-373.8646966	134.6	14.5	14.9
	HApp	def2QZVP	4.424	1.085	1.330	52.6	0.0	-376.0201783	135.8	16.3	17.8
	$C_s ({}^1A')$	pVTZ	4.352	1.086	1.332	54.9	0.0	-373.8143174	135.7	17.6	19.4
		pVQZ	3.936	1.085	1.330	90.0	0.0	-373.8660877	0.0	18.1	-116.1

Table B56: X...C₂H₄ complex geometric parameters and D_0 values from DSD-PBEP86-D3BJ optimisations. zpe values are drawn from relevant harmonic frequency calculations.

		$R_{X \cdots }$	R_{C-H}	$R_{C=C}$	$\angle_{X \cdots - C}$	Dihedral	E_{DFT}	zpe	D_e	D_o	
		Å	Å	Å	°	°	E_h	kJ mol ⁻¹	kJ mol ⁻¹	kJ mol ⁻¹	
$Cl \cdots C_2H_4$	BifOut	def2QZVP	2.467	1.081	1.352	90.0	90.0	-538.3358857	137.8	42.9	46.4
	$C_{2v} (^2A_1)$	pVTZ	2.462	1.082	1.354	90.0	90.0	-538.3116884	138.8	44.0	48.8
		pVQZ	2.459	1.081	1.352	90.0	90.0	-538.3371778	139.1	44.5	49.4
	$C_{2v} (^2A_1)$	BifPl	3.807	1.082	1.329	90.0	0.0	-538.3208903	135.2	3.5	4.4
		pVTZ	3.774	1.083	1.331	90.0	0.0	-538.2965380	134.9	4.3	5.1
		pVQZ	3.784	1.082	1.329	90.0	0.0	-538.3217340	134.1	3.9	3.9
	$C_{2v} (^2A_1)$	End	4.496	1.082	1.329	0.0	NA	-538.3203473	134.7	2.1	2.5
		pVTZ	4.462	1.083	1.331	0.0	NA	-538.2959186	134.4	2.6	3.0
		pVQZ	4.474	1.082	1.329	0.0	NA	-538.3211460	134.6	2.4	2.8
$Br \cdots C_2H_4$	BifOut	def2QZVP	2.662	1.081	1.347	90.0	90.0	-2651.8129239	137.9	35.4	39.0
	$C_{2v} (^2A_1)$	pVTZ	2.647	1.082	1.349	92.6	90.0	-494.6496280	138.2	37.3	41.5
		pVQZ	2.658	1.081	1.348	91.1	90.0	-494.6991756	138.5	38.4	42.7
	$C_{2v} (^2A_1)$	BifPl	3.943	1.082	1.329	91.3	0.0	-2651.8010190	135.1	4.2	5.0
		pVTZ	3.880	1.083	1.331	87.4	0.0	-494.6375171	134.9	5.5	6.4
		pVQZ	3.876	1.083	1.329	87.4	0.0	-494.6867041	134.4	5.7	5.9
	$C_{2v} (^2A_1)$	End	4.641	1.081	1.329	0.0	NA	-2651.8003720	138.2	2.5	6.4
		pVTZ	4.592	1.082	1.331	0.0	NA	-494.6367236	142.7	3.4	12.1
		pVQZ	4.569	1.082	1.329	0.0	NA	-494.6858765	136.0	3.5	5.3
$I \cdots C_2H_4$	BifOut	def2QZVP	2.932	1.082	1.342	90.0	90.0	-375.9055958	137.5	27.4	30.6
	$C_{2v} (^2A_1)$	pVTZ	2.939	1.083	1.343	90.0	90.0	-373.6995452	137.5	28.5	31.9
		pVQZ	2.954	1.082	1.342	87.2	90.0	-373.7497297	137.9	30.1	33.7
	$C_{2v} (^2A_1)$	BifPl	4.146	1.082	1.329	85.4	0.0	-375.8970111	136.8	4.8	7.3
		pVTZ	4.085	1.083	1.331	86.8	0.0	-373.6911592	137.2	6.4	9.7
		pVQZ	4.082	1.083	1.329	85.5	0.0	-373.7407626	138.7	6.5	11.0
	$C_{2v} (^2A_1)$	End	4.858	1.082	1.329	0.0	NA	-375.8962746	136.7	2.9	5.3
		pVTZ	4.796	1.083	1.331	0.0	NA	-373.6902362	135.8	4.0	5.8
		pVQZ	4.788	1.083	1.329	0.0	NA	-373.7398358	135.7	4.1	5.6

Table B57: $X^- \cdots C_2H_4$ complex VDEs from DSD-PBEP86-D3BJ optimisations. zpe values are drawn from relevant harmonic frequency calculations.

			E_{VDE} E_h	$VDE_{2P_{3/2}}$ eV	$VDE_{2P_{1/2}}$ eV	$ADE_{2P_{3/2}}$ eV	$ADE_{2P_{1/2}}$ eV
$Cl^- \cdots C_2H_4$	BifOut $C_{2v} ({}^1A_1)$	def2QZVP	-538.3195724				
		pVTZ	-538.2951167				
		pVQZ	-538.3203906				
	BifPl $C_{2v} ({}^1A_1)$	def2QZVP	-538.3199428	3.817	3.926		
		pVTZ	-538.2957294	3.797	3.906		
		pVQZ	-538.3209223	3.796	3.905		
	End $C_{2v} ({}^1A_1)$	def2QZVP	-538.3195152	3.804	3.913	3.794	3.903
		pVTZ	-538.2952249	3.781	3.890		
		pVQZ	-538.3204458	3.781	3.890		
	HApp $C_{2v} ({}^1A')$	def2QZVP	-538.318339	3.874	3.983	3.836	3.945
		pVTZ	-538.2941788	3.852	3.961	3.816	3.925
		pVQZ	-538.3193586	3.851	3.960	3.813	3.922
$Br^- \cdots C_2H_4$	BifOut $C_{2v} ({}^1A_1)$	def2QZVP	-2651.8011283				
		pVTZ	-494.6374407				
		pVQZ	-494.6865335				
	BifPl $C_{2v} ({}^1A_1)$	def2QZVP	-2651.8004338	3.527	3.984		
		pVTZ	-494.6370154	3.513	3.970		
		pVQZ	-494.6862272	3.510	3.967		
	End $C_{2v} ({}^1A_1)$	def2QZVP	-2651.79982	3.518	3.975	3.550	4.007
		pVTZ	-494.6362658	3.504	3.961		
		pVQZ	-494.685444	3.503	3.960		
	HApp $C_{2v} ({}^1A')$	def2QZVP	-2651.7991695	3.566	4.023	3.583	4.040
		pVTZ	-494.6364836	3.528	3.985	3.619	4.076
		pVQZ	-494.6855081	3.532	3.989	3.547	4.004

Table B58: $\text{X}^- \cdots \text{C}_2\text{H}_4$ complex VDEs from DSD-PBEP86-D3BJ optimisations. zpe values are drawn from relevant harmonic frequency calculations.

			E_{VDE}	$VDE_{2P_{3/2}}$	$VDE_{2P_{1/2}}$	$ADE_{2P_{3/2}}$	$ADE_{2P_{1/2}}$
		E_h	eV	eV	eV	eV	eV
$\text{I}^- \cdots \text{C}_2\text{H}_4$	BifOut	def2QZVP	-375.8955505				
	$C_{2v} (^1A_1)$	pVTZ	-373.7037521				
		pVQZ	-373.7389829				
	$C_{2v} (^1A_1)$	def2QZVP	-375.8967397	3.165	4.107	3.193	4.135
		pVTZ	-373.6909003	3.167	4.109	3.200	4.142
		pVQZ	-373.7405152	3.165	4.107	3.211	4.153
	End	def2QZVP	-375.8960107	3.166	4.108	3.188	4.130
		pVTZ	-373.6900002	3.166	4.108		
	$C_{2v} (^1A_1)$	pVQZ	-373.7396115	3.165	4.107		
		def2QZVP	-375.8957326	3.190	4.132	3.207	4.149
	$C_{2v} (^1A')$	pVTZ	-373.6898328	3.187	4.129	3.201	4.143
		pVQZ	-373.7405152	3.127	4.069	4.611	5.553

Table B59: Calculated harmonic frequencies and mode assignments for the $\text{Cl}^- \cdots \text{C}_2\text{H}_4$ complex. All frequencies and intensities are in cm^{-1} and km mol^{-1} respectively.

$\text{Cl}^- \cdots \text{C}_2\text{H}_4$ $C_{2v} (^1A_1)$ BifOut vdW Complex					
	Mode	Symmetry	Frequency (cm^{-1})	Intensity (km mol^{-1})	Description
def2QZVP	ω_1	b_2	74 <i>i</i>	0.1327	In plane intermol. bend
	ω_2	b_1	62 <i>i</i>	0.5869	C_2H_4 internal rotation
	ω_3	a_1	32	17.0338	Intermolecular stretch
	ω_4	b_1	847	0.0029	CH_2 symm rock
	ω_5	b_2	945	3.7835	CH_2 asymm wag
	ω_6	a_1	963	103.0111	CH_2 symm wag
	ω_7	a_2	1051	0	CH_2 twist
	ω_8	a_2	1257	0	CH_2 asymm rock
	ω_9	a_1	1384	0.5923	CH_2 symm scissor
	ω_{10}	b_2	1486	6.6909	CH_2 asymm scissor
	ω_{11}	a_1	1685	1.4123	$\text{C}=\text{C}$ stretch
	ω_{12}	b_2	3136	21.8013	CH_2 unpair symm stretch
	ω_{13}	a_1	3151	0.0014	CH_2 pair symm stretch
	ω_{14}	a_2	3212	0	CH_2 unpair asymm stretch
	ω_{15}	b_1	3239	26.9475	CH_2 unpair asymm stretch
pVTZ		zpe	133.9		
	ω_1	b_1	156 <i>i</i>	0.8847	C_2H_4 internal rotation
	ω_2	b_2	93 <i>i</i>	0.2612	In plane intermol. bend
	ω_3	a_1	28	16.4421	Intermolecular stretch
	ω_4	b_1	827	0.0027	CH_2 symm rock
	ω_5	b_2	938	4.3216	CH_2 asymm wag
	ω_6	a_1	953	109.235	CH_2 symm wag
	ω_7	a_2	1033	0	CH_2 twist
	ω_8	a_2	1246	0	CH_2 asymm rock
	ω_9	a_1	1381	0.8956	CH_2 symm scissor
	ω_{10}	b_2	1476	6.6882	CH_2 asymm scissor
	ω_{11}	a_1	1688	1.6298	$\text{C}=\text{C}$ stretch
	ω_{12}	b_2	3152	19.7149	CH_2 unpair symm stretch
	ω_{13}	a_1	3171	0.0774	CH_2 pair symm stretch
	ω_{14}	a_2	3231	0	CH_2 unpair asymm stretch
	ω_{15}	b_1	3259	24.2869	CH_2 pair asymm stretch
pVQZ		zpe	133.9		
	ω_1	b_1	154 <i>i</i>	0.8288	C_2H_4 internal rotation
	ω_2	b_2	91 <i>i</i>	0.2596	In plane intermol. bend
	ω_3	a_1	25	16.3506	Intermolecular stretch
	ω_4	b_1	830	0.0005	CH_2 symm rock
	ω_5	b_2	950	4.1068	CH_2 asymm wag
	ω_6	a_1	958	109.0714	CH_2 symm wag
	ω_7	a_2	1047	0	CH_2 twist
	ω_8	a_2	1250	0	CH_2 asymm rock
	ω_9	a_1	1382	0.8347	CH_2 symm scissor
	ω_{10}	b_2	1478	6.903	CH_2 asymm scissor
	ω_{11}	a_1	1689	1.54	$\text{C}=\text{C}$ stretch
	ω_{12}	b_2	3153	19.2479	CH_2 unpair symm stretch
	ω_{13}	a_1	3171	0.0978	CH_2 pair symm stretch
	ω_{14}	a_2	3234	0	CH_2 unpair asymm stretch
	ω_{15}	b_1	3261	23.3394	CH_2 pair asymm stretch
		zpe	134.1		

Table B60: Calculated harmonic frequencies and mode assignments for the $\text{Cl}^- \cdots \text{C}_2\text{H}_4$ complex. All frequencies and intensities are in cm^{-1} and km mol^{-1} respectively.

$\text{Cl}^- \cdots \text{C}_2\text{H}_4$ $C_{2v} ({}^1A_1)$ BifPl vdW Complex					
	Mode	Symmetry	Frequency (cm^{-1})	Intensity (km mol^{-1})	Description
def2QZVP	ω_1	b_2	82	0.1601	In plane internal rotation
	ω_2	a_1	107	18.7355	Intermolecular stretch
	ω_3	b_1	276	0.9098	OoP internal rotation
	ω_4	a_1	853	8.8812	CH_2 symm. rock
	ω_5	a_2	959	0	CH_2 asymm. wag
	ω_6	b_1	995	75.7179	CH_2 symm. wag
	ω_7	a_2	1094	0	CH_2 twist
	ω_8	b_2	1267	0.5784	CH_2 asymm. rock
	ω_9	a_1	1371	9.7341	CH_2 symm. scissor
	ω_{10}	b_2	1448	12.6496	CH_2 asymm. scissor
	ω_{11}	a_1	1662	13.4487	$\text{C}=\text{C}$ stretch
	ω_{12}	b_2	3089	37.5647	CH_2 unpair symm. stretch
	ω_{13}	a_1	3104	102.7836	CH_2 pair symm. stretch
	ω_{14}	b_2	3189	4.2636	CH_2 unpair asymm. stretch
	ω_{15}	a_1	3211	0.9283	CH_2 pair asymm. stretch
pVTZ		zpe	135.8		
	ω_1	b_2	23	0.2517	In plane internal rotation
	ω_2	a_1	105	18.5563	Intermolecular stretch
	ω_3	b_1	234	1.015	OoP internal rotation
	ω_4	a_1	832	8.2187	CH_2 symm. rock
	ω_5	a_2	970	0	CH_2 asymm. wag
	ω_6	b_1	986	77.8935	CH_2 symm. wag
	ω_7	a_2	1075	0	CH_2 twist
	ω_8	b_2	1256	0.6603	CH_2 asymm. rock
	ω_9	a_1	1368	9.8751	CH_2 symm. scissor
	ω_{10}	b_2	1440	12.6795	CH_2 asymm. scissor
	ω_{11}	a_1	1665	15.3944	$\text{C}=\text{C}$ stretch
	ω_{12}	b_2	3108	34.0231	CH_2 unpair symm. stretch
	ω_{13}	a_1	3127	92.1963	CH_2 pair symm. stretch
	ω_{14}	b_2	3210	4.7755	CH_2 unpair asymm. stretch
	ω_{15}	a_1	3233	1.4227	CH_2 pair asymm. stretch
pVQZ		zpe	135.4		
	ω_1	b_2	28	0.2562	In plane internal rotation
	ω_2	a_1	103	18.5658	Intermolecular stretch
	ω_3	b_1	232	0.9544	OoP internal rotation
	ω_4	a_1	836	8.2506	CH_2 symm. rock
	ω_5	a_2	979	0	CH_2 asymm. wag
	ω_6	b_1	988	77.3198	CH_2 symm. wag
	ω_7	a_2	1087	0	CH_2 twist
	ω_8	b_2	1259	0.6745	CH_2 asymm. rock
	ω_9	a_1	1369	9.8461	CH_2 symm. scissor
	ω_{10}	b_2	1442	12.894	CH_2 asymm. scissor
	ω_{11}	a_1	1667	15.3793	$\text{C}=\text{C}$ stretch
	ω_{12}	b_2	3110	33.5696	CH_2 unpair symm. stretch
	ω_{13}	a_1	3126	91.0359	CH_2 pair symm. stretch
	ω_{14}	b_2	3212	4.8726	CH_2 unpair asymm. stretch
	ω_{15}	a_1	3235	1.471	CH_2 pair asymm. stretch
		zpe	135.6		

Table B61: Calculated harmonic frequencies and mode assignments for the $\text{Cl}^- \cdots \text{C}_2\text{H}_4$ complex. All frequencies and intensities are in cm^{-1} and km mol^{-1} respectively.

$\text{Cl}^- \cdots \text{C}_2\text{H}_4$ $C_{2v} (^1A_1)$ End vdW Complex					
	Mode	Symmetry	Frequency (cm^{-1})	Intensity (km mol^{-1})	Description
def2QZVP	ω_1	b_2	36	1.7546	In plane internal rotation
	ω_2	b_1	89	1.0112	OoP internal rotation
	ω_3	a_1	96	19.8357	Intermolecular stretch
	ω_4	b_2	804	0.2935	CH_2 symm. rock
	ω_5	b_1	939	49.0786	Farside CH_2 wag
	ω_6	b_1	1070	35.6888	Nearside CH_2 wag
	ω_7	a_2	1083	0	CH_2 twist
	ω_8	b_2	1228	0.9365	CH_2 asymm. rock
	ω_9	a_1	1359	35.6712	CH_2 symm. scissor
	ω_{10}	a_1	1477	28.9938	CH_2 asymm. scissor
	ω_{11}	a_1	1666	0.0673	$\text{C}=\text{C}$ stretch
	ω_{12}	a_1	3113	28.1136	Farside CH_2 symm. stretch
	ω_{13}	a_1	3161	2.68	Nearside CH_2 symm. stretch
	ω_{14}	b_2	3184	25.591	Farside CH_2 asymm. stretch
	ω_{15}	b_2	3241	8.052	Nearside CH_2 asymm. stretch
pVTZ	zpe		134.9		
	ω_1	b_2	75 <i>i</i>	1.6556	In plane internal rotation
	ω_2	b_1	68	0.9121	OoP internal rotation
	ω_3	a_1	92	19.0953	Intermolecular stretch
	ω_4	b_2	783	0.1411	CH_2 symm. rock
	ω_5	b_1	923	44.7553	Farside CH_2 wag
	ω_6	b_1	1048	38.0344	Nearside CH_2 wag
	ω_7	a_2	1058	0	CH_2 twist
	ω_8	b_2	1217	0.9833	CH_2 asymm. rock
	ω_9	a_1	1356	34.4686	CH_2 symm. scissor
	ω_{10}	a_1	1466	28.9295	CH_2 asymm. scissor
	ω_{11}	a_1	1670	0.0912	$\text{C}=\text{C}$ stretch
	ω_{12}	a_1	3132	26.1584	Farside CH_2 symm. stretch
	ω_{13}	a_1	3179	2.7962	Nearside CH_2 symm. stretch
pVQZ	ω_{14}	b_2	3205	23.4361	Farside CH_2 asymm. stretch
	ω_{15}	b_2	3260	7.7758	Nearside CH_2 asymm. stretch
	zpe		134.3		
	ω_1	b_2	74 <i>i</i>	1.6346	In plane internal rotation
	ω_2	b_1	67	0.8991	OoP internal rotation
	ω_3	a_1	91	19.1179	Intermolecular stretch
	ω_4	b_2	787	0.1583	CH_2 symm. rock
	ω_5	b_1	930	46.3071	Farside CH_2 wag
	ω_6	b_1	1052	35.797	Nearside CH_2 wag
	ω_7	a_2	1075	0	CH_2 twist
	ω_8	b_2	1221	0.9868	CH_2 asymm. rock
	ω_9	a_1	1358	34.0268	CH_2 symm. scissor
	ω_{10}	a_1	1468	29.281	CH_2 asymm. scissor
	ω_{11}	a_1	1671	0.0954	$\text{C}=\text{C}$ stretch
	ω_{12}	a_1	3133	26.3244	Farside CH_2 symm. stretch
	ω_{13}	a_1	3179	2.5644	Nearside CH_2 symm. stretch
	ω_{14}	b_2	3208	23.2194	Farside CH_2 asymm. stretch
	ω_{15}	b_2	3262	7.4027	Nearside CH_2 asymm. stretch
	zpe		134.6		

Table B62: Calculated harmonic frequencies and mode assignments for the $\text{Cl}^- \cdots \text{C}_2\text{H}_4$ complex. All frequencies and intensities are in cm^{-1} and km mol^{-1} respectively.

$\text{Cl}^- \cdots \text{C}_2\text{H}_4$ $C_s ({}^1A')$ HApp vdW Complex					
	Mode	Symmetry	Frequency (cm^{-1})	Intensity (km mol^{-1})	Description
def2QZVP	ω_1	a'	83	8.8088	In plane internal rotation
	ω_2	a'	139	18.6605	Intermolecular stretch
	ω_3	a''	230	0.0272	OoP internal rotation
	ω_4	a'	861	0.0399	CH_2 symm. rock
	ω_5	a''	940	38.4126	Farside CH_2 wag
	ω_6	a''	1039	36.8613	Nearside CH_2 wag
	ω_7	a''	1111	6.2868	$\text{C}=\text{C}$ twist
	ω_8	a'	1260	3.2527	$\text{C}=\text{C}$ rock
	ω_9	a'	1381	3.7993	CH_2 symm. scissor
	ω_{10}	a'	1494	5.7863	CH_2 asymm. scissor
	ω_{11}	a'	1671	5.177	$\text{C}=\text{C}$ stretch
	ω_{12}	a'	3036	238.5303	Nearside CH_2 symm. stretch
	ω_{13}	a'	3109	54.0287	Farside CH_2 symm. stretch
	ω_{14}	a'	3160	36.8221	Nearside CH_2 asymm. stretch
	ω_{15}	a'	3198	23.3878	Farside CH_2 asymm. stretch
pVTZ	zpe		135.8		
	ω_1	a'	54	3.5908	In plane internal rotation
	ω_2	a'	128	22.9739	Intermolecular stretch
	ω_3	a''	184	0.1205	OoP internal rotation
	ω_4	a'	840	0.162	CH_2 symm. rock
	ω_5	a''	933	41.9717	Farside CH_2 wag
	ω_6	a''	1030	30.0713	Nearside CH_2 wag
	ω_7	a''	1098	7.534	$\text{C}=\text{C}$ twist
	ω_8	a'	1249	3.0091	$\text{C}=\text{C}$ rock
	ω_9	a'	1378	3.1008	CH_2 symm. scissor
	ω_{10}	a'	1484	5.1019	CH_2 asymm. scissor
	ω_{11}	a'	1675	6.5419	$\text{C}=\text{C}$ stretch
	ω_{12}	a'	3063	209.5337	Nearside CH_2 symm. stretch
	ω_{13}	a'	3129	56.5787	Farside CH_2 symm. stretch
	ω_{14}	a'	3182	37.9033	Nearside CH_2 asymm. stretch
	ω_{15}	a'	3219	20.5623	Farside CH_2 asymm. stretch
pVQZ	zpe		135.5		
	ω_1	a'	53	3.5862	In plane internal rotation
	ω_2	a'	127	22.9131	Intermolecular stretch
	ω_3	a''	182	0.1131	OoP internal rotation
	ω_4	a'	844	0.1462	CH_2 symm. rock
	ω_5	a''	941	44.5281	Farside CH_2 wag
	ω_6	a''	1037	28.4483	Nearside CH_2 wag
	ω_7	a''	1105	5.8108	$\text{C}=\text{C}$ twist
	ω_8	a'	1252	2.8779	$\text{C}=\text{C}$ rock
	ω_9	a'	1380	2.8677	CH_2 symm. scissor
	ω_{10}	a'	1486	4.9954	CH_2 asymm. scissor
	ω_{11}	a'	1676	6.7204	$\text{C}=\text{C}$ stretch
	ω_{12}	a'	3064	207.144	Nearside CH_2 symm. stretch
	ω_{13}	a'	3130	53.2625	Farside CH_2 symm. stretch
	ω_{14}	a'	3185	37.9955	Nearside CH_2 asymm. stretch
	ω_{15}	a'	3222	19.8197	Farside CH_2 asymm. stretch
	zpe		135.7		

Table B63: Calculated harmonic frequencies and mode assignments for the $\text{Br}^- \cdots \text{C}_2\text{H}_4$ complex. All frequencies and intensities are in cm^{-1} and km mol^{-1} respectively.

$\text{Br}^- \cdots \text{C}_2\text{H}_4$ C_{2v} (1A_1) BifOut vdW Complex					
	Mode	Symmetry	Frequency (cm^{-1})	Intensity (km mol^{-1})	Description
def2QZVP	ω_1	b_2	68 <i>i</i>	0.001	In plane intermol. bend
	ω_2	b_1	40 <i>i</i>	0.3576	C_2H_4 internal rotation
	ω_3	a_1	29	5.0245	Intermolecular stretch
	ω_4	b_1	848	0.0032	CH_2 symm. rock
	ω_5	b_2	948	3.4723	CH_2 asymm. wag
	ω_6	a_1	965	107.3703	CH_2 symm. wag
	ω_7	a_2	1053	0	CH_2 twist
	ω_8	a_2	1257	0	CH_2 asymm. rock
	ω_9	a_1	1384	0.5158	CH_2 symm. scissor
	ω_{10}	b_2	1486	6.8135	CH_2 asymm. scissor
	ω_{11}	a_1	1685	1.1677	$\text{C}=\text{C}$ stretch
	ω_{12}	b_2	3136	20.5737	CH_2 unpair symm. stretch
	ω_{13}	a_1	3151	0.0001	CH_2 pair symm. stretch
	ω_{14}	a_2	3212	0	CH_2 unpair asymm. stretch
	ω_{15}	b_1	3239	25.513	CH_2 unpair asymm. stretch
pVTZ	zpe		133.9		
	ω_1	b_1	152 <i>i</i>	0.6751	C_2H_4 internal rotation
	ω_2	b_2	90 <i>i</i>	0.0199	In plane intermol. bend
	ω_3	a_1	27	4.7452	Intermolecular stretch
	ω_4	b_1	826	0.003	CH_2 symm. rock
	ω_5	b_2	938	4.2763	CH_2 asymm. wag
	ω_6	a_1	955	115.1935	CH_2 symm. wag
	ω_7	a_2	1033	0	CH_2 twist
	ω_8	a_2	1246	0	CH_2 asymm. rock
	ω_9	a_1	1381	0.8067	CH_2 symm. scissor
	ω_{10}	b_2	1476	6.5932	CH_2 asymm. scissor
	ω_{11}	a_1	1687	1.3847	$\text{C}=\text{C}$ stretch
	ω_{12}	b_2	3151	18.2079	CH_2 unpair symm. stretch
	ω_{13}	a_1	3171	0.0449	CH_2 pair symm. stretch
	ω_{14}	a_2	3231	0	CH_2 unpair asymm. stretch
	ω_{15}	b_1	3259	22.3355	CH_2 pair asymm. stretch
pVQZ	zpe		133.9		
	ω_1	b_1	151 <i>i</i>	0.6418	C_2H_4 internal rotation
	ω_2	b_2	89 <i>i</i>	0.0172	In plane intermol. bend
	ω_3	a_1	26	4.7535	Intermolecular stretch
	ω_4	b_1	830	0.0012	CH_2 symm. rock
	ω_5	b_2	950	4.2006	CH_2 asymm. wag
	ω_6	a_1	958	115.0636	CH_2 symm. wag
	ω_7	a_2	1047	0	CH_2 twist
	ω_8	a_2	1250	0	CH_2 asymm. rock
	ω_9	a_1	1382	0.7838	CH_2 symm. scissor
	ω_{10}	b_2	1478	6.7412	CH_2 asymm. scissor
	ω_{11}	a_1	1689	1.4014	$\text{C}=\text{C}$ stretch
	ω_{12}	b_2	3153	18.0504	CH_2 unpair symm. stretch
	ω_{13}	a_1	3171	0.0612	CH_2 pair symm. stretch
	ω_{14}	a_2	3234	0	CH_2 unpair asymm. stretch
	ω_{15}	b_1	3261	21.7628	CH_2 pair asymm. stretch
	zpe		134.1		

Table B64: Calculated harmonic frequencies and mode assignments for the $\text{Br}^- \cdots \text{C}_2\text{H}_4$ complex. All frequencies and intensities are in cm^{-1} and km mol^{-1} respectively.

$\text{Br}^- \cdots \text{C}_2\text{H}_4$ C_{2v} (1A_1) BifPl vdW Complex					
	Mode	Symmetry	Frequency (cm^{-1})	Intensity (km mol^{-1})	Description
def2QZVP	ω_1	a_1	87	5.418	Intermolecular stretch
	ω_2	b_2	93	0.0194	In plane internal rotation
	ω_3	b_1	264	1.316	OoP internal rotation
	ω_4	a_1	853	8.2173	CH_2 symm. rock
	ω_5	a_2	960	0	CH_2 asymm. wag
	ω_6	b_1	994	73.9266	CH_2 symm. wag
	ω_7	a_2	1092	0	CH_2 twist
	ω_8	b_2	1267	0.7501	CH_2 asymm. rock
	ω_9	a_1	1374	9.5463	CH_2 symm. scissor
	ω_{10}	b_2	1456	12.6125	CH_2 asymm. scissor
	ω_{11}	a_1	1664	13.7292	$\text{C}=\text{C}$ stretch
	ω_{12}	b_2	3094	34.5103	CH_2 unpair symm. stretch
	ω_{13}	a_1	3108	94.0627	CH_2 pair symm. stretch
	ω_{14}	b_2	3191	3.8374	CH_2 unpair asymm. stretch
	ω_{15}	a_1	3213	1.6328	CH_2 pair asymm. stretch
pVTZ		zpe	135.8		
	ω_1	b_2	38	0.0006	In plane internal rotation
	ω_2	a_1	86	5.2281	Intermolecular stretch
	ω_3	b_1	225	1.7926	OoP internal rotation
	ω_4	a_1	832	7.997	CH_2 symm. rock
	ω_5	a_2	968	0	CH_2 asymm. wag
	ω_6	b_1	985	73.0119	CH_2 symm. wag
	ω_7	a_2	1073	0	CH_2 twist
	ω_8	b_2	1255	0.9295	CH_2 asymm. rock
	ω_9	a_1	1369	10.5038	CH_2 symm. scissor
	ω_{10}	b_2	1444	13.2249	CH_2 asymm. scissor
	ω_{11}	a_1	1667	16.3686	$\text{C}=\text{C}$ stretch
	ω_{12}	b_2	3112	31.9583	CH_2 unpair symm. stretch
	ω_{13}	a_1	3130	86.5713	CH_2 pair symm. stretch
	ω_{14}	b_2	3211	4.3278	CH_2 unpair asymm. stretch
	ω_{15}	a_1	3234	2.4854	CH_2 pair asymm. stretch
pVQZ		zpe	135.4		
	ω_1	b_2	56	0.0002	In plane internal rotation
	ω_2	a_1	86	5.2135	Intermolecular stretch
	ω_3	b_1	224	1.6399	OoP internal rotation
	ω_4	a_1	836	7.9208	CH_2 symm. rock
	ω_5	a_2	982	0	CH_2 asymm. wag
	ω_6	b_1	988	72.7803	CH_2 symm. wag
	ω_7	a_2	1086	0	CH_2 twist
	ω_8	b_2	1259	0.9012	CH_2 asymm. rock
	ω_9	a_1	1371	10.2742	CH_2 symm. scissor
	ω_{10}	b_2	1449	13.3597	CH_2 asymm. scissor
	ω_{11}	a_1	1669	16.1977	$\text{C}=\text{C}$ stretch
	ω_{12}	b_2	3114	31.4401	CH_2 unpair symm. stretch
	ω_{13}	a_1	3130	84.9194	CH_2 pair symm. stretch
	ω_{14}	b_2	3213	4.437	CH_2 unpair asymm. stretch
	ω_{15}	a_1	3236	2.5801	CH_2 pair asymm. stretch
		zpe	135.8		

Table B65: Calculated harmonic frequencies and mode assignments for the $\text{Br}^- \cdots \text{C}_2\text{H}_4$ complex. All frequencies and intensities are in cm^{-1} and km mol^{-1} respectively.

$\text{Br}^- \cdots \text{C}_2\text{H}_4$ $C_{2v} (^1A_1)$ End vdW Complex					
	Mode	Symmetry	Frequency (cm^{-1})	Intensity (km mol^{-1})	Description
def2QZVP	ω_1	b_2	55	0.6514	In plane internal rotation
	ω_2	a_1	78	5.9383	Intermolecular stretch
	ω_3	b_1	87	0.2961	OoP internal rotation
	ω_4	b_2	810	0.3449	CH_2 symm. rock
	ω_5	b_1	943	48.3582	Farside CH_2 wag
	ω_6	b_1	1064	34.9266	Nearside CH_2 wag
	ω_7	a_2	1083	0	CH_2 twist
	ω_8	b_2	1232	1.0795	CH_2 asymm. rock
	ω_9	a_1	1362	32.4929	CH_2 symm. scissor
	ω_{10}	a_1	1479	30.3723	CH_2 asymm. scissor
	ω_{11}	a_1	1668	0.001	$\text{C}=\text{C}$ stretch
	ω_{12}	a_1	3116	27.3057	Farside CH_2 symm. stretch
	ω_{13}	a_1	3159	1.884	Nearside CH_2 symm. stretch
	ω_{14}	b_2	3187	22.9475	Farside CH_2 asymm. stretch
	ω_{15}	b_2	3241	8.2374	Nearside CH_2 asymm. stretch
pVTZ	zpe		135		
	ω_1	b_2	69 <i>i</i>	0.6378	In plane internal rotation
	ω_2	b_1	64	0.2007	OoP internal rotation
	ω_3	a_1	75	5.5455	Intermolecular stretch
	ω_4	b_2	788	0.2465	CH_2 symm. rock
	ω_5	b_1	927	43.5251	Farside CH_2 wag
	ω_6	b_1	1044	35.7651	Nearside CH_2 wag
	ω_7	a_2	1058	0	CH_2 twist
	ω_8	b_2	1220	1.3555	CH_2 asymm. rock
	ω_9	a_1	1359	32.8618	CH_2 symm. scissor
	ω_{10}	a_1	1468	30.6295	CH_2 asymm. scissor
	ω_{11}	a_1	1672	0.003	$\text{C}=\text{C}$ stretch
	ω_{12}	a_1	3134	26.096	Farside CH_2 symm. stretch
	ω_{13}	a_1	3177	1.9546	Nearside CH_2 symm. stretch
	ω_{14}	b_2	3208	20.9315	Farside CH_2 asymm. stretch
	ω_{15}	b_2	3259	7.9844	Nearside CH_2 asymm. stretch
pVQZ	zpe		134.3		
	ω_1	b_2	62 <i>i</i>	0.6245	In plane internal rotation
	ω_2	b_1	64	0.2016	OoP internal rotation
	ω_3	a_1	76	5.5292	Intermolecular stretch
	ω_4	b_2	793	0.2594	CH_2 symm. rock
	ω_5	b_1	933	44.9402	Farside CH_2 wag
	ω_6	b_1	1048	33.7885	Nearside CH_2 wag
	ω_7	a_2	1075	0	CH_2 twist
	ω_8	b_2	1224	1.3373	CH_2 asymm. rock
	ω_9	a_1	1361	32.2749	CH_2 symm. scissor
	ω_{10}	a_1	1470	31.3592	CH_2 asymm. scissor
	ω_{11}	a_1	1673	0.003	$\text{C}=\text{C}$ stretch
	ω_{12}	a_1	3135	26.2261	Farside CH_2 symm. stretch
	ω_{13}	a_1	3176	1.7923	Nearside CH_2 symm. stretch
	ω_{14}	b_2	3210	20.7629	Farside CH_2 asymm. stretch
	ω_{15}	b_2	3261	7.621	Nearside CH_2 asymm. stretch
	zpe		134.6		

Table B66: Calculated harmonic frequencies and mode assignments for the $\text{Br}^- \cdots \text{C}_2\text{H}_4$ complex. All frequencies and intensities are in cm^{-1} and km mol^{-1} respectively.

$\text{Br}^- \cdots \text{C}_2\text{H}_4$ $C_s ({}^1A')$ HApp vdW Complex					
	Mode	Symmetry	Frequency (cm^{-1})	Intensity (km mol^{-1})	Description
def2QZVP	ω_1	a'	69	3.5179	In plane internal rotation
	ω_2	a'	122	5.7324	Intermolecular stretch
	ω_3	a''	219	0.1357	OoP internal rotation
	ω_4	a'	858	0.0636	CH_2 symm. rock
	ω_5	a''	945	35.7507	Farside CH_2 wag
	ω_6	a''	1032	42.0203	Nearside CH_2 wag
	ω_7	a''	1101	3.9979	$\text{C}=\text{C}$ twist
	ω_8	a'	1260	2.9353	$\text{C}=\text{C}$ rock
	ω_9	a'	1381	2.3298	CH_2 symm. scissor
	ω_{10}	a'	1492	5.3354	CH_2 asymm. scissor
	ω_{11}	a'	1673	4.9219	$\text{C}=\text{C}$ stretch
	ω_{12}	a'	3062	171.4185	Nearside CH_2 symm. stretch
	ω_{13}	a'	3114	52.3683	Farside CH_2 symm. stretch
	ω_{14}	a'	3169	37.5042	Nearside CH_2 asymm. stretch
	ω_{15}	a'	3203	19.7355	Farside CH_2 asymm. stretch
pVTZ	zpe		135.8		
	ω_1	a'	71	3.1409	In plane internal rotation
	ω_2	a'	128	5.9071	Intermolecular stretch
	ω_3	a''	228	0.5296	OoP internal rotation
	ω_4	a'	856	0.2593	CH_2 symm. rock
	ω_5	a''	951	41.9635	Farside CH_2 wag
	ω_6	a''	1038	28.0875	Nearside CH_2 wag
	ω_7	a''	1101	4.3561	$\text{C}=\text{C}$ twist
	ω_8	a'	1258	2.8507	$\text{C}=\text{C}$ rock
	ω_9	a'	1379	2.1703	CH_2 symm. scissor
	ω_{10}	a'	1489	3.4935	CH_2 asymm. scissor
	ω_{11}	a'	1669	7.1271	$\text{C}=\text{C}$ stretch
	ω_{12}	a'	3058	180.2937	Nearside CH_2 symm. stretch
	ω_{13}	a'	3110	54.5539	Farside CH_2 symm. stretch
	ω_{14}	a'	3165	37.6241	Nearside CH_2 asymm. stretch
	ω_{15}	a'	3199	17.7562	Farside CH_2 asymm. stretch
pVQZ	zpe		135.8		
	ω_1	a'	41	0.9102	In plane internal rotation
	ω_2	a'	104	7.9251	Intermolecular stretch
	ω_3	a''	176	0.4621	OoP internal rotation
	ω_4	a'	841	0.2327	CH_2 symm. rock
	ω_5	a''	945	42.2846	Farside CH_2 wag
	ω_6	a''	1033	29.3688	Nearside CH_2 wag
	ω_7	a''	1097	3.4939	$\text{C}=\text{C}$ twist
	ω_8	a'	1252	2.7135	$\text{C}=\text{C}$ rock
	ω_9	a'	1379	1.7497	CH_2 symm. scissor
	ω_{10}	a'	1483	3.9627	CH_2 asymm. scissor
	ω_{11}	a'	1676	6.9636	$\text{C}=\text{C}$ stretch
	ω_{12}	a'	3082	158.3062	Nearside CH_2 symm. stretch
	ω_{13}	a'	3134	51.9974	Farside CH_2 symm. stretch
	ω_{14}	a'	3192	35.9324	Nearside CH_2 asymm. stretch
	ω_{15}	a'	3226	16.6705	Farside CH_2 asymm. stretch
	zpe		135.6		

Table B67: Calculated harmonic frequencies and mode assignments for the $\text{I}^- \cdots \text{C}_2\text{H}_4$ complex. All frequencies and intensities are in cm^{-1} and km mol^{-1} respectively.

		$\text{I}^- \cdots \text{C}_2\text{H}_4$			
		C_{2v} (1A_1)		BifOut	vdW Complex
	Mode	Symmetry	Frequency (cm^{-1})	Intensity (km mol^{-1})	Description
def2QZVP	ω_1	b_2	51 <i>i</i>	0.0012	In plane intermol. bend
	ω_2	a_1	24	2.2011	Intermolecular stretch
	ω_3	b_1	50	0.4082	C_2H_4 internal rotation
	ω_4	b_1	848	0.0023	CH_2 symm. rock
	ω_5	b_2	959	3.2336	CH_2 asymm. wag
	ω_6	a_1	970	117.535	CH_2 symm. wag
	ω_7	a_2	1058	0	CH_2 twist
	ω_8	a_2	1258	0	CH_2 asymm. rock
	ω_9	a_1	1384	0.3329	CH_2 symm. scissor
	ω_{10}	b_2	1487	6.8609	CH_2 asymm. scissor
	ω_{11}	a_1	1684	0.7235	$\text{C}=\text{C}$ stretch
	ω_{12}	b_2	3136	17.9334	CH_2 unpair symm. stretch
	ω_{13}	a_1	3151	0.0008	CH_2 pair symm. stretch
	ω_{14}	a_2	3212	0	CH_2 unpair asymm. stretch
	ω_{15}	b_1	3239	22.1829	CH_2 unpair asymm. stretch
pVTZ	zpe		134.3		
	ω_1	b_1	144 <i>i</i>	0.3006	C_2H_4 internal rotation
	ω_2	b_2	83 <i>i</i>	0.0002	In plane intermol. bend
	ω_3	a_1	23	2.0312	Intermolecular stretch
	ω_4	b_1	826	0.0008	CH_2 symm. rock
	ω_5	b_2	942	1.2288	CH_2 asymm. wag
	ω_6	a_1	957	120.4808	CH_2 symm. wag
	ω_7	a_2	1034	0	CH_2 twist
	ω_8	a_2	1246	0	CH_2 asymm. rock
	ω_9	a_1	1380	0.3621	CH_2 symm. scissor
	ω_{10}	b_2	1476	6.6515	CH_2 asymm. scissor
	ω_{11}	a_1	1687	0.9835	$\text{C}=\text{C}$ stretch
	ω_{12}	b_2	3151	16.8237	CH_2 unpair symm. stretch
	ω_{13}	a_1	3171	0.0034	CH_2 pair symm. stretch
	ω_{14}	a_2	3231	0	CH_2 unpair asymm. stretch
	ω_{15}	b_1	3259	20.6015	CH_2 pair asymm. stretch
pVQZ	zpe		133.9		
	ω_1	b_1	143 <i>i</i>	0.6651	C_2H_4 internal rotation
	ω_2	b_2	83 <i>i</i>	0.0078	In plane intermol. bend
	ω_3	a_1	27	2.0511	Intermolecular stretch
	ω_4	b_1	830	0.0012	CH_2 symm. rock
	ω_5	b_2	953	3.8432	CH_2 asymm. wag
	ω_6	a_1	961	122.3421	CH_2 symm. wag
	ω_7	a_2	1049	0	CH_2 twist
	ω_8	a_2	1250	0	CH_2 asymm. rock
	ω_9	a_1	1382	0.6204	CH_2 symm. scissor
	ω_{10}	b_2	1478	6.6923	CH_2 asymm. scissor
	ω_{11}	a_1	1688	1.0461	$\text{C}=\text{C}$ stretch
	ω_{12}	b_2	3153	16.2934	CH_2 unpair symm. stretch
	ω_{13}	a_1	3170	0.0328	CH_2 pair symm. stretch
	ω_{14}	a_2	3234	0	CH_2 unpair asymm. stretch
	ω_{15}	b_1	3261	19.6029	CH_2 pair asymm. stretch
	zpe		134.2		

Table B68: Calculated harmonic frequencies and mode assignments for the $\text{I}^- \cdots \text{C}_2\text{H}_4$ complex. All frequencies and intensities are in cm^{-1} and km mol^{-1} respectively.

		$\text{I}^- \cdots \text{C}_2\text{H}_4$ C_{2v} (1A_1) BifPl vdW Complex			
	Mode	Symmetry	Frequency (cm^{-1})	Intensity (km mol^{-1})	Description
def2QZVP	ω_1	a_1	71	2.2233	Intermolecular stretch
	ω_2	b_2	94	0.0573	In plane internal rotation
	ω_3	b_1	246	1.4124	OoP internal rotation
	ω_4	a_1	852	7.4249	CH_2 symm. rock
	ω_5	a_2	971	0	CH_2 asymm. wag
	ω_6	b_1	993	69.8222	CH_2 symm. wag
	ω_7	a_2	1089	0	CH_2 twist
	ω_8	b_2	1266	1.0065	CH_2 asymm. rock
	ω_9	a_1	1376	9.4629	CH_2 symm. scissor
	ω_{10}	b_2	1464	12.5849	CH_2 asymm. scissor
	ω_{11}	a_1	1668	13.953	$\text{C}=\text{C}$ stretch
	ω_{12}	b_2	3101	30.4278	CH_2 unpair symm. stretch
	ω_{13}	a_1	3114	81.0132	CH_2 pair symm. stretch
	ω_{14}	b_2	3194	3.4116	CH_2 unpair asymm. stretch
	ω_{15}	a_1	3216	3.4029	CH_2 unpair asymm. stretch
pVTZ			zpe	135.9	
	ω_1	b_2	52	0.0263	In plane internal rotation
	ω_2	a_1	74	2.0329	Intermolecular stretch
	ω_3	b_1	205	2.0671	OoP internal rotation
	ω_4	a_1	831	7.05	CH_2 symm. rock
	ω_5	a_2	967	0	CH_2 asymm. wag
	ω_6	b_1	983	68.5478	CH_2 symm. wag
	ω_7	a_2	1071	0	CH_2 twist
	ω_8	b_2	1254	1.2199	CH_2 asymm. rock
	ω_9	a_1	1372	10.1875	CH_2 symm. scissor
	ω_{10}	b_2	1451	13.206	CH_2 asymm. scissor
	ω_{11}	a_1	1670	16.2979	$\text{C}=\text{C}$ stretch
	ω_{12}	b_2	3118	28.6775	CH_2 unpair symm. stretch
	ω_{13}	a_1	3134	75.4815	CH_2 pair symm. stretch
	ω_{14}	b_2	3214	3.7439	CH_2 unpair asymm. stretch
	ω_{15}	a_1	3236	4.5208	CH_2 pair asymm. stretch
pVQZ			zpe	135.4	
	ω_1	b_2	56	0.0216	In plane internal rotation
	ω_2	a_1	72	2.0479	Intermolecular stretch
	ω_3	b_1	203	1.9329	OoP internal rotation
	ω_4	a_1	835	7.039	CH_2 symm. rock
	ω_5	a_2	980	0	CH_2 asymm. wag
	ω_6	b_1	987	68.2653	CH_2 symm. wag
	ω_7	a_2	1083	0	CH_2 twist
	ω_8	b_2	1257	1.2025	CH_2 asymm. rock
	ω_9	a_1	1373	10.0611	CH_2 symm. scissor
	ω_{10}	b_2	1455	13.3807	CH_2 asymm. scissor
	ω_{11}	a_1	1672	16.1334	$\text{C}=\text{C}$ stretch
	ω_{12}	b_2	3119	28.2683	CH_2 unpair symm. stretch
	ω_{13}	a_1	3134	74.4466	CH_2 pair symm. stretch
	ω_{14}	b_2	3215	3.866	CH_2 unpair asymm. stretch
	ω_{15}	a_1	3238	4.5562	CH_2 pair asymm. stretch
			zpe	135.6	

Table B69: Calculated harmonic frequencies and mode assignments for the $\text{I}^- \cdots \text{C}_2\text{H}_4$ complex. All frequencies and intensities are in cm^{-1} and km mol^{-1} respectively.

		$\text{I}^- \cdots \text{C}_2\text{H}_4$ $C_{2v} (^1A_1)$ End vdW Complex			
	Mode	Symmetry	Frequency (cm^{-1})	Intensity (km mol^{-1})	Description
def2QZVP	ω_1	a_1	66	2.5099	Intermolecular stretch
	ω_2	b_2	73	0.3937	In plane internal rotation
	ω_3	b_1	83	0.1475	OoP internal rotation
	ω_4	b_2	821	0.4136	CH_2 symm. rock
	ω_5	b_1	947	45.5989	Farside CH_2 wag
	ω_6	b_1	1051	33.5535	Nearside CH_2 wag
	ω_7	a_2	1082	0	CH_2 twist
	ω_8	b_2	1238	1.3302	CH_2 asymm. rock
	ω_9	a_1	1367	28.753	CH_2 symm. scissor
	ω_{10}	a_1	1483	32.1993	CH_2 asymm. scissor
	ω_{11}	a_1	1671	0.0731	$\text{C}=\text{C}$ stretch
	ω_{12}	a_1	3119	26.4856	Farside CH_2 symm. stretch
	ω_{13}	a_1	3155	0.9335	Nearside CH_2 symm. stretch
	ω_{14}	b_2	3191	19.1257	Farside CH_2 asymm. stretch
	ω_{15}	b_2	3240	8.4423	Nearside CH_2 asymm. stretch
pVTZ	zpe		135.1		
	ω_1	b_2	49 <i>i</i>	0.3869	In plane internal rotation
	ω_2	b_1	59	0.0591	OoP internal rotation
	ω_3	a_1	65	2.29	Intermolecular stretch
	ω_4	b_2	797	0.3232	CH_2 symm. rock
	ω_5	b_1	932	42.1444	Farside CH_2 wag
	ω_6	b_1	1036	33.5077	Nearside CH_2 wag
	ω_7	a_2	1059	0	CH_2 twist
	ω_8	b_2	1225	1.6811	CH_2 asymm. rock
	ω_9	a_1	1363	28.9663	CH_2 symm. scissor
	ω_{10}	a_1	1471	32.239	CH_2 asymm. scissor
	ω_{11}	a_1	1674	0.0512	$\text{C}=\text{C}$ stretch
	ω_{12}	a_1	3137	25.7189	Farside CH_2 symm. stretch
	ω_{13}	a_1	3174	1.1284	Nearside CH_2 symm. stretch
	ω_{14}	b_2	3212	17.6456	Farside CH_2 asymm. stretch
	ω_{15}	b_2	3258	8.3119	Nearside CH_2 asymm. stretch
pVQZ	zpe		134.4		
	ω_1	b_2	47 <i>i</i>	0.3822	In plane internal rotation
	ω_2	b_1	58	0.0639	OoP internal rotation
	ω_3	a_1	65	2.296	Intermolecular stretch
	ω_4	b_2	801	0.3347	CH_2 symm. rock
	ω_5	b_1	938	43.1679	Farside CH_2 wag
	ω_6	b_1	1039	32.1207	Nearside CH_2 wag
	ω_7	a_2	1073	0	CH_2 twist
	ω_8	b_2	1229	1.6386	CH_2 asymm. rock
	ω_9	a_1	1365	28.5159	CH_2 symm. scissor
	ω_{10}	a_1	1473	32.5609	CH_2 asymm. scissor
	ω_{11}	a_1	1675	0.0415	$\text{C}=\text{C}$ stretch
	ω_{12}	a_1	3138	25.6702	Farside CH_2 symm. stretch
	ω_{13}	a_1	3174	0.9826	Nearside CH_2 symm. stretch
	ω_{14}	b_2	3214	17.562	Farside CH_2 asymm. stretch
	ω_{15}	b_2	3260	7.8891	Nearside CH_2 asymm. stretch
	zpe		134.6		

Table B70: Calculated harmonic frequencies and mode assignments for the $\text{I}^- \cdots \text{C}_2\text{H}_4$ complex. All frequencies and intensities are in cm^{-1} and km mol^{-1} respectively.

		$\text{I}^- \cdots \text{C}_2\text{H}_4$ $C_s ({}^1A')$ HApp vdW Complex			
	Mode	Symmetry	Frequency (cm^{-1})	Intensity (km mol^{-1})	Description
def2QZVP	ω_1	a'	57	1.858	In plane internal rotation
	ω_2	a'	108	2.4205	Intermolecular stretch
	ω_3	a''	208	0.2985	OoP internal rotation
	ω_4	a'	856	0.2733	CH_2 symm. rock
	ω_5	a''	952	33.7315	Farside CH_2 wag
	ω_6	a''	1025	41.2276	Nearside CH_2 wag
	ω_7	a''	1095	1.9982	$\text{C}=\text{C}$ twist
	ω_8	a'	1261	2.6295	$\text{C}=\text{C}$ rock
	ω_9	a'	1381	0.9777	CH_2 symm. scissor
	ω_{10}	a'	1489	4.1469	CH_2 asymm. scissor
	ω_{11}	a'	1674	5.3896	$\text{C}=\text{C}$ stretch
	ω_{12}	a'	3085	105.775	Nearside CH_2 symm. stretch
	ω_{13}	a'	3119	50.6678	Farside CH_2 symm. stretch
	ω_{14}	a'	3180	32.6361	Nearside CH_2 asymm. stretch
	ω_{15}	a'	3210	15.0241	Farside CH_2 asymm. stretch
pVTZ	zpe		135.8		
	ω_1	a'	60	1.3934	In plane internal rotation
	ω_2	a'	118	2.8155	Intermolecular stretch
	ω_3	a''	218	0.8119	OoP internal rotation
	ω_4	a'	854	0.6061	CH_2 symm. rock
	ω_5	a''	957	38.4627	Farside CH_2 wag
	ω_6	a''	1029	30.6209	Nearside CH_2 wag
	ω_7	a''	1087	1.685	$\text{C}=\text{C}$ twist
	ω_8	a'	1259	2.362	$\text{C}=\text{C}$ rock
	ω_9	a'	1379	0.7782	CH_2 symm. scissor
	ω_{10}	a'	1486	2.9637	CH_2 asymm. scissor
	ω_{11}	a'	1670	7.7493	$\text{C}=\text{C}$ stretch
	ω_{12}	a'	3080	114.9046	Nearside CH_2 symm. stretch
	ω_{13}	a'	3115	53.2645	Farside CH_2 symm. stretch
	ω_{14}	a'	3175	32.7348	Nearside CH_2 asymm. stretch
	ω_{15}	a'	3206	13.1773	Farside CH_2 asymm. stretch
pVQZ	zpe		135.7		
	ω_1	b_2			
	ω_2	a_1			
	ω_3	b_1			
	ω_4	a_1			
	ω_5	a_2			
	ω_6	b_1			
	ω_7	a_2			
	ω_8	b_2			
	ω_9	a_1			
	ω_{10}	b_2			
	ω_{11}	a_1			
	ω_{12}	b_2			
	ω_{13}	a_1			
	ω_{14}	b_2			
	ω_{15}	a_1			
	zpe		0		

Table B71: Calculated harmonic frequencies and mode assignments for the Cl \cdots C₂H₄ complex. All frequencies and intensities are in cm⁻¹ and km mol⁻¹ respectively.

		Cl \cdots C ₂ H ₄			
		<i>C_{2v} (2A₁)</i>		BifOut	vdW Complex
	Mode	Symmetry	Frequency (cm ⁻¹)	Intensity (km mol ⁻¹)	Description
def2QZVP	ω_1	<i>b</i> ₂	20 <i>i</i>	0.001	In plane intermol. bend
	ω_2	<i>a</i> ₁	241	0.2475	Intermolecular stretch
	ω_3	<i>b</i> ₁	380	0.2293	C ₂ H ₄ internal rotation
	ω_4	<i>b</i> ₁	852	0.3137	CH ₂ symm. rock
	ω_5	<i>a</i> ₂	988	0	CH ₂ twist
	ω_6	<i>b</i> ₂	995	0.1957	CH ₂ asymm. wag
	ω_7	<i>a</i> ₁	1016	70.3173	CH ₂ symm. wag
	ω_8	<i>a</i> ₂	1259	0	CH ₂ asymm. rock
	ω_9	<i>a</i> ₁	1355	16.6718	CH ₂ symm. scissor
	ω_{10}	<i>b</i> ₂	1491	12.5192	CH ₂ asymm. scissor
	ω_{11}	<i>a</i> ₁	1626	35.2028	C=C stretch
	ω_{12}	<i>b</i> ₂	3157	0.3015	CH ₂ unpair symm. stretch
	ω_{13}	<i>a</i> ₁	3164	7.7897	CH ₂ pair symm. stretch
	ω_{14}	<i>a</i> ₂	3244	0	CH ₂ unpair asymm. stretch
	ω_{15}	<i>b</i> ₁	3269	0.1449	CH ₂ unpair asymm. stretch
pVTZ	zpe		137.8		
	ω_1	<i>b</i> ₂	196	0.6477	In plane intermol. bend
	ω_2	<i>a</i> ₁	234	1.4545	Intermolecular stretch
	ω_3	<i>b</i> ₁	346	0.2278	C ₂ H ₄ internal rotation
	ω_4	<i>b</i> ₁	830	0.2375	CH ₂ symm. rock
	ω_5	<i>a</i> ₂	982	0	CH ₂ twist
	ω_6	<i>b</i> ₂	1000	0.3917	CH ₂ asymm. wag
	ω_7	<i>a</i> ₁	1004	75.0721	CH ₂ symm. wag
	ω_8	<i>a</i> ₂	1247	0	CH ₂ asymm. rock
	ω_9	<i>a</i> ₁	1355	15.1216	CH ₂ symm. scissor
	ω_{10}	<i>b</i> ₂	1480	11.5028	CH ₂ asymm. scissor
	ω_{11}	<i>a</i> ₁	1627	35.7212	C=C stretch
	ω_{12}	<i>b</i> ₂	3173	0.4213	CH ₂ unpair symm. stretch
	ω_{13}	<i>a</i> ₁	3183	7.8035	CH ₂ pair symm. stretch
	ω_{14}	<i>a</i> ₂	3263	0	CH ₂ unpair asymm. stretch
	ω_{15}	<i>b</i> ₁	3288	0.1973	CH ₂ pair asymm. stretch
pVQZ	zpe		138.8		
	ω_1	<i>b</i> ₂	199	0.6545	In plane intermol. bend
	ω_2	<i>a</i> ₁	235	1.3096	Intermolecular stretch
	ω_3	<i>b</i> ₁	347	0.2219	C ₂ H ₄ internal rotation
	ω_4	<i>b</i> ₁	834	0.2528	CH ₂ symm. rock
	ω_5	<i>a</i> ₂	987	0	CH ₂ twist
	ω_6	<i>a</i> ₁	1007	73.9845	CH ₂ symm. wag
	ω_7	<i>b</i> ₂	1011	0.3803	CH ₂ asymm. wag
	ω_8	<i>a</i> ₂	1250	0	CH ₂ asymm. rock
	ω_9	<i>a</i> ₁	1355	15.5924	CH ₂ symm. scissor
	ω_{10}	<i>b</i> ₂	1482	11.7476	CH ₂ asymm. scissor
	ω_{11}	<i>a</i> ₁	1627	36.7377	C=C stretch
	ω_{12}	<i>b</i> ₂	3175	0.3614	CH ₂ unpair symm. stretch
	ω_{13}	<i>a</i> ₁	3184	7.9473	CH ₂ pair symm. stretch
	ω_{14}	<i>a</i> ₂	3266	0	CH ₂ unpair asymm. stretch
	ω_{15}	<i>b</i> ₁	3290	0.1384	CH ₂ pair asymm. stretch
	zpe		139.1		

Table B72: Calculated harmonic frequencies and mode assignments for the Cl \cdots C₂H₄ complex. All frequencies and intensities are in cm⁻¹ and km mol⁻¹ respectively.

Cl \cdots C ₂ H ₄ <i>C</i> ₂ <i>v</i> (² <i>A</i> ₁) BifPl vdW Complex					
	Mode	Symmetry	Frequency (cm ⁻¹)	Intensity (km mol ⁻¹)	Description
def2QZVP	ω_1	<i>b</i> ₁	154 <i>i</i>	2.129	OoP internal rotation
	ω_2	<i>a</i> ₁	56	0	Intermolecular stretch
	ω_3	<i>b</i> ₂	76	0.0007	In plane internal rotation
	ω_4	<i>a</i> ₁	831	0.7528	CH ₂ symm. rock
	ω_5	<i>b</i> ₁	972	116.2064	CH ₂ symm. wag
	ω_6	<i>a</i> ₂	973	0.001	CH ₂ asymm. wag
	ω_7	<i>a</i> ₂	1068	0	CH ₂ twist
	ω_8	<i>b</i> ₂	1251	0.0517	CH ₂ asymm. rock
	ω_9	<i>a</i> ₁	1381	0.9117	CH ₂ symm. scissor
	ω_{10}	<i>b</i> ₂	1479	12.2049	CH ₂ asymm. scissor
	ω_{11}	<i>a</i> ₁	1686	0.5009	C=C stretch
	ω_{12}	<i>b</i> ₂	3155	13.4547	CH ₂ unpair symm. stretch
	ω_{13}	<i>a</i> ₁	3170	0.5447	CH ₂ pair symm. stretch
	ω_{14}	<i>b</i> ₂	3238	0.0055	CH ₂ unpair asymm. stretch
	ω_{15}	<i>a</i> ₁	3263	16.936	CH ₂ pair asymm. stretch
pVTZ			zpe	135.2	
	ω_1	<i>b</i> ₁	156 <i>i</i>	2.4909	OoP internal rotation
	ω_2	<i>a</i> ₁	60	0.0004	Intermolecular stretch
	ω_3	<i>b</i> ₂	78	0.0007	In plane internal rotation
	ω_4	<i>a</i> ₁	826	0.5865	CH ₂ symm. rock
	ω_5	<i>a</i> ₂	966	0	CH ₂ asymm. wag
	ω_6	<i>b</i> ₁	970	115.0523	CH ₂ symm. wag
	ω_7	<i>a</i> ₂	1052	0	CH ₂ twist
	ω_8	<i>b</i> ₂	1248	0.0696	CH ₂ asymm. rock
	ω_9	<i>a</i> ₁	1379	1.0149	CH ₂ symm. scissor
	ω_{10}	<i>b</i> ₂	1476	12.1268	CH ₂ asymm. scissor
	ω_{11}	<i>a</i> ₁	1683	0.5422	C=C stretch
	ω_{12}	<i>b</i> ₂	3151	13.5789	CH ₂ unpair symm. stretch
	ω_{13}	<i>a</i> ₁	3168	0.6425	CH ₂ pair symm. stretch
	ω_{14}	<i>b</i> ₂	3233	0.0056	CH ₂ unpair asymm. stretch
	ω_{15}	<i>a</i> ₁	3259	17.1256	CH ₂ pair asymm. stretch
pVQZ			zpe	134.9	
	ω_1	<i>b</i> ₁	163 <i>i</i>	2.7718	OoP internal rotation
	ω_2	<i>a</i> ₁	58	0.0002	Intermolecular stretch
	ω_3	<i>b</i> ₂	79	0.0006	In plane internal rotation
	ω_4	<i>a</i> ₁	830	0.6169	CH ₂ symm. rock
	ω_5	<i>b</i> ₁	972	115.9855	CH ₂ symm. wag
	ω_6	<i>a</i> ₂	975	0.0001	CH ₂ asymm. wag
	ω_7	<i>a</i> ₂	1066	0	CH ₂ twist
	ω_8	<i>b</i> ₂	1251	0.0673	CH ₂ asymm. rock
	ω_9	<i>a</i> ₁	1380	1.0139	CH ₂ symm. scissor
	ω_{10}	<i>b</i> ₂	1478	12.2802	CH ₂ asymm. scissor
	ω_{11}	<i>a</i> ₁	1684	0.541	C=C stretch
	ω_{12}	<i>b</i> ₂	3152	13.4856	CH ₂ unpair symm. stretch
	ω_{13}	<i>a</i> ₁	3167	0.6058	CH ₂ pair symm. stretch
	ω_{14}	<i>b</i> ₂	3235	0.0062	CH ₂ unpair asymm. stretch
	ω_{15}	<i>a</i> ₁	3260	16.7999	CH ₂ pair asymm. stretch
			zpe	135.1	

Table B73: Calculated harmonic frequencies and mode assignments for the Cl \cdots C₂H₄ complex. All frequencies and intensities are in cm⁻¹ and km mol⁻¹ respectively.

		Cl \cdots C ₂ H ₄ <i>C</i> ₂ <i>v</i> (2 <i>A</i> ₁) End vdW Complex			
	Mode	Symmetry	Frequency (cm ⁻¹)	Intensity (km mol ⁻¹)	Description
def2QZVP	ω_1	<i>b</i> ₁	56 <i>i</i>	0.4679	OoP internal rotation
	ω_2	<i>b</i> ₂	29	0.001	In plane internal rotation
	ω_3	<i>a</i> ₁	45	0	Intermolecular stretch
	ω_4	<i>b</i> ₂	829	0.1638	CH ₂ symm. rock
	ω_5	<i>b</i> ₁	948	101.8515	Nearside CH ₂ wag
	ω_6	<i>b</i> ₁	975	41.8331	Farside CH ₂ wag
	ω_7	<i>a</i> ₂	1070	0	CH ₂ twist
	ω_8	<i>b</i> ₂	1249	0.1446	CH ₂ asymm. rock
	ω_9	<i>a</i> ₁	1380	0.4777	CH ₂ symm. scissor
	ω_{10}	<i>a</i> ₁	1480	13.7231	CH ₂ asymm. scissor
	ω_{11}	<i>a</i> ₁	1687	0.1567	C=C stretch
	ω_{12}	<i>a</i> ₁	3155	15.4025	CH ₂ unpair symm. stretch
	ω_{13}	<i>a</i> ₁	3171	0.0351	CH ₂ pair symm. stretch
	ω_{14}	<i>b</i> ₂	3236	0.1303	CH ₂ unpair asymm. stretch
	ω_{15}	<i>b</i> ₂	3263	16.2208	CH ₂ pair asymm. stretch
pVTZ	zpe		134.7		
	ω_1	<i>b</i> ₁	58 <i>i</i>	0.7337	OoP internal rotation
	ω_2	<i>b</i> ₂	31	0.0013	In plane internal rotation
	ω_3	<i>a</i> ₁	48	0.0001	Intermolecular stretch
	ω_4	<i>b</i> ₂	825	0.0865	CH ₂ symm. rock
	ω_5	<i>b</i> ₁	941	103.5732	Nearside CH ₂ wag
	ω_6	<i>b</i> ₁	969	49.9127	Farside CH ₂ wag
	ω_7	<i>a</i> ₂	1052	0	CH ₂ twist
	ω_8	<i>b</i> ₂	1245	0.1845	CH ₂ asymm. rock
	ω_9	<i>a</i> ₁	1378	0.5352	CH ₂ symm. scissor
	ω_{10}	<i>a</i> ₁	1478	13.7718	CH ₂ asymm. scissor
	ω_{11}	<i>a</i> ₁	1684	0.1863	C=C stretch
	ω_{12}	<i>a</i> ₁	3151	15.6816	CH ₂ unpair symm. stretch
	ω_{13}	<i>a</i> ₁	3168	0.0249	CH ₂ pair symm. stretch
pVQZ	ω_{14}	<i>b</i> ₂	3231	0.1243	CH ₂ unpair asymm. stretch
	ω_{15}	<i>b</i> ₂	3259	16.351	CH ₂ pair asymm. stretch
	zpe		134.4		
	ω_1	<i>b</i> ₁	63 <i>i</i>	0.8172	OoP internal rotation
	ω_2	<i>b</i> ₂	31	0.0012	In plane internal rotation
	ω_3	<i>a</i> ₁	47	0	Intermolecular stretch
	ω_4	<i>b</i> ₂	828	0.0969	CH ₂ symm. rock
	ω_5	<i>b</i> ₁	943	123.5851	Nearside CH ₂ wag
	ω_6	<i>b</i> ₁	976	33.4506	Farside CH ₂ wag
	ω_7	<i>a</i> ₂	1068	0	CH ₂ twist
	ω_8	<i>b</i> ₂	1249	0.1764	CH ₂ asymm. rock
	ω_9	<i>a</i> ₁	1379	0.5366	CH ₂ symm. scissor
	ω_{10}	<i>a</i> ₁	1480	13.9375	CH ₂ asymm. scissor
	ω_{11}	<i>a</i> ₁	1685	0.1756	C=C stretch
	ω_{12}	<i>a</i> ₁	3152	15.5536	CH ₂ unpair symm. stretch
	ω_{13}	<i>a</i> ₁	3168	0.0243	CH ₂ pair symm. stretch
	ω_{14}	<i>b</i> ₂	3233	0.1183	CH ₂ unpair asymm. stretch
	ω_{15}	<i>b</i> ₂	3260	15.9921	CH ₂ pair asymm. stretch
	zpe		134.6		

Table B74: Calculated harmonic frequencies and mode assignments for the Br \cdots C₂H₄ complex. All frequencies and intensities are in cm⁻¹ and km mol⁻¹ respectively.

		Br \cdots C ₂ H ₄			
		<i>C_{2v}</i> (² A ₁)		BifOut	vdW Complex
	Mode	Symmetry	Frequency (cm ⁻¹)	Intensity (km mol ⁻¹)	Description
def2QZVP	ω_1	<i>b</i> ₂	99	0.0038	In plane intermol. bend
	ω_2	<i>a</i> ₁	181	2.0234	Intermolecular stretch
	ω_3	<i>b</i> ₁	345	0.0791	C ₂ H ₄ internal rotation
	ω_4	<i>b</i> ₁	852	0.2568	CH ₂ symm. rock
	ω_5	<i>b</i> ₂	995	0.0247	CH ₂ asymm. wag
	ω_6	<i>a</i> ₂	1009	0	CH ₂ twist
	ω_7	<i>a</i> ₁	1013	84.5971	CH ₂ symm. wag
	ω_8	<i>a</i> ₂	1259	0	CH ₂ asymm. rock
	ω_9	<i>a</i> ₁	1361	17.9906	CH ₂ symm. scissor
	ω_{10}	<i>b</i> ₂	1492	11.9755	CH ₂ asymm. scissor
	ω_{11}	<i>a</i> ₁	1634	40.1003	C=C stretch
	ω_{12}	<i>b</i> ₂	3152	0.6338	CH ₂ unpair symm. stretch
	ω_{13}	<i>a</i> ₁	3159	6.4686	CH ₂ pair symm. stretch
	ω_{14}	<i>a</i> ₂	3236	0	CH ₂ unpair asymm. stretch
	ω_{15}	<i>b</i> ₁	3262	0.4207	CH ₂ unpair asymm. stretch
		zpe	137.9		
pVTZ	ω_1	<i>a</i> ₁	177	3.932	Intermolecular stretch
	ω_2	<i>b</i> ₂	204	0.3356	In plane intermol. bend
	ω_3	<i>b</i> ₁	303	0.1419	C ₂ H ₄ internal rotation
	ω_4	<i>b</i> ₁	829	0.1688	CH ₂ symm. rock
	ω_5	<i>b</i> ₂	992	0.4025	CH ₂ asymm. wag
	ω_6	<i>a</i> ₁	999	92.166	CH ₂ symm. wag
	ω_7	<i>a</i> ₂	1004	0	CH ₂ twist
	ω_8	<i>a</i> ₂	1247	0	CH ₂ asymm. rock
	ω_9	<i>a</i> ₁	1359	13.9983	CH ₂ symm. scissor
	ω_{10}	<i>b</i> ₂	1479	11.0344	CH ₂ asymm. scissor
	ω_{11}	<i>a</i> ₁	1635	35.9252	C=C stretch
	ω_{12}	<i>b</i> ₂	3167	0.7735	CH ₂ unpair symm. stretch
	ω_{13}	<i>a</i> ₁	3178	5.7996	CH ₂ pair symm. stretch
	ω_{14}	<i>a</i> ₂	3255	0	CH ₂ unpair asymm. stretch
	ω_{15}	<i>b</i> ₁	3281	0.5321	CH ₂ pair asymm. stretch
		zpe	138.2		
pVQZ	ω_1	<i>a</i> ₁	179	3.7578	Intermolecular stretch
	ω_2	<i>b</i> ₂	207	0.3376	In plane intermol. bend
	ω_3	<i>b</i> ₁	307	0.1391	C ₂ H ₄ internal rotation
	ω_4	<i>b</i> ₁	833	0.1854	CH ₂ symm. rock
	ω_5	<i>a</i> ₁	1003	90.9609	CH ₂ symm. wag
	ω_6	<i>b</i> ₂	1007	0.4023	CH ₂ asymm. wag
	ω_7	<i>a</i> ₂	1009	0	CH ₂ twist
	ω_8	<i>a</i> ₂	1250	0	CH ₂ asymm. rock
	ω_9	<i>a</i> ₁	1360	14.6331	CH ₂ symm. scissor
	ω_{10}	<i>b</i> ₂	1482	11.2706	CH ₂ asymm. scissor
	ω_{11}	<i>a</i> ₁	1635	36.8806	C=C stretch
	ω_{12}	<i>b</i> ₂	3169	0.6791	CH ₂ unpair symm. stretch
	ω_{13}	<i>a</i> ₁	3179	6.0009	CH ₂ pair symm. stretch
	ω_{14}	<i>a</i> ₂	3258	0	CH ₂ unpair asymm. stretch
	ω_{15}	<i>b</i> ₁	3283	0.4172	CH ₂ pair asymm. stretch
		zpe	138.5		

Table B75: Calculated harmonic frequencies and mode assignments for the Br \cdots C₂H₄ complex. All frequencies and intensities are in cm⁻¹ and km mol⁻¹ respectively.

Br \cdots C ₂ H ₄ <i>C_{2v}</i> (² A ₁) BifPl vdW Complex					
	Mode	Symmetry	Frequency (cm ⁻¹)	Intensity (km mol ⁻¹)	Description
def2QZVP	ω_1	<i>b</i> ₁	154 <i>i</i>	7.789	OoP internal rotation
	ω_2	<i>a</i> ₁	52	0.0078	Intermolecular stretch
	ω_3	<i>b</i> ₂	114	0.0003	In plane internal rotation
	ω_4	<i>a</i> ₁	848	0.9923	CH ₂ symm. rock
	ω_5	<i>b</i> ₁	976	132.8236	CH ₂ symm. wag
	ω_6	<i>a</i> ₂	987	0	CH ₂ asymm. wag
	ω_7	<i>a</i> ₂	1074	0	CH ₂ twist
	ω_8	<i>b</i> ₂	1259	0.0949	CH ₂ asymm. rock
	ω_9	<i>a</i> ₁	1382	1.48	CH ₂ symm. scissor
	ω_{10}	<i>b</i> ₂	1487	12.2728	CH ₂ asymm. scissor
	ω_{11}	<i>a</i> ₁	1680	0.5921	C=C stretch
	ω_{12}	<i>b</i> ₂	3135	14.0089	CH ₂ unpair symm. stretch
	ω_{13}	<i>a</i> ₁	3147	0.8678	CH ₂ pair symm. stretch
	ω_{14}	<i>b</i> ₂	3213	0.0185	CH ₂ unpair asymm. stretch
	ω_{15}	<i>a</i> ₁	3238	17.6597	CH ₂ pair asymm. stretch
pVTZ			zpe	135.1	
	ω_1	<i>b</i> ₁	156 <i>i</i>	7.7352	OoP internal rotation
	ω_2	<i>a</i> ₁	58	0.0167	Intermolecular stretch
	ω_3	<i>b</i> ₂	120	0.0005	In plane internal rotation
	ω_4	<i>a</i> ₁	844	0.896	CH ₂ symm. rock
	ω_5	<i>b</i> ₁	978	125.178	CH ₂ symm. wag
	ω_6	<i>a</i> ₂	983	0	CH ₂ asymm. wag
	ω_7	<i>a</i> ₂	1063	0	CH ₂ twist
	ω_8	<i>b</i> ₂	1257	0.1428	CH ₂ asymm. rock
	ω_9	<i>a</i> ₁	1379	1.8212	CH ₂ symm. scissor
	ω_{10}	<i>b</i> ₂	1484	12.5285	CH ₂ asymm. scissor
	ω_{11}	<i>a</i> ₁	1675	0.6932	C=C stretch
	ω_{12}	<i>b</i> ₂	3131	13.8815	CH ₂ unpair symm. stretch
	ω_{13}	<i>a</i> ₁	3144	1.0642	CH ₂ pair symm. stretch
pVQZ	ω_{14}	<i>b</i> ₂	3208	0.0274	CH ₂ unpair asymm. stretch
	ω_{15}	<i>a</i> ₁	3234	17.3631	CH ₂ pair asymm. stretch
			zpe	134.9	
	ω_1	<i>b</i> ₁	132 <i>i</i>	1.6527	OoP internal rotation
	ω_2	<i>a</i> ₁	58	0.0053	Intermolecular stretch
	ω_3	<i>b</i> ₂	89	0.0004	In plane internal rotation
	ω_4	<i>a</i> ₁	830	0.8894	CH ₂ symm. rock
	ω_5	<i>a</i>	976	108.607	CH ₂ symm. wag
	ω_6	<i>a</i>	977	0.0089	CH ₂ asymm. wag
	ω_7	<i>a</i> ₂	1068	0	CH ₂ twist
	ω_8	<i>b</i> ₂	1251	0.1288	CH ₂ asymm. rock
	ω_9	<i>a</i> ₁	1380	1.6628	CH ₂ symm. scissor
	ω_{10}	<i>b</i> ₂	1478	13.0571	CH ₂ asymm. scissor
	ω_{11}	<i>a</i> ₁	1684	1.0159	C=C stretch
	ω_{12}	<i>b</i> ₂	3152	13.3744	CH ₂ unpair symm. stretch
	ω_{13}	<i>a</i> ₁	3167	0.8095	CH ₂ pair symm. stretch
	ω_{14}	<i>b</i> ₂	3235	0.0215	CH ₂ unpair asymm. stretch
	ω_{15}	<i>a</i> ₁	3260	17.1966	CH ₂ pair asymm. stretch
			zpe	135.2	

Table B76: Calculated harmonic frequencies and mode assignments for the Br \cdots C₂H₄ complex. All frequencies and intensities are in cm⁻¹ and km mol⁻¹ respectively.

		Br \cdots C ₂ H ₄ <i>C_{2v}</i> (² A ₁) End vdW Complex			
	Mode	Symmetry	Frequency (cm ⁻¹)	Intensity (km mol ⁻¹)	Description
def2QZVP	ω_1	<i>a</i> ₁	42	0.0021	Intermolecular stretch
	ω_2	<i>b</i> ₂	87	0.0014	In plane internal rotation
	ω_3	<i>b</i> ₁	158	24.0075	OoP internal rotation
	ω_4	<i>b</i> ₂	846	0.1972	CH ₂ symm. rock
	ω_5	<i>b</i> ₁	988	25.3443	Farside CH ₂ wag
	ω_6	<i>a</i> ₂	1077	0	CH ₂ twist
	ω_7	<i>b</i> ₂	1257	0.2179	CH ₂ asymm. rock
	ω_8	<i>b</i> ₁	1369	807.377	Nearside CH ₂ wag
	ω_9	<i>a</i> ₁	1381	0.6557	CH ₂ symm. scissor
	ω_{10}	<i>a</i> ₁	1488	14.4114	CH ₂ asymm. scissor
	ω_{11}	<i>a</i> ₁	1681	0.3363	C=C stretch
	ω_{12}	<i>a</i> ₁	3134	16.9899	CH ₂ unpair symm. stretch
	ω_{13}	<i>a</i> ₁	3148	0.0539	CH ₂ pair symm. stretch
	ω_{14}	<i>b</i> ₂	3211	0.2077	CH ₂ unpair asymm. stretch
	ω_{15}	<i>b</i> ₂	3239	16.448	CH ₂ pair asymm. stretch
pVTZ			zpe	138.2	
	ω_1	<i>b</i> ₂	26	0.0022	In plane internal rotation
	ω_2	<i>a</i> ₁	44	0.0024	Intermolecular stretch
	ω_3	<i>b</i> ₁	189	75.2294	OoP internal rotation
	ω_4	<i>b</i> ₂	824	0.122	CH ₂ symm. rock
	ω_5	<i>b</i> ₁	968	28.1996	Farside CH ₂ wag
	ω_6	<i>a</i> ₂	1052	0.0003	CH ₂ twist
	ω_7	<i>b</i> ₂	1245	0.3062	CH ₂ asymm. rock
	ω_8	<i>a</i> ₁	1378	0.8856	CH ₂ symm. scissor
	ω_9	<i>a</i> ₁	1478	15.0795	CH ₂ asymm. scissor
	ω_{10}	<i>a</i> ₁	1684	0.3125	C=C stretch
	ω_{11}	<i>b</i> ₁	2155	23928.6925	Nearside CH ₂ wag
	ω_{12}	<i>a</i> ₁	3150	16.607	CH ₂ unpair symm. stretch
	ω_{13}	<i>a</i> ₁	3168	0.0338	CH ₂ pair symm. stretch
pVQZ	ω_{14}	<i>b</i> ₂	3231	0.1443	CH ₂ unpair asymm. stretch
	ω_{15}	<i>b</i> ₂	3258	15.9103	CH ₂ pair asymm. stretch
			zpe	142.7	
	ω_1	<i>b</i> ₂	34	0.002	In plane internal rotation
	ω_2	<i>a</i> ₁	47	0.0031	Intermolecular stretch
	ω_3	<i>b</i> ₁	92	4.4027	OoP internal rotation
	ω_4	<i>b</i> ₂	828	0.1379	CH ₂ symm. rock
	ω_5	<i>b</i> ₁	975	25.1879	Farside CH ₂ wag
	ω_6	<i>a</i> ₂	1069	0	CH ₂ twist
	ω_7	<i>b</i> ₁	1089	2.5998	Nearside CH ₂ wag
	ω_8	<i>b</i> ₂	1248	0.3097	CH ₂ asymm. rock
	ω_9	<i>a</i> ₁	1379	0.8865	CH ₂ symm. scissor
	ω_{10}	<i>a</i> ₁	1479	15.4219	CH ₂ asymm. scissor
	ω_{11}	<i>a</i> ₁	1685	0.3261	C=C stretch
	ω_{12}	<i>a</i> ₁	3152	16.5168	CH ₂ unpair symm. stretch
	ω_{13}	<i>a</i> ₁	3168	0.0399	CH ₂ pair symm. stretch
	ω_{14}	<i>b</i> ₂	3233	0.1533	CH ₂ unpair asymm. stretch
	ω_{15}	<i>b</i> ₂	3260	15.4899	CH ₂ pair asymm. stretch
			zpe	136	

Table B77: Calculated harmonic frequencies and mode assignments for the I...C₂H₄ complex. All frequencies and intensities are in cm⁻¹ and km mol⁻¹ respectively.

		I...C ₂ H ₄			
		<i>C_{2v} (2A₁)</i>		BifOut	vdW Complex
	Mode	Symmetry	Frequency (cm ⁻¹)	Intensity (km mol ⁻¹)	Description
def2QZVP	ω_1	<i>b</i> ₂	121	0.0323	In plane intermol. bend
	ω_2	<i>a</i> ₁	140	4.3782	Intermolecular stretch
	ω_3	<i>b</i> ₁	302	0.1909	C ₂ H ₄ internal rotation
	ω_4	<i>b</i> ₁	850	0.152	CH ₂ symm. rock
	ω_5	<i>b</i> ₂	995	0	CH ₂ asymm. wag
	ω_6	<i>a</i> ₁	1010	107.2779	CH ₂ symm. wag
	ω_7	<i>a</i> ₂	1034	0	CH ₂ twist
	ω_8	<i>a</i> ₂	1259	0	CH ₂ asymm. rock
	ω_9	<i>a</i> ₁	1367	15.0291	CH ₂ symm. scissor
	ω_{10}	<i>b</i> ₂	1491	11.0454	CH ₂ asymm. scissor
	ω_{11}	<i>a</i> ₁	1644	36.6926	C=C stretch
	ω_{12}	<i>b</i> ₂	3145	1.1709	CH ₂ unpair symm. stretch
	ω_{13}	<i>a</i> ₁	3153	3.9735	CH ₂ pair symm. stretch
	ω_{14}	<i>a</i> ₂	3228	0	CH ₂ unpair asymm. stretch
	ω_{15}	<i>b</i> ₁	3253	0.9967	CH ₂ unpair asymm. stretch
pVTZ	zpe		137.5		
	ω_1	<i>a</i> ₁	133	6.2469	Intermolecular stretch
	ω_2	<i>b</i> ₂	182	0.1979	In plane intermol. bend
	ω_3	<i>b</i> ₁	247	0.2281	C ₂ H ₄ internal rotation
	ω_4	<i>b</i> ₁	828	0.0951	CH ₂ symm. rock
	ω_5	<i>b</i> ₂	982	0.1184	CH ₂ asymm. wag
	ω_6	<i>a</i> ₁	995	115.3464	CH ₂ symm. wag
	ω_7	<i>a</i> ₂	1028	0	CH ₂ twist
	ω_8	<i>a</i> ₂	1247	0	CH ₂ asymm. rock
	ω_9	<i>a</i> ₁	1366	11.2729	CH ₂ symm. scissor
	ω_{10}	<i>b</i> ₂	1478	10.5067	CH ₂ asymm. scissor
	ω_{11}	<i>a</i> ₁	1646	31.8218	C=C stretch
	ω_{12}	<i>b</i> ₂	3160	1.3688	CH ₂ unpair symm. stretch
	ω_{13}	<i>a</i> ₁	3173	3.147	CH ₂ pair symm. stretch
	ω_{14}	<i>a</i> ₂	3246	0	CH ₂ unpair asymm. stretch
	ω_{15}	<i>b</i> ₁	3272	1.2722	CH ₂ pair asymm. stretch
pVQZ	zpe		137.5		
	ω_1	<i>a</i> ₁	139	6.1187	Intermolecular stretch
	ω_2	<i>b</i> ₂	188	0.2017	In plane intermol. bend
	ω_3	<i>b</i> ₁	255	0.2243	C ₂ H ₄ internal rotation
	ω_4	<i>b</i> ₁	831	0.1119	CH ₂ symm. rock
	ω_5	<i>a</i> ₁	1000	113.8089	CH ₂ symm. wag
	ω_6	<i>b</i> ₂	1001	0.1259	CH ₂ asymm. wag
	ω_7	<i>a</i> ₂	1033	0	CH ₂ twist
	ω_8	<i>a</i> ₂	1250	0	CH ₂ asymm. rock
	ω_9	<i>a</i> ₁	1366	11.9326	CH ₂ symm. scissor
	ω_{10}	<i>b</i> ₂	1481	10.7248	CH ₂ asymm. scissor
	ω_{11}	<i>a</i> ₁	1646	32.9532	C=C stretch
	ω_{12}	<i>b</i> ₂	3163	1.1891	CH ₂ unpair symm. stretch
	ω_{13}	<i>a</i> ₁	3173	3.3415	CH ₂ pair symm. stretch
	ω_{14}	<i>a</i> ₂	3250	0	CH ₂ unpair asymm. stretch
	ω_{15}	<i>b</i> ₁	3275	1.0342	CH ₂ pair asymm. stretch
	zpe		137.9		

Table B78: Calculated harmonic frequencies and mode assignments for the I...C₂H₄ complex. All frequencies and intensities are in cm⁻¹ and km mol⁻¹ respectively.

I...C ₂ H ₄ C _{2v} (² A ₁) BifPl vdw Complex					
	Mode	Symmetry	Frequency (cm ⁻¹)	Intensity (km mol ⁻¹)	Description
def2QZVP	ω_1	a ₁	80	0.0813	Intermolecular stretch
	ω_2	b ₂	129	0.0002	In plane internal rotation
	ω_3	b ₁	254	18.4733	OoP internal rotation
	ω_4	a ₁	828	1.9682	CH ₂ symm. rock
	ω_5	a ₂	975	0	CH ₂ asymm. wag
	ω_6	b ₁	1011	37.7752	CH ₂ symm. wag
	ω_7	a ₂	1063	0	CH ₂ twist
	ω_8	b ₂	1248	0.2034	CH ₂ asymm. rock
	ω_9	a ₁	1381	3.5477	CH ₂ symm. scissor
	ω_{10}	b ₂	1481	14.6987	CH ₂ asymm. scissor
	ω_{11}	a ₁	1686	2.3242	C=C stretch
	ω_{12}	b ₂	3154	12.6605	CH ₂ unpair symm. stretch
	ω_{13}	a ₁	3168	0.9148	CH ₂ pair symm. stretch
	ω_{14}	b ₂	3234	0.204	CH ₂ unpair asymm. stretch
	ω_{15}	a ₁	3257	19.1615	CH ₂ pair asymm. stretch
pVTZ			zpe	136.8	
	ω_1	a ₁	56	0.0191	Intermolecular stretch
	ω_2	b ₂	86	0.0002	In plane internal rotation
	ω_3	b ₁	334	51.5211	OoP internal rotation
	ω_4	a ₁	825	1.1428	CH ₂ symm. rock
	ω_5	a ₂	964	0	CH ₂ asymm. wag
	ω_6	b ₁	1039	4.9933	CH ₂ symm. wag
	ω_7	a ₂	1054	0	CH ₂ twist
	ω_8	b ₂	1248	0.2461	CH ₂ asymm. rock
	ω_9	a ₁	1378	2.5092	CH ₂ symm. scissor
	ω_{10}	b ₂	1474	13.5209	CH ₂ asymm. scissor
	ω_{11}	a ₁	1682	1.8612	C=C stretch
	ω_{12}	b ₂	3149	13.3113	CH ₂ unpair symm. stretch
	ω_{13}	a ₁	3165	0.9261	CH ₂ pair symm. stretch
	ω_{14}	b ₂	3231	0.049	CH ₂ unpair asymm. stretch
	ω_{15}	a ₁	3257	18.6624	CH ₂ pair asymm. stretch
pVQZ			zpe	137.2	
	ω_1	a ₁	55	0.0197	Intermolecular stretch
	ω_2	b ₂	89	0.0001	In plane internal rotation
	ω_3	b ₁	453	176.5691	OoP internal rotation
	ω_4	a ₁	829	1.1581	CH ₂ symm. rock
	ω_5	a ₂	976	0	CH ₂ asymm. wag
	ω_6	a ₂	1068	0	CH ₂ twist
	ω_7	b ₁	1118	55.2231	CH ₂ symm. wag
	ω_8	b ₂	1251	0.2473	CH ₂ asymm. rock
	ω_9	a ₁	1379	2.4952	CH ₂ symm. scissor
	ω_{10}	b ₂	1477	13.667	CH ₂ asymm. scissor
	ω_{11}	a ₁	1683	1.8202	C=C stretch
	ω_{12}	b ₂	3151	13.1979	CH ₂ unpair symm. stretch
	ω_{13}	a ₁	3165	0.8932	CH ₂ pair symm. stretch
	ω_{14}	b ₂	3234	0.0519	CH ₂ unpair asymm. stretch
	ω_{15}	a ₁	3258	18.3099	CH ₂ pair asymm. stretch
			zpe	138.7	

Table B79: Calculated harmonic frequencies and mode assignments for the I \cdots C₂H₄ complex. All frequencies and intensities are in cm⁻¹ and km mol⁻¹ respectively.

		I \cdots C ₂ H ₄ <i>C</i> ₂ <i>v</i> (² <i>A</i> ₁) End vdW Complex			
	Mode	Symmetry	Frequency (cm ⁻¹)	Intensity (km mol ⁻¹)	Description
def2QZVP	ω_1	<i>a</i> ₁	39	0.0076	Intermolecular stretch
	ω_2	<i>b</i> ₂	87	0.0032	In plane internal rotation
	ω_3	<i>b</i> ₁	122	8.0985	OoP internal rotation
	ω_4	<i>b</i> ₂	846	0.2821	CH ₂ symm. rock
	ω_5	<i>b</i> ₁	987	25.4804	Farside CH ₂ wag
	ω_6	<i>a</i> ₂	1077	0	CH ₂ twist
	ω_7	<i>b</i> ₁	1153	51.2417	Nearside CH ₂ wag
	ω_8	<i>b</i> ₂	1256	0.44	CH ₂ asymm. rock
	ω_9	<i>a</i> ₁	1380	1.2237	CH ₂ symm. scissor
	ω_{10}	<i>a</i> ₁	1488	16.2963	CH ₂ asymm. scissor
	ω_{11}	<i>a</i> ₁	1681	0.5518	C=C stretch
	ω_{12}	<i>a</i> ₁	3134	18.6225	CH ₂ unpair symm. stretch
	ω_{13}	<i>a</i> ₁	3147	0.0364	CH ₂ pair symm. stretch
	ω_{14}	<i>b</i> ₂	3211	0.2103	CH ₂ unpair asymm. stretch
	ω_{15}	<i>b</i> ₂	3238	15.7592	CH ₂ pair asymm. stretch
pVTZ			zpe	136.7	
	ω_1	<i>b</i> ₂	19	0.0034	In plane internal rotation
	ω_2	<i>a</i> ₁	41	0.0116	Intermolecular stretch
	ω_3	<i>b</i> ₁	98	6.4172	OoP internal rotation
	ω_4	<i>b</i> ₂	823	0.1749	CH ₂ symm. rock
	ω_5	<i>b</i> ₁	969	25.6663	Farside CH ₂ wag
	ω_6	<i>a</i> ₂	1053	0	CH ₂ twist
	ω_7	<i>b</i> ₁	1110	19.0927	Nearside CH ₂ wag
	ω_8	<i>b</i> ₂	1244	0.5078	CH ₂ asymm. rock
	ω_9	<i>a</i> ₁	1377	1.4498	CH ₂ symm. scissor
	ω_{10}	<i>a</i> ₁	1477	16.7616	CH ₂ asymm. scissor
	ω_{11}	<i>a</i> ₁	1684	0.5243	C=C stretch
	ω_{12}	<i>a</i> ₁	3150	18.0679	CH ₂ unpair symm. stretch
	ω_{13}	<i>a</i> ₁	3168	0.0301	CH ₂ pair symm. stretch
pVQZ	ω_{14}	<i>b</i> ₂	3230	0.1364	CH ₂ unpair asymm. stretch
	ω_{15}	<i>b</i> ₂	3258	15.3362	CH ₂ pair asymm. stretch
			zpe	135.8	
	ω_1	<i>b</i> ₂	23	0.0032	In plane internal rotation
	ω_2	<i>a</i> ₁	42	0.0123	Intermolecular stretch
	ω_3	<i>b</i> ₁	82	3.1727	OoP internal rotation
	ω_4	<i>b</i> ₂	827	0.188	CH ₂ symm. rock
	ω_5	<i>b</i> ₁	976	25.3677	Farside CH ₂ wag
	ω_6	<i>a</i>	1068	0	CH ₂ twist
	ω_7	<i>a</i>	1069	0.0068	Nearside CH ₂ wag
	ω_8	<i>b</i> ₂	1247	0.4953	CH ₂ asymm. rock
	ω_9	<i>a</i> ₁	1378	1.4336	CH ₂ symm. scissor
	ω_{10}	<i>a</i> ₁	1479	17.0177	CH ₂ asymm. scissor
	ω_{11}	<i>a</i> ₁	1685	0.5205	C=C stretch
	ω_{12}	<i>a</i> ₁	3152	17.9436	CH ₂ unpair symm. stretch
	ω_{13}	<i>a</i> ₁	3168	0.0294	CH ₂ pair symm. stretch
	ω_{14}	<i>b</i> ₂	3233	0.1506	CH ₂ unpair asymm. stretch
	ω_{15}	<i>b</i> ₂	3260	14.9554	CH ₂ pair asymm. stretch
			zpe	135.7	

Table B80: Cartesian coordinates of the geometries of halide-ethene complexes optimised with the DSD-PBEP86-D3BJ functional, in Å.

		$\text{Cl}^- \cdots \text{C}_2\text{H}_4$			$\text{Br}^- \cdots \text{C}_2\text{H}_4$			$\text{I}^- \cdots \text{C}_2\text{H}_4$			
		x	y	z	x	y	z	x	y	z	
C_{2v} (1A_1) BifOut	def2QZVP	X	0.000000	0.000000	1.962151	0.000000	0.000000	1.315660	0.000000	0.000000	1.043715
		C	0.000000	0.663479	-2.093215	0.000000	0.663555	-2.886023	0.000000	0.663711	-3.464378
		C	0.000000	-0.663479	-2.093215	0.000000	-0.663555	-2.886023	0.000000	-0.663711	-3.464378
		H	0.922674	1.227245	-2.059496	0.922682	1.227459	-2.853953	0.922703	1.227920	-3.436094
		H	-0.922674	1.227245	-2.059496	-0.922682	1.227459	-2.853953	-0.922703	1.227920	-3.436094
		H	-0.922674	-1.227245	-2.059496	-0.922682	-1.227459	-2.853953	-0.922703	-1.227920	-3.436094
		H	0.922674	-1.227245	-2.059496	0.922682	-1.227459	-2.853953	0.922703	-1.227920	-3.436094
		X	0.000000	0.000000	1.978033	0.000000	0.000000	1.312829	0.000000	0.000000	1.034701
pVTZ	pVQZ	C	0.000000	0.664606	-2.109803	0.000000	0.664668	-2.879630	0.000000	0.664728	-3.427448
		C	0.000000	-0.664606	-2.109803	0.000000	-0.664668	-2.879630	0.000000	-0.664728	-3.427448
		H	0.923658	1.228895	-2.077231	0.923670	1.229054	-2.848367	0.923738	1.229886	-3.427448
		H	-0.923658	1.228895	-2.077231	-0.923670	1.229054	-2.848367	-0.923738	1.229886	-3.427448
		H	-0.923658	-1.228895	-2.077231	-0.923670	-1.229054	-2.848367	-0.923738	-1.229886	-3.427448
		H	0.923658	-1.228895	-2.077231	0.923670	-1.229054	-2.848367	0.923738	-1.229886	-3.427448
		X	0.000000	0.000000	2.006689	0.000000	0.000000	1.313740	0.000000	0.000000	1.020542
		C	0.000000	0.663795	-2.140009	0.000000	0.663834	-2.881599	0.000000	0.663922	-3.387766
		C	0.000000	-0.663795	-2.140009	0.000000	-0.663834	-2.881599	0.000000	-0.663922	-3.387766
		H	0.922980	1.227833	-2.108401	0.922989	1.227915	-2.850424	0.922981	1.228206	-3.358883
		H	-0.922980	1.227833	-2.108401	-0.922989	1.227915	-2.850424	-0.922981	1.228206	-3.358883
		H	-0.922980	-1.227833	-2.108401	-0.922989	-1.227915	-2.850424	-0.922981	-1.228206	-3.358883
		H	0.922980	-1.227833	-2.108401	0.922989	-1.227915	-2.850424	0.922981	-1.228206	-3.358883

Table B81: Cartesian coordinates of the geometries of halide-ethene complexes optimised with the DSD-PBEP86-D3BJ functional, in Å.

		$\text{Cl}^- \cdots \text{C}_2\text{H}_4$			$\text{Br}^- \cdots \text{C}_2\text{H}_4$			$\text{I}^- \cdots \text{C}_2\text{H}_4$			
		x	y	z	x	y	z	x	y	z	
C_{2v} (1A_1) BifPl	def2QZVP	X	0.000000	0.000000	1.705514	0.000000	0.000000	1.160611	0.000000	0.000000	0.920649
		C	0.000000	0.665054	-1.815837	0.000000	0.664955	-2.542035	0.000000	0.664839	-3.052138
		C	0.000000	-0.665054	-1.815837	0.000000	-0.664955	-2.542035	0.000000	-0.664839	-3.052138
		H	0.000000	1.184404	-0.863744	0.000000	1.190801	-1.593869	0.000000	1.199267	-2.109200
		H	0.000000	1.237849	-2.738100	0.000000	1.236569	-3.464619	0.000000	1.234895	-3.975167
		H	0.000000	-1.184404	-0.863744	0.000000	-1.190801	-1.593869	0.000000	-1.199267	-2.109200
		H	0.000000	-1.237849	-2.738100	0.000000	-1.236569	-3.464619	0.000000	-1.234895	-3.975167
		X	0.000000	0.000000	1.709351	0.000000	0.000000	1.154560	0.000000	0.000000	0.911628
pVTZ	pVQZ	C	0.000000	0.666127	-1.819794	0.000000	0.666036	-2.528909	0.000000	0.665915	-3.022458
		C	0.000000	-0.666127	-1.819794	0.000000	-0.666036	-2.528909	0.000000	-0.665915	-3.022458
		H	0.000000	1.187028	-0.867636	0.000000	1.191276	-1.579302	0.000000	1.198706	-2.077381
		H	0.000000	1.238975	-2.743086	0.000000	1.238540	-3.452051	0.000000	1.237027	-3.946000
		H	0.000000	-1.187028	-0.867636	0.000000	-1.191276	-1.579302	0.000000	-1.198706	-2.077381
		H	0.000000	-1.238975	-2.743086	0.000000	-1.238540	-3.452051	0.000000	-1.237027	-3.946000
		X	0.000000	0.000000	1.710211	0.000000	0.000000	1.156735	0.000000	0.000000	0.912070
		C	0.000000	0.665286	-1.820646	0.000000	0.665197	-2.533493	0.000000	0.665075	-3.023811
		C	0.000000	-0.665286	-1.820646	0.000000	-0.665197	-2.533493	0.000000	-0.665075	-3.023811
		H	0.000000	1.186614	-0.869489	0.000000	1.191857	-1.585473	0.000000	1.198677	-2.080001
		H	0.000000	1.237521	-2.743431	0.000000	1.236601	-3.456431	0.000000	1.235322	-3.946998
		H	0.000000	-1.186614	-0.869489	0.000000	-1.191857	-1.585473	0.000000	-1.198677	-2.080001
		H	0.000000	-1.237521	-2.743431	0.000000	-1.236601	-3.456431	0.000000	-1.235322	-3.946998

Table B82: Cartesian coordinates of the geometries of halide-ethene complexes optimised with the DSD-PBEP86-D3BJ functional, in Å.

		$\text{Cl}^- \cdots \text{C}_2\text{H}_4$			$\text{Br}^- \cdots \text{C}_2\text{H}_4$			$\text{I}^- \cdots \text{C}_2\text{H}_4$			
		x	y	z	x	y	z	x	y	z	
C_{2v} (1A_1) End	def2QZVP	X	0.000000	0.000000	2.002709	0.000000	0.000000	1.354963	0.000000	0.000000	1.064753
		C	0.000000	0.000000	-1.465186	0.000000	0.000000	-2.298419	0.000000	0.000000	-2.863833
		C	0.000000	0.000000	-2.796607	0.000000	0.000000	-3.629542	0.000000	0.000000	-4.194555
		H	0.000000	0.904433	-0.871620	0.000000	0.914810	-1.718961	0.000000	0.909644	-2.278065
		H	0.000000	-0.904433	-0.871620	0.000000	-0.914810	-1.718961	0.000000	-0.909644	-2.278065
		H	0.000000	0.922709	-3.366027	0.000000	0.914810	-4.209000	0.000000	0.922913	-4.762727
		H	0.000000	-0.922709	-3.366027	0.000000	-0.914810	-4.209000	0.000000	-0.922913	-4.762727
	pVTZ	X	0.000000	0.000000	2.010202	0.000000	0.000000	1.351718	0.000000	0.000000	1.059733
		C	0.000000	0.000000	-1.472031	0.000000	0.000000	-2.292970	0.000000	0.000000	-2.846259
		C	0.000000	0.000000	-2.805474	0.000000	0.000000	-3.626123	0.000000	0.000000	-4.179047
		H	0.000000	0.906137	-0.879222	0.000000	0.907852	-1.702656	0.000000	0.910331	-2.259633
		H	0.000000	-0.906137	-0.879222	0.000000	-0.907852	-1.702656	0.000000	-0.910331	-2.259633
		H	0.000000	0.923758	-3.374976	0.000000	0.923846	-4.195129	0.000000	0.923955	-4.747387
		H	0.000000	-0.923758	-3.374976	0.000000	-0.923846	-4.195129	0.000000	-0.923955	-4.747387
	pVQZ	X	0.000000	0.000000	2.011456	0.000000	0.000000	1.351146	0.000000	0.000000	1.060273
		C	0.000000	0.000000	-1.474205	0.000000	0.000000	-2.292566	0.000000	0.000000	-2.848865
		C	0.000000	0.000000	-2.805932	0.000000	0.000000	-3.624005	0.000000	0.000000	-4.179943
		H	0.000000	0.905582	-0.881840	0.000000	0.907251	-1.702611	0.000000	0.909826	-2.262802
		H	0.000000	-0.905582	-0.881840	0.000000	-0.907251	-1.702611	0.000000	-0.909826	-2.262802
		H	0.000000	0.923070	-3.375128	0.000000	0.923149	-4.192721	0.000000	0.923251	-4.748017
		H	0.000000	-0.923070	-3.375128	0.000000	-0.923149	-4.192721	0.000000	-0.923251	-4.748017

Table B83: Cartesian coordinates of the geometries of halide-ethene complexes optimised with the DSD-PBEP86-D3BJ functional, in Å.

		$\text{Cl}^- \cdots \text{C}_2\text{H}_4$			$\text{Br}^- \cdots \text{C}_2\text{H}_4$			$\text{I}^- \cdots \text{C}_2\text{H}_4$			
		x	y	z	x	y	z	x	y	z	
C_s ($^1A'$) HApp	def2QZVP	X	0.000000	1.020845	-1.631978	0.000000	0.000000	1.303859	0.000000	0.000000	1.025766
		C	0.000000	-0.428009	1.623340	0.000000	-0.510495	-2.425013	0.000000	-0.528200	-2.993238
		C	0.000000	-1.741167	1.843522	0.000000	0.510648	-3.278725	0.000000	0.528010	-3.802263
		H	0.000000	0.000000	0.619669	0.000000	-1.531042	-2.794194	0.000000	-1.534003	-3.399338
		H	0.000000	0.261789	2.461836	0.000000	-0.366691	-1.345678	0.000000	-0.423988	-1.911540
		H	0.000000	-2.441037	1.016429	0.000000	0.364335	-4.353607	0.000000	0.425635	-4.881832
		H	0.000000	-2.160067	2.844519	0.000000	1.532481	-2.919152	0.000000	1.533491	-3.399887
	pVTZ	X	0.000000	1.031663	-1.627639	0.000000	0.000000	1.293398	0.000000	0.000000	1.009266
		C	0.000000	-0.437344	1.625467	0.000000	-0.517366	-2.408733	0.000000	0.545439	-2.960110
		C	0.000000	-1.754748	1.832180	0.000000	0.517270	-3.249297	0.000000	-0.544755	-3.726283
		H	0.000000	0.000000	0.625336	0.000000	-1.533571	-2.792513	0.000000	1.534673	-3.407672
		H	0.000000	0.244604	2.471550	0.000000	-0.386164	-1.326705	0.000000	0.481137	-1.874093
		H	0.000000	-2.446665	0.997135	0.000000	0.385630	-4.327084	0.000000	-0.486897	-4.810191
		H	0.000000	-2.183660	2.829959	0.000000	1.534682	-2.874462	0.000000	-1.533013	-3.280803
	pVQZ	X	0.000000	1.042316	-1.621722	0.000000	0.000000	1.296327	0.000000	0.000000	0.912070
		C	0.000000	-0.448281	1.627299	0.000000	-0.516762	-2.415738	0.000000	0.665075	-3.023811
		C	0.000000	-1.766413	1.817882	0.000000	0.516662	-3.255137	0.000000	-0.665075	-3.023811
		H	0.000000	0.000000	0.632801	0.000000	-1.532357	-2.798945	0.000000	1.235321	-3.946999
		H	0.000000	0.223447	2.480517	0.000000	-0.385567	-1.334539	0.000000	1.198678	-2.080002
		H	0.000000	-2.447701	0.975135	0.000000	0.385170	-4.332155	0.000000	-1.235321	-3.946999
		H	0.000000	-2.206958	2.809742	0.000000	1.533357	-2.880568	0.000000	-1.198678	-2.080002

Table B84: Cartesian coordinates of the geometries of halogen-ethene complexes optimised with the DSD-PBEP86-D3BJ functional, in Å.

		Cl ... C ₂ H ₄			Br ... C ₂ H ₄			I ... C ₂ H ₄		
		x	y	z	x	y	z	x	y	z
def2QZVP	X	0.000000	0.000000	1.196209	0.000000	0.000000	0.836035	0.000000	0.000000	0.680237
	C	0.000000	0.675792	-1.270972	0.000000	0.673434	-1.826412	0.000000	0.670850	-2.251371
	C	0.000000	-0.675792	-1.270972	0.000000	-0.673434	-1.826412	0.000000	-0.670850	-2.251371
	H	0.924475	1.235354	-1.270972	0.924159	1.234347	-1.836074	0.923851	1.233329	-2.259024
	H	-0.924475	1.235354	-1.270972	-0.924159	1.234347	-1.836074	-0.923851	1.233329	-2.259024
	H	-0.924475	-1.235354	-1.270972	-0.924159	-1.234347	-1.836074	-0.923851	-1.233329	-2.259024
	H	0.924475	-1.235354	-1.270972	0.924159	-1.234347	-1.836074	0.923851	-1.233329	-2.259024
	C _{2v} (² A ₁) BifOut	X	0.000000	0.000000	1.195149	0.000000	0.000000	0.831021	0.000000	0.000000
pVTZ	C	0.000000	0.676824	-1.267328	0.000000	0.674442	-1.815498	0.000000	0.671687	-2.256768
	C	0.000000	-0.676824	-1.267328	0.000000	-0.674442	-1.815498	0.000000	-0.671687	-2.256768
	H	0.925515	1.236510	-1.277401	0.925224	1.235490	-1.824938	0.924810	1.234476	-2.263931
	H	-0.925515	1.236510	-1.277401	-0.925224	1.235490	-1.824938	-0.924810	1.234476	-2.263931
	H	-0.925515	-1.236510	-1.277401	-0.925224	-1.235490	-1.824938	-0.924810	-1.234476	-2.263931
	H	0.925515	-1.236510	-1.277401	0.925224	-1.235490	-1.824938	0.924810	-1.234476	-2.263931
	pVQZ	X	0.000000	0.000000	1.193560	0.000000	0.000000	0.828732	0.000000	0.000000
	C	0.000000	0.676209	-1.265587	0.000000	0.673861	-1.810568	0.000000	0.671132	-2.243313
	C	0.000000	-0.676209	-1.265587	0.000000	-0.673861	-1.810568	0.000000	-0.671132	-2.243313
	H	0.924796	1.235586	-1.275867	0.924511	1.234608	-1.819706	0.924072	1.233639	-2.250326
	H	-0.924796	1.235586	-1.275867	-0.924511	1.234608	-1.819706	-0.924072	1.233639	-2.250326
	H	-0.924796	-1.235586	-1.275867	-0.924511	-1.234608	-1.819706	-0.924072	-1.233639	-2.250326
	H	0.924796	-1.235586	-1.275867	0.924511	-1.234608	-1.819706	0.924072	-1.233639	-2.250326

Table B85: Cartesian coordinates of the geometries of halogen-ethene complexes optimised with the DSD-PBEP86-D3BJ functional, in Å.

		Cl ... C ₂ H ₄			Br ... C ₂ H ₄			I ... C ₂ H ₄			
		x	y	z	x	y	z	x	y	z	
<i>C_{2v} (2A₁)</i> BifPl	def2QZVP	X	0.000000	0.000000	1.845778	0.000000	0.000000	1.227461	0.000000	0.000000	0.948962
		C	0.000000	0.664484	-1.961322	0.000000	0.664483	-2.685324	0.000000	0.664481	-3.143739
		C	0.000000	-0.664484	-1.961322	0.000000	-0.664483	-2.685324	0.000000	-0.664481	-3.143739
		H	0.000000	1.227130	-1.036912	0.000000	1.226540	-1.760486	0.000000	1.226376	-2.218611
		H	0.000000	1.229868	-2.884268	0.000000	1.230111	-3.608133	0.000000	1.230316	-4.066455
		H	0.000000	-1.227130	-1.036912	0.000000	-1.226540	-1.760486	0.000000	-1.226376	-2.218611
		H	0.000000	-1.229868	-2.884268	0.000000	-1.230111	-3.608133	0.000000	-1.230316	-4.066455
		X	0.000000	0.000000	1.829912	0.000000	0.000000	1.207559	0.000000	0.000000	0.934768
pVTZ	pVQZ	C	0.000000	0.665511	-1.944512	0.000000	0.665519	-2.641913	0.000000	0.665508	-3.096860
		C	0.000000	-0.665511	-1.944512	0.000000	-0.665519	-2.641913	0.000000	-0.665508	-3.096860
		H	0.000000	1.227991	-1.018864	0.000000	1.231956	-3.565398	0.000000	1.232186	-4.020225
		H	0.000000	1.231408	-2.868313	0.000000	1.226709	-1.715400	0.000000	1.226366	-2.169966
		H	0.000000	-1.227991	-1.018864	0.000000	-1.231956	-3.565398	0.000000	-1.232186	-4.020225
		H	0.000000	-1.231408	-2.868313	0.000000	-1.226709	-1.715400	0.000000	-1.226366	-2.169966
		X	0.000000	0.000000	1.834417	0.000000	0.000000	1.206360	0.000000	0.000000	0.934234
		C	0.000000	0.664662	-1.949260	0.000000	0.664678	-2.639223	0.000000	0.664666	-3.095020
		C	0.000000	-0.664662	-1.949260	0.000000	-0.664678	-2.639223	0.000000	-0.664666	-3.095020
		H	0.000000	1.227248	-1.024494	0.000000	1.226161	-1.713708	0.000000	1.225843	-2.169148
		H	0.000000	1.230068	-2.872497	0.000000	1.230453	-3.562248	0.000000	1.230671	-4.017926
		H	0.000000	-1.227248	-1.024494	0.000000	-1.226161	-1.713708	0.000000	-1.225843	-2.169148
		H	0.000000	-1.230068	-2.872497	0.000000	-1.230453	-3.562248	0.000000	-1.230671	-4.017926

Table B86: Cartesian coordinates of the geometries of halogen-ethene complexes optimised with the DSD-PBEP86-D3BJ functional, in Å.

		Cl ... C ₂ H ₄			Br ... C ₂ H ₄			I ... C ₂ H ₄			
		x	y	z	x	y	z	x	y	z	
<i>C_{2v} (2A₁)</i> End	def2QZVP	X	0.000000	0.000000	2.179989	0.000000	0.000000	1.444670	0.000000	0.000000	1.111636
		C	0.000000	0.000000	-1.652014	0.000000	0.000000	-2.496024	0.000000	0.000000	-3.018108
		C	0.000000	0.000000	-2.980887	0.000000	0.000000	-3.824909	0.000000	0.000000	-4.347022
		H	0.000000	0.921657	-1.084823	0.000000	0.921483	-1.928520	0.000000	0.921462	-2.450445
		H	0.000000	-0.921657	-1.084823	0.000000	-0.921483	-1.928520	0.000000	-0.921462	-2.450445
		H	0.000000	0.922804	-3.546380	0.000000	0.922809	-4.390407	0.000000	0.922822	-4.912515
		H	0.000000	-0.922804	-3.546380	0.000000	-0.922809	-4.390407	0.000000	-0.922822	-4.912515
		X	0.000000	0.000000	2.163470	0.000000	0.000000	1.429065	0.000000	0.000000	1.097442
pVTZ	pVQZ	C	0.000000	0.000000	-1.633466	0.000000	0.000000	-2.460912	0.000000	0.000000	-2.970169
		C	0.000000	0.000000	-2.964380	0.000000	0.000000	-3.791844	0.000000	0.000000	-4.301120
		H	0.000000	0.922545	-1.065790	0.000000	0.922276	-1.892748	0.000000	0.922025	-2.401491
		H	0.000000	-0.922545	-1.065790	0.000000	-0.922276	-1.892748	0.000000	-0.922025	-2.401491
		H	0.000000	0.923789	-3.530168	0.000000	0.923803	-4.357626	0.000000	0.923825	-4.866862
		H	0.000000	-0.923789	-3.530168	0.000000	-0.923803	-4.357626	0.000000	-0.923825	-4.866862
		X	0.000000	0.000000	2.169323	0.000000	0.000000	1.421832	0.000000	0.000000	1.095543
		C	0.000000	0.000000	-1.640520	0.000000	0.000000	-2.445963	0.000000	0.000000	-2.964709

Table B87: $X^- \cdots \text{HCOOH}$ complex geometric parameters and D_0 values from DSD-PBEP86-D3BJ optimisations. zpe values are drawn from relevant harmonic frequency calculations.

			$R_{\text{X}-\text{H}}$	$\angle_{\text{X}-\text{H}-\text{O}}$	Dh	$R_{\text{C}-\text{O}}$	$R_{\text{C}=\text{O}}$	$R_{\text{O}-\text{H}}$	$\angle_{\text{C}-\text{O}-\text{H}}$	$\angle_{\text{O}-\text{C}=\text{O}}$
			Å	°	°	Å	Å	Å	°	°
$\text{Cl}^- \cdots \text{HCOOH}$	AcidAnti	def2QZVP	1.898	172.0	0.0	1.313	1.214	1.020	107.7	124.3
	C_s ($^1A'$)	pVTZ	1.903	172.2	0.0	1.316	1.217	1.022	107.7	124.3
		pVQZ	1.905	171.9	0.0	1.313	1.214	1.019	107.8	124.3
$\text{Cl}^- \cdots \text{HCOOH}$	AcidSyn	def2QZVP	1.869	168.0	180.0	1.306	1.211	1.036	115.4	129.0
	C_s ($^1A'$)	pVTZ	1.877	168.0	180.0	1.310	1.214	1.036	115.1	129.0
		pVQZ	1.878	168.1	180.0	1.307	1.212	1.034	115.2	128.9
$\text{Br}^- \cdots \text{HCOOH}$	FormSyn	def2QZVP	2.265	177.0	0.0	1.357	1.209	0.967	104.9	121.1
	C_s ($^1A'$)	pVTZ	2.271	176.7	0.0	1.359	1.212	0.969	104.9	121.2
		pVQZ	2.274	176.7	0.0	1.357	1.209	0.967	105.0	121.2
$\text{Br}^- \cdots \text{HCOOH}$	AcidAnti	def2QZVP	2.106	170.3	0.0	1.318	1.212	1.007	107.7	123.9
	C_s ($^1A'$)	pVTZ	2.102	170.6	0.0	1.320	1.214	1.009	107.6	123.9
		pVQZ	2.090	170.6	0.0	1.318	1.212	1.008	107.8	123.9
$\text{Br}^- \cdots \text{HCOOH}$	AcidSyn	def2QZVP	2.094	166.2	180.0	1.311	1.209	1.018	114.5	128.8
	C_s ($^1A'$)	pVTZ	2.092	166.4	180.0	1.314	1.212	1.019	114.3	128.7
		pVQZ	2.078	166.7	180.0	1.311	1.210	1.019	114.4	128.7
$\text{I}^- \cdots \text{HCOOH}$	FormSyn	def2QZVP	2.474	176.4	0.0	1.355	1.208	0.967	105.1	121.5
	C_s ($^1A'$)	pVTZ	2.460	176.2	0.0	1.357	1.210	0.969	105.1	121.6
		pVQZ	2.449	176.2	0.0	1.357	1.208	0.967	105.0	121.4
$\text{I}^- \cdots \text{HCOOH}$	AcidAnti	def2QZVP	2.378	169.2	0.0	1.323	1.209	0.996	108.0	123.5
	C_s ($^1A'$)	pVTZ	2.374	169.3	0.0	1.325	1.212	0.999	107.7	123.5
		pVQZ	2.365	169.1	0.0	1.323	1.210	0.997	107.9	123.5
$\text{I}^- \cdots \text{HCOOH}$	AcidSyn	def2QZVP	2.387	164.1	180.0	1.316	1.207	1.003	113.5	128.4
	C_s ($^1A'$)	pVTZ	2.383	164.3	180.0	1.319	1.210	1.006	113.4	128.4
		pVQZ	2.373	164.5	180.0	1.316	1.207	1.004	113.5	128.3
$\text{I}^- \cdots \text{HCOOH}$	FormSyn	def2QZVP	2.767	175.6	0.0	1.352	1.206	0.967	105.3	122.1
	C_s ($^1A'$)	pVTZ	2.740	175.6	0.0	1.355	1.209	0.969	105.3	122.1
		pVQZ	2.744	175.3	0.0	1.355	1.207	0.967	105.2	121.9

Table B88: X···HCOOH complex geometric parameters and D_0 values from DSD-PBEP86-D3BJ optimisations. zpe values are drawn from relevant harmonic frequency calculations.

		R_{X-H} Å	\angle_{X-H-O} °	$Dh_{X-H-O-C}$ °	R_{C-O} Å	$R_{C=O}$ Å	R_{O-H} Å	\angle_{C-O-H} °	$\angle_{O-C=O}$ °	E_{DFT} E_h	zpe kJ mol ⁻¹	D_e kJ mol ⁻¹	D_o kJ mol ⁻¹	
HOOC···O	AcidAnti C_s ($^2A''$)	def2	2.495	171.8	0.0	1.346	1.194	0.965	109.2	122.7	-649.4234691	89.6	-8.6	-7.9
		pVTZ	2.467	173.8	0.0	1.348	1.196	0.967	109.1	122.7	-649.3811215	89.4	-7.5	-6.8
		pVQZ	2.480	172.1	0.0	1.346	1.194	0.965	109.2	122.7	-649.4254670	89.5	-7.9	-7.6
	AcidPSyn C_s ($^2A'$)	def2	2.218	138.4	0.0	1.315	1.216	0.978	107.2	126.1	-649.4255680	92.4	-3.1	0.5
		pVTZ	2.217	138.7	0.0	1.318	1.218	0.981	107.1	126.1	-649.3831184	92.1	-2.3	1.2
		pVQZ	2.214	138.3	0.0	1.315	1.216	0.979	107.2	126.1	-649.4313977	92.3	7.6	10.8
	CarbPAnti C_s ($^2A'$)	def2	2.627	117.3	0.0	1.338	1.198	0.963	109.8	122.7	-649.4299518	90.2	26.1	28.3
		pVTZ	2.632	116.9	0.0	1.341	1.201	0.965	109.7	122.6	-649.3874881	89.9	26.8	28.9
		pVQZ	2.617	117.1	0.0	1.338	1.199	0.963	109.8	122.6	-649.4276632	90.1	15.4	17.2
	CarbPSyn C_1 (2A)	def2	2.796	111.5	137.7	1.347	1.197	0.968	107.3	124.6	-649.4270581	90.0	0.8	1.9
		pVTZ	2.785	110.9	132.9	1.350	1.199	0.970	107.2	124.6	-649.3845715	89.8	1.5	2.7
		pVQZ	2.779	111.6	136.8	1.348	1.224	0.968	107.4	122.4	-649.4318934	89.8	8.9	9.6
	FormPAnti C_s ($^2A'$)	def2	2.531	104.9	180.0	1.337	1.201	0.963	109.6	121.6	-649.4234691	90.8	9.1	11.9
		pVTZ	2.537	104.7	180.0	1.340	1.204	0.965	109.6	121.5	-649.3845715	90.5	19.1	21.9
		pVQZ	2.523	104.9	180.0	1.337	1.201	0.963	109.7	121.5	-649.4291541	90.7	19.3	21.7
	FormPSyn C_s ($^2A'$)	def2	2.963	86.9	180.0	1.331	1.207	0.968	107.6	124.3	-649.4333976	91.4	17.5	20.0
		pVTZ	2.963	87.1	180.0	1.334	1.209	0.970	107.5	124.3	-649.3908721	91.1	18.1	20.6
		pVQZ	2.957	86.8	180.0	1.332	1.207	0.968	107.7	124.3	-649.4354276	91.3	18.2	20.4
	InLineSyn C_s ($^2A''$)	def2	2.508	170.6	180.0	1.339	1.200	0.970	107.6	125.2	-649.4294543	90.4	7.1	8.6
		pVTZ	2.481	170.3	180.0	1.342	1.203	0.972	107.5	125.3	-649.3870798	90.2	8.1	9.7
		pVQZ	2.491	171.2	180.0	1.340	1.200	0.971	107.6	125.2	-649.4313977	90.3	7.6	8.7
	OutPlAnti C_1 (2A)	def2	2.819	110.1	59.5	1.354	1.190	0.963	109.8	122.2	-649.4231910	89.1	8.4	9.5
		pVTZ	2.813	109.2	60.1	1.356	1.193	0.965	109.7	122.1	-649.3807418	88.8	9.1	10.2
		pVQZ	2.805	110.0	58.8	1.354	1.191	0.963	109.9	122.1	-649.4251819	89.0	8.8	9.6

Table B89: X···HCOOH complex geometric parameters and D_0 values from DSD-PBEP86-D3BJ optimisations. zpe values are drawn from relevant harmonic frequency calculations.

		R_{X-H}	\angle_{X-H-O}	$Dh_{X-H-O-C}$	R_{C-O}	$R_{C=O}$	R_{O-H}	\angle_{C-O-H}	$\angle_{O-C=O}$	E_{DFT}	zpe	D_e	D_o	
		Å	°	°	Å	Å	Å	°	°	E_h	kJ mol ⁻¹	kJ mol ⁻¹	kJ mol ⁻¹	
Br···HCOOH	AcidAnti	def2	2.611	179.8	180.0	1.344	1.194	0.966	109.2	122.8	-2762.9035135	89.4	9.5	10.9
	C_s ($^2A''$)	pVTZ	2.563	174.7	180.0	1.347	1.197	0.968	109.2	122.8	-605.7221965	88.8	11.6	12.6
		pVQZ	2.562	179.8	180.0	1.344	1.194	0.966	109.2	122.8	-605.7904078	89.5	11.2	12.5
AcidPSyn	R_{X-H} \angle_{X-H-O} $Dh_{X-H-O-C}$													
	C_s ($^2A'$)	def2	2.409	140.0	0.0	1.321	1.212	0.976	107.7	126.0	-2762.9164383	91.8	25.8	28.7
		pVTZ	2.397	140.3	0.0	1.324	1.215	0.979	107.5	126.0	-605.7352501	91.6	28.2	31.2
		pVQZ	2.375	140.2	0.0	1.321	1.213	0.978	107.6	126.0	-605.8038602	91.8	29.0	31.6
CarbPAnti	R_{X-O} $\angle_{X-O=C}$ $Dh_{X-O=C-O}$													
	C_s ($^2A'$)	def2	2.774	118.7	0.0	1.339	1.198	0.963	109.8	122.5	-2762.9057547	90.0	15.4	17.4
		pVTZ	2.760	118.3	0.0	1.341	1.200	0.965	109.8	122.5	-605.7242830	89.7	17.0	19.1
		pVQZ	2.747	118.0	0.0	1.339	1.198	0.963	109.9	122.5	-605.7927562	90.0	17.4	19.1
CarbPSyn	R_{X-O} $\angle_{X-O=C}$ $Dh_{X-O-C=O}$													
	C_s ($^2A'$)	def2	2.946	114.9	180.0	1.346	1.197	0.968	107.5	124.7	-2762.9100519	89.5	9.0	9.7
		pVTZ	2.917	113.9	180.0	1.349	1.200	0.970	107.5	124.7	-605.7285103	89.3	10.5	11.2
		pVQZ	2.905	113.3	180.0	1.347	1.197	0.968	107.6	124.6	-605.7969128	89.6	10.8	11.2
FormPAnti	R_{X-O} $\angle_{X-O=C}$ $Dh_{X-O=C-O}$													
	C_s ($^2A'$)	def2	2.691	106.4	180.0	1.338	1.200	0.963	109.6	121.7	-2762.9069348	90.5	18.5	21.0
		pVTZ	2.685	106.1	180.0	1.341	1.203	0.965	109.6	121.7	-605.7254671	90.2	20.2	22.6
		pVQZ	2.671	106.4	180.0	1.338	1.200	0.963	109.7	121.7	-605.7939753	90.5	20.6	22.8
FormPSyn	R_{X-H} $\angle_{X-O=C}$ $Dh_{X-H-C-O}$													
	C_s ($^2A'$)	def2	3.130	87.8	180.0	1.332	1.206	0.968	107.6	124.4	-2762.9132907	91.1	17.5	19.8
		pVTZ	3.114	88.0	180.0	1.335	1.208	0.970	107.5	124.5	-605.7317623	90.8	19.1	21.3
		pVQZ	3.109	87.7	180.0	1.332	1.206	0.968	107.6	124.4	-605.8002542	91.1	19.6	21.5

Table B90: X···HCOOH complex geometric parameters and D_0 values from DSD-PBEP86-D3BJ optimisations. zpe values are drawn from relevant harmonic frequency calculations.

		R_{X-H}	\angle_{X-H-O}	$Dh_{X-H-O-C}$	R_{C-O}	$R_{C=O}$	R_{O-H}	\angle_{C-O-H}	$\angle_{O-C=O}$	E_{DFT}	zpe	D_e	D_o	
		Å	°	°	Å	Å	Å	°	°	E_h	kJ mol ⁻¹	kJ mol ⁻¹	kJ mol ⁻¹	
I···HCOOH	AcidAnti	def2	2.776	171.0	0.0	1.345	1.194	0.966	109.2	122.8	-487.0001124	89.4	11.8	13.1
	C_s ($^2A''$)	pVTZ	2.730	172.4	0.0	1.347	1.197	0.969	109.0	122.8	-484.7763941	89.2	14.0	15.5
		pVQZ	2.731	171.2	0.0	1.345	1.195	0.967	109.2	122.8	-484.8451626	89.4	13.9	15.0
	AcidPSyn	def2	R_{X-H} \angle_{X-H-O} $Dh_{X-H-O-C}$											
		pVTZ	2.657	141.9	0.0	1.326	1.209	0.975	108.3	126.1	-487.0113231	91.2	23.5	25.9
		pVQZ	2.645	142.6	0.0	1.328	1.212	0.977	108.2	126.1	-484.7875874	91.0	25.8	28.1
	CarbPAnti	def2	2.628	142.0	0.0	1.325	1.210	0.976	108.3	126.0	-484.8567507	91.3	26.8	28.9
		pVTZ	R_{X-O} $\angle_{X-O=C}$ $Dh_{X-O=C-O}$											
		pVQZ	2.971	120.4	0.0	1.340	1.197	0.963	109.9	122.4	-487.0017667	89.8	16.1	17.9
I···HCOO ⁻	CarbPSyn	C_s ($^2A'$)	2.974	119.6	0.0	1.342	1.200	0.965	109.9	122.3	-484.7777178	89.5	17.5	19.3
		pVTZ	2.949	120.1	0.0	1.340	1.198	0.963	110.0	122.4	-484.8467327	89.8	18.0	19.5
		pVQZ	R_{X-O} \angle_{X-O-C} $Dh_{X-O-C=O}$											
	C_s ($^2A'$)	def2	3.130	115.1	180.0	1.347	1.197	0.968	107.5	124.7	-487.0059523	89.6	9.4	10.1
		pVTZ	3.123	113.0	180.0	1.350	1.200	0.970	107.4	124.7	-484.7819179	89.4	10.9	11.7
		pVQZ	3.094	113.7	180.0	1.348	1.197	0.968	107.5	124.6	-484.8508119	89.6	11.2	11.7
	FormPAnti	def2	R_{X-O} $\angle_{X-O=C}$ $Dh_{X-O=C-O}$											
		C_s ($^2A'$)	2.891	108.4	180.0	1.339	1.199	0.963	109.7	121.8	-487.0026840	90.2	18.5	20.7
		pVTZ	2.900	107.7	180.0	1.341	1.202	0.965	109.6	121.8	-484.7786732	89.9	20.0	22.2
	FormPSyn	pVQZ	2.876	108.1	180.0	1.339	1.200	0.963	109.7	121.8	-484.8476979	90.2	20.6	22.5
		def2	R_{X-H} \angle_{X-O-C} $Dh_{X-H-C-O}$											
		C_s ($^2A'$)	3.354	88.4	180.0	1.333	1.205	0.968	107.5	124.5	-487.0090110	90.9	17.4	19.4
	pVTZ	pVTZ	3.336	89.1	180.0	1.335	1.208	0.970	107.5	124.6	-484.7849351	90.6	18.8	20.8
		pVQZ	3.332	88.5	180.0	1.332	1.206	0.968	107.6	124.5	-484.8539484	90.8	19.5	21.1

Table B91: $\text{X}^- \cdots \text{HCOOH}$ complex VDEs from DSD-PBEP86-D3BJ optimisations. zpe values are drawn from relevant harmonic frequency calculations.

		E_{DFT}	zpe	D_e	D_o	E_{VDE}	$VDE_{2P_{3/2}}$	$VDE_{2P_{1/2}}$	$EA_{2P_{3/2}}$	$EA_{2P_{1/2}}$
		E_h	kJ mol^{-1}	kJ mol^{-1}	kJ mol^{-1}	E_h	eV	eV	eV	eV
$\text{Cl}^- \cdots \text{HCOOH}$	AcidAnti def2	-649.6010967	89.8	138.0	139.8	-649.4134411	5.188	5.297	4.946	5.055
	C_s ($^1A'$) pVTZ	-649.5595544	89.5	134.5	136.3	-649.3715186	5.131	5.240	4.900	5.009
	pVQZ	-649.6053503	89.7	133.7	135.1	-649.4159030	5.127	5.236	4.897	5.006
	AcidSyn def2	-649.5922838	87.6	97.1	95.9	-649.4169766	4.852	4.988	4.574	4.683
	C_s ($^1A'$) pVTZ	-649.5508514	87.5	94.0	92.9	-649.3753025	4.790	4.926	4.532	4.641
	pVQZ	-649.5966401	87.6	93.3	91.7	-649.4196326	4.787	4.923	4.529	4.638
$\text{Br}^- \cdots \text{HCOOH}$	FormSyn def2	-649.5741821	90.5	49.6	51.2	-649.4238775	4.181	4.312	3.956	4.065
	C_s ($^1A'$) pVTZ	-649.5333411	90.2	48.0	49.7	-649.3812581	4.161	4.292	3.933	4.042
	pVQZ	-649.5791659	90.4	47.4	48.6	-649.4257443	4.155	4.286	3.926	4.035
	AcidAnti def2	-2763.0708498	90.1	122.4	124.5	-2762.896959	4.684	5.165	4.526	4.983
	C_s ($^1A'$) pVTZ	-605.8886553	89.8	121.0	123.0	-605.7159059	4.641	5.122	4.487	4.944
	pVQZ	-605.9588771	89.9	121.3	123.0	-605.7841899	4.646	5.128	4.501	4.958
$\text{I}^- \cdots \text{HCOOH}$	AcidSyn def2	-2763.0620982	88.4	81.7	81.2	-2762.9024939	4.295	4.777	3.979	4.436
	C_s ($^1A'$) pVTZ	-605.8800436	88.2	80.8	80.3	-605.7137311	4.465	4.948	3.944	4.401
	pVQZ	-605.9502153	88.2	81.1	80.1	-605.7818835	4.472	4.955	3.940	4.397
	FormSyn def2	-2763.0472360	90.4	42.7	44.2	-2762.9046064	3.841	4.318	4.278	4.735
	C_s ($^1A'$) pVTZ	-605.8655786	90.2	42.8	44.4	-605.7231863	3.822	4.299	4.249	4.706
	pVQZ	-605.9354309	90.2	42.2	43.3	-605.7913579	3.820	4.297	4.250	4.707

Table B92: Calculated harmonic frequencies and mode assignments for the $\text{Cl}^- \cdots \text{HCOOH}$ complex. All frequencies and intensities are in cm^{-1} and km mol^{-1} respectively.

$\text{Cl}^- \cdots \text{HCOOH}$ $C_s ({}^1A')$ AcidAnti vdW Complex					
	Mode	Symmetry	Frequency (cm^{-1})	Intensity (km mol^{-1})	Description
def2QZVP	ω_1	a'	111	9.7457	In plane internal rotation
	ω_2	a''	166	32.8234	OoP internal rotation
	ω_3	a'	255	58.5546	Intermolecular stretch
	ω_4	a'	708	11.1202	$\text{O}=\text{C}-\text{O}$ bend
	ω_5	a''	997	33.3866	Acidic H wag
	ω_6	a''	1084	1.0789	Formyl H wag
	ω_7	a'	1246	124.0897	$\text{C}-\text{OH}$ stretch
	ω_8	a'	1417	17.8938	Formyl H bend
	ω_9	a'	1463	158.4102	Acidic H bend
	ω_{10}	a'	1778	635.3989	$\text{C}=\text{O}$ stretch
	ω_{11}	a'	2768	2446.6507	Acidic H stretch
	ω_{12}	a'	3020	100.8512	Formyl H stretch
	zpe		89.8		
pVTZ	ω_1	a'	110	9.434	In plane internal rotation
	ω_2	a''	166	32.4683	OoP internal rotation
	ω_3	a'	252	59.571	Intermolecular stretch
	ω_4	a'	703	11.2813	$\text{O}=\text{C}-\text{O}$ bend
	ω_5	a''	991	28.7096	Acidic H wag
	ω_6	a''	1079	0.4862	Formyl H wag
	ω_7	a'	1242	125.2696	$\text{C}-\text{OH}$ stretch
	ω_8	a'	1410	18.073	Formyl H bend
	ω_9	a'	1458	149.6864	Acidic H bend
	ω_{10}	a'	1769	664.2714	$\text{C}=\text{O}$ stretch
	ω_{11}	a'	2770	2504.7336	Acidic H stretch
	ω_{12}	a'	3018	93.2322	Formyl H stretch
	zpe		89.5		
pVQZ	ω_1	a'	110	9.3829	In plane internal rotation
	ω_2	a''	166	32.3517	OoP internal rotation
	ω_3	a'	252	59.3582	Intermolecular stretch
	ω_4	a'	706	10.9735	$\text{O}=\text{C}-\text{O}$ bend
	ω_5	a''	991	28.3726	Acidic H wag
	ω_6	a''	1082	0.5926	Formyl H wag
	ω_7	a'	1243	126.0268	$\text{C}-\text{OH}$ stretch
	ω_8	a'	1414	18.0525	Formyl H bend
	ω_9	a'	1459	149.9385	Acidic H bend
	ω_{10}	a'	1773	660.9776	$\text{C}=\text{O}$ stretch
	ω_{11}	a'	2782	2472.4127	Acidic H stretch
	ω_{12}	a'	3019	96.4658	Formyl H stretch
	zpe		89.7		

Table B93: Calculated harmonic frequencies and mode assignments for the $\text{Cl}^- \cdots \text{HCOOH}$ complex. All frequencies and intensities are in cm^{-1} and km mol^{-1} respectively.

$\text{Cl}^- \cdots \text{HCOOH}$ $C_s ({}^1A')$ AcidSyn vdW Complex					
	Mode	Symmetry	Frequency (cm^{-1})	Intensity (km mol^{-1})	Description
def2QZVP	ω_1	a'	107	1.6647	In plane internal rotation
	ω_2	a''	178	5.0905	OoP internal rotation
	ω_3	a'	261	98.1138	Intermolecular stretch
	ω_4	a'	698	41.2244	$\text{O}=\text{C}-\text{O}$ bend
	ω_5	a''	1014	31.9186	Acidic H wag
	ω_6	a''	1099	16.8962	Formyl H wag
	ω_7	a'	1256	291.3672	$\text{C}-\text{OH}$ stretch
	ω_8	a'	1369	11.4201	Acidic H bend
	ω_9	a'	1424	39.3859	Formyl H bend
	ω_{10}	a'	1759	615.3097	$\text{C}=\text{O}$ stretch
	ω_{11}	a'	2527	3274.953	Acidic H stretch
	ω_{12}	a'	2954	103.8487	Formyl H stretch
	zpe		87.6		
pVTZ	ω_1	a'	106	1.6475	In plane internal rotation
	ω_2	a''	177	5.1081	OoP internal rotation
	ω_3	a'	257	98.067	Intermolecular stretch
	ω_4	a'	693	40.9312	$\text{O}=\text{C}-\text{O}$ bend
	ω_5	a''	1005	27.8697	Acidic H wag
	ω_6	a''	1094	13.4791	Formyl H wag
	ω_7	a'	1252	283.7654	$\text{C}-\text{OH}$ stretch
	ω_8	a'	1365	10.6312	Acidic H bend
	ω_9	a'	1419	40.5178	Formyl H bend
	ω_{10}	a'	1752	614.7495	$\text{C}=\text{O}$ stretch
	ω_{11}	a'	2546	3306.6377	Acidic H stretch
	ω_{12}	a'	2957	98.2896	Formyl H stretch
	zpe		87.5		
pVQZ	ω_1	a'	106	1.6473	In plane internal rotation
	ω_2	a''	177	5.07	OoP internal rotation
	ω_3	a'	257	97.6713	Intermolecular stretch
	ω_4	a'	695	41.2376	$\text{O}=\text{C}-\text{O}$ bend
	ω_5	a''	1007	27.7526	Acidic H wag
	ω_6	a''	1095	12.7135	Formyl H wag
	ω_7	a'	1252	286.5623	$\text{C}-\text{OH}$ stretch
	ω_8	a'	1366	10.1394	Acidic H bend
	ω_9	a'	1422	39.1323	Formyl H bend
	ω_{10}	a'	1755	611.5292	$\text{C}=\text{O}$ stretch
	ω_{11}	a'	2553	3290.0983	Acidic H stretch
	ω_{12}	a'	2958	96.5491	Formyl H stretch
	zpe		87.6		

Table B94: Calculated harmonic frequencies and mode assignments for the $\text{Cl}^- \cdots \text{HCOOH}$ complex. All frequencies and intensities are in cm^{-1} and km mol^{-1} respectively.

$\text{Cl}^- \cdots \text{HCOOH}$ $C_s ({}^1A')$ FormSyn vdW Complex					
	Mode	Symmetry	Frequency (cm^{-1})	Intensity (km mol^{-1})	Description
def2QZVP	ω_1	a'	88	3.6824	In plane internal rotation
	ω_2	a'	135	31.2161	Intermolecular stretch
	ω_3	a''	168	0.8281	OoP internal rotation
	ω_4	a'	631	67.7333	$\text{O}=\text{C}-\text{O}$ bend
	ω_5	a''	684	122.2421	Acidic H wag
	ω_6	a'	1093	324.6937	$\text{C}-\text{OH}$ stretch
	ω_7	a''	1152	1.5085	Formyl H wag
	ω_8	a'	1289	10.3903	Acidic H bend
	ω_9	a'	1442	20.0407	Formyl H bend
	ω_{10}	a'	1754	383.5942	$\text{C}=\text{O}$ stretch
	ω_{11}	a'	2923	371.9731	Formyl H stretch
	ω_{12}	a'	3764	23.3295	Acidic H stretch
	zpe		90.5		
pVTZ	ω_1	a'	88	3.597	In plane internal rotation
	ω_2	a'	134	31.0247	Intermolecular stretch
	ω_3	a''	172	0.7365	OoP internal rotation
	ω_4	a'	628	66.4866	$\text{O}=\text{C}-\text{O}$ bend
	ω_5	a''	679	117.5984	Acidic H wag
	ω_6	a'	1092	319.3971	$\text{C}-\text{OH}$ stretch
	ω_7	a''	1150	1.4497	Formyl H wag
	ω_8	a'	1285	9.9472	Acidic H bend
	ω_9	a'	1439	20.7269	Formyl H bend
	ω_{10}	a'	1748	388.2159	$\text{C}=\text{O}$ stretch
	ω_{11}	a'	2928	382.1225	Formyl H stretch
	ω_{12}	a'	3745	23.0205	Acidic H stretch
	zpe		90.2		
pVQZ	ω_1	a'	87	3.5485	In plane internal rotation
	ω_2	a'	134	31.0388	Intermolecular stretch
	ω_3	a''	168	0.7159	OoP internal rotation
	ω_4	a'	631	66.6196	$\text{O}=\text{C}-\text{O}$ bend
	ω_5	a''	682	117.4516	Acidic H wag
	ω_6	a'	1094	318.5852	$\text{C}-\text{OH}$ stretch
	ω_7	a''	1150	1.3496	Formyl H wag
	ω_8	a'	1287	10.0449	Acidic H bend
	ω_9	a'	1439	20.3944	Formyl H bend
	ω_{10}	a'	1751	387.7219	$\text{C}=\text{O}$ stretch
	ω_{11}	a'	2929	373.904	Formyl H stretch
	ω_{12}	a'	3757	23.9349	Acidic H stretch
	zpe		90.4		

Table B95: Calculated harmonic frequencies and mode assignments for the $\text{Br}^- \cdots \text{HCOOH}$ complex. All frequencies and intensities are in cm^{-1} and km mol^{-1} respectively.

$\text{Br}^- \cdots \text{HCOOH}$ $C_s ({}^1A')$ AcidAnti vdW Complex					
	Mode	Symmetry	Frequency (cm^{-1})	Intensity (km mol^{-1})	Description
def2QZVP	ω_1	a'	95	5.0774	In plane internal rotation
	ω_2	a''	162	30.6552	OoP internal rotation
	ω_3	a'	201	23.248	Intermolecular stretch
	ω_4	a'	703	4.9974	$\text{O}=\text{C}-\text{O}$ bend
	ω_5	a''	924	30.833	Acidic H wag
	ω_6	a''	1081	0.2409	Formyl H wag
	ω_7	a'	1230	123.0028	$\text{C}-\text{OH}$ stretch
	ω_8	a'	1418	18.686	Formyl H bend
	ω_9	a'	1434	154.302	Acidic H bend
	ω_{10}	a'	1786	588.5718	$\text{C}=\text{O}$ stretch
	ω_{11}	a'	2993	1706.3917	Acidic H stretch
	ω_{12}	a'	3034	520.9151	Formyl H stretch
	zpe		90.1		
pVTZ	ω_1	a'	92	4.6469	In plane internal rotation
	ω_2	a''	163	29.1791	OoP internal rotation
	ω_3	a'	201	23.4696	Intermolecular stretch
	ω_4	a'	698	5.3167	$\text{O}=\text{C}-\text{O}$ bend
	ω_5	a''	926	21.9497	Acidic H wag
	ω_6	a''	1078	0.0703	Formyl H wag
	ω_7	a'	1227	126.3719	$\text{C}-\text{OH}$ stretch
	ω_8	a'	1411	20.7791	Formyl H bend
	ω_9	a'	1431	136.0448	Acidic H bend
	ω_{10}	a'	1778	626.873	$\text{C}=\text{O}$ stretch
	ω_{11}	a'	2977	1974.7653	Acidic H stretch
	ω_{12}	a'	3029	327.3794	Formyl H stretch
	zpe		89.8		
pVQZ	ω_1	a'	95	4.6024	In plane internal rotation
	ω_2	a''	163	28.9496	OoP internal rotation
	ω_3	a'	204	23.7071	Intermolecular stretch
	ω_4	a'	702	5.5658	$\text{O}=\text{C}-\text{O}$ bend
	ω_5	a''	932	21.6441	Acidic H wag
	ω_6	a''	1080	0.109	Formyl H wag
	ω_7	a'	1230	127.9505	$\text{C}-\text{OH}$ stretch
	ω_8	a'	1416	19.1608	Formyl H bend
	ω_9	a'	1434	138.4097	Acidic H bend
	ω_{10}	a'	1780	631.0495	$\text{C}=\text{O}$ stretch
	ω_{11}	a'	2968	2037.2741	Acidic H stretch
	ω_{12}	a'	3028	289.7328	Formyl H stretch
	zpe		89.9		

Table B96: Calculated harmonic frequencies and mode assignments for the $\text{Br}^- \cdots \text{HCOOH}$ complex. All frequencies and intensities are in cm^{-1} and km mol^{-1} respectively.

$\text{Br}^- \cdots \text{HCOOH}$ $C_s ({}^1A')$ AcidSyn vdW Complex					
	Mode	Symmetry	Frequency (cm^{-1})	Intensity (km mol^{-1})	Description
def2QZVP	ω_1	a'	88	0.5016	In plane internal rotation
	ω_2	a''	169	5.7385	OoP internal rotation
	ω_3	a'	204	40.8374	Intermolecular stretch
	ω_4	a'	686	50.4025	$\text{O}=\text{C}-\text{O}$ bend
	ω_5	a''	956	42.6213	Acidic H wag
	ω_6	a''	1081	5.1701	Formyl H wag
	ω_7	a'	1232	294.0572	$\text{C}-\text{OH}$ stretch
	ω_8	a'	1358	3.8743	Acidic H bend
	ω_9	a'	1426	25.4849	Formyl H bend
	ω_{10}	a'	1773	522.388	$\text{C}=\text{O}$ stretch
	ω_{11}	a'	2827	2945.868	Acidic H stretch
	ω_{12}	a'	2977	30.6134	Formyl H stretch
	zpe		88.4		
pVTZ	ω_1	a'	87	0.4913	In plane internal rotation
	ω_2	a''	170	6.2016	OoP internal rotation
	ω_3	a'	203	41.5445	Intermolecular stretch
	ω_4	a'	681	49.7884	$\text{O}=\text{C}-\text{O}$ bend
	ω_5	a''	954	29.7089	Acidic H wag
	ω_6	a''	1079	4.0961	Formyl H wag
	ω_7	a'	1229	284.8898	$\text{C}-\text{OH}$ stretch
	ω_8	a'	1353	5.7773	Acidic H bend
	ω_9	a'	1421	27.6681	Formyl H bend
	ω_{10}	a'	1765	520.0975	$\text{C}=\text{O}$ stretch
	ω_{11}	a'	2818	3009.3767	Acidic H stretch
	ω_{12}	a'	2977	32.401	Formyl H stretch
	zpe		88.2		
pVQZ	ω_1	a'	87	0.4289	In plane internal rotation
	ω_2	a''	171	6.1581	OoP internal rotation
	ω_3	a'	207	42.457	Intermolecular stretch
	ω_4	a'	684	49.4776	$\text{O}=\text{C}-\text{O}$ bend
	ω_5	a''	958	29.1813	Acidic H wag
	ω_6	a''	1081	3.8263	Formyl H wag
	ω_7	a'	1232	287.9472	$\text{C}-\text{OH}$ stretch
	ω_8	a'	1355	6.1199	Acidic H bend
	ω_9	a'	1424	27.9619	Formyl H bend
	ω_{10}	a'	1766	524.6785	$\text{C}=\text{O}$ stretch
	ω_{11}	a'	2802	3050.5817	Acidic H stretch
	ω_{12}	a'	2976	36.3755	Formyl H stretch
	zpe		88.2		

Table B97: Calculated harmonic frequencies and mode assignments for the $\text{Br}^- \cdots \text{HCOOH}$ complex. All frequencies and intensities are in cm^{-1} and km mol^{-1} respectively.

$\text{Br}^- \cdots \text{HCOOH}$ $C_s ({}^1A')$ FormSyn vdW Complex					
	Mode	Symmetry	Frequency (cm^{-1})	Intensity (km mol^{-1})	Description
def2QZVP	ω_1	a'	77	3.118	In plane internal rotation
	ω_2	a'	100	8.5577	Intermolecular stretch
	ω_3	a''	150	0.3743	OoP internal rotation
	ω_4	a'	632	65.5607	$\text{O}=\text{C}-\text{O}$ bend
	ω_5	a''	683	122.9308	Acidic H wag
	ω_6	a'	1102	312.3493	$\text{C}-\text{OH}$ stretch
	ω_7	a''	1135	1.2747	Formyl H wag
	ω_8	a'	1292	11.7849	Acidic H bend
	ω_9	a'	1434	17.6277	Formyl H bend
	ω_{10}	a'	1761	378.0368	$\text{C}=\text{O}$ stretch
	ω_{11}	a'	2976	258.6564	Formyl H stretch
	ω_{12}	a'	3767	27.0993	Acidic H stretch
	zpe		90.4		
pVTZ	ω_1	a'	77	2.8139	In plane internal rotation
	ω_2	a'	103	8.5561	Intermolecular stretch
	ω_3	a''	161	0.1954	OoP internal rotation
	ω_4	a'	629	65.0371	$\text{O}=\text{C}-\text{O}$ bend
	ω_5	a''	678	116.0499	Acidic H wag
	ω_6	a'	1099	304.3194	$\text{C}-\text{OH}$ stretch
	ω_7	a''	1139	0.897	Formyl H wag
	ω_8	a'	1289	11.1906	Acidic H bend
	ω_9	a'	1432	19.3465	Formyl H bend
	ω_{10}	a'	1755	380.6314	$\text{C}=\text{O}$ stretch
	ω_{11}	a'	2973	279.8671	Formyl H stretch
	ω_{12}	a'	3748	26.2908	Acidic H stretch
	zpe		90.2		
pVQZ	ω_1	a'	77	2.9635	In plane internal rotation
	ω_2	a'	101	8.6109	Intermolecular stretch
	ω_3	a''	156	0.1932	OoP internal rotation
	ω_4	a'	631	65.6433	$\text{O}=\text{C}-\text{O}$ bend
	ω_5	a''	680	115.9062	Acidic H wag
	ω_6	a'	1100	304.9475	$\text{C}-\text{OH}$ stretch
	ω_7	a''	1139	0.8276	Formyl H wag
	ω_8	a'	1289	11.3538	Acidic H bend
	ω_9	a'	1433	19.3303	Formyl H bend
	ω_{10}	a'	1757	380.8994	$\text{C}=\text{O}$ stretch
	ω_{11}	a'	2965	283.3538	Formyl H stretch
	ω_{12}	a'	3759	26.9693	Acidic H stretch
	zpe		90.2		

Table B98: Calculated harmonic frequencies and mode assignments for the $\text{I}^- \cdots \text{HCOOH}$ complex. All frequencies and intensities are in cm^{-1} and km mol^{-1} respectively.

$\text{I}^- \cdots \text{HCOOH}$ $C_s ({}^1\text{A}')$ AcidAnti vdW Complex					
	Mode	Symmetry	Frequency (cm^{-1})	Intensity (km mol^{-1})	Description
def2QZVP	ω_1	a'	84	3.4132	In plane internal rotation
	ω_2	a''	155	29.3415	OoP internal rotation
	ω_3	a'	169	12.8271	Intermolecular stretch
	ω_4	a'	698	2.3291	$\text{O}=\text{C}-\text{O}$ bend
	ω_5	a''	852	22.7348	Acidic H wag
	ω_6	a''	1078	0.0789	Formyl H wag
	ω_7	a'	1213	120.5413	$\text{C}-\text{OH}$ stretch
	ω_8	a'	1403	134.0451	Acidic H bend
	ω_9	a'	1421	28.0215	Formyl H bend
	ω_{10}	a'	1794	579.1053	$\text{C}=\text{O}$ stretch
	ω_{11}	a'	3032	17.3591	Formyl H stretch
	ω_{12}	a'	3189	1928.5338	Acidic H stretch
	zpe		90.3		
pVTZ	ω_1	a'	87	3.0997	In plane internal rotation
	ω_2	a''	159	27.3138	OoP internal rotation
	ω_3	a'	178	13.1131	Intermolecular stretch
	ω_4	a'	698	2.9728	$\text{O}=\text{C}-\text{O}$ bend
	ω_5	a''	878	15.9108	Acidic H wag
	ω_6	a''	1079	0.0445	Formyl H wag
	ω_7	a'	1216	128.5179	$\text{C}-\text{OH}$ stretch
	ω_8	a'	1409	112.8081	Acidic H bend
	ω_9	a'	1418	36.9924	Formyl H bend
	ω_{10}	a'	1787	624.9662	$\text{C}=\text{O}$ stretch
	ω_{11}	a'	3026	15.8306	Formyl H stretch
	ω_{12}	a'	3113	2119.2068	Acidic H stretch
	zpe		90		
pVQZ	ω_1	a'	84	3.2057	In plane internal rotation
	ω_2	a''	157	27.9742	OoP internal rotation
	ω_3	a'	171	12.9743	Intermolecular stretch
	ω_4	a'	696	2.375	$\text{O}=\text{C}-\text{O}$ bend
	ω_5	a''	858	17.3723	Acidic H wag
	ω_6	a''	1077	0.0375	Formyl H wag
	ω_7	a'	1213	124.4764	$\text{C}-\text{OH}$ stretch
	ω_8	a'	1404	121.7109	Acidic H bend
	ω_9	a'	1417	31.1044	Formyl H bend
	ω_{10}	a'	1789	608.541	$\text{C}=\text{O}$ stretch
	ω_{11}	a'	3030	12.9357	Formyl H stretch
	ω_{12}	a'	3166	1982.3967	Acidic H stretch
	zpe		90.1		

Table B99: Calculated harmonic frequencies and mode assignments for the $\text{I}^- \cdots \text{HCOOH}$ complex. All frequencies and intensities are in cm^{-1} and km mol^{-1} respectively.

$\text{I}^- \cdots \text{HCOOH}$ $C_s ({}^1A')$ AcidSyn vdW Complex					
	Mode	Symmetry	Frequency (cm^{-1})	Intensity (km mol^{-1})	Description
def2QZVP	ω_1	a'	74	0.2282	In plane internal rotation
	ω_2	a''	158	5.5414	OoP internal rotation
	ω_3	a'	167	21.8737	Intermolecular stretch
	ω_4	a'	672	59.9135	$\text{O}=\text{C}-\text{O}$ bend
	ω_5	a''	893	38.4546	Acidic H wag
	ω_6	a''	1075	1.938	Formyl H wag
	ω_7	a'	1209	295.0647	$\text{C}-\text{OH}$ stretch
	ω_8	a'	1346	10.6669	Acidic H bend
	ω_9	a'	1426	20.2052	Formyl H bend
	ω_{10}	a'	1783	457.5414	$\text{C}=\text{O}$ stretch
	ω_{11}	a'	2984	587.7832	Formyl H stretch
	ω_{12}	a'	3090	1958.9768	Acidic H stretch
	zpe		89		
pVTZ	ω_1	a'	74	0.2415	In plane internal rotation
	ω_2	a''	159	6.1607	OoP internal rotation
	ω_3	a'	169	22.285	Intermolecular stretch
	ω_4	a'	669	59.7262	$\text{O}=\text{C}-\text{O}$ bend
	ω_5	a''	893	28.0078	Acidic H wag
	ω_6	a''	1072	1.6134	Formyl H wag
	ω_7	a'	1208	292.5372	$\text{C}-\text{OH}$ stretch
	ω_8	a'	1343	11.2347	Acidic H bend
	ω_9	a'	1421	21.9574	Formyl H bend
	ω_{10}	a'	1775	460.2136	$\text{C}=\text{O}$ stretch
	ω_{11}	a'	2982	722.0393	Acidic H stretch
	ω_{12}	a'	3068	1884.6705	Formyl H stretch
	zpe		88.7		
pVQZ	ω_1	a'	74	0.2383	In plane internal rotation
	ω_2	a''	157	5.9654	OoP internal rotation
	ω_3	a'	168	22.4094	Intermolecular stretch
	ω_4	a'	671	60.109	$\text{O}=\text{C}-\text{O}$ bend
	ω_5	a''	890	28.2361	Acidic H wag
	ω_6	a''	1073	1.3279	Formyl H wag
	ω_7	a'	1208	292.7416	$\text{C}-\text{OH}$ stretch
	ω_8	a'	1344	12.7328	Acidic H bend
	ω_9	a'	1424	21.6357	Formyl H bend
	ω_{10}	a'	1777	460.5677	$\text{C}=\text{O}$ stretch
	ω_{11}	a'	2981	760.5757	Formyl H stretch
	ω_{12}	a'	3066	1859.2229	Acidic H stretch
	zpe		88.7		

Table B100: Calculated harmonic frequencies and mode assignments for the $\text{I}^- \cdots \text{HCOOH}$ complex. All frequencies and intensities are in cm^{-1} and km mol^{-1} respectively.

$\text{I}^- \cdots \text{HCOOH}$ $C_s ({}^1\text{A}')$ FormAnti vdW Complex					
	Mode	Symmetry	Frequency (cm^{-1})	Intensity (km mol^{-1})	Description
def2QZVP	ω_1	a'	67	3.4626	In plane internal rotation
	ω_2	a'	79	2.2057	Intermolecular stretch
	ω_3	a''	133	0.1569	OoP internal rotation
	ω_4	a'	632	65.0057	$\text{O}=\text{C}-\text{O}$ bend
	ω_5	a''	681	121.3898	Acidic H wag
	ω_6	a'	1110	291.8537	$\text{C}-\text{OH}$ stretch
	ω_7	a''	1119	0.9322	Formyl H wag
	ω_8	a'	1296	13.4266	Acidic H bend
	ω_9	a'	1427	16.6146	Formyl H bend
	ω_{10}	a'	1770	367.3344	$\text{C}=\text{O}$ stretch
	ω_{11}	a'	3023	147.943	Formyl H stretch
	ω_{12}	a'	3770	32.6726	Acidic H stretch
		zpe	90.4		
pVTZ	ω_1	a'	68	2.9815	In plane internal rotation
	ω_2	a'	83	2.5804	Intermolecular stretch
	ω_3	a''	140	0.0748	OoP internal rotation
	ω_4	a'	629	64.2551	$\text{O}=\text{C}-\text{O}$ bend
	ω_5	a''	677	114.606	Acidic H wag
	ω_6	a'	1107	287.7821	$\text{C}-\text{OH}$ stretch
	ω_7	a''	1123	0.5986	Formyl H wag
	ω_8	a'	1292	12.5284	Acidic H bend
	ω_9	a'	1426	17.8648	Formyl H bend
	ω_{10}	a'	1763	369.8949	$\text{C}=\text{O}$ stretch
	ω_{11}	a'	3016	169.0224	Formyl H stretch
	ω_{12}	a'	3750.9663	31.4301	Acidic H stretch
		zpe	90.2		
pVQZ	ω_1	a'	67	3.142	In plane internal rotation
	ω_2	a'	80	2.4586	Intermolecular stretch
	ω_3	a''	132	0.0751	OoP internal rotation
	ω_4	a'	631	64.3507	$\text{O}=\text{C}-\text{O}$ bend
	ω_5	a''	679	114.6748	Acidic H wag
	ω_6	a'	1109	286.7053	$\text{C}-\text{OH}$ stretch
	ω_7	a''	1120	0.5394	Formyl H wag
	ω_8	a'	1294	12.7997	Acidic H bend
	ω_9	a'	1425	18.1632	Formyl H bend
	ω_{10}	a'	1765	370.1541	$\text{C}=\text{O}$ stretch
	ω_{11}	a'	3015	162.5688	Formyl H stretch
	ω_{12}	a'	3762	32.6795	Acidic H stretch
		zpe	90.2		

Table B101: Calculated harmonic frequencies and mode assignments for the Cl...HCOOH complex. All frequencies and intensities are in cm^{-1} and km mol^{-1} respectively.

Cl...HCOOH C_s ($^2A''$) AcidAnti vdW Complex					
	Mode	Symmetry	Frequency (cm^{-1})	Intensity (km mol^{-1})	Description
def2QZVP	ω_1	a'	36	5.9228	In plane internal rotation
	ω_2	a''	56	47.4152	OoP internal rotation
	ω_3	a'	91	3.8251	Intermolecular stretch
	ω_4	a'	566	66.4222	Acidic H wag
	ω_5	a''	670	5.3195	$\text{O}=\text{C}-\text{O}$ bend
	ω_6	a''	1045	0.0004	Formyl H wag
	ω_7	a'	1136	74.3592	$\text{C}-\text{OH}$ stretch
	ω_8	a'	1307	254.8261	Acidic H bend
	ω_9	a'	1426	0.7696	Formyl H bend
	ω_{10}	a'	1851	338.6601	$\text{C}=\text{O}$ stretch
	ω_{11}	a'	3009	68.5927	Formyl H stretch
	ω_{12}	a'	3786	275.5965	Acidic H stretch
	zpe		89.6		
pVTZ	ω_1	a'	35	5.8454	In plane internal rotation
	ω_2	a''	61	46.0425	OoP internal rotation
	ω_3	a'	95	3.4753	Intermolecular stretch
	ω_4	a'	568	63.1466	Acidic H wag
	ω_5	a''	666	5.4027	$\text{O}=\text{C}-\text{O}$ bend
	ω_6	a''	1041	0.0278	Formyl H wag
	ω_7	a'	1134	76.8239	$\text{C}-\text{OH}$ stretch
	ω_8	a'	1306	251.9152	Acidic H bend
	ω_9	a'	1420	0.8152	Formyl H bend
	ω_{10}	a'	1843	345.0486	$\text{C}=\text{O}$ stretch
	ω_{11}	a'	3007	64.8542	Formyl H stretch
	ω_{12}	a'	3763	289.8399	Acidic H stretch
	zpe		89.4		
pVQZ	ω_1	a'	35	5.8051	In plane internal rotation
	ω_2	a''	58	46.538	OoP internal rotation
	ω_3	a'	93	3.7038	Intermolecular stretch
	ω_4	a'	569	63.639	Acidic H wag
	ω_5	a''	669	5.2722	$\text{O}=\text{C}-\text{O}$ bend
	ω_6	a''	1044	0.0122	Formyl H wag
	ω_7	a'	1135	76.3206	$\text{C}-\text{OH}$ stretch
	ω_8	a'	1307	251.6603	Acidic H bend
	ω_9	a'	1424	0.9241	Formyl H bend
	ω_{10}	a'	1847	345.5069	$\text{C}=\text{O}$ stretch
	ω_{11}	a'	3008	65.6589	Formyl H stretch
	ω_{12}	a'	3776	280.7916	Acidic H stretch
	zpe		89.5		

Table B102: Calculated harmonic frequencies and mode assignments for the Cl...HCOOH complex. All frequencies and intensities are in cm^{-1} and km mol^{-1} respectively.

Cl...HCOOH C_s ($^2A'$) AcidPSyn vdW Complex					
	Mode	Symmetry	Frequency (cm^{-1})	Intensity (km mol^{-1})	Description
def2QZVP	ω_1	a'	156	5.0093	Intermolecular stretch
	ω_2	a''	186	2.7813	OoP internal rotation
	ω_3	a'	240	32.6209	In plane internal rotation
	ω_4	a'	677	41.735	$\text{O}=\text{C}-\text{O}$ bend
	ω_5	a''	779	94.0598	Acidic H wag
	ω_6	a''	1064	3.2223	Formyl H wag
	ω_7	a'	1209	192.7091	$\text{C}-\text{OH}$ stretch
	ω_8	a'	1339	11.9725	Acidic H bend
	ω_9	a'	1413	1.451	Formyl H bend
	ω_{10}	a'	1724	531.714	$\text{C}=\text{O}$ stretch
	ω_{11}	a'	3115	25.7853	Formyl H stretch
	ω_{12}	a'	3551	87.0881	Acidic H stretch
	zpe		92.4		
pVTZ	ω_1	a'	155	5.2568	Intermolecular stretch
	ω_2	a''	185	2.8733	OoP internal rotation
	ω_3	a'	237	32.2708	In plane internal rotation
	ω_4	a'	674	40.9681	$\text{O}=\text{C}-\text{O}$ bend
	ω_5	a''	775	89.6972	Acidic H wag
	ω_6	a''	1060	3.2367	Formyl H wag
	ω_7	a'	1207	187.7472	$\text{C}-\text{OH}$ stretch
	ω_8	a'	1335	11.7295	Acidic H bend
	ω_9	a'	1409	1.5237	Formyl H bend
	ω_{10}	a'	1719	524.6424	$\text{C}=\text{O}$ stretch
	ω_{11}	a'	3112	24.8862	Formyl H stretch
	ω_{12}	a'	3532	88.139	Acidic H stretch
	zpe		92.1		
pVQZ	ω_1	a'	158	4.7928	Intermolecular stretch
	ω_2	a''	187	2.8363	OoP internal rotation
	ω_3	a'	242	32.4941	In plane internal rotation
	ω_4	a'	677	41.2441	$\text{O}=\text{C}-\text{O}$ bend
	ω_5	a''	780	89.9504	Acidic H wag
	ω_6	a''	1063	3.1291	Formyl H wag
	ω_7	a'	1209	189.4156	$\text{C}-\text{OH}$ stretch
	ω_8	a'	1337	12.1105	Acidic H bend
	ω_9	a'	1411	1.654	Formyl H bend
	ω_{10}	a'	1720	528.5155	$\text{C}=\text{O}$ stretch
	ω_{11}	a'	3113	24.6881	Formyl H stretch
	ω_{12}	a'	3539	88.5754	Acidic H stretch
	zpe		92.3		

Table B103: Calculated harmonic frequencies and mode assignments for the Cl···HCOOH complex. All frequencies and intensities are in cm^{-1} and km mol^{-1} respectively.

Cl···HCOOH C_s ($^2A'$) CarbPAnti vdW Complex					
	Mode	Symmetry	Frequency (cm^{-1})	Intensity (km mol^{-1})	Description
def2QZVP	ω_1	a'	69	2.7875	Carb. intermol. stretch
	ω_2	a''	74	55.0428	OoP internal rotation
	ω_3	a'	132	26.3145	Hydroxyl intermol. stretch
	ω_4	a''	543	85.3225	Acidic H wag
	ω_5	a'	669	13.5862	$\text{O}=\text{C}-\text{O}$ bend
	ω_6	a''	1043	0.0219	Formyl H wag
	ω_7	a'	1147	23.9396	$\text{C}-\text{OH}$ stretch
	ω_8	a'	1289	304.4301	Acidic H bend
	ω_9	a'	1421	1.8538	Formyl H bend
	ω_{10}	a'	1825	379.2457	$\text{C}=\text{O}$ stretch
	ω_{11}	a'	3031	68.2598	Formyl H stretch
	ω_{12}	a'	3832	96.6043	Acidic H stretch
	zpe		90.2		
pVTZ	ω_1	a'	70	2.8932	Carb. intermol. stretch
	ω_2	a''	75	53.3968	OoP internal rotation
	ω_3	a'	132	25.8338	Hydroxyl intermol. stretch
	ω_4	a''	540	83.1908	Acidic H wag
	ω_5	a'	665	13.6948	$\text{O}=\text{C}-\text{O}$ bend
	ω_6	a''	1039	0.0892	Formyl H wag
	ω_7	a'	1144	24.2181	$\text{C}-\text{OH}$ stretch
	ω_8	a'	1286	300.0301	Acidic H bend
	ω_9	a'	1415	1.8483	Formyl H bend
	ω_{10}	a'	1817	374.6835	$\text{C}=\text{O}$ stretch
	ω_{11}	a'	3030	65.3763	Formyl H stretch
	ω_{12}	a'	3813	93.53	Acidic H stretch
	zpe		89.9		
pVQZ	ω_1	a'	71	2.7618	Carb. intermol. stretch
	ω_2	a''	76	53.3732	OoP internal rotation
	ω_3	a'	135	26.8564	Hydroxyl intermol. stretch
	ω_4	a''	544	83.6075	Acidic H wag
	ω_5	a'	668	13.7585	$\text{O}=\text{C}-\text{O}$ bend
	ω_6	a''	1042	0.0526	Formyl H wag
	ω_7	a'	1146	23.9199	$\text{C}-\text{OH}$ stretch
	ω_8	a'	1288	301.7887	Acidic H bend
	ω_9	a'	1419	1.9494	Formyl H bend
	ω_{10}	a'	1820	379.9374	$\text{C}=\text{O}$ stretch
	ω_{11}	a'	3030	65.9606	Formyl H stretch
	ω_{12}	a'	3824	96.0506	Acidic H stretch
	zpe		90.1		

Table B104: Calculated harmonic frequencies and mode assignments for the Cl···HCOOH complex. All frequencies and intensities are in cm^{-1} and km mol^{-1} respectively.

Cl···HCOOH C_1 (2A) CarbPSyn vdW Complex					
	Mode	Symmetry	Frequency (cm^{-1})	Intensity (km mol^{-1})	Description
def2QZVP	ω_1	<i>a</i>	21	1.8506	OoP internal rotation
	ω_2	<i>a</i>	51	1.2528	OoP internal rotation
	ω_3	<i>a</i>	93	2.6528	Intermolecular stretch
	ω_4	<i>a</i>	629	37.0005	$\text{O}=\text{C}-\text{O}$ bend
	ω_5	<i>a</i>	670	128.633	Acidic H wag
	ω_6	<i>a</i>	1059	2.5611	Formyl H wag
	ω_7	<i>a</i>	1124	279.6576	$\text{C}-\text{OH}$ stretch
	ω_8	<i>a</i>	1296	15.5884	Acidic H bend
	ω_9	<i>a</i>	1411	1.567	Formyl H bend
	ω_{10}	<i>a</i>	1819	370.6535	$\text{C}=\text{O}$ stretch
	ω_{11}	<i>a</i>	3105	26.9746	Formyl H stretch
	ω_{12}	<i>a</i>	3761	84.8346	Acidic H stretch
	zpe		90		
pVTZ	ω_1	<i>a</i>	25	1.8502	OoP internal rotation
	ω_2	<i>a</i>	55	1.3947	OoP internal rotation
	ω_3	<i>a</i>	98	2.8485	Intermolecular stretch
	ω_4	<i>a</i>	626	35.4187	$\text{O}=\text{C}-\text{O}$ bend
	ω_5	<i>a</i>	668	125.0774	Acidic H wag
	ω_6	<i>a</i>	1055	2.7704	Formyl H wag
	ω_7	<i>a</i>	1121	279.6262	$\text{C}-\text{OH}$ stretch
	ω_8	<i>a</i>	1293	14.8413	Acidic H bend
	ω_9	<i>a</i>	1407	1.4535	Formyl H bend
	ω_{10}	<i>a</i>	1812	372.2372	$\text{C}=\text{O}$ stretch
	ω_{11}	<i>a</i>	3103	25.0401	Formyl H stretch
	ω_{12}	<i>a</i>	3742	82.4455	Acidic H stretch
	zpe		89.8		
pVQZ	ω_1	<i>a</i>	20	1.9355	OoP internal rotation
	ω_2	<i>a</i>	52	1.37	OoP internal rotation
	ω_3	<i>a</i>	96	2.909	Intermolecular stretch
	ω_4	<i>a</i>	628	35.6095	$\text{O}=\text{C}-\text{O}$ bend
	ω_5	<i>a</i>	669	124.9884	Acidic H wag
	ω_6	<i>a</i>	1057	2.646	Formyl H wag
	ω_7	<i>a</i>	1123	279.4402	$\text{C}-\text{OH}$ stretch
	ω_8	<i>a</i>	1294	15.6921	Acidic H bend
	ω_9	<i>a</i>	1409	1.5428	Formyl H bend
	ω_{10}	<i>a</i>	1815	374.3723	$\text{C}=\text{O}$ stretch
	ω_{11}	<i>a</i>	3103	25.3101	Formyl H stretch
	ω_{12}	<i>a</i>	3753	84.7726	Acidic H stretch
	zpe		89.8		

Table B105: Calculated harmonic frequencies and mode assignments for the Cl...HCOOH complex. All frequencies and intensities are in cm^{-1} and km mol^{-1} respectively.

Cl...HCOOH C_s ($^2A'$) FormPAnti vdW Complex					
	Mode	Symmetry	Frequency (cm^{-1})	Intensity (km mol^{-1})	Description
def2QZVP	ω_1	a''	86	21.9815	OoP internal rotation
	ω_2	a'	103	0.5352	Intermolecular stretch
	ω_3	a'	153	51.2147	In plane internal rotation
	ω_4	a''	546	86.4284	Acidic H wag
	ω_5	a'	676	7.4704	$\text{O}=\text{C}-\text{O}$ bend
	ω_6	a''	1054	0.0074	Formyl H wag
	ω_7	a'	1157	29.7967	$\text{C}-\text{OH}$ stretch
	ω_8	a'	1296	408.9151	Acidic H bend
	ω_9	a'	1424	2.502	Formyl H bend
	ω_{10}	a'	1807	512.1326	$\text{C}=\text{O}$ stretch
	ω_{11}	a'	3055	28.0099	Formyl H stretch
	ω_{12}	a'	3830	101.7744	Acidic H stretch
	zpe		90.8		
pVTZ	ω_1	a''	85	21.8941	OoP internal rotation
	ω_2	a'	102	0.6779	Intermolecular stretch
	ω_3	a'	151	50.6631	In plane internal rotation
	ω_4	a''	542	83.8545	Acidic H wag
	ω_5	a'	671	7.1582	$\text{O}=\text{C}-\text{O}$ bend
	ω_6	a''	1050	0.0602	Formyl H wag
	ω_7	a'	1154	31.4201	$\text{C}-\text{OH}$ stretch
	ω_8	a'	1293	408.2905	Acidic H bend
	ω_9	a'	1418	2.3332	Formyl H bend
	ω_{10}	a'	1800	508.853	$\text{C}=\text{O}$ stretch
	ω_{11}	a'	3053	26.3129	Formyl H stretch
	ω_{12}	a'	3810	98.9885	Acidic H stretch
	zpe		90.5		
pVQZ	ω_1	a''	86	21.6715	OoP internal rotation
	ω_2	a'	104	0.6328	Intermolecular stretch
	ω_3	a'	155	51.8106	In plane internal rotation
	ω_4	a''	546	84.4962	Acidic H wag
	ω_5	a'	675	7.1322	$\text{O}=\text{C}-\text{O}$ bend
	ω_6	a''	1053	0.0338	Formyl H wag
	ω_7	a'	1157	30.7085	$\text{C}-\text{OH}$ stretch
	ω_8	a'	1295	412.7698	Acidic H bend
	ω_9	a'	1421	2.426	Formyl H bend
	ω_{10}	a'	1802	514.8234	$\text{C}=\text{O}$ stretch
	ω_{11}	a'	3054	26.5121	Formyl H stretch
	ω_{12}	a'	3822	101.5189	Acidic H stretch
	zpe		90.7		

Table B106: Calculated harmonic frequencies and mode assignments for the Cl…HCOOH complex. All frequencies and intensities are in cm^{-1} and km mol^{-1} respectively.

Cl…HCOOH $C_s ({}^2A')$ FormPSyn vdW Complex					
	Mode	Symmetry	Frequency (cm^{-1})	Intensity (km mol^{-1})	Description
def2QZVP	ω_1	a''	76	0.1625	OoP internal rotation
	ω_2	a'	95	0.4984	Formyl H intermol.
	ω_3	a'	146	23.1884	Carb. intermol. stretch
	ω_4	a'	646	62.8433	$\text{O}=\text{C}-\text{O}$ bend
	ω_5	a''	689	138.9582	Acidic H wag
	ω_6	a''	1073	2.9619	Formyl H wag
	ω_7	a'	1162	283.8047	$\text{C}-\text{OH}$ stretch
	ω_8	a'	1331	19.4452	Acidic H bend
	ω_9	a'	1407	5.5815	Formyl H bend
	ω_{10}	a'	1770	604.933	$\text{C}=\text{O}$ stretch
	ω_{11}	a'	3130	14.7994	Formyl H stretch
	ω_{12}	a'	3762	105.4534	Acidic H stretch
	zpe		91.4		
pVTZ	ω_1	a''	75	0.1349	OoP internal rotation
	ω_2	a'	95	0.3879	Formyl H intermol.
	ω_3	a'	145	23.1658	Carb. intermol. stretch
	ω_4	a'	643	61.8897	$\text{O}=\text{C}-\text{O}$ bend
	ω_5	a''	685	135.0279	Acidic H wag
	ω_6	a''	1069	3.1229	Formyl H wag
	ω_7	a'	1160	284.3114	$\text{C}-\text{OH}$ stretch
	ω_8	a'	1328	19.4039	Acidic H bend
	ω_9	a'	1404	5.299	Formyl H bend
	ω_{10}	a'	1764	601.9674	$\text{C}=\text{O}$ stretch
	ω_{11}	a'	3127	14.0387	Formyl H stretch
	ω_{12}	a'	3744	103.1393	Acidic H stretch
	zpe		91.1		
pVQZ	ω_1	a''	77	0.1373	OoP internal rotation
	ω_2	a'	96	0.4373	Formyl H intermol.
	ω_3	a'	149	23.8435	Carb. intermol. stretch
	ω_4	a'	645	62.6175	$\text{O}=\text{C}-\text{O}$ bend
	ω_5	a''	688	135.4245	Acidic H wag
	ω_6	a''	1072	3.0172	Formyl H wag
	ω_7	a'	1162	285.8117	$\text{C}-\text{OH}$ stretch
	ω_8	a'	1330	20.0416	Acidic H bend
	ω_9	a'	1405	5.5405	Formyl H bend
	ω_{10}	a'	1765	609.1021	$\text{C}=\text{O}$ stretch
	ω_{11}	a'	3128	14.2081	Formyl H stretch
	ω_{12}	a'	3755	105.8821	Acidic H stretch
	zpe		91.3		

Table B107: Calculated harmonic frequencies and mode assignments for the Cl...HCOOH complex. All frequencies and intensities are in cm^{-1} and km mol^{-1} respectively.

Cl...HCOOH C_s ($^2A''$) InlineSyn vdW Complex					
	Mode	Symmetry	Frequency (cm^{-1})	Intensity (km mol^{-1})	Description
def2QZVP	ω_1	a'	35	1.076	In plane internal rotation
	ω_2	a''	75	0.9649	OoP internal rotation
	ω_3	a'	90	3.8625	Intermolecular stretch
	ω_4	a'	639	44.0283	$\text{O}=\text{C}-\text{O}$ bend
	ω_5	a''	699	110.2289	Acidic H wag
	ω_6	a''	1065	2.0858	Formyl H wag
	ω_7	a'	1148	256.195	$\text{C}-\text{OH}$ stretch
	ω_8	a'	1323	14.9041	Acidic H bend
	ω_9	a'	1415	4.7092	Formyl H bend
	ω_{10}	a'	1810	327.2176	$\text{C}=\text{O}$ stretch
	ω_{11}	a'	3091	49.7707	Formyl H stretch
	ω_{12}	a'	3715	286.2537	Acidic H stretch
	zpe		90.4		
pVTZ	ω_1	a'	37	1.1422	In plane internal rotation
	ω_2	a''	82	1.2519	OoP internal rotation
	ω_3	a'	95	4.005	Intermolecular stretch
	ω_4	a'	638	43.128	$\text{O}=\text{C}-\text{O}$ bend
	ω_5	a''	701	104.4058	Acidic H wag
	ω_6	a''	1061	2.3331	Formyl H wag
	ω_7	a'	1148	255.483	$\text{C}-\text{OH}$ stretch
	ω_8	a'	1321	14.0352	Acidic H bend
	ω_9	a'	1412	5.0459	Formyl H bend
	ω_{10}	a'	1803	326.6872	$\text{C}=\text{O}$ stretch
	ω_{11}	a'	3089	48.1848	Formyl H stretch
	ω_{12}	a'	3693	298.7531	Acidic H stretch
	zpe		90.2		
pVQZ	ω_1	a'	36	1.1619	In plane internal rotation
	ω_2	a''	77	1.1669	OoP internal rotation
	ω_3	a'	93	3.9829	Intermolecular stretch
	ω_4	a'	639	42.9702	$\text{O}=\text{C}-\text{O}$ bend
	ω_5	a''	700	104.4654	Acidic H wag
	ω_6	a''	1063	2.142	Formyl H wag
	ω_7	a'	1148	254.4842	$\text{C}-\text{OH}$ stretch
	ω_8	a'	1321	15.2885	Acidic H bend
	ω_9	a'	1414	4.9331	Formyl H bend
	ω_{10}	a'	1806	326.1244	$\text{C}=\text{O}$ stretch
	ω_{11}	a'	3090	48.5574	Formyl H stretch
	ω_{12}	a'	3704	295.7677	Acidic H stretch
	zpe		90.3		

Table B108: Calculated harmonic frequencies and mode assignments for the Cl···HCOOH complex. All frequencies and intensities are in cm^{-1} and km mol^{-1} respectively.

Cl···HCOOH C_1 (2A) OutPlAnti vdW Complex					
	Mode	Symmetry	Frequency (cm^{-1})	Intensity (km mol^{-1})	Description
def2QZVP	ω_1	<i>a</i>	30	15.1853	OoP internal rotation
	ω_2	<i>a</i>	32	34.5365	OoP internal rotation
	ω_3	<i>a</i>	96	6.1625	Intermolecular stretch
	ω_4	<i>a</i>	530	87.8737	Acidic H wag
	ω_5	<i>a</i>	662	8.7064	$\text{O}=\text{C}-\text{O}$ bend
	ω_6	<i>a</i>	1037	0.1877	Formyl H wag
	ω_7	<i>a</i>	1104	84.5059	$\text{C}-\text{OH}$ stretch
	ω_8	<i>a</i>	1277	312.2931	Acidic H bend
	ω_9	<i>a</i>	1422	0.5587	Formyl H bend
	ω_{10}	<i>a</i>	1856	275.2737	$\text{C}=\text{O}$ stretch
	ω_{11}	<i>a</i>	3021	61.3993	Formyl H stretch
	ω_{12}	<i>a</i>	3825	76.9859	Acidic H stretch
	zpe		89.1		
pVTZ	ω_1	<i>a</i>	31	3.6424	OoP internal rotation
	ω_2	<i>a</i>	38	46.1937	OoP internal rotation
	ω_3	<i>a</i>	100	5.9724	Intermolecular stretch
	ω_4	<i>a</i>	527	87.0114	Acidic H wag
	ω_5	<i>a</i>	658	8.2334	$\text{O}=\text{C}-\text{O}$ bend
	ω_6	<i>a</i>	1033	0.3374	Formyl H wag
	ω_7	<i>a</i>	1101	85.46	$\text{C}-\text{OH}$ stretch
	ω_8	<i>a</i>	1274	307.5189	Acidic H bend
	ω_9	<i>a</i>	1416	0.5869	Formyl H bend
	ω_{10}	<i>a</i>	1848	273.9623	$\text{C}=\text{O}$ stretch
	ω_{11}	<i>a</i>	3021	57.6869	Formyl H stretch
	ω_{12}	<i>a</i>	3806	74.6551	Acidic H stretch
	zpe		88.8		
pVQZ	ω_1	<i>a</i>	30	3.4332	OoP internal rotation
	ω_2	<i>a</i>	35	46.1187	OoP internal rotation
	ω_3	<i>a</i>	99	5.8763	Intermolecular stretch
	ω_4	<i>a</i>	530	86.5224	Acidic H wag
	ω_5	<i>a</i>	661	8.2325	$\text{O}=\text{C}-\text{O}$ bend
	ω_6	<i>a</i>	1036	0.2853	Formyl H wag
	ω_7	<i>a</i>	1103	86.2557	$\text{C}-\text{OH}$ stretch
	ω_8	<i>a</i>	1276	309.9235	Acidic H bend
	ω_9	<i>a</i>	1419	0.6189	Formyl H bend
	ω_{10}	<i>a</i>	1852	274.7907	$\text{C}=\text{O}$ stretch
	ω_{11}	<i>a</i>	3021	58.3979	Formyl H stretch
	ω_{12}	<i>a</i>	3817	76.1307	Acidic H stretch
	zpe		89		

Table B109: Calculated harmonic frequencies and mode assignments for the Br...HCOOH complex. All frequencies and intensities are in cm^{-1} and km mol^{-1} respectively.

Br ...HCOOH C_s ($^2A''$) AcidAnti vdW Complex					
	Mode	Symmetry	Frequency (cm^{-1})	Intensity (km mol^{-1})	Description
def2QZVP	ω_1	a'	27	5.525	In plane internal rotation
	ω_2	a''	54	45.4992	OoP internal rotation
	ω_3	a'	79	3.7688	Intermolecular stretch
	ω_4	a''	569	61.1631	Acidic H wag
	ω_5	a'	671	6.2254	$\text{O}=\text{C}-\text{O}$ bend
	ω_6	a''	1046	0	Formyl H wag
	ω_7	a'	1140	73.575	$\text{C}-\text{OH}$ stretch
	ω_8	a'	1307	269.3644	Acidic H bend
	ω_9	a'	1427	0.7201	Formyl H bend
	ω_{10}	a'	1852	348.7487	$\text{C}=\text{O}$ stretch
	ω_{11}	a'	3005	68.2173	Formyl H stretch
	ω_{12}	a'	3767	341.5823	Acidic H stretch
	zpe		89.4		
pVTZ	ω_1	a'	28	13.3501	In plane internal rotation
	ω_2	a'	51	0.0546	Intermolecular stretch
	ω_3	a''	57	48.9677	OoP internal rotation
	ω_4	a''	525	72.1691	Acidic H wag
	ω_5	a'	661	9.9976	$\text{O}=\text{C}-\text{O}$ bend
	ω_6	a''	1037	0.0644	Formyl H wag
	ω_7	a'	1122	32.2641	$\text{C}-\text{OH}$ stretch
	ω_8	a'	1285	304.3958	Acidic H bend
	ω_9	a'	1418	0.5998	Formyl H bend
	ω_{10}	a'	1852	280.8939	$\text{C}=\text{O}$ stretch
	ω_{11}	a'	2988	74.2252	Formyl H stretch
	ω_{12}	a'	3816	65.4934	Acidic H stretch
	zpe		88.8		
pVQZ	ω_1	a'	22	6.1321	In plane internal rotation
	ω_2	a''	74	39.5867	OoP internal rotation
	ω_3	a'	82	3.4174	Intermolecular stretch
	ω_4	a''	608	52.1661	Acidic H wag
	ω_5	a'	671	5.618	$\text{O}=\text{C}-\text{O}$ bend
	ω_6	a''	1042	0.0011	Formyl H wag
	ω_7	a'	1140	74.6021	$\text{C}-\text{OH}$ stretch
	ω_8	a'	1301	271.4372	Acidic H bend
	ω_9	a'	1424	0.942	Formyl H bend
	ω_{10}	a'	1847	359.9749	$\text{C}=\text{O}$ stretch
	ω_{11}	a'	3000	73.383	Formyl H stretch
	ω_{12}	a'	3748	370.1762	Acidic H stretch
	zpe		89.5		

Table B110: Calculated harmonic frequencies and mode assignments for the Br...HCOOH complex. All frequencies and intensities are in cm^{-1} and km mol^{-1} respectively.

Br ...HCOOH C_s ($^2A'$) AcidPSyn vdW Complex					
	Mode	Symmetry	Frequency (cm^{-1})	Intensity (km mol^{-1})	Description
def2QZVP	ω_1	a'	115	2.8694	Intermolecular stretch
	ω_2	a''	159	2.6009	OoP internal rotation
	ω_3	a'	191	28.2509	In plane internal rotation
	ω_4	a'	671	35.9332	$\text{O}=\text{C}-\text{O}$ bend
	ω_5	a''	749	91.1129	Acidic H wag
	ω_6	a''	1065	2.6379	Formyl H wag
	ω_7	a'	1195	197.4556	$\text{C}-\text{OH}$ stretch
	ω_8	a'	1340	1.5729	Acidic H bend
	ω_9	a'	1414	2	Formyl H bend
	ω_{10}	a'	1744	467.827	$\text{C}=\text{O}$ stretch
	ω_{11}	a'	3109	33.8148	Formyl H stretch
	ω_{12}	a'	3594	142.5592	Acidic H stretch
	zpe		91.8		
pVTZ	ω_1	a'	117	2.6831	Intermolecular stretch
	ω_2	a''	161	2.8691	OoP internal rotation
	ω_3	a'	191	27.5285	In plane internal rotation
	ω_4	a'	669	34.8096	$\text{O}=\text{C}-\text{O}$ bend
	ω_5	a''	748	83.7786	Acidic H wag
	ω_6	a''	1062	2.6805	Formyl H wag
	ω_7	a'	1193	190.6678	$\text{C}-\text{OH}$ stretch
	ω_8	a'	1337	1.5391	Acidic H bend
	ω_9	a'	1411	1.9804	Formyl H bend
	ω_{10}	a'	1739	450.1297	$\text{C}=\text{O}$ stretch
	ω_{11}	a'	3108	33.3904	Formyl H stretch
	ω_{12}	a'	3570	153.5025	Acidic H stretch
	zpe		91.6		
pVQZ	ω_1	a'	121	2.7573	Intermolecular stretch
	ω_2	a''	167	3.0044	OoP internal rotation
	ω_3	a'	195	28.1126	In plane internal rotation
	ω_4	a'	673	34.9473	$\text{O}=\text{C}-\text{O}$ bend
	ω_5	a''	758	82.9512	Acidic H wag
	ω_6	a''	1065	2.5632	Formyl H wag
	ω_7	a'	1198	190.6212	$\text{C}-\text{OH}$ stretch
	ω_8	a'	1340	1.5502	Acidic H bend
	ω_9	a'	1413	2.0997	Formyl H bend
	ω_{10}	a'	1739	454.6428	$\text{C}=\text{O}$ stretch
	ω_{11}	a'	3109	33.1176	Formyl H stretch
	ω_{12}	a'	3567	157.3642	Acidic H stretch
	zpe		91.8		

Table B111: Calculated harmonic frequencies and mode assignments for the Br \cdots HCOOH complex. All frequencies and intensities are in cm^{-1} and km mol^{-1} respectively.

Br \cdots HCOOH C_s ($^2A'$) CarbPAnti vdW Complex					
	Mode	Symmetry	Frequency (cm^{-1})	Intensity (km mol^{-1})	Description
def2QZVP	ω_1	a'	57	2.8574	Carb. intermol. stretch
	ω_2	a''	69	55.3347	OoP internal rotation
	ω_3	a'	116	22.5435	Hydroxyl intermol. stretch
	ω_4	a''	542	85.2427	Acidic H wag
	ω_5	a'	669	13.9588	O=C–O bend
	ω_6	a''	1044	0.0215	Formyl H wag
	ω_7	a'	1145	24.1263	C–OH stretch
	ω_8	a'	1288	302.5445	Acidic H bend
	ω_9	a'	1422	1.1317	Formyl H bend
	ω_{10}	a'	1828	365.3429	C=O stretch
	ω_{11}	a'	3031	69.8987	Formyl H stretch
	ω_{12}	a'	3832	95.981	Acidic H stretch
	zpe		90		
pVTZ	ω_1	a'	59	3.0632	Carb. intermol. stretch
	ω_2	a''	72	53.0238	OoP internal rotation
	ω_3	a'	119	22.076	Hydroxyl intermol. stretch
	ω_4	a''	540	82.9637	Acidic H wag
	ω_5	a'	664	14.2844	O=C–O bend
	ω_6	a''	1040	0.09	Formyl H wag
	ω_7	a'	1142	23.5746	C–OH stretch
	ω_8	a'	1286	296.1627	Acidic H bend
	ω_9	a'	1416	1.1098	Formyl H bend
	ω_{10}	a'	1820	358.1274	C=O stretch
	ω_{11}	a'	3031	66.9842	Formyl H stretch
	ω_{12}	a'	3813	93.0631	Acidic H stretch
	zpe		89.7		
pVQZ	ω_1	a'	60	2.9394	Carb. intermol. stretch
	ω_2	a''	74	53.093	OoP internal rotation
	ω_3	a'	120	22.861	Hydroxyl intermol. stretch
	ω_4	a''	543	83.2524	Acidic H wag
	ω_5	a'	668	14.4304	O=C–O bend
	ω_6	a''	1043	0.0542	Formyl H wag
	ω_7	a'	1145	23.2275	C–OH stretch
	ω_8	a'	1288	297.3924	Acidic H bend
	ω_9	a'	1420	1.1612	Formyl H bend
	ω_{10}	a'	1823	361.3928	C=O stretch
	ω_{11}	a'	3031	67.5524	Formyl H stretch
	ω_{12}	a'	3824	95.4232	Acidic H stretch
	zpe		90		

Table B112: Calculated harmonic frequencies and mode assignments for the Br...HCOOH complex. All frequencies and intensities are in cm^{-1} and km mol^{-1} respectively.

Br ...HCOOH C_s ($^2A'$) CarbPSyn vdW Complex					
	Mode	Symmetry	Frequency (cm^{-1})	Intensity (km mol^{-1})	Description
def2QZVP	ω_1	a''	14 <i>i</i>	1.2571	OoP internal rotation
	ω_2	a'	36	1.4203	In plane internal rotation
	ω_3	a'	74	2.0724	Intermolecular stretch
	ω_4	a'	630	37.6733	O=C–O bend
	ω_5	a''	660	134.9961	Acidic H wag
	ω_6	a''	1061	2.2813	Formyl H wag
	ω_7	a'	1128	266.217	C–OH stretch
	ω_8	a'	1296	15.1341	Acidic H bend
	ω_9	a'	1411	2.8223	Formyl H bend
	ω_{10}	a'	1819	380.2226	C=O stretch
	ω_{11}	a'	3102	28.5712	Formyl H stretch
	ω_{12}	a'	3764	86.0264	Acidic H stretch
	zpe		89.6		
pVTZ	ω_1	a''	10 <i>i</i>	1.3328	OoP internal rotation
	ω_2	a'	39	1.5155	In plane internal rotation
	ω_3	a'	79	2.2183	Intermolecular stretch
	ω_4	a'	627	36.0542	O=C–O bend
	ω_5	a''	655	129.681	Acidic H wag
	ω_6	a''	1057	2.4109	Formyl H wag
	ω_7	a'	1126	259.9098	C–OH stretch
	ω_8	a'	1291	14.3003	Acidic H bend
	ω_9	a'	1406	3.1699	Formyl H bend
	ω_{10}	a'	1812	385.8248	C=O stretch
	ω_{11}	a'	3099	26.5862	Formyl H stretch
	ω_{12}	a'	3745	84.7072	Acidic H stretch
	zpe		89.3		
pVQZ	ω_1	a''	11	1.2921	OoP internal rotation
	ω_2	a'	43	1.4854	In plane internal rotation
	ω_3	a'	79	2.3266	Intermolecular stretch
	ω_4	a'	629	36.3123	O=C–O bend
	ω_5	a''	657	129.9958	Acidic H wag
	ω_6	a''	1060	2.2758	Formyl H wag
	ω_7	a'	1127	260.5441	C–OH stretch
	ω_8	a'	1292	14.6533	Acidic H bend
	ω_9	a'	1409	3.2873	Formyl H bend
	ω_{10}	a'	1816	386.1875	C=O stretch
	ω_{11}	a'	3100	26.793	Formyl H stretch
	ω_{12}	a'	3756	87.0447	Acidic H stretch
	zpe		89.6		

Table B113: Calculated harmonic frequencies and mode assignments for the Br...HCOOH complex. All frequencies and intensities are in cm^{-1} and km mol^{-1} respectively.

Br ...HCOOH $C_s ({}^2A')$ FormPAnti vdW Complex					
	Mode	Symmetry	Frequency (cm^{-1})	Intensity (km mol^{-1})	Description
def2QZVP	ω_1	a''	77	20.855	OoP internal rotation
	ω_2	a'	82	0.5399	Intermolecular stretch
	ω_3	a'	126	41.1341	In plane internal rotation
	ω_4	a''	546	86.1536	Acidic H wag
	ω_5	a'	675	7.2671	$\text{O}=\text{C}-\text{O}$ bend
	ω_6	a''	1053	0.0032	Formyl H wag
	ω_7	a'	1154	34.8178	$\text{C}-\text{OH}$ stretch
	ω_8	a'	1295	407.56	Acidic H bend
	ω_9	a'	1426	2.01	Formyl H bend
	ω_{10}	a'	1815	471.6004	$\text{C}=\text{O}$ stretch
	ω_{11}	a'	3047	29.1001	Formyl H stretch
	ω_{12}	a'	3830	99.43	Acidic H stretch
	zpe		90.5		
pVTZ	ω_1	a''	77	20.7468	OoP internal rotation
	ω_2	a'	83	1.0612	Intermolecular stretch
	ω_3	a'	127	40.2059	In plane internal rotation
	ω_4	a''	543	83.3484	Acidic H wag
	ω_5	a'	670	6.8702	$\text{O}=\text{C}-\text{O}$ bend
	ω_6	a''	1050	0.0439	Formyl H wag
	ω_7	a'	1151	36.2507	$\text{C}-\text{OH}$ stretch
	ω_8	a'	1292	408.4421	Acidic H bend
	ω_9	a'	1420	1.8847	Formyl H bend
	ω_{10}	a'	1808	463.4947	$\text{C}=\text{O}$ stretch
	ω_{11}	a'	3046	26.355	Formyl H stretch
	ω_{12}	a'	3811	96.9667	Acidic H stretch
	zpe		90.2		
pVQZ	ω_1	a''	84	21.0673	OoP internal rotation
	ω_2	a'	88	0.2047	Intermolecular stretch
	ω_3	a'	130	41.3818	In plane internal rotation
	ω_4	a''	549	83.3029	Acidic H wag
	ω_5	a'	674	6.8722	$\text{O}=\text{C}-\text{O}$ bend
	ω_6	a''	1053	0.0215	Formyl H wag
	ω_7	a'	1154	34.5278	$\text{C}-\text{OH}$ stretch
	ω_8	a'	1295	411.7962	Acidic H bend
	ω_9	a'	1424	2.1405	Formyl H bend
	ω_{10}	a'	1810	470.051	$\text{C}=\text{O}$ stretch
	ω_{11}	a'	3046	26.4793	Formyl H stretch
	ω_{12}	a'	3822	99.1755	Acidic H stretch
	zpe		90.5		

Table B114: Calculated harmonic frequencies and mode assignments for the Br...HCOOH complex. All frequencies and intensities are in cm^{-1} and km mol^{-1} respectively.

Br ...HCOOH $C_s ({}^2A')$ FormPSyn vdW Complex					
	Mode	Symmetry	Frequency (cm^{-1})	Intensity (km mol^{-1})	Description
def2QZVP	ω_1	a''	68	0.2612	OoP internal rotation
	ω_2	a'	77	0.3252	Formyl H intermol.
	ω_3	a'	121	15.597	Carb. intermol. stretch
	ω_4	a'	644	61.5119	$\text{O}=\text{C}-\text{O}$ bend
	ω_5	a''	689	137.7132	Acidic H wag
	ω_6	a''	1072	2.7946	Formyl H wag
	ω_7	a'	1160	288.9404	$\text{C}-\text{OH}$ stretch
	ω_8	a'	1330	20.3597	Acidic H bend
	ω_9	a'	1410	5.1924	Formyl H bend
	ω_{10}	a'	1776	568.3736	$\text{C}=\text{O}$ stretch
	ω_{11}	a'	3124	14.8849	Formyl H stretch
	ω_{12}	a'	3763	101.9659	Acidic H stretch
	zpe		91.1		
pVTZ	ω_1	a''	68	0.2285	OoP internal rotation
	ω_2	a'	77	0.1849	Formyl H intermol.
	ω_3	a'	123	15.5321	Carb. intermol. stretch
	ω_4	a'	641	60.9539	$\text{O}=\text{C}-\text{O}$ bend
	ω_5	a''	685	133.189	Acidic H wag
	ω_6	a''	1069	2.9289	Formyl H wag
	ω_7	a'	1158	289.8472	$\text{C}-\text{OH}$ stretch
	ω_8	a'	1327	20.6749	Acidic H bend
	ω_9	a'	1405	5.115	Formyl H bend
	ω_{10}	a'	1770	561.3176	$\text{C}=\text{O}$ stretch
	ω_{11}	a'	3121	13.5617	Formyl H stretch
	ω_{12}	a'	3744	99.654	Acidic H stretch
	zpe		90.8		
pVQZ	ω_1	a''	77	0.1907	OoP internal rotation
	ω_2	a'	83	0.4483	Formyl H intermol.
	ω_3	a'	125	15.5903	Carb. intermol. stretch
	ω_4	a'	644	61.3758	$\text{O}=\text{C}-\text{O}$ bend
	ω_5	a''	690	133.8507	Acidic H wag
	ω_6	a''	1072	2.9334	Formyl H wag
	ω_7	a'	1160	288.4611	$\text{C}-\text{OH}$ stretch
	ω_8	a'	1329	21.4504	Acidic H bend
	ω_9	a'	1408	5.5617	Formyl H bend
	ω_{10}	a'	1772	568.9655	$\text{C}=\text{O}$ stretch
	ω_{11}	a'	3122	13.51	Formyl H stretch
	ω_{12}	a'	3755	101.1571	Acidic H stretch
	zpe		91.1		

Table B115: Calculated harmonic frequencies and mode assignments for the I...HCOOH complex. All frequencies and intensities are in cm^{-1} and km mol^{-1} respectively.

I...HCOOH $C_s ({}^2A'')$ AcidAnti vdW Complex					
	Mode	Symmetry	Frequency (cm^{-1})	Intensity (km mol^{-1})	Description
def2QZVP	ω_1	a'	37	4.1121	In plane internal rotation
	ω_2	a''	61	43.5955	OoP internal rotation
	ω_3	a'	76	5.2359	Intermolecular stretch
	ω_4	a''	573	50.3857	Acidic H wag
	ω_5	a'	671	4.248	$\text{O}=\text{C}-\text{O}$ bend
	ω_6	a''	1046	0.0014	Formyl H wag
	ω_7	a'	1137	82.8435	$\text{C}-\text{OH}$ stretch
	ω_8	a'	1308	221.31	Acidic H bend
	ω_9	a'	1426	1.6413	Formyl H bend
	ω_{10}	a'	1849	377.5807	$\text{C}=\text{O}$ stretch
	ω_{11}	a'	3009	67.7259	Formyl H stretch
	ω_{12}	a'	3747	382.0774	Acidic H stretch
	zpe		89.4		
pVTZ	ω_1	a'	37	4.2267	In plane internal rotation
	ω_2	a''	69	41.7693	OoP internal rotation
	ω_3	a'	88	4.7208	Intermolecular stretch
	ω_4	a''	581	47.917	Acidic H wag
	ω_5	a'	667	4.1476	$\text{O}=\text{C}-\text{O}$ bend
	ω_6	a''	1043	0.0096	Formyl H wag
	ω_7	a'	1136	87.499	$\text{C}-\text{OH}$ stretch
	ω_8	a'	1309	216.6985	Acidic H bend
	ω_9	a'	1419	1.7266	Formyl H bend
	ω_{10}	a'	1841	387.7568	$\text{C}=\text{O}$ stretch
	ω_{11}	a'	3007	63.9233	Formyl H stretch
	ω_{12}	a'	3718	421.3702	Acidic H stretch
	zpe		89.2		
pVQZ	ω_1	a'	39	4.0272	In plane internal rotation
	ω_2	a''	67	42.2856	OoP internal rotation
	ω_3	a'	88	5.0746	Intermolecular stretch
	ω_4	a''	583	48.4623	Acidic H wag
	ω_5	a'	670	4.0144	$\text{O}=\text{C}-\text{O}$ bend
	ω_6	a''	1046	0.0011	Formyl H wag
	ω_7	a'	1138	87.4771	$\text{C}-\text{OH}$ stretch
	ω_8	a'	1311	216.0616	Acidic H bend
	ω_9	a'	1423	1.9027	Formyl H bend
	ω_{10}	a'	1844	388.0276	$\text{C}=\text{O}$ stretch
	ω_{11}	a'	3007	64.8598	Formyl H stretch
	ω_{12}	a'	3730	413.7455	Acidic H stretch
	zpe		89.4		

Table B116: Calculated harmonic frequencies and mode assignments for the I...HCOOH complex. All frequencies and intensities are in cm^{-1} and km mol^{-1} respectively.

I...HCOOH C_s ($^2A'$) AcidPSyn vdW Complex					
	Mode	Symmetry	Frequency (cm^{-1})	Intensity (km mol^{-1})	Description
def2QZVP	ω_1	a'	91	1.3372	Intermolecular stretch
	ω_2	a''	133	2.3344	OoP internal rotation
	ω_3	a'	153	26.0864	In plane internal rotation
	ω_4	a'	664	32.2055	$\text{O}=\text{C}-\text{O}$ bend
	ω_5	a''	725	81.0642	Acidic H wag
	ω_6	a''	1067	2.0107	Formyl H wag
	ω_7	a'	1182	192.3838	$\text{C}-\text{OH}$ stretch
	ω_8	a'	1337	9.9188	Acidic H bend
	ω_9	a'	1416	1.5096	Formyl H bend
	ω_{10}	a'	1761	400.831	$\text{C}=\text{O}$ stretch
	ω_{11}	a'	3106	43.8416	Formyl H stretch
	ω_{12}	a'	3621	209.4583	Acidic H stretch
	zpe		91.2		
pVTZ	ω_1	a'	95	1.6379	Intermolecular stretch
	ω_2	a''	134	2.6173	OoP internal rotation
	ω_3	a'	153	25.6587	In plane internal rotation
	ω_4	a'	662	31.1101	$\text{O}=\text{C}-\text{O}$ bend
	ω_5	a''	725	76.253	Acidic H wag
	ω_6	a''	1063	2.1764	Formyl H wag
	ω_7	a'	1181	187.4234	$\text{C}-\text{OH}$ stretch
	ω_8	a'	1334	10.6144	Acidic H bend
	ω_9	a'	1413	1.6705	Formyl H bend
	ω_{10}	a'	1755	390.8881	$\text{C}=\text{O}$ stretch
	ω_{11}	a'	3104	43.2326	Formyl H stretch
	ω_{12}	a'	3596	224.0859	Acidic H stretch
	zpe		91		
pVQZ	ω_1	a'	98	1.4774	Intermolecular stretch
	ω_2	a''	140	2.644	OoP internal rotation
	ω_3	a'	160	26.8066	In plane internal rotation
	ω_4	a'	666	31.2211	$\text{O}=\text{C}-\text{O}$ bend
	ω_5	a''	731	75.9052	Acidic H wag
	ω_6	a''	1066	2.0421	Formyl H wag
	ω_7	a'	1185	188.43	$\text{C}-\text{OH}$ stretch
	ω_8	a'	1337	9.987	Acidic H bend
	ω_9	a'	1415	1.7096	Formyl H bend
	ω_{10}	a'	1756	397.644	$\text{C}=\text{O}$ stretch
	ω_{11}	a'	3105	42.8216	Formyl H stretch
	ω_{12}	a'	3599	225.2343	Acidic H stretch
	zpe		91.3		

Table B117: Calculated harmonic frequencies and mode assignments for the I...HCOOH complex. All frequencies and intensities are in cm^{-1} and km mol^{-1} respectively.

I...HCOOH C_s ($^2A'$) CarbPAnti vdW Complex					
	Mode	Symmetry	Frequency (cm^{-1})	Intensity (km mol^{-1})	Description
def2QZVP	ω_1	a'	50	3.2015	Carb. intermol. stretch
	ω_2	a''	60	52.7191	OoP internal rotation
	ω_3	a'	101	20.2175	Hydroxyl intermol. stretch
	ω_4	a''	541	84.3211	Acidic H wag
	ω_5	a'	669	15.3358	$\text{O}=\text{C}-\text{O}$ bend
	ω_6	a''	1044	0.0192	Formyl H wag
	ω_7	a'	1143	23.0502	$\text{C}-\text{OH}$ stretch
	ω_8	a'	1288	293.7607	Acidic H bend
	ω_9	a'	1423	0.5809	Formyl H bend
	ω_{10}	a'	1831	346.4641	$\text{C}=\text{O}$ stretch
	ω_{11}	a'	3032	73.1252	Formyl H stretch
	ω_{12}	a'	3832	96.0051	Acidic H stretch
	zpe		89.8		
pVTZ	ω_1	a'	51	3.4152	Carb. intermol. stretch
	ω_2	a''	62	51.1888	OoP internal rotation
	ω_3	a'	103	19.9236	Hydroxyl intermol. stretch
	ω_4	a''	539	82.2371	Acidic H wag
	ω_5	a'	664	15.4585	$\text{O}=\text{C}-\text{O}$ bend
	ω_6	a''	1041	0.0906	Formyl H wag
	ω_7	a'	1140	23.4235	$\text{C}-\text{OH}$ stretch
	ω_8	a'	1285	289.2526	Acidic H bend
	ω_9	a'	1417	0.6006	Formyl H bend
	ω_{10}	a'	1823	341.5392	$\text{C}=\text{O}$ stretch
	ω_{11}	a'	3032	70.2813	Formyl H stretch
	ω_{12}	a'	3813	92.8965	Acidic H stretch
	zpe		89.5		
pVQZ	ω_1	a'	51	3.3627	Carb. intermol. stretch
	ω_2	a''	65	51.3964	OoP internal rotation
	ω_3	a'	106	20.6933	Hydroxyl intermol. stretch
	ω_4	a''	543	82.4202	Acidic H wag
	ω_5	a'	668	15.5031	$\text{O}=\text{C}-\text{O}$ bend
	ω_6	a''	1044	0.0542	Formyl H wag
	ω_7	a'	1143	22.7528	$\text{C}-\text{OH}$ stretch
	ω_8	a'	1287	291.3355	Acidic H bend
	ω_9	a'	1421	0.636	Formyl H bend
	ω_{10}	a'	1826	347.7571	$\text{C}=\text{O}$ stretch
	ω_{11}	a'	3032	70.8106	Formyl H stretch
	ω_{12}	a'	3824	95.656	Acidic H stretch
	zpe		89.8		

Table B118: Calculated harmonic frequencies and mode assignments for the I...HCOOH complex. All frequencies and intensities are in cm^{-1} and km mol^{-1} respectively.

I...HCOOH C_s ($^2A'$) CarbPSyn vdW Complex					
	Mode	Symmetry	Frequency (cm^{-1})	Intensity (km mol^{-1})	Description
def2QZVP	ω_1	a''	10	1.3114	OoP internal rotation
	ω_2	a'	37	1.4942	In plane internal rotation
	ω_3	a'	69	2.1995	Intermolecular stretch
	ω_4	a'	630	34.9846	$\text{O}=\text{C}-\text{O}$ bend
	ω_5	a''	662	129.2888	Acidic H wag
	ω_6	a''	1061	2.1186	Formyl H wag
	ω_7	a'	1126	261.1047	$\text{C}-\text{OH}$ stretch
	ω_8	a'	1297	13.4842	Acidic H bend
	ω_9	a'	1411	3.4041	Formyl H bend
	ω_{10}	a'	1819	393.7706	$\text{C}=\text{O}$ stretch
	ω_{11}	a'	3100	29.136	Formyl H stretch
	ω_{12}	a'	3762	84.9057	Acidic H stretch
	zpe		89.6		
pVTZ	ω_1	a''	20	1.2956	OoP internal rotation
	ω_2	a'	41	1.492	In plane internal rotation
	ω_3	a'	73	2.1992	Intermolecular stretch
	ω_4	a'	627	34.4773	$\text{O}=\text{C}-\text{O}$ bend
	ω_5	a''	657	126.09	Acidic H wag
	ω_6	a''	1057	2.2016	Formyl H wag
	ω_7	a'	1124	254.3251	$\text{C}-\text{OH}$ stretch
	ω_8	a'	1293	11.8841	Acidic H bend
	ω_9	a'	1407	4.2545	Formyl H bend
	ω_{10}	a'	1813	396.9914	$\text{C}=\text{O}$ stretch
	ω_{11}	a'	3097	28.1038	Formyl H stretch
	ω_{12}	a'	3744	83.7604	Acidic H stretch
	zpe		89.4		
pVQZ	ω_1	a''	23	1.3469	OoP internal rotation
	ω_2	a'	42	1.5602	In plane internal rotation
	ω_3	a'	75	2.4129	Intermolecular stretch
	ω_4	a'	629	34.3885	$\text{O}=\text{C}-\text{O}$ bend
	ω_5	a''	660	126.0804	Acidic H wag
	ω_6	a''	1060	2.1011	Formyl H wag
	ω_7	a'	1125	257.4264	$\text{C}-\text{OH}$ stretch
	ω_8	a'	1293	13.09	Acidic H bend
	ω_9	a'	1409	4.0071	Formyl H bend
	ω_{10}	a'	1816	398.3785	$\text{C}=\text{O}$ stretch
	ω_{11}	a'	3098	27.7344	Formyl H stretch
	ω_{12}	a'	3755	85.9334	Acidic H stretch
	zpe		89.6		

Table B119: Calculated harmonic frequencies and mode assignments for the I...HCOOH complex. All frequencies and intensities are in cm^{-1} and km mol^{-1} respectively.

I...HCOOH C_s ($^2A'$) FormPAnti vdW Complex					
	Mode	Symmetry	Frequency (cm^{-1})	Intensity (km mol^{-1})	Description
def2QZVP	ω_1	a''	69	19.1224	OoP internal rotation
	ω_2	a'	71	1.3452	Intermolecular stretch
	ω_3	a'	108	36.2549	In plane internal rotation
	ω_4	a''	547	85.2287	Acidic H wag
	ω_5	a'	674	6.5562	$\text{O}=\text{C}-\text{O}$ bend
	ω_6	a''	1053	0	Formyl H wag
	ω_7	a'	1152	39.705	$\text{C}-\text{OH}$ stretch
	ω_8	a'	1295	416.1611	Acidic H bend
	ω_9	a'	1428	2.3938	Formyl H bend
	ω_{10}	a'	1821	435.5117	$\text{C}=\text{O}$ stretch
	ω_{11}	a'	3038	29.3957	Formyl H stretch
	ω_{12}	a'	3830	98.7865	Acidic H stretch
	zpe		90.2		
pVTZ	ω_1	a''	70	19.4737	OoP internal rotation
	ω_2	a'	71	1.9358	Intermolecular stretch
	ω_3	a'	109	35.8225	In plane internal rotation
	ω_4	a''	543	82.6795	Acidic H wag
	ω_5	a'	669	6.3292	$\text{O}=\text{C}-\text{O}$ bend
	ω_6	a''	1050	0.026	Formyl H wag
	ω_7	a'	1149	41.4678	$\text{C}-\text{OH}$ stretch
	ω_8	a'	1292	416.3043	Acidic H bend
	ω_9	a'	1421	2.2007	Formyl H bend
	ω_{10}	a'	1814	429.9248	$\text{C}=\text{O}$ stretch
	ω_{11}	a'	3037	27.0586	Formyl H stretch
	ω_{12}	a'	3811	96.1108	Acidic H stretch
	zpe		89.9		
pVQZ	ω_1	a''	72	19.0421	OoP internal rotation
	ω_2	a'	72	1.9666	Intermolecular stretch
	ω_3	a'	113	36.6959	In plane internal rotation
	ω_4	a''	547	83.2858	Acidic H wag
	ω_5	a'	673	6.2793	$\text{O}=\text{C}-\text{O}$ bend
	ω_6	a''	1053	0.0085	Formyl H wag
	ω_7	a'	1151	40.3187	$\text{C}-\text{OH}$ stretch
	ω_8	a'	1295	420.9147	Acidic H bend
	ω_9	a'	1424	2.3099	Formyl H bend
	ω_{10}	a'	1817	437.787	$\text{C}=\text{O}$ stretch
	ω_{11}	a'	3038	27.0103	Formyl H stretch
	ω_{12}	a'	3822	98.7256	Acidic H stretch
	zpe		90.2		

Table B120: Calculated harmonic frequencies and mode assignments for the I...HCOOH complex. All frequencies and intensities are in cm^{-1} and km mol^{-1} respectively.

I...HCOOH $C_s ({}^2A')$ FormPSyn vdW Complex					
	Mode	Symmetry	Frequency (cm^{-1})	Intensity (km mol^{-1})	Description
def2QZVP	ω_1	a''	61	0.3354	OoP internal rotation
	ω_2	a'	66	0.1224	Formyl H intermol.
	ω_3	a'	104	12.7296	Carb. intermol. stretch
	ω_4	a'	642	61.9051	$\text{O}=\text{C}-\text{O}$ bend
	ω_5	a''	690	134.1108	Acidic H wag
	ω_6	a''	1072	2.5272	Formyl H wag
	ω_7	a'	1158	298.4912	$\text{C}-\text{OH}$ stretch
	ω_8	a'	1330	22.33	Acidic H bend
	ω_9	a'	1411	5.8648	Formyl H bend
	ω_{10}	a'	1782	539.2952	$\text{C}=\text{O}$ stretch
	ω_{11}	a'	3117	14.8102	Formyl H stretch
	ω_{12}	a'	3763	99.7152	Acidic H stretch
	zpe		90.9		
pVTZ	ω_1	a''	61	0.2949	OoP internal rotation
	ω_2	a'	66	0.1071	Formyl H intermol.
	ω_3	a'	105	12.9465	Carb. intermol. stretch
	ω_4	a'	639	61.6232	$\text{O}=\text{C}-\text{O}$ bend
	ω_5	a''	685	130.5905	Acidic H wag
	ω_6	a''	1069	2.6769	Formyl H wag
	ω_7	a'	1156	299.5934	$\text{C}-\text{OH}$ stretch
	ω_8	a'	1326	22.4472	Acidic H bend
	ω_9	a'	1406	5.738	Formyl H bend
	ω_{10}	a'	1776	533.105	$\text{C}=\text{O}$ stretch
	ω_{11}	a'	3114	13.7082	Formyl H stretch
	ω_{12}	a'	3745	97.5301	Acidic H stretch
	zpe		90.6		
pVQZ	ω_1	a''	64	0.2988	OoP internal rotation
	ω_2	a'	67	0.1081	Formyl H intermol.
	ω_3	a'	109	13.3972	Carb. intermol. stretch
	ω_4	a'	642	62.471	$\text{O}=\text{C}-\text{O}$ bend
	ω_5	a''	688	130.9955	Acidic H wag
	ω_6	a''	1071	2.5933	Formyl H wag
	ω_7	a'	1158	300.1443	$\text{C}-\text{OH}$ stretch
	ω_8	a'	1328	23.3888	Acidic H bend
	ω_9	a'	1408	5.8881	Formyl H bend
	ω_{10}	a'	1777	543.636	$\text{C}=\text{O}$ stretch
	ω_{11}	a'	3116	13.712	Formyl H stretch
	ω_{12}	a'	3755	100.3768	Acidic H stretch
	zpe		90.8		

Table B121: Cartesian coordinates of the geometries of halide-formic acid complexes optimised with the DSD-PBEP86-D3BJ functional, in Å.

			Cl ⁻ ...HCOOH			Br ⁻ ...HCOOH			I ⁻ ...HCOOH			
			x	y	z	x	y	z	x	y	z	
<i>C_s</i> (¹ A')	AcidAnti	def2QZVP	C	-1.112923	-0.861954	0.000000	1.882446	0.951381	0.000000	-0.350468	-2.586369	0.000000
			O	-0.995783	0.445557	0.000000	0.708971	1.550756	0.000000	0.848572	-2.028292	0.000000
			H	0.000000	0.668324	0.000000	0.000000	0.835871	0.000000	0.727114	-1.039660	0.000000
			O	-2.172235	-1.454656	0.000000	2.941964	1.538994	0.000000	-0.530678	-3.781974	0.000000
			H	-0.141554	-1.379670	0.000000	1.803338	-0.145721	0.000000	-1.167455	-1.850562	0.000000
			X	1.891955	0.820933	0.000000	-1.208729	-0.889041	0.000000	0.000000	1.224350	0.000000
		pVTZ	C	-1.115211	-0.864601	0.000000	1.884873	0.949669	0.000000	-0.350869	-2.584231	0.000000
			O	-0.997291	0.445630	0.000000	0.708425	1.548867	0.000000	0.851216	-2.026894	0.000000
			H	0.000000	0.667315	0.000000	0.000000	0.830045	0.000000	0.727309	-1.035821	0.000000
			O	-2.177759	-1.457073	0.000000	2.945843	1.540398	0.000000	-0.533111	-3.782430	0.000000
			H	-0.144033	-1.383882	0.000000	1.807321	-0.148241	0.000000	-1.166926	-1.846368	0.000000
			X	1.896217	0.823277	0.000000	-1.210020	-0.888398	0.000000	0.000000	1.223814	0.000000
		pVQZ	C	-1.118882	-0.857701	0.000000	1.884056	0.940714	0.000000	0.350480	-2.577937	0.000000
			O	-0.995632	0.449921	0.000000	0.710072	1.539080	0.000000	-0.848811	-2.020231	0.000000
			H	0.000000	0.668977	0.000000	0.000000	0.823000	0.000000	-0.726864	-1.030388	0.000000
			O	-2.182096	-1.444153	0.000000	2.943483	1.529804	0.000000	0.530879	-3.774170	0.000000
			H	-0.150345	-1.380991	0.000000	1.806654	-0.156876	0.000000	1.167444	-1.841683	0.000000
			X	1.899145	0.812475	0.000000	-1.209698	-0.881757	0.000000	0.000000	1.220659	0.000000

Table B122: Cartesian coordinates of the geometries of halide-formic acid complexes optimised with the DSD-PBEP86-D3BJ functional, in Å.

			Cl ⁻ ...HCOOH			Br ⁻ ...HCOOH			I ⁻ ...HCOOH			
			x	y	z	x	y	z	x	y	z	
<i>C_s</i> (¹ A')	AcidSyn	def2QZVP	C	-1.704052	-0.534849	0.000000	1.488596	2.025228	0.000000	-0.084238	-3.047339	0.000000
			O	-1.031344	0.585022	0.000000	0.209175	1.738385	0.000000	-0.919161	-2.029985	0.000000
			H	0.000000	0.483536	0.000000	0.000000	0.742495	0.000000	-0.462401	-1.136856	0.000000
			O	-1.290004	-1.673274	0.000000	2.433337	1.270840	0.000000	1.122357	-3.026831	0.000000
			H	-2.788006	-0.318247	0.000000	1.619511	3.121299	0.000000	-0.657739	-3.988742	0.000000
			X	1.857830	0.691166	0.000000	-0.905462	-1.145399	0.000000	0.000000	1.204984	0.000000
		pVTZ	C	-1.712756	-0.518504	0.000000	1.501305	2.014664	0.000000	-0.082950	-3.045260	0.000000
			O	-1.030176	0.599031	0.000000	0.216066	1.741123	0.000000	-0.924250	-2.029894	0.000000
			H	0.000000	0.485296	0.000000	0.000000	0.744892	0.000000	-0.467964	-1.133614	0.000000
			O	-1.304899	-1.662074	0.000000	2.439269	1.247383	0.000000	1.126440	-3.018385	0.000000
			H	-2.795280	-0.293895	0.000000	1.644459	3.109557	0.000000	-0.651859	-3.989990	0.000000
			X	1.867789	0.671998	0.000000	-0.911285	-1.138585	0.000000	0.000000	1.203423	0.000000
		pVQZ	C	-1.713319	-0.513443	0.000000	1.510338	1.996513	0.000000	-0.082865	-3.036453	0.000000
			O	-1.028052	0.599858	0.000000	0.225827	1.732010	0.000000	-0.922153	-2.022491	0.000000
			H	0.000000	0.484785	0.000000	0.000000	0.738304	0.000000	-0.468307	-1.126364	0.000000
			O	-1.309496	-1.655926	0.000000	2.441264	1.224128	0.000000	1.124243	-3.009640	0.000000
			H	-2.794802	-0.285985	0.000000	1.661891	3.089934	0.000000	-0.651223	-3.981042	0.000000
			X	1.869123	0.666494	0.000000	-0.916018	-1.127326	0.000000	0.000000	1.199683	0.000000

Table B123: Cartesian coordinates of the geometries of halide-formic acid complexes optimised with the DSD-PBEP86-D3BJ functional, in Å.

			Cl ⁻ ...HCOOH			Br ⁻ ...HCOOH			I ⁻ ...HCOOH		
			x	y	z	x	y	z	x	y	z
<i>C_s</i> (¹ A')	def2QZVP	C	-1.061067	0.459065	0.000000	0.195655	1.943483	0.000000	-0.153570	-2.528224	0.000000
		O	-1.899033	-0.608625	0.000000	1.525059	2.204679	0.000000	1.115225	-2.995156	0.000000
		H	-2.787428	-0.227635	0.000000	1.592149	3.168906	0.000000	1.033088	-3.958174	0.000000
		O	-1.490675	1.589019	0.000000	-0.622324	2.832070	0.000000	-1.107841	-3.266363	0.000000
		H	0.000000	0.142732	0.000000	0.000000	0.857599	0.000000	-0.170738	-1.428417	0.000000
	FormSyn	X	2.133617	-0.618391	0.000000	-0.285370	-1.599468	0.000000	0.000000	1.332983	0.000000
		C	-1.059466	0.469467	0.000000	0.204589	1.934917	0.000000	0.147352	-2.511024	0.000000
		O	-1.903211	-0.596335	0.000000	1.538581	2.184396	0.000000	-1.125078	-2.975631	0.000000
		H	-2.792127	-0.210975	0.000000	1.614619	3.150188	0.000000	-1.044669	-3.941014	0.000002
		O	-1.483213	1.604449	0.000000	-0.608022	2.832079	0.000000	1.102018	-3.253252	0.000000
	pVTZ	H	0.000000	0.147227	0.000000	0.000000	0.849814	0.000000	0.166605	-1.410127	-0.000001
		X	2.131783	-0.636351	0.000000	-0.293904	-1.592609	0.000000	0.003367	1.325441	0.000000
		C	-1.055326	0.481329	0.000000	0.203174	1.928865	0.000000	-0.154589	-2.512720	0.000000
		O	-1.910428	-0.572376	0.000000	1.534453	2.181092	0.000000	1.115562	-2.976655	0.000000
		H	-2.793502	-0.178264	0.000000	1.609123	3.145172	0.000000	1.036556	-3.940328	0.000000
	pVQZ	O	-1.464704	1.619102	0.000000	-0.609386	2.823055	0.000000	-1.107374	-3.253646	0.000000
		H	0.000000	0.147396	0.000000	0.000000	0.843571	0.000000	-0.174519	-1.412371	0.000000
		X	2.125089	-0.660642	0.000000	-0.292249	-1.588432	0.000000	0.000000	1.325876	0.000000

Table B124: Cartesian coordinates of the geometries of halogen-formic acid complexes optimised with the DSD-PBEP86-D3BJ functional, in Å.

		Cl … HCOOH			Br … HCOOH			I … HCOOH			
		x	y	z	x	y	z	x	y	z	
<i>C_s</i> (² <i>A''</i>) AcidAnti	def2QZVP	C	-1.604253	-0.286351	-0.000019	1.702723	1.821210	0.000000	-0.365928	-2.868667	0.000000
		O	-0.929321	0.877698	-0.000003	0.359830	1.883892	0.000000	0.847634	-2.288882	0.000000
		H	0.017809	0.694581	-0.000037	0.000000	0.987941	0.000000	0.738725	-1.328721	0.000000
		O	-2.796532	-0.340906	0.000021	2.395764	2.793008	0.000000	-0.516003	-4.053192	0.000000
		H	-0.949804	-1.171999	-0.000071	2.093766	0.791403	0.000000	-1.196202	-2.145288	0.000000
		X	2.374373	-0.123459	0.000005	-0.981567	-1.432051	0.000000	0.000000	1.347596	0.000000
	pVTZ	C	-1.611971	-0.290487	-0.000024	1.592258	1.947071	0.000000	-0.368109	-2.856003	0.000000
		O	-0.911686	0.861317	-0.000005	0.249431	1.845834	0.000000	0.838268	-2.256446	0.000000
		H	0.033474	0.656926	-0.000054	0.000000	0.910398	0.000000	0.711966	-1.295637	0.000000
		O	-2.807980	-0.319453	0.000028	2.162445	2.998993	0.000000	-0.499905	-4.045639	0.000000
		H	-0.976485	-1.190570	-0.000092	2.106998	0.972595	0.000000	-1.210223	-2.145491	0.000000
		X	2.374833	-0.121079	0.000006	-0.884444	-1.494973	0.000000	0.000000	1.339506	0.000000
	pVQZ	C	-1.602378	-0.287356	0.000081	1.720111	1.762883	0.000000	-0.366514	-2.842826	0.000000
		O	-0.921856	0.873749	0.000014	0.378846	1.853367	0.000000	0.844181	-2.257032	0.000000
		H	0.025123	0.686890	0.000175	0.000000	0.964284	0.000000	0.730476	-1.296482	0.000000
		O	-2.795433	-0.335419	-0.000091	2.433265	2.720765	0.000000	-0.510517	-4.028699	0.000000
		H	-0.952701	-1.176721	0.000309	2.090462	0.725205	0.000000	-1.200700	-2.123642	0.000000
		X	2.369421	-0.123098	-0.000021	-0.997372	-1.395996	0.000000	0.000000	1.335150	0.000000

Table B125: Cartesian coordinates of the geometries of halogen-formic acid complexes optimised with the DSD-PBEP86-D3BJ functional, in Å.

			Cl … HCOOH			Br … HCOOH			I … HCOOH		
			x	y	z	x	y	z	x	y	z
<i>C_s</i> (² <i>A'</i>) AcidPSyn	def2QZVP	C	1.171797	0.902633	0.000000	-0.199533	-2.062765	0.000000	-0.207021	-2.513855	0.000000
		O	1.635705	-0.328159	0.000000	1.105023	-1.854334	0.000000	1.104305	-2.319286	0.000000
		H	0.863030	-0.928415	0.000000	1.251848	-0.889351	0.000000	1.267695	-1.358531	0.000000
		O	0.000000	1.226115	0.000000	-1.058082	-1.207528	0.000000	-1.052381	-1.649611	0.000000
		H	1.977261	1.641515	0.000000	-0.430178	-3.131609	0.000000	-0.440971	-3.582288	0.000000
		X	-1.350395	-0.783091	0.000000	0.000000	1.168355	0.000000	0.000000	0.976889	0.000000
	pVTZ	C	1.174031	0.904697	0.000000	-0.198683	-2.061581	0.000000	-0.204118	-2.519583	0.000000
		O	1.637274	-0.329251	0.000000	1.107756	-1.848071	0.000000	1.107961	-2.312675	0.000000
		H	0.860760	-0.928176	0.000000	1.248410	-0.879636	0.000000	1.260021	-1.347486	0.000000
		O	0.000000	1.230255	0.000000	-1.061621	-1.206878	0.000000	-1.058847	-1.660729	0.000000
		H	1.981293	1.642566	0.000000	-0.425385	-3.131892	0.000000	-0.428229	-3.590797	0.000000
		X	-1.352026	-0.785330	0.000000	0.000000	1.166303	0.000000	0.000000	0.978170	0.000000
	pVQZ	C	1.172027	0.899686	0.000000	-0.197302	-2.048461	0.000000	-0.204679	-2.500062	0.000000
		O	1.633740	-0.331866	0.000000	1.105552	-1.833037	0.000000	1.105041	-2.298121	0.000000
		H	0.859490	-0.931154	0.000000	1.244920	-0.865516	0.000000	1.262354	-1.335207	0.000000
		O	0.000000	1.225003	0.000000	-1.060108	-1.196028	0.000000	-1.055007	-1.639374	0.000000
		H	1.978120	1.638166	0.000000	-0.424665	-3.118135	0.000000	-0.434553	-3.569543	0.000000
		X	-1.349393	-0.779425	0.000000	0.000000	1.157341	0.000000	0.000000	0.969907	0.000000

Table B126: Cartesian coordinates of the geometries of halogen-formic acid complexes optimised with the DSD-PBEP86-D3BJ functional, in Å.

			Cl … HCOOH			Br … HCOOH			I … HCOOH		
			x	y	z	x	y	z	x	y	z
<i>C_s</i> (² <i>A'</i>) CarbPAnti	def2QZVP	C	1.186809	1.035349	0.000000	-0.246848	-2.194973	0.000000	-0.248214	-2.647196	0.000000
		O	1.748524	-0.179303	0.000000	1.081076	-2.023548	0.000000	1.080547	-2.476808	0.000000
		H	2.707377	-0.094434	0.000000	1.520638	-2.879916	0.000000	1.520365	-3.333074	0.000000
		O	0.000000	1.198653	0.000000	-1.014872	-1.276068	0.000000	-1.013063	-1.726039	0.000000
		H	1.904358	1.868311	0.000000	-0.569184	-3.246043	0.000000	-0.570953	-3.698100	0.000000
		X	-1.512987	-0.949458	0.000000	0.000000	1.305507	0.000000	0.000000	1.066738	0.000000
	pVTZ	C	1.188700	1.035702	0.000000	-0.245546	-2.185079	0.000000	-0.245683	-2.644847	0.000000
		O	1.743574	-0.185051	0.000000	1.083644	-2.004213	0.000000	1.083676	-2.459020	0.000000
		H	2.705071	-0.105379	0.000000	1.529364	-2.859888	0.000000	1.533420	-3.312598	0.000000
		O	0.000000	1.205467	0.000000	-1.020393	-1.268147	0.000000	-1.021387	-1.729188	0.000000
		H	1.911247	1.865007	0.000000	-0.562103	-3.238377	0.000000	-0.557633	-3.699506	0.000000
		X	-1.5111595	-0.949245	0.000000	0.000000	1.296789	0.000000	0.000000	1.063903	0.000000
	pVQZ	C	1.186554	1.028268	0.000000	-0.244962	-2.175340	0.000000	-0.247555	-2.630398	0.000000
		O	1.740775	-0.189969	0.000000	1.081696	-1.994538	0.000000	1.080710	-2.455843	0.000000
		H	2.700650	-0.112093	0.000000	1.528531	-2.847632	0.000000	1.524483	-3.310540	0.000000
		O	0.000000	1.197913	0.000000	-1.018842	-1.260433	0.000000	-1.014534	-1.710195	0.000000
		H	1.908264	1.857755	0.000000	-0.561589	-3.228182	0.000000	-0.568564	-3.681887	0.000000
		X	-1.509084	-0.939931	0.000000	0.000000	1.290504	0.000000	0.000000	1.058549	0.000000

Table B127: Cartesian coordinates of the geometries of halogen-formic acid complexes optimised with the DSD-PBEP86-D3BJ functional, in Å.

			Cl … HCOOH			Br … HCOOH			I … HCOOH		
			x	y	z	x	y	z	x	y	z
<i>C_s</i> (² <i>A'</i>) CarbPSyn	def2QZVP	C	1.437991	-0.264909	0.266506	-1.318519	-1.756581	0.000000	-0.414845	-2.639290	0.000000
		O	0.570468	0.762155	0.176974	0.000000	-1.483702	0.000000	0.657273	-1.823844	0.000000
		H	0.953434	1.411361	-0.430405	0.472408	-2.328314	0.000000	1.447182	-2.383073	0.000000
		O	2.491162	-0.317148	-0.299580	-1.785574	-2.858657	0.000000	-0.360491	-3.834887	0.000000
		H	1.033008	-1.033515	0.931491	-1.888568	-0.822455	0.000000	-1.332361	-2.042654	0.000000
		X	-2.065143	-0.138144	-0.065840	0.674625	1.383689	0.000000	0.000000	1.236440	0.000000
	pVTZ	C	1.435045	-0.240101	0.297747	-1.327250	-1.715933	0.000000	-0.412922	-2.606769	0.000000
		O	0.5666724	0.785980	0.170128	0.000000	-1.473668	0.000000	0.683692	-1.820110	0.000000
		H	0.920358	1.378861	-0.511653	0.452828	-2.331421	0.000000	1.458854	-2.403217	0.000000
		O	2.457840	-0.348555	-0.319418	-1.821135	-2.809183	0.000000	-0.392207	-3.806150	0.000000
		H	1.063135	-0.947631	1.045701	-1.874607	-0.767560	0.000000	-1.313198	-1.983214	0.000000
		X	-2.046487	-0.146472	-0.066248	0.684410	1.361640	0.000000	0.000000	1.227116	0.000000
	pVQZ	C	1.434091	-0.261763	0.271874	-1.328034	-1.697266	0.000000	-0.413773	-2.597010	0.000000
		O	0.562379	0.762051	0.178666	0.000000	-1.471563	0.000000	0.672617	-1.799683	0.000000
		H	0.936650	1.405062	-0.441281	0.443158	-2.332349	0.000000	1.453609	-2.371995	0.000000
		O	2.481938	-0.317194	-0.304491	-1.833417	-2.782660	0.000000	-0.378849	-3.793671	0.000000
		H	1.038448	-1.023894	0.950141	-1.864244	-0.743027	0.000000	-1.321111	-1.984619	0.000000
		X	-2.054952	-0.139379	-0.066677	0.687332	1.351222	0.000000	0.000000	1.220481	0.000000

Table B128: Cartesian coordinates of the geometries of halogen-formic acid complexes optimised with the DSD-PBEP86-D3BJ functional, in Å.

			Cl … HCOOH			Br … HCOOH			I … HCOOH		
			x	y	z	x	y	z	x	y	z
<i>C_s</i> (² <i>A'</i>) FormPAnti	def2QZVP	C	1.077332	0.351405	0.000000	1.199735	1.370363	0.000000	0.266629	-2.289004	0.000000
		O	2.208994	1.063445	0.000000	1.909780	2.504443	0.000000	0.235497	-3.627225	0.000000
		H	2.965815	0.468302	0.000000	2.850017	2.297480	0.000000	1.134448	-3.971825	0.000000
		O	0.000000	0.881825	0.000000	0.000000	1.376770	0.000000	-0.736705	-1.632548	0.000000
		H	1.213152	-0.737582	0.000000	1.799380	0.450383	0.000000	1.275448	-1.853383	0.000000
		X	-1.665583	-1.023606	0.000000	-0.775030	-1.200564	0.000000	0.000000	1.162970	0.000000
	pVTZ	C	1.078189	0.351686	0.000000	1.202422	1.359024	0.000000	0.265013	-2.286805	0.000000
		O	2.213440	1.063093	0.000000	1.922041	2.490092	0.000000	0.245765	-3.627883	0.000000
		H	2.970270	0.464427	0.000000	2.862668	2.274873	0.000000	1.150131	-3.964309	0.000000
		O	0.000000	0.886432	0.000000	0.000000	1.375512	0.000000	-0.747025	-1.638813	0.000000
		H	1.211480	-0.738236	0.000000	1.794514	0.433495	0.000000	1.269872	-1.840691	0.000000
		X	-1.668142	-1.025442	0.000000	-0.778515	-1.193924	0.000000	0.000000	1.163385	0.000000
	pVQZ	C	1.076275	0.345747	0.000000	1.200368	1.354542	0.000000	0.266452	-2.275116	0.000000
		O	2.209331	1.055914	0.000000	1.913217	2.486963	0.000000	0.238415	-3.613419	0.000000
		H	2.966058	0.459974	0.000000	2.853569	2.278600	0.000000	1.138199	-3.956999	0.000000
		O	0.000000	0.879692	0.000000	0.000000	1.365421	0.000000	-0.739723	-1.621830	0.000000
		H	1.208806	-0.743788	0.000000	1.796240	0.431922	0.000000	1.273556	-1.835221	0.000000
		X	-1.665127	-1.016207	0.000000	-0.775936	-1.190196	0.000000	0.000000	1.157074	0.000000

Table B129: Cartesian coordinates of the geometries of halogen-formic acid complexes optimised with the DSD-PBEP86-D3BJ functional, in Å.

			Cl … HCOOH			Br … HCOOH			I … HCOOH		
			x	y	z	x	y	z	x	y	z
<i>C_s</i> (² <i>A'</i>) FormPSyn	def2QZVP	C	1.102406	0.359457	0.000000	1.205166	1.400880	0.000000	-0.321466	-2.313306	0.000000
		O	2.235319	1.058974	0.000000	1.925282	2.521666	0.000000	-0.347432	-3.645641	0.000000
		H	2.000074	1.997911	0.000000	1.306763	3.266192	0.000000	0.569753	-3.954903	0.000000
		O	0.000000	0.849785	0.000000	0.000000	1.364670	0.000000	0.684258	-1.649323	0.000000
		H	1.302829	-0.713965	0.000000	1.852539	0.520827	0.000000	-1.335570	-1.905432	0.000000
		X	-1.635287	-1.100633	0.000000	-0.736930	-1.236657	0.000000	0.000000	1.171696	0.000000
	pVTZ	C	1.102795	0.358924	0.000000	1.208223	1.388137	0.000000	-0.318864	-2.309032	0.000000
		O	2.241012	1.054704	0.000000	1.940337	2.504029	0.000000	-0.360894	-3.643467	0.000000
		H	2.008136	1.996454	0.000000	1.326567	3.255263	0.000000	0.554983	-3.963150	0.000000
		O	0.000000	0.854959	0.000000	0.000000	1.363126	0.000000	0.696750	-1.655285	0.000000
		H	1.299228	-0.715975	0.000000	1.847566	0.501383	0.000000	-1.328652	-1.888754	0.000000
		X	-1.638367	-1.100666	0.000000	-0.741319	-1.229220	0.000000	0.000000	1.171625	0.000000
	pVQZ	C	1.101357	0.353234	0.000000	1.205992	1.383336	0.000000	-0.321394	-2.298883	0.000000
		O	2.236115	1.049896	0.000000	1.930319	2.501344	0.000000	-0.349622	-3.631073	0.000000
		H	2.003652	1.989925	0.000000	1.314660	3.248743	0.000000	0.567296	-3.942325	0.000000
		O	0.000000	0.847396	0.000000	0.000000	1.352670	0.000000	0.686539	-1.637084	0.000000
		H	1.297922	-0.721123	0.000000	1.848665	0.499572	0.000000	-1.334267	-1.887442	0.000000
		X	-1.635214	-1.092149	0.000000	-0.738338	-1.225155	0.000000	0.000000	1.165440	0.000000

Table B130: Cartesian coordinates of the geometries of halogen-formic acid complexes optimised with the DSD-PBEP86-D3BJ functional, in Å.

		Cl...HCOOH			Cl...HCOOH					
		x	y	z		x	z			
C_s ($^2A''$) InLineSyn	def2QZVP	C	-1.875893	0.657476	0.000000	def2QZVP	C	1.671331	0.164369	0.229680
		O	-0.711532	1.319419	0.000000		O	0.640775	0.879312	-0.279360
		H	0.000000	0.660146	0.000000		H	0.605730	1.745101	0.140869
		O	-1.993525	-0.536451	0.000000		O	1.904226	-0.949646	-0.119502
		H	-2.708399	1.368667	0.000000		H	2.255808	0.715230	0.981572
		X	2.094365	-0.719848	0.000000		X	-1.955855	-0.169639	0.040610
	pVTZ	C	-1.878758	0.623915	0.000000	C_s (1A) OutPlAnti	C	1.662781	0.162179	0.234143
		O	-0.721432	1.302677	0.000000		O	0.639379	0.886915	-0.282628
		H	0.000000	0.650795	0.000000		H	0.602262	1.750526	0.146903
		O	-1.980683	-0.574320	0.000000		O	1.894663	-0.952515	-0.122900
		H	-2.721320	1.324211	0.000000		H	2.241376	0.704021	0.997768
		X	2.094753	-0.679138	0.000000		X	-1.946627	-0.170754	0.040865
	pVQZ	C	-1.876324	0.627438	0.000000	pVQZ	C	1.668998	-0.166400	-0.227025
		O	-0.724644	1.311503	0.000000		O	0.633318	-0.878139	0.277376
		H	0.000000	0.665816	0.000000		H	0.599572	-1.746560	-0.138527
		O	-1.970807	-0.569060	0.000000		O	1.898108	0.950091	0.118127
		H	-2.722924	1.322112	0.000000		H	2.260783	-0.721544	-0.970165
		X	2.090852	-0.687770	0.000000		X	-1.948574	0.170052	-0.040776

Appendix C

Tables and Data: Halide-Propene Complexes

Table C1: Peak positions and assignments of 50 kPa C₃H₆:CCl₄:argon gas mix.

Position (<i>m/z</i>)	Assignment
34.9	³⁵ Cl ⁻
36.9	³⁷ Cl ⁻
77.1	³⁵ Cl ⁻ ...C ₃ H ₆
79.0	³⁷ Cl ⁻ ...C ₃ H ₆ , ⁷⁹ Br ⁻
81.0	⁸¹ Br ⁻
119.4	³⁵ Cl ⁻ ...(C ₃ H ₆) ₂
121.3	³⁷ Cl ⁻ ...(C ₃ H ₆) ₂ , ⁷⁹ Br ⁻ ...C ₃ H ₆
123.2	⁸¹ Br ⁻ ...C ₃ H ₆
126.9	I ⁻

Table C2: Peak positions and assignments of 50 kPa C₃H₆:CH₂Br₂:argon gas mix.

Position (<i>m/z</i>)	Assignment
35.1	³⁵ Cl ⁻
37.0	³⁷ Cl ⁻
77.1	³⁵ Cl ⁻ ...C ₃ H ₆
79.0	³⁷ Cl ⁻ ...C ₃ H ₆ , ⁷⁹ Br ⁻
80.9	⁸¹ Br ⁻
118.0	CHCl ₃ ⁻ (³⁵ Cl: ³⁷ Cl=3:0)
119.3	³⁵ Cl ⁻ ...(C ₃ H ₆) ₂
121.2	³⁷ Cl ⁻ ...(C ₃ H ₆) ₂ , ⁷⁹ Br ⁻ ...C ₃ H ₆
123.2	⁸¹ Br ⁻ ...C ₃ H ₆
127.1	I ⁻
152.1	CCl ₄ ⁻ (³⁵ Cl: ³⁷ Cl=4:0)
153.1	CHCl ₄ ⁻ (³⁵ Cl: ³⁷ Cl=4:0)
154.2	CCl ₄ ⁻ (³⁵ Cl: ³⁷ Cl=3:1)
155.2	CHCl ₄ ⁻ (³⁵ Cl: ³⁷ Cl=3:1)
156.2	CCl ₄ ⁻ (³⁵ Cl: ³⁷ Cl=2:2)
160.2	CCl ₄ ⁻ (³⁵ Cl: ³⁷ Cl=1:3)
161.4	CCl ₄ ⁻ (³⁵ Cl: ³⁷ Cl=0:4)
162.2	³⁵ Cl ⁻ ...(C ₃ H ₆) ₃
163.4	³⁷ Cl ⁻ ...(C ₃ H ₆) ₃ , ⁷⁹ Br ⁻ ...(C ₃ H ₆) ₂
165.3	⁸¹ Br ⁻ ...(C ₃ H ₆) ₂
169.2	I ⁻ ...C ₃ H ₆
172.1	⁷⁹ Br ⁻ ...CH ₂ ⁷⁹ Br
174.1	⁷⁹ Br ⁻ ...CH ₂ ⁸¹ Br, ⁸¹ Br ⁻ ...CH ₂ ⁷⁹ Br
176.1	⁸¹ Br ⁻ ...CH ₂ ⁸¹ Br

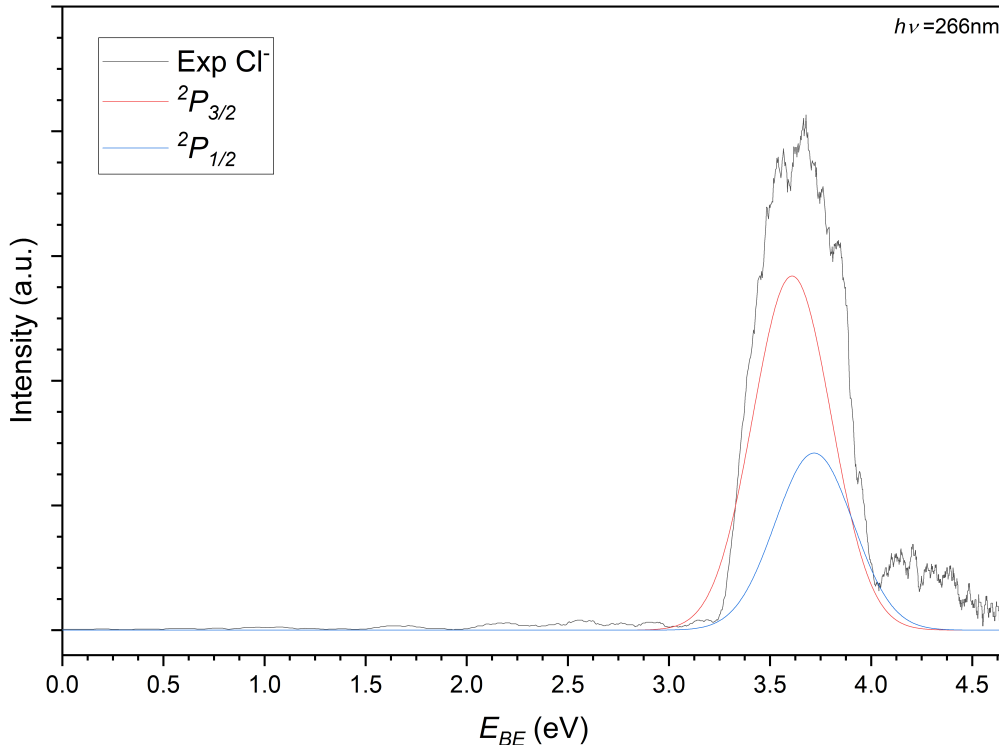
Table C3: Peak positions and assignments of 50 kPa $\text{C}_3\text{H}_6:\text{CH}_3\text{I}:\text{argon}$ gas mix.

Position (m/z)	Assignment
126.9	I^-
169.3	$\text{I}^- \cdots \text{C}_3\text{H}_6$
211.6	$\text{I}^- \cdots (\text{C}_3\text{H}_6)_2$
253.9	$\text{I}^- \cdots (\text{C}_3\text{H}_6)_3$
269.8	$\text{I}^- \cdots \text{CH}_3\text{I}$
311.9	$\text{I}^- \cdots (\text{CH}_3\text{I})(\text{C}_3\text{H}_6)$
354.4	$\text{I}^- \cdots (\text{CH}_3\text{I})(\text{C}_3\text{H}_6)_2$
395.0	$\text{I}^- \cdots (\text{CH}_3\text{I})(\text{C}_3\text{H}_6)_3$
412.7	$\text{I}^- \cdots (\text{CH}_3\text{I})_2$

Table C4: Calibration details from the each of the bare halide PES spectra.

Halide Source	Calibration Mass Peak	A^\dagger	B^\dagger
CH_2Br_2	$^{81}\text{Br}^-$	7.463E-12	-0.2496
CH_3I	I^-	8.053E-12	-0.3842
CCl_4	I^-	7.920E-12	-0.6378

$$\dagger: E_{BE} = h\nu + \frac{A}{TOF^2} + B$$

Figure C.1: An example Cl^- PES recorded during the halide-propene suite of experiments.

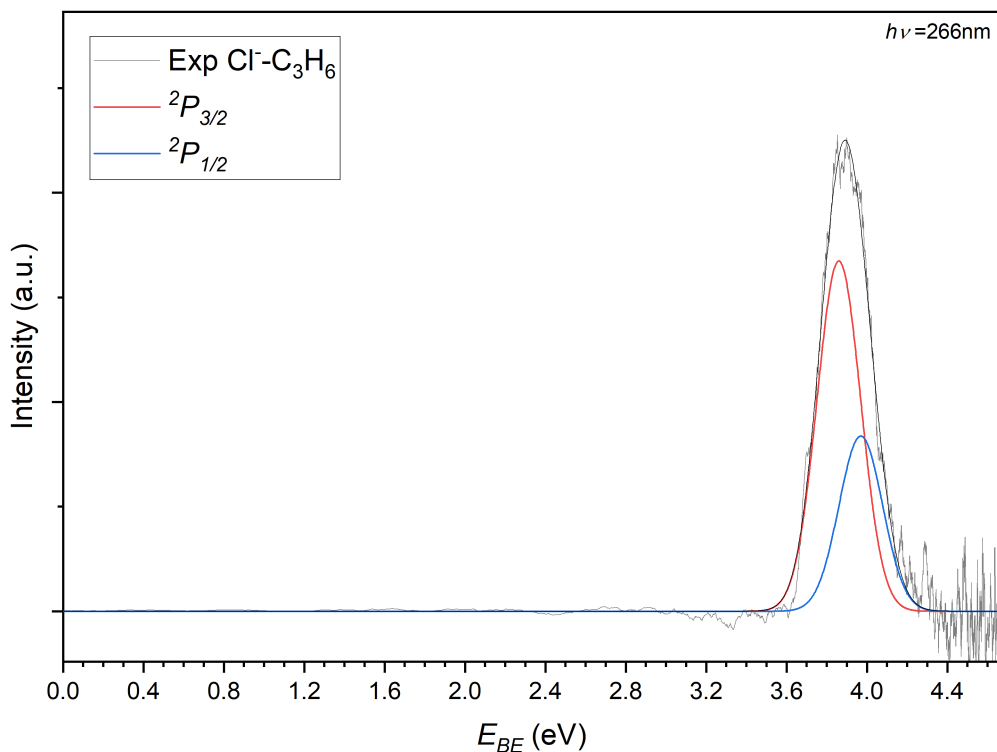


Figure C.2: Additional $\text{Cl}^- \cdots \text{C}_3\text{H}_6$ PES spectrum recorded. The peak has also been deconvoluted into two Gaussian functions yielding E_{BE} : $^2P_{3/2} = 3.86$ eV and $^2P_{1/2} = 3.97$ eV.

Table C5: $X^- \cdots C_3H_6$ complex geometric parameters and D_0 values from DSD-PBEP86-D3BJ optimisations. zpe values are drawn from relevant harmonic frequency calculations.

		R_{X-H}	\angle_{H-X-H}	E_{DFT}	zpe	D_e	D_o	E_{VDE}	VDE $^2P_{3/2}$	VDE $^2P_{1/2}$	
		\AA	$^\circ$	E_h	kJ mol^{-1}	kJ mol^{-1}	kJ mol^{-1}	E_h	eV	eV	
$Cl^- \cdots C_3H_6$	BiDent	def2QZVP pVTZ	2.664	53.2	-577.7214109	211.1	31.0	32.2	-577.5800396	3.942	4.051
			2.667	53.2	-577.6919627	211.0	29.1	30.4	-577.5493893	3.906	4.018
	Bif	def2QZVP pVTZ	R_{X-H}		\angle_{H-X-C}						
			2.659	37.6	-577.7212976	210.3	30.7	31.1	-577.5804888	3.934	4.043
	HApp	def2QZVP pVTZ	2.655	37.3	-577.6917547	210.1	28.6	28.9	-577.5497483	3.898	4.007
			R_{X-H}		\angle_{X-H-C}						
$Br^- \cdots C_3H_6$	BiDent	def2QZVP pVTZ	2.487	175.2	-577.7177605	210.5	21.5	22.0	-577.5799972	3.850	3.959
			2.494	175.0	-577.6884721	210.3	19.9	20.6	-577.5492608	3.821	3.930
			R_{X-H}		\angle_{H-X-H}						
	Bif	def2QZVP pVTZ	2.848	49.7	-2691.1955646	211.0	27.0	28.1	-2691.0609970	3.624	4.081
			2.812	50.3	-534.0253488	211.0	26.9	28.1	-533.8911496	3.601	4.058
	I-	def2QZVP pVTZ	R_{X-H}		\angle_{X-H-C}						
			2.865	35.9	-2691.1957939	210.2	27.6	28.0	-2691.0613613	3.627	4.084
$I^- \cdots C_3H_6$	BiDent	def2QZVP pVTZ	2.821	35.6	-534.0252992	210.1	26.7	27.1	-533.8914016	3.600	4.057
			R_{X-H}		\angle_{H-X-H}						
	Bif	def2QZVP pVTZ	3.127	45.3	-415.2834016	210.9	20.9	21.8	-415.1576975	3.232	4.174
			3.081	46.0	-413.0711450	210.8	22.7	23.8	-412.9453864	3.230	4.172
	I-	def2QZVP pVTZ	R_{X-H}		\angle_{X-H-C}						
			3.158	33.5	-415.2839787	210.3	22.4	22.7	-415.1577898	3.250	4.192
			3.108	33.5	-413.0715007	210.1	23.6	24.0	-412.9454346	3.244	4.186

Table C6: X···C₃H₆ complex geometric parameters and D_0 values from DSD-PBEP86-D3BJ optimisations. zpe values are drawn from relevant harmonic frequency calculations.

			R_{X-H} Å	\angle_{H-X-H} °	E_{DFT} E_h	zpe kJ mol ⁻¹	D_e kJ mol ⁻¹	D_o kJ mol ⁻¹
Cl···C ₃ H ₆	BiDent	def2QZVP pVTZ	3.204	45.3	-577.5821952	211.0	3.0	4.1
			R_{X-C}	\angle_{X-C-H}				
	MePoc	def2QZVP pVTZ	3.763	66.0	-577.5818040	210.5	2.0	2.6
			3.724	65.7	-577.5508222	210.3	2.6	3.2
	Perp	def2QZVP pVTZ	R_{X-C}	\angle_{X-C-C}				
			1.839	110.5	-577.6172780	213.4	95.1	98.6
Br···C ₃ H ₆	Bif	def2QZVP pVTZ	1.843	110.4	-577.5863091	213.2	95.8	99.3
			R_{X-H}	\angle_{H-X-H}				
	MePoc	def2QZVP pVTZ	3.310	38.3	-2691.0631763	210.6	5.9	6.6
			3.267	39.0	-533.8932934	210.3	7.8	8.4
	Perp	def2QZVP pVTZ	R_{X-C}	\angle_{X-C-H}				
			3.866	66.2	-2691.0618654	210.4	2.5	3.0
I···C ₃ H ₆	End	def2QZVP pVTZ	3.816	65.1	-533.8916923	210.4	3.6	4.3
			R_{X-C}	\angle_{X-C-C}				
	MePoc	def2QZVP pVTZ	2.688	79.7	-2691.0777652	213.2	44.2	47.5
			2.676	79.4	-533.9079853	212.9	46.4	49.6
	Perp	def2QZVP pVTZ	R_{X-H}	\angle_{H-X-H}				
			3.688	29.2	-415.1577891	210.8	2.9	3.8
	MePoc	def2QZVP pVTZ	3.702	29.5	-412.9452053	210.5	4.2	5.0
			R_{X-C}	\angle_{X-C-H}				
	Perp	def2QZVP pVTZ	4.038	66.3	-415.1577946	210.4	3.0	3.5
			3.987	64.4	-412.9452577	210.3	4.3	4.9
	Perp	def2QZVP pVTZ	R_{X-C}	\angle_{X-C-C}				
			2.946	80.7	-415.1696451	212.8	34.1	36.9
			2.948	80.5	-412.9573379	212.5	36.0	38.9

Table C7: Cartesian coordinates of the geometries of halide-propene complexes optimised with the DSD-PBEP86-D3BJ functional, in Å.

		Cl ⁻ ... C ₃ H ₆			Br ⁻ ... C ₃ H ₆			I ⁻ ... C ₃ H ₆			
		x	y	z	x	y	z	x	y	z	
def2QZVP	BiDent	H	3.034471	0.523704	0.000000	-2.964427	2.458629	0.000000	-0.170655	-4.423255	0.000000
		C	1.963427	0.322903	0.000000	-2.129604	1.758758	0.000000	-0.131856	-3.335010	0.000000
		C	1.533894	-0.939035	0.000000	-2.376685	0.449130	0.000000	-1.271591	-2.644982	0.000000
		H	2.241002	-1.762154	0.000000	-3.396406	0.079232	0.000000	-2.228481	-3.154800	0.000000
		H	0.467453	-1.155886	0.000000	-1.559293	-0.267640	0.000000	-1.264852	-1.558984	0.000000
		C	1.040991	1.503570	0.000000	-0.748439	2.338372	0.000000	1.224286	-2.700323	0.000000
		H	0.000000	1.169745	0.000000	0.000000	1.542759	0.000000	1.141933	-1.612039	0.000000
		H	1.214626	2.133002	-0.878801	-0.592376	2.971899	0.878758	1.798513	-3.008831	-0.878716
		H	1.214626	2.133002	0.878801	-0.592376	2.971899	-0.878758	1.798513	-3.008831	0.878716
		X	-2.082474	-0.492120	0.000000	1.160950	-1.058124	0.000000	0.000000	1.299031	0.000000
AVTZ	BiDent	H	3.037582	0.525126	0.000000	0.178165	3.827965	0.000000	-4.391090	0.166143	0.000000
		C	1.965757	0.323381	0.000000	0.134007	2.738471	0.000000	-3.301728	0.129418	0.000000
		C	1.537328	-0.940997	0.000000	1.270666	2.038819	0.000000	-2.612860	1.272223	0.000000
		H	2.246029	-1.763975	0.000000	2.231554	2.544255	0.000000	-3.125304	2.228876	0.000000
		H	0.470478	-1.159317	0.000000	1.248848	0.950833	0.000000	-1.525744	1.265888	0.000000
		C	1.041792	1.504527	0.000000	-1.225079	2.105462	0.000000	-2.663051	-1.226462	0.000000
		H	0.000000	1.169755	0.000000	-1.137757	1.015196	0.000000	-1.573647	-1.139933	0.000000
		H	1.215585	2.134350	-0.879941	-1.799184	2.416288	-0.879975	-2.970773	-1.801677	-0.879878
		H	1.215585	2.134350	0.879941	-1.799184	2.416288	0.879975	-2.970774	-1.801678	0.879878
		X	-2.085560	-0.491868	0.000000	0.000000	-1.556210	0.000000	1.283456	0.000591	0.000000

Table C8: Cartesian coordinates of the geometries of halide-propene complexes optimised with the DSD-PBEP86-D3BJ functional, in Å.

		Cl ⁻ ... C ₃ H ₆			Br ⁻ ... C ₃ H ₆			I ⁻ ... C ₃ H ₆			
		x	y	z	x	y	z	x	y	z	
def2QZVP	H	-0.802780	-0.406590	0.000000	-1.145058	0.824477	0.000096	-1.538742	1.151099	0.000000	
	C	-1.125712	0.631758	0.000000	-2.058247	0.235209	0.000033	-1.417175	2.230674	0.000000	
	C	-2.417746	0.963174	0.000000	-3.256978	0.819541	-0.000017	-2.481385	3.033652	0.000000	
	H	-3.193873	0.207396	0.000000	-3.358744	1.897896	0.000006	-3.488373	2.635261	0.000000	
	H	-2.737540	2.001215	0.000000	-4.172322	0.235279	-0.000087	-2.374923	4.114022	0.000000	
	C	0.000000	1.610970	0.000000	-1.833041	-1.239681	0.000001	0.000000	2.697723	0.000000	
	H	-0.357335	2.644410	0.000000	-1.231878	-1.522511	-0.865667	0.065384	3.788478	0.000000	
	H	0.640882	1.434554	-0.865336	-1.232007	-1.522573	0.865740	0.526530	2.294766	-0.866906	
	H	0.640882	1.434554	0.865336	-2.774934	-1.794464	-0.000084	0.526530	2.294766	0.866906	
	X	1.592382	-1.561818	0.000000	1.622987	0.085471	-0.000003	0.559905	-1.208503	0.000000	
Bif	AVTZ	C	1.073749	0.715818	0.000000	-1.111717	-0.793705	0.000093	-1.688699	-0.823697	-0.000032
		C	1.949537	1.724208	0.000000	-2.042092	-0.229698	0.000034	-2.605904	-0.239467	-0.000011
		H	0.000000	0.893120	0.000000	-3.226431	-0.846519	-0.000017	-3.797512	-0.841331	0.000006
		H	1.621073	2.759056	0.000000	-3.298642	-1.928226	0.000009	-3.883284	-1.921848	-0.000003
		H	3.020190	1.543923	0.000000	-4.157836	-0.286241	-0.000089	-4.721117	-0.268865	0.000030
		C	1.452043	-0.729340	0.000000	-1.856123	1.252367	0.000000	-2.399138	1.239823	0.000000
		H	2.539644	-0.839699	0.000000	-2.813435	1.782657	-0.000134	-1.805003	1.533969	-0.868544
		H	1.023042	-1.236694	0.868104	-1.263735	1.551525	-0.867927	-3.349926	1.780978	0.000041
		H	1.023042	-1.236694	-0.868104	-1.263953	1.551597	0.868052	-1.804937	1.533946	0.868506
		X	-2.122292	-0.714537	0.000000	1.618777	-0.083843	-0.000003	1.322043	-0.052616	0.000001

Table C9: Cartesian coordinates of the geometries of halide-propene complexes optimised with the DSD-PBEP86-D3BJ functional, in Å.

		$\text{Cl}^- \cdots \text{C}_3\text{H}_6$			
		x	y	z	
def2QZVP	HApp	H	-0.403974	1.802275	0.000000
		C	-1.253204	1.124407	0.000000
		C	-1.013548	-0.185150	0.000000
		H	0.000000	-0.587083	0.000000
		H	-1.845976	-0.885207	0.000000
		C	-2.615765	1.750360	0.000000
		H	-3.394624	0.985445	0.000000
		H	-2.764864	2.386074	-0.878016
		H	-2.764864	2.386074	0.878016
		X	2.380553	-1.307370	0.000000
AVTZ	HApp	H	0.417421	-1.798051	0.000000
		C	1.263808	-1.115035	0.000000
		C	1.016559	0.195012	0.000000
		H	0.000000	0.590655	0.000000
		H	1.845339	0.900819	0.000000
		C	2.630699	-1.734636	0.000000
		H	3.406492	-0.964878	0.000000
		H	2.782102	-2.370197	-0.879210
		H	2.782102	-2.370197	0.879210
		X	-2.394109	1.290577	0.000000

Table C10: Cartesian coordinates of the geometries of halogen-propene complexes optimised with the DSD-PBEP86-D3BJ functional, in Å.

		Cl···C ₃ H ₆				Br···C ₃ H ₆				I···C ₃ H ₆			
		x	y	z		x	y	z		x	y	z	
def2QZVP	BiDent	H	-3.286352	0.203741	0.000280		1.502122	1.146196	0.000000		-4.183205	1.545457	0.000255
		C	-2.201738	0.145594	0.000075		2.185647	0.302262	0.000000		-3.749861	0.549511	0.000057
		C	-1.498919	1.275687	-0.000054		3.495625	0.533837	0.000000		-2.424869	0.426578	-0.000148
		H	-1.985605	2.241870	0.000041		3.890401	1.540866	0.000000		-1.774986	1.291367	-0.000121
		H	-0.415395	1.262943	-0.000258		4.210521	-0.280678	0.000000		-1.949036	-0.547162	-0.000349
		C	-1.605472	-1.225952	-0.000041		1.566657	-1.059234	0.000000		-4.709750	-0.597142	0.000035
		H	-0.516577	-1.181639	-0.000255		0.935756	-1.202803	0.881600		-4.182562	-1.551126	-0.000171
		H	-1.927980	-1.791546	-0.877089		0.935758	-1.202803	-0.881601		-5.359630	-0.562858	-0.877145
		H	-1.927636	-1.791545	0.877135		2.326341	-1.841203	0.000000		-5.359382	-0.563099	0.877408
		X	2.464489	-0.006812	0.000016		-1.636813	0.090835	0.000000		1.662560	-0.035590	0.000009
AVTZ	Bif	H				Bif	-1.476122	-1.149426	0.000025	End	1.427047	-4.233302	0.000000
		C					-2.156289	-0.301545	0.000008		0.464302	-3.728319	0.000000
		C					-3.469194	-0.526845	-0.000006		0.437948	-2.396007	0.000000
		H					-3.868852	-1.533032	-0.000001		1.348665	-1.810168	0.000000
		H					-4.180664	0.291995	-0.000022		-0.499110	-1.849648	0.000000
		C					-1.528994	1.057689	0.000003		-0.750101	-4.603247	0.000000
		H					-2.285034	1.844999	-0.000012		-1.663969	-4.006970	0.000000
		H					-0.897099	1.196996	-0.883205		-0.762765	-5.254208	0.878468
		H					-0.897117	1.197011	0.883220		-0.762765	-5.254208	-0.878468
		X					1.615193	-0.092124	-0.000001		0.000000	1.637244	0.000000

Table C11: Cartesian coordinates of the geometries of halogen-propene complexes optimised with the DSD-PBEP86-D3BJ functional, in Å.

		Cl···C ₃ H ₆			Br···C ₃ H ₆			I···C ₃ H ₆			
		x	y	z	x	y	z	x	y	z	
def2QZVP	MePoc	H	-2.747793	-1.458953	0.000620	-3.706591	-1.452225	-0.000006	4.313588	-1.446665	-0.000247
		C	-2.333373	-0.454990	0.000161	-3.282464	-0.452316	-0.000002	3.883716	-0.449206	-0.000066
		C	-3.167235	0.581964	0.000094	-4.106262	0.592666	-0.000001	4.701479	0.600521	-0.000039
		H	-4.240171	0.444328	0.000485	-5.180488	0.465460	-0.000005	5.776427	0.479520	-0.000195
		H	-2.796467	1.600347	-0.000356	-3.725607	1.607397	0.000004	4.314950	1.613031	0.000141
		C	-0.842330	-0.346698	-0.000354	-1.790479	-0.358378	0.000004	2.391218	-0.363785	0.000140
		H	-0.520954	0.694652	-0.000790	-1.458832	0.679747	0.000013	2.053386	0.672407	0.000321
		H	-0.413469	-0.837911	-0.876575	-1.365736	-0.853391	-0.876096	1.969095	-0.861293	0.876162
		H	-0.412896	-0.837366	0.875890	-1.365741	-0.853407	0.876097	1.968862	-0.861071	-0.875895
		X	2.893493	0.100779	0.000078	2.053664	0.048988	0.000000	-1.627449	0.031677	-0.000009
AVTZ	MePoc	H	-2.706902	-1.464045	-0.018994	-3.692644	-1.446984	0.000273	-4.304063	-1.435385	0.000000
		C	-2.305411	-0.456174	0.003213	-3.254778	-0.451916	0.000074	-3.850652	-0.447300	0.000000
		C	-3.148048	0.578894	-0.001278	-4.066036	0.605185	0.000038	-4.645197	0.622429	0.000000
		H	-4.215501	0.421065	-0.029229	-5.142810	0.491538	0.000208	-5.723631	0.525760	0.000000
		H	-2.801017	1.611167	0.029261	-3.671514	1.615701	-0.000161	-4.234705	1.626560	0.000000
		C	-0.827722	-0.337827	0.011136	-1.760309	-0.377902	-0.000154	-2.355239	-0.396523	0.000000
		H	-0.505783	0.701175	-0.024796	-1.414790	0.656988	-0.000364	-1.993323	0.632773	0.000000
		H	-0.402620	-0.843579	-0.881319	-1.342375	-0.879315	-0.877454	-1.944589	-0.904132	-0.877235
		H	-0.377563	-0.866434	0.866635	-1.342125	-0.879043	0.877184	-1.944589	-0.904132	0.877236
		X	2.864498	0.101841	-0.001175	2.031228	0.051112	0.000016	1.608518	0.033715	0.000000

Table C12: Cartesian coordinates of the geometries of halogen-propene complexes optimised with the DSD-PBEP86-D3BJ functional, in Å.

		Cl...C ₃ H ₆			Br...C ₃ H ₆			I...C ₃ H ₆			
		x	y	z	x	y	z	x	y	z	
Perp	def2QZVP	C	0.145684	0.882511	0.305448	-1.099276	1.345951	-0.209853	2.029621	0.254912	0.466608
		C	-1.101663	0.533891	-0.378744	-1.574943	0.277392	0.467154	1.624305	1.344403	-0.211243
		H	-1.233685	0.881166	-1.394856	-1.515415	0.286150	1.550261	1.955877	0.263882	1.549498
		H	0.564045	1.830321	-0.017826	-0.691049	2.201877	0.307997	1.233364	2.211816	0.304072
		H	0.052878	0.859654	1.388659	-1.156189	1.390363	-1.289774	1.677612	1.384544	-1.291213
		C	-1.962278	-0.562676	0.130061	-2.212244	-0.907713	-0.169112	2.578960	-0.978224	-0.166543
		H	-1.547681	-1.541115	-0.143946	-3.261046	-0.972499	0.131287	2.009095	-1.856104	0.140789
		H	-2.969049	-0.509225	-0.282631	-1.724088	-1.825767	0.159378	2.542938	-0.902084	-1.254099
		H	-2.028673	-0.541984	1.219838	-2.159726	-0.851747	-1.255199	3.613198	-1.140921	0.139650
		X	1.451277	-0.358893	-0.065284	1.137894	-0.129204	-0.003802	-0.951498	-0.069579	-0.002295
Perp	AVTZ	C	0.144549	0.884782	0.305662	-1.088839	1.349010	-0.209402	-1.624056	1.345655	-0.210172
		C	-1.103003	0.534183	-0.379482	-1.563710	0.277991	0.467671	-2.024211	0.250792	0.465521
		H	-1.233550	0.879024	-1.397708	-1.502543	0.285913	1.551665	-1.961514	0.261450	1.550011
		H	0.564208	1.832487	-0.019319	-0.678013	2.203852	0.310248	-1.262097	2.224331	0.307310
		H	0.052542	0.861153	1.389840	-1.146645	1.394748	-1.290201	-1.684109	1.388003	-1.291571
		C	-1.963881	-0.563834	0.130444	-2.206036	-0.906138	-0.169154	-2.587813	-0.977158	-0.167685
		H	-1.546242	-1.542954	-0.141274	-3.258033	-0.962563	0.126297	-3.628075	-1.114196	0.141605
		H	-2.970821	-0.511873	-0.285049	-1.725060	-1.827441	0.164440	-2.035641	-1.863236	0.151983
		H	-2.032285	-0.540243	1.221235	-2.147387	-0.852525	-1.256296	-2.550250	-0.915157	-1.255628
		X	1.452950	-0.359317	-0.065145	1.131691	-0.130490	-0.004024	0.953550	-0.069753	-0.002447

Table C13: Calculated harmonic frequencies and mode assignments for the $\text{X}^- \cdots \text{C}_3\text{H}_6$ BiDent complexes. All frequencies and intensities are in cm^{-1} and km mol^{-1} and zero-point energies are in kJ mol^{-1} .

Cl ⁻ ...C ₃ H ₆				Br ⁻ ...C ₃ H ₆				I ⁻ ...C ₃ H ₆				
	Mode	Symmetry	Frequency (cm^{-1})	Intensity (km mol^{-1})		Symmetry	Frequency (cm^{-1})	Intensity (km mol^{-1})		Symmetry	Frequency (cm^{-1})	Intensity (km mol^{-1})
def2QZVP	ω_1	a'	90	3.3256	a'	79	6.5627	a'	65	3.7468		
	ω_2	a'	105	24.6974	a'	85	2.0685	a'	73	0.04		
	ω_3	a''	133	0.104	a''	121	0.004	a''	105	0.051		
	ω_4	a''	224	0.4346	a''	219	0.4927	a''	214	0.4669		
	ω_5	a'	446	5.1353	a'	442	3.7719	a'	437	2.7758		
	ω_6	a''	595	15.9601	a''	594	15.3112	a''	592	14.6189		
	ω_7	a'	937	5.925	a'	937	5.5184	a'	937	5.0114		
	ω_8	a'	963	1.3491	a'	960	1.3123	a'	957	1.338		
	ω_9	a''	969	17.6593	a''	967	20.279	a''	964	21.4298		
	ω_{10}	a''	1051	24.382	a''	1047	21.4968	a''	1043	17.7694		
	ω_{11}	a''	1082	2.1612	a''	1081	2.5494	a''	1080	3.0814		
	ω_{12}	a'	1208	0.9062	a'	1207	0.5864	a'	1206	0.3122		
	ω_{13}	a'	1336	0.1639	a'	1335	0.1048	a'	1334	0.1103		
	ω_{14}	a'	1415	0.6794	a'	1416	0.5257	a'	1416	0.4044		
	ω_{15}	a'	1455	1.9559	a'	1456	1.5657	a'	1457	1.2532		
	ω_{16}	a'	1501	2.1762	a'	1502	2.9078	a''	1501	1.8897		
	ω_{17}	a''	1507	2.9097	a''	1504	2.7595	a'	1502	3.9248		
	ω_{18}	a'	1699	15.6093	a'	1701	14.1942	a'	1704	12.4485		
	ω_{19}	a'	3003	97.8324	a'	3009	85.2186	a'	3017	69.9263		
	ω_{20}	a''	3066	41.2494	a''	3071	37.5093	a''	3076	31.3927		
	ω_{21}	a'	3088	7.0437	a'	3096	22.5526	a'	3105	29.6864		
	ω_{22}	a'	3096	145.695	a'	3107	100.8075	a'	3119	54.0079		
	ω_{23}	a'	3114	40.1046	a'	3120	42.2127	a'	3128	49.1996		
	ω_{24}	a'	3206	17.3553	a'	3213	14.4542	a'	3221	11.1601		
	zpe		211.1		zpe	211.0		zpe	210.9			
AVTZ	ω_1	a'	90	3.3751	a'	83	6.418	a	69	3.6386		
	ω_2	a'	105	24.5551	a'	88	2.0604	a	77	0.0281		
	ω_3	a''	134	0.0868	a''	131	0.0326	a	111	0.1174		
	ω_4	a''	226	0.4041	a''	223	0.5105	a	217	0.5069		
	ω_5	a'	443	5.3645	a'	440	4.2427	a	435	2.9781		
	ω_6	a''	596	16.8573	a''	598	16.5919	a	593	15.7184		
	ω_7	a'	936	5.8282	a'	936	5.5367	a	936	4.8944		
	ω_8	a'	961	1.6435	a'	960	1.5335	a	956	1.5468		
	ω_9	a''	978	14.9906	a''	977	15.5232	a	972	17.6738		
	ω_{10}	a''	1049	24.9763	a''	1048	21.2081	a	1042	17.0956		
	ω_{11}	a''	1083	2.1346	a''	1082	2.5958	a	1081	3.2452		
	ω_{12}	a'	1207	0.9157	a'	1206	0.6648	a	1205	0.3379		
	ω_{13}	a'	1333	0.198	a'	1332	0.1917	a	1331	0.226		
	ω_{14}	a'	1415	0.4255	a'	1416	0.2645	a	1416	0.188		
	ω_{15}	a'	1454	2.0865	a'	1455	1.9789	a	1456	1.443		
	ω_{16}	a'	1503	2.3185	a'	1503	2.874	a	1503	0.9617		
	ω_{17}	a''	1509	1.9791	a''	1506	1.3298	a	1503	3.9995		
	ω_{18}	a'	1696	17.1664	a'	1697	15.6412	a	1700	13.4432		
	ω_{19}	a'	3001	97.9615	a'	3006	89.8712	a	3013	73.7342		
	ω_{20}	a''	3063	39.0963	a''	3067	35.4061	a	3072	30.3294		
	ω_{21}	a'	3086	12.5406	a'	3091	24.3528	a	3099	30.5143		
	ω_{22}	a'	3095	133.2193	a'	3103	97.3228	a	3113	51.9914		
	ω_{23}	a'	3111	44.2773	a'	3115	50.3489	a	3123	56.9595		
	ω_{24}	a'	3204	16.9612	a'	3209	14.347	a	3217	11.4101		
	zpe		211.0		zpe	211.0		zpe	210.8			

Table C14: Calculated harmonic frequencies and mode assignments for the $X^- \cdots C_3H_6$ Bif complexes. All frequencies and intensities are in cm^{-1} and km mol^{-1} and zero-point energies are in kJ mol^{-1} .

Cl ⁻ ...C ₃ H ₆				Br ⁻ ...C ₃ H ₆				I ⁻ ...C ₃ H ₆				
	Mode	Symmetry	Frequency (cm^{-1})	Intensity (km mol^{-1})		Symmetry	Frequency (cm^{-1})	Intensity (km mol^{-1})		Symmetry	Frequency (cm^{-1})	Intensity (km mol^{-1})
def2QZVP	ω_1	a''	43	1.2728	<i>a</i>	39	0.5398	a''	44	0.282		
	ω_2	a'	64	3.0224	<i>a</i>	63	0.7519	a'	57	0.5467		
	ω_3	a'	104	24.6244	<i>a</i>	81	7.6758	a'	66	3.1355		
	ω_4	a''	202	0.1794	<i>a</i>	201	0.3111	a''	203	0.4013		
	ω_5	a'	419	0.9361	<i>a</i>	420	1.0745	a'	421	1.1874		
	ω_6	a''	608	8.228	<i>a</i>	606	8.2096	a''	604	7.7897		
	ω_7	a''	893	50.6949	<i>a</i>	898	49.9987	a''	902	47.6077		
	ω_8	a'	940	1.2677	<i>a</i>	940	1.8601	a'	940	2.8243		
	ω_9	a'	951	21.4307	<i>a</i>	952	20.3009	a'	952	19.2858		
	ω_{10}	a''	1050	2.9706	<i>a</i>	1049	3.5426	a''	1047	3.9063		
	ω_{11}	a''	1105	8.446	<i>a</i>	1099	7.4151	a''	1093	5.6876		
	ω_{12}	a'	1204	0.641	<i>a</i>	1204	0.5144	a'	1204	0.3745		
	ω_{13}	a'	1306	30.5497	<i>a</i>	1311	26.3507	a'	1316	22.9852		
	ω_{14}	a'	1405	4.0862	<i>a</i>	1407	4.3634	a'	1409	4.529		
	ω_{15}	a'	1447	2.7751	<i>a</i>	1448	2.3439	a'	1449	1.6275		
	ω_{16}	a''	1465	7.612	<i>a</i>	1467	8.3916	a''	1471	9.6868		
	ω_{17}	a'	1489	33.5786	<i>a</i>	1490	37.3231	a'	1491	42.4944		
	ω_{18}	a'	1698	21.5049	<i>a</i>	1699	20.637	a'	1701	19.3801		
	ω_{19}	a'	3031	50.1636	<i>a</i>	3033	45.1303	a'	3035	37.6464		
	ω_{20}	a'	3116	43.9359	<i>a</i>	3117	7.8204	a''	3115	7.0271		
	ω_{21}	a''	3118	8.4973	<i>a</i>	3118	39.9743	a'	3118	39.9232		
	ω_{22}	a'	3126	32.7956	<i>a</i>	3129	30.5254	a'	3133	28.5791		
	ω_{23}	a'	3152	26.2691	<i>a</i>	3159	17.8014	a'	3162	9.129		
	ω_{24}	a'	3215	30.5834	<i>a</i>	3218	29.0673	a'	3222	26.5615		
		zpe	210.3		zpe	210.2		zpe	210.3			
AVTZ	ω_1	a''	52	1.0124	<i>a</i>	53	0.3315	<i>a</i>	46	0.1901		
	ω_2	a'	60	3.0465	<i>a</i>	57	0.825	<i>a</i>	57	0.3549		
	ω_3	a'	103	24.3815	<i>a</i>	81	7.3887	<i>a</i>	68	3.1313		
	ω_4	a''	205	0.2291	<i>a</i>	205	0.4266	<i>a</i>	204	0.5304		
	ω_5	a'	416	0.9681	<i>a</i>	417	0.9936	<i>a</i>	418	1.1251		
	ω_6	a''	608	7.6445	<i>a</i>	609	7.2091	<i>a</i>	605	7.0751		
	ω_7	a''	892	49.4245	<i>a</i>	898	48.2667	<i>a</i>	903	46.5684		
	ω_8	a'	938	0.8403	<i>a</i>	938	1.3823	<i>a</i>	938	2.194		
	ω_9	a'	949	22.7808	<i>a</i>	949	22.1513	<i>a</i>	949	21.0195		
	ω_{10}	a''	1050	2.5651	<i>a</i>	1049	2.4947	<i>a</i>	1048	2.901		
	ω_{11}	a''	1104	7.9709	<i>a</i>	1102	6.6347	<i>a</i>	1095	5.2412		
	ω_{12}	a'	1202	0.5873	<i>a</i>	1202	0.4672	<i>a</i>	1202	0.3839		
	ω_{13}	a'	1304	33.8674	<i>a</i>	1308	31.3063	<i>a</i>	1312	26.0076		
	ω_{14}	a'	1404	3.5657	<i>a</i>	1406	4.016	<i>a</i>	1408	4.388		
	ω_{15}	a'	1446	2.1845	<i>a</i>	1447	1.6558	<i>a</i>	1448	1.2094		
	ω_{16}	a''	1469	8.1368	<i>a</i>	1471	9.0434	<i>a</i>	1473	10.242		
	ω_{17}	a'	1491	33.3839	<i>a</i>	1492	36.3066	<i>a</i>	1493	41.9456		
	ω_{18}	a'	1695	22.0115	<i>a</i>	1697	21.0559	<i>a</i>	1699	20.0712		
	ω_{19}	a'	3028	49.9034	<i>a</i>	3029	45.2616	<i>a</i>	3031	38.6468		
	ω_{20}	a'	3111	45.5815	<i>a</i>	3111	7.7554	<i>a</i>	3110	6.6684		
	ω_{21}	a''	3112	8.1116	<i>a</i>	3112	44.5505	<i>a</i>	3113	42.8188		
	ω_{22}	a'	3123	33.2938	<i>a</i>	3125	31.8617	<i>a</i>	3129	29.7519		
	ω_{23}	a'	3148	28.2179	<i>a</i>	3151	21.621	<i>a</i>	3156	11.1743		
	ω_{24}	a'	3211	30.0037	<i>a</i>	3214	28.3083	<i>a</i>	3218	26.2627		
		zpe	210.1		zpe	210.1		zpe	210.1			

Table C15: Calculated harmonic frequencies and mode assignments for the $\text{X}^- \cdots \text{C}_3\text{H}_6$ HApp complexes. All frequencies and intensities are in cm^{-1} and km mol^{-1} and zero-point energies are in kJ mol^{-1} .

Cl ⁻ ...C ₃ H ₆				
	Mode	Symmetry	Frequency (cm ⁻¹)	Intensity (km mol ⁻¹)
def2QZVP	ω_1	a'	32	4.1982
	ω_2	a''	78	0.152
	ω_3	a'	111	26.4963
	ω_4	a''	210	0.4785
	ω_5	a'	437	0.3888
	ω_6	a''	622	7.8004
	ω_7	a'	936	10.0601
	ω_8	a'	958	1.1021
	ω_9	a''	1002	46.5108
	ω_{10}	a''	1052	0.3398
	ω_{11}	a''	1073	3.8172
	ω_{12}	a'	1192	0.6881
	ω_{13}	a'	1322	0.7359
	ω_{14}	a'	1403	1.5228
	ω_{15}	a'	1472	0.3741
	ω_{16}	a''	1490	4.1846
	ω_{17}	a'	1506	8.8291
	ω_{18}	a'	1703	1.0886
	ω_{19}	a'	3021	69.8356
	ω_{20}	a'	3061	221.428
	ω_{21}	a''	3073	35.8006
	ω_{22}	a'	3106	27.2675
	ω_{23}	a'	3154	18.428
	ω_{24}	a'	3178	65.2542
		zpe	210.5	
AVTZ	ω_1	a'	31	4.0342
	ω_2	a''	78	0.1228
	ω_3	a'	110	26.0547
	ω_4	a''	209	0.4926
	ω_5	a'	434	0.4543
	ω_6	a''	622	6.872
	ω_7	a'	935	9.5394
	ω_8	a'	955	1.2702
	ω_9	a''	1003	45.0913
	ω_{10}	a''	1055	0.0986
	ω_{11}	a''	1074	3.7523
	ω_{12}	a'	1190	0.8803
	ω_{13}	a'	1319	0.5526
	ω_{14}	a'	1403	1.6437
	ω_{15}	a'	1470	0.6298
	ω_{16}	a''	1492	4.2594
	ω_{17}	a'	1508	8.3546
	ω_{18}	a'	1700	0.9019
	ω_{19}	a'	3018	70.581
	ω_{20}	a'	3063	216.8383
	ω_{21}	a''	3069	34.6115
	ω_{22}	a'	3102	27.1834
	ω_{23}	a'	3150	17.8764
	ω_{24}	a'	3176	65.1027
		zpe	210.3	

Table C16: Calculated harmonic frequencies and mode assignments for the Cl \cdots C₃H₆ BiDent complexes. All frequencies and intensities are in cm⁻¹ and km mol⁻¹ and zero-point energies are in kJ mol⁻¹.

Cl \cdots C ₃ H ₆				
	Mode	Symmetry	Frequency (cm ⁻¹)	Intensity (km mol ⁻¹)
def2QZVP	ω_1	<i>a</i>	41	0.1128
	ω_2	<i>a</i>	44	0.0778
	ω_3	<i>a</i>	45	0.0005
	ω_4	<i>a</i>	211	0.4897
	ω_5	<i>a</i>	426	1.0148
	ω_6	<i>a</i>	595	12.8786
	ω_7	<i>a</i>	939	2.8068
	ω_8	<i>a</i>	948	40.1101
	ω_9	<i>a</i>	950	2.6525
	ω_{10}	<i>a</i>	1034	11.7839
	ω_{11}	<i>a</i>	1077	3.5817
	ω_{12}	<i>a</i>	1201	0.2079
	ω_{13}	<i>a</i>	1332	0.0015
	ω_{14}	<i>a</i>	1414	1.4506
	ω_{15}	<i>a</i>	1459	0.3585
	ω_{16}	<i>a</i>	1493	5.0208
	ω_{17}	<i>a</i>	1505	11.4552
	ω_{18}	<i>a</i>	1711	12.1385
	ω_{19}	<i>a</i>	3043	21.8158
	ω_{20}	<i>a</i>	3103	15.8139
	ω_{21}	<i>a</i>	3134	4.9312
	ω_{22}	<i>a</i>	3153	15.13
	ω_{23}	<i>a</i>	3164	13.5783
	ω_{24}	<i>a</i>	3248	12.0585
	zpe		211.0	

Table C17: Calculated harmonic frequencies and mode assignments for the Br \cdots C₃H₆ Bif complexes. All frequencies and intensities are in cm $^{-1}$ and km mol $^{-1}$ and zero-point energies are in kJ mol $^{-1}$.

Br \cdots C ₃ H ₆				
	Mode	Symmetry	Frequency (cm $^{-1}$)	Intensity (km mol $^{-1}$)
def2QZVP	ω_1	<i>a</i>	32	0.0955
	ω_2	<i>a</i>	37	0.0224
	ω_3	<i>a</i>	68	0.6047
	ω_4	<i>a</i>	220	0.8778
	ω_5	<i>a</i>	427	0.6077
	ω_6	<i>a</i>	590	11.7722
	ω_7	<i>a</i>	937	4.9739
	ω_8	<i>a</i>	945	2.3969
	ω_9	<i>a</i>	948	43.6421
	ω_{10}	<i>a</i>	1031	11.0996
	ω_{11}	<i>a</i>	1074	3.678
	ω_{12}	<i>a</i>	1197	0.5516
	ω_{13}	<i>a</i>	1331	0.1301
	ω_{14}	<i>a</i>	1407	3.7194
	ω_{15}	<i>a</i>	1459	0.3626
	ω_{16}	<i>a</i>	1488	6.9108
	ω_{17}	<i>a</i>	1505	29.6201
	ω_{18}	<i>a</i>	1712	11.4085
	ω_{19}	<i>a</i>	3030	32.9991
	ω_{20}	<i>a</i>	3078	19.1419
	ω_{21}	<i>a</i>	3125	15.1872
	ω_{22}	<i>a</i>	3153	15.6986
	ω_{23}	<i>a</i>	3164	9.2861
	ω_{24}	<i>a</i>	3247	12.452
	zpe		210.6	
AVTZ	ω_1	<i>a</i>	31	0.0852
	ω_2	<i>a</i>	39	0.0295
	ω_3	<i>a</i>	73	0.7249
	ω_4	<i>a</i>	215	0.987
	ω_5	<i>a</i>	424	0.6078
	ω_6	<i>a</i>	591	10.9561
	ω_7	<i>a</i>	936	4.6135
	ω_8	<i>a</i>	942	2.7319
	ω_9	<i>a</i>	946	42.1971
	ω_{10}	<i>a</i>	1029	10.8894
	ω_{11}	<i>a</i>	1074	3.4411
	ω_{12}	<i>a</i>	1195	0.6207
	ω_{13}	<i>a</i>	1328	0.1627
	ω_{14}	<i>a</i>	1406	3.7796
	ω_{15}	<i>a</i>	1458	0.3344
	ω_{16}	<i>a</i>	1490	7.4678
	ω_{17}	<i>a</i>	1506	30.6022
	ω_{18}	<i>a</i>	1710	11.5241
	ω_{19}	<i>a</i>	3026	34.2603
	ω_{20}	<i>a</i>	3072	18.2904
	ω_{21}	<i>a</i>	3119	15.5744
	ω_{22}	<i>a</i>	3149	16.3262
	ω_{23}	<i>a</i>	3160	8.1191
	ω_{24}	<i>a</i>	3243	12.6428
	zpe		210.3	

Table C18: Calculated harmonic frequencies and mode assignments for the I...C₃H₆ End complexes. All frequencies and intensities are in cm⁻¹ and km mol⁻¹ and zero-point energies are in kJ mol⁻¹.

I...C ₃ H ₆				
	Mode	Symmetry	Frequency (cm ⁻¹)	Intensity (km mol ⁻¹)
def2QZVP	ω_1	<i>a</i>	20	0.0559
	ω_2	<i>a</i>	36	0.0374
	ω_3	<i>a</i>	41	0.8143
	ω_4	<i>a</i>	209	0.062
	ω_5	<i>a</i>	426	0.955
	ω_6	<i>a</i>	593	8.0162
	ω_7	<i>a</i>	938	2.8575
	ω_8	<i>a</i>	947	4.5714
	ω_9	<i>a</i>	975	11.9345
	ω_{10}	<i>a</i>	1032	10.9936
	ω_{11}	<i>a</i>	1076	2.6461
	ω_{12}	<i>a</i>	1199	0.4448
	ω_{13}	<i>a</i>	1329	0.9645
	ω_{14}	<i>a</i>	1413	2.0084
	ω_{15}	<i>a</i>	1457	2.8267
	ω_{16}	<i>a</i>	1491	5.4449
	ω_{17}	<i>a</i>	1504	18.3376
	ω_{18}	<i>a</i>	1710	19.4154
	ω_{19}	<i>a</i>	3043	23.7136
	ω_{20}	<i>a</i>	3104	14.9856
	ω_{21}	<i>a</i>	3130	8.4104
	ω_{22}	<i>a</i>	3153	20.9241
	ω_{23}	<i>a</i>	3163	11.0151
	ω_{24}	<i>a</i>	3247	11.4304
	zpe		210.8	
AVTZ	ω_1	<i>a'</i>	15	0.08
	ω_2	? <i>a</i>	39	0.0405
	ω_3	? <i>a</i>	41	0.6796
	ω_4	<i>a''</i>	210	0.0987
	ω_5	<i>a'</i>	423	0.8709
	ω_6	<i>a''</i>	592	9.138
	ω_7	<i>a'</i>	936	1.3273
	ω_8	<i>a'</i>	945	6.2952
	ω_9	<i>a''</i>	967	14.69
	ω_{10}	<i>a''</i>	1030	11.4866
	ω_{11}	<i>a''</i>	1076	2.7679
	ω_{12}	<i>a'</i>	1197	0.5239
	ω_{13}	<i>a'</i>	1326	1.2198
	ω_{14}	<i>a'</i>	1413	1.7253
	ω_{15}	<i>a'</i>	1455	3.5909
	ω_{16}	<i>a''</i>	1493	5.4904
	ω_{17}	<i>a'</i>	1506	18.2022
	ω_{18}	<i>a'</i>	1707	20.0401
	ω_{19}	<i>a'</i>	3040	24.1209
	ω_{20}	<i>a''</i>	3100	15.0809
	ω_{21}	<i>a'</i>	3126	8.436
	ω_{22}	<i>a'</i>	3149	23.0115
	ω_{23}	<i>a'</i>	3159	9.2513
	ω_{24}	<i>a'</i>	3242	11.6235
	zpe		210.5	

Table C19: Calculated harmonic frequencies and mode assignments for the X···C₃H₆ MePoc complexes. All frequencies and intensities are in cm⁻¹ and km mol⁻¹ and zero-point energies are in kJ mol⁻¹.

	Cl···C ₃ H ₆			Br···C ₃ H ₆			I···C ₃ H ₆			
	Mode	Symmetry	Frequency (cm ⁻¹)	Intensity (km mol ⁻¹)	Symmetry	Frequency (cm ⁻¹)	Intensity (km mol ⁻¹)	Symmetry	Frequency (cm ⁻¹)	Intensity (km mol ⁻¹)
def2QZVP	ω_1	<i>a</i>	20	0.079	? <i>a</i>	20	0.0806	<i>a</i>	21	0.0831
	ω_2	<i>a</i>	23	0.0104	? <i>a</i>	22	0.0094	<i>a</i>	21	0.0134
	ω_3	<i>a</i>	40	0.0036	<i>a'</i>	36	0.007	<i>a</i>	36	0.0128
	ω_4	<i>a</i>	207	0.4187	<i>a''</i>	207	0.3943	<i>a</i>	207	0.3915
	ω_5	<i>a</i>	426	1.1582	<i>a'</i>	426	1.1643	<i>a</i>	426	1.1782
	ω_6	<i>a</i>	592	12.2359	<i>a''</i>	592	12.1579	<i>a</i>	592	12.1511
	ω_7	<i>a</i>	939	2.5281	<i>a'</i>	939	2.5413	<i>a</i>	939	2.5625
	ω_8	<i>a</i>	944	42.8544	<i>a''</i>	944	42.6101	<i>a</i>	944	42.0521
	ω_9	<i>a</i>	948	3.6776	<i>a'</i>	948	3.7509	<i>a</i>	948	3.9908
	ω_{10}	<i>a</i>	1032	13.857	<i>a''</i>	1032	13.6076	<i>a</i>	1031	13.4908
	ω_{11}	<i>a</i>	1073	1.8674	<i>a''</i>	1071	2.0735	<i>a</i>	1070	1.9694
	ω_{12}	<i>a</i>	1199	0.0705	<i>a'</i>	1199	0.064	<i>a</i>	1199	0.0654
	ω_{13}	<i>a</i>	1331	0.1392	<i>a'</i>	1331	0.1655	<i>a</i>	1331	0.2382
	ω_{14}	<i>a</i>	1411	3.2964	<i>a'</i>	1410	3.9346	<i>a</i>	1410	5.3478
	ω_{15}	<i>a</i>	1458	1.3927	<i>a'</i>	1458	1.59	<i>a</i>	1458	2.0681
	ω_{16}	<i>a</i>	1492	1.1432	<i>a''</i>	1489	0.7833	<i>a</i>	1487	0.4597
	ω_{17}	<i>a</i>	1503	12.8384	<i>a'</i>	1503	12.368	<i>a</i>	1502	11.1487
	ω_{18}	<i>a</i>	1712	14.15	<i>a'</i>	1712	14.5944	<i>a</i>	1711	15.6492
	ω_{19}	<i>a</i>	3044	27.3135	<i>a'</i>	3044	28.7347	<i>a</i>	3043	31.2958
	ω_{20}	<i>a</i>	3107	7.9256	<i>a''</i>	3107	7.5366	<i>a</i>	3106	6.8344
	ω_{21}	<i>a</i>	3132	6.7525	<i>a'</i>	3132	6.4031	<i>a</i>	3131	5.8054
	ω_{22}	<i>a</i>	3152	17.3752	<i>a'</i>	3152	17.2831	<i>a</i>	3152	16.8631
	ω_{23}	<i>a</i>	3163	11.6452	<i>a'</i>	3163	11.7399	<i>a</i>	3163	11.8019
	ω_{24}	<i>a</i>	3246	14.7671	<i>a'</i>	3246	14.8847	<i>a</i>	3246	15.0772
	zpe		210.5		zpe	210.4		zpe	210.4	
AVTZ	ω_1	<i>a</i>	20	0.0654	<i>a</i>	19	0.0839	<i>a</i>	20	0.0847
	ω_2	<i>a</i>	22	0.0249	<i>a</i>	36	0.0738	<i>a</i>	29	0.0088
	ω_3	<i>a</i>	43	0.0033	<i>a</i>	40	0.0208	<i>a</i>	40	0.0158
	ω_4	<i>a</i>	208	0.4197	<i>a</i>	209	0.1655	<i>a</i>	209	0.4124
	ω_5	<i>a</i>	424	1.1754	<i>a</i>	424	1.2455	<i>a</i>	424	1.2029
	ω_6	<i>a</i>	590	11.9308	<i>a</i>	592	11.0221	<i>a</i>	592	11.9221
	ω_7	<i>a</i>	938	1.8415	<i>a</i>	938	2.0286	<i>a</i>	938	1.9198
	ω_8	<i>a</i>	942	42.0289	<i>a</i>	942	43.1401	<i>a</i>	942	41.4191
	ω_9	<i>a</i>	946	4.3667	<i>a</i>	946	4.6931	<i>a</i>	946	4.7203
	ω_{10}	<i>a</i>	1030	15.0572	<i>a</i>	1030	12.9544	<i>a</i>	1029	14.0871
	ω_{11}	<i>a</i>	1074	1.4805	<i>a</i>	1075	3.519	<i>a</i>	1072	1.8757
	ω_{12}	<i>a</i>	1198	0.0465	<i>a</i>	1197	0.0515	<i>a</i>	1197	0.0263
	ω_{13}	<i>a</i>	1328	0.1581	<i>a</i>	1328	0.1846	<i>a</i>	1328	0.2702
	ω_{14}	<i>a</i>	1411	3.1695	<i>a</i>	1411	4.1865	<i>a</i>	1410	5.2323
	ω_{15}	<i>a</i>	1457	1.5464	<i>a</i>	1459	2.4296	<i>a</i>	1457	2.2216
	ω_{16}	<i>a</i>	1494	0.9726	<i>a</i>	1493	4.4447	<i>a</i>	1491	0.5444
	ω_{17}	<i>a</i>	1504	12.282	<i>a</i>	1504	13.5711	<i>a</i>	1503	10.8879
	ω_{18}	<i>a</i>	1709	14.6456	<i>a</i>	1709	14.9167	<i>a</i>	1709	16.3323
	ω_{19}	<i>a</i>	3040	28.4007	<i>a</i>	3044	38.2326	<i>a</i>	3040	32.2625
	ω_{20}	<i>a</i>	3103	7.3404	<i>a</i>	3099	15.541	<i>a</i>	3102	6.7874
	ω_{21}	<i>a</i>	3127	6.5937	<i>a</i>	3127	9.1614	<i>a</i>	3127	5.5378
	ω_{22}	<i>a</i>	3148	18.6231	<i>a</i>	3148	17.3731	<i>a</i>	3148	18.0589
	ω_{23}	<i>a</i>	3159	10.4608	<i>a</i>	3160	10.3317	<i>a</i>	3159	10.9123
	ω_{24}	<i>a</i>	3241	15.2505	<i>a</i>	3241	15.3822	<i>a</i>	3241	15.6187
	zpe		210.3		zpe	210.4		zpe	210.3	

Table C20: Calculated harmonic frequencies and mode assignments for the X···C₃H₆ Perp complexes. All frequencies and intensities are in cm⁻¹ and km mol⁻¹ and zero-point energies are in kJ mol⁻¹.

Cl···C ₃ H ₆				Br···C ₃ H ₆			I···C ₃ H ₆					
	Mode	Symmetry	Frequency (cm ⁻¹)	Intensity (km mol ⁻¹)		Symmetry	Frequency (cm ⁻¹)	Intensity (km mol ⁻¹)		Symmetry	Frequency (cm ⁻¹)	Intensity (km mol ⁻¹)
def2QZVP	ω_1	<i>a</i>	91	1.1185	<i>a</i>	107	1.2351	<i>a</i>	94	0.2726		
	ω_2	<i>a</i>	117	1.9072	<i>a</i>	153	1.7897	<i>a</i>	143	0.2365		
	ω_3	<i>a</i>	286	6.644	<i>a</i>	198	5.3498	<i>a</i>	161	11.0808		
	ω_4	<i>a</i>	405	3.0687	<i>a</i>	226	0.2644	<i>a</i>	226	0.3251		
	ω_5	<i>a</i>	538	4.4411	<i>a</i>	423	0.2871	<i>a</i>	425	0.4774		
	ω_6	<i>a</i>	630	86.2164	<i>a</i>	634	8.054	<i>a</i>	625	12.3364		
	ω_7	<i>a</i>	883	4.4166	<i>a</i>	934	12.0901	<i>a</i>	934	9.0311		
	ω_8	<i>a</i>	917	8.8271	<i>a</i>	952	2.4303	<i>a</i>	952	2.6477		
	ω_9	<i>a</i>	1009	0.6689	<i>a</i>	975	47.6393	<i>a</i>	969	67.1585		
	ω_{10}	<i>a</i>	1092	1.5176	<i>a</i>	995	10.9681	<i>a</i>	1011	9.1808		
	ω_{11}	<i>a</i>	1179	4.1001	<i>a</i>	1069	2.9508	<i>a</i>	1073	6.0389		
	ω_{12}	<i>a</i>	1235	0.4849	<i>a</i>	1208	0.529	<i>a</i>	1207	0.2467		
	ω_{13}	<i>a</i>	1264	18.7216	<i>a</i>	1325	11.2881	<i>a</i>	1326	8.7509		
	ω_{14}	<i>a</i>	1397	1.555	<i>a</i>	1410	10.0188	<i>a</i>	1411	9.6029		
	ω_{15}	<i>a</i>	1427	6.8112	<i>a</i>	1453	14.5862	<i>a</i>	1455	11.0392		
	ω_{16}	<i>a</i>	1486	5.508	<i>a</i>	1484	9.087	<i>a</i>	1486	8.7238		
	ω_{17}	<i>a</i>	1494	11.0992	<i>a</i>	1500	20.2302	<i>a</i>	1500	21.1504		
	ω_{18}	<i>a</i>	1504	2.2667	<i>a</i>	1650	126.6081	<i>a</i>	1664	118.6545		
	ω_{19}	<i>a</i>	3008	9.9561	<i>a</i>	3049	7.2497	<i>a</i>	3051	8.8409		
	ω_{20}	<i>a</i>	3083	15.6722	<i>a</i>	3117	3.3201	<i>a</i>	3124	5.6122		
	ω_{21}	<i>a</i>	3108	12.5788	<i>a</i>	3149	6.7566	<i>a</i>	3135	7.0757		
	ω_{22}	<i>a</i>	3135	15.027	<i>a</i>	3169	4.8866	<i>a</i>	3163	3.7763		
	ω_{23}	<i>a</i>	3177	1.5803	<i>a</i>	3184	6.9539	<i>a</i>	3175	6.9858		
	ω_{24}	<i>a</i>	3208	11.9783	<i>a</i>	3271	0.8533	<i>a</i>	3261	1.4483		
	zpe		213.4		zpe	213.2		zpe	212.8			
AVTZ	ω_1	<i>a</i>	92	1.1763	<i>a</i>	108	1.2002	<i>a</i>	94	0.2335		
	ω_2	<i>a</i>	118	1.8108	<i>a</i>	154	1.5493	<i>a</i>	147	0.7951		
	ω_3	<i>a</i>	283	6.9152	<i>a</i>	200	5.0315	<i>a</i>	160	10.0406		
	ω_4	<i>a</i>	403	3.0727	<i>a</i>	228	0.2612	<i>a</i>	227	0.3023		
	ω_5	<i>a</i>	535	4.5075	<i>a</i>	420	0.2706	<i>a</i>	420	0.4652		
	ω_6	<i>a</i>	625	87.0184	<i>a</i>	631	8.1829	<i>a</i>	622	12.8423		
	ω_7	<i>a</i>	883	4.7567	<i>a</i>	933	10.5114	<i>a</i>	933	8.8051		
	ω_8	<i>a</i>	917	8.5177	<i>a</i>	950	3.0602	<i>a</i>	949	3.5498		
	ω_9	<i>a</i>	1009	0.7624	<i>a</i>	975	44.82	<i>a</i>	967	58.176		
	ω_{10}	<i>a</i>	1092	1.4988	<i>a</i>	992	13.8016	<i>a</i>	1009	13.817		
	ω_{11}	<i>a</i>	1178	4.3052	<i>a</i>	1069	2.8649	<i>a</i>	1073	5.4689		
	ω_{12}	<i>a</i>	1235	0.4754	<i>a</i>	1206	0.4333	<i>a</i>	1204	0.2451		
	ω_{13}	<i>a</i>	1263	18.5705	<i>a</i>	1322	9.5319	<i>a</i>	1324	7.9071		
	ω_{14}	<i>a</i>	1397	1.2338	<i>a</i>	1411	9.3903	<i>a</i>	1412	8.711		
	ω_{15}	<i>a</i>	1426	7.0627	<i>a</i>	1453	13.6381	<i>a</i>	1454	11.0283		
	ω_{16}	<i>a</i>	1487	5.5099	<i>a</i>	1485	9.2658	<i>a</i>	1487	8.9138		
	ω_{17}	<i>a</i>	1495	10.7199	<i>a</i>	1502	20.563	<i>a</i>	1502	21.2402		
	ω_{18}	<i>a</i>	1506	2.3479	<i>a</i>	1647	114.4989	<i>a</i>	1661	110.0241		
	ω_{19}	<i>a</i>	3005	10.0683	<i>a</i>	3046	7.8265	<i>a</i>	3046	9.5962		
	ω_{20}	<i>a</i>	3079	15.7583	<i>a</i>	3114	3.3553	<i>a</i>	3112	4.8872		
	ω_{21}	<i>a</i>	3106	12.312	<i>a</i>	3144	6.7619	<i>a</i>	3140	6.4835		
	ω_{22}	<i>a</i>	3131	15.1623	<i>a</i>	3165	4.4507	<i>a</i>	3159	3.8524		
	ω_{23}	<i>a</i>	3175	1.3666	<i>a</i>	3179	6.6381	<i>a</i>	3172	6.7468		
	ω_{24}	<i>a</i>	3204	12.0851	<i>a</i>	3266	0.8843	<i>a</i>	3257	1.4496		
	zpe		213.2		zpe	212.9		zpe	212.5			

Table C21: Energies, Intensities and Franck-Condon factors calculated from ezSpectrum 3.0 for photodetachment of the $\text{Br}^- \cdots \text{C}_3\text{H}_6$ Bif complex. Notation for the transition, 5_0^1 indicates the transition in ω_5 from $v'' = 0$ to $v' = 1$ with modes numbered according to Table C17. The band origin is the ADE from in text.

E eV	Intensity	FCF	Assignment	E eV	Intensity	FCF	Assignment
3.5630	1.59E-01	3.98E-01	ADE	3.9870	2.73E-04	1.65E-02	18_0^2
3.6156	1.06E-04	-1.03E-02	5_0^1	3.9907	8.31E-04	-2.88E-02	$5_0^1 19_0^1$
3.6629	3.42E-04	-1.85E-02	$4_0^1 6_0^1$	4.0023	9.35E-04	-3.06E-02	$5_0^1 21_0^1$
3.6682	1.42E-04	-1.19E-02	5_0^2	4.0060	9.09E-04	3.02E-02	$5_0^1 22_0^1$
3.6790	4.61E-03	6.79E-02	7_0^1	4.0071	1.05E-04	-1.02E-02	$7_0^2 18_0^1$
3.6798	2.92E-04	-1.71E-02	8_0^1	4.0074	4.91E-04	2.21E-02	$5_0^1 23_0^1$
3.7172	7.31E-04	-2.70E-02	$4_0^1 10_0^1$	4.0171	2.11E-04	-1.45E-02	$6_0^1 20_0^1$
3.7228	2.80E-03	-5.29E-02	$4_0^1 11_0^1$	4.0550	7.76E-04	2.79E-02	$8_0^1 19_0^1$
3.7317	2.62E-03	-5.12E-02	$5_0^1 7_0^1$	4.0658	3.04E-04	1.74E-02	$7_0^1 21_0^1$
3.7324	1.27E-04	-1.13E-02	$5_0^1 8_0^1$	4.0666	2.26E-04	1.50E-02	$8_0^1 21_0^1$
3.7374	2.73E-04	1.65E-02	14_0^1	4.0695	4.10E-04	2.02E-02	$7_0^1 22_0^1$
3.7438	5.07E-04	-2.25E-02	15_0^1	4.0703	3.40E-03	5.83E-02	$8_0^1 22_0^1$
3.7497	7.88E-04	2.81E-02	17_0^1	4.0708	1.04E-03	3.22E-02	$7_0^1 23_0^1$
3.7638	3.45E-04	-1.86E-02	$5_0^1 12_0^1$	4.0811	4.52E-04	2.13E-02	$7_0^1 24_0^1$
3.7744	1.41E-03	-3.76E-02	$4_0^1 16_0^1$	4.0863	4.41E-04	2.10E-02	$12_0^1 19_0^1$
3.7750	2.99E-04	-1.73E-02	18_0^1	4.0979	6.80E-04	2.61E-02	$12_0^1 21_0^1$
3.7802	2.29E-04	-1.51E-02	$5_0^1 13_0^1$	4.1016	7.86E-04	-2.80E-02	$12_0^1 22_0^1$
3.7951	1.90E-03	4.36E-02	7_0^2	4.1180	1.09E-04	-1.04E-02	$13_0^1 22_0^1$
3.7967	2.84E-04	-1.69E-02	8_0^2	4.1194	1.08E-03	3.29E-02	$13_0^1 23_0^1$
3.8023	7.43E-04	2.73E-02	$5_0^1 17_0^1$	4.1241	7.72E-04	2.78E-02	$14_0^1 21_0^1$
3.8210	1.20E-04	1.09E-02	$6_0^1 16_0^1$	4.1286	2.07E-04	-1.44E-02	$16_0^1 20_0^1$
3.8237	1.05E-04	1.02E-02	$10_0^1 11_0^1$	4.1292	1.49E-04	-1.22E-02	$14_0^1 23_0^1$
3.8272	2.53E-04	1.59E-02	$7_0^1 12_0^1$	4.1355	1.36E-04	1.17E-02	$15_0^1 23_0^1$
3.8276	1.03E-03	-3.22E-02	$5_0^1 18_0^1$	4.1364	1.34E-04	1.16E-02	$17_0^1 21_0^1$
3.8294	3.33E-04	1.82E-02	11_0^2	4.1394	1.26E-04	-1.12E-02	$14_0^1 24_0^1$
3.8437	6.32E-04	-2.51E-02	$7_0^1 13_0^1$	4.1415	1.10E-04	-1.05E-02	$17_0^1 23_0^1$
3.8477	1.70E-04	-1.31E-02	$5_0^1 7_0^2$	4.1458	1.24E-03	3.52E-02	$15_0^1 24_0^1$
3.8665	1.36E-04	-1.16E-02	$8_0^1 17_0^1$	4.1517	2.48E-04	1.57E-02	$17_0^1 24_0^1$
3.8809	2.61E-04	1.62E-02	$11_0^1 16_0^1$	4.1617	2.03E-04	-1.43E-02	$18_0^1 21_0^1$
3.8910	1.41E-03	-3.76E-02	$7_0^1 18_0^1$	4.1668	9.26E-04	-3.04E-02	$18_0^1 23_0^1$
3.9111	1.27E-04	1.13E-02	7_0^3	4.3249	1.22E-04	1.11E-02	$19_0^1 21_0^1$
3.9396	6.98E-04	2.64E-02	$13_0^1 18_0^1$	4.3365	2.96E-04	1.72E-02	21_0^2
3.9497	4.04E-04	2.01E-02	21_0^1	4.3439	5.64E-04	2.38E-02	22_0^2
3.9534	2.13E-04	-1.46E-02	22_0^1	4.3466	4.31E-04	2.08E-02	23_0^2
3.9651	1.09E-03	3.31E-02	24_0^1	4.3671	2.36E-04	1.54E-02	24_0^2
3.9705	6.38E-04	-2.53E-02	$4_0^1 20_0^1$				

Appendix D

Tables and Data: Halide-Butadiene Complexes

Table D1: Peak positions and assignments of 50 kPa C₄H₆:CCl₄:argon gas mix.

Position (<i>m/z</i>)	Assignment
35.0	³⁵ Cl ⁻
37.0	³⁷ Cl ⁻
78.9	⁷⁹ Br ⁻
81.0	⁸¹ Br ⁻
89.0	³⁵ Cl ⁻ ...C ₄ H ₆
90.9	³⁷ Cl ⁻ ...C ₄ H ₆
126.9	I ⁻
132.9	⁷⁹ Br ⁻ ...C ₄ H ₆
134.9	⁸¹ Br ⁻ ...C ₄ H ₆
142.8	³⁵ Cl ⁻ ...(C ₄ H ₆) ₂
144.9	³⁷ Cl ⁻ ...(C ₄ H ₆) ₂
151.8	CCl ₄ ⁻ (³⁵ Cl: ³⁷ Cl=4:0)
153.8	CCl ₄ ⁻ (³⁵ Cl: ³⁷ Cl=3:1)
180.8	I ⁻ ...C ₄ H ₆
186.8	⁷⁹ Br ⁻ ...(C ₄ H ₆) ₂
188.8	⁸¹ Br ⁻ ...(C ₄ H ₆) ₂
196.9	³⁵ Cl ⁻ ...(C ₄ H ₆) ₃
198.8	³⁷ Cl ⁻ ...(C ₄ H ₆) ₃
205.9	CCl ₄ ⁻ ...C ₄ H ₆ (³⁵ Cl: ³⁷ Cl=4:0)
207.9	CCl ₄ ⁻ ...C ₄ H ₆ (³⁵ Cl: ³⁷ Cl=3:1)
234.8	I ⁻ ...(C ₄ H ₆) ₂
240.8	⁷⁹ Br ⁻ ...(C ₄ H ₆) ₃
242.9	⁸¹ Br ⁻ ...(C ₄ H ₆) ₃
251.0	³⁵ Cl ⁻ ...(C ₄ H ₆) ₄
260.1	CCl ₄ ⁻ ...(C ₄ H ₆) ₂ (³⁵ Cl: ³⁷ Cl=4:0)
261.8	CCl ₄ ⁻ ...(C ₄ H ₆) ₂ (³⁵ Cl: ³⁷ Cl=3:1)

Table D2: Peak positions and assignments of 50 kPa C₄H₆:CH₂Br₂:argon gas mix.

Position (<i>m/z</i>)	Assignment
79.0	⁷⁹ Br ⁻
80.8	⁸¹ Br ⁻
127.3	I ⁻
133.1	⁷⁹ Br ⁻ ...C ₄ H ₆
135.0	⁸¹ Br ⁻ ...C ₄ H ₆
173.0	⁷⁹ Br ⁻ ...CH ⁸¹ ₂ Br, ⁸¹ Br ⁻ ...CH ⁷⁹ ₂ Br
181.1	I ⁻ ...C ₄ H ₆
187.1	⁷⁹ Br ⁻ ...(C ₄ H ₆) ₂
189.0	⁸¹ Br ⁻ ...(C ₄ H ₆) ₂
226.0	⁷⁹ Br ⁻ ...(CH ⁷⁹ ₂ Br)(C ₄ H ₆)
227.8	⁷⁹ Br ⁻ ...(CH ⁸¹ ₂ Br)(C ₄ H ₆), ⁸¹ Br ⁻ ...(CH ⁷⁹ ₂ Br)(C ₄ H ₆)
229.8	⁸¹ Br ⁻ ...(CH ⁸¹ ₂ Br)(C ₄ H ₆)
234.9	I ⁻ ...(C ₄ H ₆) ₂
241.2	⁷⁹ Br ⁻ ...(C ₄ H ₆) ₃
243.0	⁸¹ Br ⁻ ...(C ₄ H ₆) ₃
252.9	CH ₂ Br ₃ ⁻
261.3	I ⁻ ...(CH ₂ Br)(C ₄ H ₆)
280.0	⁷⁹ Br ⁻ ...(CH ⁷⁹ ₂ Br)(C ₄ H ₆) ₂
281.8	⁷⁹ Br ⁻ ...(CH ⁸¹ ₂ Br)(C ₄ H ₆) ₂ , ⁸¹ Br ⁻ ...(CH ⁷⁹ ₂ Br)(C ₄ H ₆) ₂
283.8	⁸¹ Br ⁻ ...(CH ⁸¹ ₂ Br)(C ₄ H ₆) ₂
289.0	I ⁻ ...(C ₄ H ₆) ₃
295.3	⁷⁹ Br ⁻ ...(C ₄ H ₆) ₄
297.1	⁸¹ Br ⁻ ...(C ₄ H ₆) ₄
307.0	Br ⁻ ...(CH ₂ Br)(C ₄ H ₆) ₂
308.7	Br ⁻ ...(CH ₂ Br)(C ₄ H ₆) ₂
315.9	I ⁻ ...(CH ₂ Br)(C ₄ H ₆) ₂
334.1	⁷⁹ Br ⁻ ...(CH ⁷⁹ ₂ Br)(C ₄ H ₆) ₃
336.0	⁷⁹ Br ⁻ ...(CH ⁸¹ ₂ Br)(C ₄ H ₆) ₃ , ⁸¹ Br ⁻ ...(CH ⁷⁹ ₂ Br)(C ₄ H ₆) ₃
337.7	⁸¹ Br ⁻ ...(CH ⁸¹ ₂ Br)(C ₄ H ₆) ₃
342.9	I ⁻ ...(C ₄ H ₆) ₄
349.1	⁷⁹ Br ⁻ ...(C ₄ H ₆) ₅
350.9	⁸¹ Br ⁻ ...(C ₄ H ₆) ₅

Table D3: Peak positions and assignments of 50 kPa C₄H₆:CH₃I:argon gas mix.

Position (<i>m/z</i>)	Assignment
128.7	I ⁻
182.5	I ⁻ ...C ₄ H ₆
236.4	I ⁻ ...(C ₄ H ₆) ₂
270.0	I ⁻ ...CH ₃ I
290.3	I ⁻ ...(C ₄ H ₆) ₃
324.1	I ⁻ ...(CH ₃ I)(C ₄ H ₆)
344.5	I ⁻ ...(C ₄ H ₆) ₄
377.7	I ⁻ ...(CH ₃ I)(C ₄ H ₆) ₂
398.3	I ⁻ ...(C ₄ H ₆) ₅
411.4	I ⁻ ...(CH ₃ I) ₂
431.9	I ⁻ ...(CH ₃ I)(C ₄ H ₆) ₃
452.0	I ⁻ ...(C ₄ H ₆) ₆
465.6	I ⁻ ...(CH ₃ I) ₂ (C ₄ H ₆)
486.0	I ⁻ ...(CH ₃ I)(C ₄ H ₆) ₄
505.9	I ⁻ ...(C ₄ H ₆) ₇
519.9	I ⁻ ...(CH ₃ I) ₂ (C ₄ H ₆) ₂
539.5	I ⁻ ...(CH ₃ I)(C ₄ H ₆) ₅
553.7	I ⁻ ...(CH ₃ I) ₃
559.9	I ⁻ ...(C ₄ H ₆) ₈
573.9	I ⁻ ...(CH ₃ I) ₂ (C ₄ H ₆) ₃
593.8	I ⁻ ...(CH ₃ I)(C ₄ H ₆) ₆
607.5	I ⁻ ...(CH ₃ I) ₃ (C ₄ H ₆)
613.9	I ⁻ ...(C ₄ H ₆) ₉
627.6	I ⁻ ...(CH ₃ I) ₂ (C ₄ H ₆) ₄
648.1	I ⁻ ...(CH ₃ I)(C ₄ H ₆) ₇
661.5	I ⁻ ...(CH ₃ I) ₃ (C ₄ H ₆) ₂
667.7	I ⁻ ...(C ₄ H ₆) ₁₀
681.4	I ⁻ ...(CH ₃ I) ₂ (C ₄ H ₆) ₅
702.0	I ⁻ ...(CH ₃ I)(C ₄ H ₆) ₈

Table D4: $X^- \cdots C_4H_6$ complex geometric parameters and D_0 values from DSD-PBEP86-D3BJ optimisations. zpe values are drawn from relevant harmonic frequency calculations.

			$R_{X-\parallel}$ Å	$\angle_{H-\parallel-C}$ °	E_{DFT} E_h	zpe kJ mol ⁻¹	D_e kJ mol ⁻¹	D_o kJ mol ⁻¹	E_{VDE} E_h	VDE $^2P_{3/2}$ eV	VDE $^2P_{1/2}$ eV
$1cis$	def2QZVP	3.467	90.0	-615.7464816	223.2	30.6	30.6				
		AVTZ	3.474	90.0	-615.7113439	222.8	28.9	29.2			
$2cis$	def2QZVP	$R_{X-\mid}$	$\angle_{X-\mid-C}$								
		AVTZ	2.410	90.0	-615.7496270	223.7	38.9	39.3			
$3cis$	def2QZVP	R_{X-H}	\angle_{H-X-H}								
		AVTZ	2.528	51.6	-615.7510512	223.8	42.6	43.2			
$Cl^- \cdots C_4H_6$	$5cis$	def2QZVP	R_{X-H}	\angle_{X-H-C}							
			2.415	180.0	-615.7464112	223.2	30.4	30.4			
	AVTZ		2.421	180.0	-615.7113491	222.9	28.9	29.3			
	$R_{X-\parallel}$	$\angle_{X-\parallel-C}$									
	$1trans$	def2QZVP	3.446	89.0	-615.7526373	224.3	30.9	31.2	-615.6125908	3.911	4.020
			3.465	90.4	-615.7174981	224.1	29.1	29.8	-615.5761248	3.879	3.988
	$2trans$	def2QZVP	R_{X-H}	\angle_{H-X-H}							
			2.569	55.5	-615.7564366	224.9	40.9	41.8	-615.6108422	4.056	4.165
$4trans$	$def2QZVP$	AVTZ	2.576	55.5	-615.7212027	224.8	38.9	40.2	-615.5745205	4.018	4.127
			R_{X-H}	\angle_{X-H-C}							
	AVTZ	2.414	172.2	-615.7527055	224.9	31.1	32.0	-615.6107409	3.964	4.073	
		2.421	172.6	-615.7176104	224.1	29.4	30.1	-615.5742934	3.933	4.042	

Table D5: $X^- \cdots C_4H_6$ complex geometric parameters and D_0 values from DSD-PBEP86-D3BJ optimisations. zpe values are drawn from relevant harmonic frequency calculations.

			$R_{X-\parallel}$ Å	$\angle_{H-\parallel-C}$ °	E_{DFT} E_h	zpe kJ mol ⁻¹	D_e kJ mol ⁻¹	D_o kJ mol ⁻¹	E_{VDE} E_h	VDE $^2P_{3/2}$ eV	VDE $^2P_{1/2}$ eV
$1cis$	def2QZVP	AVTZ	3.645	90.0	-2729.2209949	223.2	27.6	27.5			
			3.627	90.0	-572.0449191	222.8	27.1	27.4			
$2cis$	def2QZVP	AVTZ	$R_{X-\parallel}$	$\angle_{X-\parallel-C}$							
			3.579	90.0	-572.0449191	223.1	27.1	27.8			
$3cis$	def2QZVP	AVTZ	R_{X-H}	\angle_{H-X-H}							
			2.720	47.9	-2729.2246108	223.6	37.1	37.4			
$Br^- \cdots C_4H_6$	$5cis$	def2QZVP	2.689	48.7	-572.0487947	223.4	37.3	38.3			
			R_{X-H}	\angle_{X-H-C}							
	$1trans$	def2QZVP	2.614	180.0	-2729.2205213	223.1	26.3	26.2			
			2.591	180.0	-572.0446156	222.9	26.3	26.7			
	$1trans$	AVTZ	$R_{X-\parallel}$	$\angle_{X-\parallel-C}$							
			3.638	89.9	-2729.2271176	224.3	27.8	28.0	-2729.0931894	3.611	4.068
	$2trans$	def2QZVP	3.620	91.8	-572.0510616	224.1	27.4	28.0	-571.9175605	3.588	4.045
			R_{X-H}	\angle_{H-X-H}							
	$2trans$	AVTZ	2.760	51.8	-2729.2301879	224.8	35.8	36.6	-2729.0920531	3.722	4.179
			2.735	52.4	-572.0542769	224.8	35.8	37.1	-571.916575	3.697	4.154
	$4trans$	def2QZVP	R_{X-H}	\angle_{X-H-C}							
			2.601	164.3	-572.0508961	224.1	26.9	27.6	-571.9162254	3.620	4.077

Table D6: $\text{X}^- \cdots \text{C}_4\text{H}_6$ complex geometric parameters and D_0 values from DSD-PBEP86-D3BJ optimisations. zpe values are drawn from relevant harmonic frequency calculations.

		$R_{X-\parallel}$	$\angle_{H-\parallel-C}$	E_{DFT}	zpe	D_e	D_o	E_{VDE}	VDE $^2P_{3/2}$	VDE $^2P_{1/2}$
		\AA	$^\circ$	E_h	kJ mol^{-1}	kJ mol^{-1}	kJ mol^{-1}	E_h	eV	eV
$\text{I}^- \cdots \text{C}_4\text{H}_6$	$1cis$	def2QZVP AVTZ	3.913	90.0	-453.3092258	223.3	22.4	22.5		
			3.879	90.0	-451.0911249	222.8	24.0	24.4		
	$2cis$	def2QZVP AVTZ	$R_{X-\parallel}$	$\angle_{X-\parallel-C}$						
			3.872	90.0	-453.3113466	223.6	28.0	28.4		
	$3cis$	def2QZVP AVTZ	3.839	90.0	-451.0932590	223.0	29.6	30.2		
			R_{X-H}	\angle_{H-X-H}						
	$5cis$	def2QZVP AVTZ	3.003	43.4	-453.3117279	223.5	29.0	29.3		
			2.956	44.2	-451.0939409	223.5	31.4	32.4		
	$1trans$	def2QZVP AVTZ	R_{X-H}	\angle_{X-H-C}						
			2.903	180.0	-453.3085161	223.2	20.6	20.6		
	$2trans$	def2QZVP AVTZ	2.864	180.0	-451.0904067	222.7	22.1	22.4		
			$R_{X-\parallel}$	$\angle_{X-\parallel-C}$						
	$1trans$	def2QZVP AVTZ	3.899	90.6	-453.3153149	224.4	22.5	22.9	-453.1896164	3.235
			3.871	90.9	-451.0972285	224.1	24.2	24.8	-450.9715760	3.230
	$2trans$	def2QZVP AVTZ	R_{X-H}	\angle_{H-X-H}						
			3.038	47.1	-453.3174781	224.7	28.2	28.9	-453.1889925	3.308
			3.001	47.9	-451.0995706	224.5	30.3	31.3	-450.9709958	3.307

Table D7: X...C₄H₆ complex geometric parameters and D_0 values from DSD-PBEP86-D3BJ optimisations. zpe values are drawn from relevant harmonic frequency calculations.

			$R_{X-\parallel}$ Å	$\angle_{X-\parallel-C}$ °	E_{DFT} E_h	zpe kJ mol ⁻¹	D_e kJ mol ⁻¹	D_o kJ mol ⁻¹
Cl...C ₃ H ₆	<i>1cis</i>	def2QZVP AVTZ	3.575	90.0	-615.6075875	227.0	3.5	7.2
			$R_{X-\parallel}$	$\angle_{X-\parallel-C}$				
	<i>7cis</i>	def2QZVP AVTZ	2.482	90.0	-615.6246764	230.3	48.3	55.4
			2.479	90.0	-615.5881608	229.6	49.5	56.7
	<i>1trans</i>	def2QZVP AVTZ	R_{X-H}	\angle_{H-X-H}				
			2.980	50.2	-615.5770219	224.5	4.4	5.5
	<i>2trans</i>	def2QZVP AVTZ	R_{X-H}	\angle_{H-X-H}				
			3.073	47.700	-615.5770724	224.5	4.6	5.6
	<i>7trans</i>	def2QZVP AVTZ	$R_{X-\parallel}$	$\angle_{X-\parallel-C}$				
			2.492	90.0	-615.6304045	230.1	47.5	53.6
			2.490	90.0	-615.5938722	229.5	48.7	54.7

Table D8: X...C₄H₆ complex geometric parameters and D_0 values from DSD-PBEP86-D3BJ optimisations. zpe values are drawn from relevant harmonic frequency calculations.

			$R_{X- }$ Å	$\angle_{X- -C}$ °	E_{DFT} E_h	zpe kJ mol ⁻¹	D_e kJ mol ⁻¹	D_o kJ mol ⁻¹
Br...C ₃ H ₆	<i>1cis</i>	def2QZVP AVTZ	3.670	90.0	-2729.0877923	225.1	4.3	6.1
			3.410	90.0	-571.9121692	225.4	6.2	9.2
	<i>4cis</i>	def2QZVP AVTZ	R_{X-H} \angle_{H-X-H}					
			2.924	31.3	-571.9113004	230.1	3.9	11.6
	<i>7cis</i>	def2QZVP AVTZ	$R_{X- }$ $\angle_{X- -C}$					
			2.671	90.0	-2729.1013282	230.2	39.9	46.8
	<i>3trans</i>	def2QZVP AVTZ	2.407	90.0	-571.9257889	229.5	42.0	49.1
			R_{X-H} \angle_{H-X-H}					
	<i>7trans</i>	def2QZVP AVTZ	3.472	30.8	-2729.0932480	224.5	2.8	3.3
			2.923	31.3	-571.9173054	228.2	3.8	8.6
			$R_{X- }$ $\angle_{X- -C}$					
	<i>7trans</i>	def2QZVP AVTZ	2.683	90.0	-2729.1071082	229.5	39.2	44.7
			2.420	90.0	-571.9315454	229.0	41.2	46.8

Table D9: X...C₄H₆ complex geometric parameters and D_0 values from DSD-PBEP86-D3BJ optimisations. zpe values are drawn from relevant harmonic frequency calculations.

		$R_{X-\parallel}$	$\angle_{X-\parallel-C}$	E_{DFT}	zpe	D_e	D_o
		Å	°	E_h	kJ mol ⁻¹	kJ mol ⁻¹	kJ mol ⁻¹
I...C ₃ H ₆	<i>1cis</i>	def2QZVP AVTZ	3.852	90.0	-450.9658668	223.9	7.3
			$R_{X-\parallel}$	$\angle_{X-\parallel-C}$			
	<i>7cis</i>	def2QZVP AVTZ	2.932	90.0	-453.1937310	230.5	31.1
			2.713	90.0	-450.9755807	229.8	32.8
	<i>1trans</i>	def2QZVP AVTZ	R_{X-H}	\angle_{H-X-H}			
			3.186	45.6	-453.1896328	245.9	4.4
		def2QZVP AVTZ	3.333	43.1	-450.9719372	224.3	7.4
			R_{X-H}	\angle_{H-X-H}			
	<i>3trans</i>	def2QZVP AVTZ	3.652	29.3	-453.1891727	224.7	3.2
			3.114	29.8	-450.9708574	224.9	4.6
	<i>7trans</i>	def2QZVP AVTZ	$R_{X-\parallel}$	$\angle_{X-\parallel-C}$			
			2.948	90.0	-453.1994965	229.0	30.3
			2.728	90.0	-450.9813569	228.4	32.1
							35.4
							37.1

Table D10: Cartesian coordinates of the geometries of halide-butadiene complexes optimised with the DSD-PBEP86-D3BJ functional, in Å.

		Cl ⁻ ... C ₄ H ₆			Br ⁻ ... C ₄ H ₆			I ⁻ ... C ₄ H ₆			
		x	y	z	x	y	z	x	y	z	
1 <i>cis</i>	def2QZVP	C	1.246967	0.226266	0.000000	-1.812523	0.034962	0.000000	2.036059	1.158945	0.000000
		C	0.000000	0.706167	0.000000	-1.077965	1.150834	0.000000	0.979232	1.975837	0.000000
		H	1.418449	-0.844995	0.000000	-1.331545	-0.937158	0.000000	1.901098	0.083157	0.000000
		H	2.092391	0.906165	0.000000	-2.895600	0.092432	0.000000	3.043128	1.560621	0.000000
		H	-0.794396	-0.035266	0.000000	0.000000	1.016569	0.000000	0.000000	1.506534	0.000000
		C	-0.381475	2.122985	0.000000	-1.592269	2.525202	0.000000	1.019088	3.443004	0.000000
		H	-1.451541	2.311540	0.000000	-0.832111	3.301302	0.000000	0.048429	3.930300	0.000000
		C	0.428693	3.189117	0.000000	-2.871934	2.918374	0.000000	2.103251	4.227567	0.000000
		H	0.034825	4.197777	0.000000	-3.140473	3.967305	0.000000	2.019238	5.306969	0.000000
		H	1.505995	3.079817	0.000000	-3.683108	2.201181	0.000000	3.102291	3.810331	0.000000
	AVTZ	X	-0.621814	-2.769544	0.000000	1.600314	-1.411939	0.000000	-0.885660	-1.528868	0.000000
		C	1.249418	0.229390	0.000000	1.804993	0.010421	0.000000	2.034127	1.121796	0.000000
		C	0.000000	0.708217	0.000000	1.079895	1.134770	0.000000	0.983235	1.949447	0.000000
		H	1.422949	-0.842454	0.000000	1.313976	-0.957786	0.000000	1.888237	0.046368	0.000000
		H	2.094840	0.910731	0.000000	2.889534	0.058297	0.000000	3.045411	1.515665	0.000000
		H	-0.794043	-0.034732	0.000000	0.000000	1.008288	0.000000	0.000000	1.486067	0.000000
		C	-0.385458	2.124900	0.000000	1.604757	2.505965	0.000000	1.034090	3.417001	0.000000
		H	-1.456976	2.310554	0.000000	0.849507	3.288173	0.000000	0.066031	3.911563	0.000000
		C	0.422893	3.194727	0.000000	2.889019	2.890470	0.000000	2.125109	4.195317	0.000000
		H	0.025606	4.203151	0.000000	3.165047	3.938525	0.000000	2.048033	5.276274	0.000000
		H	1.501486	3.087991	0.000000	3.695575	2.166537	0.000000	3.122131	3.770637	0.000000
		X	-0.618528	-2.775214	0.000000	-1.605304	-1.392908	0.000000	-0.891117	-1.511471	0.000000

Table D11: Cartesian coordinates of the geometries of halide-butadiene complexes optimised with the DSD-PBEP86-D3BJ functional, in Å.

		$\text{Cl}^- \cdots \text{C}_4\text{H}_6$			$\text{Br}^- \cdots \text{C}_4\text{H}_6$			$\text{I}^- \cdots \text{C}_4\text{H}_6$			
		x	y	z	x	y	z	x	y	z	
def2QZVP	C	0.091201	-2.474219	0.000000				-3.344399	1.525931	0.000000	
	C	0.000000	-1.139829	0.000000				-2.266530	0.734815	0.000000	
	H	-0.791217	-3.103449	0.000000				-3.254834	2.605588	0.000000	
	H	1.051026	-2.977538	0.000000				-4.347543	1.116808	0.000000	
	H	-0.968132	-0.646065	0.000000				-1.272033	1.171180	0.000000	
	C	1.123670	-0.191263	0.000000				-2.266530	-0.734815	0.000000	
	H	0.799388	0.846001	0.000000				-1.272033	-1.171181	0.000000	
	C	2.423830	-0.505104	0.000000				-3.344400	-1.525931	0.000000	
	H	3.192225	0.259203	0.000000				-3.254835	-2.605587	0.000000	
	H	2.758940	-1.535782	0.000000				-4.347544	-1.116808	0.000000	
2cis	X	-1.639673	1.942360	0.000000				1.605283	0.000000	0.000000	
	C	0.000000	1.529194	-1.952851	1.621965	2.689435	0.000000	0.000000	-1.529132	-3.323733	
	C	0.000000	0.735653	-0.873884	1.079992	1.464863	0.000000	0.000000	-0.735221	-2.245608	
	H	0.000000	2.610219	-1.862594	1.006251	3.582364	0.000000	0.000000	-2.609666	-3.232009	
	H	0.000000	1.120956	-2.957890	2.696904	2.834113	0.000000	0.000000	-1.120840	-4.328354	
	H	0.000000	1.157308	0.128614	0.000000	1.338116	0.000000	0.000000	-1.169306	-1.248950	
	AVTZ	C	0.000000	-0.735653	-0.873884	1.810206	0.188010	0.000000	0.000000	0.735221	-2.245608
		H	0.000000	-1.157308	0.128614	1.153317	-0.678560	0.000000	0.000000	1.169306	-1.248950
		C	0.000000	-1.529194	-1.952851	3.140482	0.034120	0.000000	0.000000	1.529132	-3.323733
		H	0.000000	-2.610219	-1.862594	3.597836	-0.949371	0.000000	0.000000	2.609666	-3.232009
		H	0.000000	-1.120956	-2.957890	3.810298	0.887215	0.000000	0.000000	1.120840	-4.328354
		X	0.000000	0.000000	2.547332	-1.662299	-0.950641	0.000000	0.000000	0.000000	1.593409

Table D12: Cartesian coordinates of the geometries of halide-butadiene complexes optimised with the DSD-PBEP86-D3BJ functional, in Å.

		Cl ⁻ ... C ₄ H ₆			Br ⁻ ... C ₄ H ₆			I ⁻ ... C ₄ H ₆			
		x	y	z	x	y	z	x	y	z	
3cis	def2QZVP	C	1.047907	-1.397785	0.000000	0.658636	-2.140685	0.000000	-1.523084	-2.238446	0.000000
		C	2.021639	-0.479461	0.000000	1.989537	-2.002229	0.000000	-0.734513	-3.318914	0.000000
		H	1.274307	-2.460762	0.000000	0.191800	-3.121063	0.000000	-2.604367	-2.325806	0.000000
		H	0.000000	-1.109569	0.000000	0.000000	-1.277392	0.000000	-1.110187	-1.235291	0.000000
		H	3.057420	-0.812753	0.000000	2.608475	-2.896723	0.000000	-1.198454	-4.302280	0.000000
		C	1.833211	0.977853	0.000000	2.726293	-0.731067	0.000000	0.734510	-3.318914	0.000000
		H	2.750178	1.563606	0.000000	3.810112	-0.823527	0.000000	1.198457	-4.302278	0.000000
		C	0.657979	1.618405	0.000000	2.184991	0.492638	0.000000	1.523085	-2.238449	0.000000
		H	0.606646	2.704011	0.000000	2.803698	1.384976	0.000000	2.604368	-2.325810	0.000000
		H	-0.282206	1.073217	0.000000	1.108532	0.635124	0.000000	1.110195	-1.235291	0.000000
	AVTZ	X	-2.398280	-0.310107	0.000000	-1.596553	0.925334	0.000000	0.000000	1.555002	0.000000
		C	1.048960	-1.400193	0.000000	0.672299	-2.123942	0.000000	1.525506	2.206128	0.000000
		C	2.023132	-0.479521	0.000000	2.002841	-1.964470	0.000000	0.734925	3.287607	0.000000
		H	1.277014	-2.463716	0.000000	0.220893	-3.112787	0.000000	2.607895	2.294942	0.000000
		H	0.000000	-1.112496	0.000000	0.000000	-1.269778	0.000000	1.112427	1.201728	0.000000
		H	3.059912	-0.812717	0.000000	2.635846	-2.850281	0.000000	1.198774	4.272154	0.000000
		C	1.834457	0.978640	0.000000	2.721291	-0.681934	0.000000	-0.734924	3.287608	0.000000
		H	2.752300	1.564730	0.000000	3.807295	-0.759141	0.000000	-1.198772	4.272154	0.000000
		C	0.658072	1.621110	0.000000	2.162516	0.536072	0.000000	-1.525507	2.206129	0.000000
		H	0.607978	2.707654	0.000000	2.770121	1.437395	0.000000	-2.607895	2.294945	0.000000
		H	-0.283152	1.075963	0.000000	1.083002	0.663410	0.000000	-1.112429	1.201729	0.000000
		X	-2.400105	-0.310566	0.000000	-1.596310	0.894195	0.000000	0.000000	-1.537028	0.000000

Table D13: Cartesian coordinates of the geometries of halide-butadiene complexes optimised with the DSD-PBEP86-D3BJ functional, in Å.

		Cl ⁻ ... C ₄ H ₆			Br ⁻ ... C ₄ H ₆			I ⁻ ... C ₄ H ₆			
		x	y	z	x	y	z	x	y	z	
5 <i>cis</i>	def2QZVP	C	0.000000	0.528601	0.000000	0.874781	1.020462	0.000000	0.266371	2.008085	0.000000
		C	-1.246360	0.043094	0.000000	2.111341	0.511635	0.000000	1.544227	2.400304	0.000000
		H	0.862909	-0.135664	0.000000	0.000000	0.374472	0.000000	0.000000	0.955366	0.000000
		H	0.186200	1.601536	0.000000	0.707991	2.095043	0.000000	-0.544726	2.730092	0.000000
		H	-1.363350	-1.035479	0.000000	2.209023	-0.568766	0.000000	2.306960	1.629057	0.000000
		C	-2.491871	0.819928	0.000000	3.370364	1.266540	0.000000	2.034947	3.784001	0.000000
		H	-3.406847	0.233056	0.000000	4.274711	0.663818	0.000000	3.115809	3.894590	0.000000
		C	-2.618799	2.152410	0.000000	3.518793	2.596499	0.000000	1.301198	4.902672	0.000000
		H	-3.592428	2.625595	0.000000	4.499819	3.054024	0.000000	1.764693	5.880811	0.000000
		H	-1.752018	2.800907	0.000000	2.662774	3.259047	0.000000	0.219382	4.867224	0.000000
5 <i>cis</i>	AVTZ	X	2.776924	-1.609067	0.000000	-2.103028	-1.178527	0.000000	-0.712124	-1.859010	0.000000
		C	0.000000	0.530064	0.000000	0.895833	0.985528	0.000000	0.274888	1.982270	0.000000
		C	-1.248494	0.045037	0.000000	2.116987	0.436256	0.000000	1.557763	2.364318	0.000000
		H	0.862857	-0.135432	0.000000	0.000000	0.367227	0.000000	0.000000	0.930554	0.000000
		H	0.187289	1.603530	0.000000	0.764112	2.066019	0.000000	-0.530598	2.712244	0.000000
		H	-1.366593	-1.034395	0.000000	2.179435	-0.647756	0.000000	2.314279	1.585562	0.000000
		C	-2.494363	0.823067	0.000000	3.400933	1.149762	0.000000	2.061444	3.744248	0.000000
		H	-3.410326	0.235973	0.000000	4.285643	0.516882	0.000000	3.144279	3.844857	0.000000
		C	-2.621380	2.157438	0.000000	3.594154	2.475901	0.000000	1.337743	4.871761	0.000000
		H	-3.596022	2.630918	0.000000	4.591037	2.900426	0.000000	1.811613	5.846078	0.000000
		H	-1.753573	2.806299	0.000000	2.759854	3.167233	0.000000	0.254591	4.846695	0.000000
		X	2.780105	-1.614149	0.000000	-2.132215	-1.104420	0.000000	-0.724249	-1.840407	0.000000

Table D14: Cartesian coordinates of the geometries of halide-butadiene complexes optimised with the DSD-PBEP86-D3BJ functional, in Å.

		Cl ⁻ ... C ₄ H ₆			Br ⁻ ... C ₄ H ₆			I ⁻ ... C ₄ H ₆			
		x	y	z	x	y	z	x	y	z	
1 <i>trans</i>	def2QZVP	C	0.553030	1.479648	0.000000	1.995204	0.404532	0.000000	2.079553	1.413935	0.000000
		C	0.838363	0.172872	0.000000	1.030926	1.331173	0.000000	0.926143	2.090320	0.000000
		H	1.357103	2.208743	0.000000	3.037926	0.704466	0.000000	3.025663	1.944195	0.000000
		H	-0.481767	1.807228	0.000000	1.737001	-0.649299	0.000000	2.078688	0.329361	0.000000
		H	0.000000	-0.520015	0.000000	0.000000	0.985129	0.000000	0.000000	1.521020	0.000000
		C	2.195909	-0.343298	0.000000	1.300627	2.758527	0.000000	0.854348	3.541473	0.000000
		H	2.996068	0.394584	0.000000	2.347521	3.055688	0.000000	1.802064	4.075801	0.000000
		C	2.516469	-1.644002	0.000000	0.357392	3.709332	0.000000	-0.286744	4.241865	0.000000
		H	3.550526	-1.965817	0.000000	0.621194	4.759624	0.000000	-0.279045	5.324680	0.000000
		H	1.750373	-2.409466	0.000000	-0.694975	3.453934	0.000000	-1.248760	3.744799	0.000000
1 <i>cis</i>	AVTZ	X	-2.693819	0.146672	0.000000	-1.004387	-1.758026	0.000000	-0.506008	-1.597461	0.000000
		C	0.536603	1.515326	0.000000	2.018880	0.435216	0.000000	2.080709	1.389356	0.000000
		C	0.833516	0.209273	0.000000	1.016137	1.322871	0.000000	0.924703	2.064960	0.000000
		H	1.334068	2.252760	0.000000	3.049454	0.777284	0.000000	3.026533	1.922220	0.000000
		H	-0.501298	1.835515	0.000000	1.804359	-0.629243	0.000000	2.080653	0.303756	0.000000
		H	0.000000	-0.491083	0.000000	0.000000	0.931976	0.000000	0.000000	1.491133	0.000000
		C	2.196147	-0.296581	0.000000	1.225823	2.761295	0.000000	0.848558	3.516825	0.000000
		H	2.991950	0.447457	0.000000	2.259852	3.103826	0.000000	1.795223	4.055088	0.000000
		C	2.526061	-1.596789	0.000000	0.240945	3.671573	0.000000	-0.296353	4.214570	0.000000
		H	3.563391	-1.911425	0.000000	0.459678	4.733214	0.000000	-0.291736	5.298425	0.000000
		H	1.764236	-2.367940	0.000000	-0.800217	3.370064	0.000000	-1.257533	3.713674	0.000000
		X	-2.688607	0.073373	0.000000	-0.965252	-1.755224	0.000000	-0.503752	-1.582992	0.000000

Table D15: Cartesian coordinates of the geometries of halide-butadiene complexes optimised with the DSD-PBEP86-D3BJ functional, in Å.

		$\text{Cl}^- \cdots \text{C}_4\text{H}_6$			$\text{Br}^- \cdots \text{C}_4\text{H}_6$			$\text{I}^- \cdots \text{C}_4\text{H}_6$			
		x	y	z	x	y	z	x	y	z	
def2QZVP	C	0.851468	-1.663531	0.000000	2.295798	-0.150294	0.000000	-1.736799	-2.123673	0.000000	
	C	1.634880	-0.577668	0.000000	2.164235	1.181899	0.000000	-0.691075	-2.958848	0.000000	
	H	-0.230150	-1.558550	0.000000	1.418462	-0.790177	0.000000	-1.587303	-1.049009	0.000000	
	H	1.292177	-2.656856	0.000000	3.281352	-0.606203	0.000000	-2.751808	-2.507088	0.000000	
	H	2.719438	-0.676713	0.000000	3.044029	1.823352	0.000000	-0.848431	-4.035837	0.000000	
	C	1.088673	0.772232	0.000000	0.864430	1.837727	0.000000	0.687538	-2.492226	0.000000	
	H	0.000000	0.836738	0.000000	0.000000	1.174499	0.000000	0.826663	-1.412752	0.000000	
	C	1.857176	1.869216	0.000000	0.719001	3.168854	0.000000	1.739788	-3.319661	0.000000	
	H	1.422254	2.862384	0.000000	-0.262843	3.628276	0.000000	2.754617	-2.939363	0.000000	
	H	2.939168	1.799693	0.000000	1.578480	3.829445	0.000000	1.609546	-4.395552	0.000000	
2trans	X	-2.396239	-0.176952	0.000000	-1.294865	-1.293952	0.000000	0.000000	1.541624	0.000000	
	C	0.854197	-1.667058	0.000000	2.284522	-0.187086	0.000000	-1.740537	-2.095666	0.000000	
	C	1.637181	-0.578563	0.000000	2.165221	1.148194	0.000000	-0.691029	-2.929225	0.000000	
	H	-0.228384	-1.563589	0.000000	1.400002	-0.818726	0.000000	-1.592760	-1.019660	0.000000	
	H	1.296574	-2.660532	0.000000	3.267005	-0.651919	0.000000	-2.755155	-2.483195	0.000000	
	H	2.722727	-0.677216	0.000000	3.052008	1.781672	0.000000	-0.845950	-4.007638	0.000000	
	AVTZ	C	1.089485	0.771831	0.000000	0.870214	1.815695	0.000000	0.687081	-2.457714	0.000000
		H	0.000000	0.835668	0.000000	0.000000	1.158113	0.000000	0.821547	-1.376345	0.000000
		C	1.856957	1.871697	0.000000	0.734524	3.149644	0.000000	1.743919	-3.282229	0.000000
		H	1.419502	2.864850	0.000000	-0.244919	3.616591	0.000000	2.758214	-2.897514	0.000000
		H	2.940060	1.803823	0.000000	1.599881	3.804246	0.000000	1.617503	-4.359642	0.000000
		X	-2.398671	-0.175909	0.000000	-1.297168	-1.269962	0.000000	0.000000	1.523264	0.000000

Table D16: Cartesian coordinates of the geometries of halide-butadiene complexes optimised with the DSD-PBEP86-D3BJ functional, in Å.

		Cl ⁻ ... C ₄ H ₆			Br ⁻ ... C ₄ H ₆			
		x	y	z	x	y	z	
4 <i>trans</i>	def2QZVP	C	0.000000	0.946361	0.000000			
		C	-1.065230	0.135801	0.000000			
		H	-0.126050	2.028343	0.000000			
		H	1.009208	0.536397	0.000000			
		H	-0.904348	-0.938277	0.000000			
		C	-2.439582	0.606724	0.000000			
		H	-2.573866	1.686093	0.000000			
		C	-3.524102	-0.179839	0.000000			
		H	-4.522506	0.239753	0.000000			
		H	-3.435378	-1.259188	0.000000			
		X	3.101554	-0.667495	0.000000			
		C	0.000000	0.943332	0.000000	0.430704	1.319180	0.000000
4 <i>trans</i>	AVTZ	C	-1.070245	0.136472	0.000000	0.430704	2.658277	0.000000
		H	-0.120805	2.026612	0.000000	1.336835	0.726433	0.000000
		H	1.008201	0.529063	0.000000	-0.475427	0.726433	0.000000
		H	-0.913935	-0.939302	0.000000	1.384403	3.179349	0.000000
		C	-2.443843	0.613069	0.000000	-0.758050	3.522000	0.000000
		H	-2.574528	1.693881	0.000000	-0.559831	4.591649	0.000000
		C	-3.532849	-0.170375	0.000000	-2.038268	3.128054	0.000000
		H	-4.530485	0.253683	0.000000	-2.847961	3.847846	0.000000
		H	-3.447951	-1.251067	0.000000	-2.303217	2.077576	0.000000
		X	3.109478	-0.673404	0.000000	0.430704	-2.254696	0.000000

Table D17: Cartesian coordinates of the geometries of halogen-butadiene complexes optimised with the DSD-PBEP86-D3BJ functional, in Å.

		Cl ... C ₄ H ₆			Br ... C ₄ H ₆			I ... C ₄ H ₆		
		x	y	z	x	y	z	x	y	z
def2QZVP	C	1.255021	0.288459	0.000000	1.823575	0.057689	0.000000			
	C	0.000000	0.745708	0.000000	1.080712	1.167766	0.000000			
	H	1.473139	-0.771483	0.000000	1.373967	-0.926690	0.000000			
	H	2.103860	0.959671	0.000000	2.905024	0.097891	0.000000			
	H	-0.812019	0.025504	0.000000	0.000000	1.066032	0.000000			
	C	-0.415450	2.154531	0.000000	1.576907	2.550156	0.000000			
	H	-1.486542	2.324642	0.000000	0.812760	3.319707	0.000000			
	C	0.392272	3.218012	0.000000	2.856730	2.931527	0.000000			
	H	-0.000423	4.226084	0.000000	3.135015	3.976982	0.000000			
	H	1.468750	3.110234	0.000000	3.661875	2.208920	0.000000			
1 <i>cis</i>	X	-0.596343	-2.842054	0.000000	-1.597605	-1.428162	0.000000			
	C				1.790419	-0.027576	0.000000	-2.053472	1.252369	0.000000
	C				1.084506	1.108556	0.000000	-0.979001	2.049166	0.000000
	H				1.306796	-0.996886	0.000000	-1.955298	0.173735	0.000000
	H				2.873671	-0.023338	0.000000	-3.057120	1.659529	0.000000
	H				0.000000	1.041670	0.000000	0.000000	1.579860	0.000000
	C				1.624937	2.475160	0.000000	-0.980152	3.518734	0.000000
	H				0.884719	3.269063	0.000000	0.000132	3.985372	0.000000
	C				2.917851	2.816538	0.000000	-2.055723	4.313803	0.000000
	H				3.228892	3.853780	0.000000	-1.961552	5.392645	0.000000
AVTZ	H				3.700393	2.068042	0.000000	-3.059496	3.907344	0.000000
	X				-1.614307	-1.355668	0.000000	0.876291	-1.575527	0.000000

Table D18: Cartesian coordinates of the geometries of halogen-butadiene complexes optimised with the DSD-PBEP86-D3BJ functional, in Å.

			Br ... C ₄ H ₆		
			x	y	z
4 <i>cis</i>	AVTZ	C	0.429008	1.473559	0.000000
		C	0.429008	2.810053	0.000000
		H	1.350840	0.905242	0.000000
		H	-0.492825	0.905242	0.000000
		H	1.386301	3.322185	0.000000
		C	-0.754416	3.683424	0.000000
		H	-0.547460	4.749177	0.000000
		C	-2.031624	3.289928	0.000000
		H	-2.843933	4.006135	0.000000
		H	-2.300039	2.240761	0.000000
		X	0.429008	-2.390587	0.000000

Table D19: Cartesian coordinates of the geometries of halogen-butadiene complexes optimised with the DSD-PBEP86-D3BJ functional, in Å.

		Cl...C ₄ H ₆			Br...C ₄ H ₆			I...C ₄ H ₆			
		x	y	z	x	y	z	x	y	z	
7 <i>cis</i>	def2QZVP	C	0.154030	1.441447	-0.492577	-0.697102	1.571830	-0.496130	-1.285167	1.594872	-0.498298
		C	-0.408481	0.842030	0.590382	-1.130513	0.880000	0.584637	-1.648530	0.871374	0.579278
		H	0.914901	2.199782	-0.380002	-0.103456	2.468165	-0.387126	-0.782628	2.546396	-0.393465
		H	-0.143907	1.176418	-1.496400	-0.931838	1.248406	-1.500127	-1.484455	1.247158	-1.502447
		H	-0.065695	1.152785	1.569981	-0.861136	1.256710	1.564593	-1.420308	1.274791	1.559678
		C	-1.444265	-0.194787	0.571965	-1.938928	-0.344961	0.571145	-2.333345	-0.429402	0.570500
		H	-1.765519	-0.548867	1.543762	-2.185277	-0.749800	1.545185	-2.539896	-0.851858	1.546607
		C	-1.995290	-0.710352	-0.520687	-2.374538	-0.970134	-0.517734	-2.705709	-1.103452	-0.514381
		H	-2.757409	-1.475610	-0.462688	-2.968132	-1.872000	-0.452768	-3.207497	-2.059001	-0.441980
		H	-1.702605	-0.384319	-1.509549	-2.151707	-0.600372	-1.509480	-2.520497	-0.720964	-1.509120
	AVTZ	X	1.628487	-0.611189	-0.009388	1.315658	-0.244901	-0.003194	1.128147	-0.132771	-0.001545
		C	0.159513	1.441876	-0.492935	-0.680511	1.572794	-0.496404	-1.288887	1.597304	-0.498626
		C	-0.405858	0.842396	0.590748	-1.118777	0.881940	0.584936	-1.652757	0.872075	0.579373
		H	0.922914	2.198928	-0.378990	-0.081178	2.466380	-0.386071	-0.786434	2.549869	-0.392585
		H	-0.139018	1.177738	-1.497923	-0.917200	1.250855	-1.501493	-1.487783	1.249756	-1.503978
		H	-0.062253	1.152264	1.571441	-0.847106	1.257020	1.565941	-1.424840	1.275561	1.560863
		C	-1.444976	-0.192621	0.572315	-1.935082	-0.339548	0.571432	-2.337382	-0.430022	0.570752
		H	-1.767077	-0.545965	1.545180	-2.183658	-0.743036	1.546548	-2.543738	-0.852522	1.547933
		C	-1.998503	-0.707959	-0.521157	-2.375409	-0.963593	-0.518089	-2.710223	-1.106010	-0.514708
		H	-2.763195	-1.472046	-0.462102	-2.974715	-1.862824	-0.451843	-3.211925	-2.062659	-0.440927
		H	-1.705070	-0.382617	-1.511168	-2.150612	-0.595128	-1.511000	-2.525276	-0.723661	-1.510664
		X	1.626626	-0.613556	-0.009427	1.308947	-0.248081	-0.003238	1.130481	-0.132763	-0.001536

Table D20: Cartesian coordinates of the geometries of halogen-butadiene complexes optimised with the DSD-PBEP86-D3BJ functional, in Å.

		Cl ... C ₄ H ₆			I ... C ₄ H ₆				Cl ... C ₄ H ₆		
		x	y	z	x	y	z		x	y	z
def2QZVP	C				2.094127	1.568462	0.000000	2trans			
	C				0.926376	2.219226	0.000000				
	H				3.034647	2.104310	0.000000				
	H				2.133191	0.486710	0.000000				
	H				0.000000	1.652668	0.000000				
	C				0.808802	3.668425	0.000000				
	H				1.736142	4.233393	0.000000				
	C				-0.359811	4.317511	0.000000				
	H				-0.402080	5.399003	0.000000				
	H				-1.300289	3.781870	0.000000				
1 <i>trans</i>	X				-0.490917	-1.666032	0.000000				
	C	1.044992	-1.302424	0.000000	2.094525	1.505774	0.000000		-1.406790	-1.429950	0.000000
	C	0.973676	0.034392	0.000000	0.931834	2.169244	0.000000		-1.901894	-0.186077	0.000000
	H	2.000296	-1.813308	0.000000	3.040929	2.033233	0.000000		-0.338404	-1.609083	0.000000
	H	0.149465	-1.912045	0.000000	2.121880	0.422655	0.000000		-2.059844	-2.294275	0.000000
	H	0.000000	0.516801	0.000000	0.000000	1.609819	0.000000		-2.978552	-0.036645	0.000000
	AVTZ	C	2.138283	0.906675	0.000000	0.827227	3.620446	0.000000	-1.076224	1.012433	0.000000
	AVTZ	H	3.111349	0.422479	0.000000	1.760249	4.177943	0.000000	0.000000	0.862772	0.000000
	AVTZ	C	2.065645	2.243266	0.000000	-0.336998	4.281054	0.000000	-1.572402	2.255678	0.000000
	AVTZ	H	2.959646	2.855128	0.000000	-0.369142	5.363915	0.000000	-0.921118	3.121458	0.000000
2 <i>trans</i>	H	1.110600	2.754640	0.000000	-1.283068	3.753254	0.000000	-2.640835	2.435120	0.000000	
	X	-2.745114	-0.830303	0.000000	-0.497554	-1.638112	0.000000	2.628389	-0.728932	0.000000	

Table D21: Cartesian coordinates of the geometries of halogen-butadiene complexes optimised with the DSD-PBEP86-D3BJ functional, in Å.

		Br … C ₄ H ₆			I … C ₄ H ₆			
		x	y	z	x	y	z	
def2QZVP	C	-0.279289	1.303282	0.000000	-0.218744	1.987638	0.000000	
	C	-0.279289	2.640039	0.000000	-0.218744	3.324429	0.000000	
	H	0.644117	0.738838	0.000000	0.704631	1.423018	0.000000	
	H	-1.202695	0.738838	0.000000	-1.142120	1.423018	0.000000	
	H	-1.223050	3.177112	0.000000	-1.162508	3.861511	0.000000	
	C	0.930304	3.446928	0.000000	0.990898	4.131213	0.000000	
	H	1.873825	2.909510	0.000000	1.934352	3.593670	0.000000	
	C	0.931450	4.783610	0.000000	0.992193	5.467907	0.000000	
	H	1.856742	5.345039	0.000000	1.917550	6.029232	0.000000	
	H	0.007123	5.346625	0.000000	0.067926	6.031024	0.000000	
3trans	X	-0.279289	-2.608546	0.000000	-0.218744	-2.109973	0.000000	
	C	-0.279508	1.273767	0.000000	-0.218971	1.945630	0.000000	
	C	-0.279508	2.612337	0.000000	-0.218971	3.284217	0.000000	
	H	0.644730	0.708700	0.000000	0.705023	1.380069	0.000000	
	H	-1.203747	0.708700	0.000000	-1.142964	1.380069	0.000000	
	H	-1.224442	3.149379	0.000000	-1.163857	3.821339	0.000000	
	AVTZ	C	0.930711	3.420186	0.000000	0.991410	4.091776	0.000000
		H	1.875233	2.882481	0.000000	1.935704	3.553670	0.000000
		C	0.932427	4.758662	0.000000	0.993609	5.430258	0.000000
		H	1.858950	5.320040	0.000000	1.920333	5.991304	0.000000
		H	0.007346	5.322414	0.000000	0.068733	5.994346	0.000000
		X	-0.279508	-2.585184	0.000000	-0.218971	-2.087398	0.000000

Table D22: Cartesian coordinates of the geometries of halogen-butadiene complexes optimised with the DSD-PBEP86-D3BJ functional, in Å.

		Cl ... C ₄ H ₆			Br ... C ₄ H ₆			I ... C ₄ H ₆			
		x	y	z	x	y	z	x	y	z	
3 ^{trans}	def2QZVP	C	0.553491	1.58509	0.086362	-0.394349	1.838462	0.090905	-1.050935	1.898978	0.094761
		C	-0.422229	0.778779	-0.413156	-1.154386	0.833337	-0.410444	-1.683577	0.816782	-0.408422
		H	0.64498	1.754135	1.149786	-0.337225	2.016419	1.155761	-1.009667	2.077097	1.160879
		H	1.259541	2.075112	-0.568765	0.173446	2.486941	-0.561732	-0.568414	2.616852	-0.554753
		H	-0.485963	0.630551	-1.485422	-1.189412	0.682266	-1.484155	-1.706233	0.668041	-1.483367
		C	-1.400892	0.091497	0.407252	-1.940023	-0.072439	0.407342	-2.350309	-0.183745	0.406474
		H	-1.337236	0.239652	1.479384	-1.905537	0.077927	1.480797	-2.328384	-0.036231	1.481068
		C	-2.344705	-0.691863	-0.113098	-2.679018	-1.053045	-0.113298	-2.969826	-1.246289	-0.113156
		H	-3.066027	-1.19615	0.516313	-3.256706	-1.716178	0.517043	-3.458548	-1.976078	0.518839
		H	-2.419092	-0.848011	-1.181205	-2.723681	-1.215735	-1.182099	-3.002207	-1.410249	-1.182234
	AVTZ	X	1.593518	-0.778606	0.016809	1.321308	-0.331701	0.006496	1.139648	-0.182147	0.003427
		C	0.558683	1.584461	0.086345	-0.375660	1.837139	0.090924	-1.056308	1.901401	0.094918
		C	-0.420078	0.779077	-0.413340	-1.142768	0.835555	-0.410832	-1.688619	0.817399	-0.408478
		H	0.650576	1.753612	1.150755	-0.317898	2.014984	1.156775	-1.015005	2.079697	1.162013
		H	1.266167	2.073086	-0.569962	0.196811	2.482163	-0.562701	-0.574300	2.620245	-0.555559
		H	-0.483934	0.630863	-1.486646	-1.177986	0.684790	-1.485564	-1.711003	0.669049	-1.484453
		C	-1.401222	0.093235	0.407491	-1.935442	-0.066244	0.407243	-2.354880	-0.184973	0.406558
		H	-1.337448	0.241372	1.480648	-1.900348	0.084340	1.481696	-2.333177	-0.037767	1.482215
		C	-2.347863	-0.689161	-0.113245	-2.681541	-1.043639	-0.113333	-2.974256	-1.249580	-0.113268
		H	-3.070811	-1.192172	0.517099	-3.263923	-1.703156	0.518228	-3.462429	-1.980290	0.519817
		H	-2.422562	-0.845403	-1.182363	-2.727139	-1.206782	-1.183055	-3.006740	-1.413794	-1.183327
		X	1.591817	-0.780414	0.016880	1.314370	-0.335234	0.006589	1.142397	-0.181936	0.003413

Table D23: Calculated harmonic frequencies and mode assignments for the X...C₄H₆ 1*cis* def2QZVP complexes. All frequencies and intensities are in cm⁻¹ and km mol⁻¹ and zero-point energies are in kJ mol⁻¹.

Cl ⁻ ...C ₄ H ₆				Br ⁻ ...C ₄ H ₆				I ⁻ ...C ₄ H ₆				
	Mode	Symmetry	Frequency (cm ⁻¹)	Intensity (km mol ⁻¹)	Mode	Symmetry	Frequency (cm ⁻¹)	Intensity (km mol ⁻¹)	Mode	Symmetry	Frequency (km mol ⁻¹)	Intensity
def2QZVP	ω_1	a''	159 <i>i</i>	0.9803	ω_1	a''	159 <i>i</i>	0.6846	ω_1	a''	157 <i>i</i>	0.4939
	ω_2	a'	24	2.7237	ω_2	a'	31	0.6234	ω_2	a'	33	0.3219
	ω_3	a''	72	0.6492	ω_3	a''	63	0.0328	ω_3	a''	56	0.0021
	ω_4	a'	103	27.0339	ω_4	a'	79	8.7582	ω_4	a'	66	3.8818
	ω_5	a'	298	1.7348	ω_5	a'	300	1.3649	ω_5	a'	301	1.0364
	ω_6	a''	556	11.9947	ω_6	a''	552	11.6741	ω_6	a''	550	11.2488
	ω_7	a'	559	5.2136	ω_7	a'	559	5.1654	ω_7	a'	560	5.1032
	ω_8	a''	752	0.4882	ω_8	a''	751	0.5173	ω_8	a''	752	0.5322
	ω_9	a''	882	30.2771	ω_9	a''	886	29.3901	ω_9	a'	890	1.0335
	ω_{10}	a'	889	0.9674	ω_{10}	a'	889	1.0251	ω_{10}	a''	892	29.4014
	ω_{11}	a''	955	45.041	ω_{11}	a''	952	44.0567	ω_{11}	a''	955	40.7991
	ω_{12}	a''	1033	5.6733	ω_{12}	a''	1033	5.4166	ω_{12}	a''	1035	6.7031
	ω_{13}	a'	1058	6.4863	ω_{13}	a''	1057	17.0946	ω_{13}	a''	1056	14.5641
	ω_{14}	a''	1060	16.6406	ω_{14}	a'	1060	5.3	ω_{14}	a'	1062	4.2285
	ω_{15}	a'	1114	32.3375	ω_{15}	a'	1115	32.2775	ω_{15}	a'	1116	31.9787
	ω_{16}	a'	1319	5.701	ω_{16}	a'	1320	5.1194	ω_{16}	a'	1320	4.351
	ω_{17}	a'	1358	4.7566	ω_{17}	a'	1360	5.2376	ω_{17}	a'	1361	5.7616
	ω_{18}	a'	1419	7.7455	ω_{18}	a'	1424	6.4245	ω_{18}	a'	1430	4.9562
	ω_{19}	a'	1461	12.4616	ω_{19}	a'	1463	13.2434	ω_{19}	a'	1465	13.6643
	ω_{20}	a'	1664	39.3699	ω_{20}	a'	1666	37.1481	ω_{20}	a'	1668	33.717
	ω_{21}	a'	1685	1.0757	ω_{21}	a'	1687	1.206	ω_{21}	a'	1689	1.2446
	ω_{22}	a'	3123	57.4202	ω_{22}	a'	3127	53.1277	ω_{22}	a'	3133	46.7474
	ω_{23}	a'	3143	25.8776	ω_{23}	a'	3145	24.043	ω_{23}	a'	3148	21.4907
	ω_{24}	a'	3155	3.311	ω_{24}	a'	3157	4.5128	ω_{24}	a'	3159	6.2553
	ω_{25}	a'	3163	27.7264	ω_{25}	a'	3166	23.67	ω_{25}	a'	3169	18.1037
	ω_{26}	a'	3229	2.2547	ω_{26}	a'	3230	1.4344	ω_{26}	a'	3233	0.8024
	ω_{27}	a'	3237	26.8867	ω_{27}	a'	3238	25.6532	ω_{27}	a'	3240	23.1477
		zpe	223.2			zpe	223.2			zpe	223.3	

Table D24: Calculated harmonic frequencies and mode assignments for the X...C₄H₆ 1*cis* AVTZ complexes. All frequencies and intensities are in cm⁻¹ and km mol⁻¹ and zero-point energies are in kJ mol⁻¹.

Cl ⁻ ...C ₄ H ₆				Br ⁻ ...C ₄ H ₆				I ⁻ ...C ₄ H ₆				
	Mode	Symmetry	Frequency (cm ⁻¹)	Intensity (km mol ⁻¹)	Mode	Symmetry	Frequency (cm ⁻¹)	Intensity (km mol ⁻¹)	Mode	Symmetry	Frequency (cm ⁻¹)	Intensity (km mol ⁻¹)
AVTZ	ω_1	a''	163 <i>i</i>	1.0146	ω_1	a''	162 <i>i</i>	0.8233	ω_1	a''	165 <i>i</i>	0.7446
	ω_2	a'	22	2.9501	ω_2	a'	26	0.6313	ω_2	a'	33	0.3427
	ω_3	a''	74	0.6479	ω_3	a''	68	0.0096	ω_3	a''	58	0.0086
	ω_4	a'	102	26.9125	ω_4	a'	81	8.6544	ω_4	a'	69	3.7348
	ω_5	a'	296	1.6518	ω_5	a'	297	1.2938	ω_5	a'	298	1.0239
	ω_6	a'	556	5.1551	ω_6	a''	554	11.1204	ω_6	a''	549	10.2767
	ω_7	a''	557	12.3652	ω_7	a'	556	5.1232	ω_7	a'	557	5.1678
	ω_8	a''	740	0.4891	ω_8	a''	739	0.6139	ω_8	a''	738	0.7004
	ω_9	a'	887	1.0361	ω_9	a'	887	1.2067	ω_9	a'	888	1.2498
	ω_{10}	a''	891	33.9576	ω_{10}	a''	894	33.2744	ω_{10}	a''	897	31.9322
	ω_{11}	a''	964	41.891	ω_{11}	a''	963	39.0624	ω_{11}	a''	959	36.6103
	ω_{12}	a''	1020	6.0267	ω_{12}	a''	1020	5.4901	ω_{12}	a''	1018	4.2719
	ω_{13}	a'	1055	7.1003	ω_{13}	a'	1056	6.4736	ω_{13}	a''	1051	17.0361
	ω_{14}	a''	1059	15.415	ω_{14}	a''	1056	15.7514	ω_{14}	a'	1058	5.0404
	ω_{15}	a'	1111	32.5271	ω_{15}	a'	1111	33.6038	ω_{15}	a'	1112	33.5108
	ω_{16}	a'	1316	6.092	ω_{16}	a'	1316	5.8541	ω_{16}	a'	1317	5.0738
	ω_{17}	a'	1356	4.9917	ω_{17}	a'	1356	5.8094	ω_{17}	a'	1358	6.1404
	ω_{18}	a'	1417	7.2554	ω_{18}	a'	1421	6.7219	ω_{18}	a'	1426	5.2536
	ω_{19}	a'	1460	12.5728	ω_{19}	a'	1461	13.1497	ω_{19}	a'	1463	13.7918
	ω_{20}	a'	1662	41.9934	ω_{20}	a'	1664	41.0121	ω_{20}	a'	1666	37.8484
	ω_{21}	a'	1681	1.284	ω_{21}	a'	1682	1.3896	ω_{21}	a'	1684	1.4689
	ω_{22}	a'	3120	55.8315	ω_{22}	a'	3123	53.5211	ω_{22}	a'	3128	47.6849
	ω_{23}	a'	3139	25.795	ω_{23}	a'	3140	23.9903	ω_{23}	a'	3143	21.5976
	ω_{24}	a'	3151	4.0031	ω_{24}	a'	3152	3.3967	ω_{24}	a'	3154	4.4752
	ω_{25}	a'	3161	25.9133	ω_{25}	a'	3161	24.9529	ω_{25}	a'	3164	20.4342
	ω_{26}	a'	3225	1.531	ω_{26}	a'	3226	1.0925	ω_{26}	a'	3228	0.67
	ω_{27}	a'	3232	27.8469	ω_{27}	a'	3234	26.4218	ω_{27}	a'	3235	24.3417
	zpe		222.8		zpe		222.8		zpe		222.8	

Table D25: Calculated harmonic frequencies and mode assignments for the X...C₄H₆ 2*cis* def2QZVP complexes. All frequencies and intensities are in cm⁻¹ and km mol⁻¹ and zero-point energies are in kJ mol⁻¹.

Cl ⁻ ...C ₄ H ₆				I ⁻ ...C ₄ H ₆				
	Mode	Symmetry	Frequency (cm ⁻¹)	Intensity (km mol ⁻¹)	Mode	Symmetry	Frequency (cm ⁻¹)	Intensity (km mol ⁻¹)
def2QZVP	ω_1	a''	166 <i>i</i>	0	ω_1	a_2	167 <i>i</i>	0
	ω_2	a'	62	3.8485	ω_2	b_2	55	0.2821
	ω_3	a''	79	0.9785	ω_3	b_1	58	0.0651
	ω_4	a'	111	30.2483	ω_4	a_1	68	4.6305
	ω_5	a'	304	0.2315	ω_5	a_1	304	0.0874
	ω_6	a''	537	13.5892	ω_6	b_1	534	13.149
	ω_7	a'	551	4.6372	ω_7	b_2	554	4.3326
	ω_8	a''	759	0	ω_8	a_2	758	0
	ω_9	a'	885	1.2253	ω_9	a_1	887	0.6219
	ω_{10}	a''	894	0.0028	ω_{10}	a_2	902	0
	ω_{11}	a''	906	83.1123	ω_{11}	b_1	913	78.2739
	ω_{12}	a''	1076	0.0047	ω_{12}	a_2	1071	0
	ω_{13}	a'	1078	8.4302	ω_{13}	b_1	1073	17.1965
	ω_{14}	a''	1084	19.6311	ω_{14}	a_1	1075	6.9044
	ω_{15}	a'	1119	9.0875	ω_{15}	b_2	1118	6.317
	ω_{16}	a'	1290	5.8345	ω_{16}	b_2	1304	3.3748
	ω_{17}	a'	1347	52.7426	ω_{17}	a_1	1356	44.1467
	ω_{18}	a'	1439	2.4493	ω_{18}	b_2	1441	2.6752
	ω_{19}	a'	1467	23.2853	ω_{19}	a_1	1470	23.8593
	ω_{20}	a'	1670	1.9556	ω_{20}	a_1	1672	1.4763
	ω_{21}	a'	1691	5.8967	ω_{21}	b_2	1694	5.5133
	ω_{22}	a'	3140	10.4431	ω_{22}	b_2	3145	7.3294
	ω_{23}	a'	3144	29.906	ω_{23}	a_1	3149	27.8743
	ω_{24}	a'	3154	7.2923	ω_{24}	b_2	3161	7.1769
	ω_{25}	a'	3159	82.193	ω_{25}	a_1	3165	53.6269
	ω_{26}	a'	3222	31.3513	ω_{26}	b_2	3229	24.2792
	ω_{27}	a'	3225	8.2069	ω_{27}	a_1	3232	8.4173
		zpe	223.7			zpe	223.6	

Table D26: Calculated harmonic frequencies and mode assignments for the X...C₄H₆ 2*cis* AVTZ complexes. All frequencies and intensities are in cm⁻¹ and km mol⁻¹ and zero-point energies are in kJ mol⁻¹.

Cl ⁻ ...C ₄ H ₆				Br ⁻ ...C ₄ H ₆				I ⁻ ...C ₄ H ₆				
	Mode	Symmetry	Frequency (cm ⁻¹)	Intensity (km mol ⁻¹)	Mode	Symmetry	Frequency (cm ⁻¹)	Intensity (km mol ⁻¹)	Mode	Symmetry	Frequency (cm ⁻¹)	Intensity (km mol ⁻¹)
AVTZ	ω_1	<i>a</i> ₂	171 <i>i</i>	0	ω_1	<i>a</i> ["]	170 <i>i</i>	0	ω_1	<i>a</i> ₂	171 <i>i</i>	0
	ω_2	<i>b</i> ₂	61	3.8319	ω_2	<i>a</i> [']	57	0.8152	ω_2	<i>b</i> ₂	55	0.2622
	ω_3	<i>b</i> ₁	81	0.8153	ω_3	<i>a</i> ["]	76	0.0904	ω_3	<i>b</i> ₁	63	0.0061
	ω_4	<i>a</i> ₁	110	30.0357	ω_4	<i>a</i> [']	86	9.8984	ω_4	<i>a</i> ₁	71	4.514
	ω_5	<i>a</i> ₁	302	0.2123	ω_5	<i>a</i> [']	301	0.1153	ω_5	<i>a</i> ₁	301	0.0743
	ω_6	<i>b</i> ₁	537	13.8494	ω_6	<i>a</i> ["]	536	12.9767	ω_6	<i>b</i> ₁	533	12.3425
	ω_7	<i>b</i> ₂	548	4.6048	ω_7	<i>a</i> [']	549	4.3661	ω_7	<i>b</i> ₂	551	4.2209
	ω_8	<i>a</i> ₂	743	0	ω_8	<i>a</i> ["]	743	0	ω_8	<i>a</i> ₂	740	0
	ω_9	<i>a</i> ₁	883	1.3207	ω_9	<i>a</i> [']	884	1.0403	ω_9	<i>a</i> ₁	885	0.6948
	ω_{10}	<i>a</i> ₂	892	0	ω_{10}	<i>a</i> ["]	894	0.0008	ω_{10}	<i>a</i> ₂	898	0
	ω_{11}	<i>b</i> ₁	906	81.0414	ω_{11}	<i>a</i> ["]	909	79.3648	ω_{11}	<i>b</i> ₁	912	76.7642
	ω_{12}	<i>a</i> ₂	1065	0	ω_{12}	<i>a</i> ["]	1062	0.0001	ω_{12}	<i>a</i> ₂	1050	0
	ω_{13}	<i>a</i> ₁	1075	9.1799	ω_{13}	<i>a</i> [']	1075	8.9941	ω_{13}	<i>b</i> ₁	1073	14.5331
	ω_{14}	<i>b</i> ₁	1083	19.2831	ω_{14}	<i>a</i> ["]	1081	16.5538	ω_{14}	<i>a</i> ₁	1073	8.0432
	ω_{15}	<i>b</i> ₂	1115	8.0662	ω_{15}	<i>a</i> [']	1115	6.7157	ω_{15}	<i>b</i> ₂	1115	5.2639
	ω_{16}	<i>b</i> ₂	1287	6.1026	ω_{16}	<i>a</i> [']	1292	5.2061	ω_{16}	<i>b</i> ₂	1299	3.6668
	ω_{17}	<i>a</i> ₁	1345	56.7892	ω_{17}	<i>a</i> [']	1349	55.878	ω_{17}	<i>a</i> ₁	1352	50.2478
	ω_{18}	<i>b</i> ₂	1437	2.4547	ω_{18}	<i>a</i> [']	1437	2.4774	ω_{18}	<i>b</i> ₂	1438	2.5003
	ω_{19}	<i>a</i> ₁	1466	23.3257	ω_{19}	<i>a</i> [']	1467	24.0714	ω_{19}	<i>a</i> ₁	1468	24.1221
	ω_{20}	<i>a</i> ₁	1668	1.8523	ω_{20}	<i>a</i> [']	1669	1.5083	ω_{20}	<i>a</i> ₁	1670	1.2852
	ω_{21}	<i>b</i> ₂	1688	6.4964	ω_{21}	<i>a</i> [']	1688	6.3167	ω_{21}	<i>b</i> ₂	1689	6.2194
	ω_{22}	<i>b</i> ₂	3136	10.246	ω_{22}	<i>a</i> [']	3138	9.2458	ω_{22}	<i>b</i> ₂	3140	7.592
	ω_{23}	<i>a</i> ₁	3140	27.5419	ω_{23}	<i>a</i> [']	3142	27.6767	ω_{23}	<i>a</i> ₁	3144	26.8301
	ω_{24}	<i>b</i> ₂	3150	6.4775	ω_{24}	<i>a</i> [']	3151	7.0898	ω_{24}	<i>b</i> ₂	3154	7.2028
	ω_{25}	<i>a</i> ₁	3157	82.1605	ω_{25}	<i>a</i> [']	3157	73.8042	ω_{25}	<i>a</i> ₁	3159	58.4594
	ω_{26}	<i>b</i> ₂	3218	31.1012	ω_{26}	<i>a</i> [']	3220	28.333	ω_{26}	<i>b</i> ₂	3223	24.6062
	ω_{27}	<i>a</i> ₁	3221	7.8745	ω_{27}	<i>a</i> [']	3223	8.1034	ω_{27}	<i>a</i> ₁	3227	8.4097
	zpe		223.2		zpe		223.1		zpe		223.0	

Table D27: Calculated harmonic frequencies and mode assignments for the X...C₄H₆ 3*cis* def2QZVP complexes. All frequencies and intensities are in cm⁻¹ and km mol⁻¹ and zero-point energies are in kJ mol⁻¹.

Cl ⁻ ...C ₄ H ₆				Br ⁻ ...C ₄ H ₆				I ⁻ ...C ₄ H ₆				
	Mode	Symmetry	Frequency (cm ⁻¹)	Intensity (km mol ⁻¹)	Mode	Symmetry	Frequency (cm ⁻¹)	Intensity (km mol ⁻¹)	Mode	Symmetry	Frequency (km mol ⁻¹)	Intensity
def2QZVP	ω_1	<i>a''</i>	54 <i>i</i>	0	ω_1	<i>a''</i>	83 <i>i</i>	0	ω_1	<i>a''</i>	102 <i>i</i>	0
	ω_2	<i>a''</i>	80	0.4002	ω_2	<i>a''</i>	65	0.0191	ω_2	<i>a''</i>	51	0.0072
	ω_3	<i>a'</i>	104	2.0486	ω_3	<i>a'</i>	84	10.6855	ω_3	<i>a'</i>	67	4.9983
	ω_4	<i>a'</i>	113	31.4698	ω_4	<i>a'</i>	90	0.2211	ω_4	<i>a'</i>	75	0.0038
	ω_5	<i>a'</i>	318	2.4854	ω_5	<i>a'</i>	313	1.1628	ω_5	<i>a'</i>	309	0.5399
	ω_6	<i>a''</i>	532	25.4621	ω_6	<i>a''</i>	529	24.3866	ω_6	<i>a''</i>	525	24.0998
	ω_7	<i>d'</i>	585	6.2194	ω_7	<i>a'</i>	581	6.1489	ω_7	<i>a'</i>	576	6.0758
	ω_8	<i>a''</i>	745	0	ω_8	<i>a''</i>	745	0	ω_8	<i>a''</i>	744	0
	ω_9	<i>a'</i>	895	0.5248	ω_9	<i>a'</i>	893	0.3	ω_9	<i>a'</i>	891	0.1128
	ω_{10}	<i>a''</i>	961	0.0001	ω_{10}	<i>a''</i>	960	0.0002	ω_{10}	<i>a''</i>	960	0
	ω_{11}	<i>a''</i>	983	17.8609	ω_{11}	<i>a''</i>	979	23.607	ω_{11}	<i>a''</i>	976	25.2801
	ω_{12}	<i>a''</i>	1034	0.0003	ω_{12}	<i>a''</i>	1030	0.0008	ω_{12}	<i>a''</i>	1028	0
	ω_{13}	<i>a''</i>	1057	57.2056	ω_{13}	<i>a''</i>	1051	52.9074	ω_{13}	<i>a''</i>	1046	46.1797
	ω_{14}	<i>a'</i>	1068	1.4311	ω_{14}	<i>a'</i>	1066	1.7744	ω_{14}	<i>a'</i>	1064	2.2367
	ω_{15}	<i>a'</i>	1114	2.2406	ω_{15}	<i>a'</i>	1113	2.2485	ω_{15}	<i>a'</i>	1111	2.0632
	ω_{16}	<i>a'</i>	1322	0.0639	ω_{16}	<i>a'</i>	1321	0.0903	ω_{16}	<i>a'</i>	1320	0.2322
	ω_{17}	<i>a'</i>	1364	6.3013	ω_{17}	<i>a'</i>	1363	6.9563	ω_{17}	<i>a'</i>	1362	7.8246
	ω_{18}	<i>a'</i>	1460	1.6464	ω_{18}	<i>a'</i>	1457	1.3836	ω_{18}	<i>a'</i>	1454	0.778
	ω_{19}	<i>a'</i>	1488	6.7348	ω_{19}	<i>a'</i>	1485	7.3783	ω_{19}	<i>a'</i>	1483	7.7442
	ω_{20}	<i>a'</i>	1671	0.1163	ω_{20}	<i>a'</i>	1672	0.0359	ω_{20}	<i>a'</i>	1673	0.0012
	ω_{21}	<i>a'</i>	1687	1.9384	ω_{21}	<i>a'</i>	1688	1.4679	ω_{21}	<i>a'</i>	1690	0.871
	ω_{22}	<i>a'</i>	3086	41.0782	ω_{22}	<i>a'</i>	3102	26.236	ω_{22}	<i>a'</i>	3118	6.1809
	ω_{23}	<i>a'</i>	3097	126.7056	ω_{23}	<i>a'</i>	3110	89.2875	ω_{23}	<i>a'</i>	3125	46.8208
	ω_{24}	<i>a'</i>	3114	27.5122	ω_{24}	<i>a'</i>	3119	31.4243	ω_{24}	<i>a'</i>	3127	40.1177
	ω_{25}	<i>a'</i>	3135	162.2812	ω_{25}	<i>a'</i>	3140	153.936	ω_{25}	<i>a'</i>	3147	145.0511
	ω_{26}	<i>a'</i>	3195	24.228	ω_{26}	<i>a'</i>	3206	21.7487	ω_{26}	<i>a'</i>	3219	18.4975
	ω_{27}	<i>a'</i>	3203	52.3773	ω_{27}	<i>a'</i>	3213	42.9546	ω_{27}	<i>a'</i>	3225	28.7384
zpe				223.8	zpe				223.6	zpe		223.5

Table D28: Calculated harmonic frequencies and mode assignments for the X...C₄H₆ 3*cis* AVTZ complexes. All frequencies and intensities are in cm⁻¹ and km mol⁻¹ and zero-point energies are in kJ mol⁻¹.

Cl ⁻ ...C ₄ H ₆				Br ⁻ ...C ₄ H ₆				I ⁻ ...C ₄ H ₆				
	Mode	Symmetry	Frequency (cm ⁻¹)	Intensity (km mol ⁻¹)	Mode	Symmetry	Frequency (cm ⁻¹)	Intensity (km mol ⁻¹)	Mode	Symmetry	Frequency (cm ⁻¹)	Intensity (km mol ⁻¹)
AVTZ	ω_1	a''	49 <i>i</i>	0	ω_1	a''	50 <i>i</i>	0	ω_1	a_2	93 <i>i</i>	0
	ω_2	a''	82	0.3085	ω_2	a''	75	0.0006	ω_2	b_1	57	0.0581
	ω_3	a'	103	2.023	ω_3	a'	87	10.6354	ω_3	a_1	71	4.9498
	ω_4	a'	113	31.5322	ω_4	a'	93	0.1431	ω_4	b_2	80	0.0002
	ω_5	a'	315	2.4244	ω_5	a'	311	1.2588	ω_5	a_1	307	0.5363
	ω_6	a''	535	28.3687	ω_6	a''	534	28.3051	ω_6	b_1	528	27.225
	ω_7	a'	581	6.7862	ω_7	a'	578	6.9351	ω_7	b_2	575	6.823
	ω_8	a''	743	0	ω_8	a''	743	0	ω_8	a_2	748	0
	ω_9	a'	893	0.5465	ω_9	a'	891	0.3302	ω_9	a_1	890	0.1142
	ω_{10}	a''	977	0	ω_{10}	a''	977	0	ω_{10}	a_2	978	0
	ω_{11}	a''	992	11.3724	ω_{11}	a''	990	12.7491	ω_{11}	b_1	987	16.3979
	ω_{12}	a''	1022	0.0002	ω_{12}	a''	1021	0.0001	ω_{12}	a_2	1032	0
	ω_{13}	a''	1056	57.2667	ω_{13}	a''	1054	50.6118	ω_{13}	b_1	1047	43.8407
	ω_{14}	a'	1065	1.5343	ω_{14}	a'	1064	1.8462	ω_{14}	a_1	1062	2.3678
	ω_{15}	a'	1111	2.0612	ω_{15}	a'	1109	1.8079	ω_{15}	b_2	1109	1.7592
	ω_{16}	a'	1318	0.1291	ω_{16}	a'	1317	0.3086	ω_{16}	b_2	1317	0.4788
	ω_{17}	a'	1361	6.6468	ω_{17}	a'	1360	7.5633	ω_{17}	a_1	1359	8.5793
	ω_{18}	a'	1457	1.0138	ω_{18}	a'	1455	0.5426	ω_{18}	b_2	1453	0.2375
	ω_{19}	a'	1485	6.0357	ω_{19}	a'	1484	6.1983	ω_{19}	a_1	1482	7.2249
	ω_{20}	a'	1669	0.3652	ω_{20}	a'	1670	0.2887	ω_{20}	a_1	1671	0.0829
	ω_{21}	a'	1683	2.5908	ω_{21}	a'	1684	1.753	ω_{21}	b_2	1686	1.0355
	ω_{22}	a'	3085	38.4197	ω_{22}	a'	3096	27.2872	ω_{22}	b_2	3111	7.8674
	ω_{23}	a'	3095	123.7431	ω_{23}	a'	3105	98.4379	ω_{23}	a_1	3118	55.4911
	ω_{24}	a'	3109	28.8652	ω_{24}	a'	3113	31.7236	ω_{24}	b_2	3121	38.7952
	ω_{25}	a'	3132	169.6811	ω_{25}	a'	3135	165.2486	ω_{25}	a_1	3142	155.6527
	ω_{26}	a'	3193	23.4247	ω_{26}	a'	3201	20.9826	ω_{26}	b_2	3212	18.6807
	ω_{27}	a'	3201	52.9197	ω_{27}	a'	3208	45.0553	ω_{27}	a_1	3219	31.1975
	zpe		223.6		zpe		223.4		zpe		223.5	

Table D29: Calculated harmonic frequencies and mode assignments for the X...C₄H₆ 5*cis* def2QZVP complexes. All frequencies and intensities are in cm⁻¹ and km mol⁻¹ and zero-point energies are in kJ mol⁻¹.

Cl ⁻ ...C ₄ H ₆				Br ⁻ ...C ₄ H ₆				I ⁻ ...C ₄ H ₆				
	Mode	Symmetry	Frequency (cm ⁻¹)	Intensity (km mol ⁻¹)	Mode	Symmetry	Frequency (cm ⁻¹)	Intensity (km mol ⁻¹)	Mode	Symmetry	Frequency (km mol ⁻¹)	Intensity
def2QZVP	ω_1	a''	133 <i>i</i>	0.571	ω_1	a''	141 <i>i</i>	0.323	ω_1	a''	148 <i>i</i>	0.261
	ω_2	a'	32	4.1862	ω_2	a'	24	1.3722	ω_2	a'	15	0.6779
	ω_3	a''	62	1.3297	ω_3	a''	54	0.2336	ω_3	a''	48	0.0674
	ω_4	a'	107	32.5168	ω_4	a'	82	10.9749	ω_4	a'	67	5.0249
	ω_5	a'	310	8.5857	ω_5	a'	308	5.2842	ω_5	a'	306	3.3924
	ω_6	a''	545	15.9733	ω_6	a''	540	16.0016	ω_6	a''	537	14.9518
	ω_7	a'	571	3.3551	ω_7	a'	569	4.0728	ω_7	a'	567	4.7917
	ω_8	a''	749	0.4111	ω_8	a''	748	0.3953	ω_8	a''	748	0.4663
	ω_9	a''	887	34.4896	ω_9	a''	891	33.4431	ω_9	a'	892	0.4081
	ω_{10}	a'	895	0.6953	ω_{10}	a'	893	0.5504	ω_{10}	a''	897	32.7446
	ω_{11}	a''	1016	31.8713	ω_{11}	a''	1007	44.4603	ω_{11}	a''	1001	41.5119
	ω_{12}	a''	1026	24.175	ω_{12}	a''	1022	1.0911	ω_{12}	a''	1025	1.5201
	ω_{13}	a''	1047	4.7294	ω_{13}	a''	1041	16.8466	ω_{13}	a''	1041	17.865
	ω_{14}	a'	1060	1.253	ω_{14}	a'	1060	1.2018	ω_{14}	a'	1060	1.2316
	ω_{15}	a'	1120	2.3639	ω_{15}	a'	1119	2.947	ω_{15}	a'	1118	3.9448
	ω_{16}	a'	1314	0.4317	ω_{16}	a'	1315	0.2983	ω_{16}	a'	1316	0.1243
	ω_{17}	a'	1354	0.7426	ω_{17}	a'	1355	0.4666	ω_{17}	a'	1356	0.1607
	ω_{18}	a'	1445	2.4644	ω_{18}	a'	1445	2.7656	ω_{18}	a'	1445	3.355
	ω_{19}	a'	1486	14.5702	ω_{19}	a'	1483	13.429	ω_{19}	a'	1481	10.7724
	ω_{20}	a'	1663	40.8519	ω_{20}	a'	1665	35.614	ω_{20}	a'	1667	29.8591
	ω_{21}	a'	1688	1.6496	ω_{21}	a'	1689	1.6729	ω_{21}	a'	1691	1.8757
	ω_{22}	a'	3059	297.6576	ω_{22}	a'	3084	221.7145	ω_{22}	a'	3108	149.6231
	ω_{23}	a'	3139	30.3203	ω_{23}	a'	3141	25.9964	ω_{23}	a'	3145	22.6588
	ω_{24}	a'	3157	34.8166	ω_{24}	a'	3158	24.1517	ω_{24}	a'	3160	20.6709
	ω_{25}	a'	3171	37.7099	ω_{25}	a'	3175	14.7528	ω_{25}	a'	3177	13.1824
	ω_{26}	a'	3177	68.6839	ω_{26}	a'	3192	87.0112	ω_{26}	a'	3211	64.1744
	ω_{27}	a'	3242	21.0545	ω_{27}	a'	3243	20.9274	ω_{27}	a'	3244	20.9615
		zpe	223.2			zpe	223.1			zpe	223.2	

Table D30: Calculated harmonic frequencies and mode assignments for the X...C₄H₆ 5*cis* AVTZ complexes. All frequencies and intensities are in cm⁻¹ and km mol⁻¹ and zero-point energies are in kJ mol⁻¹.

Cl ⁻ ...C ₄ H ₆				Br ⁻ ...C ₄ H ₆				I ⁻ ...C ₄ H ₆				
	Mode	Symmetry	Frequency (cm ⁻¹)	Intensity (km mol ⁻¹)	Mode	Symmetry	Frequency (cm ⁻¹)	Intensity (km mol ⁻¹)	Mode	Symmetry	Frequency (cm ⁻¹)	Intensity (km mol ⁻¹)
AVTZ	ω_1	a''	139 <i>i</i>	0.5671	ω_1	a''	143 <i>i</i>	0.4268	ω_1	a''	153 <i>i</i>	0.3512
	ω_2	a'	32	4.1141	ω_2	a'	24	1.2827	ω_2	a'	13	0.6216
	ω_3	a''	62	1.3174	ω_3	a''	59	0.1462	ω_3	a''	50	0.0338
	ω_4	a'	106	32.197	ω_4	a'	85	10.7674	ω_4	a'	69	5.0173
	ω_5	a'	308	8.3321	ω_5	a'	307	5.4197	ω_5	a'	305	3.4966
	ω_6	a''	546	15.8887	ω_6	a''	545	14.5622	ω_6	a''	539	13.528
	ω_7	a'	568	3.5326	ω_7	a'	566	4.225	ω_7	a'	564	4.9498
	ω_8	a''	741	0.3775	ω_8	a''	741	0.5394	ω_8	a''	735	0.7472
	ω_9	a'	893	0.6981	ω_9	a'	892	0.57	ω_9	a'	890	0.4358
	ω_{10}	a''	893	36.298	ω_{10}	a''	896	35.5736	ω_{10}	a''	900	34.2174
	ω_{11}	a''	999	7.7554	ω_{11}	a''	998	8.6445	ω_{11}	a''	994	8.7986
	ω_{12}	a''	1026	50.5175	ω_{12}	a''	1022	45.2187	ω_{12}	a''	1010	29.6937
	ω_{13}	a''	1053	0.1112	ω_{13}	a''	1047	2.8476	ω_{13}	a''	1038	17.3686
	ω_{14}	a'	1057	1.245	ω_{14}	a'	1057	1.3052	ω_{14}	a'	1057	1.2847
	ω_{15}	a'	1117	2.349	ω_{15}	a'	1115	2.9827	ω_{15}	a'	1114	3.8903
	ω_{16}	a'	1311	0.3353	ω_{16}	a'	1312	0.1931	ω_{16}	a'	1313	0.0823
	ω_{17}	a'	1351	0.6691	ω_{17}	a'	1352	0.3656	ω_{17}	a'	1353	0.132
	ω_{18}	a'	1443	2.5779	ω_{18}	a'	1443	2.9798	ω_{18}	a'	1443	3.4591
	ω_{19}	a'	1484	13.1598	ω_{19}	a'	1482	11.4711	ω_{19}	a'	1479	10.0242
	ω_{20}	a'	1661	43.1078	ω_{20}	a'	1663	39.2168	ω_{20}	a'	1666	33.3538
	ω_{21}	a'	1684	2.0023	ω_{21}	a'	1685	2.1224	ω_{21}	a'	1687	2.1876
	ω_{22}	a'	3061	293.8446	ω_{22}	a'	3080	235.2896	ω_{22}	a'	3101	164.5028
	ω_{23}	a'	3134	29.101	ω_{23}	a'	3136	25.8335	ω_{23}	a'	3139	22.5869
	ω_{24}	a'	3153	32.5628	ω_{24}	a'	3154	25.1971	ω_{24}	a'	3155	21.5685
	ω_{25}	a'	3167	23.6284	ω_{25}	a'	3170	13.681	ω_{25}	a'	3172	12.5623
	ω_{26}	a'	3175	85.8366	ω_{26}	a'	3188	91.6744	ω_{26}	a'	3204	69.1798
	ω_{27}	a'	3237	21.8179	ω_{27}	a'	3238	21.8219	ω_{27}	a'	3239	21.9076
		zpe	222.9			zpe	222.9			zpe	222.7	

Table D31: Calculated harmonic frequencies and mode assignments for the X...C₄H₆ 1*trans* def2QZVP complexes. All frequencies and intensities are in cm⁻¹ and km mol⁻¹ and zero-point energies are in kJ mol⁻¹.

Cl ⁻ ...C ₄ H ₆				Br ⁻ ...C ₄ H ₆				I ⁻ ...C ₄ H ₆				
	Mode	Symmetry	Frequency (cm ⁻¹)	Intensity (km mol ⁻¹)	Mode	Symmetry	Frequency (cm ⁻¹)	Intensity (km mol ⁻¹)	Mode	Symmetry	Frequency (km mol ⁻¹)	Intensity
def2QZVP	ω_1	<i>a'</i>	21	3.3909	ω_1	<i>a'</i>	25	0.6865	ω_1	<i>a'</i>	27	0.298
	ω_2	<i>a'</i>	110	25.9286	ω_2	<i>a'</i>	86	8.6856	ω_2	<i>a'</i>	72	3.9254
	ω_3	<i>a''</i>	111	0	ω_3	<i>a''</i>	105	0.1647	ω_3	<i>a''</i>	95	0.2842
	ω_4	<i>a''</i>	170	0.547	ω_4	<i>a''</i>	170	0.509	ω_4	<i>a''</i>	169	0.5221
	ω_5	<i>a'</i>	290	2.128	ω_5	<i>a'</i>	291	2.342	ω_5	<i>a'</i>	293	2.4363
	ω_6	<i>a'</i>	515	1.1097	ω_6	<i>a'</i>	515	0.8519	ω_6	<i>a'</i>	515	0.631
	ω_7	<i>a''</i>	574	6.4142	ω_7	<i>a''</i>	571	6.2633	ω_7	<i>a''</i>	566	5.9581
	ω_8	<i>a''</i>	791	2.0571	ω_8	<i>a''</i>	790	1.899	ω_8	<i>a''</i>	789	1.9101
	ω_9	<i>a''</i>	896	41.2271	ω_9	<i>a''</i>	900	40.5224	ω_9	<i>a''</i>	906	39.2089
	ω_{10}	<i>a'</i>	910	1.0947	ω_{10}	<i>a'</i>	910	1.0181	ω_{10}	<i>a'</i>	910	0.9526
	ω_{11}	<i>a''</i>	953	33.9216	ω_{11}	<i>a''</i>	948	33.583	ω_{11}	<i>a''</i>	949	31.8633
	ω_{12}	<i>a'</i>	1004	13.8023	ω_{12}	<i>a'</i>	1005	12.9009	ω_{12}	<i>a'</i>	1005	12.1275
	ω_{13}	<i>a''</i>	1013	5.3036	ω_{13}	<i>a''</i>	1012	4.4574	ω_{13}	<i>a''</i>	1012	4.6371
	ω_{14}	<i>a''</i>	1074	24.6503	ω_{14}	<i>a''</i>	1072	24.9557	ω_{14}	<i>a''</i>	1071	23.2338
	ω_{15}	<i>a'</i>	1220	4.8712	ω_{15}	<i>a'</i>	1223	4.5637	ω_{15}	<i>a'</i>	1226	3.9572
	ω_{16}	<i>a'</i>	1313	0.4259	ω_{16}	<i>a'</i>	1314	0.3337	ω_{16}	<i>a'</i>	1315	0.3145
	ω_{17}	<i>a'</i>	1318	13.4927	ω_{17}	<i>a'</i>	1321	14.2676	ω_{17}	<i>a'</i>	1323	14.7183
	ω_{18}	<i>a'</i>	1399	10.9216	ω_{18}	<i>a'</i>	1403	9.8913	ω_{18}	<i>a'</i>	1408	9.4499
	ω_{19}	<i>a'</i>	1463	2.4932	ω_{19}	<i>a'</i>	1466	2.2163	ω_{19}	<i>a'</i>	1470	1.8989
	ω_{20}	<i>a'</i>	1638	23.2644	ω_{20}	<i>a'</i>	1640	23.7712	ω_{20}	<i>a'</i>	1642	24.0227
	ω_{21}	<i>a'</i>	1698	37.6289	ω_{21}	<i>a'</i>	1700	33.6407	ω_{21}	<i>a'</i>	1702	29.5395
	ω_{22}	<i>a'</i>	3116	52.9192	ω_{22}	<i>a'</i>	3122	41.7763	ω_{22}	<i>a'</i>	3128	28.4332
	ω_{23}	<i>a'</i>	3127	45.8944	ω_{23}	<i>a'</i>	3129	48.7224	ω_{23}	<i>a'</i>	3133	50.9494
	ω_{24}	<i>a'</i>	3152	24.2082	ω_{24}	<i>a'</i>	3152	23.9228	ω_{24}	<i>a'</i>	3154	21.488
	ω_{25}	<i>a'</i>	3156	0.9389	ω_{25}	<i>a'</i>	3156	0.4157	ω_{25}	<i>a'</i>	3158	0.2313
	ω_{26}	<i>a'</i>	3226	9.0666	ω_{26}	<i>a'</i>	3229	7.1156	ω_{26}	<i>a'</i>	3232	5.6124
	ω_{27}	<i>a'</i>	3240	19.9831	ω_{27}	<i>a'</i>	3241	19.2511	ω_{27}	<i>a'</i>	3243	18.5262
		zpe	224.3			zpe	224.3			zpe	224.4	

Table D32: Calculated harmonic frequencies and mode assignments for the X...C₄H₆ 1*trans* AVTZ complexes. All frequencies and intensities are in cm⁻¹ and km mol⁻¹ and zero-point energies are in kJ mol⁻¹.

Cl ⁻ ...C ₄ H ₆				Br ⁻ ...C ₄ H ₆				I ⁻ ...C ₄ H ₆				
	Mode	Symmetry	Frequency (cm ⁻¹)	Intensity (km mol ⁻¹)	Mode	Symmetry	Frequency (cm ⁻¹)	Intensity (km mol ⁻¹)	Mode	Symmetry	Frequency (cm ⁻¹)	Intensity (km mol ⁻¹)
AVTZ	ω_1	<i>a'</i>	20	3.3341	ω_1	<i>a'</i>	21	0.5513	ω_1	<i>a'</i>	29	0.3097
	ω_2	<i>a'</i>	108	25.6296	ω_2	<i>a'</i>	86	8.3468	ω_2	<i>a'</i>	76	3.6974
	ω_3	<i>a''</i>	114	0.0003	ω_3	<i>a''</i>	111	0.2622	ω_3	<i>a''</i>	100	0.4306
	ω_4	<i>a''</i>	169	0.6495	ω_4	<i>a''</i>	170	0.6542	ω_4	<i>a''</i>	168	0.649
	ω_5	<i>a'</i>	288	2.4402	ω_5	<i>a'</i>	289	2.7183	ω_5	<i>a'</i>	292	2.4489
	ω_6	<i>a'</i>	513	1.0385	ω_6	<i>a'</i>	512	0.789	ω_6	<i>a'</i>	513	0.6893
	ω_7	<i>a''</i>	573	6.2336	ω_7	<i>a''</i>	572	5.4415	ω_7	<i>a''</i>	566	5.0732
	ω_8	<i>a''</i>	788	2.0474	ω_8	<i>a''</i>	788	2.1931	ω_8	<i>a''</i>	787	2.1849
	ω_9	<i>a''</i>	902	40.8078	ω_9	<i>a''</i>	906	39.8281	ω_9	<i>a'</i>	908	1.0667
	ω_{10}	<i>a'</i>	908	0.9875	ω_{10}	<i>a'</i>	907	0.9656	ω_{10}	<i>a''</i>	910	38.9487
	ω_{11}	<i>a''</i>	959	32.1651	ω_{11}	<i>a''</i>	955	30.7514	ω_{11}	<i>a''</i>	953	28.3811
	ω_{12}	<i>a'</i>	1000	13.9076	ω_{12}	<i>a'</i>	1001	13.6016	ω_{12}	<i>a'</i>	1002	12.5961
	ω_{13}	<i>a''</i>	1012	9.118	ω_{13}	<i>a''</i>	1012	8.256	ω_{13}	<i>a''</i>	1010	6.4127
	ω_{14}	<i>a''</i>	1075	21.7004	ω_{14}	<i>a''</i>	1077	20.6078	ω_{14}	<i>a''</i>	1070	21.3373
	ω_{15}	<i>a'</i>	1218	5.7922	ω_{15}	<i>a'</i>	1220	6.0546	ω_{15}	<i>a'</i>	1223	4.6689
	ω_{16}	<i>a'</i>	1311	0.3917	ω_{16}	<i>a'</i>	1311	0.3137	ω_{16}	<i>a'</i>	1312	0.292
	ω_{17}	<i>a'</i>	1317	15.1218	ω_{17}	<i>a'</i>	1319	16.7186	ω_{17}	<i>a'</i>	1320	15.9394
	ω_{18}	<i>a'</i>	1398	10.1637	ω_{18}	<i>a'</i>	1401	9.6832	ω_{18}	<i>a'</i>	1405	9.9441
	ω_{19}	<i>a'</i>	1462	2.353	ω_{19}	<i>a'</i>	1464	2.0076	ω_{19}	<i>a'</i>	1467	1.9024
	ω_{20}	<i>a'</i>	1635	24.7516	ω_{20}	<i>a'</i>	1637	25.5049	ω_{20}	<i>a'</i>	1639	24.9065
	ω_{21}	<i>a'</i>	1696	38.7757	ω_{21}	<i>a'</i>	1697	35.7817	ω_{21}	<i>a'</i>	1699	32.9788
	ω_{22}	<i>a'</i>	3116	37.671	ω_{22}	<i>a'</i>	3120	20.6922	ω_{22}	<i>a'</i>	3124	21.5343
	ω_{23}	<i>a'</i>	3123	57.1399	ω_{23}	<i>a'</i>	3124	70.4976	ω_{23}	<i>a'</i>	3128	59.8301
	ω_{24}	<i>a'</i>	3147	25.5911	ω_{24}	<i>a'</i>	3145	21.3147	ω_{24}	<i>a'</i>	3149	19.3227
	ω_{25}	<i>a'</i>	3150	2.1426	ω_{25}	<i>a'</i>	3151	6.4172	ω_{25}	<i>a'</i>	3153	3.3729
	ω_{26}	<i>a'</i>	3224	7.9393	ω_{26}	<i>a'</i>	3226	6.4161	ω_{26}	<i>a'</i>	3227	5.8445
	ω_{27}	<i>a'</i>	3236	20.3693	ω_{27}	<i>a'</i>	3237	19.8451	ω_{27}	<i>a'</i>	3238	19.4477
	zpe		224.1		zpe		224.1		zpe		224.1	

Table D33: Calculated harmonic frequencies and mode assignments for the X...C₄H₆ 2*trans* def2QZVP complexes. All frequencies and intensities are in cm⁻¹ and km mol⁻¹ and zero-point energies are in kJ mol⁻¹.

Cl ⁻ ...C ₄ H ₆				Br ⁻ ...C ₄ H ₆				I ⁻ ...C ₄ H ₆				
	Mode	Symmetry	Frequency (cm ⁻¹)	Intensity (km mol ⁻¹)	Mode	Symmetry	Frequency (cm ⁻¹)	Intensity (km mol ⁻¹)	Mode	Symmetry	Frequency (km mol ⁻¹)	Intensity
def2QZVP	ω_1	<i>a'</i>	73	5.5452	ω_1	<i>a'</i>	62	2.0503	ω_1	<i>a'</i>	49	1.0413
	ω_2	<i>a'</i>	117	28.3525	ω_2	<i>a'</i>	92	9.0563	ω_2	<i>a'</i>	74	4.1334
	ω_3	<i>a''</i>	140	0.0914	ω_3	<i>a''</i>	127	0.0054	ω_3	<i>a''</i>	111	0.0766
	ω_4	<i>a''</i>	178	0.4572	ω_4	<i>a''</i>	176	0.4302	ω_4	<i>a''</i>	174	0.4424
	ω_5	<i>a'</i>	303	3.4384	ω_5	<i>a'</i>	301	3.1667	ω_5	<i>a'</i>	299	2.9171
	ω_6	<i>a'</i>	520	2.9638	ω_6	<i>a'</i>	519	2.1684	ω_6	<i>a'</i>	517	1.5723
	ω_7	<i>a''</i>	559	12.0695	ω_7	<i>a''</i>	556	11.8961	ω_7	<i>a''</i>	553	11.3126
	ω_8	<i>a''</i>	791	1.0649	ω_8	<i>a''</i>	790	0.9112	ω_8	<i>a''</i>	789	0.8311
	ω_9	<i>a''</i>	891	48.8076	ω_9	<i>a''</i>	896	47.9157	ω_9	<i>a''</i>	901	45.1736
	ω_{10}	<i>a'</i>	912	2.1775	ω_{10}	<i>a'</i>	911	1.6912	ω_{10}	<i>a'</i>	910	1.1731
	ω_{11}	<i>a''</i>	973	13.3308	ω_{11}	<i>a''</i>	969	15.6664	ω_{11}	<i>a''</i>	967	16.7918
	ω_{12}	<i>a'</i>	1018	1.0333	ω_{12}	<i>a'</i>	1016	0.8293	ω_{12}	<i>a'</i>	1013	0.6509
	ω_{13}	<i>a''</i>	1027	11.876	ω_{13}	<i>a''</i>	1023	9.1689	ω_{13}	<i>a''</i>	1019	7.437
	ω_{14}	<i>a''</i>	1101	24.3	ω_{14}	<i>a''</i>	1093	24.262	ω_{14}	<i>a''</i>	1086	21.9008
	ω_{15}	<i>a'</i>	1236	0.8119	ω_{15}	<i>a'</i>	1237	0.5862	ω_{15}	<i>a'</i>	1236	0.3285
	ω_{16}	<i>a'</i>	1320	9.0963	ω_{16}	<i>a'</i>	1321	6.5085	ω_{16}	<i>a'</i>	1321	5.0215
	ω_{17}	<i>a'</i>	1333	3.4713	ω_{17}	<i>a'</i>	1332	3.3316	ω_{17}	<i>a'</i>	1330	2.7453
	ω_{18}	<i>a'</i>	1416	0.205	ω_{18}	<i>a'</i>	1417	0.2511	ω_{18}	<i>a'</i>	1417	0.4072
	ω_{19}	<i>a'</i>	1478	9.0494	ω_{19}	<i>a'</i>	1478	7.5557	ω_{19}	<i>a'</i>	1479	6.3197
	ω_{20}	<i>a'</i>	1640	21.2615	ω_{20}	<i>a'</i>	1641	20.1851	ω_{20}	<i>a'</i>	1643	18.7831
	ω_{21}	<i>a'</i>	1701	4.7811	ω_{21}	<i>a'</i>	1703	4.4459	ω_{21}	<i>a'</i>	1705	4.1102
	ω_{22}	<i>a'</i>	3091	39.3279	ω_{22}	<i>a'</i>	3103	26.0235	ω_{22}	<i>a'</i>	3115	12.0783
	ω_{23}	<i>a'</i>	3107	200.3151	ω_{23}	<i>a'</i>	3117	183.0056	ω_{23}	<i>a'</i>	3127	140.784
	ω_{24}	<i>a'</i>	3122	18.494	ω_{24}	<i>a'</i>	3129	10.2215	ω_{24}	<i>a'</i>	3139	14.2021
	ω_{25}	<i>a'</i>	3136	27.9997	ω_{25}	<i>a'</i>	3139	27.5291	ω_{25}	<i>a'</i>	3142	29.1517
	ω_{26}	<i>a'</i>	3206	28.1016	ω_{26}	<i>a'</i>	3214	22.6772	ω_{26}	<i>a'</i>	3224	15.7885
	ω_{27}	<i>a'</i>	3221	20.2546	ω_{27}	<i>a'</i>	3224	18.4836	ω_{27}	<i>a'</i>	3229	16.5417
zpe				224.9	zpe				224.8	zpe		224.7

Table D34: Calculated harmonic frequencies and mode assignments for the X...C₄H₆ 2*trans* AVTZ complexes. All frequencies and intensities are in cm⁻¹ and km mol⁻¹ and zero-point energies are in kJ mol⁻¹.

Cl ⁻ ...C ₄ H ₆				Br ⁻ ...C ₄ H ₆				I ⁻ ...C ₄ H ₆				
	Mode	Symmetry	Frequency (cm ⁻¹)	Intensity (km mol ⁻¹)	Mode	Symmetry	Frequency (cm ⁻¹)	Intensity (km mol ⁻¹)	Mode	Symmetry	Frequency (cm ⁻¹)	Intensity (km mol ⁻¹)
AVTZ	ω_1	<i>a'</i>	73	5.6962	ω_1	<i>a'</i>	65	2.0903	ω_1	<i>a'</i>	53	0.9976
	ω_2	<i>a'</i>	117	28.1357	ω_2	<i>a'</i>	96	8.813	ω_2	<i>a'</i>	78	4.0314
	ω_3	<i>a''</i>	143	0.0344	ω_3	<i>a''</i>	140	0.0994	ω_3	<i>a''</i>	118	0.239
	ω_4	<i>a''</i>	177	0.5674	ω_4	<i>a''</i>	177	0.5368	ω_4	<i>a''</i>	174	0.5232
	ω_5	<i>a'</i>	301	3.4389	ω_5	<i>a'</i>	300	3.1257	ω_5	<i>a'</i>	298	2.859
	ω_6	<i>a'</i>	517	3.1099	ω_6	<i>a'</i>	517	2.5025	ω_6	<i>a'</i>	515	1.7763
	ω_7	<i>a''</i>	559	11.9737	ω_7	<i>a''</i>	559	11.7536	ω_7	<i>a''</i>	553	11.3609
	ω_8	<i>a''</i>	790	1.2049	ω_8	<i>a''</i>	790	1.3338	ω_8	<i>a''</i>	786	1.1523
	ω_9	<i>a''</i>	891	47.0669	ω_9	<i>a''</i>	895	45.5888	ω_9	<i>a''</i>	901	43.4369
	ω_{10}	<i>a'</i>	910	2.3265	ω_{10}	<i>a'</i>	909	1.948	ω_{10}	<i>a'</i>	908	1.3433
	ω_{11}	<i>a''</i>	988	8.6134	ω_{11}	<i>a''</i>	987	9.6797	ω_{11}	<i>a''</i>	979	12.7325
	ω_{12}	<i>a'</i>	1014	0.9503	ω_{12}	<i>a'</i>	1012	0.6798	ω_{12}	<i>a'</i>	1010	0.4777
	ω_{13}	<i>a''</i>	1023	15.1567	ω_{13}	<i>a''</i>	1024	12.9624	ω_{13}	<i>a''</i>	1016	9.2426
	ω_{14}	<i>a''</i>	1101	23.3535	ω_{14}	<i>a''</i>	1099	20.3715	ω_{14}	<i>a''</i>	1087	18.6096
	ω_{15}	<i>a'</i>	1234	0.8071	ω_{15}	<i>a'</i>	1234	0.5815	ω_{15}	<i>a'</i>	1234	0.3229
	ω_{16}	<i>a'</i>	1317	9.8519	ω_{16}	<i>a'</i>	1318	7.7886	ω_{16}	<i>a'</i>	1318	5.8376
	ω_{17}	<i>a'</i>	1330	4.2207	ω_{17}	<i>a'</i>	1329	4.191	ω_{17}	<i>a'</i>	1326	2.9818
	ω_{18}	<i>a'</i>	1414	0.125	ω_{18}	<i>a'</i>	1415	0.1226	ω_{18}	<i>a'</i>	1415	0.1779
	ω_{19}	<i>a'</i>	1476	10.003	ω_{19}	<i>a'</i>	1477	9.2973	ω_{19}	<i>a'</i>	1477	7.413
	ω_{20}	<i>a'</i>	1637	22.455	ω_{20}	<i>a'</i>	1638	21.2635	ω_{20}	<i>a'</i>	1640	19.6006
	ω_{21}	<i>a'</i>	1699	5.1052	ω_{21}	<i>a'</i>	1700	4.9818	ω_{21}	<i>a'</i>	1702	4.7958
	ω_{22}	<i>a'</i>	3090	33.2253	ω_{22}	<i>a'</i>	3099	22.2848	ω_{22}	<i>a'</i>	3109	12.1904
	ω_{23}	<i>a'</i>	3105	203.7414	ω_{23}	<i>a'</i>	3112	193.8479	ω_{23}	<i>a'</i>	3121	155.8923
	ω_{24}	<i>a'</i>	3119	16.3313	ω_{24}	<i>a'</i>	3124	12.5183	ω_{24}	<i>a'</i>	3131	10.1809
	ω_{25}	<i>a'</i>	3133	29.9672	ω_{25}	<i>a'</i>	3135	30.4634	ω_{25}	<i>a'</i>	3138	32.9146
	ω_{26}	<i>a'</i>	3204	27.573	ω_{26}	<i>a'</i>	3211	22.7311	ω_{26}	<i>a'</i>	3219	16.1659
	ω_{27}	<i>a'</i>	3217	20.0955	ω_{27}	<i>a'</i>	3219	18.6065	ω_{27}	<i>a'</i>	3223	16.8383
	zpe		224.8		zpe		224.8		zpe		224.5	

Table D35: Calculated harmonic frequencies and mode assignments for the X...C₄H₆ 4*trans* def2QZVP complexes. All frequencies and intensities are in cm⁻¹ and km mol⁻¹ and zero-point energies are in kJ mol⁻¹.

Cl ⁻ ...C ₄ H ₆				
	Mode	Symmetry	Frequency (cm ⁻¹)	Intensity (km mol ⁻¹)
def2QZVP	ω_1	<i>a'</i>	22	5.3577
	ω_2	<i>a''</i>	88	0.3754
	ω_3	<i>a'</i>	119	35.507
	ω_4	<i>a''</i>	178	0.5115
	ω_5	<i>a'</i>	303	0.117
	ω_6	<i>a'</i>	519	4.3976
	ω_7	<i>a''</i>	567	8.3949
	ω_8	<i>a''</i>	790	1.1395
	ω_9	<i>a''</i>	888	45.1181
	ω_{10}	<i>a'</i>	916	0.3374
	ω_{11}	<i>a''</i>	991	10.5662
	ω_{12}	<i>a'</i>	1011	2.4457
	ω_{13}	<i>a''</i>	1030	29.5465
	ω_{14}	<i>a''</i>	1063	19.0873
	ω_{15}	<i>a'</i>	1229	5.0643
	ω_{16}	<i>a'</i>	1309	2.1284
	ω_{17}	<i>a'</i>	1314	3.3957
	ω_{18}	<i>a'</i>	1423	1.0249
	ω_{19}	<i>a'</i>	1489	0.5477
	ω_{20}	<i>a'</i>	1640	9.7799
	ω_{21}	<i>a'</i>	1698	51.662
	ω_{22}	<i>a'</i>	3055	284.6219
	ω_{23}	<i>a'</i>	3137	15.153
	ω_{24}	<i>a'</i>	3154	14.2318
	ω_{25}	<i>a'</i>	3163	29.2919
	ω_{26}	<i>a'</i>	3174	87.3283
	ω_{27}	<i>a'</i>	3238	21.9854
		zpe	224.3	

Table D36: Calculated harmonic frequencies and mode assignments for the X...C₄H₆ 4*trans* AVTZ complexes. All frequencies and intensities are in cm⁻¹ and km mol⁻¹ and zero-point energies are in kJ mol⁻¹.

Cl ⁻ ...C ₄ H ₆				Br ⁻ ...C ₄ H ₆				
	Mode	Symmetry	Frequency (cm ⁻¹)	Intensity (km mol ⁻¹)	Mode	Symmetry	Frequency (cm ⁻¹)	Intensity (km mol ⁻¹)
AVTZ	ω_1	<i>a'</i>	22	5.2613	ω_1	<i>a'</i>	8	1.429
	ω_2	<i>a''</i>	88	0.3444	ω_2	<i>a''</i>	92	0.0158
	ω_3	<i>a'</i>	118	35.0704	ω_3	<i>a'</i>	102	12.83
	ω_4	<i>a''</i>	176	0.5288	ω_4	<i>a''</i>	174	0.4908
	ω_5	<i>a'</i>	302	0.0902	ω_5	<i>a'</i>	300	0.2361
	ω_6	<i>a'</i>	517	4.503	ω_6	<i>a'</i>	516	3.528
	ω_7	<i>a''</i>	565	8.1192	ω_7	<i>a''</i>	568	6.961
	ω_8	<i>a''</i>	788	1.1786	ω_8	<i>a''</i>	789	1.5409
	ω_9	<i>a''</i>	890	44.3099	ω_9	<i>a''</i>	895	43.0369
	ω_{10}	<i>a'</i>	914	0.3577	ω_{10}	<i>a'</i>	914	0.4383
	ω_{11}	<i>a''</i>	985	8.3169	ω_{11}	<i>a''</i>	984	10.4818
	ω_{12}	<i>a'</i>	1008	2.6353	ω_{12}	<i>a'</i>	1008	5.1586
	ω_{13}	<i>a''</i>	1038	41.8276	ω_{13}	<i>a''</i>	1029	30.5661
	ω_{14}	<i>a''</i>	1063	9.0787	ω_{14}	<i>a''</i>	1062	16.5129
	ω_{15}	<i>a'</i>	1226	4.7349	ω_{15}	<i>a'</i>	1226	2.0521
	ω_{16}	<i>a'</i>	1306	1.9509	ω_{16}	<i>a'</i>	1308	1.9279
	ω_{17}	<i>a'</i>	1311	3.4573	ω_{17}	<i>a'</i>	1312	3.6365
	ω_{18}	<i>a'</i>	1421	0.7532	ω_{18}	<i>a'</i>	1419	2.7438
	ω_{19}	<i>a'</i>	1487	0.2617	ω_{19}	<i>a'</i>	1482	0.8026
	ω_{20}	<i>a'</i>	1637	9.5472	ω_{20}	<i>a'</i>	1638	10.6844
	ω_{21}	<i>a'</i>	1696	54.0451	ω_{21}	<i>a'</i>	1698	50.8915
	ω_{22}	<i>a'</i>	3056	281.2455	ω_{22}	<i>a'</i>	3077	208.4803
	ω_{23}	<i>a'</i>	3133	14.9009	ω_{23}	<i>a'</i>	3133	16.3506
	ω_{24}	<i>a'</i>	3150	13.4448	ω_{24}	<i>a'</i>	3151	12.0202
	ω_{25}	<i>a'</i>	3158	20.7886	ω_{25}	<i>a'</i>	3161	8.6858
	ω_{26}	<i>a'</i>	3173	96.0755	ω_{26}	<i>a'</i>	3190	77.1545
	ω_{27}	<i>a'</i>	3233	22.3046	ω_{27}	<i>a'</i>	3235	21.2793
		zpe	224.1			zpe	224.1	

Table D37: Calculated harmonic frequencies and mode assignments for the X...C₄H₆ 1*cis* def2QZVP complexes. All frequencies and intensities are in cm⁻¹ and km mol⁻¹ and zero-point energies are in kJ mol⁻¹.

Cl...C ₄ H ₆				Br...C ₄ H ₆				
	Mode	Symmetry	Frequency (cm ⁻¹)	Intensity (km mol ⁻¹)	Mode	Symmetry	Frequency (cm ⁻¹)	Intensity (km mol ⁻¹)
def2QZVP	ω_1	a''	123 <i>i</i>	2.1527	ω_1	a''	150 <i>i</i>	0.3945
	ω_2	a'	65	0.0011	ω_2	a'	60	0.0076
	ω_3	a'	82	0.0639	ω_3	a''	76	1.1215
	ω_4	a''	181	21.7969	ω_4	a'	77	0.0628
	ω_5	a'	311	0.0223	ω_5	a'	311	0.0255
	ω_6	a'	563	4.8398	ω_6	a''	557	3.7525
	ω_7	a''	636	13.1678	ω_7	a'	563	4.7252
	ω_8	a''	793	52.2384	ω_8	a''	761	5.4252
	ω_9	a'	889	0.1759	ω_9	a'	889	0.2398
	ω_{10}	a''	939	34.4837	ω_{10}	a''	938	22.7792
	ω_{11}	a''	977	0.1433	ω_{11}	a''	961	23.1329
	ω_{12}	a''	1034	19.9757	ω_{12}	a''	1030	0.0298
	ω_{13}	a'	1066	0.4317	ω_{13}	a''	1040	41.4506
	ω_{14}	a''	1079	6.7719	ω_{14}	a'	1066	0.5973
	ω_{15}	a'	1114	13.3328	ω_{15}	a'	1114	14.6042
	ω_{16}	a'	1321	0.2682	ω_{16}	a'	1321	0.3937
	ω_{17}	a'	1366	1.586	ω_{17}	a'	1364	2.3874
	ω_{18}	a'	1446	3.7367	ω_{18}	a'	1445	3.6759
	ω_{19}	a'	1481	15.9299	ω_{19}	a'	1478	16.2169
	ω_{20}	a'	1697	2.4555	ω_{20}	a'	1690	2.9156
	ω_{21}	a'	1718	1.9311	ω_{21}	a'	1698	1.5852
	ω_{22}	a'	3162	1.6718	ω_{22}	a'	3162	1.8371
	ω_{23}	a'	3167	15.427	ω_{23}	a'	3167	13.2371
	ω_{24}	a'	3169	9.0076	ω_{24}	a'	3168	10.7472
	ω_{25}	a'	3184	7.0881	ω_{25}	a'	3184	7.4646
	ω_{26}	a'	3252	7.5009	ω_{26}	a'	3251	7.447
	ω_{27}	a'	3256	7.8137	ω_{27}	a'	3256	8.1411
zpe				227.0	zpe			

Table D38: Calculated harmonic frequencies and mode assignments for the X...C₄H₆ 1*cis* AVTZ complexes. All frequencies and intensities are in cm⁻¹ and km mol⁻¹ and zero-point energies are in kJ mol⁻¹.

Br...C ₄ H ₆				I...C ₄ H ₆				
	Mode	Symmetry	Frequency (cm ⁻¹)	Intensity (km mol ⁻¹)	Mode	Symmetry	Frequency (cm ⁻¹)	Intensity (km mol ⁻¹)
AVTZ	ω_1	a''	144 <i>i</i>	1.6317	ω_1	a''	156 <i>i</i>	1.3633
	ω_2	a'	68	0.0211	ω_2	a'	39	0.0038
	ω_3	a'	86	0.1094	ω_3	a'	52	0.0249
	ω_4	a''	111	4.3285	ω_4	a''	74	1.6298
	ω_5	a'	311	0.0284	ω_5	a'	304	0.0172
	ω_6	a'	560	4.9186	ω_6	a''	550	3.9453
	ω_7	a''	571	0.7954	ω_7	a'	559	5.3305
	ω_8	a''	738	3.6967	ω_8	a''	738	2.5778
	ω_9	a'	888	0.3207	ω_9	a'	887	0.2273
	ω_{10}	a''	934	17.6424	ω_{10}	a''	932	12.1942
	ω_{11}	a''	957	31.8361	ω_{11}	a''	951	39.2685
	ω_{12}	a''	1007	2.3604	ω_{12}	a''	1004	1.0034
	ω_{13}	a''	1038	22.1458	ω_{13}	a''	1037	24.5421
	ω_{14}	a'	1064	0.6735	ω_{14}	a'	1060	0.7829
	ω_{15}	a'	1110	15.3908	ω_{15}	a'	1110	14.9759
	ω_{16}	a'	1318	0.6126	ω_{16}	a'	1317	0.4043
	ω_{17}	a'	1367	2.157	ω_{17}	a'	1361	2.205
	ω_{18}	a'	1442	3.5834	ω_{18}	a'	1440	3.5663
	ω_{19}	a'	1483	17.8206	ω_{19}	a'	1475	16.2079
	ω_{20}	a'	1693	2.4653	ω_{20}	a'	1691	1.9386
	ω_{21}	a'	1779	1.6928	ω_{21}	a'	1699	2.9211
	ω_{22}	a'	3157	2.5791	ω_{22}	a'	3156	1.8532
	ω_{23}	a'	3163	9.1336	ω_{23}	a'	3161	15.654
	ω_{24}	a'	3164	15.155	ω_{24}	a'	3164	10.9465
	ω_{25}	a'	3180	6.037	ω_{25}	a'	3180	6.4813
	ω_{26}	a'	3246	7.2362	ω_{26}	a'	3247	9.3204
	ω_{27}	a'	3251	8.3395	ω_{27}	a'	3251	7.8784
		zpe	225.4			zpe	223.9	

Table D39: Calculated harmonic frequencies and mode assignments for the X...C₄H₆ 4*cis* AVTZ complexes. All frequencies and intensities are in cm⁻¹ and km mol⁻¹ and zero-point energies are in kJ mol⁻¹.

Br...C ₄ H ₆				
	Mode	Symmetry	Frequency (cm ⁻¹)	Intensity (km mol ⁻¹)
AVTZ	ω_1	<i>a''</i>	177 <i>i</i>	1.4356
	ω_2	<i>a'</i>	10	0.0002
	ω_3	<i>a'</i>	43	0.0017
	ω_4	<i>a''</i>	99	25.2218
	ω_5	<i>a'</i>	303	0.0415
	ω_6	<i>a''</i>	535	0.3001
	ω_7	<i>a'</i>	559	5.4148
	ω_8	<i>a''</i>	741	22.5611
	ω_9	<i>a'</i>	885	0.1604
	ω_{10}	<i>a''</i>	939	38.6298
	ω_{11}	<i>a''</i>	998	0.0152
	ω_{12}	<i>a''</i>	1035	39.0717
	ω_{13}	<i>a'</i>	1060	0.2522
	ω_{14}	<i>a'</i>	1110	8.7448
	ω_{15}	<i>a'</i>	1319	0.8885
	ω_{16}	<i>a'</i>	1378	0.4121
	ω_{17}	<i>a'</i>	1441	6.7868
	ω_{18}	<i>a'</i>	1491	22.0598
	ω_{19}	<i>a''</i>	1491	3139.9708
	ω_{20}	<i>a'</i>	1701	5.2765
	ω_{21}	<i>a'</i>	2164	12.3884
	ω_{22}	<i>a'</i>	3156	2.5045
	ω_{23}	<i>a'</i>	3164	9.8509
	ω_{24}	<i>a'</i>	3167	28.5462
	ω_{25}	<i>a'</i>	3188	1.3027
	ω_{26}	<i>a'</i>	3248	9.6509
	ω_{27}	<i>a'</i>	3252	7.1456
		zpe	230.1	

Table D40: Calculated harmonic frequencies and mode assignments for the X...C₄H₆ 7*cis* def2QZVP complexes. All frequencies and intensities are in cm⁻¹ and km mol⁻¹ and zero-point energies are in kJ mol⁻¹.

Cl...C ₄ H ₆				Br...C ₄ H ₆				I...C ₄ H ₆				
	Mode	Symmetry	Frequency (cm ⁻¹)	Intensity (km mol ⁻¹)	Mode	Symmetry	Frequency (cm ⁻¹)	Intensity (km mol ⁻¹)	Mode	Symmetry	Frequency (km mol ⁻¹)	Intensity
def2QZVP	ω_1	<i>a</i>	122 <i>i</i>	0.1728	ω_1	<i>a</i>	126 <i>i</i>	0.05	ω_1	<i>a</i>	132 <i>i</i>	0.0339
	ω_2	<i>a</i>	135	5.4046	ω_2	<i>a</i>	108	1.4407	ω_2	<i>a</i>	88	0.1916
	ω_3	<i>a</i>	235	0.3848	ω_3	<i>a</i>	180	4.4357	ω_3	<i>a</i>	138	8.6449
	ω_4	<i>a</i>	277	19.2037	ω_4	<i>a</i>	292	7.7063	ω_4	<i>a</i>	289	6.1638
	ω_5	<i>a</i>	306	5.4185	ω_5	<i>a</i>	313	14.6147	ω_5	<i>a</i>	316	10.8321
	ω_6	<i>a</i>	558	9.6848	ω_6	<i>a</i>	554	10.5442	ω_6	<i>a</i>	551	12.9701
	ω_7	<i>a</i>	566	3.6755	ω_7	<i>a</i>	567	5.494	ω_7	<i>a</i>	565	7.9535
	ω_8	<i>a</i>	746	2.5761	ω_8	<i>a</i>	752	0.6956	ω_8	<i>a</i>	759	1.4263
	ω_9	<i>a</i>	891	8.0286	ω_9	<i>a</i>	890	4.8811	ω_9	<i>a</i>	889	1.9804
	ω_{10}	<i>a</i>	961	48.6801	ω_{10}	<i>a</i>	963	38.8054	ω_{10}	<i>a</i>	966	9.6394
	ω_{11}	<i>a</i>	996	49.1989	ω_{11}	<i>a</i>	987	62.772	ω_{11}	<i>a</i>	981	89.456
	ω_{12}	<i>a</i>	1025	2.8723	ω_{12}	<i>a</i>	1036	2.0482	ω_{12}	<i>a</i>	1040	1.0136
	ω_{13}	<i>a</i>	1050	11.1581	ω_{13}	<i>a</i>	1045	11.9203	ω_{13}	<i>a</i>	1045	18.896
	ω_{14}	<i>a</i>	1068	1.2203	ω_{14}	<i>a</i>	1067	0.8158	ω_{14}	<i>a</i>	1065	0.488
	ω_{15}	<i>a</i>	1115	13.8932	ω_{15}	<i>a</i>	1115	15.702	ω_{15}	<i>a</i>	1114	16.149
	ω_{16}	<i>a</i>	1316	16.0964	ω_{16}	<i>a</i>	1318	15.4672	ω_{16}	<i>a</i>	1322	9.5069
	ω_{17}	<i>a</i>	1376	4.4397	ω_{17}	<i>a</i>	1377	5.7367	ω_{17}	<i>a</i>	1378	6.0712
	ω_{18}	<i>a</i>	1448	6.2333	ω_{18}	<i>a</i>	1448	6.0819	ω_{18}	<i>a</i>	1447	5.4387
	ω_{19}	<i>a</i>	1498	30.6463	ω_{19}	<i>a</i>	1500	25.1514	ω_{19}	<i>a</i>	1502	19.8046
	ω_{20}	<i>a</i>	1644	162.6252	ω_{20}	<i>a</i>	1661	181.8574	ω_{20}	<i>a</i>	1686	139.8021
	ω_{21}	<i>a</i>	1980	222.8588	ω_{21}	<i>a</i>	2032	323.5052	ω_{21}	<i>a</i>	2137	508.8677
	ω_{22}	<i>a</i>	3176	2.7022	ω_{22}	<i>a</i>	3175	1.6692	ω_{22}	<i>a</i>	3170	2.7901
	ω_{23}	<i>a</i>	3184	6.4909	ω_{23}	<i>a</i>	3179	9.8203	ω_{23}	<i>a</i>	3176	13.3944
	ω_{24}	<i>a</i>	3191	7.5913	ω_{24}	<i>a</i>	3187	6.3793	ω_{24}	<i>a</i>	3180	3.7227
	ω_{25}	<i>a</i>	3206	7.197	ω_{25}	<i>a</i>	3202	10.7695	ω_{25}	<i>a</i>	3198	16.8299
	ω_{26}	<i>a</i>	3263	4.6745	ω_{26}	<i>a</i>	3262	4.963	ω_{26}	<i>a</i>	3260	5.1029
	ω_{27}	<i>a</i>	3284	0.4254	ω_{27}	<i>a</i>	3277	0.6048	ω_{27}	<i>a</i>	3268.3771	1.0619
	zpe		230.3		zpe		230.2		zpe		230.5	

Table D41: Calculated harmonic frequencies and mode assignments for the X...C₄H₆ 7*cis* AVTZ complexes. All frequencies and intensities are in cm⁻¹ and km mol⁻¹ and zero-point energies are in kJ mol⁻¹.

Cl...C ₄ H ₆				Br...C ₄ H ₆				I...C ₄ H ₆				
	Mode	Symmetry	Frequency (cm ⁻¹)	Intensity (km mol ⁻¹)	Mode	Symmetry	Frequency (cm ⁻¹)	Intensity (km mol ⁻¹)	Mode	Symmetry	Frequency (cm ⁻¹)	Intensity (km mol ⁻¹)
AVTZ	ω_1	<i>a</i>	132 <i>i</i>	0.1493	ω_1	<i>a</i>	140 <i>i</i>	0.0611	ω_1	<i>a</i>	148 <i>i</i>	0.0617
	ω_2	<i>a</i>	134	5.6246	ω_2	<i>a</i>	108	1.7258	ω_2	<i>a</i>	87	0.3512
	ω_3	<i>a</i>	235	0.1496	ω_3	<i>a</i>	180	3.8409	ω_3	<i>a</i>	135	8.2517
	ω_4	<i>a</i>	260	16.6642	ω_4	<i>a</i>	277	9.9927	ω_4	<i>a</i>	267	7.3345
	ω_5	<i>a</i>	304	3.352	ω_5	<i>a</i>	306	5.1063	ω_5	<i>a</i>	306	2.6674
	ω_6	<i>a</i>	555	8.7355	ω_6	<i>a</i>	551	9.2724	ω_6	<i>a</i>	548	11.677
	ω_7	<i>a</i>	562	4.163	ω_7	<i>a</i>	562	6.855	ω_7	<i>a</i>	561	9.2814
	ω_8	<i>a</i>	737	2.8593	ω_8	<i>a</i>	741	0.8445	ω_8	<i>a</i>	747	1.3295
	ω_9	<i>a</i>	889	8.3173	ω_9	<i>a</i>	888	4.3663	ω_9	<i>a</i>	887	1.5645
	ω_{10}	<i>a</i>	959	51.614	ω_{10}	<i>a</i>	962	33.5059	ω_{10}	<i>a</i>	960	5.9311
	ω_{11}	<i>a</i>	994	45.2285	ω_{11}	<i>a</i>	985	65.9307	ω_{11}	<i>a</i>	980	98.1133
	ω_{12}	<i>a</i>	1015	9.6387	ω_{12}	<i>a</i>	1016	10.7328	ω_{12}	<i>a</i>	1020	5.8375
	ω_{13}	<i>a</i>	1039	12.2797	ω_{13}	<i>a</i>	1037	11.7654	ω_{13}	<i>a</i>	1040	17.2189
	ω_{14}	<i>a</i>	1064	1.3235	ω_{14}	<i>a</i>	1063	0.77	ω_{14}	<i>a</i>	1062	0.4217
	ω_{15}	<i>a</i>	1112	12.3975	ω_{15}	<i>a</i>	1111	14.2489	ω_{15}	<i>a</i>	1110	15.1556
	ω_{16}	<i>a</i>	1313	13.8304	ω_{16}	<i>a</i>	1315	13.0399	ω_{16}	<i>a</i>	1319	8.3615
	ω_{17}	<i>a</i>	1374	4.8439	ω_{17}	<i>a</i>	1375	6.0048	ω_{17}	<i>a</i>	1376	6.3102
	ω_{18}	<i>a</i>	1445	6.2799	ω_{18}	<i>a</i>	1444	6.0998	ω_{18}	<i>a</i>	1444	5.5138
	ω_{19}	<i>a</i>	1498	32.2596	ω_{19}	<i>a</i>	1501	25.6795	ω_{19}	<i>a</i>	1502	20.3847
	ω_{20}	<i>a</i>	1641	161.5686	ω_{20}	<i>a</i>	1659	175.1954	ω_{20}	<i>a</i>	1683	138.7014
	ω_{21}	<i>a</i>	1979	220.4422	ω_{21}	<i>a</i>	2044	337.9873	ω_{21}	<i>a</i>	2156	527.0134
	ω_{22}	<i>a</i>	3172	2.8739	ω_{22}	<i>a</i>	3170	1.6812	ω_{22}	<i>a</i>	3166	1.49
	ω_{23}	<i>a</i>	3179	6.4757	ω_{23}	<i>a</i>	3174	8.4712	ω_{23}	<i>a</i>	3171	11.1161
	ω_{24}	<i>a</i>	3186	6.8303	ω_{24}	<i>a</i>	3181	5.6169	ω_{24}	<i>a</i>	3174	3.6438
	ω_{25}	<i>a</i>	3202	9.0455	ω_{25}	<i>a</i>	3198	13.0761	ω_{25}	<i>a</i>	3194	18.7549
	ω_{26}	<i>a</i>	3259	4.8752	ω_{26}	<i>a</i>	3257	5.4257	ω_{26}	<i>a</i>	3255	5.794
	ω_{27}	<i>a</i>	3279	0.4192	ω_{27}	<i>a</i>	3272	0.6602	ω_{27}	<i>a</i>	3263	1.193
		zpe	229.6		zpe		229.5		zpe		229.8	

Table D42: Calculated harmonic frequencies and mode assignments for the X...C₄H₆ 1*trans* def2QZVP complexes. All frequencies and intensities are in cm⁻¹ and km mol⁻¹ and zero-point energies are in kJ mol⁻¹.

I...C ₄ H ₆				
	Mode	Symmetry	Frequency (cm ⁻¹)	Intensity (km mol ⁻¹)
def2QZVP	ω_1	a'	54	0
	ω_2	a''	93	0
	ω_3	a'	120	0
	ω_4	a''	237	0
	ω_5	a'	436	0
	ω_6	a'	544	0
	ω_7	a''	629	0
	ω_8	a''	788	0
	ω_9	a'	1045	0
	ω_{10}	a''	1116	0
	ω_{11}	a''	1155	0
	ω_{12}	a'	1254	0
	ω_{13}	a''	1262	0
	ω_{14}	a''	1310	0
	ω_{15}	a'	1339	0
	ω_{16}	a'	1372	0
	ω_{17}	a'	1415	0
	ω_{18}	a'	1640	0
	ω_{19}	a'	1847	0
	ω_{20}	a'	1983	0
	ω_{21}	a'	2282	0
	ω_{22}	a'	3144	0
	ω_{23}	a'	3163	0
	ω_{24}	a'	3179	0
	ω_{25}	a'	3191	0
	ω_{26}	a'	3252	0
	ω_{27}	a'	3262	0
		zpe	245.9	

Table D43: Calculated harmonic frequencies and mode assignments for the X...C₄H₆ 1*trans* AVTZ complexes. All frequencies and intensities are in cm⁻¹ and km mol⁻¹ and zero-point energies are in kJ mol⁻¹.

Cl...C ₄ H ₆				I...C ₄ H ₆				
	Mode	Symmetry	Frequency (cm ⁻¹)	Intensity (km mol ⁻¹)	Mode	Symmetry	Frequency (cm ⁻¹)	Intensity (km mol ⁻¹)
AVTZ	ω_1	<i>a'</i>	37	0.0007	ω_1	<i>a'</i>	33	0.0027
	ω_2	<i>a''</i>	57	0.0728	ω_2	<i>a''</i>	40	0.0649
	ω_3	<i>a'</i>	60	0.0049	ω_3	<i>a'</i>	55	0.0215
	ω_4	<i>a''</i>	168	0.7529	ω_4	<i>a''</i>	167	0.718
	ω_5	<i>a'</i>	297	2.7813	ω_5	<i>a'</i>	297	2.8017
	ω_6	<i>a'</i>	513	0.0363	ω_6	<i>a'</i>	513	0.0632
	ω_7	<i>a''</i>	545	9.5621	ω_7	<i>a''</i>	543	8.9758
	ω_8	<i>a''</i>	779	0.0676	ω_8	<i>a''</i>	779	0.1885
	ω_9	<i>a'</i>	905	0.0965	ω_9	<i>a'</i>	905	0.2384
	ω_{10}	<i>a''</i>	937	15.3064	ω_{10}	<i>a''</i>	937	8.9701
	ω_{11}	<i>a''</i>	940	61.5469	ω_{11}	<i>a''</i>	940	62.6183
	ω_{12}	<i>a''</i>	997	0.2584	ω_{12}	<i>a''</i>	996	0.0246
	ω_{13}	<i>a'</i>	999	2.7626	ω_{13}	<i>a'</i>	998	3.8738
	ω_{14}	<i>a''</i>	1055	32.8145	ω_{14}	<i>a''</i>	1054	32.9935
	ω_{15}	<i>a'</i>	1231	0.4428	ω_{15}	<i>a'</i>	1230	1.0812
	ω_{16}	<i>a'</i>	1314	0.6663	ω_{16}	<i>a'</i>	1314	1.7885
	ω_{17}	<i>a'</i>	1318	3.3289	ω_{17}	<i>a'</i>	1317	3.7584
	ω_{18}	<i>a'</i>	1417	5.6055	ω_{18}	<i>a'</i>	1416	7.052
	ω_{19}	<i>a'</i>	1479	0.1368	ω_{19}	<i>a'</i>	1478	0.2864
	ω_{20}	<i>a'</i>	1647	20.7495	ω_{20}	<i>a'</i>	1646	20.9809
	ω_{21}	<i>a'</i>	1709	0.087	ω_{21}	<i>a'</i>	1708	0.8263
	ω_{22}	<i>a'</i>	3152	2.2647	ω_{22}	<i>a'</i>	3151	0.5927
	ω_{23}	<i>a'</i>	3156	11.761	ω_{23}	<i>a'</i>	3155	14.038
	ω_{24}	<i>a'</i>	3164	1.6861	ω_{24}	<i>a'</i>	3162	0.3384
	ω_{25}	<i>a'</i>	3169	7.0454	ω_{25}	<i>a'</i>	3167	8.7163
	ω_{26}	<i>a'</i>	3248	9.1022	ω_{26}	<i>a'</i>	3247	5.2318
	ω_{27}	<i>a'</i>	3249	10.0008	ω_{27}	<i>a'</i>	3248	14.8051
		zpe	224.5			zpe	224.3	

Table D44: Calculated harmonic frequencies and mode assignments for the X...C₄H₆ 2*trans* AVTZ complexes. All frequencies and intensities are in cm⁻¹ and km mol⁻¹ and zero-point energies are in kJ mol⁻¹.

Cl...C ₄ H ₆				
	Mode	Symmetry	Frequency (cm ⁻¹)	Intensity (km mol ⁻¹)
AVTZ	ω_1	<i>a'</i>	36	0.0021
	ω_2	<i>a''</i>	47	0.0715
	ω_3	<i>a'</i>	51	0.0391
	ω_4	<i>a''</i>	169	0.6758
	ω_5	<i>a'</i>	292	2.3657
	ω_6	<i>a'</i>	513	0.1196
	ω_7	<i>a''</i>	542	11.8179
	ω_8	<i>a''</i>	779	0.0771
	ω_9	<i>a'</i>	905	0.0381
	ω_{10}	<i>a''</i>	937	32.4107
	ω_{11}	<i>a''</i>	942	42.2822
	ω_{12}	<i>a''</i>	998	0.2236
	ω_{13}	<i>a'</i>	1001	1.1026
	ω_{14}	<i>a''</i>	1058	32.0716
	ω_{15}	<i>a'</i>	1232	0.0363
	ω_{16}	<i>a'</i>	1316	0.1185
	ω_{17}	<i>a'</i>	1319	0.815
	ω_{18}	<i>a'</i>	1418	2.572
	ω_{19}	<i>a'</i>	1481	0.4434
	ω_{20}	<i>a'</i>	1647	18.8068
	ω_{21}	<i>a'</i>	1710	0.0396
	ω_{22}	<i>a'</i>	3151	1.2558
	ω_{23}	<i>a'</i>	3155	9.9907
	ω_{24}	<i>a'</i>	3164	3.5412
	ω_{25}	<i>a'</i>	3170	6.1626
	ω_{26}	<i>a'</i>	3247	8.9177
	ω_{27}	<i>a'</i>	3250	8.4587
		zpe	224.5	

Table D45: Calculated harmonic frequencies and mode assignments for the X...C₄H₆ 3*trans* def2QZVP complexes. All frequencies and intensities are in cm⁻¹ and km mol⁻¹ and zero-point energies are in kJ mol⁻¹.

Cl...C ₄ H ₆				I...C ₄ H ₆				
	Mode	Symmetry	Frequency (cm ⁻¹)	Intensity (km mol ⁻¹)	Mode	Symmetry	Frequency (cm ⁻¹)	Intensity (km mol ⁻¹)
def2QZVP	ω_1	<i>a'</i>	13	0.0006	ω_1	<i>a'</i>	11	0.0013
	ω_2	<i>a''</i>	24	0.0083	ω_2	<i>a'</i>	32	0.0081
	ω_3	<i>a'</i>	36	0.0015	ω_3	<i>a''</i>	36	0.413
	ω_4	<i>a''</i>	171	0.5649	ω_4	<i>a''</i>	176	0.0047
	ω_5	<i>a'</i>	295	2.7309	ω_5	<i>a'</i>	295	2.7539
	ω_6	<i>a'</i>	516	0.0086	ω_6	<i>a'</i>	516	0.0106
	ω_7	<i>a''</i>	545	11.2494	ω_7	<i>a''</i>	543	8.2429
	ω_8	<i>a''</i>	784	0.0063	ω_8	<i>a''</i>	785	0.8431
	ω_9	<i>a'</i>	906	0.0603	ω_9	<i>a'</i>	906	0.1152
	ω_{10}	<i>a''</i>	939	37.8244	ω_{10}	<i>a''</i>	939	40.0203
	ω_{11}	<i>a''</i>	945	38.5771	ω_{11}	<i>a''</i>	980	7.0784
	ω_{12}	<i>a'</i>	1001	1.9996	ω_{12}	<i>a'</i>	1001	2.2251
	ω_{13}	<i>a''</i>	1003	0.0023	ω_{13}	<i>a''</i>	1003	0.0002
	ω_{14}	<i>a''</i>	1058	32.695	ω_{14}	<i>a''</i>	1059	29.982
	ω_{15}	<i>a'</i>	1233	0.0476	ω_{15}	<i>a'</i>	1233	0.0993
	ω_{16}	<i>a'</i>	1316	0.2469	ω_{16}	<i>a'</i>	1316	0.494
	ω_{17}	<i>a'</i>	1321	1.9885	ω_{17}	<i>a'</i>	1320	1.9172
	ω_{18}	<i>a'</i>	1419	6.9886	ω_{18}	<i>a'</i>	1418	8.2517
	ω_{19}	<i>a'</i>	1481	0.5563	ω_{19}	<i>a'</i>	1481	0.9775
	ω_{20}	<i>a'</i>	1650	24.9637	ω_{20}	<i>a'</i>	1650	27.2718
	ω_{21}	<i>a'</i>	1713	0.1048	ω_{21}	<i>a'</i>	1715	0.162
	ω_{22}	<i>a'</i>	3156	0.0177	ω_{22}	<i>a'</i>	3155	0.0717
	ω_{23}	<i>a'</i>	3160	14.3313	ω_{23}	<i>a'</i>	3159	15.5839
	ω_{24}	<i>a'</i>	3168	0.0284	ω_{24}	<i>a'</i>	3167	0.0215
	ω_{25}	<i>a'</i>	3172	9.7708	ω_{25}	<i>a'</i>	3171	9.7297
	ω_{26}	<i>a'</i>	3253	8.9245	ω_{26}	<i>a'</i>	3252	7.2358
	ω_{27}	<i>a'</i>	3254	8.7034	ω_{27}	<i>a'</i>	3253	9.9427
		zpe	224.5			zpe	224.7	

Table D46: Calculated harmonic frequencies and mode assignments for the X...C₄H₆ 3*trans* AVTZ complexes. All frequencies and intensities are in cm⁻¹ and km mol⁻¹ and zero-point energies are in kJ mol⁻¹.

Cl...C ₄ H ₆				I...C ₄ H ₆				
	Mode	Symmetry	Frequency (cm ⁻¹)	Intensity (km mol ⁻¹)	Mode	Symmetry	Frequency (cm ⁻¹)	Intensity (km mol ⁻¹)
AVTZ	ω_1	<i>a'</i>	13	0.0008	ω_1	<i>a'</i>	9	0.0012
	ω_2	<i>a'</i>	39	0.0047	ω_2	<i>a'</i>	36	0.014
	ω_3	<i>a''</i>	80	6.46	ω_3	<i>a''</i>	53	1.8042
	ω_4	<i>a''</i>	224	29.9653	ω_4	<i>a''</i>	185	1.4866
	ω_5	<i>a'</i>	293	2.7123	ω_5	<i>a'</i>	292	2.7567
	ω_6	<i>a'</i>	514	0.0093	ω_6	<i>a'</i>	514	0.0097
	ω_7	<i>a''</i>	543	0.7986	ω_7	<i>a''</i>	541	5.5095
	ω_8	<i>a''</i>	784	11.8764	ω_8	<i>a''</i>	781	3.6044
	ω_9	<i>a'</i>	904	0.0803	ω_9	<i>a'</i>	903	0.1307
	ω_{10}	<i>a''</i>	936	40.8465	ω_{10}	<i>a''</i>	936	39.8483
	ω_{11}	<i>a''</i>	993	0.0005	ω_{11}	<i>a''</i>	994	0.0011
	ω_{12}	<i>a'</i>	997	1.9316	ω_{12}	<i>a'</i>	996	2.0915
	ω_{13}	<i>a''</i>	1050	41.7914	ω_{13}	<i>a''</i>	1038	38.4457
	ω_{14}	<i>a'</i>	1231	0.0668	ω_{14}	<i>a''</i>	1071	0.0484
	ω_{15}	<i>a'</i>	1314	0.3966	ω_{15}	<i>a'</i>	1231	0.114
	ω_{16}	<i>a'</i>	1317	1.8343	ω_{16}	<i>a'</i>	1314	0.6377
	ω_{17}	<i>a'</i>	1417	7.0525	ω_{17}	<i>a'</i>	1317	1.7749
	ω_{18}	<i>a'</i>	1479	0.7002	ω_{18}	<i>a'</i>	1416	8.1782
	ω_{19}	<i>a''</i>	1531	3370.4944	ω_{19}	<i>a'</i>	1479	1.1152
	ω_{20}	<i>a'</i>	1647	26.458	ω_{20}	<i>a'</i>	1647	28.5143
	ω_{21}	<i>a'</i>	1715	0.0891	ω_{21}	<i>a'</i>	1715	0.1604
	ω_{22}	<i>a'</i>	3151	0.0034	ω_{22}	<i>a'</i>	3151	0.0345
	ω_{23}	<i>a'</i>	3155	15.7477	ω_{23}	<i>a'</i>	3155	16.3884
	ω_{24}	<i>a'</i>	3164	0.0442	ω_{24}	<i>a'</i>	3164	0.0127
	ω_{25}	<i>a'</i>	3167	8.9886	ω_{25}	<i>a'</i>	3167	9.0921
	ω_{26}	<i>a'</i>	3248	8.6197	ω_{26}	<i>a'</i>	3248	7.7308
	ω_{27}	<i>a'</i>	3250	9.4089	ω_{27}	<i>a'</i>	3249	9.7687
		zpe	228.2			zpe	224.9	

Table D47: Calculated harmonic frequencies and mode assignments for the X...C₄H₆ 7*trans* def2QZVP complexes. All frequencies and intensities are in cm⁻¹ and km mol⁻¹ and zero-point energies are in kJ mol⁻¹.

Cl...C ₄ H ₆				Br...C ₄ H ₆				I...C ₄ H ₆				
	Mode	Symmetry	Frequency (cm ⁻¹)	Intensity (km mol ⁻¹)	Mode	Symmetry	Frequency (cm ⁻¹)	Intensity (km mol ⁻¹)	Mode	Symmetry	Frequency (km mol ⁻¹)	Intensity
def2QZVP	ω_1	<i>a</i>	107	3.2449	ω_1	<i>a</i>	94	1.6503	ω_1	<i>a</i>	85	0.4295
	ω_2	<i>a</i>	151	1.693	ω_2	<i>a</i>	131	0.419	ω_2	<i>a</i>	123	2.8562
	ω_3	<i>a</i>	232	0.4871	ω_3	<i>a</i>	179	4.6966	ω_3	<i>a</i>	143	6.9971
	ω_4	<i>a</i>	292	4.4338	ω_4	<i>a</i>	293	3.463	ω_4	<i>a</i>	294	3.0021
	ω_5	<i>a</i>	337	14.8759	ω_5	<i>a</i>	348	9.9727	ω_5	<i>a</i>	392	13.4024
	ω_6	<i>a</i>	511	3.7179	ω_6	<i>a</i>	513	2.7916	ω_6	<i>a</i>	515	2.3435
	ω_7	<i>a</i>	578	7.5784	ω_7	<i>a</i>	572	9.1847	ω_7	<i>a</i>	569	11.858
	ω_8	<i>a</i>	773	1.0983	ω_8	<i>a</i>	779	1.3074	ω_8	<i>a</i>	788	4.592
	ω_9	<i>a</i>	910	4.3214	ω_9	<i>a</i>	909	2.8944	ω_9	<i>a</i>	908	1.5428
	ω_{10}	<i>a</i>	966	14.5541	ω_{10}	<i>a</i>	967	0.6247	ω_{10}	<i>a</i>	960	14.0272
	ω_{11}	<i>a</i>	985	70.1339	ω_{11}	<i>a</i>	980	80.1924	ω_{11}	<i>a</i>	983	63.602
	ω_{12}	<i>a</i>	1004	3.9112	ω_{12}	<i>a</i>	1004	3.6497	ω_{12}	<i>a</i>	1003	2.8527
	ω_{13}	<i>a</i>	1011	2.709	ω_{13}	<i>a</i>	1020	22.3731	ω_{13}	<i>a</i>	1024	41.762
	ω_{14}	<i>a</i>	1052	16.8069	ω_{14}	<i>a</i>	1062	15.1689	ω_{14}	<i>a</i>	1072	12.5728
	ω_{15}	<i>a</i>	1249	12.7787	ω_{15}	<i>a</i>	1247	10.9765	ω_{15}	<i>a</i>	1246	8.4601
	ω_{16}	<i>a</i>	1311	19.4142	ω_{16}	<i>a</i>	1313	18.5822	ω_{16}	<i>a</i>	1316	14.9726
	ω_{17}	<i>a</i>	1333	6.2654	ω_{17}	<i>a</i>	1331	7.6625	ω_{17}	<i>a</i>	1327	7.3898
	ω_{18}	<i>a</i>	1421	20.2411	ω_{18}	<i>a</i>	1419	21.1257	ω_{18}	<i>a</i>	1417	16.5375
	ω_{19}	<i>a</i>	1492	9.7031	ω_{19}	<i>a</i>	1492	8.7187	ω_{19}	<i>a</i>	1491	5.2037
	ω_{20}	<i>a</i>	1606	133.831	ω_{20}	<i>a</i>	1612	142.5528	ω_{20}	<i>a</i>	1621	114.457
	ω_{21}	<i>a</i>	1877	172.9202	ω_{21}	<i>a</i>	1863	174.9639	ω_{21}	<i>a</i>	1812	134.5292
	ω_{22}	<i>a</i>	3168	8.6005	ω_{22}	<i>a</i>	3167	8.024	ω_{22}	<i>a</i>	3162	3.1151
	ω_{23}	<i>a</i>	3178	3.1923	ω_{23}	<i>a</i>	3173	3.6795	ω_{23}	<i>a</i>	3164	5.5473
	ω_{24}	<i>a</i>	3186	3.2838	ω_{24}	<i>a</i>	3181	5.6784	ω_{24}	<i>a</i>	3174	3.2888
	ω_{25}	<i>a</i>	3194	3.5947	ω_{25}	<i>a</i>	3189	3.4159	ω_{25}	<i>a</i>	3182	3.5121
	ω_{26}	<i>a</i>	3261	4.3623	ω_{26}	<i>a</i>	3260	4.586	ω_{26}	<i>a</i>	3259	4.9087
	ω_{27}	<i>a</i>	3281	0.3492	ω_{27}	<i>a</i>	3274	0.5515	ω_{27}	<i>a</i>	3262	0.9424
zpe				230.1	zpe				229.5	zpe		229.0

Table D48: Calculated harmonic frequencies and mode assignments for the X...C₄H₆ 7*trans* AVTZ complexes. All frequencies and intensities are in cm⁻¹ and km mol⁻¹ and zero-point energies are in kJ mol⁻¹.

Cl...C ₄ H ₆				Br...C ₄ H ₆				I...C ₄ H ₆				
	Mode	Symmetry	Frequency (cm ⁻¹)	Intensity (km mol ⁻¹)	Mode	Symmetry	Frequency (cm ⁻¹)	Intensity (km mol ⁻¹)	Mode	Symmetry	Frequency (cm ⁻¹)	Intensity (km mol ⁻¹)
AVTZ	ω_1	<i>a</i>	105	3.1642	ω_1	<i>a</i>	94	1.5823	ω_1	<i>a</i>	84	0.4688
	ω_2	<i>a</i>	148	2.0869	ω_2	<i>a</i>	129	0.4635	ω_2	<i>a</i>	113	0.9843
	ω_3	<i>a</i>	232	0.3907	ω_3	<i>a</i>	179	4.3871	ω_3	<i>a</i>	138	8.67
	ω_4	<i>a</i>	290	4.9895	ω_4	<i>a</i>	291	3.3655	ω_4	<i>a</i>	291	2.8877
	ω_5	<i>a</i>	322	10.8227	ω_5	<i>a</i>	349	10.2278	ω_5	<i>a</i>	359	7.9277
	ω_6	<i>a</i>	509	3.5942	ω_6	<i>a</i>	510	2.7198	ω_6	<i>a</i>	512	1.5214
	ω_7	<i>a</i>	574	7.2457	ω_7	<i>a</i>	566	9.3489	ω_7	<i>a</i>	563	12.2986
	ω_8	<i>a</i>	769	1.0974	ω_8	<i>a</i>	775	1.4202	ω_8	<i>a</i>	783	4.4196
	ω_9	<i>a</i>	908	4.5911	ω_9	<i>a</i>	907	2.7039	ω_9	<i>a</i>	906	1.2727
	ω_{10}	<i>a</i>	964	10.8716	ω_{10}	<i>a</i>	963	0.1975	ω_{10}	<i>a</i>	957	8.5898
	ω_{11}	<i>a</i>	985	73.7536	ω_{11}	<i>a</i>	979	70.3369	ω_{11}	<i>a</i>	978	58.0368
	ω_{12}	<i>a</i>	999	4.4919	ω_{12}	<i>a</i>	999	5.3018	ω_{12}	<i>a</i>	999	3.5186
	ω_{13}	<i>a</i>	1008	6.8417	ω_{13}	<i>a</i>	1014	31.3205	ω_{13}	<i>a</i>	1021	54.7408
	ω_{14}	<i>a</i>	1047	15.6951	ω_{14}	<i>a</i>	1053	13.9927	ω_{14}	<i>a</i>	1073	12.9835
	ω_{15}	<i>a</i>	1245	11.9777	ω_{15}	<i>a</i>	1244	10.1699	ω_{15}	<i>a</i>	1242	7.7365
	ω_{16}	<i>a</i>	1308	16.8481	ω_{16}	<i>a</i>	1310	16.484	ω_{16}	<i>a</i>	1314	12.7967
	ω_{17}	<i>a</i>	1330	6.6423	ω_{17}	<i>a</i>	1328	8.305	ω_{17}	<i>a</i>	1324	8.0553
	ω_{18}	<i>a</i>	1419	20.1085	ω_{18}	<i>a</i>	1418	19.9707	ω_{18}	<i>a</i>	1416	15.9827
	ω_{19}	<i>a</i>	1490	10.2407	ω_{19}	<i>a</i>	1491	8.859	ω_{19}	<i>a</i>	1491	6.544
	ω_{20}	<i>a</i>	1604	132.667	ω_{20}	<i>a</i>	1610	135.8665	ω_{20}	<i>a</i>	1620	110.8854
	ω_{21}	<i>a</i>	1880	175.4378	ω_{21}	<i>a</i>	1869	180.5205	ω_{21}	<i>a</i>	1820	140.2183
	ω_{22}	<i>a</i>	3164	8.8518	ω_{22}	<i>a</i>	3163	7.9535	ω_{22}	<i>a</i>	3160	3.7033
	ω_{23}	<i>a</i>	3174	3.1819	ω_{23}	<i>a</i>	3168	3.1123	ω_{23}	<i>a</i>	3163	4.3444
	ω_{24}	<i>a</i>	3181	4.9794	ω_{24}	<i>a</i>	3176	6.1694	ω_{24}	<i>a</i>	3170	5.3873
	ω_{25}	<i>a</i>	3189	3.7579	ω_{25}	<i>a</i>	3183	3.2301	ω_{25}	<i>a</i>	3177	3.0691
	ω_{26}	<i>a</i>	3256	4.4562	ω_{26}	<i>a</i>	3255	4.773	ω_{26}	<i>a</i>	3254	5.1106
	ω_{27}	<i>a</i>	3277	0.3462	ω_{27}	<i>a</i>	3269	0.5759	ω_{27}	<i>a</i>	3261	1.0491
		zpe	229.5		zpe		229.0		zpe		228.4	

Table D49: $\text{I}^- \cdots \text{C}_8\text{H}_{12}$ and $\text{I}^- \cdots (\text{C}_4\text{H}_6)_2$ complex geometric parameters and D_0 values from DSD-PBEP86-D3BJ optimisations. zpe values are drawn from relevant harmonic frequency calculations.

	R_{I-H1} Å	R_{I-H2} Å	R_{I-H3} Å	$\angle H - I - H$ °	E_{DFT} E_h	zpe kJ mol ⁻¹	D_e kJ mol ⁻¹	D_o kJ mol ⁻¹	E_{VDE} E_h	VDE $^2P_{3/2}$ eV	VDE $^2P_{1/2}$ eV	
$\text{I}^- \cdots \text{C}_8\text{H}_{12}$	1	3.215	3.254	43.6	-608.9970149	471.1	19.7	19.4	-608.8736616	3.189	4.131	
	2	2.982	3.190		3.094	-609.0030585	471.4	35.5	35.6	-608.8735983	3.351	4.293
	3	3.007	3.766		3.184	-609.0022405	470.5	33.4	32.6			
$\text{I}^- \cdots (\text{C}_4\text{H}_6)_2$	1	R_{I-H1}	R_{I-H2}	$\angle C - C - I - C$								
		3.099	3.092			90.0	-608.9409645	448.8	54.9	56.4	-608.8049649	3.520

Table D50: Cartesian coordinates of the geometries of iodide-4-vinylcyclohexene complexes optimised with the DSD-PBEP86-D3BJ functional, in Å.

		4v.1			4v.2			4v.3		
		x	y	z	x	y	z	x	y	z
def2TZVPD	C	0.835281	-0.343663	-0.209516	-2.296644	-1.385311	1.242185	-2.940397	-1.234308	-0.993228
	C	0.670592	0.953988	0.059321	-2.821968	-1.900144	0.127611	-2.323916	-2.077719	-0.161421
	H	-0.038808	-0.985425	-0.291769	-2.373729	-1.941712	2.173385	-3.539481	-1.633267	-1.808449
	H	-0.334809	1.346891	0.191423	-3.317914	-2.867040	0.170120	-2.431458	-3.149162	-0.313412
	C	1.815922	1.917426	0.191657	-2.765084	-1.206500	-1.203977	-1.475931	-1.621315	0.991888
	H	1.942687	2.189617	1.248844	-3.764533	-0.828376	-1.460738	-0.417400	-1.806051	0.761270
	H	1.574724	2.851189	-0.329251	-2.510640	-1.930493	-1.986618	-1.698266	-2.229021	1.876589
	C	3.115730	1.331234	-0.354513	-1.758570	-0.058305	-1.202459	-1.690572	-0.141872	1.302698
	H	3.079981	1.319030	-1.452063	-0.738494	-0.464644	-1.221894	-2.663783	-0.007561	1.793477
	H	3.968274	1.954776	-0.066879	-1.877388	0.556998	-2.100040	-0.926334	0.218568	1.998680
	C	3.320770	-0.103267	0.144515	-1.917228	0.806213	0.053048	-1.670102	0.695090	0.018977
	H	3.274611	-0.093539	1.242602	-2.962184	1.142602	0.107173	-0.726270	0.492644	-0.506587
	C	2.182226	-0.989227	-0.376088	-1.621453	-0.043640	1.295024	-2.827719	0.260713	-0.888479
	C	4.651903	-0.644721	-0.272408	-1.030082	2.010252	0.006401	-1.745837	2.159468	0.316926
	H	2.354036	-1.219194	-1.438075	-0.534360	-0.179658	1.394762	-3.770365	0.677209	-0.503552
	H	2.201224	-1.953994	0.143814	-1.936902	0.498444	2.193952	-2.695474	0.696391	-1.885541
	C	5.599642	-1.072187	0.561511	-1.451157	3.273743	0.057819	-0.828656	3.060483	-0.034228
	H	4.833068	-0.681266	-1.347640	0.038952	1.808447	-0.075579	-2.631048	2.486634	0.864325
	H	6.547142	-1.454456	0.197845	-0.757518	4.106508	0.019007	-0.939796	4.110869	0.211695
	H	5.451832	-1.051259	1.637706	-2.508304	3.510401	0.140976	0.063904	2.769416	-0.581126
	I	-3.169931	-0.160752	0.033897	2.211625	-0.233761	-0.030348	2.177256	-0.174149	-0.098607

Table D51: Cartesian coordinates of the geometries of iodide-2-butadiene complexes optimised with the DSD-PBEP86-D3BJ functional, in Å.

		2tb.1		
		x	y	z
def2TZVPD	C	0.000000	4.576546	0.242823
	C	0.827639	3.927849	1.070462
	H	0.858781	2.843843	1.101604
	H	1.494128	4.465056	1.736951
	C	-0.008247	5.664883	0.234576
	H	-0.914625	3.909814	-0.671802
	H	-0.906310	2.821478	-0.663487
	C	-1.742285	4.558456	-1.499462
	H	-2.408756	4.021202	-2.165933
	H	-1.773462	5.642459	-1.530639
	C	0.000000	-4.576546	0.242823
	H	-0.827639	-3.927849	1.070462
	C	-0.858781	-2.843843	1.101604
	C	-1.494128	-4.465056	1.736951
$I^- \cdots C_4H_6$	H	0.008247	-5.664883	0.234576
	H	0.914625	-3.909814	-0.671802
	C	0.906310	-2.821478	-0.663487
	H	1.742285	-4.558456	-1.499462
	H	2.408756	-4.021202	-2.165933
$I^- \cdots C_4H_6$	H	1.773462	-5.642459	-1.530639
	I	0.000000	0.000000	0.242823

Table D52: Calculated harmonic frequencies and mode assignments for the $\text{I}^- \cdots \text{C}_8\text{H}_{12}$ def2TZVPD complexes. All frequencies and intensities are in cm^{-1} and km mol^{-1} and zero-point energies are in kJ mol^{-1} .

$\text{I}^- \cdots \text{C}_8\text{H}_{12}$								
	Mode	Symmetry	Frequency (cm^{-1})	Intensity (km mol^{-1})	Mode	Symmetry	Frequency (cm^{-1})	Intensity
def2TZVPD	ω_1	<i>a</i>	9	0.3057	ω_{30}	<i>a</i>	1210	15.8808
	ω_2	<i>a</i>	13	0.2175	ω_{31}	<i>a</i>	1249	5.1379
	ω_3	<i>a</i>	48	5.387	ω_{32}	<i>a</i>	1280	4.3942
	ω_4	<i>a</i>	80	0.0046	ω_{33}	<i>a</i>	1302	0.9126
	ω_5	<i>a</i>	116	0.3622	ω_{34}	<i>a</i>	1319	1.0897
	ω_6	<i>a</i>	187	0.3438	ω_{35}	<i>a</i>	1326	1.4394
	ω_7	<i>a</i>	272	0.1956	ω_{36}	<i>a</i>	1364	1.1963
	ω_8	<i>a</i>	321	0.8897	ω_{37}	<i>a</i>	1372	1.2894
	ω_9	<i>a</i>	385	0.1443	ω_{38}	<i>a</i>	1388	0.7107
	ω_{10}	<i>a</i>	417	0.3459	ω_{39}	<i>a</i>	1414	0.6379
	ω_{11}	<i>a</i>	482	1.3477	ω_{40}	<i>a</i>	1460	1.6422
	ω_{12}	<i>a</i>	521	0.7356	ω_{41}	<i>a</i>	1479	0.7759
	ω_{13}	<i>a</i>	680	10.4516	ω_{42}	<i>a</i>	1485	5.3557
	ω_{14}	<i>a</i>	690	8.5017	ω_{43}	<i>a</i>	1498	3.0875
	ω_{15}	<i>a</i>	755	9.6138	ω_{44}	<i>a</i>	1699	23.1736
	ω_{16}	<i>a</i>	823	0.0978	ω_{45}	<i>a</i>	1711	0.0691
	ω_{17}	<i>a</i>	889	3.7026	ω_{46}	<i>a</i>	3002	31.0059
	ω_{18}	<i>a</i>	924	41.6148	ω_{47}	<i>a</i>	3012	42.5138
	ω_{19}	<i>a</i>	932	5.5634	ω_{48}	<i>a</i>	3017	5.5201
	ω_{20}	<i>a</i>	951	3.1629	ω_{49}	<i>a</i>	3028	42.6033
	ω_{21}	<i>a</i>	970	1.0789	ω_{50}	<i>a</i>	3059	37.3329
	ω_{22}	<i>a</i>	989	2.272	ω_{51}	<i>a</i>	3060	38.9
	ω_{23}	<i>a</i>	1029	0.1537	ω_{52}	<i>a</i>	3079	54.1974
	ω_{24}	<i>a</i>	1034	14.4214	ω_{53}	<i>a</i>	3126	22.3159
	ω_{25}	<i>a</i>	1066	3.3058	ω_{54}	<i>a</i>	3146	10.2488
	ω_{26}	<i>a</i>	1089	0.4816	ω_{55}	<i>a</i>	3164	1.206
	ω_{27}	<i>a</i>	1110	2.7589	ω_{56}	<i>a</i>	3174	8.2554
	ω_{28}	<i>a</i>	1157	1.1858	ω_{57}	<i>a</i>	3232	22.3558
	ω_{29}	<i>a</i>	1161	4.3392	zpe			471.1

Table D53: Calculated harmonic frequencies and mode assignments for the $\text{I}^- \cdots \text{C}_8\text{H}_{12}$ def2TZVPD complexes. All frequencies and intensities are in cm^{-1} and km mol^{-1} and zero-point energies are in kJ mol^{-1} .

$\text{I}^- \cdots \text{C}_8\text{H}_{12}$								
	Mode	Symmetry	Frequency (cm^{-1})	Intensity (km mol^{-1})	Mode	Symmetry	Frequency (cm^{-1})	Intensity
def2TZVPD	ω_1	<i>a</i>	34	1.5186	ω_{30}	<i>a</i>	1211	1.299
	ω_2	<i>a</i>	42	0.398	ω_{31}	<i>a</i>	1251	0.0393
	ω_3	<i>a</i>	68	0.7582	ω_{32}	<i>a</i>	1288	1.3183
	ω_4	<i>a</i>	72	3.3825	ω_{33}	<i>a</i>	1302	0.3518
	ω_5	<i>a</i>	119	1.1873	ω_{34}	<i>a</i>	1324	1.1365
	ω_6	<i>a</i>	186	0.4774	ω_{35}	<i>a</i>	1339	11.777
	ω_7	<i>a</i>	275	0.0462	ω_{36}	<i>a</i>	1368	1.5834
	ω_8	<i>a</i>	320	0.7863	ω_{37}	<i>a</i>	1384	1.2089
	ω_9	<i>a</i>	384	0.475	ω_{38}	<i>a</i>	1402	4.0074
	ω_{10}	<i>a</i>	413	1.0352	ω_{39}	<i>a</i>	1420	0.8923
	ω_{11}	<i>a</i>	479	5.5323	ω_{40}	<i>a</i>	1459	5.1283
	ω_{12}	<i>a</i>	519	2.0943	ω_{41}	<i>a</i>	1480	2.7918
	ω_{13}	<i>a</i>	651	29.0537	ω_{42}	<i>a</i>	1483	3.2831
	ω_{14}	<i>a</i>	694	4.9727	ω_{43}	<i>a</i>	1507	0.7112
	ω_{15}	<i>a</i>	742	5.8077	ω_{44}	<i>a</i>	1701	20.9563
	ω_{16}	<i>a</i>	821	2.8915	ω_{45}	<i>a</i>	1712	8.687
	ω_{17}	<i>a</i>	889	2.5062	ω_{46}	<i>a</i>	3002	81.9777
	ω_{18}	<i>a</i>	906	42.1646	ω_{47}	<i>a</i>	3007	65.1395
	ω_{19}	<i>a</i>	929	6.3613	ω_{48}	<i>a</i>	3011	13.5377
	ω_{20}	<i>a</i>	945	4.788	ω_{49}	<i>a</i>	3031	6.7454
	ω_{21}	<i>a</i>	969	1.0876	ω_{50}	<i>a</i>	3057	39.2742
	ω_{22}	<i>a</i>	986	0.4404	ω_{51}	<i>a</i>	3059	32.3563
	ω_{23}	<i>a</i>	991	1.3004	ω_{52}	<i>a</i>	3086	29.8534
	ω_{24}	<i>a</i>	1065	3.5152	ω_{53}	<i>a</i>	3129	33.2817
	ω_{25}	<i>a</i>	1076	7.3993	ω_{54}	<i>a</i>	3139	30.4815
	ω_{26}	<i>a</i>	1092	0.2072	ω_{55}	<i>a</i>	3143	16.7825
	ω_{27}	<i>a</i>	1112	2.0914	ω_{56}	<i>a</i>	3170	68.2135
	ω_{28}	<i>a</i>	1165	4.1637	ω_{57}	<i>a</i>	3227	20.8526
	ω_{29}	<i>a</i>	1171	0.4667	zpe		471.4	

Table D54: Calculated harmonic frequencies and mode assignments for the $\text{I}^- \cdots \text{C}_8\text{H}_{12}$ def2TZVPD complexes. All frequencies and intensities are in cm^{-1} and km mol^{-1} and zero-point energies are in kJ mol^{-1} .

$\text{I}^- \cdots \text{C}_8\text{H}_{12}$								
	Mode	Symmetry	Frequency (cm^{-1})	Intensity (km mol^{-1})	Mode	Symmetry	Frequency (cm^{-1})	Intensity
def2TZVPD	ω_1	<i>a</i>	12 <i>i</i>	0.0844	ω_{30}	<i>a</i>	1205	1.4156
	ω_2	<i>a</i>	30	0.5777	ω_{31}	<i>a</i>	1256	3.4095
	ω_3	<i>a</i>	56	4.9954	ω_{32}	<i>a</i>	1281	2.2668
	ω_4	<i>a</i>	77	0.3035	ω_{33}	<i>a</i>	1322	1.299
	ω_5	<i>a</i>	114	0.1434	ω_{34}	<i>a</i>	1324	4.1895
	ω_6	<i>a</i>	186	1.232	ω_{35}	<i>a</i>	1331	3.7081
	ω_7	<i>a</i>	260	0.4892	ω_{36}	<i>a</i>	1374	8.3852
	ω_8	<i>a</i>	317	0.9004	ω_{37}	<i>a</i>	1379	1.5001
	ω_9	<i>a</i>	384	0.6314	ω_{38}	<i>a</i>	1394	0.599
	ω_{10}	<i>a</i>	416	0.3892	ω_{39}	<i>a</i>	1420	0.3719
	ω_{11}	<i>a</i>	477	2.534	ω_{40}	<i>a</i>	1465	2.3574
	ω_{12}	<i>a</i>	520	0.5317	ω_{41}	<i>a</i>	1475	1.8057
	ω_{13}	<i>a</i>	648	31.8696	ω_{42}	<i>a</i>	1481	4.3651
	ω_{14}	<i>a</i>	674	9.5054	ω_{43}	<i>a</i>	1492	8.3918
	ω_{15}	<i>a</i>	738	3.7619	ω_{44}	<i>a</i>	1701	14.0313
	ω_{16}	<i>a</i>	817	4.1517	ω_{45}	<i>a</i>	1712	9.5623
	ω_{17}	<i>a</i>	885	4.4259	ω_{46}	<i>a</i>	2997	74.7082
	ω_{18}	<i>a</i>	926	8.7997	ω_{47}	<i>a</i>	3012	63.9866
	ω_{19}	<i>a</i>	944	31.4197	ω_{48}	<i>a</i>	3020	29.4478
	ω_{20}	<i>a</i>	950	9.7403	ω_{49}	<i>a</i>	3034	4.1048
	ω_{21}	<i>a</i>	970	0.6456	ω_{50}	<i>a</i>	3059	2.8672
	ω_{22}	<i>a</i>	983	1.0996	ω_{51}	<i>a</i>	3060	64.1098
	ω_{23}	<i>a</i>	990	1.4978	ω_{52}	<i>a</i>	3087	15.3465
	ω_{24}	<i>a</i>	1025	19.5685	ω_{53}	<i>a</i>	3116	36.8928
	ω_{25}	<i>a</i>	1066	2.747	ω_{54}	<i>a</i>	3142	17.1938
	ω_{26}	<i>a</i>	1090	1.0086	ω_{55}	<i>a</i>	3146	25.0948
	ω_{27}	<i>a</i>	1109	1.7664	ω_{56}	<i>a</i>	3169	72.7947
	ω_{28}	<i>a</i>	1160	0.3883	ω_{57}	<i>a</i>	3234	20.442
	ω_{29}	<i>a</i>	1166	5.6034	zpe		470.5	

Table D55: Calculated harmonic frequencies and mode assignments for the $\text{I}^- \cdots (\text{C}_4\text{H}_6)_2$ def2TZVPD complexes. All frequencies and intensities are in cm^{-1} and km mol^{-1} and zero-point energies are in kJ mol^{-1} .

$\text{I}^- \cdots (\text{C}_4\text{H}_6)_2$								
	Mode	Symmetry	Frequency (cm^{-1})	Intensity (km mol^{-1})	Mode	Symmetry	Frequency (cm^{-1})	Intensity
def2TZVPD	ω_1	<i>a</i>	53 <i>i</i>	0.9909	ω_{30}	<i>b</i>	1083	19.9955
	ω_2	<i>b</i>	53 <i>i</i>	0.9869	ω_{31}	<i>a</i>	1083	19.8663
	ω_3	<i>a</i>	13	0.049	ω_{32}	<i>b</i>	1238	0.4645
	ω_4	<i>b</i>	23	0.3108	ω_{33}	<i>a</i>	1238	0.0872
	ω_5	<i>a</i>	24	0.2384	ω_{34}	<i>b</i>	1322	7.2699
	ω_6	<i>a</i>	43	0.26	ω_{35}	<i>a</i>	1322	0.0272
	ω_7	<i>b</i>	46	0.4505	ω_{36}	<i>b</i>	1331	5.9197
	ω_8	<i>a</i>	62	0.0061	ω_{37}	<i>a</i>	1331	1.5043
	ω_9	<i>b</i>	77	8.3139	ω_{38}	<i>b</i>	1416	0.5045
	ω_{10}	<i>b</i>	164	0.4268	ω_{39}	<i>a</i>	1416	0.3438
	ω_{11}	<i>a</i>	165	0.4291	ω_{40}	<i>b</i>	1477	14.672
	ω_{12}	<i>b</i>	285	3.2073	ω_{41}	<i>a</i>	1478	0.1037
	ω_{13}	<i>a</i>	286	2.5181	ω_{42}	<i>b</i>	1648	17.4874
	ω_{14}	<i>b</i>	511	3.4351	ω_{43}	<i>a</i>	1648	18.2584
	ω_{15}	<i>a</i>	511	0.0294	ω_{44}	<i>b</i>	1711	5.4552
	ω_{16}	<i>b</i>	537	11.2345	ω_{45}	<i>a</i>	1711	1.9801
	ω_{17}	<i>a</i>	537	11.2283	ω_{46}	<i>b</i>	3137	17.7197
	ω_{18}	<i>b</i>	783	0.59	ω_{47}	<i>a</i>	3137	4.8501
	ω_{19}	<i>a</i>	783	0.596	ω_{48}	<i>b</i>	3148	99.06
	ω_{20}	<i>b</i>	900	43.0044	ω_{49}	<i>a</i>	3148	14.4246
	ω_{21}	<i>a</i>	900	42.9947	ω_{50}	<i>b</i>	3150	188.067
	ω_{22}	<i>b</i>	904	2.1714	ω_{51}	<i>a</i>	3151	0.0524
	ω_{23}	<i>a</i>	904	0.0266	ω_{52}	<i>b</i>	3159	12.2124
	ω_{24}	<i>b</i>	974	14.5524	ω_{53}	<i>a</i>	3159	6.1276
	ω_{25}	<i>a</i>	974	14.4458	ω_{54}	<i>b</i>	3236	28.5112
	ω_{26}	<i>a</i>	1005	0.4521	ω_{55}	<i>a</i>	3236	2.493
	ω_{27}	<i>b</i>	1005	0.8222	ω_{56}	<i>b</i>	3241	13.7792
	ω_{28}	<i>b</i>	1013	8.3901	ω_{57}	<i>a</i>	3241	9.1572
	ω_{29}	<i>a</i>	1014	8.6126	zpe		448.8	

Appendix E

Tables and Data: PH_2^- Complexes

Table E1: PH_2^- geometric parameters and VDEs from DSD-PBEP86-D3BJ optimisations.

	R_{P-H} Å	\angle_{H-P-H} °	E E_h	E_{VDE} E_h	VDE eV
PH_2^-	def2QZVP	1.430	88.5	-342.2660345	-342.2275203
	AVTZ	1.430	88.4	-342.2631546	-342.2180715
	AVQZ	1.429	88.4	-342.2718528	-342.2264677
	W1w			-342.1235804	-342.0774611
	W2w			-342.1238270	-342.0777577

Table E2: PH_2 geometric parameters and ADEs from DSD-PBEP86-D3BJ optimisations.

	R_{P-H} Å	\angle_{H-P-H} °	E E_h	ADE eV	ADE_{exp} eV	Shift eV
PH_2	def2QZVP	1.417	88.6	-342.2276487	1.062	-0.201
	pVTZ	1.419	88.6	-342.2198546	1.194	-0.069
	pVQZ	1.417	88.6	-342.2275554	1.221	1.263
	W1w			-342.0775556	1.268	0.005
	W2w			-342.0778538	1.267	0.004

Table E3: H_2S geometric parameters from DSD-PBEP86-D3BJ optimisations.

	R_{S-H} Å	\angle_{H-S-H} °	E E_h
H_2S	def2QZVP	1.337	92.5
	pVTZ	1.338	92.4
	pVQZ	1.337	92.5
	W1w		-398.9676731
	W2w		-398.9682739

Table E4: PH_3 geometric parameters from DSD-PBEP86-D3BJ optimisations.

	R_{P-H} Å	\angle_{H-P-H} °	Dihedral °	E E_h
PH_3	def2QZVP	1.414	93.7	94.0
	pVTZ	1.415	93.6	93.9
	pVQZ	1.414	93.7	94.0
	W1w			-342.8645899
	W2w			-342.8557371

Table E5: HS⁻ geometric parameters and VDEs from DSD-PBEP86-D3BJ optimisations.

		R_{S-H}	E	E_{VDE}	VDE
		Å	E_h	E_h	eV
HS ⁻	def2QZVP	1.343	-398.5406083	-398.4614591	1.989
	pVTZ	1.344	-398.5352128	-398.4521964	2.094
	pVQZ	1.344	-398.5457684	-398.4614623	2.129
	W1w		-398.4009932	-398.3145549	2.187
	W2w		-398.4012176	-398.3151608	2.177

Table E6: HS geometric parameters and ADEs from DSD-PBEP86-D3BJ optimisations.

		R_{S-H}	E	ADE	$^2\Pi_{3/2}$	$^2\Pi_{1/2}$	ADE_{exp}	Shift
		Å	E_h	eV	eV	eV	eV	eV
HS	def2QZVP	1.341	-398.4614621	2.157	2.134	2.204		-0.181
	pVTZ	1.342	-398.4521994	2.262	2.239	2.309		-0.076
	pVQZ	1.341	-398.4614654	2.297	2.274	2.344	2.315	-0.041
	W1w		-398.3145553	2.355	2.332	2.402		0.017
	W2w		-398.3151625	2.345	2.321	2.392		0.007

Table E7: CH₄ geometric parameters from DSD-PBEP86-D3BJ optimisations.

		R_{C-H}	\angle_{H-C-H}	E
		Å	°	E_h
CH ₄	def2QZVP	1.088	109.5	-40.4524081
	pVTZ	1.089	109.5	-40.4446760
	pVQZ	1.088	109.5	-40.4526926
	W1w			-40.4579153
	W2w			-40.4578898

Table E8: C₂H₄ geometric parameters from DSD-PBEP86-D3BJ optimisations.

		$R_{C=C}$	R_{C-H}	E
		Å	°	E_h
C ₂ H ₄	def2QZVP	1.329	1.082	-78.4700163
	pVTZ	1.331	1.083	-78.4564437
	pVQZ	1.329	1.082	-78.4707010
	W1w			-78.4749669
	W2w			-78.4747560

Table E9: HCCH geometric parameters from DSD-PBEP86-D3BJ optimisations.

		$R_{C\equiv C}$	R_{C-H}	E
		Å	°	E_h
HCCH	def2QZVP	1.204	1.063	-77.2198341
	pVTZ	1.206	1.063	-77.2071669
	pVQZ	1.204	1.063	-77.2204955
	W1w			-77.2218814
	W2w			-77.2217271

Table E10: CO₂ geometric parameters from DSD-PBEP86-D3BJ optimisations.

		R_{C-O}	\angle_{O-C-O}	E
		Å	°	E_h
CO ₂	def2QZVP	1.162	180.0	-188.4046748
	pVTZ	1.165	180.0	-188.3733475
	pVQZ	1.163	180.0	-188.4060983
	W1w			-188.4173803
	W2w			-188.4198120

Table E11: NH₃ geometric parameters from DSD-PBEP86-D3BJ optimisations.

		R_{N-H}	\angle_{H-N-H}	E
		Å	°	E_h
NH ₃	def2QZVP	1.012	106.9	-56.4943702
	pVTZ	1.013	106.8	-56.4845550
	pVQZ	1.012	106.9	-56.4951929
	W1w			-56.5044684
	W2w			-56.5045865

Table E12: DSD-PBEP86-D3BJ and extrapolated single-point energies for PH_2^- and PH_2 . Geometries use for CC energies are from DSD-PBEP86-D3BJ/AVQZ optimisations. All energies are in E_h .

	PH_2^- (1A_1)						
	E_{DH-DFT}	E_{SCF}	E_{CCSD}	E_{corr}	$E_{CCSD(T)}$	$E_{(T)}$	E_{Wnw}
def2QZVP	-342.2660345						
AVDZ		-341.8801766	-342.0547743	-0.1745977	-342.0611264	-0.0063521	
AVTZ	-342.2631546	-341.8910403	-342.0958121	-0.2047718	-342.1053029	-0.0094908	
AVQZ	-342.2718528	-341.8940422	-342.1067715	-0.2127293	-342.1170734	-0.0103019	
AV5Z		-341.8946082	-342.1099336	-0.2153254			
W1w		-341.8949762		-0.2179465		-0.0106576	-342.1235804
W2w		-341.8948841		-0.2180492		-0.0108938	-342.1238270
	VDE PH_2^- (2B_1)						
def2QZVP	-342.2275203						
AVDZ		-341.8779288	-342.0193047	-0.1413759	-342.0231417	-0.0038370	
AVTZ	-342.2180715	-341.8891621	-342.0558523	-0.1666902	-342.0618387	-0.0059864	
AVQZ	-342.2264677	-341.8921857	-342.0654347	-0.1732490	-342.0719873	-0.0065526	
AV5Z		-341.8927714	-342.0682096	-0.1754382			
W1w		-341.8931265		-0.1775492		-0.0067855	-342.0774611
W2w		-341.8930569		-0.1777351		-0.0069658	-342.0777577
	PH_2 (2B_1)						
def2QZVP	-342.2276487						
AVDZ		-341.8780232	-342.0191702	-0.1411470	-342.0229753	-0.0038051	
AVTZ	-342.2198546	-341.8894010	-342.0559422	-0.1665412	-342.0618936	-0.0059514	
AVQZ	-342.2275554	-341.8924427	-342.0655530	-0.1731103	-342.0720693	-0.0065163	
AV5Z		-341.8930326	-342.0683364	-0.1753038			
W1w		-341.8933891		-0.1774172		-0.0067493	-342.0775556
W2w		-341.8933201		-0.1776052		-0.0069285	-342.0778538

Table E13: DSD-PBEP86-D3BJ and extrapolated single-point energies for H₂S and PH₃. Geometries use for CC energies are from DSD-PBEP86-D3BJ/AVQZ optimisations. All energies are in E_h .

	H ₂ S (¹ A ₁)						
	E_{DH-DFT}	E_{SCF}	E_{CCSD}	E_{corr}	$E_{CCSD(T)}$	$E_{(T)}$	E_{Wnw}
def2QZVP	-399.1115618						
AVDZ		-398.7022665	-398.8826329	-0.1803664	-398.8878008	-0.0051679	
AVTZ	-399.1013798	-398.7159573	-398.9349327	-0.2189754	-398.9436174	-0.0086847	
AVQZ	-399.1118008	-398.7193525	-398.9493791	-0.2300266	-398.9589936	-0.0096145	
AV5Z		-398.7200142	-398.9537582	-0.2337440			
W1w		-398.7204089		-0.2372721		-0.0099921	-398.9676731
W2w		-398.7203367		-0.2376442		-0.0102930	-398.9682739
	PH ₃ (¹ A)						
def2QZVP	-342.8645899						
AVDZ		-342.4775713	-342.6494645	-0.1718932	-342.6542282	-0.0047637	
AVTZ	-342.8557371	-342.4905568	-342.6918670	-0.2013102	-342.6990035	-0.0071365	
AVQZ	-342.8646068	-342.4939602	-342.7031239	-0.2091637	-342.7108842	-0.0077603	
AV5Z		-342.4946352	-342.7063176	-0.2116824			
W1w		-342.4950191		-0.2143127		-0.0080186	-342.7173505
W2w		-342.4949642		-0.2143250		-0.0082155	-342.7175047

Table E14: DSD-PBEP86-D3BJ and extrapolated single-point energies for HS[−] and HS. Geometries use for CC energies are from DSD-PBEP86-D3BJ/AVQZ optimisations. All energies are in E_h .

	HS [−] ($^1\Sigma_g$)						
	E_{DH-DFT}	E_{SCF}	E_{CCSD}	E_{corr}	$E_{CCSD(T)}$	$E_{(T)}$	E_{Wnw}
def2QZVP	-398.5406083						
AVDZ		-398.1356036	-398.3148523	-0.1792487	-398.3209969	-0.0061446	
AVTZ	-398.5352128	-398.1462517	-398.3648467	-0.2185950	-398.3753736	-0.0105269	
AVQZ	-398.5457684	-398.1491970	-398.3799497	-0.2307527	-398.3915835	-0.0116338	
AV5Z		-398.1497070	-398.3843968	-0.2346898			
W1w		-398.1501134		-0.2387237		-0.0121561	-398.4009932
W2w		-398.1499556		-0.2388205		-0.0124415	-398.4012176
	VDE HS [−] ($^2\Sigma_g$)						
def2QZVP	-398.4614591						
AVDZ		-398.0944543	-398.2398388	-0.1453845	-398.2435114	-0.0036726	
AVTZ	-398.4521964	-398.1070258	-398.2865145	-0.1794887	-398.2933053	-0.0067908	
AVQZ	-398.4614623	-398.1101056	-398.2992899	-0.1891843	-398.3069315	-0.0076416	
AV5Z		-398.1106731	-398.3031584	-0.1924853			
W1w		-398.1110638		-0.1955411		-0.0079500	-398.3145549
W2w		-398.1109497		-0.1959486		-0.0082625	-398.3151608
	HS ($^2\Sigma_g$)						
def2QZVP	-398.4614621						
AVDZ		-398.0944658	-398.2398121	-0.1453463	-398.2434801	-0.0036680	
AVTZ	-398.4521994	-398.1070570	-398.2865175	-0.1794605	-398.2933026	-0.0067851	
AVQZ	-398.4614654	-398.1101387	-398.2992954	-0.1891567	-398.3069311	-0.0076357	
AV5Z		-398.1107069	-398.3031652	-0.1924583			
W1w		-398.1110975		-0.1955139		-0.0079439	-398.3145553
W2w		-398.1109838		-0.1959223		-0.0082564	-398.3151625

Table E15: DSD-PBEP86-D3BJ and extrapolated single-point energies for CH₄, C₂H₄ and HCCH. Geometries use for CC energies are from DSD-PBEP86-D3BJ/AVQZ optimisations. All energies are in E_h .

	CH ₄ (¹ A ₁)						
	E_{DH-DFT}	E_{SCF}	E_{CCSD}	E_{corr}	$E_{CCSD(T)}$	$E_{(T)}$	E_{Wnw}
def2QZVP	-40.4524081						
pVDZ		-40.1996270	-40.3907831	-0.1911561	-40.3952647	-0.0044816	
pVTZ	-40.4446760	-40.2136128	-40.4343736	-0.2207608	-40.4409199	-0.0065463	
pVQZ	-40.4526926	-40.2162385	-40.4447215	-0.2284830	-40.4517280	-0.0070065	
pV5Z		-40.2169441	-40.4477580	-0.2308139			
W1w		-40.2170555		-0.2335459		-0.0073139	-40.4579153
W2w		-40.2172880		-0.2332594		-0.0073423	-40.4578898
	C ₂ H ₄ (¹ A _g)						
def2QZVP	-78.4700163						
pVDZ		-78.0436706	-78.3572903	-0.3136197	-78.3683708	-0.0110805	
pVTZ	-78.4564437	-78.0648015	-78.4282164	-0.3634149	-78.4436728	-0.0154564	
pVQZ	-78.4707010	-78.0694983	-78.4471127	-0.3776144	-78.4635569	-0.0164442	
pV5Z		-78.0706003	-78.4525282	-0.3819279			
W1w		-78.0709597		-0.3869241		-0.0170832	-78.4749669
W2w		-78.0711374		-0.3864535		-0.0171650	-78.4747560
	HCCH (¹ Σ _g)						
def2QZVP	-77.2198341						
pVDZ		-76.8284180	-77.1074865	-0.2790685	-77.1197460	-0.0122595	
pVTZ	-77.2071669	-76.8500359	-77.1752288	-0.3251929	-77.1921220	-0.0168932	
pVQZ	-77.2204955	-76.8544380	-77.1930789	-0.3386409	-77.2109803	-0.0179014	
pV5Z		-76.8554056	-77.1982296	-0.3428240			
W1w		-76.8558077		-0.3474579		-0.0186158	-77.2218814
W2w		-76.8558772		-0.3472128		-0.0186371	-77.2217271

Table E16: DSD-PBEP86-D3BJ and extrapolated single-point energies for CO₂ and NH₃. Geometries use for CC energies are from DSD-PBEP86-D3BJ/AVQZ optimisations. All energies are in E_h .

	CO ₂ ($^1\Sigma_g$)						
	E_{DH-DFT}	E_{SCF}	E_{CCSD}	E_{corr}	$E_{CCSD(T)}$	$E_{(T)}$	E_{Wnw}
def2QZVP	-188.4046748						
pVDZ		-187.6623766	-188.1641465	-0.5017699	-188.1851906	-0.0210441	
pVTZ	-188.3733475	-187.7089326	-188.3106643	-0.6017317	-188.3405184	-0.0298541	
pVQZ	-188.4060983	-187.7216060	-188.3577475	-0.6361415	-188.3895939	-0.0318464	
pV5Z		-187.7244039	-188.3725515	-0.6481476			
W1w		-187.7255492		-0.6587017		-0.0331293	-188.4173803
W2w		-187.7257676		-0.6607442		-0.0333002	-188.4198120
	NH ₃ (1A_1)						
def2QZVP	-56.4943702						
pVDZ		-56.2054132	-56.4197554	-0.2143422	-56.4252103	-0.0054549	
pVTZ	-56.4845550	-56.2203412	-56.4722073	-0.2518661	-56.4805384	-0.0083311	
pVQZ	-56.4951929	-56.2239879	-56.4867739	-0.2627860	-56.4957260	-0.0089521	
pV5Z		-56.2248682	-56.4911180	-0.2662498			
W1w		-56.2251225		-0.2699455		-0.0094004	-56.5044684
W2w		-56.2252972		-0.2698840		-0.0094053	-56.5045865

Table E17: Calculated harmonic frequencies and mode assignments for the PH₂⁻ and PH₂. All frequencies and intensities are in cm⁻¹ and km mol⁻¹ and zero-point energies are in kJ mol⁻¹.

PH ₂ ⁻				PH ₂				
	Mode	Symmetry	Frequency (cm ⁻¹)	Intensity (km mol ⁻¹)	Mode	Symmetry	Frequency (cm ⁻¹)	Intensity (km mol ⁻¹)
def2QZVP	ω_1	<i>a</i> ₁	1095	30.6536	ω_1	<i>a</i> ₁	1140	20.2594
	ω_2	<i>a</i> ₁	2291	238.1615	ω_2	<i>a</i> ₁	2406	50.9906
	ω_3	<i>b</i> ₂	2291	272.0284	ω_3	<i>b</i> ₂	2414	64.8456
	zpe		34.0		zpe		35.7	
AVTZ	ω_1	<i>a</i> ₁	1095	30.6859	ω_1	<i>a</i> ₁	1139	20.5596
	ω_2	<i>a</i> ₁	2295	211.8099	ω_2	<i>a</i> ₁	2400	51.8748
	ω_3	<i>b</i> ₂	2297	215.643	ω_3	<i>b</i> ₂	2408	63.8038
	zpe		34.0		zpe		35.6	
AVQZ	ω_1	<i>a</i> ₁	1095	30.3185	ω_1	<i>a</i> ₁	1140	20.7439
	ω_2	<i>a</i> ₁	2300	200.5837	ω_2	<i>a</i> ₁	2405	51.2822
	ω_3	<i>b</i> ₂	2302	203.2941	ω_3	<i>b</i> ₂	2413	62.7292
	zpe		34.1		zpe		35.6	

Table E18: Calculated harmonic frequencies and mode assignments for the H₂S. All frequencies and intensities are in cm⁻¹ and km mol⁻¹ and zero-point energies are in kJ mol⁻¹.

H ₂ S				
	Mode	Symmetry	Frequency (cm ⁻¹)	Intensity (km mol ⁻¹)
def2QZVP	ω_1	<i>a</i> ₁	1221	0.7181
	ω_2	<i>a</i> ₁	2728	0.0001
	ω_3	<i>b</i> ₂	2742	0.0234
	zpe		40.0	
AVTZ	ω_1	<i>a</i> ₁	1221	0.7489
	ω_2	<i>a</i> ₁	2724	0.0049
	ω_3	<i>b</i> ₂	2738	0.0739
	zpe		40.0	
AVQZ	ω_1	<i>a</i> ₁	1221	0.7573
	ω_2	<i>a</i> ₁	2725	0.0003
	ω_3	<i>b</i> ₂	2740	0.1222
	zpe		40.0	

Table E19: Calculated harmonic frequencies and mode assignments for the HS⁻ and HS. All frequencies and intensities are in cm⁻¹ and km mol⁻¹ and zero-point energies are in kJ mol⁻¹.

HS				HS ⁻				
	Mode	Symmetry	Frequency (cm ⁻¹)	Intensity (km mol ⁻¹)	Mode	Symmetry	Frequency (cm ⁻¹)	Intensity (km mol ⁻¹)
def2QZVP	ω_1	σ	2712	0.1523	ω_1	σ	2656	93.9452
		zpe	16.2			zpe	15.9	
AVTZ	ω_1	σ	2709	0.1286	ω_1	σ	2657	71.1739
		zpe	16.2			zpe	15.9	
AVQZ	ω_1	σ	2710	0.0848	ω_1	σ	2659	67.5488
		zpe	16.2			zpe	15.9	

Table E20: Calculated harmonic frequencies and mode assignments for the PH₃. All frequencies and intensities are in cm⁻¹ and km mol⁻¹ and zero-point energies are in kJ mol⁻¹.

PH ₃				
	Mode	Symmetry	Frequency (cm ⁻¹)	Intensity (km mol ⁻¹)
def2QZVP	ω_1	a	1026	21.4036
	ω_2	a	1154	12.7195
	ω_3	a	1154	12.7192
	ω_4	a	2425	29.7905
	ω_5	a	2432	56.7152
	ω_6	a	2432	56.7174
		zpe	63.5	
AVTZ	ω_1	a	1025	21.6363
	ω_2	a	1154	13.105
	ω_3	a	1154	13.1068
	ω_4	a	2418	31.6186
	ω_5	a	2425	56.1637
	ω_6	a	2425	56.1592
		zpe	63.4	
AVQZ	ω_1	a	1025	21.8617
	ω_2	a	1154	13.2741
	ω_3	a	1154	13.2755
	ω_4	a	2423	31.2424
	ω_5	a	2430	55.3308
	ω_6	a	2430	55.337
		zpe	63.5	

Table E21: Calculated harmonic frequencies and mode assignments for the CH₄. All frequencies and intensities are in cm⁻¹ and km mol⁻¹ and zero-point energies are in kJ mol⁻¹.

CH ₄				
	Mode	Symmetry	Frequency (cm ⁻¹)	Intensity (km mol ⁻¹)
def2QZVP	ω_1	t_2	1357	11.4189
	ω_2	t_2	1357	11.4189
	ω_3	t_2	1357	11.4189
	ω_4	e	1576	0
	ω_5	e	1576	0
	ω_6	a_1	3035	0
	ω_7	t_2	3147	21.3011
	ω_8	t_2	3147	21.3011
	ω_9	t_2	3147	21.3011
		zpe	117.8	
AVTZ	ω_1	t_2	1357	10.761
	ω_2	t_2	1357	10.761
	ω_3	t_2	1357	10.761
	ω_4	e	1577	0
	ω_5	e	1577	0
	ω_6	a_1	3031	0
	ω_7	t_2	3141	21.512
	ω_8	t_2	3141	21.512
	ω_9	t_2	3141	21.512
		zpe	117.7	
AVQZ	ω_1	t_2	1356	10.9466
	ω_2	t_2	1356	10.9466
	ω_3	t_2	1356	10.9466
	ω_4	e	1576	0
	ω_5	e	1576	0
	ω_6	a_1	3033	0
	ω_7	t_2	3144	21.1518
	ω_8	t_2	3144	21.1518
	ω_9	t_2	3144	21.1518
		zpe	117.8	

Table E22: Calculated harmonic frequencies and mode assignments for the CO₂. All frequencies and intensities are in cm⁻¹ and km mol⁻¹ and zero-point energies are in kJ mol⁻¹.

CO ₂				
	Mode	Symmetry	Frequency (cm ⁻¹)	Intensity (km mol ⁻¹)
def2QZVP	ω_1	π_u	669	28.13
	ω_2	π_u	669	28.13
	ω_3	σ_g	1346	0
	ω_4	σ_u	2394	606.0406
	zpe		30.4	
AVTZ	ω_1	π_u	667	27.2036
	ω_2	π_u	667	27.2036
	ω_3	σ_g	1339	0
	ω_4	σ_u	2381	609.4681
	zpe		30.2	
AVQZ	ω_1	π_u	669	27.3437
	ω_2	π_u	669	27.3437
	ω_3	σ_g	1344	0
	ω_4	σ_u	2390	613.015
	zpe		30.3	

Table E23: Calculated harmonic frequencies and mode assignments for the NH₃. All frequencies and intensities are in cm⁻¹ and km mol⁻¹ and zero-point energies are in kJ mol⁻¹.

NH ₃				
	Mode	Symmetry	Frequency (cm ⁻¹)	Intensity (km mol ⁻¹)
def2QZVP	ω_1	a'	1051	155.9012
	ω_2	a'	1676	16.898
	ω_3	a'	1676	16.8977
	ω_4	a'	3501	2.2242
	ω_5	a'	3636	4.7337
	ω_6	a'	3636 90.8	4.7341
AVTZ	ω_1	a_1	1055	137.8448
	ω_2	e	1676	14.7135
	ω_3	e	1676	14.7139
	ω_4	a_1	3474	4.2058
	ω_5	e	3600	4.623
	ω_6	e	3600	4.623
		zpe	90.2	
AVQZ	ω_1	a'	1044	140.796
	ω_2	a'	1674	15.0035
	ω_3	a'	1674	15.0039
	ω_4	a'	3495	3.916
	ω_5	a'	3630	5.1724
	ω_6	a'	3630	5.1722
		zpe	90.6	

Table E24: Cartesian coordinates of the geometries of PH_2^- optimised with the DSD-PBEP86-D3BJ functional, in Å.

		PH_2^-			PH_2		
		x	y	z	x	y	z
def2QZVP	P	0.000000	0.000000	0.116840	0.000000	0.000000	0.115835
	H	0.000000	1.029387	-0.876299	0.000000	1.019599	-0.868763
	H	0.000000	-1.029387	-0.876299	0.000000	-1.019599	-0.868763
AVTZ	P	0.000000	0.000000	0.116679	0.000000	0.000000	0.115978
	H	0.000000	1.030698	-0.875092	0.000000	1.020091	-0.869837
	H	0.000000	-1.030698	-0.875092	0.000000	-1.020091	-0.869837
AVQZ	P	0.000000	0.000000	0.116504	0.000000	0.000000	0.115839
	H	0.000000	1.030477	-0.873781	0.000000	1.019699	-0.868789
	H	0.000000	-1.030477	-0.873781	0.000000	-1.019699	-0.868789

Table E25: Cartesian coordinates of the geometries of H_2S optimised with the DSD-PBEP86-D3BJ functional, in Å.

		H_2S			PH_3			
		x	y	z	x	y	z	
def2QZVP	S	0.000000	0.000000	0.102781	P	0.000000	0.000001	-0.126975
	H	0.000000	0.965545	-0.822245	H	-1.043024	0.575049	0.634876
	H	0.000000	-0.965545	-0.822245	H	1.019524	0.615753	0.634875
AVTZ	S	0.000000	0.000000	0.102886	H	0.023501	-1.190812	0.634869
	H	0.000000	0.965934	-0.823091	P	0.000000	0.000000	-0.127250
	H	0.000000	-0.965934	-0.823091	H	-1.170366	-0.222913	0.636254
AVQZ	S	0.000000	0.000000	0.102797	H	0.392134	1.125026	0.636249
	H	0.000000	0.965779	-0.822380	H	0.778235	-0.902107	0.636253
	H	0.000000	-0.965779	-0.822380	P	0.000000	0.000000	-0.126986

Table E26: Cartesian coordinates of the geometries of HS^- optimised with the DSD-PBEP86-D3BJ functional, in Å.

		HS^-			HS		
		x	y	z	x	y	z
def2QZVP	S	0.000000	0.000000	0.079021	0.000000	0.000000	0.078877
	H	0.000000	0.000000	-1.264337	0.000000	0.000000	-1.262031
AVTZ	S	0.000000	0.000000	0.079079	0.000000	0.000000	0.078932
	H	0.000000	0.000000	-1.265257	0.000000	0.000000	-1.262910
AVQZ	S	0.000000	0.000000	0.082784	0.000000	0.000000	0.078888
	H	0.000000	0.000000	-1.324546	0.000000	0.000000	-1.262214

Table E27: Cartesian coordinates of the geometries of CH₄, CO₂ and NH₃ optimised with the DSD-PBEP86-D3BJ functional, in Å.

		CH ₄			
		x	y	z	
def2QZVP	C	0.000000	0.000000	0.000000	
	H	-0.627934	-0.627934	0.627934	
	H	0.627934	0.627934	0.627934	
	H	0.627934	-0.627934	-0.627934	
	H	-0.627934	0.627934	-0.627934	
	C	0.000000	0.000000	0.000000	
	H	0.628704	-0.628704	0.628704	
	H	-0.628704	0.628704	0.628704	
AVTZ	H	0.628704	0.628704	-0.628704	
	C	0.000000	0.000000	0.000000	
	H	0.628091	-0.628091	0.628091	
	H	-0.628091	0.628091	0.628091	
	H	0.628091	0.628091	-0.628091	
	H	-0.628091	-0.628091	-0.628091	
AVQZ		CO ₂			
		x	y	z	
	def2QZVP	C	0.000000	0.000000	0.000000
		O	0.000000	0.000000	1.162232
		O	0.000000	0.000000	-1.162232
	AVTZ	C	0.000000	0.000000	0.000000
		O	0.000000	0.000000	1.165021
		O	0.000000	0.000000	-1.165021
AVQZ	AVQZ	C	0.000000	0.000000	0.000000
		O	0.000000	0.000000	1.162538
		O	0.000000	0.000000	-1.162538
def2QZVP		NH ₃			
		x	y	z	
		N	0.000000	0.000000	-0.113482
		H	0.000000	0.938126	0.264794
		H	0.812442	-0.469063	0.264791
		H	-0.812442	-0.469063	0.264791
		N	0.000000	0.000000	0.113958
	AVTZ	H	0.000000	0.939421	-0.265901
		H	0.813563	-0.469711	-0.265901
		H	-0.813563	-0.469711	-0.265901
		N	0.000000	0.000000	0.113455
	AVQZ	H	0.000000	0.938681	-0.264726
		H	0.812921	-0.469340	-0.264728
		H	-0.812921	-0.469340	-0.264728

Table E28: PH₂⁻...CH₄ complex geometric parameters from DSD-PBEP86-D3BJ optimisations. zpe values are drawn from relevant harmonic frequency calculations.

		R _{P-H} Å	∠ _{H-P-H} °	R _{P-HC} Å	∠ _{H-P-HC} °	∠ _{H-P-HC-H} °	E E _h	zpe kJ mol ⁻¹	D _e kJ mol ⁻¹	D ₀ kJ mol ⁻¹	E _{VDE} E _h	VDE eV
1a: C _s (¹ A')	def2QZVP	1.430	92.1	3.083	86.2	46.2	-382.7233549	154.8	12.9	15.9	-382.6805931	1.154
	AVTZ	1.431	92.1	3.090	59.8	56.4	-382.7114078	154.7	9.4	12.4	-382.6652806	1.247
	AVQZ	1.429	92.1	3.102	59.9	56.3	-382.7279731	154.9	9.0	12.0	-382.6809052	1.281
	W1w						-382.5847342		8.5	11.5	-382.5358873	1.329
	W2w						-382.5849780		8.6	11.6	-382.5361853	1.328
1b: C _s (¹ A')	def2QZVP	1.430	92.1	3.083	86.2	46.2	-382.7233549	154.8	12.9	15.9	-382.6805931	1.154
	AVTZ	1.430	92.4	2.962	131.2	106.5	-382.7114930	154.3	9.4	11.9	-382.6649229	1.033
	AVQZ	1.428	92.5	2.975	130.9	107.1	-382.7280826	154.4	9.3	12.3	-382.6805700	1.293
	W1w						-382.5848299		8.8	11.4	-382.5355584	1.341
	W2w						-382.5850850		8.8	11.4	-382.5358724	1.339
		R _{P-H} Å	∠ _{H-P-H} °	R _{P-HC} Å	∠ _{H-P-HC} °	∠ _{H-P-HC-H} °	E E _h	zpe kJ mol ⁻¹	D _e kJ mol ⁻¹	D ₀ kJ mol ⁻¹	ADE eV	ADE _{shift} eV
1c: C ₁ (² A)	def2QZVP	1.417	90.8	3.832	71.0	29.6	-382.6811472	156.1	2.9	5.5	1.162	1.363
	AVTZ	1.419	91.9	3.796	67.0	51.4	-382.6658038	156.0	3.3	6.0	1.254	1.323
	AVQZ	1.417	92.0	3.806	66.5	51.6	-382.6814248	156.2	3.1	6.0	1.281	1.322
	W1w						-382.5363871		2.4	5.3	1.330	1.324
	W2w						-382.5366800		2.5	5.3	1.328	1.324
1d: C _s (² A'')	def2QZVP	1.417	92.0	2.971	180.0	0.0	-382.6811347	155.5	2.8	4.8	1.156	1.357
	AVTZ	1.418	92.0	2.937	180.0	0.0	-382.6655370	155.5	2.6	4.8	1.256	1.324
	AVQZ	1.417	92.0	2.949	180.0	0.0	-382.6811585	155.2	2.4	4.2	1.277	1.319
	W1w						-382.5362373		2.0	3.8	1.323	1.317
	W2w						-382.5365265		2.1	3.9	1.322	1.317
1e: C _s (² A')	def2QZVP	1.417	92.1	3.747	60.3	180.0	-382.6810515	156.3	2.6	5.4	1.166	1.367
	AVTZ	1.418	92.1	3.722	61.1	180.0	-382.6659195	156.1	3.6	6.5	1.252	1.321
	AVQZ	1.417	92.2	3.735	60.5	180.0	-382.6815348	156.3	3.4	6.3	1.278	1.320
	W1w						-382.5365107		2.7	5.6	1.327	1.321
	W2w						-382.5368122		2.8	5.7	1.325	1.321

Table E29: DSD-PBEP86-D3BJ and extrapolated single-point energies for $\text{PH}_2^- \cdots \text{CH}_4$ complexes. Geometries use for CC energies are from DSD-PBEP86-D3BJ/AVQZ optimisations. All energies are in E_h .

	1a: $\text{PH}_2^- \cdots \text{CH}_4$ (${}^1A'$)						
	E_{DH-DFT}	E_{SCF}	E_{CCSD}	E_{corr}	$E_{CCSD(T)}$	$E_{(T)}$	E_{Wnw}
def2QZVP	-382.7233549						
AVDZ		-382.0802005	-382.4491184	-0.3689179	-382.4605102	-0.0113918	
AVTZ	-382.7114078	-382.1048448	-382.5332304	-0.4283856	-382.549801	-0.0165706	
AVQZ	-382.7279731	-382.1104296	-382.5543292	-0.4438996	-382.5721628	-0.0178336	
AV5Z		-382.1116808	-382.5604763	-0.4487955			
W1w		-382.1121673		-0.4540711		-0.0184959	-382.5847342
W2w		-382.1122906		-0.4539322		-0.0187552	-382.5849780
	1a: VDE $\text{PH}_2^- \cdots \text{CH}_4$ (${}^2A'$)						
def2QZVP	-382.6805931						
AVDZ		-382.0763333	-382.4110819	-0.3347486	-382.4197018	-0.0086199	
AVTZ	-382.6652806	-382.1013494	-382.4907278	-0.3893784	-382.5035697	-0.0128419	
AVQZ	-382.6809052	-382.1069602	-382.5104670	-0.4035068	-382.5243344	-0.0138674	
AV5Z		-382.1082396	-382.5162358	-0.4079962			
W1w		-382.1087059		-0.4127699		-0.0144115	-382.5358873
W2w		-382.1088632		-0.4127064		-0.0146157	-382.5361853
	1b: $\text{PH}_2^- \cdots \text{CH}_4$ (${}^1A'$)						
def2QZVP	-382.7233549						
-382.0805896	-382.4491800	-0.3685904	-382.4605012	-0.0113212			
AVTZ	-382.7114930	-382.105289	-382.5333342	-0.4280452	-382.5498457	-0.0165115	
AVQZ	-382.7280826	-382.1108776	-382.5544620	-0.4435844	-382.5722386	-0.0177766	
AV5Z		-382.1121359	-382.5606255	-0.4484896			
W1w		-382.1126164		-0.4537724		-0.0184411	-382.5848299
W2w		-382.1127492		-0.4536360		-0.0186998	-382.5850850
	1b: VDE $\text{PH}_2^- \cdots \text{CH}_4$ (${}^2A'$)						
def2QZVP	-382.6805931						
AVDZ		-382.0759714	-382.4106290	-0.3346576	-382.4192478	-0.0086188	
AVTZ	-382.6649229	-382.1010275	-382.4903753	-0.3893478	-382.5032158	-0.0128405	
AVQZ	-382.6805700	-382.1066384	-382.5101297	-0.4034913	-382.5239974	-0.0138677	
AV5Z		-382.107923	-382.5159111	-0.4079881			
W1w		-382.1083842		-0.4127643		-0.0144100	-382.5355584
W2w		-382.1085491		-0.4127061		-0.0146173	-382.5358724

Table E30: DSD-PBEP86-D3BJ and extrapolated single-point energies for $\text{PH}_2 \cdots \text{CH}_4$ complexes. Geometries use for CC energies are from DSD-PBEP86-D3BJ/AVQZ optimisations. All energies are in E_h .

	1c: $\text{PH}_2 \cdots \text{CH}_4$ ($^2A'$)						
	E_{DH-DFT}	E_{SCF}	E_{CCSD}	E_{corr}	$E_{CCSD(T)}$	$E_{(T)}$	E_{Wnw}
def2QZVP	-382.6811472						
AVDZ		-382.0800525	-382.4111893	-0.3311368	-382.4197590	-0.0085697	
AVTZ	-382.6658038	-382.1018887	-382.4911527	-0.3892640	-382.5039537	-0.0128010	
AVQZ	-382.6814248	-382.1075165	-382.5109633	-0.4034468	-382.5247942	-0.0138309	
AV5Z		-382.1087996	-382.5167486	-0.4079490			
W1w		-382.1092675		-0.4127455		-0.0143740	-382.5363871
W2w		-382.1094250		-0.4126726		-0.0145824	-382.5366800
	1d: $\text{PH}_2 \cdots \text{CH}_4$ ($^2A''$)						
def2QZVP	-382.6811347						
AVDZ		-382.0771234	-382.4112112	-0.3340878	-382.4197294	-0.0085182	
AVTZ	-382.6655370	-382.1022504	-382.4910991	-0.3888487	-382.5038357	-0.0127366	
AVQZ	-382.6811585	-382.1078947	-382.5108968	-0.4030021	-382.5246551	-0.0137583	
AV5Z		-382.1091794	-382.5166784	-0.4074990			
W1w		-382.1096509		-0.4122816		-0.0143048	-382.5362373
W2w		-382.1098055		-0.4122171		-0.0145039	-382.5365265
	1e: $\text{PH}_2 \cdots \text{CH}_4$ ($^2A''$)						
def2QZVP	-382.6810515						
AVDZ		-382.0766971	-382.4110793	-0.3343822	-382.4196488	-0.0085695	
AVTZ	-382.6659195	-382.102014	-382.4912998	-0.3892858	-382.5041084	-0.0128086	
AVQZ	-382.6815348	-382.1076449	-382.5110905	-0.4034456	-382.5249284	-0.0138379	
AV5Z		-382.1089315	-382.516876	-0.4079445			
W1w		-382.1093969		-0.4127293		-0.0143845	-382.5365107
W2w		-382.1095586		-0.4126647		-0.0145890	-382.5368122

Table E31: Cartesian coordinates of the PH₂⁻ ...CH₄ conformers optimised at DSD-PBEP86-D3BJ/def-2QZVP,AVTZ in Å.

		1a*: PH ₂ ⁻ ...CH ₄ (¹ A')			1b*: PH ₂ ⁻ ...CH ₄ (¹ A')		
		x	y	z	x	y	z
deg2QZVP	C	-0.035952	2.513407	0.000000	0.073181	2.620418	0.000000
	H	0.218045	3.576651	0.000000	0.118722	1.528180	0.000000
	H	-1.123482	2.381100	0.000000	1.082580	3.032603	0.000000
	H	0.373906	2.020440	0.879577	-0.455498	2.966064	0.888543
	H	0.373906	2.020440	-0.879577	-0.455498	2.966064	-0.888543
	P	-0.035952	-1.576763	0.000000	0.073181	-1.554760	0.000000
	H	0.456312	-0.713813	1.029114	-0.913556	-1.447006	1.029078
AVTZ	H	0.456312	-0.713813	-1.029114	-0.913556	-1.447006	-1.029078
		x	y	z	x	y	z
C	0.049035	2.570934	0.000000	0.019239	2.619923	0.000000	
C	0.182014	1.486795	0.000000	-0.073691	1.532204	0.000000	
H	1.023752	3.061318	0.000000	1.073919	2.897907	0.000000	
H	-0.506231	2.871862	0.889608	-0.462001	3.029796	0.889247	
P	-0.506231	2.871862	-0.889608	-0.462001	3.029796	-0.889247	
	H	0.049035	-1.600049	0.000000	0.019239	-1.429414	0.000000
	H	-0.611521	-0.858355	1.029521	-0.240123	-2.384016	1.031978
	H	-0.611521	-0.858355	-1.029521	-0.240123	-2.384016	-1.031978

Table E32: Cartesian coordinates of the PH₂⁻...CH₄ conformers optimised at DSD-PBEP86-D3BJ/def-2QZVP,AVnZ ($n = T, Q$) in Å.

	1a: PH ₂ ⁻ ...CH ₄ (¹ A')			1b: PH ₂ ⁻ ...CH ₄ (¹ A')			
	x	y	z	x	y	z	
def2QZVP	C	-0.073142	2.620188	0.000000			
	H	-0.117195	1.527888	0.000000			
	H	0.967321	2.945351	0.000000			
	H	-0.570646	3.009427	0.888654			
	H	-0.570646	3.009427	-0.888654			
	P	-0.073142	-1.554661	0.000000			
	H	0.913580	-1.446656	-1.029072			
	H	0.913580	-1.446656	1.029072			
	x	y	z	x	y	z	
	C	-0.048431	2.570561	0.000000	-0.019869	2.617840	0.000000
AVTZ	H	-0.180643	1.486360	0.000000	0.089137	1.531581	0.000000
	H	1.015968	2.809303	0.000000	0.964909	3.087349	0.000000
	H	-0.513920	2.997408	0.889757	-0.568927	2.931085	0.889104
	H	-0.513920	2.997408	-0.889757	-0.568927	2.931085	-0.889104
	P	-0.048431	-1.600602	0.000000	-0.019869	-1.428527	0.000000
	H	0.604783	-0.852411	-1.029499	0.250533	-2.380117	-1.031946
	H	0.604783	-0.852411	1.029499	0.250533	-2.380117	1.031946
	x	y	z	x	y	z	
	C	-0.048491	2.577705	0.000000	-0.020711	2.624637	0.000000
	H	-0.184244	1.495033	0.000000	0.092637	1.539877	0.000000
pVQZ	H	1.015701	2.812258	0.000000	0.961149	3.097747	0.000000
	H	-0.512011	3.005616	0.888933	-0.570518	2.935169	0.888248
	H	-0.512011	3.005616	-0.888933	-0.570518	2.935169	-0.888248
	P	-0.048491	-1.604482	0.000000	-0.020711	-1.433079	0.000000
	H	0.605442	-0.858760	-1.029241	0.261089	-2.379802	-1.031744
	H	0.605442	-0.858760	1.029241	0.261089	-2.379802	1.031744

Table E33: Cartesian coordinates of the PH₂ ... CH₄ conformers optimised at DSD-PBEP86-D3BJ/def-2QZVP,AVnZ ($n = T, Q$) in Å.

	1c: PH ₂ ... CH ₄ (² A')			1d: PH ₂ ... CH ₄ (² A'')			1e: PH ₂ ... CH ₄ (² A'')			
	x	y	z	x	y	z	x	y	z	
def2QZVP	C	-2.371825	0.002293	-0.021152	-0.052463	-2.712074	0.000000	2.381029	-0.003003	0.000000
	H	-3.441739	0.170226	-0.122767	-0.051785	-3.799739	0.000000	1.863143	-0.959542	0.000000
	H	-2.011967	0.489222	0.882559	0.972937	-2.348912	0.000000	3.455621	-0.171184	0.000000
	H	-1.855794	0.414812	-0.885464	-0.565570	-2.350299	0.888397	2.102421	0.559708	0.888436
	H	-2.176370	-1.066016	0.040528	-0.565570	-2.350299	-0.888397	2.102421	0.559708	-0.888436
	P	1.459377	-0.016280	-0.082759	-0.052463	0.258728	0.000000	-1.364883	-0.108313	0.000000
	H	1.015078	1.121192	0.636746	-0.052463	1.675818	0.000000	-0.697059	1.141350	0.000000
	H	0.811081	-0.898986	0.816697	1.364167	1.725693	0.000000	-2.639478	0.512678	0.000000
	x	y	z	x	y	z	x	y	z	
AVTZ	C	0.060343	2.348877	0.000000	-0.052509	-2.691408	0.000000	-0.069709	-2.364873	0.000000
	H	0.110694	3.436846	0.000000	-0.047790	-3.780400	0.000000	-1.019211	-1.831498	0.000000
	H	-0.981978	2.032986	0.000000	0.972743	-2.323815	0.000000	-0.254618	-3.438074	0.000000
	H	0.556917	1.962019	0.888838	-0.567573	-2.330990	0.889473	0.497951	-2.094592	0.889529
	H	0.556917	1.962019	-0.888838	-0.567573	-2.330990	-0.889473	0.497951	-2.094592	-0.889529
	P	0.060343	-1.446896	0.000000	-0.052509	0.245538	0.000000	-0.069709	1.356905	0.000000
	H	-0.754874	-0.891842	1.019590	-0.052509	1.663767	0.000000	1.171496	0.670953	0.000000
	H	-0.754874	-0.891842	-1.019590	1.365397	1.712603	0.000000	0.570322	2.623458	0.000000
	x	y	z	x	y	z	x	y	z	
pVQZ	C	0.059762	2.354929	0.000000	0.052466	2.698679	0.000000	0.069850	2.372245	0.000000
	H	0.117044	3.441488	0.000000	0.048017	3.786610	0.000000	0.256560	3.444057	0.000000
	H	-0.983575	2.046079	0.000000	-0.971923	2.331785	0.000000	1.017557	1.837762	0.000000
	H	0.553363	1.965317	0.888012	0.566958	2.338558	0.888639	-0.497753	2.103288	-0.888673
	H	0.553363	1.965317	-0.888012	0.566958	2.338558	-0.888639	-0.497753	2.103288	0.888673
	P	0.059762	-1.451551	0.000000	0.052466	-0.250741	0.000000	-1.162862	-0.663611	0.000000
	H	-0.747600	-0.887251	1.019224	0.052466	-1.667926	0.000000	0.069850	-1.362458	0.000000
	H	-0.747600	-0.887251	-1.019224	-1.364271	-1.717951	0.000000	-0.582597	-2.621387	0.000000

Table E34: Calculated harmonic frequencies and mode assignments for the 1a* PH₂⁻...CH₄ complex. All frequencies and intensities are in cm⁻¹ and km mol⁻¹.

1a* PH ₂ ⁻ ...CH ₄ (¹ A')					
	Mode	Symmetry	Frequency (cm ⁻¹)	Intensity (km mol ⁻¹)	Description
def2QZVP	ω_1	a''	1	0.1581	CH ₃ rotation
	ω_2	a'	68	2.4678	PH ₂ wag
	ω_3	a''	81	0.0514	PH ₂ twist
	ω_4	a'	89	10.3126	Intermolecular stretch
	ω_5	a'	168	0.2721	CH ₄ rotation
	ω_6	a''	171	0.1465	CH ₄ rotation
	ω_7	a'	1092	29.1015	PH ₂ scissor
	ω_8	a'	1309	10.7655	CH ₄ wag
	ω_9	a'	1369	3.3962	CH ₄ wag
	ω_{10}	a''	1369	3.6533	CH ₄ wag
	ω_{11}	a'	1574	0.6468	CH ₄ scissor
	ω_{12}	a''	1574	0.6123	CH ₄ twist
	ω_{13}	a'	2317	204.156	PH ₂ symm. stretch
	ω_{14}	a''	2318	236.725	PH ₂ asymm. stretch
	ω_{15}	a'	2995	149.708	CH ₄ symm. stretch
	ω_{16}	a'	3115	11.277	CH ₃ symm. stretch
	ω_{17}	a'	3137	42.9577	CH ₃ asymm. stretch
	ω_{18}	a''	3139	41.49	CH ₂ asymm. stretch
		zpe	154.8		
AVTZ	ω_1	a''	10 <i>i</i>	0.0048	CH ₃ rotation
	ω_2	a'	72	0.5828	PH ₂ wag
	ω_3	a'	76	11.0615	Intermolecular stretch
	ω_4	a''	99	0.3158	PH ₂ twist
	ω_5	a'	132	0.2368	CH ₄ rotation
	ω_6	a''	138	0.0405	CH ₄ rotation
	ω_7	a'	1092	35.7016	PH ₂ scissor
	ω_8	a'	1317	11.1405	CH ₄ wag
	ω_9	a''	1364	1.7543	CH ₄ wag
	ω_{10}	a'	1364	0.9393	CH ₄ wag
	ω_{11}	a''	1573	2.2092	CH ₄ twist
	ω_{12}	a'	1573	2.7518	CH ₄ scissor
	ω_{13}	a'	2315	198.1386	PH ₂ symm. stretch
	ω_{14}	a''	2318	188.8247	PH ₂ asymm. stretch
	ω_{15}	a'	3011	94.3277	CH ₄ symm. stretch
	ω_{16}	a'	3132	8.4113	CH ₃ symm. stretch
	ω_{17}	a'	3138	31.4523	CH ₃ asymm. stretch
	ω_{18}	a''	3139	35.0357	CH ₂ asymm. stretch
		zpe	154.6		

Table E35: Calculated harmonic frequencies and mode assignments for the 1b* PH₂⁻...CH₄ complex. All frequencies and intensities are in cm⁻¹ and km mol⁻¹.

1b* PH ₂ ⁻ ...CH ₄ (¹ A')					
	Mode	Symmetry	Frequency (cm ⁻¹)	Intensity (km mol ⁻¹)	Description
AVTZ	ω_1	a''	13 <i>i</i>	0.0384	CH ₃ rotation
	ω_2	a''	19	0.342	PH ₂ rock
	ω_3	a'	36	3.4581	PH ₂ wag
	ω_4	a'	83	13.0149	Intermolecular stretch
	ω_5	a'	118	0.6014	CH ₄ rotation
	ω_6	a''	141	0.081	CH ₄ rotation
	ω_7	a'	1090	37.2545	PH ₂ scissor
	ω_8	a'	1318	9.457	CH ₄ wag
	ω_9	a'	1363	1.3666	CH ₄ wag
	ω_{10}	a''	1368	3.0187	CH ₄ wag
	ω_{11}	a'	1573	2.6146	CH ₄ scissor
	ω_{12}	a''	1577	0.8468	CH ₄ twist
	ω_{13}	a'	2320	229.2051	PH ₂ symm. stretch
	ω_{14}	a''	2324	200.7212	PH ₂ asymm. stretch
	ω_{15}	a'	3016	68.9645	CH ₄ symm. stretch
	ω_{16}	a''	3138	38.8199	CH ₂ asymm. stretch
	ω_{17}	a'	3140	14.1356	CH ₃ asymm. stretch
	ω_{18}	a'	3142	23.2757	CH ₃ symm. stretch
	zpe		154.0		

Table E36: Calculated harmonic frequencies and mode assignments for the 1a PH₂⁻...CH₄ complex. All frequencies and intensities are in cm⁻¹ and km mol⁻¹ respectively.

1a PH ₂ ⁻ ...CH ₄ (¹ A')					
	Mode	Symmetry	Frequency (cm ⁻¹)	Intensity (km mol ⁻¹)	Description
def2QZVP	ω_1	a''	7	0.1423	CH ₃ rotation
	ω_2	a'	68	2.5872	PH ₂ wag
	ω_3	a''	82	0.0596	PH ₂ twist
	ω_4	a'	89	10.2063	Intermolecular stretch
	ω_5	a'	165	0.2649	CH ₄ rotation
	ω_6	a''	175	0.165	CH ₄ rotation
	ω_7	a'	1092	29.1229	PH ₂ scissor
	ω_8	a'	1309	10.7452	CH ₄ wag
	ω_9	a'	1369	3.7869	CH ₄ wag
	ω_{10}	a''	1370	3.113	CH ₄ wag
	ω_{11}	a'	1574	0.6306	CH ₄ scissor
	ω_{12}	a''	1575	0.5073	CH ₄ twist
	ω_{13}	a'	2317	204.3525	PH ₂ symm. stretch
	ω_{14}	a''	2318	237.1507	PH ₂ asymm. stretch
	ω_{15}	a'	2995	149.8341	CH ₄ symm. stretch
	ω_{16}	a'	3115	11.2668	CH ₃ symm. stretch
	ω_{17}	a''	3137	43.2604	CH ₂ asymm. stretch
	ω_{18}	a'	3139	41.2549	CH ₃ asymm. stretch
AVTZ	zpe		154.8		
	ω_1	a''	12	0.0059	CH ₃ rotation
	ω_2	a'	73	0.5691	PH ₂ wag
	ω_3	a'	76	11.1056	Intermolecular stretch
	ω_4	a''	99	0.2721	PH ₂ twist
	ω_5	a'	129	0.2454	CH ₄ rotation
	ω_6	a''	142	0.025	CH ₄ rotation
	ω_7	a'	1092	35.9279	PH ₂ scissor
	ω_8	a'	1317	11.2039	CH ₄ wag
	ω_9	a'	1363	1.0873	CH ₄ wag
	ω_{10}	a''	1365	1.3598	CH ₄ wag
	ω_{11}	a'	1573	2.8914	CH ₄ scissor
	ω_{12}	a''	1574	2.0488	CH ₄ twist
	ω_{13}	a'	2315	197.714	PH ₂ symm. stretch
	ω_{14}	a''	2318	189.2301	PH ₂ asymm. stretch
	ω_{15}	a'	3011	92.9888	CH ₄ symm. stretch
	ω_{16}	a'	3132	8.6751	CH ₃ symm. stretch
	ω_{17}	a''	3137	37.151	CH ₂ asymm. stretch
	ω_{18}	a'	3140	29.6626	CH ₃ asymm. stretch
	zpe		154.7		

Continued on next page

Table E37: (Continued) Calculated harmonic frequencies and mode assignments for the 1a PH₂⁻...CH₄ complex. All frequencies and intensities are in cm⁻¹ and km mol⁻¹ respectively.

1a PH ₂ ⁻ ...CH ₄ (¹ A')					
	Mode	Symmetry	Frequency (cm ⁻¹)	Intensity (km mol ⁻¹)	Description
AVQZ	ω_1	a''	29	0.0044	CH ₃ rotation
	ω_2	a'	72	0.9176	PH ₂ wag
	ω_3	a'	74	10.6424	Intermolecular stretch
	ω_4	a''	97	0.2418	PH ₂ twist
	ω_5	a'	128	0.3763	CH ₄ rotation
	ω_6	a''	142	0.0143	CH ₄ rotation
	ω_7	a'	1093	34.9205	PH ₂ scissor
	ω_8	a'	1314	11.4156	CH ₄ wag
	ω_9	a'	1360	1.1975	CH ₄ wag
	ω_{10}	a''	1363	1.5206	CH ₄ wag
	ω_{11}	a'	1571	2.7352	CH ₄ scissor
	ω_{12}	a''	1572	1.9847	CH ₄ twist
	ω_{13}	a'	2321	193.4139	PH ₂ symm. stretch
	ω_{14}	a''	2324	181.681	PH ₂ asymm. stretch
	ω_{15}	a'	3013	90.8811	CH ₄ symm. stretch
	ω_{16}	a'	3136	8.6527	CH ₃ symm. stretch
	ω_{17}	a''	3141	35.8944	CH ₂ asymm. stretch
	ω_{18}	a'	3144	28.6851	CH ₃ asymm. stretch
			zpe	154.9	

Table E38: Calculated harmonic frequencies and mode assignments for the 1b PH₂⁻...CH₄ complex. All frequencies and intensities are in cm⁻¹ and km mol⁻¹ respectively.

1b PH ₂ ⁻ ...CH ₄ (¹ A')					
	Mode	Symmetry	Frequency (cm ⁻¹)	Intensity (km mol ⁻¹)	Description
AVTZ	ω_1	a''	13	0.3994	CH ₃ rotation
	ω_2	a''	21	0.0555	PH ₂ twist
	ω_3	a'	45	3.8211	PH ₂ wag
	ω_4	a'	83	12.6362	Intermolecular stretch
	ω_5	a'	122	0.6753	CH ₄ rotation
	ω_6	a''	139	0.0662	CH ₄ rotation
	ω_7	a'	1090	37.1173	PH ₂ scissor
	ω_8	a'	1318	9.3723	CH ₄ wag
	ω_9	a'	1364	1.0765	CH ₄ wag
	ω_{10}	a''	1367	3.1573	CH ₄ wag
	ω_{11}	a'	1573	2.4469	CH ₄ scissor
	ω_{12}	a''	1576	0.7898	CH ₄ twist
	ω_{13}	a'	2320	228.556	PH ₂ symm. stretch
	ω_{14}	a''	2324	200.7732	PH ₂ asymm. stretch
	ω_{15}	a'	3016	70.3643	CH ₄ symm. stretch
	ω_{16}	a'	3139	25.8358	CH ₃ symm. stretch
	ω_{17}	a'	3140	13.2289	CH ₃ asymm. stretch
	ω_{18}	a''	3140	37.3308	CH ₂ asymm. stretch
AVQZ	zpe		154.3		
	ω_1	a''	15	0.3942	CH ₃ rotation
	ω_2	a''	37	0.0032	PH ₂ twist
	ω_3	a'	45	4.0852	PH ₂ wag
	ω_4	a'	82	12.5085	Intermolecular stretch
	ω_5	a'	121	0.5867	CH ₄ rotation
	ω_6	a''	141	0.0495	CH ₄ rotation
	ω_7	a'	1091	36.5251	PH ₂ scissor
	ω_8	a'	1316	9.6785	CH ₄ wag
	ω_9	a'	1361	1.2021	CH ₄ wag
	ω_{10}	a''	1364	3.1736	CH ₄ wag
	ω_{11}	a'	1572	2.5	CH ₄ scissor
	ω_{12}	a''	1574	0.8286	CH ₄ twist
	ω_{13}	a'	2327	219.0521	PH ₂ symm. stretch
	ω_{14}	a''	2330	191.3157	PH ₂ asymm. stretch
	ω_{15}	a'	3017	69.821	CH ₄ symm. stretch
	ω_{16}	a'	3142	22.0635	CH ₃ symm. stretch
	ω_{17}	? a	3143	16.1231	CH ₃ asymm. stretch
	ω_{18}	? a	3143	35.9165	CH ₂ asymm. stretch
	zpe		154.4		

Table E39: Calculated harmonic frequencies and mode assignments for the 1c PH₂ ··· CH₄ complex. All frequencies and intensities are in cm⁻¹ and km mol⁻¹ respectively.

1c PH ₂ ··· CH ₄ (² A')					
	Mode	Symmetry	Frequency (cm ⁻¹)	Intensity (km mol ⁻¹)	Description
def2QZVP	ω_1	<i>a</i>	21	1.0268	CH ₃ rotation
	ω_2	<i>a</i>	45	0.5739	CH ₄ rotation
	ω_3	<i>a</i>	52	0.9012	CH ₄ rotation
	ω_4	<i>a</i>	65	0.0972	CH ₄ rotation
	ω_5	<i>a</i>	79	1.5373	PH ₂ twist
	ω_6	<i>a</i>	98	5.5587	PH ₂ wag
	ω_7	<i>a</i>	1137	21.46	PH ₂ scissor
	ω_8	<i>a</i>	1346	20.195	CH ₄ wag
	ω_9	<i>a</i>	1348	11.9445	CH ₄ wag
	ω_{10}	<i>a</i>	1349	12.7396	CH ₄ wag
	ω_{11}	<i>a</i>	1572	0.6802	CH ₄ twist
	ω_{12}	<i>a</i>	1572	0.8213	CH ₄ scissor
	ω_{13}	<i>a</i>	2425	47.9591	PH ₂ symm. stretch
	ω_{14}	<i>a</i>	2434	56.8176	PH ₂ asymm. stretch
	ω_{15}	<i>a</i>	3048	0.1249	CH ₄ symm. stretch
	ω_{16}	<i>a</i>	3169	17.65	CH ₂ asymm. stretch
	ω_{17}	<i>a</i>	3170	17.0136	CH ₂ asymm. stretch
	ω_{18}	<i>a</i>	3171	26.1785	CH ₃ asymm. stretch
AVTZ	zpe		156.1		
	ω_1	<i>a''</i>	14	0.8014	CH ₃ rotation
	ω_2	<i>a''</i>	49	0.7893	PH ₂ twist
	ω_3	<i>a'</i>	52	0.8055	Intermolecular stretch
	ω_4	<i>a'</i>	64	0.1312	CH ₄ rotation
	ω_5	<i>a''</i>	89	0.4391	PH ₂ twist
	ω_6	<i>a'</i>	100	5.8726	PH ₂ wag
	ω_7	<i>a'</i>	1136	21.5108	PH ₂ scissor
	ω_8	<i>a'</i>	1347	20.0861	CH ₄ wag
	ω_9	<i>a''</i>	1349	11.2709	CH ₄ wag
	ω_{10}	<i>a'</i>	1350	11.8573	CH ₄ wag
	ω_{11}	<i>a'</i>	1573	0.8004	CH ₄ scissor
	ω_{12}	<i>a''</i>	1574	0.8788	CH ₄ twist
	ω_{13}	<i>a'</i>	2418	49.6844	PH ₂ symm. stretch
	ω_{14}	<i>a''</i>	2426	56.3115	PH ₂ asymm. stretch
	ω_{15}	<i>a'</i>	3044	0.1359	CH ₄ symm. stretch
	ω_{16}	<i>a''</i>	3164	16.2277	CH ₂ asymm. stretch
	ω_{17}	<i>a'</i>	3165	16.5118	CH ₃ asymm. stretch
	ω_{18}	<i>a'</i>	3165	29.0321	CH ₃ symm. stretch
	zpe		156.0		

Continued on next page

Table E40: Calculated harmonic frequencies and mode assignments for the 1c PH₂⋯CH₄ complex. All frequencies and intensities are in cm⁻¹ and km mol⁻¹ respectively.

1c PH ₂ ⋯CH ₄ (² A')					
	Mode	Symmetry	Frequency (cm ⁻¹)	Intensity (km mol ⁻¹)	Description
AVQZ	ω_1	a''	36	0.5843	CH ₃ rotation
	ω_2	?a	43	1.3404	PH ₂ twist
	ω_3	?a	49	0.8698	Intermolecular stretch
	ω_4	a'	64	0.2607	CH ₄ rotation
	ω_5	a''	97	0.146	PH ₂ twist
	ω_6	a'	110	5.8207	PH ₂ wag
	ω_7	a'	1137	21.5112	PH ₂ scissor
	ω_8	a'	1344	20.5647	CH ₄ wag
	ω_9	a''	1347	11.6328	CH ₄ wag
	ω_{10}	a'	1348	12.17	CH ₄ wag
	ω_{11}	a'	1571	0.7906	CH ₄ scissor
	ω_{12}	a''	1572	0.8325	CH ₄ twist
	ω_{13}	a'	2424	48.6644	PH ₂ symm. stretch
	ω_{14}	a''	2433	54.8431	PH ₂ asymm. stretch
	ω_{15}	a'	3045	0.149	CH ₄ symm. stretch
	ω_{16}	?a	3167	15.9531	CH ₂ asymm. stretch
	ω_{17}	a'	3167	16.1577	CH ₃ asymm. stretch
	ω_{18}	?a	3168	28.4659	CH ₃ symm. stretch
zpe			156.2		

Table E41: Calculated harmonic frequencies and mode assignments for the 1d PH₂ ··· CH₄ complex. All frequencies and intensities are in cm⁻¹ and km mol⁻¹ respectively.

1d PH ₂ ··· CH ₄ (² A'')					
	Mode	Symmetry	Frequency (cm ⁻¹)	Intensity (km mol ⁻¹)	Description
def2QZVP	ω_1	a''	-44	0.0878	PH ₂ twist
	ω_2	a'	-26	3.3368	PH ₂ rock
	ω_3	?a	53	0.0825	PH ₂ wag
	ω_4	?a	53	5.7252	Intermolecular stretch
	ω_5	a'	67	0.1562	CH ₄ rotation
	ω_6	a''	68	0.3107	CH ₄ rotation
	ω_7	a'	1139	23.6883	PH ₂ scissor
	ω_8	a'	1347	20.9717	CH ₄ wag
	ω_9	a'	1349	12.3862	CH ₄ wag
	ω_{10}	a''	1349	11.987	CH ₄ wag
	ω_{11}	a''	1573	0.255	CH ₄ twist
	ω_{12}	a'	1573	0.3101	CH ₄ scissor
	ω_{13}	a'	2426	46.4779	PH ₂ symm. stretch
	ω_{14}	a'	2438	45.9337	PH ₂ asymm. stretch
	ω_{15}	a'	3048	0.239	CH ₄ symm. stretch
	ω_{16}	a''	3170	17.7521	CH ₂ asymm. stretch
	ω_{17}	a'	3170	17.4547	CH ₃ asymm. stretch
	ω_{18}	a'	3172	27.3765	CH ₃ symm. stretch
AVTZ			zpe	155.5	
	ω_1	?a	3	2.9466	PH ₂ rock
	ω_2	?a	5	2.5263	Axial CH ₃ rotation
	ω_3	a''	36	2.4698	Planar CH ₃ rotation
	ω_4	a'	57	0.1207	Intermolecular stretch
	ω_5	a'	77	0.2875	CH ₄ rotation
	ω_6	a''	84	0.7545	CH ₄ rotation
	ω_7	a'	1138	24.3964	PH ₂ scissor
	ω_8	a'	1349	20.2213	CH ₄ wag
	ω_9	a'	1350	11.656	CH ₄ wag
	ω_{10}	a''	1351	11.2989	CH ₄ wag
	ω_{11}	a''	1575	0.3063	CH ₄ twist
	ω_{12}	a'	1575	0.3716	CH ₄ scissor
	ω_{13}	a'	2419	48.5192	PH ₂ symm. stretch
	ω_{14}	a'	2432	43.6817	PH ₂ asymm. stretch
	ω_{15}	a'	3044	0.281	CH ₄ symm. stretch
	ω_{16}	a''	3164	17.6433	CH ₂ asymm. stretch
	ω_{17}	a'	3165	17.5665	CH ₃ asymm. stretch
	ω_{18}	a'	3166	28.698	CH ₃ symm. stretch
			zpe	155.5	

Continued on next page

Table E42: Calculated harmonic frequencies and mode assignments for the 1d PH₂⋯CH₄ complex. All frequencies and intensities are in cm⁻¹ and km mol⁻¹ respectively.

1d PH ₂ ⋯CH ₄ (² A'')					
	Mode	Symmetry	Frequency (cm ⁻¹)	Intensity (km mol ⁻¹)	Description
AVQZ	ω_1	a''	-32	0.5393	PH ₂ twist
	ω_2	a'	-20	3.0911	PH ₂ rock
	ω_3	a''	48	5.1847	PH ₂ wag
	ω_4	a'	55	0.1029	Intermolecular stretch
	ω_5	? a	78	0.217	CH ₄ rotation
	ω_6	? a	78	0.0568	CH ₄ rotation
	ω_7	a'	1139	24.4042	PH ₂ scissor
	ω_8	a'	1346	20.5442	CH ₄ wag
	ω_9	? a	1348	11.9411	CH ₄ wag
	ω_{10}	? a	1348	11.4785	CH ₄ wag
	ω_{11}	? a	1573	0.3059	CH ₄ twist
	ω_{12}	? a	1573	0.3569	CH ₄ scissor
	ω_{13}	a'	2425	46.6648	PH ₂ symm. stretch
	ω_{14}	a'	2438	43.4458	PH ₂ asymm. stretch
	ω_{15}	a'	3045	0.272	CH ₄ symm. stretch
	ω_{16}	a''	3167	17.6732	CH ₂ asymm. stretch
	ω_{17}	a'	3167	17.335	CH ₃ asymm. stretch
	ω_{18}	a'	3169	27.897	CH ₃ symm. stretch
			zpe	155.2	

Table E43: Calculated harmonic frequencies and mode assignments for the 1e PH₂ ··· CH₄ complex. All frequencies and intensities are in cm⁻¹ and km mol⁻¹ respectively.

1e PH ₂ ··· CH ₄ (² A'')					
	Mode	Symmetry	Frequency (cm ⁻¹)	Intensity (km mol ⁻¹)	Description
def2QZVP	ω_1	a''	29	2.7853	PH ₂ wag
	ω_2	a''	44	0.4456	PH ₂ rock
	ω_3	a'	53	0.3471	PH ₂ twist
	ω_4	a'	77	0.1044	CH ₄ rotation
	ω_5	a''	83	1.882	CH ₄ rotation
	ω_6	a'	101	4.2178	PH ₂ rock
	ω_7	a'	1137	16.35	PH ₂ scissor
	ω_8	a'	1347	16.8418	CH ₄ wag
	ω_9	a'	1348	16.7974	CH ₄ wag
	ω_{10}	a''	1349	11.1787	CH ₄ wag
	ω_{11}	a''	1573	0.5949	CH ₄ twist
	ω_{12}	a'	1573	0.7199	CH ₄ scissor
	ω_{13}	a'	2424	51.6366	PH ₂ symm. stretch
	ω_{14}	a'	2435	67.0138	PH ₂ asymm. stretch
	ω_{15}	a'	3048	0.145	CH ₄ symm. stretch
	ω_{16}	a''	3169	17.2237	CH ₂ asymm. stretch
	ω_{17}	a'	3170	19.5201	CH ₄ asymm. stretch
	ω_{18}	a'	3172	23.3863	CH ₂ asymm. stretch
AVTZ		zpe	156.3		
	ω_1	a''	17	3.2193	PH ₂ wag
	ω_2	a'	50	0.6054	PH ₂ rock
	ω_3	a''	61	1.5448	PH ₂ twist
	ω_4	a'	77	0.1438	CH ₄ rotation
	ω_5	a''	78	0.1324	CH ₄ rotation
	ω_6	a'	100	3.6706	PH ₂ rock
	ω_7	a'	1137	16.441	PH ₂ scissor
	ω_8	a'	1348	15.5521	CH ₄ wag
	ω_9	a'	1350	16.833	CH ₄ wag
	ω_{10}	a''	1351	10.7087	CH ₄ wag
	ω_{11}	a''	1574	0.7388	CH ₄ twist
	ω_{12}	a'	1574	0.7404	CH ₄ scissor
	ω_{13}	a'	2417	53.7289	PH ₂ symm. stretch
	ω_{14}	a'	2428	67.417	PH ₂ asymm. stretch
	ω_{15}	a'	3044	0.1612	CH ₄ symm. stretch
	ω_{16}	a''	3163	17.3226	CH ₂ asymm. stretch
	ω_{17}	a'	3165	20.4835	CH ₄ asymm. stretch
	ω_{18}	a'	3167	23.7069	CH ₂ asymm. stretch
		zpe	156.1		

Continued on next page

Table E44: Calculated harmonic frequencies and mode assignments for the 1e PH₂⋯CH₄ complex. All frequencies and intensities are in cm⁻¹ and km mol⁻¹ respectively.

1e PH ₂ ⋯CH ₄ (² A'')					
	Mode	Symmetry	Frequency (cm ⁻¹)	Intensity (km mol ⁻¹)	Description
AVQZ	ω_1	a''	28	3.3314	PH ₂ wag
	ω_2	a''	50	0.5331	PH ₂ twist
	ω_3	a'	54	0.4272	PH ₂ rock
	ω_4	?a	78	0.1986	CH ₄ rotation
	ω_5	?a	85	1.0266	CH ₄ rotation
	ω_6	a'	103	3.9041	PH ₂ rock
	ω_7	a'	1138	16.534	PH ₂ scissor
	ω_8	a'	1346	16.5779	CH ₄ wag
	ω_9	a'	1347	16.4168	CH ₄ wag
	ω_{10}	a''	1348	10.8595	CH ₄ wag
	ω_{11}	a''	1572	0.6762	CH ₄ twist
	ω_{12}	a'	1573	0.7256	CH ₄ scissor
	ω_{13}	a'	2423	52.1266	PH ₂ symm. stretch
	ω_{14}	a'	2434	65.7813	PH ₂ asymm. stretch
	ω_{15}	a'	3045	0.1559	CH ₄ symm. stretch
	ω_{16}	a''	3166	16.9257	CH ₂ asymm. stretch
	ω_{17}	a'	3167	18.9687	CH ₄ asymm. stretch
	ω_{18}	a'	3169	24.3004	CH ₂ asymm. stretch
			zpe	156.3	

Table E45: PH₂⁻...C₂H₄ complex geometric parameters, D_0 s and VDEs from DSD-PBEP86-D3BJ optimisations. zpe values are drawn from relevant harmonic frequency calculations.

		R_{P-H} Å	\angle_{H-P-H} °	$R_{P-\parallel}$ Å	$\angle_{H-P-\parallel}$ °	$\angle_{H-P-C-C}$ °	E E_h	zpe kJ mol ⁻¹	D_e kJ mol ⁻¹	D_0 kJ mol ⁻¹	E_{VDE} E_h	VDE eV
2a: C_s ($^1A'$)	def2QZVP	1.429	88.3	3.740	133.8	99.5	-420.7440744	171.6	21.1	24.4	-420.6987569	1.222
	AVTZ	1.429	88.2	3.763	133.7	99.5	-420.7268803	171.5	19.1	22.6	-420.6777207	1.326
	AVQZ	1.428	88.2	3.767	133.7	99.4	-420.7496618	171.9	18.7	22.3	-420.6995663	1.351
	W1w						-420.6052977		17.7	21.3	-420.5536224	1.394
	W2w						-420.6053553		17.8	21.4	-420.5537311	1.393
	def2QZVP	1.429	88.5	4.340	85.9	46.1	-420.7443278	171.2	21.7	24.7	-420.6982256	1.245
2b: C_s ($^1A'$)	AVTZ	1.430	88.5	3.999	48.7	66.0	-420.7262186	171.8	17.4	21.1	-420.6779178	1.302
	AVQZ	1.429	88.5	4.007	49.1	65.0	-420.7489633	172.1	16.8	20.7	-420.6997271	1.327
	W1w						-420.6046892		16.1	20.0	-420.5536224	1.376
	W2w						-420.6047426		16.2	20.0	-420.5537311	1.375
	def2QZVP	1.430	88.5	4.380	91.8	133.9	-420.7442858	171.2	21.6	24.6	-420.6981879	1.245
	AVTZ	1.431	88.6	4.411	69.1	127.3	-420.7262186	170.7	17.4	20.0	-420.6771064	1.332
2c: C_s ($^1A'$)	AVQZ	1.430	88.5	4.422	70.1	127.8	-420.7488135	171.1	16.8	19.6	-420.6989398	1.348
	W1w						-420.6044733		15.6	18.4	-420.5528628	1.395
	W2w						-420.6045226		15.6	18.4	-420.5529692	1.394

Table E46: PH₂⋯C₂H₄ complex geometric parameters, D_0 s and ADEs from DSD-PBEP86-D3BJ optimisations. zpe values are drawn from relevant harmonic frequency calculations.

		R_{P-H} Å	\angle_{H-P-H} °	$R_{P-\parallel}$ Å	$\angle_{H-P-\parallel}$ °	$\angle_{H-P-C-C}$ °	E E_h	zpe kJ mol ⁻¹	D_e kJ mol ⁻¹	D_0 kJ mol ⁻¹	ADE eV	ADE_{shift} eV
2d: C_1 (2A)	def2QZVP	1.418	88.3	3.705	72.4	86.8	-420.6992718	172.9	4.2	7.2	1.233	1.434
	AVTZ	1.417	88.2	3.689	72.9	93.0	-420.6785858	172.5	6	8.9	1.324	1.393
	AVQZ	1.416	88.2	3.696	72.4	86.8	-420.7003992	173.2	5.6	9.0	1.354	1.396
	W1w						-420.5542191		4.5	7.8	1.404	1.398
	W2w						-420.5543516		4.6	8.0	1.402	1.398
	def2QZVP	1.417	88.6	3.638	75.2	135.7	-420.6994924	173.5	4.8	8.4	1.233	1.434
2e: C_s ($^2A'$)	AVTZ	1.418	88.6	3.619	74.7	135.7	-420.6783573	172.6	5.4	8.5	1.332	1.401
	AVQZ	1.417	88.6	3.620	74.9	135.7	-420.7001984	173.5	5.1	8.7	1.362	1.404
	W1w						-420.5538743		3.5	7.2	1.415	1.41
	W2w						-420.5539669		3.6	7.2	1.414	1.41
	def2QZVP	1.418	88.6	4.072	49.1	64.9	-420.6993358	172.8	4.4	7.2	1.240	1.441
	AVTZ	1.419	88.7	4.038	50.1	62.8	-420.6782294	172.4	5.1	7.9	1.312	1.381
2f: C_1 (2A)	AVQZ	1.418	88.6	4.034	51.4	60.6	-420.7000392	172.9	4.7	7.7	1.339	1.381
	W1w						-420.5539388		3.7	6.8	1.389	1.383
	W2w						-420.5540377		3.7	6.8	1.387	1.383
	def2QZVP	1.417	88.5	3.592	74.1	46.7	-420.6996006	173.5	5.1	8.7	1.240	1.441
	AVTZ	1.418	88.6	3.575	73.9	46.7	-420.6784722	173.3	5.7	9.0	1.326	1.395
	AVQZ	1.417	88.5	3.577	74.1	46.7	-420.7003136	173.9	5.4	9.4	1.349	1.390
2g: C_s ($^2A'$)	W1w						-420.5538414		3.5	7.5	1.407	1.401
	W2w						-420.5539430		3.5	7.5	1.405	1.401

Table E47: DSD-PBEP86-D3BJ and extrapolated single-point energies for $\text{PH}_2^- \cdots \text{C}_2\text{H}_4$ complexes. Geometries use for CC energies are from DSD-PBEP86-D3BJ/AVQZ optimisations. All energies are in E_h .

	2a: $\text{PH}_2^- \cdots \text{C}_2\text{H}_4$ (${}^1A'$)						
	E_{DH-DFT}	E_{SCF}	E_{CCSD}	E_{corr}	$E_{CCSD(T)}$	$E_{(T)}$	E_{Wnw}
def2QZVP	-420.7440744						
AVDZ		-419.9261787	-420.4188826	-0.4927039	-420.4372367	-0.0183541	
AVTZ	-420.7268803	-419.9578716	-420.5302300	-0.5723584	-420.5560868	-0.0258568	
AVQZ	-420.7496618	-419.9655068	-420.5598573	-0.5943505	-420.5875076	-0.0276503	
AV5Z		-419.9671529	-420.5683796	-0.6012267			
W1w		-419.9678824		-0.6087693		-0.0286460	-420.6052977
W2w		-419.9679552		-0.6084411		-0.0289591	-420.6053553
	2b: $\text{PH}_2^- \cdots \text{C}_2\text{H}_4$ (${}^1A'$)						
def2QZVP	-420.7443278						
AVDZ		-419.9254001	-420.4183999	-0.4929998	-420.4367701	-0.0183702	
AVTZ	-420.7262186	-419.9570668	-420.5297422	-0.5726754	-420.5556186	-0.0258764	
AVQZ	-420.6830931	-419.9647060	-420.5592848	-0.5945788	-420.5869508	-0.0276660	
AV5Z		-419.9663470	-420.5677798	-0.6014328			
W1w		-419.9670829		-0.6089394		-0.0286669	-420.6046892
W2w		-419.9671468		-0.6086239		-0.0289719	-420.6047426
	2c: $\text{PH}_2^- \cdots \text{C}_2\text{H}_4$ (${}^1A'$)						
def2QZVP	-420.7442858						
AVDZ		-419.9263070	-420.4183672	-0.4920602	-420.4365943	-0.0182271	
AVTZ	-420.7260699	-419.9579332	-420.5296645	-0.5717313	-420.5553677	-0.0257032	
AVQZ	-420.7489633	-419.9655551	-420.5592314	-0.5936763	-420.5867227	-0.0274913	
AV5Z		-419.9671947	-420.5677305	-0.6005358			
W1w		-419.9679266		-0.6080642		-0.0284825	-420.6044733
W2w		-419.9679938		-0.6077327		-0.0287961	-420.6045226

Table E48: DSD-PBEP86-D3BJ and extrapolated single-point energies for $\text{PH}_2^- \cdots \text{C}_2\text{H}_4$ complexes. Geometries use for CC energies are from DSD-PBEP86-D3BJ/AVQZ optimisations. All energies are in E_h .

	1a: VDE $\text{PH}_2^- \cdots \text{CH}_4$ ($^2A''$)						
	E_{DH-DFT}	E_{SCF}	E_{CCSD}	E_{corr}	$E_{CCSD(T)}$	$E_{(T)}$	E_{Wnw}
def2QZVP	-420.6987569						
AVDZ		-419.9193763	-420.3779149	-0.4585386	-420.3933916	-0.0154767	
AVTZ	-420.6777207	-419.9514297	-420.4848269	-0.5333972	-420.5068596	-0.0220327	
AVQZ	-420.7488135	-419.9590955	-420.5130880	-0.5539925	-420.5366836	-0.0235956	
AV5Z		-419.9607730	-420.5212320	-0.5604590			
W1w		-419.9614806		-0.5674955		-0.0244700	-420.5534461
W2w		-419.9615906		-0.5672435		-0.0247361	-420.5535702
	2b: VDE $\text{PH}_2^- \cdots \text{CH}_4$ ($^2A'$)						
def2QZVP	-420.6982256						
AVDZ		-419.9194652	-420.3781709	-0.4587057	-420.3936466	-0.0154757	
AVTZ	-420.6779178	-419.9515052	-420.4850940	-0.5335888	-420.5071360	-0.0220420	
AVQZ	-420.6997271	-419.9591703	-420.5132922	-0.5541219	-420.5368909	-0.0235987	
AV5Z		-419.9608422	-420.5214142	-0.5605720			
W1w		-419.9615552		-0.5675841		-0.0244831	-420.5536224
W2w		-419.9616571		-0.5673393		-0.0247347	-420.5537311
	2c: VDE $\text{PH}_2^- \cdots \text{CH}_4$ ($^2A'$)						
def2QZVP	-420.6981879						
AVDZ		-419.9197093	-420.3777645	-0.4580552	-420.3931326	-0.0153681	
AVTZ	-420.6771064	-419.9517407	-420.4844852	-0.5327445	-420.5063904	-0.0219052	
AVQZ	-420.6989398	-419.9593959	-420.5126794	-0.5532835	-420.5361375	-0.0234581	
AV5Z		-419.9610685	-420.5207988	-0.5597303			
W1w		-419.9617777		-0.5667496		-0.0243354	-420.5528628
W2w		-419.9618837		-0.5664942		-0.0245913	-420.5529692

Table E49: DSD-PBEP86-D3BJ and extrapolated single-point energies for $\text{PH}_2 \cdots \text{C}_2\text{H}_4$ complexes. Geometries use for CC energies are from DSD-PBEP86-D3BJ/AVQZ optimisations. All energies are in E_h .

	2d: $\text{PH}_2 \cdots \text{C}_2\text{H}_4$ (2A)						
	E_{DH-DFT}	E_{SCF}	E_{CCSD}	E_{corr}	$E_{CCSD(T)}$	$E_{(T)}$	E_{Wnw}
def2QZVP	-420.6992718						
AVDZ		-419.9206102	-420.3781346	-0.4575244	-420.3934706	-0.0153360	
AVTZ	-420.6785858	-419.9529137	-420.4857101	-0.5327964	-420.5076166	-0.0219065	
AVQZ	-420.7003992	-419.9605871	-420.5139792	-0.5533921	-420.5374458	-0.0234666	
AV5Z		-419.9622688	-420.5221347	-0.5598659			
W1w		-419.9629746		-0.5668953		-0.0243492	-420.5542191
W2w		-419.9630884		-0.5666581		-0.0246051	-420.5543516
2e: $\text{PH}_2 \cdots \text{C}_2\text{H}_4$ (${}^2A'$)							
def2QZVP	-420.6994924						
AVDZ		-419.9197420	-420.3777547	-0.4580127	-420.3931693	-0.0154146	
AVTZ	-420.6783573	-419.9520302	-420.4851760	-0.5331458	-420.5071598	-0.0219838	
AVQZ	-420.7001984	-419.9596986	-420.5135120	-0.5538134	-420.5370636	-0.0235516	
AV5Z		-419.9613729	-420.5216615	-0.5602886			
W1w		-419.9620845		-0.5673638		-0.0244260	-420.5538743
W2w		-419.9621889		-0.5670823		-0.0246957	-420.5539669
2f: $\text{PH}_2 \cdots \text{C}_2\text{H}_4$ (2A)							
def2QZVP	-420.6993358						
AVDZ		-419.9202575	-420.3781240	-0.4578665	-420.3934717	-0.0153477	
AVTZ	-420.6782294	-419.9525517	-420.4854609	-0.5329092	-420.5073646	-0.0219037	
AVQZ	-420.7000392	-419.9602431	-420.5137199	-0.5534768	-420.5371775	-0.0234576	
AV5Z		-419.9619217	-420.5218545	-0.5599328			
W1w		-419.9626362		-0.5669616		-0.0243410	-420.5539388
W2w		-419.9627398		-0.5667063		-0.0245915	-420.5540377
2g: $\text{PH}_2 \cdots \text{C}_2\text{H}_4$ (${}^2A'$)							
def2QZVP	-420.6996006						
AVDZ		-419.9197261	-420.3777384	-0.4580123	-420.3931822	-0.0154438	
AVTZ	-420.6784722	-419.9519920	-420.4851102	-0.5331182	-420.5071271	-0.0220169	
AVQZ	-420.7003136	-419.9596609	-420.5134453	-0.5537844	-420.5370366	-0.0235913	
AV5Z		-419.9613356	-420.5215941	-0.5602585			
W1w		-419.9620470		-0.5673339		-0.0244605	-420.5538414
W2w		-419.9621518		-0.5670510		-0.0247402	-420.5539430

Table E50: Cartesian coordinates of the PH₂⁻ ... C₂H₄ conformers optimised at DSD-PBEP86-D3BJ/def-2QZVP,AVnZ ($n = T, Q$) in Å.

	2a: PH ₂ ⁻ ... C ₂ H ₄ (¹ A')			2b: PH ₂ ⁻ ... C ₂ H ₄ (¹ A')			2c: PH ₂ ⁻ ... C ₂ H ₄ (¹ A')			
	x	y	z	x	y	z	x	y	z	
deg2QZVP	C	0.000000	0.665332	1.987563	-2.617607	-0.483439	-0.000006	1.544569	-2.268641	0.000000
	C	0.000000	-0.665332	1.987563	-1.841775	0.598018	0.000002	0.274965	-1.868897	0.000000
	H	0.000000	1.198710	1.043054	-2.179012	-1.474191	-0.000016	1.821366	-3.317542	0.000000
	H	0.000000	1.234254	2.912026	-3.700552	-0.419729	-0.000002	2.350978	-1.544936	0.000000
	H	0.000000	-1.198710	1.043054	-0.752752	0.523340	-0.000001	-0.529249	-2.598033	0.000000
	H	0.000000	-1.234254	2.912026	-2.283292	1.589900	0.000013	0.000000	-0.812545	0.000000
	P	0.000000	0.000000	-1.751999	2.110324	0.062673	0.000026	-0.746511	1.986188	0.000000
	H	1.031523	0.000000	-2.740467	2.008432	-0.923650	1.029386	-1.681313	1.652729	1.029094
	H	-1.031523	0.000000	-2.740467	2.008604	-0.923229	-1.029754	-1.681313	1.652729	-1.029094
	x	y	z	x	y	z	x	y	z	
AVTZ	C	-0.000004	-1.999277	0.666329	0.622006	-2.094980	0.000000	1.293846	-2.428887	0.000000
	C	-0.000004	-1.999277	-0.666329	-0.697668	-1.911371	0.000000	0.102028	-1.832297	0.000000
	H	-0.000016	-1.055646	1.202411	1.288099	-1.239789	0.000000	1.398401	-3.509386	0.000000
	H	0.000009	-2.924679	1.235304	1.061693	-3.087830	0.000000	2.206184	-1.842724	0.000000
	H	-0.000016	-1.055646	-1.202411	-1.107384	-0.905717	0.000000	-0.809779	-2.422089	0.000000
	H	0.000009	-2.924679	-1.235304	-1.383476	-2.753701	0.000000	0.000000	-0.747332	0.000000
	P	-0.000004	1.763281	0.000000	0.000000	1.995229	0.000000	-0.578461	2.091804	0.000000
	H	1.032371	2.751312	0.000000	0.297541	1.048354	1.029489	-1.246566	1.355786	1.029202
	H	-1.032247	2.751451	0.000000	0.297541	1.048354	-1.029489	-1.246566	1.355786	-1.029202
	x	y	z	x	y	z	x	y	z	
AVQZ	C	-0.000004	-2.001527	0.665481	2.019867	-0.857576	0.000000	-1.292360	2.436069	0.000000
	C	-0.000004	-2.001527	-0.665481	1.034118	-1.751481	0.000000	-0.102026	1.840243	0.000000
	H	-0.000031	-1.058740	1.201642	1.791249	0.201287	0.000000	-1.396822	3.515791	0.000000
	H	0.000022	-2.926300	1.234002	3.063004	-1.156282	0.000000	-2.204163	1.850483	0.000000
	H	-0.000031	-1.058740	-1.201642	0.000000	-1.422004	0.000000	0.809295	2.429352	0.000000
	H	0.000022	-2.926300	-1.234002	1.241056	-2.817020	0.000000	0.000000	0.755956	0.000000
	P	-0.000004	1.765596	0.000000	-1.545595	1.267398	0.000000	0.575397	-2.096481	0.000000
	H	1.032168	2.752159	0.000000	-0.617644	0.918693	1.029208	1.263527	-1.381124	1.029003
	H	-1.032034	2.752308	0.000000	-0.617644	0.918693	-1.029208	1.263527	-1.381124	-1.029003

Table E51: Cartesian coordinates of the PH₂ ... C₂H₄ conformers optimised at DSD-PBEP86-D3BJ/def-2QZVP,AVnZ ($n = T, Q$) in Å.

	2d: PH ₂ ... C ₂ H ₄ (² A)			2e: PH ₂ ... C ₂ H ₄ (² A')			
	x	y	z	x	y	z	
def2QZVP	C	-1.937848	-0.664479	0.029287	1.853021	-0.664694	-0.030631
	C	-1.937850	0.664475	0.029198	1.853062	0.664676	-0.030607
	H	-1.183997	-1.227899	0.564378	1.501039	-1.228839	-0.884588
	H	-2.691219	-1.230406	-0.503288	2.204448	-1.230305	0.822587
	H	-1.183989	1.227967	0.564198	1.501108	1.228873	-0.884540
	H	-2.691225	1.230330	-0.503450	2.204520	1.230232	0.822635
	P	1.767193	0.000050	0.072653	-1.784999	-0.000004	-0.079402
	H	3.140544	-0.000286	-0.280169	-1.436394	-1.019009	0.841334
	H	1.356178	-0.000439	-1.282368	-1.436232	1.019221	0.841027
	x	y	z	x	y	z	
AVTZ	C	-1.929774	0.665469	-0.029016	0.055258	-1.842003	-0.665699
	C	-1.929767	-0.665471	-0.029079	0.055258	-1.842003	0.665699
	H	-1.164621	1.229141	-0.549636	0.916106	-1.504562	-1.230176
	H	-2.694285	1.231722	0.489180	-0.804954	-2.178737	-1.231585
	H	-1.164610	-1.229084	-0.549752	0.916106	-1.504562	1.230176
	H	-2.694271	-1.231783	0.489063	-0.804954	-2.178737	1.231585
	P	1.758810	0.000032	-0.072529	0.055258	1.777483	0.000000
	H	1.357160	-0.000310	1.286571	-0.857132	1.404199	-1.019479
	H	3.135729	-0.000150	0.271081	-0.857132	1.404199	1.019479
	x	y	z	x	y	z	
AVQZ	C	-1.933209	-0.664633	0.029271	0.055283	-1.842593	-0.664866
	C	-1.933240	0.664631	0.029279	0.055283	-1.842593	0.664866
	H	-1.177243	-1.228147	0.561842	0.914059	-1.501839	-1.229080
	H	-2.688613	-1.230555	-0.500942	-0.802879	-2.182638	-1.230446
	H	-1.177302	1.228173	0.561857	0.914059	-1.501839	1.229080
	H	-2.688670	1.230524	-0.500926	-0.802879	-2.182638	1.230446
	P	1.762996	-0.000010	0.072712	0.055283	1.777528	0.000000
	H	1.349627	0.000040	-1.281717	-0.857496	1.408570	-1.019179
	H	3.135961	0.000131	-0.282096	-0.857496	1.408570	1.019179

Table E52: Cartesian coordinates of the PH₂ ... C₂H₄ conformers optimised at DSD-PBEP86-D3BJ/def-2QZVP,AVnZ ($n = T, Q$) in Å.

	2f: PH ₂ ... C ₂ H ₄ (² A)			2g: PH ₂ ... C ₂ H ₄ (² A')			
	x	y	z	x	y	z	
def2QZVP	C	2.091531	-0.644502	0.000104	0.532331	-1.989582	0.000000
	C	1.991291	0.680449	-0.000126	-0.755010	-1.659305	0.000000
	H	1.213400	-1.277401	0.000225	1.080133	-2.129510	0.922889
	H	3.054336	-1.138762	0.000179	1.080133	-2.129510	-0.922889
	H	1.027961	1.174446	-0.000200	-1.303518	-1.519363	0.922367
	H	2.868583	1.314210	-0.000246	-1.303518	-1.519363	-0.922367
	P	-2.030408	0.022174	-0.000016	0.000000	1.766077	0.000000
	H	-1.102674	-0.3111419	-1.018925	0.891421	1.349960	1.019604
	H	-1.102420	-0.309361	1.019334	0.891421	1.349960	-1.019604
	x	y	z	x	y	z	
AVTZ	C	-2.080565	-0.642817	-0.000001	0.534205	-1.977622	0.000000
	C	-1.969369	0.683269	-0.000009	-0.756729	-1.653458	0.000000
	H	-1.206590	-1.283121	-0.000077	1.083089	-2.114539	0.923885
	H	-3.048343	-1.129507	0.000082	1.083089	-2.114539	-0.923885
	H	-1.001048	1.169717	-0.000093	-1.306180	-1.516100	0.923375
	H	-2.842365	1.324646	0.000066	-1.306180	-1.516100	-0.923375
	P	2.012857	0.025749	0.000007	0.000000	1.758194	0.000000
	H	1.102520	-0.355327	1.019627	0.890661	1.337426	1.020061
	H	1.102578	-0.355365	-1.019651	0.890661	1.337426	-1.020061
	x	y	z	x	y	z	
AVQZ	C	-2.086175	-0.639281	-0.000009	0.532408	-1.981895	0.000000
	C	-1.963304	0.684081	0.000011	-0.755040	-1.650729	0.000000
	H	-1.218696	-1.287151	-0.000030	1.080212	-2.121904	0.923174
	H	-3.057588	-1.116979	-0.000004	1.080212	-2.121904	-0.923174
	H	-0.991434	1.161900	0.000006	-1.303448	-1.510286	0.922653
	H	-2.829902	1.332829	0.000032	-1.303448	-1.510286	-0.922653
	P	2.009491	0.030258	0.000000	0.000000	1.758465	0.000000
	H	1.126092	-0.406719	1.019339	0.891133	1.341573	1.019717
	H	1.126032	-0.406553	-1.019357	0.891133	1.341573	-1.019717

Table E53: Calculated harmonic frequencies and mode assignments for the 2a PH₂⁻...C₂H₄ complex. All frequencies and intensities are in cm⁻¹ and km mol⁻¹ respectively.

2a PH ₂ ⁻ ...C ₂ H ₄ (¹ A')					
	Mode	Symmetry	Frequency (cm ⁻¹)	Intensity (km mol ⁻¹)	Description
def2QZVP	ω_1	b_1	30	0.6953	Intermolecular PH ₂ rock
	ω_2	b_2	69	0.0474	Intermolecular C ₂ H ₄ rock
	ω_3	b_2	79	2.8661	Intermolecular PH ₂ wag
	ω_4	a_1	96	17.6427	Intermolecular stretch
	ω_5	a_2	111	0	Intermolecular PH ₂ twist
	ω_6	b_1	223	0.6128	Intermolecular C ₂ H ₄ wag
	ω_7	a_1	841	7.1397	C ₂ H ₄ paired rock
	ω_8	a_2	972	0	C ₂ H ₄ unpaired wag
	ω_9	b_1	994	69.7043	C ₂ H ₄ paired wag
	ω_{10}	a_1	1090	44.899	PH ₂ scissor
	ω_{11}	a_2	1093	0	C ₂ H ₄ twist
	ω_{12}	b_2	1260	2.2457	C ₂ H ₄ unpaired rock
	ω_{13}	a_1	1375	6.5205	C ₂ H ₄ paired scissor
	ω_{14}	b_2	1456	11.8807	C ₂ H ₄ unpaired symm. scissor
	ω_{15}	a_1	1670	14.4022	C=C stretch
	ω_{16}	a_1	2324	250.777	P-H symm. stretch
	ω_{17}	b_1	2326	230.5617	P-H asymm. stretch
	ω_{18}	b_2	3111	31.3999	C ₂ H ₄ unpaired symm. stretch
	ω_{19}	a_1	3126	106.3865	C ₂ H ₄ paired symm. stretch
	ω_{20}	b_2	3207	4.3121	C ₂ H ₄ unpaired asymm. stretch
	ω_{21}	a_1	3233	1.8886	C ₂ H ₄ paired asymm. stretch
	zpe		171.6		
pVTZ	ω_1	a'	27	0.4038	Intermolecular PH ₂ rock
	ω_2	a''	66	0.4803	Intermolecular C ₂ H ₄ rock
	ω_3	a'	93	16.5594	Intermolecular stretch
	ω_4	a''	104	0	Intermolecular PH ₂ twist
	ω_5	a''	114	7.0972	Intermolecular PH ₂ wag
	ω_6	a'	218	0.8428	Intermolecular C ₂ H ₄ wag
	ω_7	a'	836	6.6859	C ₂ H ₄ paired rock
	ω_8	a''	973	0	C ₂ H ₄ unpaired wag
	ω_9	a'	991	67.4943	C ₂ H ₄ paired wag
	ω_{10}	a''	1078	0	C ₂ H ₄ twist
	ω_{11}	a'	1090	37.2167	PH ₂ scissor
	ω_{12}	a''	1257	3.7028	C ₂ H ₄ unpaired rock
	ω_{13}	a'	1374	5.3808	C ₂ H ₄ paired scissor
	ω_{14}	a''	1456	9.4286	C ₂ H ₄ unpaired symm. scissor
	ω_{15}	a'	1668	14.8529	C=C stretch
	ω_{16}	a'	2324	229.2889	P-H symm. stretch
	ω_{17}	a'	2327	191.779	P-H asymm. stretch
	ω_{18}	a''	3111	30.4271	C ₂ H ₄ unpaired symm. stretch
	ω_{19}	a'	3128	94.9378	C ₂ H ₄ paired symm. stretch
	ω_{20}	a''	3206	4.6766	C ₂ H ₄ unpaired asymm. stretch
	ω_{21}	a'	3233	3.3929	C ₂ H ₄ paired asymm. stretch
	zpe		171.5		

Continued on next page

Table E54: (Continued) Calculated harmonic frequencies and mode assignments for the 2a PH₂⁻ ··· C₂H₄ complex. All frequencies and intensities are in cm⁻¹ and km mol⁻¹ respectively.

2a PH ₂ ⁻ ··· C ₂ H ₄ (¹ A')					
	Mode	Symmetry	Frequency (cm ⁻¹)	Intensity (km mol ⁻¹)	Description
pVQZ	ω_1	a''	29	0.3611	Intermolecular PH ₂ rock
	ω_2	a''	68	0.6311	Intermolecular C ₂ H ₄ rock
	ω_3	a''	92	16.6886	Intermolecular stretch
	ω_4	a''	109	7.393	Intermolecular PH ₂ wag
	ω_5	a''	112	0.0001	Intermolecular PH ₂ twist
	ω_6	a'	222	0.7592	Intermolecular C ₂ H ₄ wag
	ω_7	a'	839	6.7079	C ₂ H ₄ paired rock
	ω_8	a''	982	0	C ₂ H ₄ unpaired wag
	ω_9	a'	993	66.88	C ₂ H ₄ paired wag
	ω_{10}	a''	1089	0	C ₂ H ₄ twist
	ω_{11}	a'	1091	37.2379	PH ₂ scissor
	ω_{12}	a''	1260	3.715	C ₂ H ₄ unpaired rock
	ω_{13}	a'	1375	5.4839	C ₂ H ₄ paired scissor
	ω_{14}	a''	1458	9.5821	C ₂ H ₄ unpaired symm. scissor
	ω_{15}	a'	1670	14.9571	C=C stretch
	ω_{16}	a'	2331	221.9286	P-H symm. stretch
	ω_{17}	a'	2334	183.699	P-H asymm. stretch
	ω_{18}	a''	3113	30.1754	C ₂ H ₄ unpaired symm. stretch
	ω_{19}	a'	3128	94.6285	C ₂ H ₄ paired symm. stretch
	ω_{20}	a''	3209	4.8963	C ₂ H ₄ unpaired asymm. stretch
	ω_{21}	a'	3235	3.3557	C ₂ H ₄ paired asymm. stretch
	zpe		171.9		

Table E55: Calculated harmonic frequencies and mode assignments for the 2b PH₂⁻...C₂H₄ complex. All frequencies and intensities are in cm⁻¹ and km mol⁻¹ respectively.

2b PH ₂ ⁻ ...C ₂ H ₄ (¹ A')					
	Mode	Symmetry	Frequency (cm ⁻¹)	Intensity (km mol ⁻¹)	Description
def2QZVP	ω_1	<i>a</i>	16	0.8178	Intermolecular PH ₂ rock
	ω_2	<i>a</i>	45	4.1086	Intermolecular C ₂ H ₄ rock
	ω_3	<i>a</i>	96	0.0177	Intermolecular PH ₂ twist
	ω_4	<i>a</i>	101	9.4582	Intermolecular PH ₂ wag
	ω_5	<i>a</i>	105	5.2624	Intermolecular stretch
	ω_6	<i>a</i>	214	0.1199	Intermolecular C ₂ H ₄ wag
	ω_7	<i>a</i>	846	1.0147	C ₂ H ₄ paired rock
	ω_8	<i>a</i>	939	32.4043	H-side CH ₂ wag
	ω_9	<i>a</i>	1029	37.2665	P-side CH ₂ wag
	ω_{10}	<i>a</i>	1092	28.0402	PH ₂ scissor
	ω_{11}	<i>a</i>	1117	10.6221	C ₂ H ₄ twist
	ω_{12}	<i>a</i>	1255	2.9279	C ₂ H ₄ unpaired rock
	ω_{13}	<i>a</i>	1381	0.8338	C ₂ H ₄ paired scissor
	ω_{14}	<i>a</i>	1483	4.074	C ₂ H ₄ unpaired symm. scissor
	ω_{15}	<i>a</i>	1676	8.1185	C=C stretch
	ω_{16}	<i>a</i>	2321	186.6926	P-H symm. stretch
	ω_{17}	<i>a</i>	2323	227.2953	P-H asymm. stretch
	ω_{18}	<i>a</i>	3046	239.7378	P-side CH symm. stretch
	ω_{19}	<i>a</i>	3134	53.8257	H-side CH symm. stretch
	ω_{20}	<i>a</i>	3184	20.2736	C ₂ H ₄ unpaired asymm. stretch
	ω_{21}	<i>a</i>	3225	17.9119	C ₂ H ₄ paired asymm. stretch
	zpe		171.2		
pVTZ	ω_1	<i>a'</i>	35	0.4904	Intermolecular C ₂ H ₄ rock
	ω_2	<i>a'</i>	83	10.5719	Intermolecular stretch
	ω_3	<i>a''</i>	88	0.0005	Intermolecular PH ₂ twist
	ω_4	<i>a'</i>	112	5.0864	Intermolecular PH ₂ wag
	ω_5	<i>a''</i>	158	0.021	Intermolecular PH ₂ rock
	ω_6	<i>a''</i>	180	1.2015	Intermolecular C ₂ H ₄ wag
	ω_7	<i>a'</i>	837	4.0416	C ₂ H ₄ paired rock
	ω_8	<i>a''</i>	964	19.0948	H-side CH ₂ wag
	ω_9	<i>a''</i>	992	44.8473	P-side CH ₂ wag
	ω_{10}	<i>a''</i>	1069	0.1065	C ₂ H ₄ twist
	ω_{11}	<i>a'</i>	1101	37.0496	PH ₂ scissor
	ω_{12}	<i>a'</i>	1255	3.1238	C ₂ H ₄ unpaired rock
	ω_{13}	<i>a'</i>	1376	3.9294	C ₂ H ₄ paired scissor
	ω_{14}	<i>a'</i>	1462	9.3983	C ₂ H ₄ unpaired symm. scissor
	ω_{15}	<i>a'</i>	1672	11.7061	C=C stretch
	ω_{16}	<i>a'</i>	2321	190.2747	P-H symm. stretch
	ω_{17}	<i>a''</i>	2324	164.2944	P-H asymm. stretch
	ω_{18}	<i>a'</i>	3112	52.7122	P-side CH symm. stretch
	ω_{19}	<i>a'</i>	3136	61.07	H-side CH symm. stretch
	ω_{20}	<i>a'</i>	3207	5.6546	C ₂ H ₄ unpaired asymm. stretch
	ω_{21}	<i>a'</i>	3237	8.3012	C ₂ H ₄ paired asymm. stretch
	zpe		171.8		

Continued on next page

Table E56: (Continued) Calculated harmonic frequencies and mode assignments for the 2b PH₂⁻...C₂H₄ complex. All frequencies and intensities are in cm⁻¹ and km mol⁻¹ respectively.

2b PH ₂ ⁻ ...C ₂ H ₄ (¹ A')					
	Mode	Symmetry	Frequency (cm ⁻¹)	Intensity (km mol ⁻¹)	Description
pVQZ	ω_1	a'	39	0.7552	Intermolecular C ₂ H ₄ rock
	ω_2	a'	81	10.0387	Intermolecular stretch
	ω_3	a''	90	0	Intermolecular PH ₂ twist
	ω_4	a'	108	5.6099	Intermolecular PH ₂ wag
	ω_5	a''	154	0.0679	Intermolecular PH ₂ rock
	ω_6	a''	191	0.9991	Intermolecular C ₂ H ₄ wag
	ω_7	a'	840	4.1499	C ₂ H ₄ paired rock
	ω_8	a''	970	26.3037	H-side CH ₂ wag
	ω_9	a''	997	36.925	P-side CH ₂ wag
	ω_{10}	a''	1082	0.0986	C ₂ H ₄ twist
	ω_{11}	a'	1101	36.6294	PH ₂ scissor
	ω_{12}	a'	1258	3.0138	C ₂ H ₄ unpaired rock
	ω_{13}	a'	1377	3.9017	C ₂ H ₄ paired scissor
	ω_{14}	a'	1464	9.5907	C ₂ H ₄ unpaired symm. scissor
	ω_{15}	a'	1673	11.8447	C=C stretch
	ω_{16}	a'	2326	189.2413	P-H symm. stretch
	ω_{17}	a''	2330	158.6722	P-H asymm. stretch
	ω_{18}	a'	3112	56.8415	P-side CH symm. stretch
	ω_{19}	a'	3136	57.7225	H-side CH symm. stretch
	ω_{20}	a'	3209	6.0687	C ₂ H ₄ unpaired asymm. stretch
	ω_{21}	a'	3239	8.3056	C ₂ H ₄ paired asymm. stretch
	zpe		172.1		

Table E57: Calculated harmonic frequencies and mode assignments for the 2c PH₂⁻...C₂H₄ complex. All frequencies and intensities are in cm⁻¹ and km mol⁻¹ respectively.

2c PH ₂ ⁻ ...C ₂ H ₄ (¹ A')					
	Mode	Symmetry	Frequency (cm ⁻¹)	Intensity (km mol ⁻¹)	Description
def2QZVP	ω_1	a''	25	0.0747	Intermolecular PH ₂ rock
	ω_2	a'	50	5.1847	Intermolecular C ₂ H ₄ rock
	ω_3	a'	82	4.688	Intermolecular stretch
	ω_4	a''	95	0.1039	Intermolecular PH ₂ twist
	ω_5	a'	119	8.111	Intermolecular PH ₂ wag
	ω_6	a''	209	0.0847	Intermolecular C ₂ H ₄ wag
	ω_7	a'	844	0.4002	C ₂ H ₄ paired rock
	ω_8	a''	938	34.3255	Farside CH ₂ wag
	ω_9	a''	1030	35.696	Nearside CH ₂ wag
	ω_{10}	a'	1092	27.6779	PH ₂ scissor
	ω_{11}	a''	1114	9.0283	C ₂ H ₄ twist
	ω_{12}	a'	1253	3.392	C ₂ H ₄ unpaired rock
	ω_{13}	a'	1381	2.4591	C ₂ H ₄ paired scissor
	ω_{14}	a'	1484	5.1945	C ₂ H ₄ unpaired symm. scissor
	ω_{15}	a'	1677	5.7364	C=C stretch
	ω_{16}	a'	2318	196.9054	P-H symm. stretch
	ω_{17}	a''	2320	231.8103	P-H asymm. stretch
	ω_{18}	a'	3047	232.9705	Nearside CH symm. stretch
	ω_{19}	a'	3134	54.9179	Farside CH symm. stretch
	ω_{20}	a'	3185	21.5018	C ₂ H ₄ unpaired asymm. stretch
	ω_{21}	a'	3224	20.9016	C ₂ H ₄ paired asymm. stretch
	zpe		171.2		
pVTZ	ω_1	a''	25	0.1088	Intermolecular PH ₂ rock
	ω_2	a'	42	2.1666	Intermolecular C ₂ H ₄ rock
	ω_3	a'	75	7.9303	Intermolecular stretch
	ω_4	a'	100	7.0545	Intermolecular PH ₂ wag
	ω_5	a''	104	0.4792	Intermolecular PH ₂ twist
	ω_6	a''	178	1.1068	Intermolecular C ₂ H ₄ wag
	ω_7	a'	835	0.9384	C ₂ H ₄ paired rock
	ω_8	a''	940	37.3593	Farside CH ₂ wag
	ω_9	a''	1022	28.5947	Nearside CH ₂ wag
	ω_{10}	a''	1084	1.9086	C ₂ H ₄ twist
	ω_{11}	a'	1092	35.1183	PH ₂ scissor
	ω_{12}	a'	1249	2.7762	C ₂ H ₄ unpaired rock
	ω_{13}	a'	1378	1.9826	C ₂ H ₄ paired scissor
	ω_{14}	a'	1479	3.0792	C ₂ H ₄ unpaired symm. scissor
	ω_{15}	a'	1675	8.0759	C=C stretch
	ω_{16}	a'	2313	195.8579	P-H symm. stretch
	ω_{17}	a''	2315	189.1407	P-H asymm. stretch
	ω_{18}	a'	3081	146.8363	Nearside CH symm. stretch
	ω_{19}	a'	3134	56.8474	Farside CH symm. stretch
	ω_{20}	a'	3192	21.8962	C ₂ H ₄ unpaired asymm. stretch
	ω_{21}	a'	3224	17.7081	C ₂ H ₄ paired asymm. stretch
	zpe		170.7		

Continued on next page

Table E58: (Continued) Calculated harmonic frequencies and mode assignments for the 2c PH₂⁻...C₂H₄ complex. All frequencies and intensities are in cm⁻¹ and km mol⁻¹ respectively.

2c PH ₂ ⁻ ...C ₂ H ₄ (¹ A')					
	Mode	Symmetry	Frequency (cm ⁻¹)	Intensity (km mol ⁻¹)	Description
pVQZ	ω_1	a''	31	0.0824	Intermolecular PH ₂ rock
	ω_2	a'	47	2.3574	Intermolecular C ₂ H ₄ rock
	ω_3	a'	69	7.5114	Intermolecular stretch
	ω_4	a'	100	7.3257	Intermolecular PH ₂ wag
	ω_5	a''	106	0.5891	Intermolecular PH ₂ twist
	ω_6	a''	188	0.9183	Intermolecular C ₂ H ₄ wag
	ω_7	a'	840	0.8978	C ₂ H ₄ paired rock
	ω_8	a''	947	39.2545	Farside CH ₂ wag
	ω_9	a''	1028	26.1166	Nearside CH ₂ wag
	ω_{10}	a'	1093	33.9918	PH ₂ scissor
	ω_{11}	a''	1093	1.2999	C ₂ H ₄ twist
	ω_{12}	a'	1252	2.8268	C ₂ H ₄ unpaired rock
	ω_{13}	a'	1379	2.0293	C ₂ H ₄ paired scissor
	ω_{14}	a'	1481	3.2773	C ₂ H ₄ unpaired symm. scissor
	ω_{15}	a'	1676	8.0708	C=C stretch
	ω_{16}	a'	2319	191.3427	P-H symm. stretch
	ω_{17}	a''	2321	183.2535	P-H asymm. stretch
	ω_{18}	a'	3081	150.996	Nearside CH symm. stretch
	ω_{19}	a'	3135	54.2393	Farside CH symm. stretch
	ω_{20}	a'	3195	22.1135	C ₂ H ₄ unpaired asymm. stretch
	ω_{21}	a'	3226	17.4373	C ₂ H ₄ paired asymm. stretch
	zpe		171.1		

Table E59: Calculated harmonic frequencies and mode assignments for the 2d PH₂⋯C₂H₄ complex. All frequencies and intensities are in cm⁻¹ and km mol⁻¹ respectively.

2d PH ₂ ⋯C ₂ H ₄ (² A)					
	Mode	Symmetry	Frequency (cm ⁻¹)	Intensity (km mol ⁻¹)	Description
def2QZVP	ω_1	<i>a</i>	43	6.2177	Intermolecular PH ₂ wag
	ω_2	<i>a</i>	62	0.7422	Intermolecular stretch
	ω_3	<i>a</i>	73	0.1466	Intermolecular C ₂ H ₄ rock
	ω_4	<i>a</i>	75	1.7443	Intermolecular C ₂ H ₄ wag
	ω_5	<i>a</i>	77	0.2041	Intermolecular PH ₂ twist
	ω_6	<i>a</i>	109	2.7812	Intermolecular PH ₂ rock
	ω_7	<i>a</i>	830	0.3342	C ₂ H ₄ paired rock
	ω_8	<i>a</i>	977	0.0843	C ₂ H ₄ unpaired wag
	ω_9	<i>a</i>	984	98.9871	C ₂ H ₄ paired wag
	ω_{10}	<i>a</i>	1071	0.2135	C ₂ H ₄ twist
	ω_{11}	<i>a</i>	1136	18.2266	PH ₂ scissor
	ω_{12}	<i>a</i>	1250	0.1324	C ₂ H ₄ unpaired rock
	ω_{13}	<i>a</i>	1381	0.9538	C ₂ H ₄ paired scissor
	ω_{14}	<i>a</i>	1479	12.059	C ₂ H ₄ unpaired symm. scissor
	ω_{15}	<i>a</i>	1686	0.6279	C=C stretch
	ω_{16}	<i>a</i>	2424	64.4445	Farside PH stretch
	ω_{17}	<i>a</i>	2440	54.1442	Nearside PH stretch
	ω_{18}	<i>a</i>	3153	11.1389	C ₂ H ₄ unpaired symm. stretch
	ω_{19}	<i>a</i>	3167	0.0025	C ₂ H ₄ paired symm. stretch
	ω_{20}	<i>a</i>	3235	0.1878	C ₂ H ₄ unpaired asymm. stretch
	ω_{21}	<i>a</i>	3260	19.8807	C ₂ H ₄ paired asymm. stretch
	zpe		172.9		
pVTZ	ω_1	<i>a</i>	39	5.8204	Intermolecular PH ₂ wag
	ω_2	<i>a</i>	63	0.9466	Intermolecular C ₂ H ₄ wag
	ω_3	<i>a</i>	74	0.2126	Intermolecular PH ₂ twist
	ω_4	<i>a</i>	77	1.3109	Intermolecular C ₂ H ₄ rock
	ω_5	<i>a</i>	80	0.1095	Intermolecular PH ₂ twist
	ω_6	<i>a</i>	108	2.7942	Intermolecular PH ₂ rock
	ω_7	<i>a</i>	826	0.3192	C ₂ H ₄ paired rock
	ω_8	<i>a</i>	967	0.0879	C ₂ H ₄ unpaired wag
	ω_9	<i>a</i>	981	97.7435	C ₂ H ₄ paired wag
	ω_{10}	<i>a</i>	1059	0.2151	C ₂ H ₄ twist
	ω_{11}	<i>a</i>	1135	18.2576	PH ₂ scissor
	ω_{12}	<i>a</i>	1247	0.1651	C ₂ H ₄ unpaired rock
	ω_{13}	<i>a</i>	1379	1.0546	C ₂ H ₄ paired scissor
	ω_{14}	<i>a</i>	1477	11.918	C ₂ H ₄ unpaired symm. scissor
	ω_{15}	<i>a</i>	1683	0.7831	C=C stretch
	ω_{16}	<i>a</i>	2417	66.2835	Farside PH stretch
	ω_{17}	<i>a</i>	2433	54.9803	Nearside PH stretch
	ω_{18}	<i>a</i>	3148	11.1938	C ₂ H ₄ unpaired symm. stretch
	ω_{19}	<i>a</i>	3164	0.0021	C ₂ H ₄ paired symm. stretch
	ω_{20}	<i>a</i>	3229	0.2075	C ₂ H ₄ unpaired asymm. stretch
	ω_{21}	<i>a</i>	3255	20.5064	C ₂ H ₄ paired asymm. stretch
	zpe		172.5		

Continued on next page

Table E60: (Continued) Calculated harmonic frequencies and mode assignments for the 2d PH₂...C₂H₄ complex. All frequencies and intensities are in cm⁻¹ and km mol⁻¹ respectively.

2d PH ₂ ...C ₂ H ₄ (² A)					
	Mode	Symmetry	Frequency (cm ⁻¹)	Intensity (km mol ⁻¹)	Description
pVQZ	ω_1	<i>a</i>	65	0.2039	Intermolecular PH ₂ twist
	ω_2	<i>a</i>	68	0.008	Intermolecular PH ₂ twist
	ω_3	<i>a</i>	71	5.3084	Intermolecular PH ₂ wag
	ω_4	<i>a</i>	87	0.8849	Intermolecular C ₂ H ₄ wag
	ω_5	<i>a</i>	97	4.0782	Intermolecular PH ₂ rock
	ω_6	<i>a</i>	120	0.8267	Intermolecular C ₂ H ₄ rock
	ω_7	<i>a</i>	831	0.2748	C ₂ H ₄ paired rock
	ω_8	<i>a</i>	977	0.4659	C ₂ H ₄ unpaired wag
	ω_9	<i>a</i>	984	98.0703	C ₂ H ₄ paired wag
	ω_{10}	<i>a</i>	1070	0.2206	C ₂ H ₄ twist
	ω_{11}	<i>a</i>	1136	18.2698	PH ₂ scissor
	ω_{12}	<i>a</i>	1250	0.1865	C ₂ H ₄ unpaired rock
	ω_{13}	<i>a</i>	1380	0.9979	C ₂ H ₄ paired scissor
	ω_{14}	<i>a</i>	1479	11.8515	C ₂ H ₄ unpaired symm. scissor
	ω_{15}	<i>a</i>	1685	0.7019	C=C stretch
	ω_{16}	<i>a</i>	2423	64.7375	Farside PH stretch
	ω_{17}	<i>a</i>	2439	53.4009	Nearside PH stretch
	ω_{18}	<i>a</i>	3148	11.2054	C ₂ H ₄ unpaired symm. stretch
	ω_{19}	<i>a</i>	3163	0.0805	C ₂ H ₄ paired symm. stretch
	ω_{20}	<i>a</i>	3230	0.2698	C ₂ H ₄ unpaired asymm. stretch
	ω_{21}	<i>a</i>	3256	20.0324	C ₂ H ₄ paired asymm. stretch
	zpe		173.2		

Table E61: Calculated harmonic frequencies and mode assignments for the 2e PH₂ ··· C₂H₄ complex. All frequencies and intensities are in cm⁻¹ and km mol⁻¹ respectively.

2e PH ₂ ··· C ₂ H ₄ (² A')					
	Mode	Symmetry	Frequency (cm ⁻¹)	Intensity (km mol ⁻¹)	Description
def2QZVP	ω_1	a''	19	2.3039	Intermolecular PH ₂ rock
	ω_2	a'	38	0.3179	Intermolecular C ₂ H ₄ twist
	ω_3	a'	62	0.1518	Intermolecular C ₂ H ₄ wag
	ω_4	a''	67	0.4964	Intermolecular stretch
	ω_5	a''	145	0.2272	Intermolecular PH ₂ twist
	ω_6	a'	178	3.8861	Intermolecular PH ₂ wag
	ω_7	a''	830	0.0266	C ₂ H ₄ paired rock
	ω_8	a'	974	2.1281	C ₂ H ₄ unpaired wag
	ω_9	a'	985	114.3699	C ₂ H ₄ paired wag
	ω_{10}	a''	1070	0.0069	C ₂ H ₄ twist
	ω_{11}	a'	1133	19.9498	PH ₂ scissor
	ω_{12}	a''	1250	0.0057	C ₂ H ₄ unpaired rock
	ω_{13}	a'	1387	0.1909	C ₂ H ₄ paired scissor
	ω_{14}	a'	1481	9.2081	C ₂ H ₄ unpaired symm. scissor
	ω_{15}	a'	1699	0.907	C=C stretch
	ω_{16}	a'	2427	44.0113	P-H symm. stretch
	ω_{17}	a''	2436	56.4645	P-H asymm. stretch
	ω_{18}	a'	3155	9.7861	C ₂ H ₄ unpaired symm. stretch
	ω_{19}	a'	3171	0.0041	C ₂ H ₄ paired symm. stretch
	ω_{20}	a''	3236	0.0616	C ₂ H ₄ unpaired asymm. stretch
	ω_{21}	a''	3263	11.9503	C ₂ H ₄ paired asymm. stretch
	zpe		173.5		
pVTZ	ω_1	a''	18	2.135	Intermolecular PH ₂ rock
	ω_2	a''	36	0.0178	Intermolecular C ₂ H ₄ twist
	ω_3	a'	42	1.1602	Intermolecular C ₂ H ₄ wag
	ω_4	a'	61	0.1128	Intermolecular stretch
	ω_5	a''	137	0.3014	Intermolecular PH ₂ twist
	ω_6	a'	169	3.298	Intermolecular PH ₂ wag
	ω_7	a'	826	0.0215	C ₂ H ₄ paired rock
	ω_8	a''	964	0.167	C ₂ H ₄ unpaired wag
	ω_9	a'	979	114.6594	C ₂ H ₄ paired wag
	ω_{10}	a''	1060	0.0521	C ₂ H ₄ twist
	ω_{11}	a'	1133	20.7732	PH ₂ scissor
	ω_{12}	a''	1247	0.0234	C ₂ H ₄ unpaired rock
	ω_{13}	a'	1379	0.372	C ₂ H ₄ paired scissor
	ω_{14}	a''	1478	9.1025	C ₂ H ₄ unpaired symm. scissor
	ω_{15}	a'	1682	0.5888	C=C stretch
	ω_{16}	a'	2419	47.3038	P-H symm. stretch
	ω_{17}	a''	2427	51.3768	P-H asymm. stretch
	ω_{18}	a''	3149	9.8483	C ₂ H ₄ unpaired symm. stretch
	ω_{19}	a'	3167	0.0097	C ₂ H ₄ paired symm. stretch
	ω_{20}	a''	3231	0.0565	C ₂ H ₄ unpaired asymm. stretch
	ω_{21}	a'	3258	13.5557	C ₂ H ₄ paired asymm. stretch
	zpe		172.6		

Continued on next page

Table E62: (Continued) Calculated harmonic frequencies and mode assignments for the 2e PH₂ ··· C₂H₄ complex. All frequencies and intensities are in cm⁻¹ and km mol⁻¹ respectively.

2e PH ₂ ··· C ₂ H ₄ (² A')					
	Mode	Symmetry	Frequency (cm ⁻¹)	Intensity (km mol ⁻¹)	Description
pVQZ	ω_1	a''	26	1.8643	Intermolecular PH ₂ rock
	ω_2	a''	44	0.2308	Intermolecular C ₂ H ₄ twist
	ω_3	a'	57	0.4067	Intermolecular C ₂ H ₄ wag
	ω_4	a'	107	0.878	Intermolecular stretch
	ω_5	a''	138	0.4521	Intermolecular PH ₂ twist
	ω_6	a'	174	3.4203	Intermolecular PH ₂ wag
	ω_7	a'	831	0.0167	C ₂ H ₄ paired rock
	ω_8	a''	974	0.1627	C ₂ H ₄ unpaired wag
	ω_9	a'	982	114.5034	C ₂ H ₄ paired wag
	ω_{10}	a''	1067	0.0514	C ₂ H ₄ twist
	ω_{11}	a'	1134	20.9052	PH ₂ scissor
	ω_{12}	a''	1250	0.0238	C ₂ H ₄ unpaired rock
	ω_{13}	a'	1380	0.3816	C ₂ H ₄ paired scissor
	ω_{14}	a''	1480	9.3218	C ₂ H ₄ unpaired symm. scissor
	ω_{15}	a'	1683	0.6029	C=C stretch
	ω_{16}	a'	2426	45.7967	P-H symm. stretch
	ω_{17}	a''	2434	49.771	P-H asymm. stretch
	ω_{18}	a''	3151	9.7313	C ₂ H ₄ unpaired symm. stretch
	ω_{19}	a'	3167	0.0077	C ₂ H ₄ paired symm. stretch
	ω_{20}	a''	3234	0.0496	C ₂ H ₄ unpaired asymm. stretch
	ω_{21}	a'	3260	13.3326	C ₂ H ₄ paired asymm. stretch
			zpe	173.5	

Table E63: Calculated harmonic frequencies and mode assignments for the 2f PH₂⋯C₂H₄ complex. All frequencies and intensities are in cm⁻¹ and km mol⁻¹ respectively.

2f PH ₂ ⋯C ₂ H ₄ (² A)					
	Mode	Symmetry	Frequency (cm ⁻¹)	Intensity (km mol ⁻¹)	Description
def2QZVP	ω_1	<i>a</i>	22	4.7723	Intermolecular PH ₂ wag
	ω_2	<i>a</i>	48	0	Intermolecular C ₂ H ₄ wag
	ω_3	<i>a</i>	66	0.9773	Intermolecular stretch
	ω_4	<i>a</i>	74	0.3822	Intermolecular PH ₂ twist
	ω_5	<i>a</i>	101	2.3754	Intermolecular C ₂ H ₄ rock
	ω_6	<i>a</i>	111	4.3612	Intermolecular C ₂ H ₄ twist
	ω_7	<i>a</i>	829	0.6885	C ₂ H ₄ paired rock
	ω_8	<i>a</i>	974	0.1943	C ₂ H ₄ unpaired wag
	ω_9	<i>a</i>	981	80.8867	C ₂ H ₄ paired wag
	ω_{10}	<i>a</i>	1069	0.0064	C ₂ H ₄ twist
	ω_{11}	<i>a</i>	1141	18.8235	PH ₂ scissor
	ω_{12}	<i>a</i>	1249	0.1099	C ₂ H ₄ unpaired rock
	ω_{13}	<i>a</i>	1380	1.6169	C ₂ H ₄ paired scissor
	ω_{14}	<i>a</i>	1480	13.2426	C ₂ H ₄ unpaired symm. scissor
	ω_{15}	<i>a</i>	1687	1.0994	C=C stretch
	ω_{16}	<i>a</i>	2423	49.6168	P–H symm. stretch
	ω_{17}	<i>a</i>	2432	51.8723	P–H asymm. stretch
	ω_{18}	<i>a</i>	3154	13.2519	C ₂ H ₄ unpaired symm. stretch
	ω_{19}	<i>a</i>	3168	0.023	C ₂ H ₄ paired symm. stretch
	ω_{20}	<i>a</i>	3235	0.0218	C ₂ H ₄ unpaired asymm. stretch
	ω_{21}	<i>a</i>	3260	22.1461	C ₂ H ₄ paired asymm. stretch
	zpe		172.8		
pVTZ	ω_1	<i>a</i>	25	4.2235	Intermolecular PH ₂ wag
	ω_2	<i>a</i>	51	0.0008	Intermolecular C ₂ H ₄ wag
	ω_3	<i>a</i>	70	1.0913	Intermolecular stretch
	ω_4	<i>a</i>	75	0.4612	Intermolecular PH ₂ twist
	ω_5	<i>a</i>	103	2.3223	Intermolecular C ₂ H ₄ rock
	ω_6	<i>a</i>	112	4.0588	Intermolecular C ₂ H ₄ twist
	ω_7	<i>a</i>	825	0.5423	C ₂ H ₄ paired rock
	ω_8	<i>a</i>	965	0.034	C ₂ H ₄ unpaired wag
	ω_9	<i>a</i>	979	79.7567	C ₂ H ₄ paired wag
	ω_{10}	<i>a</i>	1051	0.0162	C ₂ H ₄ twist
	ω_{11}	<i>a</i>	1140	19.4353	PH ₂ scissor
	ω_{12}	<i>a</i>	1246	0.1437	C ₂ H ₄ unpaired rock
	ω_{13}	<i>a</i>	1379	1.6504	C ₂ H ₄ paired scissor
	ω_{14}	<i>a</i>	1477	13.1874	C ₂ H ₄ unpaired symm. scissor
	ω_{15}	<i>a</i>	1684	1.2946	C=C stretch
	ω_{16}	<i>a</i>	2416	50.6223	P–H symm. stretch
	ω_{17}	<i>a</i>	2425	51.945	P–H asymm. stretch
	ω_{18}	<i>a</i>	3149	13.2402	C ₂ H ₄ unpaired symm. stretch
	ω_{19}	<i>a</i>	3166	0.0238	C ₂ H ₄ paired symm. stretch
	ω_{20}	<i>a</i>	3230	0.0418	C ₂ H ₄ unpaired asymm. stretch
	ω_{21}	<i>a</i>	3256	22.6296	C ₂ H ₄ paired asymm. stretch
	zpe		172.4		

Continued on next page

Table E64: (Continued) Calculated harmonic frequencies and mode assignments for the 2f PH₂ ··· C₂H₄ complex. All frequencies and intensities are in cm⁻¹ and km mol⁻¹ respectively.

2f PH ₂ ··· C ₂ H ₄ (² A)					
	Mode	Symmetry	Frequency (cm ⁻¹)	Intensity (km mol ⁻¹)	Description
pVQZ	ω_1	<i>a</i>	48	1.8209	Intermolecular PH ₂ wag
	ω_2	<i>a</i>	59	0.22	Intermolecular C ₂ H ₄ wag
	ω_3	<i>a</i>	70	0.0816	Intermolecular PH ₂ twist
	ω_4	<i>a</i>	79	1.8174	Intermolecular stretch
	ω_5	<i>a</i>	96	4.0968	Intermolecular C ₂ H ₄ rock
	ω_6	<i>a</i>	111	4.2235	Intermolecular C ₂ H ₄ twist
	ω_7	<i>a</i>	829	0.509	C ₂ H ₄ paired rock
	ω_8	<i>a</i>	973	0.0404	C ₂ H ₄ unpaired wag
	ω_9	<i>a</i>	981	79.2714	C ₂ H ₄ paired wag
	ω_{10}	<i>a</i>	1066	0.0082	C ₂ H ₄ twist
	ω_{11}	<i>a</i>	1141	20.0633	PH ₂ scissor
	ω_{12}	<i>a</i>	1249	0.1503	C ₂ H ₄ unpaired rock
	ω_{13}	<i>a</i>	1380	1.579	C ₂ H ₄ paired scissor
	ω_{14}	<i>a</i>	1479	13.5045	C ₂ H ₄ unpaired symm. scissor
	ω_{15}	<i>a</i>	1685	1.2564	C=C stretch
	ω_{16}	<i>a</i>	2422	49.4774	P-H symm. stretch
	ω_{17}	<i>a</i>	2431	50.6143	P-H asymm. stretch
	ω_{18}	<i>a</i>	3150	13.0472	C ₂ H ₄ unpaired symm. stretch
	ω_{19}	<i>a</i>	3165	0.0533	C ₂ H ₄ paired symm. stretch
	ω_{20}	<i>a</i>	3232	0.0705	C ₂ H ₄ unpaired asymm. stretch
	ω_{21}	<i>a</i>	3258	22.0564	C ₂ H ₄ paired asymm. stretch
	zpe		172.9		

Table E65: Calculated harmonic frequencies and mode assignments for the 2g PH₂ ··· C₂H₄ complex. All frequencies and intensities are in cm⁻¹ and km mol⁻¹ respectively.

2g PH ₂ ··· C ₂ H ₄ (² A')					
	Mode	Symmetry	Frequency (cm ⁻¹)	Intensity (km mol ⁻¹)	Description
def2QZVP	ω_1	a''	27	2.292	Intermolecular PH ₂ rock
	ω_2	a'	37	0.3163	H-side Inter. C ₂ H ₄ wag
	ω_3	a'	61	0.1548	P-side Inter. C ₂ H ₄ wag
	ω_4	a''	67	0.5051	Intermolecular C ₂ H ₄ twist
	ω_5	a''	146	0.2307	Intermolecular PH ₂ twist
	ω_6	a'	179	3.8883	Intermolecular PH ₂ wag
	ω_7	a''	830	0.0266	C ₂ H ₄ paired rock
	ω_8	a'	974	2.1692	C ₂ H ₄ unpaired wag
	ω_9	a'	985	114.3195	C ₂ H ₄ paired wag
	ω_{10}	a''	1070	0.0069	C ₂ H ₄ twist
	ω_{11}	a'	1134	19.956	PH ₂ scissor
	ω_{12}	a''	1250	0.0057	C ₂ H ₄ unpaired rock
	ω_{13}	a'	1387	0.1907	C ₂ H ₄ paired scissor
	ω_{14}	a'	1481	9.2083	C ₂ H ₄ unpaired symm. scissor
	ω_{15}	a'	1699	0.9048	C=C stretch
	ω_{16}	a'	2427	44.0104	P-H symm. stretch
	ω_{17}	a''	2436	56.4618	P-H asymm. stretch
	ω_{18}	a'	3155	9.7869	C ₂ H ₄ unpaired symm. stretch
	ω_{19}	a'	3171	0.0041	C ₂ H ₄ paired symm. stretch
	ω_{20}	a''	3236	0.0614	C ₂ H ₄ unpaired asymm. stretch
	ω_{21}	a''	3263	11.9507	C ₂ H ₄ paired asymm. stretch
	zpe		173.5		
pVTZ	ω_1	a''	29	2.0396	Intermolecular PH ₂ rock
	ω_2	a'	39	0.3057	H-side Inter. C ₂ H ₄ wag
	ω_3	a'	63	0.1815	P-side Inter. C ₂ H ₄ wag
	ω_4	a''	67	0.5641	Intermolecular C ₂ H ₄ twist
	ω_5	a''	151	0.2101	Intermolecular PH ₂ twist
	ω_6	a'	184	3.419	Intermolecular PH ₂ wag
	ω_7	a''	826	0.0045	C ₂ H ₄ paired rock
	ω_8	a'	966	0.6077	C ₂ H ₄ unpaired wag
	ω_9	a'	982	116.178	C ₂ H ₄ paired wag
	ω_{10}	a''	1063	0.0068	C ₂ H ₄ twist
	ω_{11}	a'	1133	20.2285	PH ₂ scissor
	ω_{12}	a''	1247	0.0056	C ₂ H ₄ unpaired rock
	ω_{13}	a'	1386	0.1908	C ₂ H ₄ paired scissor
	ω_{14}	a'	1479	8.9093	C ₂ H ₄ unpaired symm. scissor
	ω_{15}	a'	1697	0.8681	C=C stretch
	ω_{16}	a'	2419	45.6596	P-H symm. stretch
	ω_{17}	a''	2428	56.1812	P-H asymm. stretch
	ω_{18}	a'	3150	9.6942	C ₂ H ₄ unpaired symm. stretch
	ω_{19}	a'	3168	0.012	C ₂ H ₄ paired symm. stretch
	ω_{20}	a''	3231	0.0637	C ₂ H ₄ unpaired asymm. stretch
	ω_{21}	a''	3258	12.0691	C ₂ H ₄ paired asymm. stretch
	zpe		173.3		

Continued on next page

Table E66: (Continued) Calculated harmonic frequencies and mode assignments for the 2g PH₂ ··· C₂H₄ complex. All frequencies and intensities are in cm⁻¹ and km mol⁻¹ respectively.

2g PH ₂ ··· C ₂ H ₄ (² A')					
	Mode	Symmetry	Frequency (cm ⁻¹)	Intensity (km mol ⁻¹)	Description
pVQZ	ω_1	a''	34	2.2827	Intermolecular PH ₂ rock
	ω_2	a'	43	0.3232	H-side Inter. C ₂ H ₄ wag
	ω_3	a'	64	0.1451	P-side Inter. C ₂ H ₄ wag
	ω_4	a''	106	0.2925	Intermolecular C ₂ H ₄ twist
	ω_5	a''	149	0.2964	Intermolecular PH ₂ twist
	ω_6	a'	188	3.5508	Intermolecular PH ₂ wag
	ω_7	a''	831	0.0066	C ₂ H ₄ paired rock
	ω_8	a'	977	2.945	C ₂ H ₄ unpaired wag
	ω_9	a'	985	113.5919	C ₂ H ₄ paired wag
	ω_{10}	a''	1069	0.0094	C ₂ H ₄ twist
	ω_{11}	a'	1134	20.4328	PH ₂ scissor
	ω_{12}	a''	1250	0.0058	C ₂ H ₄ unpaired rock
	ω_{13}	a'	1386	0.1885	C ₂ H ₄ paired scissor
	ω_{14}	a'	1481	9.0929	C ₂ H ₄ unpaired symm. scissor
	ω_{15}	a'	1698	0.8792	C=C stretch
	ω_{16}	a'	2426	43.9474	P-H symm. stretch
	ω_{17}	a''	2434	54.6447	P-H asymm. stretch
	ω_{18}	a'	3152	9.5722	C ₂ H ₄ unpaired symm. stretch
	ω_{19}	a'	3169	0.0117	C ₂ H ₄ paired symm. stretch
	ω_{20}	a''	3233	0.0647	C ₂ H ₄ unpaired asymm. stretch
	ω_{21}	a''	3260	11.8272	C ₂ H ₄ paired asymm. stretch
			zpe	173.9	

Table E67: $\text{PH}_2^- \cdots \text{HCCH}$ complex geometric parameters, D_0 s and VDEs from DSD-PBEP86-D3BJ optimisations. zpe values are drawn from relevant harmonic frequency calculations.

	R_{P-H} Å	\angle_{H-P-H} °	R_{P-HC} Å	\angle_{H-P-HC} °	$\angle_{H-P-H-C}$ °	E E_h	zpe kJ mol ⁻¹	D_e kJ mol ⁻¹	D_0 kJ mol ⁻¹	E_{VDE} E_h	VDE eV	
3a: C_s ($^1A'$)	def2QZVP	1.429	88.4	2.611	94.3	92.6	-419.5021193	108.0	42.7	46.3	-419.4468306	1.485
	pVTZ	1.429	88.2	2.624	103.8	96.1	-419.4842843	107.4	36.7	39.7	-419.4270719	1.540
	pVQZ	1.428	88.2	2.630	104.0	96.3	-419.5060361	107.4	35.9	39.0	-419.4479183	1.564
	W1w						-419.3585745		34.4	37.5	-419.2987551	1.611
	W2w						-419.3586718		34.4	37.5	-419.2989239	1.609
	R_{P-H} Å	\angle_{H-P-H} °	R_{P-HC} Å	\angle_{H-P-HC} °	$\angle_{H-P-H-C}$ °	E E_h	zpe kJ mol ⁻¹	D_e kJ mol ⁻¹	D_0 kJ mol ⁻¹	ADE eV	ADE_{shift} eV	
3b: C_{2v} (2B_1)	def2QZVP	1.416	88.1	2.977	133.7	180.0	-419.4493307	108.2	4.9	7.0	1.439	1.640
	pVTZ	1.417	88.1	2.944	133.7	180.0	-419.4291182	108.2	5.5	7.8	1.510	1.579
	pVQZ	1.416	88.1	2.964	133.7	180.0	-419.4499792	108.1	5.1	7.2	1.532	1.574
	W1w						-419.3010045		4.1	6.3	1.573	1.568
	W2w						-419.3011966		4.2	6.4	1.571	1.567
	R_{P-H}	\angle_{H-P-H}	$R_{P-\parallel\parallel}$	$\angle_{H-P-\parallel\parallel}$	$\angle_{H-P-C-C}$							
3c: C_s ($^2A''$)	def2QZVP	1.416	88.4	3.633	105.7	129.3	-419.4493180	108.8	4.8	7.5	1.445	1.646
	pVTZ	1.418	88.5	3.620	106.1	129.1	-419.4290451	108.6	5.3	8.1	1.516	1.585
	pVQZ	1.417	88.4	3.615	105.9	129.2	-419.4500034	108.8	5.1	8.0	1.539	1.580
	W1w						-419.3007955		3.6	6.4	1.586	1.581
	W2w						-419.3009568		3.6	6.5	1.585	1.581
3d: C_s ($^2A'$)	def2QZVP	1.418	88.1	3.786	65.1	0.0	-419.4493629	108.3	4.9	7.2	1.440	1.641
	pVTZ	1.419	88.1	3.771	65.4	0.0	-419.4290991	108.2	5.5	7.8	1.511	1.579
	pVQZ	1.418	88.1	3.768	64.9	0.0	-419.4500467	108.3	5.2	7.6	1.533	1.574
	W1w						-419.3010002		4.1	6.5	1.576	1.570
	W2w						-419.3011676		4.2	6.5	1.574	1.570

Table E68: DSD-PBEP86-D3BJ and extrapolated single-point energies for $\text{PH}_2^- \cdots \text{HCCH}$ complexes. Geometries use for CC energies are from DSD-PBEP86-D3BJ/AVQZ optimisations. All energies are in E_h .

	3a: $\text{PH}_2^- \cdots \text{HCCH}$ (${}^1\text{A}'$)						
	$E_{DH-\text{DFT}}$	E_{SCF}	E_{CCSD}	E_{corr}	$E_{CCSD(T)}$	$E_{(T)}$	E_{Wnw}
def2QZVP	-419.5021193						
AVDZ		-418.7182739	-419.1760756	-0.4578017	-419.1957249	-0.0196493	
AVTZ	-419.4842843	-418.7498433	-419.2836724	-0.5338291	-419.3110450	-0.0273726	
AVQZ	-419.5060361	-418.7570931	-419.3121544	-0.5550613	-419.3413334	-0.0291790	
AV5Z		-418.7585942	-419.3203838	-0.5617896			
W1w		-418.7593488		-0.5689819		-0.0302438	-419.3585745
W2w		-418.7593258		-0.5688488		-0.0304972	-419.3586718
	3a: VDE $\text{PH}_2^- \cdots \text{HCCH}$ (${}^2\text{A}'$)						
def2QZVP	-419.4468306						
AVDZ		-418.7027542	-419.1275453	-0.4247911	-419.1443423	-0.0167970	
AVTZ	-419.4270719	-418.7348607	-419.2303886	-0.4955279	-419.2539823	-0.0235937	
AVQZ	-419.4479183	-418.7421473	-419.2574213	-0.5152740	-419.2825902	-0.0251689	
AV5Z		-418.7436848	-419.2652527	-0.5215679			
W1w		-418.7444144		-0.5282202		-0.0261205	-419.2987551
W2w		-418.7444342		-0.5281713		-0.0263184	-419.2989239

Table E69: DSD-PBEP86-D3BJ and extrapolated single-point energies for $\text{PH}_2 \cdots \text{HCCH}$ complexes. Geometries use for CC energies are from DSD-PBEP86-D3BJ/AVQZ optimisations. All energies are in E_h .

	3b: $\text{PH}_2 \cdots \text{HCCH}$ (${}^2\text{B}_1$)						
	$E_{DH-\text{DFT}}$	E_{SCF}	E_{CCSD}	E_{corr}	$E_{CCSD(T)}$	$E_{(T)}$	E_{Wnw}
def2QZVP	-419.4493307						
AVDZ		-418.7069512	-419.1287630	-0.4218118	-419.1451310	-0.0163680	
AVTZ	-419.4291182	-418.7397456	-419.2328629	-0.4931173	-419.2559901	-0.0231272	
AVQZ	-419.4499792	-418.7471012	-419.2600643	-0.5129631	-419.2847581	-0.0246938	
AV5Z		-418.7486518	-419.2679535	-0.5193017			
W1w		-418.7493898		-0.5259747		-0.0256400	-419.3010045
W2w		-418.7494075		-0.5259520		-0.0258370	-419.3011966
	3c: $\text{PH}_2 \cdots \text{HCCH}$ (${}^2\text{A}''$)						
def2QZVP	-419.4493180						
AVDZ		-418.7048603	-419.1277545	-0.4228942	-419.1442835	-0.0165290	
AVTZ	-419.4290451	-418.7376868	-419.2321212	-0.4944344	-419.2554791	-0.0233579	
AVQZ	-419.4500034	-418.7450748	-419.2594961	-0.5144213	-419.2844489	-0.0249528	
AV5Z		-418.7466213	-419.2674080	-0.5207867			
W1w		-418.7473735		-0.5275254		-0.0258966	-419.3007955
W2w		-418.7473750		-0.5274652		-0.0261166	-419.3009568
	3d: $\text{PH}_2 \cdots \text{HCCH}$ (${}^2\text{A}'$)						
def2QZVP	-419.4493629						
AVDZ		-418.7057891	-419.1281066	-0.4223175	-419.1445441	-0.0164375	
AVTZ	-419.4290991	-418.7386388	-419.2325124	-0.4938736	-419.2557641	-0.0232517	
AVQZ	-419.4500467	-418.7460369	-419.2598442	-0.5138073	-419.2846826	-0.0248384	
AV5Z		-418.7475885	-419.2677492	-0.5201607			
W1w		-418.7483387		-0.5268765		-0.0257850	-419.3010002
W2w		-418.7483447		-0.5268266		-0.0259963	-419.3011676

Table E70: Cartesian coordinates of the PH₂⁻ ...HCCH conformers optimised at DSD-PBEP86-D3BJ/def-2QZVP,AVnZ ($n = T, Q$) in Å.

		3a: PH ₂ ⁻ ...HCCH (¹ A')		
		x	y	z
def2QZVP	C	0.121359	-1.764694	0.000000
	C	0.161335	-2.973889	0.000000
	H	0.084383	-0.669583	0.000000
	H	0.194442	-4.035284	0.000000
	P	0.000000	1.940259	0.000000
	H	-0.987482	2.016225	-1.029715
	H	-0.987482	2.016225	1.029715
		x	y	z
AVTZ	C	-0.015043	1.788503	0.000000
	C	0.000000	2.999962	0.000000
	H	-0.032775	0.696211	0.000000
	H	0.013846	4.062405	0.000000
	P	0.113148	-1.923911	0.000000
	H	-0.794029	-2.315386	1.032372
	H	-0.794029	-2.315386	-1.032372
		x	y	z
AVQZ	C	0.072675	1.790750	0.000000
	C	0.148835	2.998054	0.000000
	H	0.000000	0.701047	0.000000
	H	0.216275	4.058075	0.000000
	P	0.017564	-1.928776	0.000000
	H	-0.904396	-2.280149	1.032115
	H	-0.904396	-2.280149	-1.032115

Table E71: Cartesian coordinates of the PH₂ ... HCCH conformers optimised at DSD-PBEP86-D3BJ/def-2QZVP,AVnZ ($n = T, Q$) in Å.

	3b: PH ₂ ... HCCH (² B ₁)			3c: PH ₂ ... HCCH (² A'')			3d: PH ₂ ... HCCH (² A')			
	x	y	z	x	y	z	x	y	z	
def2QZVP	C	0.000000	0.000000	-3.211681	0.000000	2.190547	0.000000	0.968707	-1.661130	0.000000
	C	0.000000	0.000000	-2.007520	1.050980	1.602951	0.000000	2.088434	-1.218678	0.000000
	H	0.000000	0.000000	-4.274454	-0.928735	2.707589	0.000000	-0.021647	-2.047699	0.000000
	H	0.000000	0.000000	-0.942712	1.980539	1.087222	0.000000	3.077848	-0.830329	0.000000
	P	0.000000	0.000000	2.033950	-0.340205	-1.631202	0.000000	-1.298501	1.077624	0.000000
	H	0.000000	1.024185	3.011562	-1.127287	-1.043890	-1.020801	-1.921529	2.351598	0.000000
	H	0.000000	-1.024185	3.011562	-1.127287	-1.043890	1.020801	0.000000	1.640919	0.000000
	x	y	z	x	y	z	x	y	z	
AVTZ	C	0.000000	0.000000	-3.195413	0.000000	2.180130	0.000000	0.967013	-1.656175	0.000000
	C	0.000000	0.000000	-1.989124	1.055477	1.596225	0.000000	2.085681	-1.205311	0.000000
	H	0.000000	0.000000	-4.258769	-0.931905	2.692402	0.000000	-0.020963	-2.049858	0.000000
	H	0.000000	0.000000	-0.923987	1.987926	1.084799	0.000000	3.072781	-0.809925	0.000000
	P	0.000000	0.000000	2.019552	-0.342801	-1.625367	0.000000	-1.296054	1.069730	0.000000
	H	0.000000	1.024676	2.998345	-1.123473	-1.027405	-1.021236	-1.927171	2.341130	0.000000
	H	0.000000	-1.024676	2.998345	-1.123473	-1.027405	1.021236	0.000000	1.641628	0.000000
	x	y	z	x	y	z	x	y	z	
AVQZ	C	0.000000	0.000000	-3.205386	-0.448549	2.131743	0.000000	0.971829	-1.655176	0.000000
	C	0.000000	0.000000	-2.000899	0.702302	1.776543	0.000000	2.085151	-1.196004	0.000000
	H	0.000000	0.000000	-4.268366	-1.465128	2.442981	0.000000	-0.012774	-2.056694	0.000000
	H	0.000000	0.000000	-0.935861	1.719330	1.466472	0.000000	3.068832	-0.792833	0.000000
	P	0.000000	0.000000	2.028635	0.000000	-1.658629	0.000000	-1.298367	1.065830	0.000000
	H	0.000000	1.024348	3.006206	-0.888360	-1.239867	-1.020921	-1.922434	2.339479	0.000000
	H	0.000000	-1.024348	3.006206	-0.888360	-1.239867	1.020921	0.000000	1.629673	0.000000

Table E72: Calculated harmonic frequencies and mode assignments for the 3a PH₂⁻...HCCH complex. All frequencies and intensities are in cm⁻¹ and km mol⁻¹.

3a PH ₂ ⁻ ...HCCH (¹ A')					
	Mode	Symmetry	Frequency (cm ⁻¹)	Intensity (km mol ⁻¹)	Description
def2QZVP	ω_1	a'	98	0.0669	PH ₂ wag
	ω_2	a''	100	0.1846	PH ₂ twist
	ω_3	a'	119	20.3753	Intermolecular stretch
	ω_4	a'	174	1.1227	PH ₂ rock
	ω_5	a''	194	0.3863	PH ₂ twist
	ω_6	a'	633	37.6391	Far Planar C–H bend
	ω_7	a''	635	37.989	Far OoP C–H bend
	ω_8	a'	956	31.4412	Near Planar C–H bend
	ω_9	a''	967	33.2168	Near OoP C–H bend
	ω_{10}	a'	1092	30.6008	PH ₂ scissor
	ω_{11}	a'	1946	216.3244	CC stretch
	ω_{12}	a'	2325	191.3063	PH ₂ symm. Stretch
	ω_{13}	a''	2327	218.9901	PH ₂ asymm. Stretch
	ω_{14}	a'	3000	1220.2734	Near CH stretch
	ω_{15}	a'	3482	2.7652	Far CH stretch
	zpe		108.0		
AVTZ	ω_1	a'	79	4.991	PH ₂ wag
	ω_2	a''	82	0.7338	PH ₂ twist
	ω_3	a'	117	18.0825	Intermolecular stretch
	ω_4	a'	155	1.07	PH ₂ rock
	ω_5	a''	178	1.3442	PH ₂ twist
	ω_6	a'	626	37.4191	Far Planar C–H bend
	ω_7	a''	628	37.9506	Far OoP C–H bend
	ω_8	a'	930	19.3157	Near Planar C–H bend
	ω_9	a''	942	23.1222	Near OoP C–H bend
	ω_{10}	a'	1089	31.3682	PH ₂ scissor
	ω_{11}	a'	1948	211.5746	CC stretch
	ω_{12}	a'	2324	185.9409	PH ₂ symm. Stretch
	ω_{13}	a''	2327	193.0257	PH ₂ asymm. Stretch
	ω_{14}	a'	3042	1224.7893	Near CH stretch
	ω_{15}	a'	3479	1.3377	Far CH stretch
	zpe		107.4		
AVQZ	ω_1	a'	81	5.3251	PH ₂ wag
	ω_2	a''	82	0.6806	PH ₂ twist
	ω_3	a'	115	17.8483	Intermolecular stretch
	ω_4	a'	154	1.215	PH ₂ rock
	ω_5	a''	177	1.517	PH ₂ twist
	ω_6	a'	629	36.9835	Far Planar C–H bend
	ω_7	a''	631	37.4584	Far OoP C–H bend
	ω_8	a'	922	18.7784	Near Planar C–H bend
	ω_9	a''	935	22.3843	Near OoP C–H bend
	ω_{10}	a'	1090	31.4815	PH ₂ scissor
	ω_{11}	a'	1952	208.423	CC stretch
	ω_{12}	a'	2331	181.487	PH ₂ symm. Stretch
	ω_{13}	a''	2334	187.9636	PH ₂ asymm. Stretch
	ω_{14}	a'	3047	1216.715	Near CH stretch
	ω_{15}	a'	3480	2.5449	Far CH stretch
	zpe		107.4		

Table E73: Calculated harmonic frequencies and mode assignments for the 3b PH₂ ··· HCCH complex. All frequencies and intensities are in cm⁻¹ and km mol⁻¹.

3b PH ₂ ··· HCCH (² B ₁)					
	Mode	Symmetry	Frequency (cm ⁻¹)	Intensity (km mol ⁻¹)	Description
def2QZVP	ω_1	<i>b</i> ₂	25	2.1954	PH ₂ rock
	ω_2	<i>b</i> ₁	34	5.0346	PH ₂ wag
	ω_3	<i>a</i> ₁	61	0.1774	Intermolecular stretch
	ω_4	<i>b</i> ₁	68	2.8792	PH ₂ wag
	ω_5	<i>b</i> ₂	99	0.8567	PH ₂ rock
	ω_6	<i>b</i> ₁	645	2.7258	OoP HCCH bend
	ω_7	<i>b</i> ₂	648	3.3119	Planar HCCH bend
	ω_8	<i>b</i> ₁	774	77.3033	OoP CH bend
	ω_9	<i>b</i> ₂	778	76.2795	Planar CH bend
	ω_{10}	<i>a</i> ₁	1136	33.3188	PH ₂ scissor
	ω_{11}	<i>a</i> ₁	2013	2.9355	CC stretch
	ω_{12}	<i>a</i> ₁	2434	54.209	PH ₂ symm. Stretch
	ω_{13}	<i>b</i> ₂	2444	50.6488	PH ₂ asymm. Stretch
	ω_{14}	<i>a</i> ₁	3413	180.4984	Asymm. CH stretch
	ω_{15}	<i>a</i> ₁	3510	1.652	Symm. CH stretch
AVTZ		zpe	108.2		
	ω_1	<i>b</i> ₂	32	2.2652	PH ₂ rock
	ω_2	<i>b</i> ₁	45	4.9707	PH ₂ wag
	ω_3	<i>a</i> ₁	65	0.1848	Intermolecular stretch
	ω_4	<i>b</i> ₁	76	2.3255	PH ₂ wag
	ω_5	<i>b</i> ₂	99	0.5484	PH ₂ rock
	ω_6	<i>b</i> ₁	642	3.2629	OoP HCCH bend
	ω_7	<i>b</i> ₂	644	3.6967	Planar HCCH bend
	ω_8	<i>b</i> ₁	780	74.6936	OoP CH bend
	ω_9	<i>b</i> ₂	784	74.383	Planar CH bend
	ω_{10}	<i>a</i> ₁	1136	34.0574	PH ₂ scissor
	ω_{11}	<i>a</i> ₁	2009	3.2392	CC stretch
	ω_{12}	<i>a</i> ₁	2427	56.745	PH ₂ symm. Stretch
	ω_{13}	<i>b</i> ₂	2437	50.6564	PH ₂ asymm. Stretch
	ω_{14}	<i>a</i> ₁	3406	185.8532	Asymm. CH stretch
	ω_{15}	<i>a</i> ₁	3512	3.7135	Symm. CH stretch
AVQZ		zpe	108.2		
	ω_1	<i>b</i> ₂	25	2.1053	PH ₂ rock
	ω_2	<i>b</i> ₁	35	4.7437	PH ₂ wag
	ω_3	<i>a</i> ₁	62	0.1829	Intermolecular stretch
	ω_4	<i>b</i> ₁	69	2.6869	PH ₂ wag
	ω_5	<i>b</i> ₂	99	0.7432	PH ₂ rock
	ω_6	<i>b</i> ₁	644	2.6474	OoP HCCH bend
	ω_7	<i>b</i> ₂	646	3.2138	Planar HCCH bend
	ω_8	<i>b</i> ₁	772	74.9425	OoP CH bend
	ω_9	<i>b</i> ₂	776	74.404	Planar CH bend
	ω_{10}	<i>a</i> ₁	1137	33.874	PH ₂ scissor
	ω_{11}	<i>a</i> ₁	2012	3.1039	CC stretch
	ω_{12}	<i>a</i> ₁	2433	55.142	PH ₂ symm. Stretch
	ω_{13}	<i>b</i> ₂	2443	49.2342	PH ₂ asymm. Stretch
	ω_{14}	<i>a</i> ₁	3410	183.4446	Asymm. CH stretch
	ω_{15}	<i>a</i> ₁	3508	1.8084	Symm. CH stretch
		zpe	108.1		

Table E74: Calculated harmonic frequencies and mode assignments for the 3c PH₂ ··· HCCH complex. All frequencies and intensities are in cm⁻¹ and km mol⁻¹.

3c PH ₂ ··· HCCH (² A'')					
	Mode	Symmetry	Frequency (cm ⁻¹)	Intensity (km mol ⁻¹)	Description
def2QZVP	ω_1	a'	41	0.5517	H-side intermolecular bend
	ω_2	a''	46	2.6262	PH ₂ rock
	ω_3	a'	66	0.1176	P-side intermolecular bend
	ω_4	a''	114	0.1201	PH ₂ twist
	ω_5	a'	153	5.4252	PH ₂ wag
	ω_6	a'	635	0.1982	Planar HCCH bend
	ω_7	a''	637	0.0464	OoP HCCH bend
	ω_8	a'	762	113.129	Planar CH bend
	ω_9	a''	763	83.9872	OoP CH bend
	ω_{10}	a'	1135	20.157	PH ₂ scissor
	ω_{11}	a'	2017	0.3984	CC stretch
	ω_{12}	a'	2429	42.9707	PH ₂ symm. Stretch
	ω_{13}	a''	2438	54.7695	PH ₂ asymm. Stretch
	ω_{14}	a'	3428	89.981	Asymm. CH stretch
	ω_{15}	a'	3520	0.2649	Symm. CH stretch
AVTZ	zpe		108.8		
	ω_1	a'	42	0.5219	H-side intermolecular bend
	ω_2	a''	47	2.3486	PH ₂ rock
	ω_3	a'	67	0.1229	P-side intermolecular bend
	ω_4	a''	121	0.1679	PH ₂ twist
	ω_5	a'	158	4.9468	PH ₂ wag
	ω_6	a'	627	0.2396	Planar HCCH bend
	ω_7	a''	631	0.0434	OoP HCCH bend
	ω_8	a'	764	112.909	Planar CH bend
	ω_9	a''	765	83.173	OoP CH bend
	ω_{10}	a'	1135	20.6375	PH ₂ scissor
	ω_{11}	a'	2013	0.3877	CC stretch
	ω_{12}	a'	2422	44.8392	PH ₂ symm. Stretch
	ω_{13}	a''	2431	54.4903	PH ₂ asymm. Stretch
	ω_{14}	a'	3419	89.9344	Asymm. CH stretch
AVQZ	ω_{15}	a'	3521	0.2861	Symm. CH stretch
	zpe		108.6		
	ω_1	a'	42	0.5469	H-side intermolecular bend
	ω_2	a''	50	2.421	PH ₂ rock
	ω_3	a'	68	0.1257	P-side intermolecular bend
	ω_4	a''	119	0.1416	PH ₂ twist
	ω_5	a'	157	5.1144	PH ₂ wag
	ω_6	a'	634	0.2383	Planar HCCH bend
	ω_7	a''	637	0.0518	OoP HCCH bend
	ω_8	a'	761	112.5171	Planar CH bend
	ω_9	a''	762	82.7305	OoP CH bend
	ω_{10}	a'	1135	20.6348	PH ₂ scissor
	ω_{11}	a'	2016	0.3945	CC stretch
	ω_{12}	a'	2428	43.6919	PH ₂ symm. Stretch
	ω_{13}	a''	2437	53.0453	PH ₂ asymm. Stretch
	ω_{14}	a'	3425	89.444	Asymm. CH stretch
	ω_{15}	a'	3517	0.2792	Symm. CH stretch
	zpe		108.8		

Table E75: Calculated harmonic frequencies and mode assignments for the 3d PH₂ ··· HCCH complex. All frequencies and intensities are in cm⁻¹ and km mol⁻¹.

3d PH ₂ ··· HCCH (² A')					
	Mode	Symmetry	Frequency (cm ⁻¹)	Intensity (km mol ⁻¹)	Description
def2QZVP	ω_1	a'	34	0.311	H-side intermolecular bend
	ω_2	a''	51	6.3315	PH ₂ wag
	ω_3	a''	67	0.0523	PH ₂ twist
	ω_4	a'	79	0.1758	P-side intermolecular bend
	ω_5	a'	118	4.9254	PH ₂ rock
	ω_6	a'	636	0.2494	Planar HCCH bend
	ω_7	a''	637	0.233	OoP HCCH bend
	ω_8	a'	763	116.4601	Planar CH bend
	ω_9	a''	763	84.8815	OoP CH bend
	ω_{10}	a'	1135	16.0898	PH ₂ scissor
	ω_{11}	a'	2016	0.0568	CC stretch
	ω_{12}	a'	2422	66.7145	Farside PH stretch
	ω_{13}	a'	2443	54.7202	Nearside PH stretch
	ω_{14}	a'	3428	87.8505	Asymm. CH stretch
	ω_{15}	a'	3519	0.2172	Symm. CH stretch
	zpe		108.3		
AVTZ	ω_1	a'	35	0.3252	H-side intermolecular bend
	ω_2	a''	58	5.4065	PH ₂ wag
	ω_3	a''	72	0.447	PH ₂ twist
	ω_4	a'	82	0.1663	P-side intermolecular bend
	ω_5	a'	123	4.6491	PH ₂ rock
	ω_6	a'	628	0.3253	Planar HCCH bend
	ω_7	a''	631	0.2141	OoP HCCH bend
	ω_8	a'	763	115.2781	Planar CH bend
	ω_9	a''	765	83.56	OoP CH bend
	ω_{10}	a'	1135	16.201	PH ₂ scissor
	ω_{11}	a'	2011	0.0472	CC stretch
	ω_{12}	a'	2415	69.1021	Farside PH stretch
	ω_{13}	a'	2436	55.6119	Nearside PH stretch
	ω_{14}	a'	3419	87.8926	Asymm. CH stretch
	ω_{15}	a'	3521	0.2127	Symm. CH stretch
	zpe		108.2		
AVQZ	ω_1	a'	35	0.3134	H-side intermolecular bend
	ω_2	a''	53	5.9903	PH ₂ wag
	ω_3	a''	68	0.0001	PH ₂ twist
	ω_4	a'	80	0.1854	P-side intermolecular bend
	ω_5	a'	122	4.7515	PH ₂ rock
	ω_6	a'	635	0.2886	Planar HCCH bend
	ω_7	a''	638	0.2366	OoP HCCH bend
	ω_8	a'	761	114.6782	Planar CH bend
	ω_9	a''	762	83.1086	OoP CH bend
	ω_{10}	a'	1135	16.1913	PH ₂ scissor
	ω_{11}	a'	2014	0.0491	CC stretch
	ω_{12}	a'	2421	67.6536	Farside PH stretch
	ω_{13}	a'	2442	53.8812	Nearside PH stretch
	ω_{14}	a'	3425	87.3621	Asymm. CH stretch
	ω_{15}	a'	3517	0.2269	Symm. CH stretch
	zpe		108.3		

Table E76: $\text{PH}_2^- \cdots \text{CO}_2$ complex geometric parameters, D_0 s and VDEs from DSD-PBEP86-D3BJ optimisations. zpe values are drawn from relevant harmonic frequency calculations.

	R_{P-H} Å	\angle_{H-P-H} °	R_{P-C} Å	\angle_{H-P-C} °	$\angle_{H-P-C-O}$ °	\angle_{O-C-O} °	E E_h	zpe kJ mol ⁻¹	D_e kJ mol ⁻¹	D_0 kJ mol ⁻¹	E_{VDE} E_h	VDE eV	
4a: C_s ($^1A'$)	def2QZVP	1.429	88.3	3.345	95.7	43.6	180.0	-530.6818382	66.9	29.2	31.8	-530.6335276	1.301
	AVTZ	1.429	88.2	3.349	102.4	42.3	180.0	-530.6461856	66.5	25.4	27.7	-530.5947214	1.388
	AVQZ	1.428	88.2	3.348	103.0	42.1	180.0	-530.6875884	66.8	25.3	27.7	-530.6351408	1.414
	W1w						-530.5503573		24.7	27.1	-530.4960965	1.463	
	W2w						-530.5530225		24.6	27.1	-530.4988091	1.462	
4b: C_s ($^1A'$)	def2QZVP	1.417	87.1	1.945	99.1	43.9	132.8	-530.7112142	75.3	106.3	117.4	-530.5820139	3.516
	AVTZ	1.418	87.1	1.947	99.0	43.9	132.8	-530.6740789	75.0	98.7	109.4	-530.5434711	3.554
	AVQZ	1.417	87.1	1.943	99.1	43.8	132.7	-530.7153744	75.3	98.3	109.1	-530.5837826	3.581
	W1w						-530.5781690		97.7	108.5	-530.4429959	3.678	
	W2w						-530.5809081		97.8	108.7	-530.4457681	3.677	
	R_{P-H} Å	\angle_{H-P-H} °	R_{P-C} Å	\angle_{H-P-C} °	$\angle_{H-P-C-O}$ °	\angle_{O-C-O} °	E E_h	zpe kJ mol ⁻¹	D_e kJ mol ⁻¹	D_0 kJ mol ⁻¹	ADE eV	ADE_{shift} eV	
4c: C_{2v} (2B_1)	def2QZVP	1.416	88.2	3.489	133.7	0.0	180.0	-530.6345054	68.2	5.7	7.9	2.014	2.215
	AVTZ	1.418	88.2	3.476	133.8	0.0	180.0	-530.5955495	68.0	6.2	8.4	2.065	2.134
	AVQZ	1.416	88.2	3.469	133.7	0.0	180.0	-530.6359683	68.4	6.1	8.5	2.089	2.131
	W1w						-530.4970098		5.4	7.8	2.137	2.131	
	W2w						-530.4997243		5.4	7.8	2.138	2.134	
4d: C_{2v} (2B_1)	def2QZVP	1.418	88.4	3.928	46.1	0.0	180.0	-530.6337367	68.0	3.7	5.7	2.032	2.233
	AVTZ	1.419	88.4	3.904	46.1	0.0	180.0	-530.5948351	67.9	4.3	6.4	2.083	2.152
	AVQZ	1.418	88.3	3.913	46.1	0.0	180.0	-530.6352059	68.1	4.1	6.2	2.107	2.149
	W1w						-530.4963584		3.7	5.9	2.152	2.147	
	W2w						-530.4990421		3.6	5.8	2.154	2.149	

Table E77: DSD-PBEP86-D3BJ and extrapolated single-point energies for $\text{PH}_2^- \cdots \text{CO}_2$ complexes. Geometries use for CC energies are from DSD-PBEP86-D3BJ/AVQZ optimisations. All energies are in E_h .

	4a: $\text{PH}_2^- \cdots \text{CO}_2$ (${}^1\text{A}'$)						
	E_{DH-DFT}	E_{SCF}	E_{CCSD}	E_{corr}	$E_{CCSD(T)}$	$E_{(T)}$	E_{Wnw}
def2QZVP	-530.6818382						
AVDZ		-529.5465097	-530.2272331	-0.6807234	-530.2556851	-0.0284520	
AVTZ	-530.6461856	-529.6036661	-530.4147501	-0.8110840	-530.4551799	-0.0404298	
AVQZ	-530.6875884	-529.6192898	-530.4727984	-0.8535086	-530.5160569	-0.0432585	
AV5Z		-529.6226186	-530.4907429	-0.8681243			
W1w		-529.6241510		-0.8813236		-0.0448827	-530.5503573
W2w		-529.6242410		-0.8834588		-0.0453227	-530.5530225
	4a: VDE $\text{PH}_2^- \cdots \text{CO}_2$ (${}^2\text{A}'$)						
def2QZVP	-530.6335276						
AVDZ		-529.5379981	-530.1843696	-0.6463715	-530.2098703	-0.0255007	
AVTZ	-530.5947214	-529.5956152	-530.3672306	-0.7716154	-530.4037297	-0.0364991	
AVQZ	-530.6351408	-529.6112494	-530.4238034	-0.8125540	-530.4628829	-0.0390795	
AV5Z		-529.6146052	-530.4413365	-0.8267313			
W1w		-529.6161138		-0.8393948		-0.0405879	-530.4960965
W2w		-529.6162408		-0.8416058		-0.0409625	-530.4988091
	4b: PH_2COO^- (${}^1\text{A}'$)						
def2QZVP	-530.7112142						
AVDZ		-529.5642625	-530.2534287	-0.6891662	-530.2828406	-0.0294119	
AVTZ	-530.6740789211	-529.6196238	-530.4407444	-0.8211206	-530.4821960	-0.0414516	
AVQZ	-530.7153744	-529.6346681	-530.4991388	-0.8644707	-530.5434658	-0.0443270	
AV5Z		-529.6379758	-530.5172935	-0.8793177			
W1w		-529.6393490		-0.8928925		-0.0459275	-530.5781690
W2w		-529.6395879		-0.8948949		-0.0464253	-530.5809081
	4b: VDE PH_2COO^- (${}^2\text{A}'$)						
def2QZVP	-530.5820139						
AVDZ		-529.4502380	-530.1241321	-0.6738941	-530.1562620	-0.0321299	
AVTZ	-530.5434711	-529.5065997	-530.3067905	-0.8001908	-530.3506246	-0.0438341	
AVQZ	-530.5837826	-529.5217997	-530.3631172	-0.8413175	-530.4097641	-0.0466469	
AV5Z		-529.5251434	-530.3806022	-0.8554588			
W1w		-529.5265290		-0.8682816		-0.0481853	-530.4429959
W2w		-529.5267731		-0.8702956		-0.0486995	-530.4457681

Table E78: DSD-PBEP86-D3BJ and extrapolated single-point energies for $\text{PH}_2 \cdots \text{CO}_2$ complexes. Geometries use for CC energies are from DSD-PBEP86-D3BJ/AVQZ optimisations. All energies are in E_h .

	4c: $\text{PH}_2 \cdots \text{CO}_2$ (${}^2\text{B}_1$)						
	E_{DH-DFT}	E_{SCF}	E_{CCSD}	E_{corr}	$E_{CCSD(T)}$	$E_{(T)}$	E_{Wnw}
def2QZVP	-530.6345054						
AVDZ		-529.5402433	-530.1851386	-0.6448953	-530.2103999	-0.0252613	
AVTZ	-530.5955495	-529.5980494	-530.3683556	-0.7703062	-530.4045815	-0.0362259	
AVQZ	-530.6359683	-529.6137406	-530.4249850	-0.8112444	-530.4637813	-0.0387963	
AV5Z		-529.6171072	-530.4425328	-0.8254256			
W1w		-529.6186228		-0.8380849		-0.0403021	-530.4970098
W2w		-529.6187480		-0.8403042		-0.0406720	-530.4997243
	4d: $\text{PH}_2 \cdots \text{CO}_2$ (${}^2\text{B}_1$)						
def2QZVP	-530.6337367						
AVDZ		-529.5393626	-530.1846489	-0.6452863	-530.2099386	-0.0252897	
AVTZ	-530.5948351	-529.5971688	-530.3677835	-0.7706147	-530.4040475	-0.0362640	
AVQZ	-530.6352059	-529.6128397	-530.4243356	-0.8114959	-530.4631631	-0.0388275	
AV5Z		-529.6162006	-530.4418531	-0.8256525			
W1w		-529.6177155		-0.8382990		-0.0403438	-530.4963584
W2w		-529.6178387		-0.8405053		-0.0406982	-530.4990421

Table E79: Cartesian coordinates of the $\text{PH}_2^- \cdots \text{CO}_2$ conformers optimised at DSD-PBEP86-D3BJ/def-2QZVP,AV n Z ($n = T, Q$) in Å.

		4a: $\text{PH}_2 \cdots \text{CO}_2$ (${}^1A'$)			4b: $\text{PH}_2 \cdots \text{CO}_2$ (${}^1A'$)		
		x	y	z	x	y	z
def2QZVP	C	-1.466371	0.000027	0.004120	-0.024952	0.656629	0.000000
	O	-1.466533	-1.164083	0.004136	-0.052155	1.151921	-1.136536
	O	-1.466209	1.164137	0.004104	-0.052155	1.151921	1.136536
	P	1.876777	-0.000004	-0.119871	-0.052155	-1.287939	0.000000
	H	2.053788	1.030158	0.854073	0.883264	-1.525707	-1.037290
	H	2.054724	-1.030689	0.853348	0.883264	-1.525707	1.037290
		x	y	z	x	y	z
AVTZ	C	-1.476123	0.000004	0.007497	0.025299	0.656755	0.000000
	O	-1.476098	1.166809	0.007493	0.052201	1.154114	1.139073
	O	-1.476148	-1.166801	0.007502	0.052201	1.154114	-1.139073
	P	1.870122	0.000001	-0.118803	0.052201	-1.290354	0.000000
	H	2.211365	1.032274	0.808638	-0.885009	-1.525525	1.037905
	H	2.211504	-1.032380	0.808465	-0.885009	-1.525525	-1.037905
		x	y	z	x	y	z
AVQZ	C	1.476753	0.000001	0.007740	-0.655590	0.000000	0.009533
	O	1.476751	-1.164306	0.007736	-1.153180	1.136843	0.008950
	O	1.476755	1.164307	0.007745	-1.153180	-1.136843	0.008950
	P	-1.869312	-0.000015	-0.118314	1.282972	-0.000001	-0.120171
	H	-2.224445	-1.032071	0.802345	1.569916	1.037687	0.801077
	H	-2.224444	1.032281	0.802076	1.569917	-1.037677	0.801090

Table E80: Cartesian coordinates of the PH₂⋯CO₂ conformers optimised at DSD-PBEP86-D3BJ/def-2QZVP,AVnZ ($n = T, Q$) in Å.

		4c: PH ₂ ⋯CO ₂ (² B ₁)			4d: PH ₂ ⋯CO ₂ (² B ₁)		
		x	y	z	x	y	z
def2QZVP	C	0.000000	0.000000	-1.570899	0.000000	0.000000	-1.661680
	O	0.000000	1.162222	-1.570899	0.000000	1.162275	-1.661680
	O	0.000000	-1.162222	-1.570899	0.000000	-1.162275	-1.661680
	P	0.000000	0.000000	1.917714	0.000000	0.000000	2.266127
	H	0.000000	1.023180	2.897035	0.000000	1.021585	1.282529
	H	0.000000	-1.023180	2.897035	0.000000	-1.021585	1.282529
		x	y	z	x	y	z
AVTZ	C	0.000000	0.000000	-1.565364	0.000000	0.000000	-1.651335
	O	0.000000	1.165010	-1.565364	0.000000	1.165072	-1.651335
	O	0.000000	-1.165010	-1.565364	0.000000	-1.165072	-1.651335
	P	0.000000	0.000000	1.910413	0.000000	0.000000	2.252892
	H	0.000000	1.023734	2.890901	0.000000	1.022068	1.267999
	H	0.000000	-1.023734	2.890901	0.000000	-1.022068	1.267999
		x	y	z	x	y	z
AVQZ	C	0.000000	0.000000	-1.559810	0.000000	0.000000	-1.655322
	O	0.000000	1.162531	-1.565689	0.000000	1.162598	-1.655519
	O	0.000000	-1.162531	-1.565689	0.000000	-1.162598	-1.655519
	P	0.000000	0.000000	1.908917	0.000000	0.000000	2.258087
	H	0.000000	1.023445	2.888065	0.000000	1.021762	1.274470
	H	0.000000	-1.023445	2.888065	0.000000	-1.021762	1.274470

Table E81: Calculated harmonic frequencies and mode assignments for the 4a PH₂⁻...CO₂ complex. All frequencies and intensities are in cm⁻¹ and km mol⁻¹.

4a PH ₂ ⁻ ...CO ₂ (¹ A')					
	Mode	Symmetry	Frequency (cm ⁻¹)	Intensity (km mol ⁻¹)	Description
def2QZVP	ω_1	<i>a</i>	45	1.0065	PH ₂ rock
	ω_2	<i>a</i>	83	27.6512	Intermolecular stretch
	ω_3	<i>a</i>	84	0.1032	PH ₂ twist
	ω_4	<i>a</i>	128	0.0719	PH ₂ wag
	ω_5	<i>a</i>	207	0.8877	PH ₂ twist
	ω_6	<i>a</i>	528	128.0676	CO ₂ planar bend
	ω_7	<i>a</i>	644	14.6889	CO ₂ OoP bend
	ω_8	<i>a</i>	1094	29.1645	PH ₂ scissor
	ω_9	<i>a</i>	1338	15.6392	CO ₂ symm. stretch
	ω_{10}	<i>a</i>	2325	199.4075	PH ₂ symm. stretch
	ω_{11}	<i>a</i>	2326	156.2214	PH ₂ asymm. stretch
	ω_{12}	<i>a</i>	2391	567.3114	CO ₂ asymm stretch
	zpe		66.9		
AVTZ	ω_1	<i>a</i>	49	2.4802	PH ₂ twist
	ω_2	<i>a</i>	71	0.0003	PH ₂ rock
	ω_3	<i>a</i>	81	25.7791	Intermolecular stretch
	ω_4	<i>a</i>	91	0.6447	PH ₂ wag
	ω_5	<i>a</i>	196	2.3713	PH ₂ twist
	ω_6	<i>a</i>	536	124.9385	CO ₂ planar bend
	ω_7	<i>a</i>	642	12.5408	CO ₂ OoP bend
	ω_8	<i>a</i>	1092	28.7251	PH ₂ scissor
	ω_9	<i>a</i>	1334	19.7172	CO ₂ symm. stretch
	ω_{10}	<i>a</i>	2324	188.2665	PH ₂ symm. stretch
	ω_{11}	<i>a</i>	2327	130.2623	PH ₂ asymm. stretch
	ω_{12}	<i>a</i>	2380	552.2771	CO ₂ asymm stretch
	zpe		66.5		
AVQZ	ω_1	<i>a''</i>	58	2.3844	PH ₂ twist
	ω_2	<i>a''</i>	75	0.0886	PH ₂ rock
	ω_3	<i>a'</i>	82	25.2338	Intermolecular stretch
	ω_4	<i>a'</i>	91	1.1352	PH ₂ wag
	ω_5	<i>a''</i>	197	2.5268	PH ₂ twist
	ω_6	<i>a'</i>	542	125.8444	CO ₂ planar bend
	ω_7	<i>a'</i>	647	12.5257	CO ₂ OoP bend
	ω_8	<i>a'</i>	1092	28.7893	PH ₂ scissor
	ω_9	<i>a'</i>	1338	19.4295	CO ₂ symm. stretch
	ω_{10}	<i>a'</i>	2331	183.122	PH ₂ symm. stretch
	ω_{11}	<i>a''</i>	2334	127.4736	PH ₂ asymm. stretch
	ω_{12}	<i>a''</i>	2388	551.1642	CO ₂ asymm stretch
	zpe		66.8		

Table E82: Calculated harmonic frequencies and mode assignments for the 4b PH₂⁻...CO₂ complex. All frequencies and intensities are in cm⁻¹ and km mol⁻¹.

4b PH ₂ ⁻ ...CO ₂ (¹ A')					
	Mode	Symmetry	Frequency (cm ⁻¹)	Intensity (km mol ⁻¹)	Description
def2QZVP	ω_1	a''	144	4.2514	PH ₂ rock
	ω_2	a''	286	0.8196	PH ₂ twist
	ω_3	a'	371	9.1934	P-C stretch
	ω_4	a'	554	12.1745	PH ₂ wag
	ω_5	a'	751	233.5998	CO ₂ planar bend
	ω_6	a''	760	16.5842	PH ₂ twist
	ω_7	a'	795	1.993	PH ₂ wag
	ω_8	a'	1122	32.0138	PH ₂ scissor
	ω_9	a'	1271	501.6755	CO ₂ symm. stretch
	ω_{10}	a''	1725	520.3643	CO ₂ asymm. stretch
	ω_{11}	a'	2406	99.8302	PH ₂ symm. stretch
	ω_{12}	a''	2410	122.5782	PH ₂ asymm. stretch
	zpe		75.3		
AVTZ	ω_1	a''	141	4.8191	PH ₂ rock
	ω_2	a''	286	0.8635	PH ₂ twist
	ω_3	a'	371	9.6321	P-C stretch
	ω_4	a'	553	12.6536	PH ₂ wag
	ω_5	a'	743	236.9494	CO ₂ planar bend
	ω_6	a''	757	19.9476	PH ₂ twist
	ω_7	a'	789	3.8843	PH ₂ wag
	ω_8	a'	1120	32.9916	PH ₂ scissor
	ω_9	a'	1264	512.9572	CO ₂ symm. stretch
	ω_{10}	a''	1712	563.8963	CO ₂ asymm. stretch
	ω_{11}	a'	2398	102.6451	PH ₂ symm. stretch
	ω_{12}	a''	2402	115.7435	PH ₂ asymm. stretch
	zpe		75.0		
AVQZ	ω_1	a''	152	4.6757	PH ₂ rock
	ω_2	a''	287	0.9458	PH ₂ twist
	ω_3	a'	373	9.0871	P-C stretch
	ω_4	a'	557	12.4647	PH ₂ wag
	ω_5	a'	747	233.776	CO ₂ planar bend
	ω_6	a''	761	19.7734	PH ₂ twist
	ω_7	a'	793	3.8517	PH ₂ wag
	ω_8	a'	1121	33.6437	PH ₂ scissor
	ω_9	a'	1267	509.425	CO ₂ symm. stretch
	ω_{10}	a''	1713	564.693	CO ₂ asymm. stretch
	ω_{11}	a'	2405	101.0097	PH ₂ symm. stretch
	ω_{12}	a''	2408	114.7416	PH ₂ asymm. stretch
	zpe		75.3		

Table E83: Calculated harmonic frequencies and mode assignments for the 4c PH₂ ··· CO₂ complex. All frequencies and intensities are in cm⁻¹ and km mol⁻¹.

4c PH ₂ ··· CO ₂ (² B ₁)					
	Mode	Symmetry	Frequency (cm ⁻¹)	Intensity (km mol ⁻¹)	Description
def2QZVP	ω_1	<i>b</i> ₂	23	1.5018	PH ₂ rock
	ω_2	<i>b</i> ₁	53	7.6095	PH ₂ wag
	ω_3	<i>a</i> ₂	60	0	PH ₂ twist
	ω_4	<i>a</i> ₁	61	0.0121	Intermolecular stretch
	ω_5	<i>b</i> ₂	103	0.6766	PH ₂ rock
	ω_6	<i>a</i> ₁	664	47.6851	CO ₂ planar bend
	ω_7	<i>b</i> ₁	673	23.1012	CO ₂ OoP bend
	ω_8	<i>a</i> ₁	1137	26.7961	PH ₂ scissor
	ω_9	<i>a</i> ₁	1352	0.0201	CO ₂ symm. stretch
	ω_{10}	<i>b</i> ₂	2409	492.0007	PH ₂ symm. stretch
	ω_{11}	<i>a</i> ₁	2431	51.8258	PH ₂ asymm. stretch
	ω_{12}	<i>b</i> ₂	2441	87.6108	CO ₂ asymm stretch
	zpe		68.2		
AVTZ	ω_1	<i>b</i> ₂	19	1.4326	PH ₂ rock
	ω_2	<i>b</i> ₁	61	6.9572	PH ₂ wag
	ω_3	<i>a</i> ₁	62	0.0112	Intermolecular stretch
	ω_4	<i>a</i> ₂	64	0	PH ₂ twist
	ω_5	<i>b</i> ₂	103	0.5578	PH ₂ rock
	ω_6	<i>a</i> ₁	659	46.8534	CO ₂ planar bend
	ω_7	<i>b</i> ₁	668	22.0147	CO ₂ OoP bend
	ω_8	<i>a</i> ₁	1137	27.6168	PH ₂ scissor
	ω_9	<i>a</i> ₁	1347	0.0247	CO ₂ symm. stretch
	ω_{10}	<i>b</i> ₂	2398	493.9327	PH ₂ symm. stretch
	ω_{11}	<i>a</i> ₁	2424	54.6594	PH ₂ asymm. stretch
	ω_{12}	<i>b</i> ₂	2434	84.8248	CO ₂ asymm stretch
	zpe		68.0		
AVQZ	ω_1	<i>b</i> ₂	38	1.2601	PH ₂ rock
	ω_2	<i>a</i> ₂	55	0	PH ₂ twist
	ω_3	<i>a</i> ₁	63	0.0158	Intermolecular stretch
	ω_4	<i>b</i> ₁	66	7.0601	PH ₂ wag
	ω_5	<i>b</i> ₂	111	0.7985	PH ₂ rock
	ω_6	<i>a</i> ₁	663	47.8538	CO ₂ planar bend
	ω_7	<i>b</i> ₁	671	22.1253	CO ₂ OoP bend
	ω_8	<i>a</i> ₁	1137	27.9008	PH ₂ scissor
	ω_9	<i>a</i> ₁	1351	0.0379	CO ₂ symm. stretch
	ω_{10}	<i>b</i> ₂	2405	497.7455	PH ₂ symm. stretch
	ω_{11}	<i>a</i> ₁	2430	53.0216	PH ₂ asymm. stretch
	ω_{12}	<i>b</i> ₂	2440	82.9745	CO ₂ asymm stretch
	zpe		68.4		

Table E84: Calculated harmonic frequencies and mode assignments for the 4d PH₂ ··· CO₂ complex. All frequencies and intensities are in cm⁻¹ and km mol⁻¹.

4d PH ₂ ··· CO ₂ (² B ₁)					
	Mode	Symmetry	Frequency (cm ⁻¹)	Intensity (km mol ⁻¹)	Description
def2QZVP	ω_1	<i>b</i> ₁	27	8.1082	PH ₂ wag
	ω_2	<i>a</i> ₂	29	0	PH ₂ twist
	ω_3	<i>b</i> ₂	39	0.2543	CO ₂ planar rot.
	ω_4	<i>a</i> ₁	55	0.0095	Intermolecular stretch
	ω_5	<i>b</i> ₂	116	4.7081	PH ₂ rock
	ω_6	<i>a</i> ₁	669	39.5817	CO ₂ planar bend
	ω_7	<i>b</i> ₁	672	24.1284	CO ₂ OoP bend
	ω_8	<i>a</i> ₁	1150	18.9422	PH ₂ scissor
	ω_9	<i>a</i> ₁	1352	0.0014	CO ₂ symm. stretch
	ω_{10}	<i>b</i> ₂	2408	487.5491	PH ₂ symm. stretch
	ω_{11}	<i>a</i> ₁	2422	45.032	PH ₂ asymm. stretch
	ω_{12}	<i>b</i> ₂	2431	78.7101	CO ₂ asymm stretch
	zpe		68.0		
AVTZ	ω_1	<i>b</i> ₂	39	0.3268	CO ₂ planar rot.
	ω_2	<i>b</i> ₁	40	7.4393	PH ₂ wag
	ω_3	<i>a</i> ₂	41	0	PH ₂ twist
	ω_4	<i>a</i> ₁	58	0.0151	Intermolecular stretch
	ω_5	<i>b</i> ₂	115	4.3612	PH ₂ rock
	ω_6	<i>a</i> ₁	664	38.6844	CO ₂ planar bend
	ω_7	<i>b</i> ₁	668	23.0077	CO ₂ OoP bend
	ω_8	<i>a</i> ₁	1149	19.1362	PH ₂ scissor
	ω_9	<i>a</i> ₁	1346	0.0008	CO ₂ symm. stretch
	ω_{10}	<i>b</i> ₂	2397	489.605	PH ₂ symm. stretch
	ω_{11}	<i>a</i> ₁	2415	45.5477	PH ₂ asymm. stretch
	ω_{12}	<i>b</i> ₂	2424	74.6021	CO ₂ asymm stretch
	zpe		67.9		
AVQZ	ω_1	<i>a</i> ₂	20	0	PH ₂ twist
	ω_2	<i>b</i> ₂	41	0.245	CO ₂ planar rot.
	ω_3	<i>b</i> ₁	46	7.6204	PH ₂ wag
	ω_4	<i>a</i> ₁	57	0.0128	Intermolecular stretch
	ω_5	<i>b</i> ₂	131	4.3785	PH ₂ rock
	ω_6	<i>a</i> ₁	668	39.0188	CO ₂ planar bend
	ω_7	<i>b</i> ₁	671	23.1924	CO ₂ OoP bend
	ω_8	<i>a</i> ₁	1150	19.3107	PH ₂ scissor
	ω_9	<i>a</i> ₁	1350	0.0007	CO ₂ symm. stretch
	ω_{10}	<i>b</i> ₂	2404	493.0445	PH ₂ symm. stretch
	ω_{11}	<i>a</i> ₁	2421	44.4927	PH ₂ asymm. stretch
	ω_{12}	<i>b</i> ₂	2430	73.8753	CO ₂ asymm stretch
	zpe		68.1		

Table E85: HS⁻ ··· PH₃ complex geometric parameters, D_0 s and VDEs from DSD-PBEP86-D3BJ optimisations. zpe values are drawn from relevant harmonic frequency calculations.

	R_{P-H} Å	\angle_{H-P-H} °	R_{P-HS} Å	R_{PH-S} Å	\angle_{P-H-S} °	$\angle_{P-H-S-H}$ °	\angle_{H-S-H} °	E E_h	zpe kJ mol ⁻¹	D_e kJ mol ⁻¹	D_0 kJ mol ⁻¹	E_{VDE} E_h	VDE eV
5a: C_s ($^1A'$)	def2QZVP	1.417	93.4	1.444	2.398	176.2	0.0	86.8 -741.4172135	82.1	31.5	34.2	-741.3266070	2.442
	pVTZ	1.418	93.4	1.442	2.423	176.2	0.0	86.8 -741.4018413	82.1	28.6	31.4	-741.3091042	2.500
	pVQZ	1.417	93.4	1.441	2.427	176.2	0.0	87.1 -741.4210843	82.2	28.1	30.9	-741.3269358	2.539
	W1w							-741.1282222		25.9	28.8	-741.0319843	2.595
	W2w							-741.1286566		26.1	28.9	-741.0327810	2.586
5b: C_s ($^1A'$)	def2QZVP	1.417	93.4	1.445	2.395	179.1	180.0	86.4 -741.4172421	82.1	31.6	34.3	-741.3267399	2.463
	pVTZ	1.418	93.4	1.442	2.420	179.1	180.0	86.9 -741.4018921	82.2	28.7	31.6	-741.3002829	2.765
	pVQZ	1.417	93.4	1.441	2.424	179.3	180.0	87.1 -741.4211343	82.3	28.2	31.1	-741.3270689	2.560
	W1w							-741.1282663		26.1	28.9	-741.0321132	2.616
	W2w							-741.1287004		26.2	29.1	-741.0329115	2.606
5c: C_s ($^1A'$)		R_{P-H}	\angle_{H-P-H}	R_{P-S}	R_{P-H}	\angle_{S-P-H}	$\angle_{H-P-S-H}$	\angle_{H-S-P}					
	def2QZVP	1.406	96.0	3.255	1.444	157.7	0.0	92.2 -741.4165067	84.1	29.7	34.3	-741.3268151	2.429
	pVTZ	1.408	95.8	3.290	1.443	158.2	0.0	96.1 -741.4008582	83.8	26.0	30.5	-741.2967501	2.821
	pVQZ	1.407	95.9	3.283	1.442	158.2	0.0	96.2 -741.4202512	83.9	25.9	30.4	-741.3271357	2.510
	W1w							-741.1273991		23.8	28.3	-741.0322297	2.566
5d: C_s ($^1A'$)	def2QZVP	1.406	96.0	3.226	1.446	159.0	180.0	90.0 -741.4167390	84.3	30.3	35.1	-741.3277082	2.423
	pVTZ	1.408	95.8	3.269	1.445	158.2	180.0	91.1 -741.4010655	84.0	26.6	31.2	-741.3099052	2.481
	pVQZ	1.407	95.9	3.262	1.443	158.2	180.0	91.4 -741.4204578	84.1	26.5	31.2	-741.3279797	2.516
	W1w							-741.1275398		24.1	28.9	-741.0330081	2.572
	W2w							-741.1280381		24.5	29.2	-741.0338603	2.563

Table E86: PH₂…H₂S and HS…PH₃ complex geometric parameters, D_0 s and VDEs from DSD-PBEP86-D3BJ optimisations. zpe values are drawn from relevant harmonic frequency calculations.

	R_{P-H} Å	\angle_{H-P-H} °	R_{P-S} Å	R_{P-H} Å	\angle_{S-P-H} °	$\angle_{H-P-S-H}$ °	\angle_{H-S-P} °	E E_h	zpe kJ mol ⁻¹	D_e kJ mol ⁻¹	D_0 kJ mol ⁻¹	ADE eV	ADE_{shift} eV
5e: C ₁ (² A)	def2QZVP	1.416	92.1	3.703	1.337	78.8	107.7	70.0	-741.3412040	80.0	5.2	9.6	2.047
	pVTZ	1.418	92.0	3.723	1.338	78.2	88.9	72.6	-741.3214706	79.9	0.6	5.0	2.164
	pVQZ	1.417	92.1	3.678	1.338	78.7	74.9	76.1	-741.3414545	79.6	5.5	9.5	2.140
	W1w								-741.0466947		3.8	7.9	2.192
	W2w								-741.0476229		3.9	7.9	2.178
5f: C ₁ (² A)	def2QZVP	1.418	92.6	3.857	1.337	76.0	123.2	59.4	-741.3413284	79.3	5.6	9.2	2.036
	pVTZ	1.419	92.5	3.846	1.338	75.7	123.2	59.4	-741.3235045	79.4	6.0	9.8	2.103
	pVQZ	1.418	92.6	3.848	1.338	75.7	123.2	59.4	-741.3415376	79.5	5.7	9.6	2.136
	W1w								-741.0469858		4.6	8.4	2.182
	W2w								-741.0479148		4.7	8.5	2.164
rg: C ₁ (² A)	def2QZVP	1.414	94.0	3.656	1.340	69.7	0.0	78.0	-741.3285714	83.0	6.6	13.9	2.421
	pVTZ	1.416	93.9	3.663	1.341	68.5	0.0	75.7	-741.3088681	83.0	2.4	9.9	2.539
	pVQZ	1.415	94.1	3.641	1.341	69.8	0.0	77.9	-741.3288062	83.2	7.2	14.7	2.521
	W1w								-741.0339440		5.4	12.9	2.575
	W2w								-741.0347538		5.5	13.0	2.565

Table E87: PH₂...H₂S and HS...PH₃ complex geometric parameters, D_0 s and VDEs from DSD-PBEP86-D3BJ optimisations. zpe values are drawn from relevant harmonic frequency calculations.

	R_{P-H} Å	\angle_{H-P-H} °	R_{P-HS} Å	R_{PH-S} Å	\angle_{P-H-S} °	$\angle_{P-H-S-H}$ °	\angle_{H-S-H} °	E E_h	zpe kJ mol ⁻¹	D_e kJ mol ⁻¹	D_0 kJ mol ⁻¹	ADE eV	ADE_{shift} eV
5h: C ₁ (² A)	pVTZ	1.417	92.6	2.893	1.340	178.5	-179.0	92.5	-741.3217126	79.3	1.3	5.0	2.107
	pVQZ	1.416	92.7	2.901	1.339	179.0	-179.0	92.5	-741.3414963	79.4	5.6	9.4	2.096
	W1w								-741.0469868		4.6	8.4	2.141
	W2w								-741.0479099		4.7	8.5	2.130
5i: C ₁ (² A) 5j: C ₁ (² A)	R_{P-H}	\angle_{H-P-H}	R_{P-S}	R_{P-H}	\angle_{S-P-H}	$\angle_{H-P-S-H}$	\angle_{H-S-P}						
	pVTZ	1.417	92.5	3.664	1.338	82.8	141.8	66.3	-741.3215899	79.3	0.9	4.7	2.114
	pVQZ	1.416	92.5	3.608	1.337	83.3	144.9	70.1	-741.3415530	79.6	5.8	9.8	2.101
	W1w								-741.0469511		4.5	8.5	2.146
	W2w								-741.0478830		4.6	8.6	2.135
5k: C ₁ (² A) 5j: C ₁ (² A)	pVTZ	1.403	99.0	2.416	1.338	161.6	-58.1	91.6	-741.3176870	90.8	25.6	40.8	2.336
	pVQZ	1.402	99.2	2.405	1.338	161.3	-58.1	91.7	-741.3387307	91.0	33.2	48.6	2.291
	W1w								-741.0416316		25.5	40.9	2.407
	W2w								-741.0428243		26.7	42.0	2.388
5l: C ₁ (² A)	pVTZ	1.418	92.2	3.588	1.337	88.0	133.8	77.5	-741.3214629	79.0	0.6	4.1	2.155
	pVQZ	1.417	92.3	3.543	1.337	89.9	134.3	78.2	-741.3414947	78.7	5.6	8.7	2.130
	W1w								-741.0467996		4.1	7.2	2.179
	W2w								-741.0477223		4.2	7.3	2.166

Table E88: DSD-PBEP86-D3BJ and extrapolated single-point energies for HS⁻ ...PH₃ complexes. Geometries use for CC energies are from DSD-PBEP86-D3BJ/AVQZ optimisations. All energies are in E_h ..

	5a: HS ⁻ ...PH ₃ (¹ A')						
	E_{DH-DFT}	E_{SCF}	E_{CCSD}	E_{corr}	$E_{CCSD(T)}$	$E_{(T)}$	E_{Wnw}
def2QZVP	-741.4172135						
AVDZ		-740.6160983	-740.9730938	-0.3569955	-740.9852474	-0.0121536	
AVTZ	-741.4018413	-740.6393958	-741.0656447	-0.4262489	-741.0846771	-0.0190324	
AVQZ	-741.4210843	-740.6456481	-741.0917022	-0.4460541	-741.1124887	-0.0207865	
AV5Z		-740.6468078	-741.0992854	-0.4524776			
W1w		-740.6475934		-0.4590391		-0.0215897	-741.1282222
W2w		-740.6473730		-0.4592170		-0.0220665	-741.1286566
	5b: HS ⁻ ...PH ₃ (¹ A)						
def2QZVP	-741.4172421						
AVDZ		-740.6160864	-740.9731364	-0.3570500	-740.9852993	-0.0121629	
AVTZ	-741.4018921	-740.6393788	-741.0656779	-0.4262991	-741.0847218	-0.0190439	
AVQZ	-741.4211343	-740.6456305	-741.0917344	-0.4461039	-741.1125330	-0.0207986	
AV5Z		-740.6467903	-741.0993172	-0.4525269			
W1w		-740.6475757		-0.4590886		-0.0216020	-741.1282663
W2w		-740.6473556		-0.4592658		-0.0220791	-741.1287004
	5c: HS ⁻ ...PH ₃ (¹ A')						
def2QZVP	-741.4165067						
AVDZ		-740.6154401	-740.9715924	-0.3561523	-740.9835366	-0.0119442	
AVTZ	-741.4008582	-740.6390661	-741.0645973	-0.4255312	-741.0834454	-0.0188481	
AVQZ	-741.4202512	-740.6454143	-741.0909159	-0.4455016	-741.1115502	-0.0206343	
AV5Z		-740.6466061	-741.0985786	-0.4519725			
W1w		-740.6473895		-0.4585949		-0.0214147	-741.1273991
W2w		-740.6471870		-0.4587616		-0.0219377	-741.1278864
	5d: HS ⁻ ...PH ₃ (¹ A')						
def2QZVP	-741.4167390						
AVDZ		-740.6153965	-740.9717260	-0.3563295	-740.9837070	-0.0119810	
AVTZ	-741.4010655	-740.6390167	-741.0646935	-0.4256768	-741.0835813	-0.0188878	
AVQZ	-741.4204578	-740.6453587	-741.0910131	-0.4456544	-741.1116874	-0.0206743	
AV5Z		-740.6465516	-741.0986831	-0.4521315			
W1w		-740.6473319		-0.4587524		-0.0214555	-741.1275398
W2w		-740.6471330		-0.4589271		-0.0219780	-741.1280381

Table E89: DSD-PBEP86-D3BJ and extrapolated single-point energies for HS⁻ ...PH₃ complexes. Geometries use for CC energies are from DSD-PBEP86-D3BJ/AVQZ optimisations. All energies are in E_h ..

	5a: HS ⁻ ...PH ₃ (² A')						
	E_{DH-DFT}	E_{SCF}	E_{CCSD}	E_{corr}	$E_{CCSD(T)}$	$E_{(T)}$	E_{Wnw}
def2QZVP	-741.3266070						
AVDZ		-740.5672312	-740.8893676	-0.3221364	-740.8985524	-0.0091848	
AVTZ	-741.3091042	-740.5925045	-740.9779859	-0.3854814	-740.9927705	-0.0147846	
AVQZ	-741.3269358	-740.5989159	-741.0017476	-0.4028317	-741.0180304	-0.0162828	
AV5Z		-740.6001416	-741.0087484	-0.4086068			
W1w		-740.6009107		-0.4142072		-0.0168664	-741.0319843
W2w		-740.6007390		-0.4146659		-0.0173761	-741.0327810
	5b: HS ⁻ ...PH ₃ (² A)						
def2QZVP	-741.3267399						
AVDZ		-740.5672493	-740.8894955	-0.3222462	-740.8986974	-0.0092019	
AVTZ	-741.3002829	-740.5925267	-740.9781026	-0.3855759	-740.9929083	-0.0148057	
AVQZ	-741.3270689	-740.5989375	-741.0018579	-0.4029204	-741.0181631	-0.0163052	
AV5Z		-740.6001640	-741.0088574	-0.4086934			
W1w		-740.6009322		-0.4142920		-0.0168890	-741.0321132
W2w		-740.6007618		-0.4147503		-0.0173994	-741.0329115
	5c: HS ⁻ ...PH ₃ (² A')						
def2QZVP	-741.3268151						
AVDZ		-740.5667259	-740.8885043	-0.3217784	-740.8976459	-0.0091416	
AVTZ	-741.2967501	-740.5922272	-740.9778865	-0.3856593	-740.9926864	-0.0147999	
AVQZ	-741.3271357	-740.5986534	-741.0018372	-0.4031838	-741.0181696	-0.0163324	
AV5Z		-740.599884	-741.0089027	-0.4090187			
W1w		-740.6006528		-0.4146735		-0.0169034	-741.0322297
W2w		-740.6004838		-0.4151406		-0.0174507	-741.0330751
	5d: HS ⁻ ...PH ₃ (² A')						
def2QZVP	-741.3277082						
AVDZ		-740.5673326	-740.8892194	-0.3218868	-740.8983978	-0.0091784	
AVTZ	-741.3099052	-740.5927926	-740.978581	-0.3857884	-740.993424	-0.0148430	
AVQZ	-741.3279797	-740.5992111	-741.0025533	-0.4033422	-741.018932	-0.0163787	
AV5Z		-740.6004409	-741.0096286	-0.4091877			
W1w		-740.6012081		-0.4148511		-0.0169489	-741.0330081
W2w		-740.6010403		-0.4153207		-0.0174993	-741.0338603

Table E90: DSD-PBEP86-D3BJ and extrapolated single-point energies for $\text{PH}_2 \cdots \text{H}_2\text{S}$ and $\text{HS} \cdots \text{PH}_3$ complexes. Geometries use for CC energies are from DSD-PBEP86-D3BJ/AVQZ optimisations. All energies are in E_h .

	5e: $\text{PH}_2 \cdots \text{H}_2\text{S}$ (2A)						
	E_{DH-DFT}	E_{SCF}	E_{CCSD}	E_{corr}	$E_{CCSD(T)}$	$E_{(T)}$	E_{Wnw}
def2QZVP	-741.3412040						
AVDZ		-740.5783337	-740.9026939	-0.3243602	-740.9121363	-0.0094424	
AVTZ	-741.3214706	-740.6031701	-740.9918377	-0.3886676	-741.0070480	-0.0152103	
AVQZ	-741.3414545	-740.6095380	-741.0158141	-0.4062761	-741.0325530	-0.0167389	
AV5Z		-740.6107747	-741.0229629	-0.4121882			
W1w		-740.6115193		-0.4178208		-0.0173546	-741.0466947
W2w		-740.6113775		-0.4183911		-0.0178544	-741.0476229
	5f: $\text{PH}_2 \cdots \text{H}_2\text{S}$ (2A)						
def2QZVP	-741.3413284						
AVDZ		-740.5795989	-740.9032469	-0.3236480	-740.912582	-0.0093351	
AVTZ	-741.3235045	-740.6044997	-740.9923915	-0.3878918	-741.0074599	-0.0150684	
AVQZ	-741.3415376	-740.610883	-741.0163059	-0.4054229	-741.0328892	-0.0165833	
AV5Z		-740.6121249	-741.0234394	-0.4113145			
W1w		-740.6128691		-0.4169169		-0.0171998	-741.0469858
W2w		-740.6127302		-0.4174959		-0.0176888	-741.0479148
	5g: $\text{HS} \cdots \text{PH}_3$ (2A)						
def2QZVP	-741.3285714						
AVDZ		-740.5689416	-740.8905001	-0.3215585	-740.8996462	-0.0091461	
AVTZ	-741.3088681	-740.5943267	-740.9796341	-0.3853074	-740.9944084	-0.0147743	
AVQZ	-741.3288062	-740.6007646	-741.0035893	-0.4028247	-741.0198864	-0.0162971	
AV5Z		-740.6019931	-741.0106391	-0.4086460			
W1w		-740.6027677		-0.4143096		-0.0168667	-741.0339440
W2w		-740.6025919		-0.4147536		-0.0174083	-741.0347538

Table E91: DSD-PBEP86-D3BJ and extrapolated single-point energies for $\text{PH}_2 \cdots \text{H}_2\text{S}$ and $\text{HS} \cdots \text{PH}_3$ complexes. Geometries use for CC energies are from DSD-PBEP86-D3BJ/AVQZ optimisations. All energies are in E_h .

	5h: $\text{PH}_2 \cdots \text{H}_2\text{S}$ (2A)						
	E_{DH-DFT}	E_{SCF}	E_{CCSD}	E_{corr}	$E_{CCSD(T)}$	$E_{(T)}$	E_{Wnw}
AVDZ		-740.5800040	-740.9035134	-0.3235094	-740.9128363	-0.0093229	
AVTZ	-741.3217126	-740.6049689	-740.9924472	-0.3874783	-741.0074701	-0.0150229	
AVQZ	-741.3414963	-740.6113660	-741.0163664	-0.4050004	-741.0328892	-0.0165228	
AV5Z		-740.6126099	-741.0235034	-0.4108935			
W1w		-740.6133564		-0.4164885		-0.0171419	-741.0469868
W2w		-740.6132162		-0.4170764		-0.0176173	-741.0479099
	5i: $\text{PH}_2 \cdots \text{H}_2\text{S}$ (2A)						
AVDZ		-740.5793969	-740.9031358	-0.3237389	-740.9124742	-0.0093384	
AVTZ	-741.3215899	-740.6042722	-740.9922795	-0.3880073	-741.0073709	-0.0150914	
AVQZ	-741.3415530	-740.6106768	-741.0162267	-0.4055499	-741.0328345	-0.0166078	
AV5Z		-740.6119237	-741.0233722	-0.4114485			
W1w		-740.6126695		-0.4170514		-0.0172301	-741.0469511
W2w		-740.6125314		-0.4176372		-0.0177144	-741.0478830
	5j: $\text{PH}_2 \cdots \text{H}_2\text{S}$ (2A)						
AVDZ		-740.5557612	-740.8878303	-0.3320691	-740.8993518	-0.0115215	
AVTZ	-741.3176870	-740.5826220	-740.9813783	-0.3987563	-740.9992183	-0.0178400	
AVQZ	-741.3387307	-740.5891179	-741.0069287	-0.4178108	-741.0265165	-0.0195878	
AV5Z		-740.5904375	-741.0146263	-0.4241888			
W1w		-740.5911390		-0.4303036		-0.0201890	-741.0416316
W2w		-740.5910807		-0.4308805		-0.0208632	-741.0428243
	5k: $\text{PH}_2 \cdots \text{H}_2\text{S}$ (2A)						
AVDZ		-740.5787442	-740.9028769	-0.3241327	-740.9122579	-0.0093810	
AVTZ	-741.3214629	-740.6036309	-740.9919883	-0.3883574	-741.0071308	-0.0151425	
AVQZ	-741.3414947	-740.6100322	-741.0159864	-0.4059542	-741.0326516	-0.0166652	
AV5Z		-740.6112747	-741.0231393	-0.4118646			
W1w		-740.6120239		-0.4174913		-0.0172844	-741.0467996
W2w		-740.6118803		-0.4180657		-0.0177764	-741.0477223

Table E92: Cartesian coordinates of the HS⁻ ...PH₃ conformers optimised at DSD-PBEP86-D3BJ/def-2QZVP,AVnZ ($n = T, Q$) in Å.

		5a: HS ⁻ ...PH ₃ (¹ A')			5b: HS ⁻ ...PH ₃ (¹ A)		
		x	y	z	x	y	z
def2QZVP	S	-0.018681	1.948205	0.000000	0.093402	1.943922	0.000000
	P	-0.018681	-1.890435	0.000000	0.093402	-1.896300	0.000000
	H	0.934480	-2.082045	1.030961	-0.868847	-2.034420	1.030940
	H	0.934480	-2.082045	-1.030961	-0.868847	-2.034420	-1.030940
	H	-1.353049	1.797706	0.000000	0.088974	-0.451353	0.000000
	H	0.063202	-0.448368	0.000000	-1.246755	1.861934	0.000000
		x	y	z	x	y	z
AVTZ	S	0.018146	-1.958378	0.000000	0.093738	1.955178	0.000000
	P	0.018146	1.904505	0.000000	0.093738	-1.907297	0.000000
	H	-0.939411	2.077167	1.031688	-0.868759	-2.049249	1.031701
	H	-0.939411	2.077167	-1.031688	-0.868759	-2.049249	-1.031701
	H	1.357824	-1.851494	0.000000	0.080191	-0.464976	0.000000
	H	-0.041524	0.463628	0.000000	-1.248468	1.890071	0.000000
		x	y	z	x	y	z
AVQZ	S	-0.018052	1.959861	0.000000	0.093572	1.956539	0.000000
	P	-0.018052	-1.905983	0.000000	0.093572	-1.908708	0.000000
	H	0.937866	-2.080219	1.031439	-0.867642	-2.050311	1.031423
	H	0.937866	-2.080219	-1.031439	-0.867642	-2.050311	-1.031423
	H	-1.357467	1.858642	0.000000	0.082603	-0.467487	0.000000
	H	0.041353	-0.466247	0.000000	-1.248065	1.894100	0.000000

Table E93: Cartesian coordinates of the HS⁻ ...PH₃ conformers optimised at DSD-PBEP86-D3BJ/def-2QZVP,AVnZ ($n = T, Q$) in Å.

		5c: HS ⁻ ...PH ₃ (¹ A')			5d: HS ⁻ ...PH ₃ (¹ A')		
		x	y	z	x	y	z
def2QZVP	S	0.101909	-1.686234	0.000000	-0.024983	-1.674340	0.000000
	P	0.101909	1.568643	0.000000	-0.024983	1.551547	0.000000
	H	-0.736612	1.141039	-1.044817	0.494300	2.901018	0.000000
	H	-0.736612	1.141039	1.044817	0.823516	1.145349	1.045151
	H	-1.240462	-1.737149	0.000000	-1.366850	-1.675487	0.000000
	H	-0.445503	2.905174	0.000000	0.823516	1.145349	-1.045151
		x	y	z	x	y	z
AVTZ	S	-0.101707	-1.701901	0.000000	-0.025208	-1.694518	0.000000
	P	-0.101707	1.587888	0.000000	-0.025208	1.574017	0.000000
	H	0.741843	1.164292	1.044454	0.510095	2.915670	0.000000
	H	0.741843	1.164292	-1.044454	0.819694	1.153749	1.044632
	H	1.235155	-1.844502	0.000000	-1.368023	-1.721138	0.000000
	H	0.434056	2.928021	0.000000	0.819694	1.153749	-1.044632
		x	y	z	x	y	z
AVQZ	S	0.101553	-1.698055	0.000000	-0.025116	-1.690716	0.000000
	P	0.101553	1.584514	0.000000	-0.025116	1.570873	0.000000
	H	-0.740166	1.160566	-1.044484	0.510333	2.911213	0.000000
	H	-0.740166	1.160566	1.044484	0.817692	1.149808	1.044700
	H	-1.234275	-1.843618	0.000000	-1.367107	-1.722473	0.000000
	H	-0.433542	2.923649	0.000000	0.817692	1.149808	-1.044700

Table E94: Cartesian coordinates of the PH₂⋯H₂S and HS⋯PH₃ conformers optimised at DSD-PBEP86-D3BJ/def-2QZVP,AVnZ ($n = T, Q$) in Å.

	5e: PH ₂ ⋯H ₂ S (² A)			5f: PH ₂ ⋯H ₂ S (² A)			5g: HS⋯PH ₃ (² A)			
	x	y	z	x	y	z	x	y	z	
def2QZVP	S	1.802973	0.025363	-0.079156	1.941545	0.058873	-0.000005	0.051224	1.824858	0.000000
	P	-1.895941	0.017927	0.096449	-1.913297	-0.080530	0.000003	0.051224	-1.831548	0.000000
	H	-1.670601	-1.150459	-0.672616	-3.312023	0.151319	-0.000007	0.473798	-0.964838	-1.034795
	H	-1.675467	0.859040	-1.021434	-1.619527	1.304312	-0.000041	-1.275502	-1.341480	0.000000
	H	1.544262	-1.129441	0.543676	1.283132	-0.594882	-0.963239	-1.260037	1.546654	0.000000
	H	1.393352	0.746150	0.970144	1.283155	-0.594764	0.963325	0.473798	-0.964838	1.034795
	x	y	z	x	y	z	x	y	z	
AVTZ	S	1.811944	0.005676	-0.081539	1.935802	0.058980	0.000024	0.052843	1.829196	0.000000
	P	-1.906975	0.003527	0.097249	-1.907507	-0.080808	-0.000003	0.052843	-1.833801	0.000000
	H	-1.664225	-1.048761	-0.821408	-3.306541	0.156597	-0.000112	-1.287215	-1.377853	0.000000
	H	-1.665696	0.990030	-0.891911	-1.608655	1.304170	0.000263	0.451288	-0.953674	1.034697
	H	1.489810	-1.006023	0.732860	1.277545	-0.595822	-0.963873	-1.253462	1.525076	0.000000
	H	1.453619	0.921034	0.826346	1.277412	-0.596497	0.963371	0.451288	-0.953674	-1.034697
	x	y	z	x	y	z	x	y	z	
AVQZ	S	-1.789024	-0.010452	-0.082920	-1.936727	0.058920	-0.000003	-1.816193	0.069430	0.000001
	P	1.884883	-0.007018	0.097868	1.908618	-0.080724	-0.000007	1.824182	0.033072	-0.000010
	H	1.650345	1.075118	-0.786000	3.306667	0.156015	0.000083	0.961302	0.462985	-1.035315
	H	1.654696	-0.959739	-0.924844	1.609694	1.303143	-0.000006	1.322361	-1.289452	0.000486
	H	-1.505557	1.038918	0.696553	-1.279035	-0.595498	0.963642	-1.548609	-1.244254	0.000006
	H	-1.448333	-0.881795	0.872984	-1.278961	-0.595526	-0.963578	0.961300	0.463757	1.034971

Table E95: Cartesian coordinates of the PH₂...H₂S and HS...PH₃ conformers optimised at DSD-PBEP86-D3BJ/def-2QZVP,AVnZ ($n = T, Q$) in Å.

	5h: PH ₂ ...H ₂ S (² A)			5i: PH ₂ ...H ₂ S (² A)			5j: PH ₂ ...H ₂ S (² A)			5k: PH ₂ ...H ₂ S (² A)			
	x	y	z	x	y	z	x	y	z	x	y	z	
AVTZ	S	2.146393	-0.000002	-0.080338	1.792048	0.070420	-0.072365	-1.286306	0.072857	-0.004416	1.708790	-0.079339	-0.000003
	P	-2.085371	0.000043	0.009433	-1.867535	-0.084548	0.014153	1.126374	-0.045236	0.044325	-1.874441	0.112920	0.000240
	H	-3.063476	1.024369	-0.040490	-1.735627	1.250291	0.471277	1.370037	-0.306284	-1.312448	-1.875327	-0.872160	1.019995
	H	-3.062490	-1.025211	-0.040735	-3.209851	0.123102	-0.395040	1.231303	1.352505	0.022142	-1.877613	-0.868209	-1.023314
	H	0.807562	0.000441	-0.027970	1.314117	-1.109090	0.339015	-1.391325	-1.244921	0.204820	1.489898	1.240029	0.000649
	H	2.256687	-0.000225	1.253100	2.971618	-0.122804	0.530286	2.475270	-0.288480	0.491267	3.039020	0.075960	-0.000885
	x	y	z	x	y	z	x	y	z	x	y	z	
AVQZ	S	2.150200	0.000194	-0.080134	-1.761079	0.071341	-0.066062	1.280384	0.072814	0.004507	1.689066	-0.079759	-0.000073
	P	-2.089192	0.000000	0.010857	1.842695	-0.085133	0.019702	-1.120825	-0.044886	-0.043733	-1.848575	0.113972	-0.001114
	H	-3.064862	-1.024534	-0.051317	1.725841	1.261351	0.442240	-1.368304	-0.310009	1.310622	-1.899606	-0.876286	-1.013059
	H	-3.065389	1.024276	-0.047149	3.167905	0.110327	-0.444420	-1.226628	1.351810	-0.022414	-1.905306	-0.856151	1.029850
	H	2.253336	-0.003208	1.253332	-1.368334	-1.146383	0.321470	1.388582	-1.243837	-0.207373	1.487417	1.241740	-0.003607
	H	0.811589	0.000370	-0.035584	-2.988569	-0.089768	0.442182	-2.467423	-0.289704	-0.496959	3.021060	0.057251	0.004702

Table E96: Calculated harmonic frequencies and mode assignments for the 5a HS⁻ ...PH₃ complex. All frequencies and intensities are in cm⁻¹ and km mol⁻¹.

5a: HS ⁻ ...PH ₃ (¹ A')					
	Mode	Symmetry	Frequency (cm ⁻¹)	Intensity (km mol ⁻¹)	Description
def2QZVP	ω_1	a''	101	6.3395	PH ₂ rock
	ω_2	a'	110	49.5953	Intermolecular stretch
	ω_3	a'	167	24.4223	PH ₂ wag
	ω_4	a''	201	5.0865	PH ₂ twist
	ω_5	a'	311	1.3123	PH ₃ rotation
	ω_6	a'	1036	36.1399	PH ₃ symm. scissor
	ω_7	a''	1141	15.7099	PH ₃ twist
	ω_8	a'	1149	31.3244	PH ₃ asymm. scissor
	ω_9	a'	2048	1405.8565	H-transfer stretch
	ω_{10}	a'	2398	68.1505	PH ₂ symm. stretch
	ω_{11}	a''	2400	92.2241	PH ₂ asymm. stretch
	ω_{12}	a'	2665	61.5653	SH stretch
	zpe		82.1		
AVTZ	ω_1	a'	106	49.7468	Intermolecular stretch
	ω_2	a''	108	4.8953	PH ₂ rock
	ω_3	a'	161	19.972	PH ₂ wag
	ω_4	a''	206	5.0057	PH ₂ twist
	ω_5	a'	301	1.0876	PH ₃ rotation
	ω_6	a'	1031	43.5992	PH ₃ symm. scissor
	ω_7	a''	1142	22.1657	PH ₃ twist
	ω_8	a'	1148	26.607	PH ₃ asymm. scissor
	ω_9	a'	2079	1357.7105	H-transfer stretch
	ω_{10}	a'	2393	65.0988	PH ₂ symm. stretch
	ω_{11}	a''	2395	78.6423	PH ₂ asymm. stretch
	ω_{12}	a'	2662	50.2719	SH stretch
	zpe		82.1		
AVQZ	ω_1	a'	105	48.9479	Intermolecular stretch
	ω_2	a''	111	4.8055	PH ₂ rock
	ω_3	a'	160	19.9333	PH ₂ wag
	ω_4	a''	205	5.1397	PH ₂ twist
	ω_5	a'	299	1.1462	PH ₃ rotation
	ω_6	a'	1031	44.2145	PH ₃ symm. scissor
	ω_7	a''	1141	21.8485	PH ₃ twist
	ω_8	a'	1148	27.2077	PH ₃ asymm. scissor
	ω_9	a'	2085	1337.6901	H-transfer stretch
	ω_{10}	a'	2398	64.4786	PH ₂ symm. stretch
	ω_{11}	a''	2399	77.285	PH ₂ asymm. stretch
	ω_{12}	a'	2664	48.505	SH stretch
	zpe		82.2		

Table E97: Calculated harmonic frequencies and mode assignments for the 5b HS⁻ ...PH₃ complex. All frequencies and intensities are in cm⁻¹ and km mol⁻¹.

5b: HS ⁻ ...PH ₃ (¹ A)					
	Mode	Symmetry	Frequency (cm ⁻¹)	Intensity (km mol ⁻¹)	Description
def2QZVP	ω_1	a''	99	0.1863	PH ₂ rock
	ω_2	a'	110	54.2765	Intermolecular stretch
	ω_3	a'	170	12.005	PH ₂ wag
	ω_4	a''	203	5.915	PH ₂ twist
	ω_5	a'	313	6.0496	PH ₃ rotation
	ω_6	a'	1035	29.4911	PH ₃ symm. scissor
	ω_7	a''	1142	15.9354	PH ₃ twist
	ω_8	a'	1149	19.0293	PH ₃ asymm. scissor
	ω_9	a'	2043	1439.5407	H-transfer stretch
	ω_{10}	a'	2399	65.3293	PH ₂ symm. stretch
	ω_{11}	a''	2401	91.0515	PH ₂ asymm. stretch
	ω_{12}	a'	2666	60.9368	SH stretch
	zpe		82.1		
AVTZ	ω_1	a'	107	53.4377	Intermolecular stretch
	ω_2	a''	107	0.0323	PH ₂ rock
	ω_3	a'	166	10.3198	PH ₂ wag
	ω_4	a''	207	5.3125	PH ₂ twist
	ω_5	a'	304	6.7526	PH ₃ rotation
	ω_6	a'	1031	41.4567	PH ₃ symm. scissor
	ω_7	a''	1142	22.2253	PH ₃ twist
	ω_8	a'	1148	20.6478	PH ₃ asymm. scissor
	ω_9	a'	2076	1372.2545	H-transfer stretch
	ω_{10}	a'	2393	62.8812	PH ₂ symm. stretch
	ω_{11}	a''	2395	77.7641	PH ₂ asymm. stretch
	ω_{12}	a'	2663	49.4888	SH stretch
	zpe		82.2		
AVQZ	ω_1	a'	106	52.7459	Intermolecular stretch
	ω_2	a''	109	0.0229	PH ₂ rock
	ω_3	a'	164	10.3776	PH ₂ wag
	ω_4	a''	206	5.4397	PH ₂ twist
	ω_5	a'	302	6.3914	PH ₃ rotation
	ω_6	a'	1030	41.2577	PH ₃ symm. scissor
	ω_7	a''	1142	21.9646	PH ₃ twist
	ω_8	a'	1148	20.4574	PH ₃ asymm. scissor
	ω_9	a'	2082	1353.506	H-transfer stretch
	ω_{10}	a'	2399	61.5569	PH ₂ symm. stretch
	ω_{11}	a''	2400	76.2166	PH ₂ asymm. stretch
	ω_{12}	a'	2665	47.8762	SH stretch
	zpe		82.3		

Table E98: Calculated harmonic frequencies and mode assignments for the 5c HS⁻ ...PH₃ complex. All frequencies and intensities are in cm⁻¹ and km mol⁻¹.

5c: HS ⁻ ...PH ₃ (¹ A')					
	Mode	Symmetry	Frequency (cm ⁻¹)	Intensity (km mol ⁻¹)	Description
def2QZVP	ω_1	a'	93	44.0542	Intermolecular stretch
	ω_2	a''	115	0.7272	PH ₂ rock
	ω_3	a'	174	1.1347	PH ₂ wag
	ω_4	a''	279	0.0577	PH ₂ twist
	ω_5	a'	323	1.4007	PH ₃ rotation
	ω_6	a'	1022	24.0391	PH ₃ symm. scissor
	ω_7	a'	1104	34.804	PH ₃ asymm. scissor
	ω_8	a''	1139	12.8811	PH ₃ wag
	ω_9	a'	2207	749.5134	PH stretch
	ω_{10}	a'	2463	37.8891	PH ₂ symm. stretch
	ω_{11}	a''	2476	43.9198	PH ₂ asymm. stretch
	ω_{12}	a'	2659	63.6137	SH stretch
	zpe		84.1		
AVTZ	ω_1	a'	89	42.3004	Intermolecular stretch
	ω_2	a''	119	0.734	PH ₂ rock
	ω_3	a'	158	1.8805	PH ₂ wag
	ω_4	a''	269	0.0818	PH ₂ twist
	ω_5	a'	311	2.45	PH ₃ rotation
	ω_6	a'	1020	20.5543	PH ₃ symm. scissor
	ω_7	a'	1107	36.6241	PH ₃ asymm. scissor
	ω_8	a''	1139	9.2564	PH ₃ wag
	ω_9	a'	2217	751.5673	PH stretch
	ω_{10}	a'	2454	37.3323	PH ₂ symm. stretch
	ω_{11}	a''	2467	35.2113	PH ₂ asymm. stretch
	ω_{12}	a'	2657	53.8806	SH stretch
	zpe		83.8		
AVQZ	ω_1	a'	89	42.708	Intermolecular stretch
	ω_2	a''	120	0.6211	PH ₂ rock
	ω_3	a'	159	1.8548	PH ₂ wag
	ω_4	a''	271	0.0779	PH ₂ twist
	ω_5	a'	313	2.4893	PH ₃ rotation
	ω_6	a'	1020	20.6293	PH ₃ symm. scissor
	ω_7	a'	1107	37.3923	PH ₃ asymm. scissor
	ω_8	a''	1139	9.0067	PH ₃ wag
	ω_9	a'	2221	748.697	PH stretch
	ω_{10}	a'	2459	36.6313	PH ₂ symm. stretch
	ω_{11}	a''	2471	34.8685	PH ₂ asymm. stretch
	ω_{12}	a'	2659	51.7621	SH stretch
	zpe		83.9		

Table E99: Calculated harmonic frequencies and mode assignments for the 5d HS⁻ ...PH₃ complex. All frequencies and intensities are in cm⁻¹ and km mol⁻¹.

5d: HS ⁻ ...PH ₃ (¹ A')					
	Mode	Symmetry	Frequency (cm ⁻¹)	Intensity (km mol ⁻¹)	Description
def2QZVP	ω_1	a'	96	42.9977	Intermolecular stretch
	ω_2	a''	107	6.1764	PH ₂ rock
	ω_3	a'	178	12.0447	PH ₂ wag
	ω_4	a''	293	0.0216	PH ₂ rotation
	ω_5	a'	337	2.2874	PH ₃ rotation
	ω_6	a'	1022	24.7156	PH ₃ symm. scissor
	ω_7	a'	1105	42.6211	PH ₃ asymm. scissor
	ω_8	a''	1141	13.4942	PH ₂ twist
	ω_9	a'	2196	816.5295	PH stretch
	ω_{10}	a'	2463	34.1756	PH ₂ symm. stretch
	ω_{11}	a''	2476	44.5712	PH ₂ asymm. stretch
	ω_{12}	a'	2672	56.2692	SH stretch
	zpe		84.3		
AVTZ	ω_1	a'	90	40.1291	Intermolecular stretch
	ω_2	a''	116	4.348	PH ₂ rock
	ω_3	a'	162	11.6993	PH ₂ wag
	ω_4	a''	280	0.0427	PH ₂ rotation
	ω_5	a'	324	3.1811	PH ₃ rotation
	ω_6	a'	1020	20.6383	PH ₃ symm. scissor
	ω_7	a'	1108	42.5328	PH ₃ asymm. scissor
	ω_8	a''	1141	9.4824	PH ₂ twist
	ω_9	a'	2208	814.6315	PH stretch
	ω_{10}	a'	2454	34.0205	PH ₂ symm. stretch
	ω_{11}	a''	2467	35.7282	PH ₂ asymm. stretch
	ω_{12}	a'	2669	47.2566	SH stretch
	zpe		84.0		
AVQZ	ω_1	a'	90	40.4033	Intermolecular stretch
	ω_2	a''	119	4.3803	PH ₂ rock
	ω_3	a'	163	11.7167	PH ₂ wag
	ω_4	a''	283	0.038	PH ₂ rotation
	ω_5	a'	327	3.2068	PH ₃ rotation
	ω_6	a'	1020	20.7759	PH ₃ symm. scissor
	ω_7	a'	1108	43.4813	PH ₃ asymm. scissor
	ω_8	a''	1141	9.2116	PH ₂ twist
	ω_9	a'	2212	811.5028	PH stretch
	ω_{10}	a'	2459	33.4057	PH ₂ symm. stretch
	ω_{11}	a''	2471	35.4546	PH ₂ asymm. stretch
	ω_{12}	a'	2671	45.4751	SH stretch
	zpe		84.1		

Table E100: Calculated harmonic frequencies and mode assignments for the 5e PH₂ ··· H₂S complex. All frequencies and intensities are in cm⁻¹ and km mol⁻¹.

5e: PH ₂ ··· H ₂ S (² A)					
	Mode	Symmetry	Frequency (cm ⁻¹)	Intensity (km mol ⁻¹)	Description
def2QZVP	ω_1	<i>a</i>	50	4.1594	Intermolecular stretch
	ω_2	<i>a</i>	74	12.3268	Intermolecular rock
	ω_3	<i>a</i>	118	14.7527	H ₂ S twist
	ω_4	<i>a</i>	128	34.2865	H ₂ S twist
	ω_5	<i>a</i>	159	0.1494	PH ₂ twist
	ω_6	<i>a</i>	196	0.3994	PH ₂ wag
	ω_7	<i>a</i>	1135	18.7083	PH ₂ scissor
	ω_8	<i>a</i>	1219	0.8893	H ₂ S scissor
	ω_9	<i>a</i>	2410	45.135	PH ₂ symm. stretch
	ω_{10}	<i>a</i>	2419	53.748	PH ₂ asymm. stretch
	ω_{11}	<i>a</i>	2727	0.8428	H ₂ S symm. stretch
	ω_{12}	<i>a</i>	2741	0.3482	H ₂ S asymm. stretch
	zpe		80.0		
AVTZ	ω_1	<i>a</i>	50	3.061	Intermolecular stretch
	ω_2	<i>a</i>	73	12.0106	Intermolecular rock
	ω_3	<i>a</i>	116	2.2319	H ₂ S twist
	ω_4	<i>a</i>	130	45.0636	H ₂ S twist
	ω_5	<i>a</i>	163	0.0975	PH ₂ twist
	ω_6	<i>a</i>	196	0.2612	PH ₂ wag
	ω_7	<i>a</i>	1135	19.7862	PH ₂ scissor
	ω_8	<i>a</i>	1219	0.925	H ₂ S scissor
	ω_9	<i>a</i>	2404	44.7704	PH ₂ symm. stretch
	ω_{10}	<i>a</i>	2412	54.6675	PH ₂ asymm. stretch
	ω_{11}	<i>a</i>	2724	0.7448	H ₂ S symm. stretch
	ω_{12}	<i>a</i>	2737	0.3409	H ₂ S asymm. stretch
	zpe		79.9		
AVQZ	ω_1	<i>a</i>	14	12.5289	Intermolecular stretch
	ω_2	<i>a</i>	53	4.4573	Intermolecular rock
	ω_3	<i>a</i>	101	9.6816	H ₂ S twist
	ω_4	<i>a</i>	106	38.9463	H ₂ S twist
	ω_5	<i>a</i>	142	0.0834	PH ₂ twist
	ω_6	<i>a</i>	182	0.2374	PH ₂ wag
	ω_7	<i>a</i>	1133	19.3638	PH ₂ scissor
	ω_8	<i>a</i>	1216	0.7318	H ₂ S scissor
	ω_9	<i>a</i>	2428	41.5577	PH ₂ symm. stretch
	ω_{10}	<i>a</i>	2436	50.9223	PH ₂ asymm. stretch
	ω_{11}	<i>a</i>	2743	0.8108	H ₂ S symm. stretch
	ω_{12}	<i>a</i>	2759	0.6679	H ₂ S asymm. stretch
	zpe		79.6		

Table E101: Calculated harmonic frequencies and mode assignments for the 5f PH₂ ··· H₂S complex. All frequencies and intensities are in cm⁻¹ and km mol⁻¹.

5f: PH ₂ ··· H ₂ S (² A)					
	Mode	Symmetry	Frequency (cm ⁻¹)	Intensity (km mol ⁻¹)	Description
def2QZVP	ω_1	<i>a</i>	60	0.9571	Intermolecular stretch
	ω_2	<i>a</i>	76	14.6231	Intermolecular rock
	ω_3	<i>a</i>	86	4.8566	H ₂ S twist
	ω_4	<i>a</i>	115	24.0563	PH ₂ rock
	ω_5	<i>a</i>	123	0.2733	H ₂ S twist
	ω_6	<i>a</i>	154	20.7619	H ₂ S rock
	ω_7	<i>a</i>	1137	18.6528	PH ₂ scissor
	ω_8	<i>a</i>	1218	0.7497	H ₂ S scissor
	ω_9	<i>a</i>	2405	73.5169	P–H stretch
	ω_{10}	<i>a</i>	2423	51.0112	P–H stretch
	ω_{11}	<i>a</i>	2727	0.0818	H ₂ S symm. stretch
	ω_{12}	<i>a</i>	2740	0.0972	H ₂ S asymm. stretch
	zpe		79.3		
AVTZ	ω_1	<i>a</i>	62	0.9046	Intermolecular stretch
	ω_2	<i>a</i>	80	15.4168	Intermolecular rock
	ω_3	<i>a</i>	96	2.499	H ₂ S twist
	ω_4	<i>a</i>	121	25.9222	PH ₂ rock
	ω_5	<i>a</i>	124	0.1687	H ₂ S twist
	ω_6	<i>a</i>	156	16.3265	H ₂ S rock
	ω_7	<i>a</i>	1137	18.4937	PH ₂ scissor
	ω_8	<i>a</i>	1217	0.7575	H ₂ S scissor
	ω_9	<i>a</i>	2399	75.0088	P–H stretch
	ω_{10}	<i>a</i>	2416	50.5665	P–H stretch
	ω_{11}	<i>a</i>	2723	0.0624	H ₂ S symm. stretch
	ω_{12}	<i>a</i>	2736	0.143	H ₂ S asymm. stretch
	zpe		79.4		
AVQZ	ω_1	<i>a</i>	61	0.8069	Intermolecular stretch
	ω_2	<i>a</i>	82	14.8771	Intermolecular rock
	ω_3	<i>a</i>	95	2.8224	H ₂ S twist
	ω_4	<i>a</i>	121	26.3932	PH ₂ rock
	ω_5	<i>a</i>	128	0.333	H ₂ S twist
	ω_6	<i>a</i>	157	15.858	H ₂ S rock
	ω_7	<i>a</i>	1138	18.5855	PH ₂ scissor
	ω_8	<i>a</i>	1218	0.7674	H ₂ S scissor
	ω_9	<i>a</i>	2404	74.2325	P–H stretch
	ω_{10}	<i>a</i>	2421	49.5052	P–H stretch
	ω_{11}	<i>a</i>	2724	0.0521	H ₂ S symm. stretch
	ω_{12}	<i>a</i>	2737	0.1985	H ₂ S asymm. stretch
	zpe		79.5		

Table E102: Calculated harmonic frequencies and mode assignments for the 5g PH₂ ··· H₂S complex. All frequencies and intensities are in cm⁻¹ and km mol⁻¹.

5g: HS ··· PH ₃ (² A)					
	Mode	Symmetry	Frequency (cm ⁻¹)	Intensity (km mol ⁻¹)	Description
def2QZVP	ω_1	a'	63	1.13	Intermolecular stretch
	ω_2	a''	75	4.7493	Intermolecular rock
	ω_3	a''	104	8.2138	PH ₃ rotation
	ω_4	a'	126	5.1049	PH ₃ rotation
	ω_5	a'	199	11.8887	P–S–H bend
	ω_6	a'	1015	3.1226	PH ₃ symm. scissor
	ω_7	a'	1155	13.5149	PH ₃ asymm. scissor
	ω_8	a''	1155	14.3742	PH ₂ twist
	ω_9	a'	2420	40.0161	PH ₃ symm. stretch
	ω_{10}	a''	2424	43.3119	PH ₂ asymm. stretch
	ω_{11}	a'	2428	47.7917	PH ₂ symm. stretch
	ω_{12}	a'	2714	0.8549	SH stretch
	zpe		83.0		
AVTZ	ω_1	a'	63	1.0152	Intermolecular stretch
	ω_2	a''	90	3.7408	Intermolecular rock
	ω_3	a''	100	7.4515	PH ₃ rotation
	ω_4	a'	136	4.7965	PH ₃ rotation
	ω_5	a'	203	10.5001	P–S–H bend
	ω_6	a'	1015	3.7689	PH ₃ symm. scissor
	ω_7	a'	1154	13.9893	PH ₃ asymm. scissor
	ω_8	a''	1154	13.9586	PH ₂ twist
	ω_9	a'	2413	42.2052	PH ₃ symm. stretch
	ω_{10}	a''	2416	47.8122	PH ₂ asymm. stretch
	ω_{11}	a'	2422	47.7252	PH ₂ symm. stretch
	ω_{12}	a'	2711	0.8973	SH stretch
	zpe		83.0		
AVQZ	ω_1	a	65	1.2388	Intermolecular stretch
	ω_2	a	90	4.8452	Intermolecular rock
	ω_3	a	109	7.1923	PH ₃ rotation
	ω_4	a	137	4.9102	PH ₃ rotation
	ω_5	a	207	10.7028	P–S–H bend
	ω_6	a	1014	3.0007	PH ₃ symm. scissor
	ω_7	a	1155	14.811	PH ₃ asymm. scissor
	ω_8	a	1155	14.0796	PH ₂ twist
	ω_9	a	2417	40.879	PH ₃ symm. stretch
	ω_{10}	a	2421	42.0499	PH ₂ asymm. stretch
	ω_{11}	a	2426	45.7031	PH ₂ symm. stretch
	ω_{12}	a	2712	0.7519	SH stretch
	zpe		83.2		

Table E103: Calculated harmonic frequencies and mode assignments for the 5h PH₂⋯H₂S complex. All frequencies and intensities are in cm⁻¹ and km mol⁻¹.

5h: PH ₂ ⋯H ₂ S (² A)					
	Mode	Symmetry	Frequency (cm ⁻¹)	Intensity (km mol ⁻¹)	Description
AVTZ	ω_1	<i>a</i>	61	0.3303	Intermolecular stretch
	ω_2	<i>a</i>	84	3.4591	PH ₂ rock
	ω_3	<i>a</i>	86	5.525	PH ₂ wag
	ω_4	<i>a</i>	86	3.7433	PH ₂ twist
	ω_5	<i>a</i>	108	11.0993	H ₂ S rock
	ω_6	<i>a</i>	212	6.8962	H–S wag
	ω_7	<i>a</i>	1136	40.0042	PH ₂ scissor
	ω_8	<i>a</i>	1223	3.4625	H ₂ S scissor
	ω_9	<i>a</i>	2407	65.0399	PH ₂ symm. stretch
	ω_{10}	<i>a</i>	2417	51.4918	PH ₂ asymm. stretch
	ω_{11}	<i>a</i>	2707	36.6035	S–H stretch
	ω_{12}	<i>a</i>	2733	3.7045	S–H stretch
	zpe		79.3		
AVQZ	ω_1	<i>a</i>	60	0.378	Intermolecular stretch
	ω_2	<i>a</i>	83	6.8663	PH ₂ twist
	ω_3	<i>a</i>	87	6.0081	PH ₂ wag
	ω_4	<i>a</i>	93	0.4437	PH ₂ rock
	ω_5	<i>a</i>	109	10.2227	H ₂ S rock
	ω_6	<i>a</i>	208	6.8461	H–S wag
	ω_7	<i>a</i>	1137	39.409	PH ₂ scissor
	ω_8	<i>a</i>	1223	3.1582	H ₂ S scissor
	ω_9	<i>a</i>	2412	63.5433	PH ₂ symm. stretch
	ω_{10}	<i>a</i>	2422	49.6324	PH ₂ asymm. stretch
	ω_{11}	<i>a</i>	2707	37.484	S–H stretch
	ω_{12}	<i>a</i>	2734	3.9236	S–H stretch
	zpe		79.4		

Table E104: Calculated harmonic frequencies and mode assignments for the 5i PH₂⋯H₂S complex. All frequencies and intensities are in cm⁻¹ and km mol⁻¹.

5i: PH ₂ ⋯H ₂ S (² A)					
	Mode	Symmetry	Frequency (cm ⁻¹)	Intensity (km mol ⁻¹)	Description
AVTZ	ω_1	<i>a</i>	52	2.0872	Intermolecular stretch
	ω_2	<i>a</i>	91	8.2002	PH ₂ twist
	ω_3	<i>a</i>	100	16.9674	PH ₂ rock
	ω_4	<i>a</i>	109	1.3691	PH ₂ wag
	ω_5	<i>a</i>	118	18.1194	H ₂ S rock
	ω_6	<i>a</i>	157	0.2414	H ₂ S twist
	ω_7	<i>a</i>	1137	20.2805	PH ₂ scissor
	ω_8	<i>a</i>	1218	0.1497	H ₂ S scissor
	ω_9	<i>a</i>	2401	67.5277	P–H stretch
	ω_{10}	<i>a</i>	2415	52.5189	P–H stretch
	ω_{11}	<i>a</i>	2722	0.4414	S–H stretch
	ω_{12}	<i>a</i>	2739	0.5507	S–H stretch
	zpe		79.3		
AVQZ	ω_1	<i>a</i>	58	1.3322	Intermolecular stretch
	ω_2	<i>a</i>	90	1.0188	PH ₂ twist
	ω_3	<i>a</i>	105	21.317	PH ₂ rock
	ω_4	<i>a</i>	119	9.5468	PH ₂ wag
	ω_5	<i>a</i>	129	14.1471	H ₂ S rock
	ω_6	<i>a</i>	170	0.8847	H ₂ S twist
	ω_7	<i>a</i>	1138	19.929	PH ₂ scissor
	ω_8	<i>a</i>	1218	0.0943	H ₂ S scissor
	ω_9	<i>a</i>	2405	67.7602	P–H stretch
	ω_{10}	<i>a</i>	2419	50.2307	P–H stretch
	ω_{11}	<i>a</i>	2721	0.5888	S–H stretch
	ω_{12}	<i>a</i>	2741	0.7564	S–H stretch
	zpe		79.6		

Table E105: Calculated harmonic frequencies and mode assignments for the 5j HS ... PH₃ complex. All frequencies and intensities are in cm⁻¹ and km mol⁻¹.

5j: HS ... PH ₃ (² A)					
	Mode	Symmetry	Frequency (cm ⁻¹)	Intensity (km mol ⁻¹)	Description
AVTZ	ω_1	<i>a</i>	198	9.8758	SH rock
	ω_2	<i>a</i>	219	16.0244	Intermolecular stretch
	ω_3	<i>a</i>	411	0.2488	PH ₃ twist
	ω_4	<i>a</i>	464	11.9691	PH ₃ rock
	ω_5	<i>a</i>	715	0.5116	P-S-H bend
	ω_6	<i>a</i>	1011	90.5815	PH ₃ symm. scissor
	ω_7	<i>a</i>	1125	72.8762	PH ₃ asymm. scissor
	ω_8	<i>a</i>	1148	8.8178	PH ₂ twist
	ω_9	<i>a</i>	2186	184.4707	P-H stretch
	ω_{10}	<i>a</i>	2484	14.0728	PH ₂ symm. stretch
	ω_{11}	<i>a</i>	2501	15.5179	PH ₂ asymm. stretch
	ω_{12}	<i>a</i>	2719	1.1869	S-H stretch
	zpe		90.8		
AVQZ	ω_1	<i>a</i>	202	9.5086	SH rock
	ω_2	<i>a</i>	224	18.1139	Intermolecular stretch
	ω_3	<i>a</i>	413	0.2273	PH ₃ twist
	ω_4	<i>a</i>	469	11.244	PH ₃ rock
	ω_5	<i>a</i>	722	0.4225	P-S-H bend
	ω_6	<i>a</i>	1011	87.7534	PH ₃ symm. scissor
	ω_7	<i>a</i>	1125	75.7902	PH ₃ asymm. scissor
	ω_8	<i>a</i>	1149	8.9191	PH ₂ twist
	ω_9	<i>a</i>	2180	189.434	P-H stretch
	ω_{10}	<i>a</i>	2489	13.4076	PH ₂ symm. stretch
	ω_{11}	<i>a</i>	2505	14.5698	PH ₂ asymm. stretch
	ω_{12}	<i>a</i>	2720	1.1805	S-H stretch
	zpe		91.0		

Table E106: Calculated harmonic frequencies and mode assignments for the 5k PH₂⋯H₂S complex. All frequencies and intensities are in cm⁻¹ and km mol⁻¹.

5k: PH ₂ ⋯H ₂ S (² A)					
	Mode	Symmetry	Frequency (cm ⁻¹)	Intensity (km mol ⁻¹)	Description
AVTZ	ω_1	<i>a</i>	53	0.7493	Intermolecular stretch
	ω_2	<i>a</i>	59	29.8152	H ₂ S wag
	ω_3	<i>a</i>	98	0.005	PH ₂ twist
	ω_4	<i>a</i>	115	19.5232	PH ₂ wag
	ω_5	<i>a</i>	131	0.7719	H ₂ S twist
	ω_6	<i>a</i>	132	3.6838	H ₂ S rock
	ω_7	<i>a</i>	1138	18.2818	PH ₂ scissor
	ω_8	<i>a</i>	1218	0.409	H ₂ S scissor
	ω_9	<i>a</i>	2404	42.0239	PH ₂ symm. stretch
	ω_{10}	<i>a</i>	2413	51.8238	PH ₂ asymm. stretch
	ω_{11}	<i>a</i>	2716	2.1276	H ₂ S symm. stretch
	ω_{12}	<i>a</i>	2738	1.345	H ₂ S asymm. stretch
	zpe		79.0		
AVQZ	ω_1	<i>a</i>	12	22.1289	PH ₂ rock
	ω_2	<i>a</i>	51	7.4723	Intermolecular stretch
	ω_3	<i>a</i>	55	9.778	PH ₂ twist
	ω_4	<i>a</i>	75	12.9537	PH ₂ wag
	ω_5	<i>a</i>	128	5.9461	H ₂ S rock
	ω_6	<i>a</i>	131	0.406	H ₂ S twist
	ω_7	<i>a</i>	1137	17.6485	PH ₂ scissor
	ω_8	<i>a</i>	1215	0.4214	H ₂ S scissor
	ω_9	<i>a</i>	2428	38.5474	PH ₂ symm. stretch
	ω_{10}	<i>a</i>	2437	48.1511	PH ₂ asymm. stretch
	ω_{11}	<i>a</i>	2734	1.4971	H ₂ S symm. stretch
	ω_{12}	<i>a</i>	2759	1.4663	H ₂ S asymm. stretch
	zpe		78.7		

Table E107: PH₂⁻...NH₃ complex geometric parameters, D_0 s and VDEs from DSD-PBEP86-D3BJ optimisations. zpe values are drawn from relevant harmonic frequency calculations.

		R_{P-H} Å	\angle_{H-P-H} °	R_{P-HN} Å	\angle_{H-P-HN} °	$\angle_{H-N-H-P}$ °	E E_h	zpe kJ mol ⁻¹	D_e kJ mol ⁻¹	D_0 kJ mol ⁻¹	E_{VDE} E_h	VDE eV
6a: C_1 (¹ A)	def2QZVP	1.429	92.1	2.649	92.0	63.6	-398.7748616	130.1	38.0	43.3	-398.7221340	1.417
	pVTZ	1.429	92.3	2.662	98.3	62.6	-398.7603057	129.3	33.1	38.1	-398.7048751	1.493
	pVQZ	1.428	92.4	2.667	96.5	63.0	-398.7794691	129.4	32.6	37.4	-398.7230940	1.518
	W1w						-398.6399975		31.4	36.1	-398.5819002	1.565
	W2w						-398.6403453		31.3	36.1	-398.5823315	1.563
		R_{P-H} Å	\angle_{H-P-H} °	R_{P-N} Å	\angle_{H-P-N} °	$\angle_{H-N-P-H}$ °	E E_h	zpe kJ mol ⁻¹	D_e kJ mol ⁻¹	D_0 kJ mol ⁻¹	ADE eV	ADE_{shift} eV
6b: C_{2v} (² A)	def2QZVP	1.414	92.8	3.377	73.6	0.0	-398.7244508	130.2	6.4	10.2	1.374	1.575
	pVTZ	1.415	92.8	3.370	74.1	0.0	-398.7069361	129.9	6.6	10.7	1.458	1.527
	pVQZ	1.414	92.8	3.375	73.4	0.0	-398.7251821	129.9	6.4	10.1	1.482	1.524
	W1w						-398.5841337		5.5	9.2	1.525	1.520
	W2w						-398.5845747		5.6	9.3	1.523	1.519
6c: C_s (² A)	def2QZVP	1.417	92.0	3.693	80.0	132.8	-398.7233846	129.3	3.6	6.4	1.393	1.594
	pVTZ	1.419	92.0	3.694	80.0	133.1	-398.7058123	128.9	3.7	6.8	1.478	1.547
	pVQZ	1.417	92.0	3.695	80.2	132.8	-398.7240790	129.0	3.5	6.3	1.503	1.544
	W1w						-398.5829341		2.4	5.2	1.548	1.543
	W2w						-398.5833737		2.5	5.2	1.546	1.542
6d: C_s (² A)	def2QZVP	1.416	92.2	3.263	77.0	47.7	-398.7242556	130.8	5.9	10.3	1.385	1.586
	pVTZ	1.417	92.2	3.268	77.1	47.7	-398.7067106	130.5	6.0	10.7	1.471	1.539
	pVQZ	1.416	92.2	3.255	77.2	47.8	-398.7249982	130.7	5.9	10.4	1.495	1.536
	W1w						-398.5837632		4.6	9.0	1.543	1.537
	W2w						-398.5841837		4.6	9.0	1.541	1.537

Table E108: DSD-PBEP86-D3BJ and extrapolated single-point energies for $\text{PH}_2^- \cdots \text{NH}_3$ complexes. Geometries use for CC energies are from DSD-PBEP86-D3BJ/AVQZ optimisations. All energies are in E_h .

	6a: $\text{PH}_2^- \cdots \text{HCCH}$ (1A)						
	E_{DH-DFT}	E_{SCF}	E_{CCSD}	E_{corr}	$E_{CCSD(T)}$	$E_{(T)}$	E_{Wnw}
def2QZVP	-398.7748616						
pVDZ		-398.0922301	-398.4860109	-0.3937808	-398.4987571	-0.0127462	
pVTZ	-398.7603057	-398.1175713	-398.5792824	-0.4617111	-398.5981054	-0.0188230	
pVQZ	-398.7794691	-398.1241327	-398.6045859	-0.4804532	-398.6248425	-0.0202566	
pV5Z		-398.1255533	-398.6120302	-0.4864769			
W1w		-398.1261742		-0.4927412		-0.0210821	-398.6399975
W2w		-398.1262457		-0.4927968		-0.0213027	-398.6403453
	3a: VDE $\text{PH}_2^- \cdots \text{HCCH}$ (2A)						
def2QZVP	-398.7221340						
pVDZ		-398.0797959	-398.4391471	-0.3593512	-398.4490023	-0.0098552	
pVTZ	-398.7048751	-398.1056752	-398.5277858	-0.4221106	-398.5427329	-0.0149471	
pVQZ	-398.7230940	-398.1122560	-398.5516687	-0.4394127	-398.5678133	-0.0161446	
pV5Z		-398.1137079	-398.5587252	-0.4450173			
W1w		-398.1143035		-0.4507566		-0.0168401	-398.5819002
W2w		-398.1144155		-0.4508975		-0.0170185	-398.5823315

Table E109: DSD-PBEP86-D3BJ and extrapolated single-point energies for $\text{PH}_2 \cdots \text{HCCH}$ complexes. Geometries use for CC energies are from DSD-PBEP86-D3BJ/AVQZ optimisations. All energies are in E_h .

	6b: $\text{PH}_2 \cdots \text{HCCH}$ (2A)						
	E_{DH-DFT}	E_{SCF}	E_{CCSD}	E_{corr}	$E_{CCSD(T)}$	$E_{(T)}$	E_{Wnw}
def2QZVP	-398.7244508						
pVDZ		-398.0836628	-398.4409675	-0.3573047	-398.4505470	-0.0095795	
pVTZ	-398.7069361	-398.1096871	-398.5300896	-0.4204025	-398.5447391	-0.0146495	
pVQZ	-398.7251821	-398.1163211	-398.5541258	-0.4378047	-398.5699718	-0.0158460	
pV5Z		-398.1177870	-398.5612278	-0.4434408			
W1w		-398.1183852		-0.4492142		-0.0165343	-398.5841337
W2w		-398.1185015		-0.4493541		-0.0167191	-398.5845747
	6c: $\text{PH}_2 \cdots \text{HCCH}$ (2A)						
def2QZVP	-398.7233846						
pVDZ		-398.0819647	-398.4395972	-0.3576325	-398.4492324	-0.0096352	
pVTZ	-398.7058123	-398.1081417	-398.5287644	-0.4206227	-398.5434785	-0.0147141	
pVQZ	-398.7240790	-398.1147894	-398.5528383	-0.4380489	-398.5687528	-0.0159145	
pV5Z		-398.1162502	-398.5599463	-0.4436961			
W1w		-398.1168578		-0.4494741		-0.0166022	-398.5829341
W2w		-398.1169622		-0.4496210		-0.0167905	-398.5833737
	6d: $\text{PH}_2 \cdots \text{HCCH}$ (2A)						
def2QZVP	-398.7242556						
pVDZ		-398.0822362	-398.4403214	-0.3580852	-398.4500493	-0.0097279	
pVTZ	-398.7067106	-398.1082368	-398.5294017	-0.4211649	-398.5442200	-0.0148183	
pVQZ	-398.7249982	-398.1148862	-398.5535263	-0.4386401	-398.5695531	-0.0160268	
pV5Z		-398.1163464	-398.5606360	-0.4442896			
W1w		-398.1169551		-0.4500974		-0.0167107	-398.5837632
W2w		-398.1170581		-0.4502169		-0.0169087	-398.5841837

Table E110: Cartesian coordinates of the PH₂⁻ ...NH₃ conformers optimised at DSD-PBEP86-D3BJ/def-2QZVP,AVnZ ($n = T, Q$) in Å.

		6a: PH ₂ ⁻ ...NH ₃ (¹ A)		
		x	y	z
def2QZVP	N	2.334696	0.038149	-0.113124
	P	-1.328518	-0.085430	-0.076760
	H	1.312804	0.020003	-0.251399
	H	2.463557	0.669898	0.670349
	H	2.552559	-0.882395	0.254126
	H	-1.307977	-0.132343	1.351643
	H	-1.436049	1.339244	-0.081443
		x	y	z
AVTZ	N	-2.35375	-0.02918	-0.11872
	P	1.32210	0.11448	-0.03122
	H	-2.52748	-0.74745	0.57871
	H	-2.55712	0.85028	0.34803
	H	-1.32874	-0.02841	-0.23461
	H	1.41327	-0.46314	1.27354
	H	1.64476	-1.12428	-0.66634
		x	y	z
AVQZ	N	-2.355453	-0.028270	-0.118795
	P	1.321606	0.114787	-0.029377
	H	-2.527106	-0.752725	0.570742
	H	-2.553668	0.845905	0.357069
	H	-1.332614	-0.029183	-0.241384
	H	1.412808	-0.479354	1.266659
	H	1.664659	-1.108562	-0.680857

Table E111: Cartesian coordinates of the PH₂⋯NH₃ conformers optimised at DSD-PBEP86-D3BJ/def-2QZVP,AVnZ ($n = T, Q$) in Å.

	6b: PH ₂ ⋯NH ₃ (² A)			6c: PH ₂ ⋯NH ₃ (² A)			6d: PH ₂ ⋯NH ₃ (² A)			
	x	y	z	x	y	z	x	y	z	
def2QZVP	N	0.027481	2.139188	0.000000	2.348386	0.000206	0.046152	1.992787	0.000000	-0.013655
	P	-0.182184	3.129158	0.000000	-1.344142	-0.000143	0.101978	-1.268435	0.000000	0.096394
	H	0.605671	1.959926	0.810957	1.748345	0.002737	0.861040	2.658359	-0.000002	-0.775806
	H	0.605671	1.959926	-0.810957	2.100365	-0.814936	-0.499360	2.191406	0.812815	0.555015
	H	0.027481	-1.237770	0.000000	2.099427	0.811175	-0.505124	2.191406	-0.812813	0.555018
	H	-0.304791	-2.617429	0.000000	-1.112587	1.020673	-0.853632	-0.982078	-1.020277	-0.842280
	H	-1.328955	-0.839375	0.000000	-1.112118	-1.018943	-0.855664	-0.982078	1.020278	-0.842279
	x	y	z	x	y	z	x	y	z	
AVTZ	N	0.08924	-2.13749	0.00000	-2.348950	-0.000018	0.050337	1.996525	0.000008	-0.017339
	P	0.88911	-1.50773	0.00000	1.344910	0.000013	0.101621	-1.269582	0.000007	0.096215
	H	-0.54115	-1.96434	-0.77794	-1.723339	-0.000347	0.847963	2.694247	0.000696	-0.752574
	H	-0.54115	-1.96434	0.77794	-2.115543	0.814314	-0.505958	2.173388	0.813345	0.560781
	H	-1.00750	0.27387	0.00000	-2.115530	-0.813876	-0.506645	2.173726	-0.814111	0.559576
	H	0.08924	1.18611	0.00000	1.111719	-1.020310	-0.855924	-0.986651	-1.020804	-0.844759
	H	-0.76256	2.33329	0.00000	1.111687	1.020152	-0.856112	-0.986645	1.020714	-0.844870
	x	y	z	x	y	z	x	y	z	
AVQZ	N	2.136111	0.070786	0.000017	-2.349833	-0.000404	0.050210	1.988379	0.000020	-0.016514
	P	-1.235233	-0.085281	-0.000005	1.345084	0.000288	0.101769	-1.264420	0.000022	0.096253
	H	3.110797	0.344236	0.000041	-1.724261	-0.003438	0.846231	2.678428	0.001811	-0.757178
	H	1.994147	-0.517745	0.811453	-2.120608	0.816246	-0.502025	2.167944	0.812128	0.560202
	H	1.994098	-0.517419	-0.811647	-2.118107	-0.810737	-0.510225	2.168791	-0.814130	0.557052
	H	-0.895273	1.287096	0.000103	1.118112	-1.021697	-0.853875	-0.983780	-1.020587	-0.843973
	H	-2.628046	0.187543	0.000012	1.117429	1.018135	-0.858111	-0.983730	1.020316	-0.844296

Table E112: Calculated harmonic frequencies and mode assignments for the 6a PH₂⁻...NH₃ complex. All frequencies and intensities are in cm⁻¹ and km mol⁻¹.

3a PH ₂ ⁻ ...NH ₃ (¹ A)					
	Mode	Symmetry	Frequency (cm ⁻¹)	Intensity (km mol ⁻¹)	Description
def2QZVP	ω_1	<i>a</i>	25	21.2191	Intermolecular rock
	ω_2	<i>a</i>	123	9.952	Intermolecular wag
	ω_3	<i>a</i>	138	10.3663	P-H wag
	ω_4	<i>a</i>	150	1.1526	P-H wag
	ω_5	<i>a</i>	279	20.3244	NH ₃ rotation
	ω_6	<i>a</i>	367	59.5918	NH ₃ wag
	ω_7	<i>a</i>	1093	28.0885	PH ₂ scissor
	ω_8	<i>a</i>	1207	128.9069	NH ₃ symm. scissor
	ω_9	<i>a</i>	1662	24.5431	NH ₃ asymm. scissor
	ω_{10}	<i>a</i>	1704	1.2023	NH ₃ twist
	ω_{11}	<i>a</i>	2322	202.8731	P-H stretch
	ω_{12}	<i>a</i>	2327	213.7291	P-H stretch
	ω_{13}	<i>a</i>	3251	608.1636	H-transfer stretch
	ω_{14}	<i>a</i>	3512	13.6066	NH ₂ symm. stretch
	ω_{15}	<i>a</i>	3586	0.2605	NH ₂ asymm. stretch
AVTZ	zpe		130.1		
	ω_1	<i>a</i>	39	19.1371	Intermolecular rock
	ω_2	<i>a</i>	102	7.0483	Intermolecular wag
	ω_3	<i>a</i>	112	9.6307	P-H wag
	ω_4	<i>a</i>	129	6.0468	P-H wag
	ω_5	<i>a</i>	260	16.0494	NH ₃ rotation
	ω_6	<i>a</i>	355	55.35	NH ₃ wag
	ω_7	<i>a</i>	1090	28.0044	PH ₂ scissor
	ω_8	<i>a</i>	1180	101.0088	NH ₃ symm. scissor
	ω_9	<i>a</i>	1659	26.7189	NH ₃ asymm. scissor
	ω_{10}	<i>a</i>	1693	2.676	NH ₃ twist
	ω_{11}	<i>a</i>	2320	186.4415	P-H stretch
	ω_{12}	<i>a</i>	2327	189.8758	P-H stretch
	ω_{13}	<i>a</i>	3261	647.8296	H-transfer stretch
	ω_{14}	<i>a</i>	3506	15.7044	NH ₂ symm. stretch
	ω_{15}	<i>a</i>	3579	0.1528	NH ₂ asymm. stretch
AVQZ	zpe		129.3		
	ω_1	<i>a</i>	39	18.6998	Intermolecular rock
	ω_2	<i>a</i>	101	8.4824	Intermolecular wag
	ω_3	<i>a</i>	111	9.0554	P-H wag
	ω_4	<i>a</i>	128	5.9846	P-H wag
	ω_5	<i>a</i>	257	16.1856	NH ₃ rotation
	ω_6	<i>a</i>	352	55.0939	NH ₃ wag
	ω_7	<i>a</i>	1091	28.3559	PH ₂ scissor
	ω_8	<i>a</i>	1180	102.9597	NH ₃ symm. scissor
	ω_9	<i>a</i>	1660	27.7614	NH ₃ asymm. scissor
	ω_{10}	<i>a</i>	1694	2.8201	NH ₃ twist
	ω_{11}	<i>a</i>	2327	181.0523	P-H stretch
	ω_{12}	<i>a</i>	2334	184.6298	P-H stretch
	ω_{13}	<i>a</i>	3268	644.2961	H-transfer stretch
	ω_{14}	<i>a</i>	3513	16.5124	NH ₂ symm. stretch
	ω_{15}	<i>a</i>	3586	0.1936	NH ₂ asymm. stretch
	zpe		129.4		

Table E113: Calculated harmonic frequencies and mode assignments for the 6b PH₂ ··· NH₃ complex. All frequencies and intensities are in cm⁻¹ and km mol⁻¹.

3b PH ₂ ··· NH ₃ (² A)					
	Mode	Symmetry	Frequency (cm ⁻¹)	Intensity (km mol ⁻¹)	Description
def2QZVP	ω_1	a''	49	4.0456	PH ₂ wag
	ω_2	a'	80	0.3593	Intermolecular stretch
	ω_3	a''	81	13.7815	P–H wag
	ω_4	a'	99	79.9398	Intermolecular rock
	ω_5	a''	130	27.9904	PH ₂ twist
	ω_6	a'	165	16.7278	Intermolecular rock
	ω_7	a'	1063	162.1381	NH ₃ scissor
	ω_8	a'	1136	18.3194	PH ₂ scissor
	ω_9	a''	1671	24.8899	NH ₃ asymm. scissor
	ω_{10}	a'	1675	19.5987	NH ₂ symm. scissor
	ω_{11}	a'	2417	80.6696	P–H stretch
	ω_{12}	a'	2454	42.9787	P–H stretch
	ω_{13}	a'	3496	1.9503	NH ₃ symm. stretch
	ω_{14}	a''	3630	5.2942	NH ₂ asymm. stretch
	ω_{15}	a'	3631	3.5983	NH ₂ symm. stretch
AVTZ	zpe		130.2		
	ω_1	a''	43	3.0535	PH ₂ wag
	ω_2	a'	81	1.6878	Intermolecular stretch
	ω_3	a''	86	15.8324	P–H wag
	ω_4	a'	97	77.2217	Intermolecular rock
	ω_5	a''	127	23.7078	PH ₂ twist
	ω_6	a'	164	13.081	Intermolecular rock
	ω_7	a'	1060	154.1574	NH ₃ scissor
	ω_8	a'	1136	18.2882	PH ₂ scissor
	ω_9	a''	1670	23.8144	NH ₃ asymm. scissor
	ω_{10}	a'	1671	17.5165	NH ₂ symm. scissor
	ω_{11}	a'	2410	82.9888	P–H stretch
	ω_{12}	a'	2446	43.6537	P–H stretch
	ω_{13}	a'	3485	3.4502	NH ₃ symm. stretch
	ω_{14}	a''	3618	5.4085	NH ₂ asymm. stretch
	ω_{15}	a'	3619	3.3345	NH ₂ symm. stretch
AVQZ	zpe		129.9		
	ω_1	a	39	2.7498	PH ₂ wag
	ω_2	a	77	14.9568	P–H wag
	ω_3	a	79	2.4604	Intermolecular stretch
	ω_4	a	96	76.9818	Intermolecular rock
	ω_5	a	125	25.3912	PH ₂ twist
	ω_6	a	163	11.88	Intermolecular rock
	ω_7	a	1057	156.7274	NH ₃ scissor
	ω_8	a	1136	18.3764	PH ₂ scissor
	ω_9	a	1670	24.0556	NH ₃ asymm. scissor
	ω_{10}	a	1672	17.3746	NH ₂ symm. scissor
	ω_{11}	a	2415	81.4229	P–H stretch
	ω_{12}	a	2452	42.342	P–H stretch
	ω_{13}	a	3490	3.1959	NH ₃ symm. stretch
	ω_{14}	a	3624	5.8005	NH ₂ asymm. stretch
	ω_{15}	a	3626	3.7813	NH ₂ symm. stretch
	zpe		129.9		

Table E114: Calculated harmonic frequencies and mode assignments for the 6c PH₂ ··· NH₃ complex. All frequencies and intensities are in cm⁻¹ and km mol⁻¹.

3c PH ₂ ··· NH ₃ (² A)					
	Mode	Symmetry	Frequency (cm ⁻¹)	Intensity (km mol ⁻¹)	Description
def2QZVP	ω_1	<i>a</i>	29	4.3787	Intermolecular rock
	ω_2	<i>a</i>	51	12.153	Intermolecular wag
	ω_3	<i>a</i>	76	57.1885	Intermolecular twist
	ω_4	<i>a</i>	83	40.173	Intermolecular wag
	ω_5	<i>a</i>	108	1.1194	PH ₂ twist
	ω_6	<i>a</i>	133	19.6046	PH ₂ wag
	ω_7	<i>a</i>	1035	244.367	NH ₃ scissor
	ω_8	<i>a</i>	1136	19.4381	PH ₂ scissor
	ω_9	<i>a</i>	1672	13.1952	NH ₂ symm. scissor
	ω_{10}	<i>a</i>	1673	8.2181	NH ₃ asymm. scissor
	ω_{11}	<i>a</i>	2425	44.9941	PH ₂ symm. stretch
	ω_{12}	<i>a</i>	2433	57.563	PH ₂ asymm. stretch
	ω_{13}	<i>a</i>	3497	9.928	NH ₃ symm. stretch
	ω_{14}	<i>a</i>	3631	4.8786	NH ₂ symm. stretch
	ω_{15}	<i>a</i>	3634	4.543	NH ₂ asymm. stretch
AVTZ	zpe		129.3		
	ω_1	<i>a</i>	27	7.6047	Intermolecular rock
	ω_2	<i>a</i>	50	16.7968	Intermolecular wag
	ω_3	<i>a</i>	69	50.9939	Intermolecular twist
	ω_4	<i>a</i>	80	34.0419	Intermolecular wag
	ω_5	<i>a</i>	106	0.3292	PH ₂ twist
	ω_6	<i>a</i>	131	17.686	PH ₂ wag
	ω_7	<i>a</i>	1034	228.6472	NH ₃ scissor
	ω_8	<i>a</i>	1136	19.5225	PH ₂ scissor
	ω_9	<i>a</i>	1671	12.3451	NH ₂ symm. scissor
	ω_{10}	<i>a</i>	1671	6.8053	NH ₃ asymm. scissor
	ω_{11}	<i>a</i>	2417	46.5574	PH ₂ symm. stretch
	ω_{12}	<i>a</i>	2426	57.1869	PH ₂ asymm. stretch
	ω_{13}	<i>a</i>	3486	10.9842	NH ₃ symm. stretch
	ω_{14}	<i>a</i>	3618	4.7158	NH ₂ symm. stretch
	ω_{15}	<i>a</i>	3622	4.6588	NH ₂ asymm. stretch
AVQZ	zpe		128.9		
	ω_1	<i>a</i>	27	7.8032	Intermolecular rock
	ω_2	<i>a</i>	49	15.1511	Intermolecular wag
	ω_3	<i>a</i>	68	50.5682	Intermolecular twist
	ω_4	<i>a</i>	81	33.6948	Intermolecular wag
	ω_5	<i>a</i>	105	0.6342	PH ₂ twist
	ω_6	<i>a</i>	131	19.963	PH ₂ wag
	ω_7	<i>a</i>	1031	231.4757	NH ₃ scissor
	ω_8	<i>a</i>	1136	19.6063	PH ₂ scissor
	ω_9	<i>a</i>	1671	12.733	NH ₂ symm. scissor
	ω_{10}	<i>a</i>	1672	7.0579	NH ₃ asymm. scissor
	ω_{11}	<i>a</i>	2423	45.3734	PH ₂ symm. stretch
	ω_{12}	<i>a</i>	2432	55.5676	PH ₂ asymm. stretch
	ω_{13}	<i>a</i>	3491	10.5012	NH ₃ symm. stretch
	ω_{14}	<i>a</i>	3625	5.1127	NH ₂ symm. stretch
	ω_{15}	<i>a</i>	3628	5.0282	NH ₂ asymm. stretch
	zpe		129.0		

Table E115: Calculated harmonic frequencies and mode assignments for the 6d PH₂⋯NH₃ complex. All frequencies and intensities are in cm⁻¹ and km mol⁻¹.

3d PH ₂ ⋯NH ₃ (² A)					
	Mode	Symmetry	Frequency (cm ⁻¹)	Intensity (km mol ⁻¹)	Description
def2QZVP	ω_1	<i>a</i>	15	0.6527	Intermolecular rock
	ω_2	<i>a</i>	70	2.9725	Intermolecular stretch
	ω_3	<i>a</i>	87	46.9389	NH ₃ wag
	ω_4	<i>a</i>	109	35.7407	NH ₃ rotation
	ω_5	<i>a</i>	184	0.9015	PH ₂ twist
	ω_6	<i>a</i>	240	3.5227	PH ₂ wag
	ω_7	<i>a</i>	1050	138.5484	NH ₃ scissor
	ω_8	<i>a</i>	1131	20.1087	PH ₂ scissor
	ω_9	<i>a</i>	1671	21.2384	NH ₃ asymm. scissor
	ω_{10}	<i>a</i>	1673	14.6191	NH ₂ symm. scissor
	ω_{11}	<i>a</i>	2433	48.9833	PH ₂ symm. stretch
	ω_{12}	<i>a</i>	2441	63.1882	PH ₂ asymm. stretch
	ω_{13}	<i>a</i>	3497	1.4039	NH ₃ symm. stretch
	ω_{14}	<i>a</i>	3633	7.231	NH ₂ symm. stretch
	ω_{15}	<i>a</i>	3634	7.3456	NH ₂ asymm. stretch
AVTZ	zpe		130.8		
	ω_1	<i>a</i>	17	0.8313	Intermolecular rock
	ω_2	<i>a</i>	71	5.5784	Intermolecular stretch
	ω_3	<i>a</i>	85	45.5062	NH ₃ wag
	ω_4	<i>a</i>	108	33.5951	NH ₃ rotation
	ω_5	<i>a</i>	182	0.6637	PH ₂ twist
	ω_6	<i>a</i>	237	2.7796	PH ₂ wag
	ω_7	<i>a</i>	1050	137.589	NH ₃ scissor
	ω_8	<i>a</i>	1130	20.5437	PH ₂ scissor
	ω_9	<i>a</i>	1669	20.2621	NH ₃ asymm. scissor
	ω_{10}	<i>a</i>	1672	12.8588	NH ₂ symm. scissor
	ω_{11}	<i>a</i>	2425	49.679	PH ₂ symm. stretch
	ω_{12}	<i>a</i>	2434	62.0659	PH ₂ asymm. stretch
	ω_{13}	<i>a</i>	3486	2.952	NH ₃ symm. stretch
	ω_{14}	<i>a</i>	3621	6.6708	NH ₂ symm. stretch
	ω_{15}	<i>a</i>	3622	7.1448	NH ₂ asymm. stretch
AVQZ	zpe		130.5		
	ω_1	<i>a</i>	15	0.8879	Intermolecular rock
	ω_2	<i>a</i>	71	6.281	Intermolecular stretch
	ω_3	<i>a</i>	88	44.3244	NH ₃ wag
	ω_4	<i>a</i>	110	33.3329	NH ₃ rotation
	ω_5	<i>a</i>	185	0.7115	PH ₂ twist
	ω_6	<i>a</i>	240	2.8274	PH ₂ wag
	ω_7	<i>a</i>	1047	139.4813	NH ₃ scissor
	ω_8	<i>a</i>	1130	20.6529	PH ₂ scissor
	ω_9	<i>a</i>	1670	20.657	NH ₃ asymm. scissor
	ω_{10}	<i>a</i>	1672	13.1729	NH ₂ symm. scissor
	ω_{11}	<i>a</i>	2431	48.7142	PH ₂ symm. stretch
	ω_{12}	<i>a</i>	2440	60.6286	PH ₂ asymm. stretch
	ω_{13}	<i>a</i>	3492	2.6415	NH ₃ symm. stretch
	ω_{14}	<i>a</i>	3628	7.2297	NH ₂ symm. stretch
	ω_{15}	<i>a</i>	3629	7.7045	NH ₂ asymm. stretch
	zpe		130.7		

Table E116: Energies, Intensities and Franck-Condon factors calculated from ezSpectrum 3.0 for the $2g \leftarrow 2a$ transition. Notation for the transition, 4_0^1 indicates the transition in ω_4 from $v'' = 0$ to $v' = 1$ with modes numbered according to Table E65. The band origin is the ADE from Table E46.

<i>E</i> eV	Intensity	FCF	Assignment
2.2297	1.18E-29	3.43E-15	$4_0^1 6_0^3 11_0^3 16_0^1$
2.2399	6.70E-30	2.59E-15	$6_0^4 11_0^3 16_0^1$
2.3469	1.69E-29	-4.11E-15	$4_0^1 6_0^2 11_0^4 16_0^1$
2.3571	1.45E-29	-3.80E-15	$6_0^3 11_0^4 16_0^1$
2.3796	7.89E-30	2.81E-15	$4_0^2 6_0^2 11_0^2 16_0^2$
2.3899	1.85E-29	4.30E-15	$4_0^1 6_0^3 11_0^2 16_0^2$
2.4001	1.02E-29	3.19E-15	$6_0^4 11_0^2 16_0^2$
2.4640	1.18E-29	3.43E-15	$4_0^1 6_0^1 11_0^5 16_0^1$
2.4743	1.68E-29	4.10E-15	$6_0^2 11_0^5 16_0^1$
2.4939	6.22E-30	-2.49E-15	$6_0^2 11_0^3 16_0^2$
2.4968	8.89E-30	-2.98E-15	$4_0^2 6_0^1 11_0^3 16_0^2$
2.5071	3.48E-29	-5.90E-15	$4_0^1 6_0^2 11_0^3 16_0^2$
2.5173	2.90E-29	-5.38E-15	$6_0^3 11_0^3 16_0^2$
2.5398	6.36E-30	2.52E-15	$4_0^2 6_0^2 11_0^1 16_0^3$
2.5501	1.45E-29	3.81E-15	$4_0^1 6_0^3 11_0^1 16_0^3$
2.5603	7.73E-30	2.78E-15	$6_0^4 11_0^1 16_0^3$
2.5915	9.92E-30	-3.15E-15	$6_0^1 11_0^6 16_0^1$
2.6111	5.32E-30	2.31E-15	$6_0^1 11_0^4 16_0^2$
2.6243	2.98E-29	5.46E-15	$4_0^1 6_0^1 11_0^4 16_0^2$
2.6345	4.14E-29	6.43E-15	$6_0^2 11_0^4 16_0^2$
2.6439	5.33E-30	-2.31E-15	$4_0^1 6_0^1 11_0^2 16_0^3$
2.6541	7.16E-30	-2.68E-15	$6_0^2 11_0^2 16_0^3$
2.6570	1.05E-29	-3.24E-15	$4_0^2 6_0^1 11_0^2 16_0^3$
2.6673	4.01E-29	-6.33E-15	$4_0^1 6_0^2 11_0^2 16_0^3$
2.6775	3.24E-29	-5.70E-15	$6_0^3 11_0^2 16_0^3$
2.7415	9.45E-30	-3.07E-15	$4_0^1 11_0^5 16_0^2$
2.7517	2.87E-29	-5.36E-15	$6_0^1 11_0^5 16_0^2$
2.7713	8.00E-30	2.83E-15	$6_0^1 11_0^3 16_0^3$
2.7742	5.34E-30	2.31E-15	$4_0^2 11_0^3 16_0^3$
2.7845	4.49E-29	6.70E-15	$4_0^1 6_0^1 11_0^3 16_0^3$
2.7947	6.07E-29	7.79E-15	$6_0^2 11_0^3 16_0^3$
2.8172	6.93E-30	-2.63E-15	$4_0^2 6_0^1 11_0^1 16_0^4$
2.8275	2.58E-29	-5.08E-15	$4_0^1 6_0^2 11_0^1 16_0^4$
2.8377	2.02E-29	-4.50E-15	$6_0^3 11_0^1 16_0^4$

Table E117: Energies, Intensities and Franck-Condon factors calculated from ezSpectrum 3.0 for the $2f \leftarrow 2b$ transition. Notation for the transition, 5_0^1 indicates the transition in ω_5 from $v'' = 0$ to $v' = 1$ with modes numbered according to Table E63. The band origin is the ADE from Table E46.

Table E118: Energies, Intensities and Franck-Condon factors calculated from ezSpectrum 3.0 for the 3b \leftarrow 3a transition. Notation for the transition, 2₀¹ indicates the transition in ω_2 from $v'' = 0$ to $v' = 1$ with modes numbered according to Table E73. The band origin is the ADE from Table E67.

E eV	Intensity	FCF	Assignment	E eV	Intensity	FCF	Assignment
1.5670	1.06E-02	1.03E-01	ADE	1.6004	9.31E-04	-3.05E-02	2 ₀ ⁴ 3 ₀ ¹ 4 ₀ ¹
1.5713	1.31E-03	-3.62E-02	2 ₀ ¹	1.6013	6.50E-04	-2.55E-02	2 ₀ ² 4 ₀ ³
1.5731	2.95E-03	-5.43E-02	1 ₀ ²	1.6013	5.99E-04	2.45E-02	2 ₀ ⁶ 4 ₀ ¹
1.5747	8.39E-03	9.16E-02	3 ₀ ¹	1.6078	9.16E-04	3.03E-02	3 ₀ ¹ 4 ₀ ⁵ 2 ₀ ⁰
1.5756	7.48E-03	-8.65E-02	4 ₀ ¹	1.6090	5.20E-04	-2.28E-02	2 ₀ ² 3 ₀ ¹ 4 ₀ ³
1.5756	2.10E-03	-4.58E-02	2 ₀ ²	1.8488	6.49E-04	2.55E-02	10 ₀ ²
1.5790	9.92E-04	-3.15E-02	2 ₀ ¹ 3 ₀ ¹	1.8566	5.16E-04	2.27E-02	3 ₀ ¹ 10 ₀ ²
1.5792	1.22E-03	3.50E-02	1 ₀ ⁴	1.8729	5.94E-04	2.44E-02	1 ₀ ¹ 13 ₀ ¹
1.5798	9.91E-04	3.14E-02	2 ₀ ³	1.8821	6.20E-04	2.49E-02	5 ₀ ¹ 13 ₀ ¹
1.5809	2.32E-03	-4.82E-02	1 ₀ ²	2.0096	1.97E-03	-4.44E-02	10 ₀ ¹ 12 ₀ ¹
1.5817	2.07E-03	4.55E-02	1 ₀ ² 4 ₀ ¹	2.0157	5.46E-04	2.34E-02	1 ₀ ² 10 ₀ ¹ 12 ₀ ¹
1.5817	5.82E-04	2.41E-02	1 ₀ ² 2 ₀ ²	2.0173	1.53E-03	-3.91E-02	3 ₀ ¹ 10 ₀ ¹ 12 ₀ ¹
1.5825	1.28E-03	3.58E-02	3 ₀ ²	2.0181	1.50E-03	3.87E-02	4 ₀ ¹ 10 ₀ ¹ 12 ₀ ¹
1.5833	5.88E-03	-7.67E-02	3 ₀ ¹ 4 ₀ ¹	2.0259	1.16E-03	3.41E-02	3 ₀ ¹ 4 ₀ ¹ 10 ₀ ¹ 12 ₀ ¹
1.5833	1.68E-03	-4.10E-02	2 ₀ ² 3 ₀ ¹	2.1703	1.92E-03	4.38E-02	12 ₀ ²
1.5841	2.47E-03	4.97E-02	2 ₀ ² 4 ₀ ¹	2.1727	2.29E-03	4.79E-02	13 ₀ ²
1.5841	5.90E-04	2.43E-02	2 ₀ ⁴	2.1764	5.31E-04	-2.31E-02	1 ₀ ² 12 ₀ ²
1.5854	5.67E-04	-2.38E-02	1 ₀ ⁶	2.1780	1.49E-03	3.86E-02	3 ₀ ¹ 12 ₀ ²
1.5870	9.68E-04	3.11E-02	1 ₀ ⁴ 3 ₀ ¹	2.1789	1.45E-03	-3.80E-02	4 ₀ ¹ 12 ₀ ²
1.5876	7.54E-04	2.74E-02	2 ₀ ³ 3 ₀ ¹	2.1804	1.81E-03	4.25E-02	3 ₀ ¹ 13 ₀ ²
1.5878	8.63E-04	-2.93E-02	1 ₀ ⁴ 4 ₀ ¹	2.1813	1.61E-03	-4.01E-02	4 ₀ ¹ 13 ₀ ²
1.5884	6.44E-04	2.53E-02	2 ₀ ¹ 4 ₀ ²	2.1866	1.11E-03	-3.34E-02	3 ₀ ¹ 4 ₀ ¹ 12 ₀ ²
1.5884	6.23E-04	-2.49E-02	2 ₀ ⁵	2.1890	1.27E-03	-3.56E-02	3 ₀ ¹ 4 ₀ ¹ 13 ₀ ²
1.5894	1.63E-03	4.03E-02	1 ₀ ² 3 ₀ ¹ 4 ₀ ¹	2.1898	5.32E-04	2.31E-02	2 ₀ ² 4 ₀ ¹ 13 ₀ ²
1.5902	6.85E-04	-2.61E-02	1 ₀ ² 2 ₀ ⁰ 4 ₀ ¹	2.4521	8.87E-04	2.98E-02	10 ₀ ² 12 ₀ ²
1.5910	8.94E-04	-2.99E-02	3 ₀ ² 4 ₀ ¹	2.4599	6.87E-04	2.62E-02	3 ₀ ¹ 10 ₀ ² 12 ₀ ²
1.5915	1.65E-03	-4.07E-02	5 ₀ ²	2.4607	7.03E-04	-2.65E-02	4 ₀ ¹ 10 ₀ ² 12 ₀ ²
1.5919	1.95E-03	4.41E-02	2 ₀ ² 3 ₀ ¹ 4 ₀ ¹	2.4684	5.43E-04	-2.33E-02	3 ₀ ¹ 4 ₀ ¹ 10 ₀ ² 12 ₀ ²
1.5927	1.84E-03	4.29E-02	4 ₀ ³	2.6129	1.06E-03	-3.25E-02	10 ₀ ¹ 12 ₀ ³
1.5927	1.17E-03	-3.42E-02	2 ₀ ⁴ 4 ₀ ¹	2.6206	8.13E-04	-2.85E-02	3 ₀ ¹ 10 ₀ ¹ 12 ₀ ³
1.5955	6.79E-04	-2.61E-02	1 ₀ ⁴ 3 ₀ ¹ 4 ₀ ¹	2.6214	8.60E-04	2.93E-02	4 ₀ ¹ 10 ₀ ¹ 12 ₀ ³
1.5961	5.09E-04	2.26E-02	2 ₀ ¹ 3 ₀ ¹ 4 ₀ ²	2.6292	6.56E-04	2.56E-02	3 ₀ ¹ 4 ₀ ¹ 10 ₀ ¹ 12 ₀ ³
1.5970	5.02E-04	-2.24E-02	2 ₀ ³ 4 ₀ ²	2.7736	5.17E-04	2.27E-02	12 ₀ ⁴
1.5977	6.16E-04	2.48E-02	1 ₀ ² 5 ₀ ²	2.7784	7.41E-04	2.72E-02	13 ₀ ⁴
1.5980	5.41E-04	-2.33E-02	1 ₀ ² 2 ₀ ⁰ 3 ₀ ¹	2.7862	5.84E-04	2.42E-02	3 ₀ ¹ 13 ₀ ⁴
1.5988	5.11E-04	-2.26E-02	1 ₀ ² 4 ₀ ³	2.7870	5.20E-04	-2.28E-02	4 ₀ ¹ 13 ₀ ⁴
1.5993	1.31E-03	-3.61E-02	3 ₀ ¹ 5 ₀ ²	3.0555	6.39E-04	2.53E-02	10 ₀ ² 12 ₀ ⁴
1.6001	1.16E-03	3.41E-02	3 ₀ ¹ 5 ₀ ²	3.0640	5.43E-04	-2.33E-02	4 ₀ ¹ 10 ₀ ² 12 ₀ ⁴
1.6004	1.45E-03	3.81E-02	3 ₀ ¹ 4 ₀ ³				

Table E119: Energies, Intensities and Franck-Condon factors calculated from ezSpectrum 3.0 for the 4c \leftarrow 4b transition. Notation for the transition, 3₀⁵ indicates the transition in ω_3 from $v'' = 0$ to $v' = 5$ with modes numbered according to Table E83. The band origin is the ADE from Table E76.

E eV	Intensity	FCF	Assignment
2.2550	1.03E-07	3.21E-04	3 ₀ ⁵ 6 ₀ ¹
2.2627	2.42E-07	4.92E-04	3 ₀ ⁶ 6 ₀ ¹
2.2631	1.32E-07	3.63E-04	3 ₀ ⁵ 4 ₀ ¹ 6 ₀ ¹
2.2705	4.28E-07	6.54E-04	3 ₀ ⁷ 6 ₀ ¹
2.2709	3.10E-07	5.57E-04	3 ₀ ⁶ 4 ₀ ¹ 6 ₀ ¹
2.3294	1.24E-07	3.52E-04	3 ₀ ⁴ 6 ₀ ²
2.3371	3.92E-07	6.26E-04	3 ₀ ⁵ 6 ₀ ²
2.3375	1.59E-07	3.99E-04	3 ₀ ⁴ 4 ₀ ¹ 6 ₀ ²
2.3449	9.24E-07	9.61E-04	3 ₀ ⁶ 6 ₀ ²
2.3453	5.02E-07	7.08E-04	3 ₀ ⁵ 4 ₀ ¹ 6 ₀ ²
2.3960	1.65E-07	4.07E-04	3 ₀ ⁵ 6 ₀ ¹ 8 ₀ ¹
2.4038	3.89E-07	6.23E-04	3 ₀ ⁶ 6 ₀ ¹ 8 ₀ ¹
2.4041	2.07E-07	4.55E-04	3 ₀ ⁵ 4 ₀ ¹ 6 ₀ ¹ 8 ₀ ¹
2.4115	2.99E-07	5.47E-04	3 ₀ ⁴ 6 ₀ ³
2.4193	9.45E-07	9.72E-04	3 ₀ ⁵ 6 ₀ ³
2.4197	3.83E-07	6.19E-04	3 ₀ ⁴ 4 ₀ ¹ 6 ₀ ³
2.4704	2.00E-07	4.48E-04	3 ₀ ⁴ 6 ₀ ² 8 ₀ ¹
2.4781	6.33E-07	7.95E-04	3 ₀ ⁵ 6 ₀ ² 8 ₀ ¹
2.4785	2.51E-07	5.01E-04	3 ₀ ⁴ 4 ₀ ¹ 6 ₀ ² 8 ₀ ¹
2.4859	1.17E-07	3.43E-04	3 ₀ ³ 6 ₀ ⁴
2.4937	5.12E-07	7.15E-04	3 ₀ ⁴ 6 ₀ ⁴
2.4940	1.51E-07	3.88E-04	3 ₀ ³ 4 ₀ ¹ 6 ₀ ⁴
2.5370	1.41E-07	3.76E-04	3 ₀ ⁵ 6 ₀ ¹ 8 ₀ ²
2.5448	1.12E-07	3.35E-04	3 ₀ ³ 6 ₀ ² 8 ₀ ¹
2.5525	4.86E-07	6.97E-04	3 ₀ ⁴ 6 ₀ ³ 8 ₀ ¹
2.5529	1.40E-07	3.75E-04	3 ₀ ³ 4 ₀ ¹ 6 ₀ ³ 8 ₀ ¹
2.5641	2.33E-07	-4.82E-04	3 ₀ ⁶ 6 ₀ ¹ 11 ₀ ¹
2.5644	1.48E-07	-3.84E-04	3 ₀ ⁵ 4 ₀ ¹ 6 ₀ ¹ 11 ₀ ¹
2.5681	1.51E-07	3.89E-04	3 ₀ ³ 6 ₀ ⁵
2.6114	1.72E-07	4.15E-04	3 ₀ ⁴ 6 ₀ ² 8 ₀ ²
2.6269	1.92E-07	4.39E-04	3 ₀ ³ 6 ₀ ⁴ 8 ₀ ¹
2.6307	1.22E-07	-3.50E-04	3 ₀ ⁴ 6 ₀ ² 11 ₀ ¹
2.6385	3.83E-07	-6.19E-04	3 ₀ ⁵ 6 ₀ ² 11 ₀ ¹
2.6388	1.81E-07	-4.26E-04	3 ₀ ⁴ 4 ₀ ¹ 6 ₀ ² 11 ₀ ¹
2.6973	2.11E-07	-4.60E-04	3 ₀ ⁵ 6 ₀ ¹ 8 ₀ ¹ 11 ₀ ¹
2.7129	2.98E-07	-5.46E-04	3 ₀ ⁴ 6 ₀ ³ 11 ₀ ¹
2.7132	1.02E-07	-3.20E-04	3 ₀ ³ 4 ₀ ¹ 6 ₀ ³ 11 ₀ ¹
2.7717	2.60E-07	-5.10E-04	3 ₀ ⁴ 6 ₀ ² 8 ₀ ¹ 11 ₀ ¹
2.7872	1.19E-07	-3.45E-04	3 ₀ ³ 6 ₀ ⁴ 11 ₀ ¹
2.8461	1.47E-07	-3.84E-04	3 ₀ ³ 6 ₀ ³ 8 ₀ ¹ 11 ₀ ¹
2.9320	1.12E-07	3.35E-04	3 ₀ ⁴ 6 ₀ ² 11 ₀ ²

Table E120: Energies, Intensities and Franck-Condon factors calculated from ezSpectrum 3.0 for the $4d \leftarrow 4b$ transition. Notation for the transition, 3_0^5 indicates the transition in ω_3 from $v'' = 0$ to $v' = 5$ with modes numbered according to Table E84. The band origin is the ADE from Table E76.

<i>E</i> eV	Intensity	FCF	Assignment
2.2055	1.12E-11	3.35E-06	4_0^8
2.2742	1.18E-11	3.44E-06	$4_0^6 6_0^1$
2.2798	1.71E-11	4.14E-06	$3_0^1 4_0^6 6_0^1$
2.2812	3.71E-11	6.09E-06	$4_0^7 6_0^1$
2.3410	1.62E-11	-4.03E-06	$4_0^7 8_0^1$
2.3499	1.20E-11	3.46E-06	$4_0^5 6_0^2$
2.3556	1.73E-11	4.16E-06	$3_0^1 4_0^5 6_0^2$
2.3570	4.71E-11	6.86E-06	$4_0^6 6_0^2$
2.4097	1.09E-11	-3.30E-06	$4_0^5 6_0^1 8_0^1$
2.4154	1.48E-11	-3.85E-06	$3_0^1 4_0^5 6_0^1 8_0^1$
2.4167	4.30E-11	-6.56E-06	$4_0^6 6_0^1 8_0^1$
2.4327	3.02E-11	5.49E-06	$4_0^5 6_0^3$
2.4911	1.16E-11	-3.40E-06	$3_0^1 4_0^4 6_0^2 8_0^1$
2.4925	4.32E-11	-6.57E-06	$4_0^5 6_0^2 8_0^1$
2.4986	1.22E-11	-3.49E-06	$4_0^7 11_0^1$
2.5085	1.07E-11	3.28E-06	$4_0^4 6_0^4$
2.5523	1.99E-11	4.46E-06	$4_0^5 6_0^1 8_0^2$
2.5683	2.14E-11	-4.63E-06	$4_0^5 6_0^3 8_0^1$
2.5729	1.20E-11	-3.47E-06	$3_0^1 4_0^5 6_0^1 11_0^1$
2.5743	3.23E-11	-5.68E-06	$4_0^6 6_0^1 11_0^1$
2.6280	1.54E-11	3.93E-06	$4_0^5 6_0^2 8_0^1$
2.6341	1.59E-11	3.98E-06	$4_0^6 8_0^1 11_0^1$
2.6501	3.25E-11	-5.70E-06	$4_0^5 6_0^2 11_0^1$
2.7098	3.33E-11	5.77E-06	$4_0^5 6_0^1 8_0^1 11_0^1$
2.7258	1.62E-11	-4.02E-06	$4_0^4 6_0^3 11_0^1$
2.7856	2.60E-11	5.10E-06	$4_0^4 6_0^2 8_0^1 11_0^1$
2.8454	1.33E-11	-3.65E-06	$4_0^4 6_0^1 8_0^2 11_0^1$
2.8674	1.45E-11	3.81E-06	$4_0^5 6_0^1 11_0^1$
2.9431	1.14E-11	3.37E-06	$4_0^4 6_0^2 11_0^1$
3.0029	1.27E-11	-3.56E-06	$4_0^4 6_0^2 8_0^1 11_0^2$

Table E121: Energies, Intensities and Franck-Condon factors calculated from ezSpectrum 3.0 for the $5g \leftarrow 5b$ transition. Notation for the transition, 3_0^1 indicates the transition in ω_3 from $v'' = 0$ to $v' = 1$ with modes numbered according to Table E102. The band origin is the ADE from Table E86.

E eV	Intensity	FCF	Assignment	E eV	Intensity	FCF	Assignment	E eV	Intensity	FCF	Assignment
2.5660	2.2426E-04	1.4975E-02	ADE	3.4957	3.1766E-04	1.7823E-02	$3_0^1 4_0^1 9_0^3$	4.0818	1.1530E-04	1.0738E-02	$3_0^1 4_0^1 7_0^2 9_0^4$
2.5741	1.2399E-04	-1.1135E-02	1_0^1	3.5037	1.4710E-04	-1.2128E-02	$1_0^1 3_0^1 4_0^1 9_0^3$	4.0862	1.7271E-04	-1.3142E-02	$1_0^1 3_0^1 9_0^5$
2.5795	1.5129E-04	1.2300E-02	3_0^1	3.5227	1.1322E-04	-1.0641E-02	$3_0^3 4_0^1 9_0^3$	4.0896	1.4957E-04	-1.2230E-02	$1_0^1 4_0^1 9_0^5$
2.5830	2.6163E-04	1.6175E-02	4_0^1	3.5909	1.0388E-04	1.0192E-02	$6_0^1 9_0^3$	4.0951	3.5612E-04	1.8871E-02	$3_0^1 4_0^1 9_0^5$
2.5910	1.2760E-04	-1.1296E-02	$1_0^1 4_0^1$	3.6045	1.0073E-04	1.0036E-02	$3_0^1 6_0^1 9_0^3$	4.1032	1.6527E-04	-1.2856E-02	$1_0^1 3_0^1 4_0^1 9_0^5$
2.5965	1.4840E-04	1.2182E-02	$3_0^1 4_0^1$	3.6084	1.4293E-04	1.1955E-02	$7_0^1 9_0^3$	4.1904	1.0214E-04	1.0106E-02	$6_0^1 9_0^5$
2.8657	2.1074E-04	1.4517E-02	9_0^1	3.6219	1.9009E-04	1.3787E-02	$3_0^1 7_0^1 9_0^3$	4.2039	1.1609E-04	1.0774E-02	$3_0^1 6_0^1 9_0^5$
2.8738	1.1605E-04	-1.0773E-02	$1_0^1 9_0^1$	3.6253	1.8558E-04	1.3623E-02	$4_0^1 7_0^1 9_0^3$	4.2078	1.8513E-04	1.3606E-02	$7_0^1 9_0^5$
2.8793	1.9598E-04	1.3999E-02	$3_0^1 9_0^1$	3.6300	1.0521E-04	-1.0257E-02	$1_0^1 3_0^1 7_0^1 9_0^3$	4.2159	1.0514E-04	-1.0254E-02	$1_0^1 7_0^1 9_0^5$
2.8827	2.5239E-04	1.5887E-02	$4_0^1 9_0^1$	3.6389	2.1848E-04	1.4781E-02	$3_0^1 4_0^1 7_0^1 9_0^3$	4.2213	2.7666E-04	1.6633E-02	$3_0^1 7_0^1 9_0^5$
2.8873	1.0398E-04	-1.0197E-02	$1_0^1 3_0^1 9_0^1$	3.6469	1.0619E-04	-1.0305E-02	$1_0^1 3_0^1 4_0^1 7_0^1 9_0^3$	4.2248	2.4168E-04	1.5546E-02	$4_0^1 7_0^1 9_0^5$
2.8908	1.2278E-04	-1.1081E-02	$1_0^1 4_0^1 9_0^1$	3.7649	2.6692E-04	1.6338E-02	9_0^4	4.2294	1.5226E-04	-1.2339E-02	$1_0^1 3_0^1 7_0^1 9_0^5$
2.8962	2.0225E-04	1.4221E-02	$3_0^1 4_0^1 9_0^1$	3.7730	1.4645E-04	-1.2102E-02	$1_0^1 9_0^4$	4.2328	1.2201E-04	-1.1046E-02	$1_0^1 4_0^1 7_0^1 9_0^5$
3.1654	2.6578E-04	1.6303E-02	9_0^2	3.7784	3.2113E-04	1.7920E-02	$3_0^1 9_0^4$	4.2383	3.2235E-04	1.7954E-02	$3_0^1 4_0^1 7_0^1 9_0^5$
3.1735	1.4623E-04	-1.2093E-02	$1_0^1 9_0^2$	3.7818	3.2744E-04	1.8095E-02	$4_0^1 9_0^4$	4.3643	2.3094E-04	1.5197E-02	9_0^6
3.1790	2.6361E-04	1.6236E-02	$3_0^1 9_0^2$	3.7865	1.7047E-04	-1.3056E-02	$1_0^1 3_0^1 9_0^4$	4.3646	1.2315E-04	1.1097E-02	$3_0^1 7_0^1 9_0^5$
3.1824	3.2014E-04	1.7893E-02	$4_0^1 9_0^2$	3.7899	1.5890E-04	-1.2606E-02	$1_0^1 4_0^1 9_0^4$	4.3724	1.2643E-04	-1.1244E-02	$1_0^1 9_0^6$
3.1871	1.3985E-04	-1.1826E-02	$1_0^1 3_0^1 9_0^2$	3.7954	3.4703E-04	1.8629E-02	$3_0^1 4_0^1 9_0^4$	4.3779	3.1843E-04	1.7845E-02	$3_0^1 9_0^6$
3.1905	1.5564E-04	-1.2476E-02	$1_0^1 4_0^1 9_0^2$	3.8035	1.6085E-04	-1.2683E-02	$1_0^1 3_0^1 4_0^1 9_0^4$	4.3813	2.8726E-04	1.6949E-02	$4_0^1 9_0^6$
3.1959	2.7587E-04	1.6609E-02	$3_0^1 4_0^1 9_0^2$	3.8225	1.0972E-04	-1.0475E-02	$3_0^1 4_0^1 9_0^4$	4.3859	1.6904E-04	-1.3001E-02	$1_0^1 3_0^1 9_0^6$
3.2040	1.2743E-04	-1.1288E-02	$1_0^1 3_0^1 4_0^1 9_0^2$	3.8906	1.0697E-04	1.0343E-02	$6_0^1 9_0^4$	4.3894	1.3920E-04	-1.1798E-02	$1_0^1 4_0^1 9_0^6$
3.2230	1.1263E-04	-1.0613E-02	$3_0^1 4_0^1 9_0^2$	3.9042	1.1158E-04	1.0563E-02	$3_0^1 6_0^1 9_0^4$	4.3948	3.5213E-04	1.8765E-02	$3_0^1 4_0^1 9_0^6$
3.2912	1.0140E-04	1.0070E-02	$6_0^1 9_0^2$	3.9081	1.6679E-04	1.2915E-02	$7_0^1 9_0^4$	4.5036	1.1611E-04	1.0776E-02	$3_0^1 6_0^1 9_0^6$
3.3086	1.0608E-04	1.0299E-02	$7_0^1 9_0^2$	3.9216	2.3798E-04	1.5427E-02	$3_0^1 7_0^1 9_0^4$	4.5075	1.9217E-04	1.3862E-02	$7_0^1 9_0^6$
3.3222	1.3496E-04	1.1617E-02	$3_0^1 7_0^1 9_0^2$	3.9250	2.1745E-04	1.4746E-02	$4_0^1 7_0^1 9_0^4$	4.5156	1.0881E-04	-1.0431E-02	$1_0^1 7_0^1 9_0^6$
3.3256	1.3818E-04	1.1755E-02	$4_0^1 7_0^1 9_0^2$	3.9297	1.3134E-04	-1.1460E-02	$1_0^1 3_0^1 7_0^1 9_0^4$	4.5211	3.0295E-04	1.7405E-02	$3_0^1 7_0^1 9_0^6$
3.3391	1.5447E-04	1.2428E-02	$3_0^1 4_0^1 7_0^1 9_0^2$	3.9331	1.1023E-04	-1.0499E-02	$1_0^1 4_0^1 7_0^1 9_0^4$	4.5245	2.5177E-04	1.5867E-02	$4_0^1 7_0^1 9_0^6$
3.4652	2.6355E-04	1.6234E-02	9_0^3	3.9386	2.7567E-04	1.6603E-02	$3_0^1 4_0^1 7_0^1 9_0^4$	4.6640	2.0560E-04	1.4339E-02	9_0^7
3.4732	1.4474E-04	-1.2031E-02	$1_0^1 9_0^3$	3.9467	1.3368E-04	-1.1562E-02	$1_0^1 3_0^1 4_0^1 7_0^1 9_0^4$	4.6721	1.1245E-04	-1.0604E-02	$1_0^1 9_0^7$
3.4787	2.9751E-04	1.7249E-02	$3_0^1 9_0^3$	4.0646	2.4942E-04	1.5793E-02	9_0^5	4.6776	3.0106E-04	1.7351E-02	$3_0^1 9_0^7$
3.4821	3.2131E-04	1.7925E-02	$4_0^1 9_0^3$	4.0727	1.3667E-04	-1.1691E-02	$1_0^1 9_0^5$	4.6810	2.5738E-04	1.6043E-02	$4_0^1 9_0^7$
3.4868	1.5794E-04	-1.2567E-02	$1_0^1 3_0^1 9_0^3$	4.0781	3.2530E-04	1.8036E-02	$3_0^1 9_0^5$	4.8072	1.9287E-04	1.3888E-02	$7_0^1 9_0^7$
3.4902	1.5603E-04	-1.2491E-02	$1_0^1 4_0^1 9_0^3$	4.0816	3.0846E-04	1.7563E-02	$4_0^1 9_0^5$	4.9638	1.8067E-04	1.3441E-02	9_0^8

Table E122: Energies, Intensities and Franck-Condon factors calculated from ezSpectrum 3.0 for the $6d \leftarrow 6a$ transition. Notation for the transition, 3_0^1 indicates the transition in ω_3 from $v'' = 0$ to $v' = 1$ with modes numbered according to Table E115. The band origin is the ADE from Table E107.

E eV	Intensity	FCF	Assignment	E eV	Intensity	FCF	Assignment
1.5642	2.1619E-08	1.4703E-04	4_0^2	2.8398	2.1069E-08	-1.4515E-04	$2_0^1 4_0^1 10_0^2 13_0^2$
1.9971	2.9312E-08	-1.7121E-04	$4_0^2 13_0^1$	2.8446	6.2062E-08	2.4912E-04	$4_0^2 10_0^2 13_0^2$
2.1908	2.3254E-08	-1.5249E-04	$4_0^1 10_0^1 13_0^1$	2.8483	2.9441E-08	-1.7158E-04	$1_0^2 4_0^2 10_0^2 13_0^2$
2.2044	4.0403E-08	2.0100E-04	$4_0^2 10_0^1 13_0^1$	2.8493	2.6821E-08	1.6377E-04	$4_0^1 13_0^3$
2.2132	2.3623E-08	1.5370E-04	$2_0^1 4_0^2 10_0^1 13_0^1$	2.8534	3.3590E-08	1.8328E-04	$2_0^1 4_0^2 10_0^2 13_0^2$
2.2180	2.2914E-08	-1.5137E-04	$4_0^3 10_0^1 13_0^1$	2.8582	3.0898E-08	-1.7578E-04	$4_0^3 10_0^2 13_0^2$
2.3981	2.0305E-08	1.4250E-04	$4_0^1 10_0^2 13_0^1$	2.8629	4.6802E-08	-2.1634E-04	$4_0^2 13_0^3$
2.4117	3.3706E-08	-1.8359E-04	$4_0^2 10_0^2 13_0^1$	2.8663	2.0538E-08	-1.4331E-04	$3_0^2 4_0^2 10_0^2 13_0^2$
2.4164	2.2645E-08	-1.5048E-04	$4_0^1 13_0^2$	2.8666	2.2350E-08	1.4950E-04	$1_0^2 4_0^2 13_0^3$
2.4300	4.0500E-08	2.0125E-04	$4_0^2 13_0^2$	2.8717	3.1563E-08	-1.7766E-04	$2_0^1 4_0^2 13_0^3$
2.4388	2.7029E-08	1.6441E-04	$2_0^1 4_0^2 13_0^2$	2.8743	2.7077E-08	1.6455E-04	$4_0^2 6_0^1 10_0^2 13_0^2$
2.4436	2.4328E-08	-1.5598E-04	$4_0^3 13_0^2$	2.8765	2.6800E-08	1.6371E-04	$4_0^3 13_0^3$
2.6190	2.2073E-08	1.4857E-04	$4_0^2 10_0^3 13_0^1$	2.8831	2.0963E-08	1.4479E-04	$2_0^1 4_0^2 6_0^1 10_0^2 13_0^2$
2.6237	3.7922E-08	1.9474E-04	$4_0^1 10_0^1 13_0^2$	2.8927	2.2769E-08	-1.5089E-04	$4_0^2 6_0^1 13_0^3$
2.6325	2.3036E-08	1.5178E-04	$2_0^1 4_0^1 10_0^1 13_0^2$	2.9014	2.0977E-08	-1.4483E-04	$2_0^1 4_0^2 6_0^1 13_0^3$
2.6373	6.4460E-08	-2.5389E-04	$4_0^2 10_0^1 13_0^2$	3.0383	2.9273E-08	1.7109E-04	$4_0^1 10_0^3 13_0^2$
2.6410	3.0679E-08	1.7515E-04	$1_0^2 4_0^2 10_0^1 13_0^2$	3.0519	4.5831E-08	-2.1408E-04	$4_0^2 10_0^3 13_0^2$
2.6461	3.8448E-08	-1.9608E-04	$2_0^1 4_0^2 10_0^1 13_0^2$	3.0566	5.2316E-08	-2.2873E-04	$4_0^1 10_0^3 13_0^3$
2.6509	3.5016E-08	1.8713E-04	$4_0^3 10_0^1 13_0^2$	3.0603	2.4954E-08	1.5797E-04	$1_0^2 4_0^1 10_0^1 13_0^3$
2.6590	2.0149E-08	1.4195E-04	$3_0^2 4_0^2 10_0^1 13_0^2$	3.0607	2.2672E-08	-1.5057E-04	$2_0^1 4_0^2 10_0^3 13_0^2$
2.6597	2.0130E-08	1.4188E-04	$2_0^1 4_0^3 10_0^1 13_0^2$	3.0654	3.2357E-08	-1.7988E-04	$2_0^1 4_0^1 10_0^1 13_0^3$
2.6670	2.9647E-08	-1.7218E-04	$4_0^2 6_0^1 10_0^1 13_0^2$	3.0655	2.0998E-08	1.4491E-04	$4_0^3 10_0^3 13_0^2$
2.6758	2.4737E-08	-1.5728E-04	$2_0^1 4_0^2 6_0^1 10_0^1 13_0^2$	3.0702	8.7248E-08	2.9538E-04	$4_0^2 10_0^1 13_0^3$
2.8310	3.8109E-08	-1.9522E-04	$4_0^1 10_0^2 13_0^2$	3.0739	4.1549E-08	-2.0384E-04	$1_0^2 4_0^2 10_0^1 13_0^3$

Appendix F

Additional Appendices

F.1 List of Publications

The following articles were published during candidature, however do not form a part of this thesis:

1. **Watson, P.**, Yong, H., Lapere, K. M. L., Kettner, M., McKinley, A. & Wild, D., *Chemical Physics Letters*. **2016**, *654*, 119-124.
2. Corkish, T. R., 't Hart, D. B., **Watson, P. D.**, McKinley, A. J. & Wild, D. A., *Journal of Molecular Spectroscopy*. **2019**, *364*, 111178.
3. Haakansson, C. T., Corkish, T. R., **Watson, P. D.**, McKinley, A. J. & Wild, D. A., *Chemical Physics Letters*. **2020**, *761*, 138060.
4. **Watson, P. D.**, McKinley, A. J. & Wild, D. A., *Journal of Molecular Spectroscopy*. **2020**, *372*, 111320.
5. Corkish, T., Haakansson, C., **Watson, P. D.**, Robinson, H., McKinley, A. & Wild, D., *ChemPhysChem*. **2021**, *22*, 1316-1320
6. Haakansson, C. T., Corkish, T. R., **Watson, P. D.**, Robinson, H. T., Tsui, T., McKinley, A. J. & Wild, D. A., *ChemPhysChem*. **2021**, *22*, 808-812

7. Corkish, T. R., Haakansson, C. T., **Watson, P. D.**, McKinley, A. J. & Wild, D. A., *ChemPhysChem.* **2021**, *22*, 69-75

F.2 SEVI Chamber Volume

The interior volume of the SEVI apparatus can be estimated by determining the volume of the individual chambers:

4-way cross is described by two intersecting cylinders where the intersecting region is described by a Steinmetz solid.

$$V = 2\pi r^2 \ell - \frac{16}{3}r^3 \quad (\text{F.1})$$

Similarly the 6-way cross is 3 intersecting cylinders with 2 tricylinders removed.

$$V = 3\pi r^2 \ell - 2 \times 8(2 - \sqrt{2})r^3 \quad (\text{F.2})$$

The Tee chambers are similar to the 4-way cross however one of the intersecting cylinders (and the Steinmetz solid) is halved.

$$V = \pi r^2 \ell + \pi r^2 \frac{\ell}{2} - \frac{1}{2} \times \frac{16}{3}r^3 = \frac{3}{2}\pi r^2 \ell - \frac{16}{6}r^3 \quad (\text{F.3})$$

With the flight tube a simple cylinder of length L . Combining these volumes to estimate the total volume of the SEVI apparatus yields the following:

$$\begin{aligned} V &= 2\pi r^2 \ell - \frac{16}{3}r^3 + 3\pi r^2 \ell - 2 \times 8(2 - \sqrt{2})r^3 + 2(\frac{3}{2}\pi r^2 \ell - \frac{16}{6}r^3) + \pi r^2 L \\ &= 8\pi r^2 \ell - \frac{32}{3}r^3 - 16(2 - \sqrt{2})r^3 + \pi r^2 L \\ &= r^2(8\pi \ell - 16r(\frac{8}{3} - \sqrt{2}) + \pi L) \end{aligned} \quad (\text{F.4})$$

where $\ell = 21.9456 \text{ cm}$, $r = 9.628 \text{ cm}$ and $L = 26.9748 \text{ cm}$.ⁱ The subsequent estimated volume is then 12510 cm^3 (4 s.f.).

ⁱChamber lengths are taken from specifications available through *Kurt Lesker* (example part number is C6-0600S in the case of the 6-way cross). Chamber radius is determined by measurement of the interior diameter with vernier callipers.